# SANDIA REPORT

SAND88–0196 • UC–721
Unlimited Release
Printed August 1991



# Hydrogeochemical Studies of the Rustler Formation and Related Rocks in the Waste Isolation Pilot Plant Area, Southeastern New Mexico

M. D. Siegel, S. J. Lambert, K. L. Robinson, Editors



**Prepared by**
**Sandia National Laboratories**
**Albuquerque, New Mexico 87185 and Livermore, California 94550**
**for the United States Department of Energy**
**under Contract DE-AC04-76DP00789**

Issued by Sandia National Laboratories, operated for the United States Department of Energy by Sandia Corporation.



Available to DOE and DOE contractors from
Office of Scientific and Technical Information
PO Box 62
Oak Ridge, TN 37831

Prices available from (615) 576-8401, FTS 626-8401

Available to the public from
National Technical Information Service
US Department of Commerce
5285 Port Royal Rd
Springfield, VA 22161

NTIS price codes
Printed copy: A99
Microfiche copy: A01

SAND88-0196
Unlimited Release
Printed August 1991

Distribution
Category UC-721

# Hydrogeochemical Studies of the Rustler Formation and Related Rocks in the Waste Isolation Pilot Plant Area, Southeastern New Mexico

M. D. Siegel, S. J. Lambert, and K. L. Robinson, Editors
Sandia National Laboratories
Albuquerque, New Mexico 87185

## ABSTRACT

Chemical, mineralogical, isotopic, and hydrological studies of the Culebra dolomite member of the Rustler Formation and related rocks are used to delineate hydrochemical facies and form the basis for a conceptual model for post-Pleistocene groundwater flow and chemical evolution. Modern flow within the Culebra in the Waste Isolation Pilot Plant (WIPP) area appears to be largely north-to-south; however, these flow directions under confined conditions are not consistent with the salinity distribution in the region surrounding the WIPP Site. Isotopic, mineralogical, and hydrological data suggest that vertical recharge to the Culebra in the WIPP area and to the immediate east and south has not occurred for several thousand years. Eastward-increasing $^{234}U/^{238}U$ activity ratios suggest recharge from a near-surface Pleistocene infiltration zone flowing from the west-northwest and imply a change in flow direction in the last 30,000 to 12,000 years.

Culebra groundwaters are in chemical equilibrium with gypsum and are undersaturated with halite and anhydrite. A partial-equilibrium model for the chemical evolution of the groundwater suggests that Na, Cl, Mg, K, and $SO_4$ are added to the Culebra by dissolution of evaporite salts in adjacent strata. Equilibrium is maintained with gypsum and calcite, but dolomite supersaturation increases as the salinity of the water increases. Stable-isotope compositions of carbonates are consistent with this model and indicate that no recrystallization of dolomite in equilibrium with the groundwater has occurred. Major and minor element correlations are consistent with several plausible mechanisms of water/rock interaction, including sorption of lithium and boron by clays and dissolution of Mg-rich clays.

# ACKNOWLEDGMENTS

In addition to the authors of component chapters of this report, the editors thank several individuals whose valuable discussions and critical reviews have improved this report, specifically R. L. Beauheim, D. G. Brookins, W. H. Casey, P. B. Davies, B. F. Jones, J. L. Krumhansl, A. R. Lappin, and L. N. Plummer. D. G. Brookins and W. H. Casey provided detailed reviews of most chapters. J. L. Krumhansl provided an additional review of the chapter on mineralogy. A. R. Lappin provided text and figures summarizing the physical hydrology.

I. J. Hall assisted with the principal component analysis. S. E. Bayley helped with the reduction of the data from that analysis and preparation of several of the figures. P. James and M. Adams prepared the element ratio and factor score contour plots. L. N. Plummer allowed us to use an unreleased version of the PHRQPITZ code used in the saturation index calculations and provided some instruction in its use. S. Anderholm assisted in the reaction path calculations using PHRQPITZ. T. Johnson helped to coordinate preparation of the final figures. Suggestions by B. F. Jones, L. N. Plummer, D. G. Brookins, and W. H. Casey led to extensive revisions, which greatly improved this report.

# GENERAL CONTENTS

# EXECUTIVE SUMMARY

An understanding of the geological history of the Rustler Formation in the northern Delaware Basin of southeastern New Mexico is considered fundamental to the evaluation of the ability of the bedded evaporite environment at the Waste Isolation Pilot Plant (WIPP) to isolate waste radionuclides from the accessible environment for long periods of time. The Rustler is deemed important because it (1) is the uppermost evaporite-bearing unit in the Ochoan (Permian) sequence, (2) is experiencing active dissolution where it outcrops west of the WIPP Site, (3) immediately overlies the Salado Formation, where the WIPP Facility is being mined, and (4) contains interbeds of brittle fractured rock that contain the most abundant and regionally persistent occurrences of groundwater associated with the evaporites.

The US Department of Energy agreed to carry out several supplementary geotechnical studies as part of the WIPP Site characterization program. This report has been prepared to satisfy part of that agreement, as specified in Appendix II to the November 1984 Modification to the Working Agreement.

An extensive geochemical data base, including analyses of major and minor solutes, redox data, mineralogical studies of intact core samples, and isotopic studies of waters, carbonates, and sulfates, has been assembled for the Rustler Formation and adjacent units in the northern Delaware Basin. These data were evaluated to compare the aqueous geochemistry with host rock mineralogies, to delineate hydrochemical facies in the Culebra member of the Rustler Formation, and to determine the consistency of these facies with groundwater flow patterns derived from site stratigraphy and hydrology. The resulting synthesis of data and current hypotheses concerning the origin, composition, and history of waters in the Culebra member of the Rustler Formation and related units provides a tentative conceptual model for groundwater flow in the Rustler during the last 12,000 to 16,000 years. This model can form part of the basis for assessing the long-term performance of the geological containment

system at the WIPP, which is developed in the underlying evaporites of the Salado Formation.

Based on the available hydrological data, modern flow within the Culebra at and near the WIPP Site is interpreted to be largely north-to-south, except in relatively low-transmissivity areas directly affected by either a high-transmissivity zone in the southeastern portion of the WIPP Site or by Nash Draw west of the WIPP Site. The amount of modern vertical flow into and out of the Culebra near site-center remains indeterminate; however, with the exception of the region in and near Nash Draw, this flow may be negligible, making the assumption of confined flow within the Culebra adequate for modeling purposes on some limited time scale. Specifically, it is assumed that the steady-state confined flow is adequate on the time scale of hydrological testing and disturbances due to the sinking of the WIPP shafts, probably 100 years or less. This does not preclude a limited amount of localized downward flow through the Tamarisk member from the Magenta to the Culebra over longer time periods, as facilitated by higher potentiometric levels in the Magenta than in the Culebra.

The measurement of modern head potentials, transmissivities, and/or fluid densities, however, does not give any direct indication of time scales on which the system might be transient. The geochemical and isotopic data suggest that inferences about flow direction and velocity based on present hydrologic conditions and modeling alone may not be uniformly applicable to directions and velocities during the past 10,000 years. In particular, present-day steady-state (north-to-south) regional water flow directions under confined conditions are not consistent with the salinity distribution at the WIPP Site, if the salinity distribution itself is assumed to be at steady state (i.e., fixed in place). For example, a hydrochemical facies having low salinity, with element ratios inconsistent with ongoing halite dissolution, lies downgradient along the modern flow directions from more saline water to the north.

Arguments that the observed solute distribution is generally consistent with the current hydrological flow field must rely heavily on the assumption of extensive vertical recharge and on the resultant subsurface mixing of at least two solute assemblages, especially in the southern part of the site. This would be required to provide fresher fluids to dilute the saline brines entering from the less permeable, halite-rich strata east of the sixteen-square-mile area delineating the WIPP.

Isotopic data, however, indicate that vertical recharge to the Culebra in the WIPP area and to the east and south has not occurred for several thousand years. Specifically, the three available radiocarbon dates in the Culebra are in excess of 12,000 to 16,000 years in both northern and southern portions of the study area, with no apparent regionally consistent or statistically significant age gradient.

Mineralogical and isotopic studies of sulfates in overlying layers also show that no significant amounts of either solutes or water have permeated vertically downward from the surface to recharge the Culebra. Specifically, much of the anhydrite in the Tamarisk member between the Magenta and Culebra members has not been hydrated to gypsum by recrystallization in the presence of fresh water, D/H ratios in gypsum throughout the Rustler are not consistent with a pervasively large water/rock ratio accompanying such hydration, and comparison of $^{87}Sr/^{86}Sr$ ratios of gypsums and carbonates in Rustler, Dewey Lake, and surface rocks shows that secondary sulfates and carbonates in the Rustler did not form in a hydrological regime that was uniformly interconnected with overlying rocks and the surface. Thus, the available mineralogical, hydrological, and isotopic data indicate no significant vertical connection between the Culebra and overlying strata.

The apparent discrepancy between modern flow direction and solute distribution can be explained by a change in flow direction in the last 30,000, or perhaps 12,000 years. Such a model is consistent with generally eastward-increasing $^{234}U/^{238}U$ activity ratios that indicate recharge from a near-surface Pleistocene infiltration zone,

flowing from the west-northwest. The model is also consistent with the cessation of recharge in the late Pleistocene, as indicated by the radiocarbon dates. A likely explanation for the less saline waters south of the WIPP Site is that at the time of influx of the present generation of Culebra groundwater from the west-northwest, Rustler halite was absent adjacent to the Culebra in that area, and did not provide a source of NaCl. Thus, the postulated paleoflow direction (from the west-northwest) is consistent with both flow perpendicular to the $^{234}U/^{238}U$ contours and flow parallel to the hydrochemical facies boundary between more saline water in the north and less saline water south of the WIPP.

A model for the chemical evolution of waters in the Culebra tentatively identifies the major sources and sinks for many of the solutes. It is proposed that: (1) solutes are added to the Culebra by dissolution of evaporite minerals; (2) the solubilities of gypsum and calcite increase as the salinity increases, and these minerals dissolve as chemical equilibrium is maintained between them and the groundwater; (3) equilibrium is not maintained between the waters and dolomite, and sufficient Mg is added to the waters by dissolution of accessory carnallite or polyhalite so that the degree of dolomite supersaturation increases with ionic strength; (4) clays within the fractures and rock matrix exert some control on the distribution of Li, B, Mg, and Si via sorption, ion exchange, and dissolution.

Increase of salinity in Culebra waters due to dissolution of evaporite salts in adjacent rock units is an irreversible chemical process affecting the water chemistry. The solubilities of gypsum, dolomite, and calcite increase with salinity up to 3 molal ionic strength and then decrease. Thus, even if the saturation indices for gypsum and calcite are near zero, the waters may still be capable of dissolving significant amounts of these phases if the salinity increases. Computer modeling of several hypothetical reaction paths shows that addition of solutes (Mg, $SO_4$, K, and Cl) to the Culebra from evaporite minerals such as polyhalite and carnallite in a

partial equilibrium system is consistent with the observed groundwater compositions, if dolomite does not precipitate from supersaturated solutions.

Isotopic studies of minerals and waters provide some support for this model. Stable-isotope compositions of carbonate minerals indicate that calcite has precipitated in equilibrium with the groundwater now found in the Culebra in some areas, but that dolomite has not extensively recrystallized or exchanged isotopes with meteoric groundwater of any age. There is also isotopic evidence that calcium sulfate has recrystallized (dissolved and reprecipitated) in the presence of Rustler ground-waters.

The results of principal component analysis (PCA) suggest that reactions with clay minerals may exert an observable influence on the water's minor-element chemistry throughout the study area. When the effects of solute addition associated with halite dissolution are factored out prior to the PCA, a Mg-$SiO_2$-alkalinity association is left that is negatively correlated with a pH-B-Li association. These correlations are consistent with several plausible mechanisms, including uptake of Li by vacant octahedral sites in a clay lattice, sorption of B by surface sites of clays, and dissolution of a reactive amorphous Si-Mg-rich layer in corrensite, the dominant Culebra clay mineral.

Investigations that could further elucidate the hypotheses proposed here include collection and analysis of isotopic and chemical data from additional boreholes, systematic examination of the mineralogy of samples from highly transmissive zones (containing core rubble rather than intact core), and more rigorous calculations of the extent of mass transfer that could result from precipitation, dissolution, ion exchange, and sorption.

# CHAPTER 1:

# SUMMARY OF HYDROGEOCHEMICAL CONSTRAINTS ON GROUNDWATER FLOW AND EVOLUTION IN THE RUSTLER FORMATION

Malcolm D. Siegel and Steven J. Lambert
Sandia National Laboratories

## ABSTRACT

Chemical, mineralogical, isotopic, and hydrological data from the Culebra dolomite member of the Rustler Formation and related rocks were evaluated to delineate hydrochemical facies in the Culebra dolomite, to compare these facies with host rock mineralogies and hydrological flow patterns, and to formulate a conceptual model for post-Pleistocene groundwater flow and chemical evolution in the Rustler. Modern flow within the Culebra at and near the Waste Isolation Pilot Plant (WIPP) Site appears to be largely north-to-south; however, these inferences about flow direction and velocity may not be uniformly applicable to directions and velocities during the past 10,000 years. Present-day regional water flow directions are not consistent with the salinity distribution at the WIPP Site, assuming confined hydrological flow. In particular, a hydrochemical facies with low salinity and element ratios inconsistent with halite dissolution lies downgradient from more saline water to the north.

Isotopic, mineralogical, and hydrological data suggest that vertical recharge to the Culebra in the WIPP area and to the immediate east and south has not occurred for several thousand years. These data are consistent with the view that the apparent discrepancy between modern flow direction and solute distribution can be explained by a change in flow direction during the last 30,000, or perhaps 12,000 years. This model is consistent with generally eastward-increasing $^{234}U/^{238}U$ activity ratios that

suggest recharge from a near-surface Pleistocene infiltration zone, flowing from the west-northwest. Culebra groundwaters are in chemical equilibrium with gypsum and undersaturated with respect to halite and anhydrite. A partial-equilibrium model for the chemical evolution of the groundwater suggests that Na, Cl, Mg, K, and $SO_4$ are added to the Culebra by dissolution of evaporite salts in adjacent strata. Equilibrium is maintained with gypsum and calcite, but dolomite supersaturation increases as the salinity of the water increases. Isotopic studies of minerals and waters provide some support for this model. Stable-isotope compositions of carbonates indicate no recrystallization of dolomite in equilibrium with the groundwater now found in the Culebra, but local precipitation of calcite has apparently occurred. There is isotopic as well as mineralogical indication that calcium sulfate has recrystallized (dissolved and reprecipitated) in the presence of Rustler groundwaters.

Controls on the distribution of minor and trace elements are more problematic. Reactions with clay minerals may exert an observable influence on the water's minor-element chemistry. Major and minor element correlations are consistent with several plausible mechanisms, including sorption of lithium and boron by clays and silicate dissolution.

# CONTENTS

# CONTENTS (Continued)



# FIGURES

# FIGURES (Continued)

# TABLES

# CHAPTER 1.0

## 1.1 INTRODUCTION

### 1.1.1 Purpose and Scope

In the "Agreement for Consultation and Cooperation between [the] Department of Energy and the State of New Mexico on the Waste Isolation Pilot Plant," the United States Department of Energy (DOE) agreed to conduct geotechnical studies as part of its site characterization program for the Waste Isolation Pilot Plant (WIPP). The Agreement was enacted on July 1, 1981 and was subsequently modified in November 1984 and August 1987. The DOE agreed to provide the State with a report entitled "Hydrogeochemical Facies in the Rustler Formation at the WIPP." The report was to "compare the solutes with host rock mineralogies at and between various well sites" and "... attempt to delineate hydrochemical facies in the Rustler Formation." In addition, "comparison of these facies with flow patterns derived solely from physical hydrology [was to] be made for the purpose of examining internal consistency" (United States Department of Energy and the State of New Mexico, 1988).

This report synthesizes current data and hypotheses concerning the origin of the composition of waters in the Culebra member of the Rustler Formation. Progress is described in attempts to compare the aqueous geochemistry with host rock mineralogies and geochemistry at and between various well sites and to delineate hydrochemical facies in the Culebra member. These facies are then compared to modern groundwater flow patterns derived from site stratigraphy and hydrology. Although the emphasis is on the properties of waters in the Culebra member, preliminary results from work dealing with the Magenta member, Rustler/Salado contact zone, and the Dewey Lake Red Beds are also included where relevant.

The area included in this study is shown in Figures 1-1 and 1-2. As shown in Figure 1-1, the WIPP Site is located in southeastern New Mexico, in the northern portion of the Delaware Basin. As used in this report, the term "WIPP Site" refers to the 16 square miles of T22S, R31E contained within WIPP Zone 3 as shown in these Figures. Figure 1-2 shows the locations of all wells and boreholes from which water and/or rock samples were taken and described in this report. Table 1-2 describes the kinds of data available from each of these locations.

The information collected in the independent studies described in Chapters 2 through 6 has been integrated in this chapter. The techniques used and specific data examined by the different research groups have led to alternative interpretations and hypotheses concerning the origins of solutes and water in the Culebra. The primary purpose of this chapter is to summarize the results of these investigations, present these differing views, point out the areas of disagreement, and discuss investigations that might resolve the controversies.

### 1.1.2 Geological Setting

The general stratigraphy in the vicinity of the WIPP Site has been described in detail, particularly in relation to occurrences and manifestations of groundwater, by Powers et al. (1978) and Lambert (1983). The need to consider groundwater geochemistry in its geological context warrants the following brief discussion of the stratigraphy (Figure 1-3) and geological features relevant to the geochemical results subsequently presented. The chemical formulae of minerals mentioned in this section are given in Table 1-2.

The Delaware Basin became a distinct structure by the late Pennsylvanian Period to early Permian Period, around 280 million years (Ma) ago. About 250 Ma ago, fringing reef-type structures began to grow around the margins of the developing basin. Now termed the Goat Seep Dolomite and Capitan Limestone, these carbonates interfinger with the basinal deposits of sandstones, shales, and carbonates now called the Delaware Mountain Group, the uppermost of which is the Bell Canyon Formation. The Bell Canyon contains

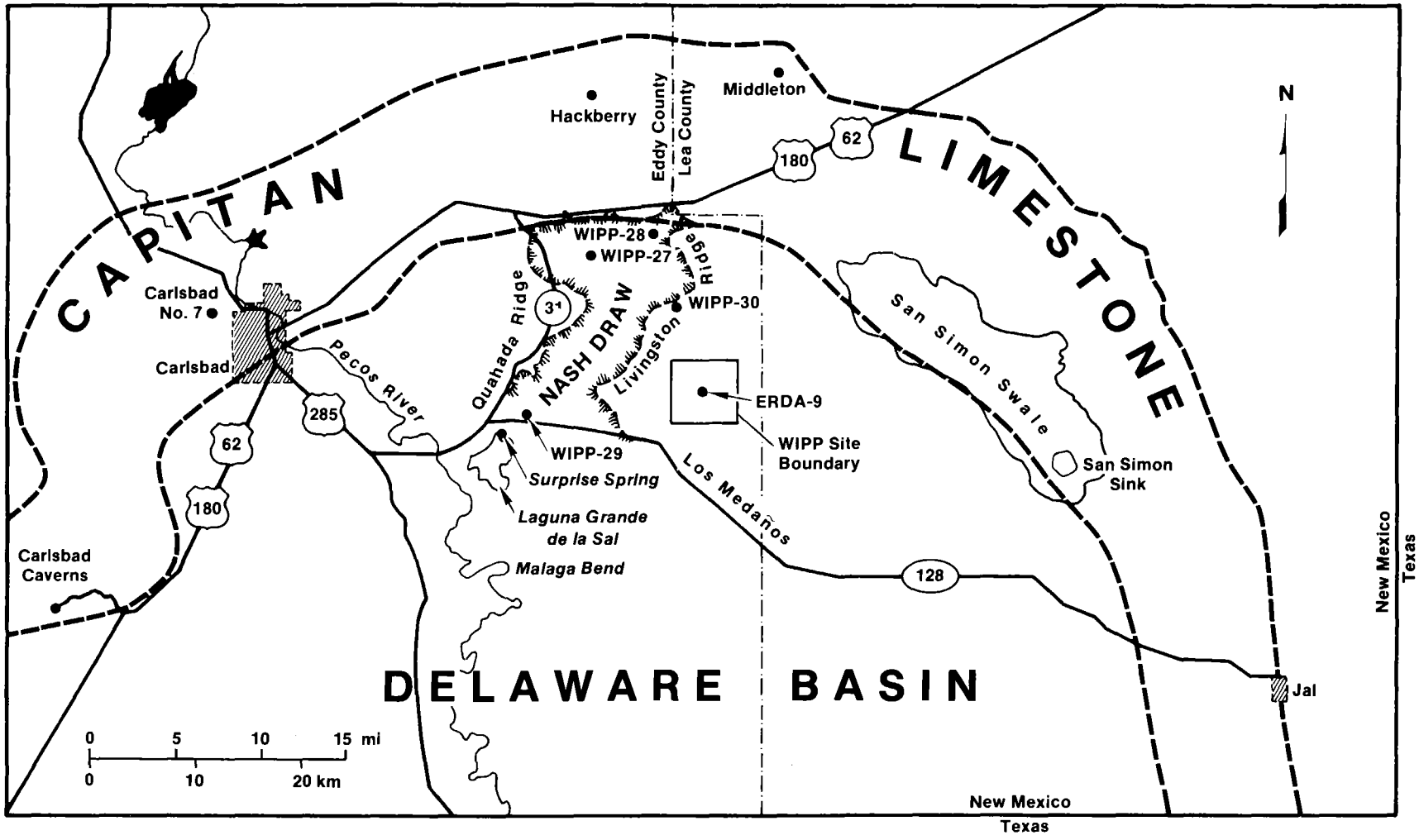


TRI-6330-72-1

Figure 1-1. Setting of the WIPP Site relative to the northern Delaware Basin, including selected geomorphic features and boreholes (modified by Lappin [1988] from Figure 6-1 of Lambert [1983]).

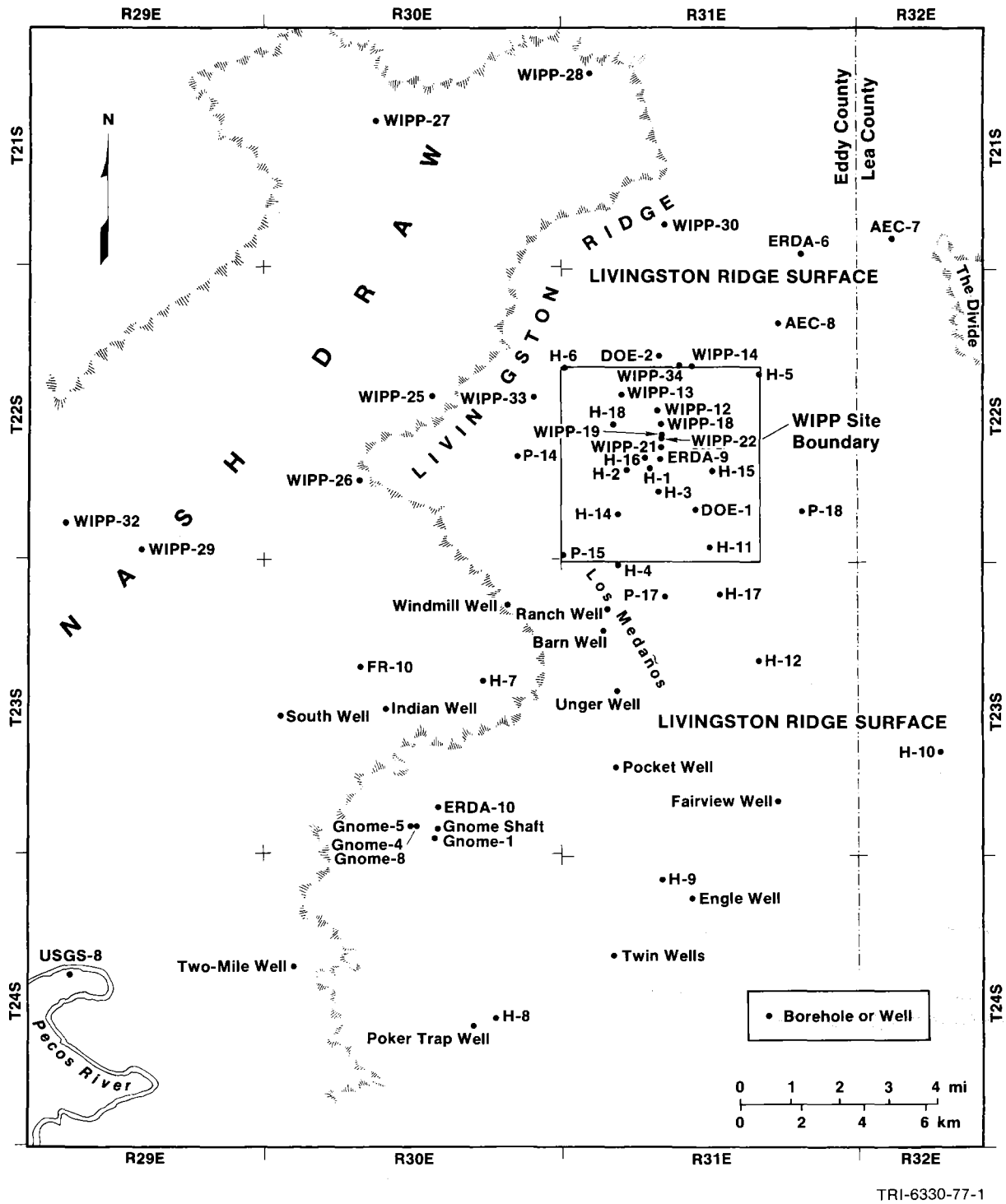


Figure 1-2. Map showing location of wells mentioned in this document.

## Table 1-1. Chapters in This Report Containing Discussion of Various Types of Data Available at Each Well

| Well | Unit[1] | Waters | | | | | | | | Rocks | | | | | |
|---|---|---|---|---|---|---|---|---|---|---|---|---|---|---|---|
| | | Solutes | Eh | TOC | PMC | $^3H$ | $\delta D$ | $\delta^{18}O$ | A.R. | Mnrlgy | $^{87}/^{86}Sr$ | $\delta^{13}C$ | $\delta^{18}O$ | $\delta D$ | $\Delta$ Head[2] |
| Zone A: | | | | | | | | | | | | | | | |
| DOE-1 | Mag | | | | | | | | | | | | | | + |
| DOE-1 | Cul | 2,4 | 6 | 6 | | | 5 | 5 | | | | | | | |
| H-5 | Mag | 2,4 | | | | | | | | | | | | | + |
| H-5 | Cul | 2,4 | 6 | 6 | | 5 | | 5 | 5 | | | 5 | 5 | | |
| H-5 | R/S | 4 | | | | | 5 | 5 | | | | | | | |
| P-18 | Cul | 4 | | | | | 5 | 5 | | | | | | | |
| P-18 | R/S | 4 | | | | | 5 | 5 | | | | | | | |
| H-11 | Cul | 2,4 | 6 | 6 | | | | 5 | | 3 | | | | | |
| H-12 | Cul | 2,4 | 6 | 6 | | 5 | | 5 | | | | | | | |
| Zone B: | | | | | | | | | | | | | | | |
| ENGLE | Cul | 2,4 | 6 | 6 | | 5 | 5 | 5 | | | | | | | |
| H-7 | Mag | | | | | | | | | | | | | | + |
| H-7 | Cul | 2,4 | 6 | 6 | | | | | | 3 | | | | | |
| H-7 | R/S | 4 | | | | | | | | | | | | | - |
| H-8 | Mag | 4 | | | | | | | | | | | | | + |
| H-8 | Cul | 2,4 | 6 | 6 | | | | | | | | | | | |
| H-8 | R/S | 4 | | | | | | | | | | | | | 0 |
| H-9 | Mag | 4 | | | | | | | | | | | | | + |
| H-9 | Cul | 2,4 | 6 | 6 | 5 | | 5 | 5 | | | | | | | |
| H-9 | R/S | 4 | | | | | | | | | | | | | |

## Table 1-1. Chapters in This Report Containing Discussion of Various Types of Data Available at Each Well (Continued)

| Well | Unit[1] | Waters | | | | | | | | Rocks | | | | | |
|---|---|---|---|---|---|---|---|---|---|---|---|---|---|---|---|
| | | Solutes | Eh | TOC | PMC | $^3H$ | $\delta D$ | $\delta^{18}O$ | A.R. | Mnrlgy | $^{87}/^{86}Sr$ | $\delta^{13}C$ | $\delta^{18}O$ | $\delta D$ | $\Delta$ Head[2] |
| FR-10 | Cul | | | | | | 5 | 5 | | | | | | | |
| Ranch | DL | 2 | | | | | 5 | | | | | | | | |
| Twin P. | DL | 2,4 | | | | | | | | | | | | | |
| Indian | Cul | 4 | | | | | | | | | | | | | |
| Two Mile | Cul | 4 | | | | | | | | | | | | | |
| Pocket | DL | 4 | | | 5 | | 5 | | | | | | | | |
| Windmill | Cul | 4 | | | | | | | | | | | | | |
| Gnome-SH | Cul | 4 | | | | | | | | | | | | | |
| Gnome-1 | Cul | 4 | | | | | | | | | | | | | |
| Gnome-4 | Cul | 4 | | | | | | | | | | | | | |
| Gnome-5 | Mag | 4 | | | | | | | | | | | | | |
| Gnome-5 | R/S | 4 | | | | | | | | | | | | | |
| Gnome-8 | Cul | 4 | | | | | | | | | | | | | |
| Unger | DL | | | | | 5 | | | | | | | | | |
| South Fairview | Cul<br>DL | 4 | | | | | 5 | | | | | | | | |

## Table 1-1. Chapters in This Report Containing Discussion of Various Types of Data Available at Each Well (Continued)

| Well | Unit[1] | Waters | | | | | | | | Rocks | | | | | |
|---|---|---|---|---|---|---|---|---|---|---|---|---|---|---|---|
| | | Solutes | Eh | TOC | PMC | $^3H$ | $\delta D$ | $\delta^{18}O$ | A.R. | Mnrlgy | $^{87}Sr/^{86}Sr$ | $\delta^{13}C$ | $\delta^{18}O$ | $\delta D$ | $\Delta$ Head[2] |
| Zone C: | | | | | | | | | | | | | | | |
| AEC-8 | DL | | | | | | | | | | 5 | | | 5 | |
| AEC-8 | Tam | | | | | | | | | | | | | 5 | |
| AEC-8 | BC | | | | | | | | | | | 5 | 5 | | |
| DOE-2 | 49r | | | | | | | | | | | | | | 0 |
| DOE-2 | Mag | | | | | | | | | | | | | | + |
| DOE-2 | Cul | 2,4 | 6 | 6 | | | 5 | 5 | | | | | | | |
| DOE-2 | BC | 2 | | | | | | | | | | | | | |
| H-1 | Mag | 4 | | | | | 5 | 5 | | | | | | | + |
| H-1 | Cul | 4 | | | | | 5 | 5 | | | | | | | |
| H-1 | lwr | | | | | | | | | | | | | | |
| H-1 | R/S | 4 | | | | | 5 | 5 | | | | | | | |
| H-2 | Mag | 4 | | | | | 5 | 5 | | | | | | | + |
| H-2 | Cul | 2,4 | | 6 | | | 5 | 5 | | | | | | | |
| H-2 | R/S | 4 | | | | | 5 | 5 | | | | | | | + |
| H-3 | 49r | | | | | | | | | | | | | | - |
| H-3 | Mag | 2,4 | | | | | 5 | 5 | | | | | | | + |
| H-3 | Cul | 2,4 | 6 | 6 | | 5 | 5 | 5 | | 3 | | | | | |
| H-3 | R/S | 4 | | | | | 5 | 5 | | | | | | | |
| H-4 | Mag | 2,4 | | | | | | | | | | | | | + |
| H-4 | Cul | 2,4 | 6 | 6 | 5 | 5 | 5 | 5 | 5 | 3 | | 5 | 5 | | |
| H-4 | R/S | 4 | | | | | 5 | 5 | | | | | | | |
| H-6 | Mag | 2,4 | | | | | | | | | | | | | 0 |
| H-6 | Cul | 2,4 | 6 | 6 | 5 | | 5 | 5 | 5 | 3 | | 5 | 5 | | |
| H-6 | R/S | 4 | | | | | 5 | 5 | | | | | | | - |

## Table 1-1. Chapters in This Report Containing Discussion of Various Types of Data Available at Each Well (Continued)

| Well | Unit[1] | Waters | | | | | | | | Rocks | | | | | |
|---|---|---|---|---|---|---|---|---|---|---|---|---|---|---|---|
| | | Solutes | Eh | TOC | PMC | $^3H$ | $\delta D$ | $\delta^{18}O$ | A.R. | Mnrlgy | $^{87/86}Sr$ | $\delta^{13}C$ | $\delta^{18}O$ | $\delta D$ | $\Delta$ Head[2] |
| H-10 | Mag | 4 | | | | | | | | | | | | | + |
| H-10 | Cul | 4 | | | | | | | | 3 | | | | | |
| H-10 | R/S | 4 | | | | | | | | | | | | | |
| H-14 | 49r | | | | | | | | | | | | | | (-) |
| H-14 | Mag | | | | | | | | | | | | | | + |
| H-14 | Cul | | 6 | 6 | | | | | | | | | | | |
| H-15 | Cul | | 6 | 6 | | | | | | | | | | | |
| H-16 | 49r | | | | | | | | | | | | | | (-) |
| H-16 | Mag | | | | | | | | | | | | | | + |
| H-16 | R/S | | | | | | | | | | | | | | (+) |
| H-17 | Cul | | 6 | | | | | | | | | | | | |
| H-18 | Cul | | 6 | | | | | | | | | | | | |
| P-14 | Cul | 2,4 | 6 | 6 | | | 5 | 5 | | | | | | | |
| P-14 | R/S | 4 | | | | | 5 | 5 | | | | | | | |
| P-15 | Cul | 4 | | | | | 5 | 5 | | | | | | | |
| P-15 | R/S | 4 | | | | | 5 | 5 | | | | | | | |
| P-17 | Cul | 2,4 | 6 | 6 | | | 5 | 5 | | | | | | | |
| P-17 | R/S | 4 | | | | | 5 | 5 | | | | | | | |
| WIPP-12 | Cul | | | | | | | | | 3 | | | | | |
| WIPP-13 | Mag | | | | | | | | | | 5 | | | | |
| WIPP-13 | Tam | | | | | | | | | | 5 | | | | |
| WIPP-13 | Cul | 2 | | | | | | | | | 5 | | | | |

## Table 1-1. Chapters in This Report Containing Discussion of Various Types of Data Available at Each Well (Continued)

| Well | Unit[1] | Waters | | | | | | | | Rocks | | | | | |
|---|---|---|---|---|---|---|---|---|---|---|---|---|---|---|---|
| | | Solutes | Eh | TOC | PMC | $^3H$ | $\delta D$ | $\delta^{18}O$ | A.R. | Mnrlgy | $^{87/86}Sr$ | $\delta^{13}C$ | $\delta^{18}O$ | $\delta D$ | $\Delta$ Head[2] |
| WIPP-14 | DL | | | | | | | | | | 5 | | | 5 | |
| WIPP-19 | DL | | | | | | | | | | 5 | | | 5 | |
| WIPP-19 | Cul | | 6 | 6 | | | | | | 3 | | | | | |
| WIPP-25 | DL | | | | | | | | | | 5 | | | | |
| WIPP-25 | 49r | | | | | | | | | | 5 | | | | |
| WIPP-25 | Mag | 2,4 | | | | | 5 | 5 | 5 | | 5 | 5 | 5 | | 0 |
| WIPP-25 | Cul | 2,4 | 6 | 6 | | | 5 | 5 | 5 | 3 | 5 | 5 | 5 | | |
| WIPP-25 | lwr | | | | | | | | | | 5 | | | | |
| WIPP-25 | R/S | 2,4 | | | | | 5 | 5 | 5 | | | | | | (-) |
| WIPP-26 | Mag | | | | | | | | | | 5 | | | | |
| WIPP-26 | Tam | | | | | | | | | | 5 | | | | |
| WIPP-26 | Cul | 2,4 | 6 | 6 | | | 5 | 5 | 5 | 3 | 5 | 5 | 5 | | |
| WIPP-26 | R/S | 2,4 | | | | | 5 | 5 | 5 | | | | | | (-) |
| WIPP-28 | Mag | | | | | | | | | | | 5 | 5 | | + |
| WIPP-28 | Cul | 2,4 | | | | | 5 | 5 | 5 | | | 5 | 5 | | |
| WIPP-28 | R/S | 2,4 | | | | | 5 | 5 | 5 | | | | | | 0 |
| WIPP-30 | Mag | 4 | | | | | 5 | 5 | | | | 5 | 5 | | + |
| WIPP-30 | Cul | 2,4 | | | | | 5 | 5 | 5 | | | 5 | 5 | | |
| WIPP-30 | R/S | 2,4 | | | | | 5 | 5 | 5 | | | | | | - |
| WIPP-33 | 49r | | | | | | | | | | 5 | | | 5 | |
| WIPP-33 | Mag | | | | | | | | | | 5 | 5 | 5 | | |
| WIPP-33 | Cul | | | | | | | | | | 5 | | | | |
| WIPP-33 | lwr | | | | | | | | | | 5 | | | | |
| WIPP-34 | 49r | | | | | | | | | | 5 | | | 5 | |
| WIPP-34 | Mag | | | | | | | | | | 5 | | | 5 | |
| WIPP-34 | lwr | | | | | | | | | | 5 | | | 5 | |

## Table 1-1. Chapters in This Report Containing Discussion of Various Types of Data Available at Each Well (Continued)

| Well | Unit[1] | Waters | | | | | | | | Rocks | | | | | | |
|---|---|---|---|---|---|---|---|---|---|---|---|---|---|---|---|---|
| | | Solutes | Eh | TOC | PMC | $^3H$ | $\delta D$ | $\delta^{18}O$ | A.R. | Mnrlgy | $^{87}Sr/^{86}Sr$ | $\delta^{13}C$ | $\delta^{18}O$ | $\delta D$ | $\Delta$ Head[2] |
| Zone D: | | | | | | | | | | | | | | | |
| WIPP-27 | Mag | 2,4 | | | | | 5 | 5 | 5 | | | | | | + |
| WIPP-27 | Cul | 2,4 | | | | | 5 | 5 | 5 | | | 5 | 5 | | |
| WIPP-27 | R/S | 4 | | | | | 5 | 5 | | | | | | | |
| WIPP-29 | Cul | 2,4 | | 6 | | | 5 | 5 | 5 | 3 | | 5 | | | |
| WIPP-29 | R/S | 2,4 | | | | | 5 | 5 | 5 | | | | | | - |
| S.Spring | Tam | 4 | | | | | | 5 | 5 | | | | | | |

1. Unit abbreviations:
   - DL: Dewey Lake Red Beds
   - 49r: Rustler Fm., Forty-niner member
   - Mag: Rustler Fm., Magenta dolomite member
   - Tam: Rustler Fm., Tamarisk member
   - Cul: Rustler Fm., Culebra dolomite member
   - lwr: Rustler Fm., lower member
   - BC: Bell Canyon Fm.
2. Comparison of hydraulic heads for nearby units.
   - For Mag and R/S:
     - "+": unit's head is higher than that of Culebra; potential for flow into Culebra.
     - "-": unit's head is lower than that of Culebra; potential for flow from Culebra.
   - For 49r:
     - "-": unit's head is lower than that of Magenta; potential for flow from Magenta into Forty-niner.
   - For all:
     - "0": approximately equivalent heads in units being compared.
     - "()": potential flow direction is based on reported lower or upper limit for head of one of the units (see Beauheim, 1987).

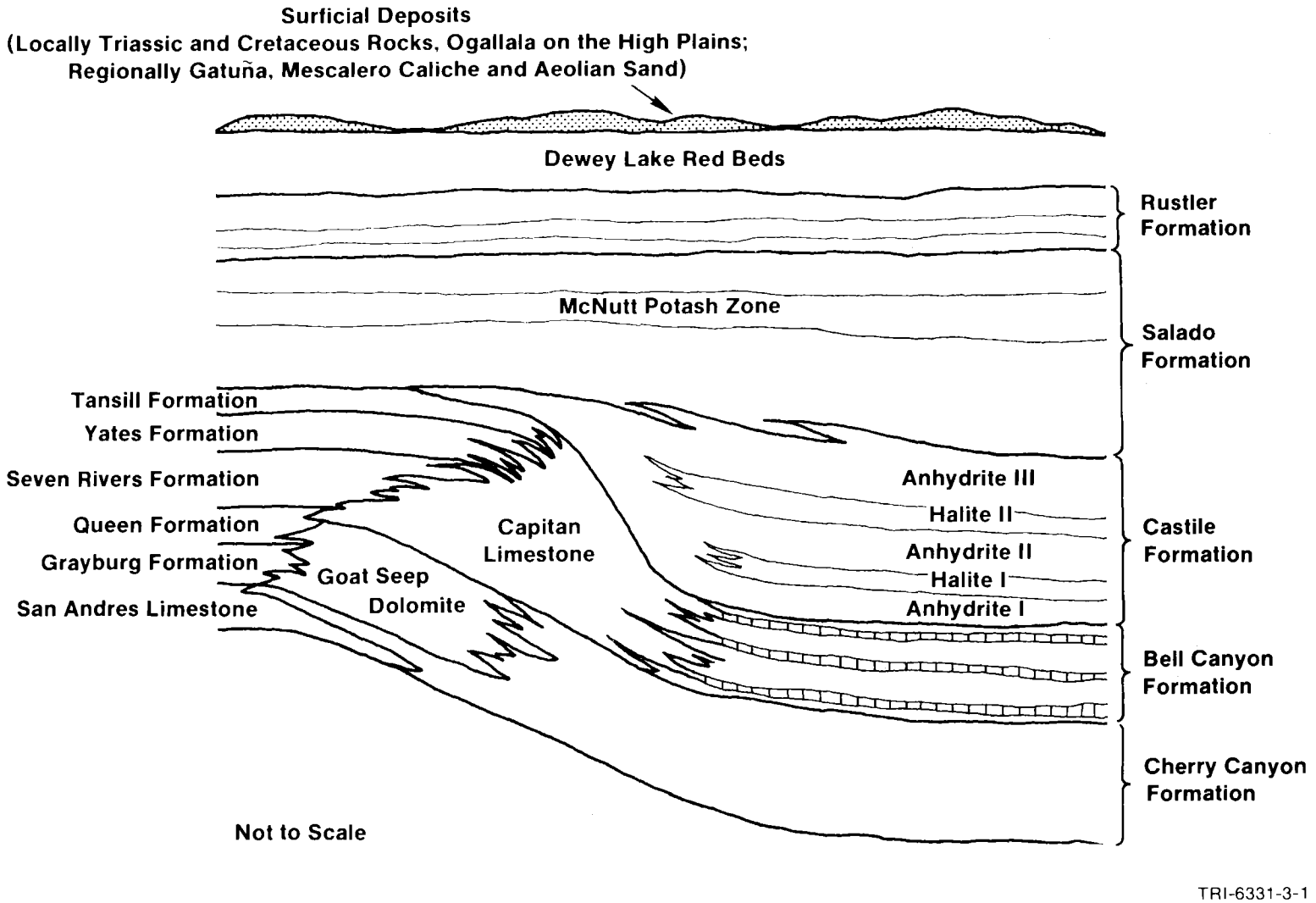


Figure 1-3. Generalized stratigraphy of Guadalupian (Permian) and younger rocks in the Delaware Basin.
A. Idealized north-south section, looking east, at the northern apex of the Capitan Limestone, near the Eddy-Lea County line (from Lambert, 1983).

| System | Series | Group | Formation | Member |
|---|---|---|---|---|
| Recent | Recent | | Surficial Deposits | |
| Quater-nary | Pleisto-cene | | Mescalero Caliche | |
| | | | Gatuña | |
| Triassic | | Dockum | Undivided | |
| Permian | Ochoan | | Dewey Lake Red Beds | |
| | | | Rustler | Forty-niner |
| | | | | Magenta Dolomite |
| | | | | Tamarisk |
| | | | | Culebra Dolomite |
| | | | | lower |
| | | | Salado | |
| | | | Castile | |
| | Guadalupian | Delaware Mountain | Bell Canyon | |
| | | | Cherry Canyon | |
| | | | Brushy Canyon | |

TRI-6330-89-2

Figure 1-3. B. Stratigraphic column of Guadalupian and younger rocks, exclusive of the Capitan complex, including members of the Rustler Formation (from Lappin, 1988).

## Table 1-2. Chemical Formulae[1] of Minerals Mentioned in This Chapter

| Mineral | Formula |
|---|---|
| Amesite | $(Mg_4Al_2)(Si_2Al_2)O_{10}(OH)_8$ |
| Anhydrite | $CaSO_4$ |
| Calcite | $CaCO_3$ |
| Carnallite | $KMgCl_3 \cdot 6H_2O$ |
| Chlorite | $(Mg,Al,Fe)_{12}(Si,Al)_8O_{20}(OH)_{16}$ |
| Corrensite | mixed-layer chlorite/smectite |
| Dolomite | $CaMg(CO_3)_2$ |
| Feldspar | $(K,Na,Ca)(Si,Al)_4O_8$ |
| Glauberite | $Na_2Ca(SO_4)_2$ |
| Gypsum | $CaSO_4 \cdot 2H_2O$ |
| Halite | $NaCl$ |
| Illite | $K_{1-1.5}Al_4[Si_{7-6.5}Al_{1-1.5}O_{20}](OH)_4$ |
| Kainite | $KMgClSO_4 \cdot 3H_2O$ |
| Kieserite | $MgSO_4 \cdot H_2O$ |
| Langbeinite | $K_2Mg_2(SO_4)_3$ |
| Magnesite | $MgCO_3$ |
| Polyhalite | $K_2Ca_2Mg(SO_4)_4 \cdot 2H_2O$ |
| Pyrite | $FeS_2$ |
| Quartz | $SiO_2$ |
| Serpentine | $Mg_3Si_2O_5(OH)_4$ |
| Smectite | $(Ca/2,Na)_{0.7}(Al,Mg,Fe)_4(Si,Al)_8O_{20}(OH)_4 \cdot nH_2O$ |
| Sylvite | $KCl$ |

1. Formulae are taken from Fleischer (1987) and Deer, Howie, and Zussman (1962).

local occurrences of economically important hydrocarbons and sporadically distributed oilfield-type brines, and forms the substrate for later evaporite deposition. The Capitan Limestone has a locally developed cavernous porosity displaying the classic features of limestone karst and includes Carlsbad Caverns.

The sandstones and shales of the Bell Canyon Formation grade upward into the alternating sequence of sulfate and carbonate laminations characteristic of the Castile Formation. The thick Castile sequences of sulfate/carbonate are interrupted two (and locally three) times by comparably thick sequences of bedded rock salt containing glauberite as an accessory mineral. The Salado Formation overlying the Castile consists dominantly of halite, interrupted at various intervals of meters to tens of meters by beds of anhydrite, polyhalite, mudstone, and local potash mineralization (sylvite or langbeinite, with or without accessory carnallite, kieserite, kainite, and glauberite, all in a halite matrix) of economic importance. The nonhalitic units, on the order of 0.1 to 1 m thick, have been numbered (in some cases named) for convenience as "marker" beds, where uniquely identifiable, to facilitate cross-basinal stratigraphic correlation. The WIPP mined facility is being emplaced just above Marker Bed 139 in the Salado, at an approximate depth of 660 m. Radiometric dates on sylvites (Register and Brookins, 1980) and polyhalites (Brookins et al., 1980) give generally concordant post-Permian ages of crystallization and/or recrystallization of 214 ± 15 Ma and 195-205 Ma, respectively. Clay minerals from the WIPP Facility in the Salado preserve a possibly detrital geochemical signature, unaltered by deposition and diagenesis, and having a radiometric age of 428 ± 7 Ma (Brookins and Lambert, 1987; 1988).

The Rustler Formation, overlying the Salado, contains five members according to the regional stratigraphic nomenclature, in ascending stratigraphic sequence: (1) a lower member (unnamed) consisting of siltstone/mudstone, anhydrite locally altered to gypsum, and containing halite under most of the WIPP Site; (2) the relatively permeable Culebra dolomite member, containing dominantly dolomite with subordinate anhydrite and/or gypsum; (3) the Tamarisk member, dominantly anhydrite/gypsum, with subordinate

fine-grained clastics, containing halite to the east of the WIPP Site; (4) the Magenta member, another dolomite/sulfate unit containing sporadic occurrences of groundwater near the WIPP Site; and (5) the Forty-niner member, similar in lithology to the other nondolomitic units, but containing halite only in the easternmost part of the study area. The Culebra member is the first major water-bearing unit above the WIPP Facility; for this reason, the hydrochemistry and hydrology of Culebra groundwater in the study area shown in Figures 1-1 and 1-2 is the primary focus of this work.

The Dewey Lake Red Beds are the uppermost Permian unit, consisting of siltstones and claystones locally transected by concordant and discordant fractures that are either unaltered or contain gypsum (selenite and satin spar). The Dewey Lake contains sporadic occurrences of groundwater, mostly in the area south of the WIPP Site. The Triassic Dockum Group (undivided) rests on the Dewey Lake in the east half of the site and thickens eastward.

Locally throughout the area sands, gravels, and boulder conglomerates of the Gatuña Formation occur as channel and alluvial pond deposits as part of a high-energy stream system that dissected the southeastern New Mexico landscape in the middle Pleistocene. One such channel was Nash Draw, a broad, shallow solution valley west of the WIPP Site, where outcrops of the Rustler Formation have been eroded into shallow karstic landforms typical of subaerially exposed gypsum terrane. The pedogenic Mescalero caliche commonly is developed on top of the Gatuña where it occurs, and on many other rock types as well. Late Pleistocene spring deposits, dominantly of gypsite, occur just inside the eastern scarp of Nash Draw, and are thought to represent remobilization of sulfates from the Dewey Lake Red Beds and perhaps part of the upper Rustler Formation by groundwaters moving westward into Nash Draw during the late Pleistocene.

# 1.2 HYDROLOGIC SETTING OF CULEBRA AND RELATED ROCKS

## 1.2.1 Introduction

The hydrologic system in the Rustler Formation has been the subject of intense study since 1976. The results of these studies to date are summarized by Lappin (1988) and briefly reviewed here. Recent findings concerning physical hydrology within the Rustler have yielded various interpretations; consistency between interpretations based on physical hydrology and those based on geochemical and isotopic observations is a significant topic of discussion in this work.

The most important constraints on numerical models for calculating the modern or present-day flow velocities and directions in a groundwater system are the heads and transmissivities in various parts of the system. These parameters are inferred from other observations. The basic data describing the hydrologic properties of the Culebra over the study area consist of water-level measurements and observations of drawdown and/or recovery during hydraulic tests. Equivalent freshwater heads are derived from pressure data (water-level measurements) and a fluid density at each point. The time-dependent drawdown function obtained in response to pumping is then numerically simulated by varying the transmissivity until an optimized match between calculated and observed drawdown function is obtained. Assuming vertical homogeneity across the tested interval, this gives the best available estimate of transmissivity. The hydrologic testing that yielded the head and transmissivity data base is summarized by Lappin (1988).

## 1.2.2 Culebra Dolomite

Estimated Culebra transmissivities in the WIPP Site area and within Nash Draw range over approximately six orders of magnitude, from about $2 \times 10^{-9}$ $m^2/s$ a short distance east of the site to about $10^{-3}$ $m^2/s$ west of the site, on the east side of Nash Draw (Figure 1-4). Values

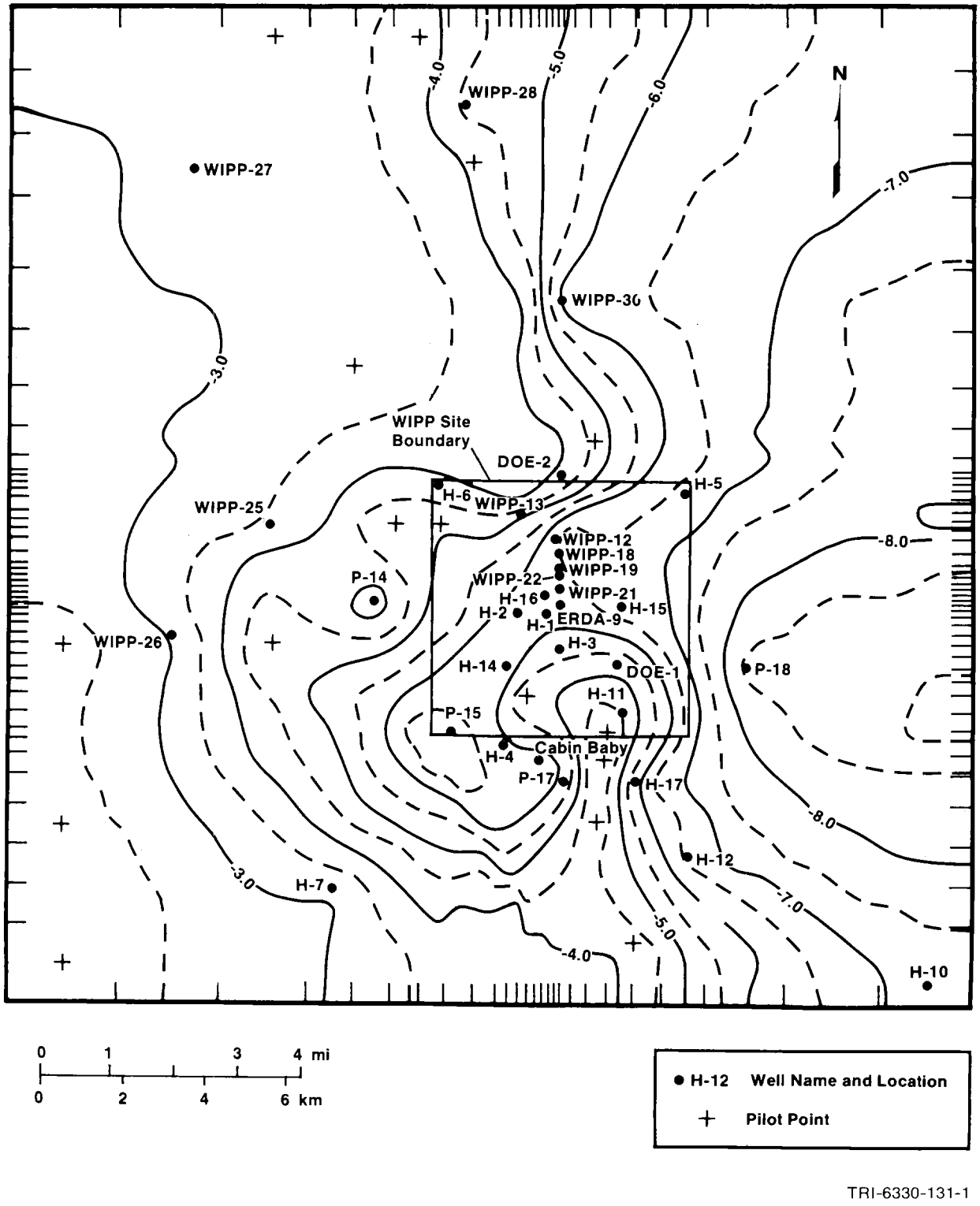


Figure 1-4. Logarithms of calculated Culebra transmissivities at and near the WIPP Site (Figure 4.3 of LaVenue et al. [1988]).

shown in Figure 1-4 are $\log_{10}$ of transmissivities in units of $m^2/s$ and are based on a steady-state calibration against the freshwater-equivalent head distribution. Culebra transmissivities in the central portion of the site, including very near the positions of all four WIPP shafts, are less than $10^{-6}$ $m^2/s$. LaVenue et al. (1988) estimate that uncertainties in transmissivity measurements are half an order of magnitude or less. They estimate that the uncertainty in calculated freshwater heads at most locations is approximately ± 2 m.

A continuous but complex zone of variable and higher Culebra transmissivities is present northwest, west, and south of the site; this zone extends into the southeast and northwest portions of the WIPP Site. In spite of the transmissivity determinations at 39 discrete locations in the Culebra, there is no direct field evidence of aqueous mass transport between the relatively high-transmissivity region in the southeast portion of the site (containing the H-4 hydropad and hole DOE-1) and the less saline groundwater system in the halite-free extensively gypsified region of the Rustler further south (containing holes H-7 and H-9). In fact, as discussed in Section 1.4.2, these two regions are geochemically dissimilar. The degree of fracturing appears to have some control over transmissivity in the Culebra, especially where the transmissivity is higher than about $10^{-6}$ $m^2/s$. The most fractured portions of the unit almost certainly carry the most groundwater.

The analytical and numerical modeling of Rustler groundwater flow has, over the years, used various assumptions to explain various observations. For example, no hydrologic-modeling studies to date consider possible reactions within the Culebra that might lead to local changes in fluid density or composition, such as halite dissolution from adjacent portions of the Rustler. Assumption of steady-state brine-density distribution (Haug et al., 1987) results in significant problems with model calibration that assumes completely confined flow. Haug et al. (1987) examine the effects of possible steady-state vertical inputs into the Culebra of fluids having different densities, from either the lower member of the Rustler or the Magenta. LaVenue et al. (1988) relax the assumption of long-term steady-state fluid compositions, but do assume that the fluid density distribution

is fixed on the time scale of local fluid-pressure changes in response to site characterization and shaft sinking (as long as 100 years). They also assume that the Culebra is completely confined on this same time scale.

The numerical modeling of the Culebra groundwater system using the measured formation pressures, a function to estimate the distribution of fluid densities, and a transmissivity distribution modified from an original kriged estimate, results in the instantaneous (present-day) flow directions and Darcy velocities within the Culebra shown in Figure 1-5. The hydrologic flow is calculated assuming the transmissivity distribution shown in Figure 1-4 and the freshwater-equivalent head distribution. Present-day flow within the Culebra at and near the WIPP Site, ignoring possible effects of both fractures and anisotropy, appears to be largely north-to-south, except in relatively low-transmissivity areas directly affected by either the high-transmissivity zone in the southeastern portion of the WIPP Site or by Nash Draw west of the WIPP Site. Calculated Darcy velocities range over six orders of magnitude, from $10^{-12}$ m/s ($m^3/m^2s$) east of the WIPP Site to as high as $10^{-6}$ m/s in central Nash Draw.

Darcy velocities do not include consideration of effective porosity and therefore do not represent actual groundwater particle velocities, nor can groundwater travel times be calculated directly from them unless effective in situ porosity values are known or assumed. Particle flowpaths and flowtimes within Nash Draw calculated by LaVenue et al. (1988) assuming steady state, the transmissivity and head distributions used to derive Figure 1-5, and a uniform effective in situ porosity of 16% are shown in Figure 1-6. They range from 450 years along a 25.1-km path in the west (particle A) to 2800 years along a 26.3-km path in the eastern part of Nash Draw (particle C). However, changes in the Nash Draw shallow groundwater system since the beginning of potash mining about 50 years ago (Hunter, 1985) make the steady-state assumption unrealistic in Nash Draw on even this short time scale.

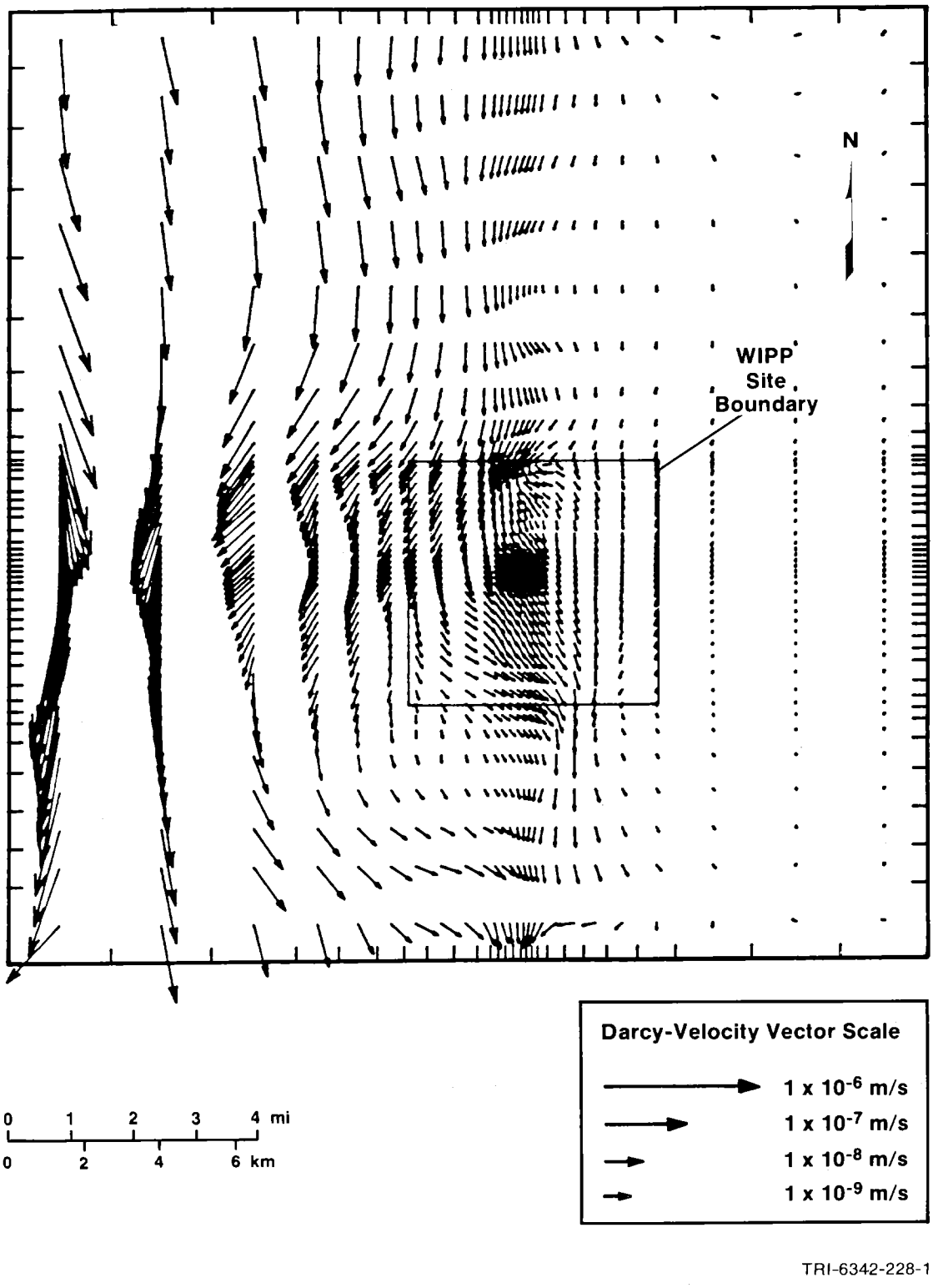


Figure 1-5. Calculated Darcy-velocity vectors in the Culebra dolomite (Figure 4.5B of LaVenue et al. [1988]).

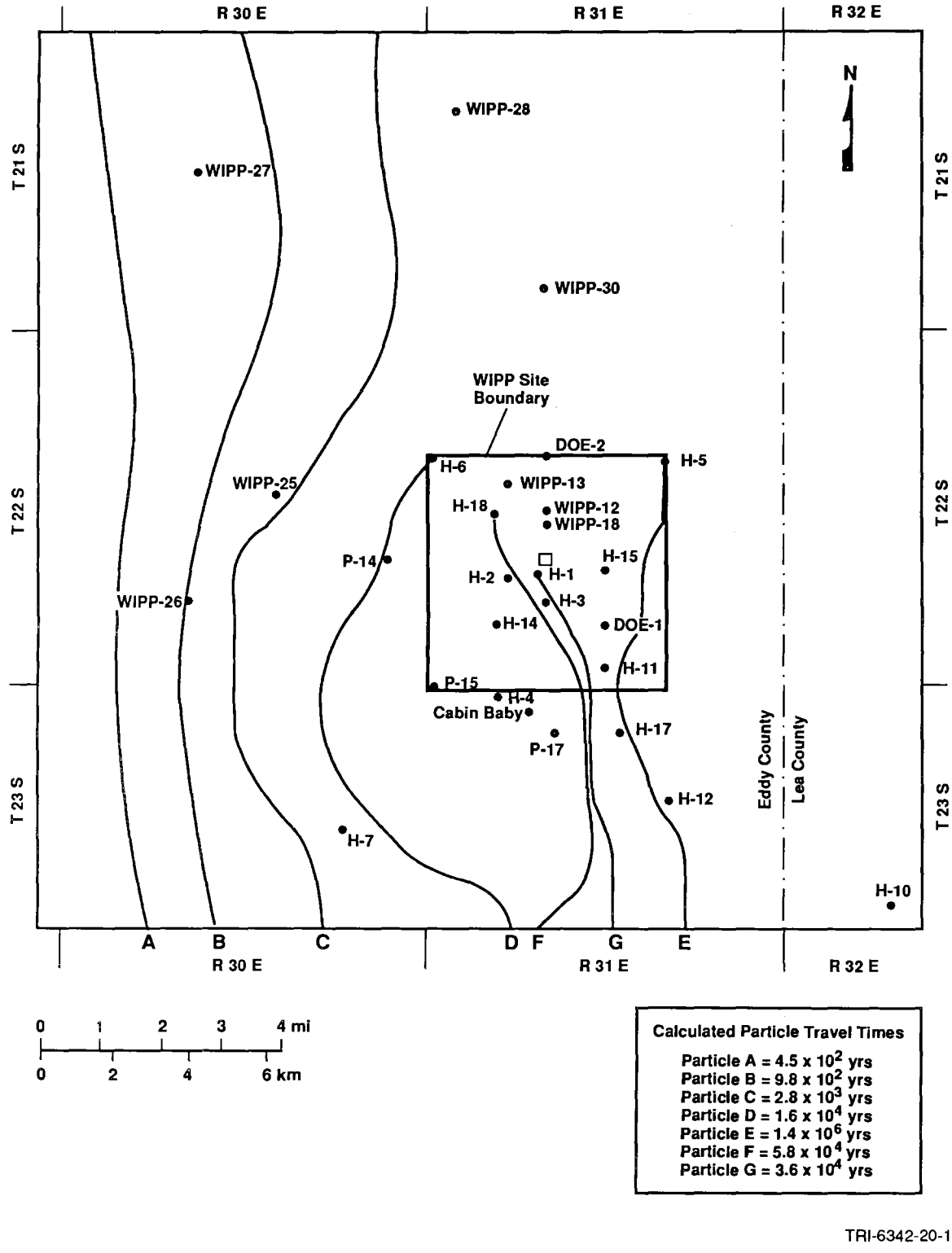


Figure 1-6. Calculated flowpaths and flow times within the Culebra dolomite (Figure 4.17 of LaVenue et al. [1988]).

LaVenue et al. (1988) calculated the particle travel time from north to south along a 13.7-km path in the eastern part of the WIPP Site (particle E) to be more than one million years. Travel time from directly above the center of the waste-emplacement panels to the southern boundary of the WIPP Site (along a 4-km segment of path G in Figure 1-6) is about 13,000 years. These results, however, cannot be used to quantitatively predict the behavior of the groundwater over the next 10,000 to one million years given the probable non-steady-state character of the Culebra hydrology, as discussed in Section 1.5.2. The amount of possible vertical flow into and out of the Culebra near site-center remains indeterminate and cannot be directly measured in the field (see Figure 1-7). At several well locations, the relationships between the heads in the Culebra and adjacent units indicate the potential for vertical flow into the Culebra (see Table 1-1). At H-16, H-3, H-2, H-1, H-14, and DOE-1, the head in the Magenta is higher than that of the Culebra. At H-2 and H-16, the measured head in the Rustler/Salado contact zone is higher than that of the Culebra. The amount of flow, however, may be negligible, making the assumption of confined transient flow within the Culebra adequate for modeling purposes, at least for short-term stresses associated with WIPP shafts and well tests. This assumption may or may not be valid for all modeling aspects over a 10,000-year time frame. In Nash Draw, for example, the development of near-surface gypsum karst has certainly allowed the Culebra to be hydraulically connected to various other Rustler horizons, including the Magenta.

At two localities near the site (holes H-3 and H-14), the Magenta head is greater than the head in claystone in the overlying Forty-niner member; therefore, any modern fluid flow between these two members at these two localities is upward, not downward. The head relationships between the Forty-niner and the Magenta at H-16 are probably similar (Beauheim, 1987). This precludes recharge of the Magenta and underlying units by direct downward infiltration from the surface at those localities. It has not been possible to measure hydraulic conductivities within the upper part of the unnamed lower member of the Rustler in borehole testing from the surface; thus, the degree of upward flow from the Rustler/Salado contact zone near the site-center (where the head relationships

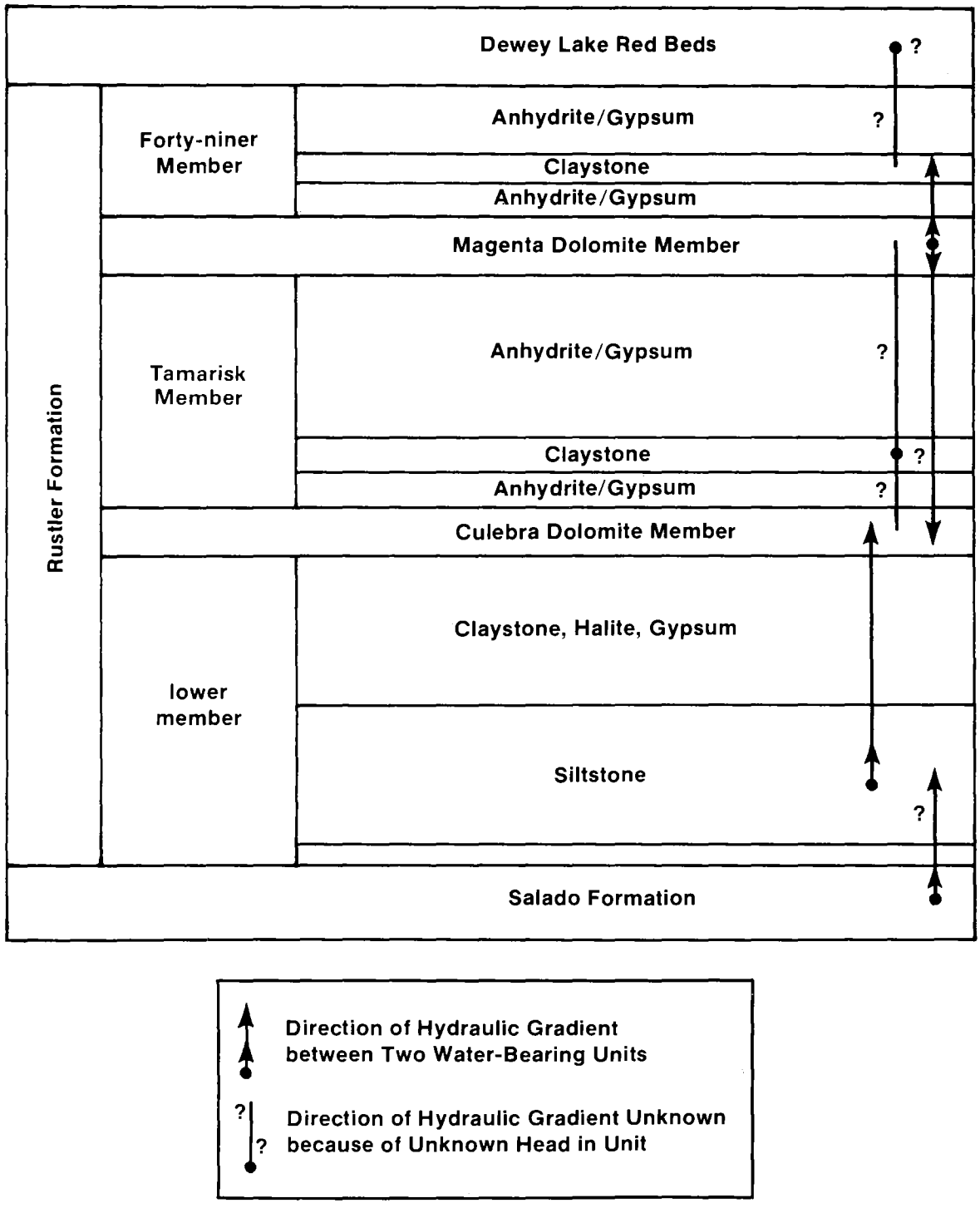


Figure 1-7. Generalized head relations among units in the Rustler Formation and between the Rustler, Dewey Lake Red Beds, and Salado at the WIPP Site (Figure 6-3 of Beauheim [1987]).

favor such a flow direction) cannot be determined. Horizontal hydraulic conductivities within the lower member claystone and siltstone range from $10^{-13}$ to $10^{-14}$ m/s. The extremely low hydraulic conductivity of the Tamarisk and relatively high transmissivity of the Culebra suggest that transient confined flow within the Culebra prevails at and near the WIPP Site.

Flow velocities calculated from a given set of heads and a given transmissivity distribution are interpretable as only a "snapshot" of instantaneous or modern behavior, unless the assumption of a steady state can be defended and the distribution of effective porosity is known. Physical measurements alone indicate only the present directions of potential fluid flow within and across the boundaries of the Rustler Formation. These inferences about flow direction and velocity may not be applicable to directions and velocities during the past 10,000 years, or during in the next 10,000 years, the interval of interest to regulatory agencies governing radioactive-waste repositories. Consequently, climatic variations and their influence on groundwater flow will be included as a factor affecting the uncertainty in the hydrologic modeling for performance assessment of the WIPP.

### 1.2.3 Related Rocks

Data for other hydrologic units of interest, including the Magenta, Dewey Lake, Triassic, and "brine aquifer" near the Rustler/Salado contact zone, are much less abundant than for the Culebra, although some of them have been used in various model calculations of hypothetical flow crossing bedding planes into or out of the Culebra. Some testing at selected points has been carried out in other horizons of the Rustler, including the Forty-niner, Tamarisk, and lower members of the Rustler (Lappin, 1988). Most of the data from non-Culebra units overlying the Salado in the study are reported by Mercer (1983) and Beauheim (1987).

# 1.3 SOURCES AND QUALITY OF GEOCHEMICAL DATA

## 1.3.1 Major and Minor Solute Data

Analyses of major and minor solutes from water samples collected by several different agencies and analyzed in different laboratories from 1976 to 1987 were considered in this work. The sources of data include the US Geological Survey (USGS) (Mercer, 1983; Mercer and Orr, 1979; Bodine et al., Chapter 4), the International Technologies (IT) Corporation (Uhland and Randall, 1986; Uhland et al., 1987; Randall et al., 1988), and Sandia National Laboratories (Robinson, 1988). In many cases, large discrepancies exist in the concentrations of major and minor solutes reported for the same location by different agencies. Much of the variation can be attributed to differences in sampling methods, to differences in analytical techniques, or to changes in the groundwater chemistry due to contamination. As discussed below, some of the inconsistencies among conceptual models proposed for the hydrochemical system at the WIPP can be attributed to discrepancies among the data sets. A list of wells from which water analyses were obtained is found in Table 1-1. Additional details concerning the solutes analyzed at each well, the dates of sample collection, and the methods of chemical analyses are found in Chapters 2, 4, and 6 and in the references cited in these chapters.

Siegel et al. (see Table 2-2) tabulate the values used for their calculations dealing with the concentrations of major and minor elements for waters in the Rustler Formation. Data from Table 2-2 were used in the saturation index calculations, factor analyses, and element ratio contours discussed below. Robinson (1988), Lambert and Harvey (1987), and Siegel et al. (Chapter 2) describe the different data sets examined and the development of a critical evaluation procedure to determine the criteria for acceptable values.

Bodine et al. (Chapter 4) used the SNORM computer code (Bodine and Jones, 1986) to evaluate data for their hydrochemical study. Their final data base for the Rustler Formation includes 161 chemical analyses from 70 sites representing 107 horizon-site

sampling points (see Table 1-1). The authors compiled data for the calculations from a variety of sources, including the data compiled in Robinson (1988), analyses reported in previous WIPP Site characterization and USGS Technical File reports, and new chemical analyses by USGS staff. In several cases, data from samples rejected by Robinson (1988) or Lambert and Harvey (1987) were accepted by Bodine et al. for use in calculating salt norms.

### 1.3.2 Evaluation of Oxidation-Reduction Potential and Occurrence of Organic Constituents in the Culebra

A data set from the WIPP Water Quality Sampling Program (WQSP) was independently evaluated by the IT Corporation and used in the calculations of Eh described below and in Chapter 6. Analyses of concentrations of members of four oxidation-reduction ("redox") couples and platinum electrode potential measurements were obtained from 21 wells in the Culebra during the period from 1985 to 1987 and used to calculate apparent Eh values (see Table 1-1). In most cases, the concentration of one of the members of a specific redox couple was below the limit of detection and only an upper or lower bound for the Eh could be calculated. Robinson (Appendix 6A) independently evaluated these redox data and compared them to a larger data set collected between 1985 and 1989.

Final groundwater samples from 21 Culebra wells listed in Table 1-1 were analyzed for total organic carbon (TOC) in acidified solutions passed through a 0.45 micron filter. Details of the sample collection and analytical techniques are found in Chapter 6.

### 1.3.3 Mineralogical Data

Mineralogical data were obtained from 12 cores from three east-west traverses in the Culebra member. Over 100 samples were analyzed by optical microscopy, quantitative x-ray diffraction (XRD), and x-ray fluorescence. Core from one borehole (WIPP-12) was examined to obtain a representation of the textural variations in the Culebra, while core from another (WIPP-19) was examined both texturally and mineralogically to obtain some

degree of representation of the entire Rustler near the center of the WIPP Site. Sample locations are listed in Table 1-1 and analysis techniques are summarized in Chapter 3. As discussed in more detail in Chapter 3, the samples examined in this study were from intact core that may not be representative of the principal water-bearing zones. The rock most recently in contact with Culebra groundwater is commonly a small fraction of the dolomite member and is likely to be reduced to rubble by partial dissolution, and hence be poorly recovered from the borehole.

### 1.3.4 Isotopic Data

Several isotopic studies have been conducted on rocks and waters from the Rustler Formation and related units. Lists of sample locations for each isotope are found in Table 1-1. Data pairs for $\delta D$-$\delta^{18}O$ are available for water samples from 70 localities: six from the Magenta, 21 from the Culebra, 17 from the Rustler/Salado contact zone, three from the Dewey Lake, four from the confined portion of the Capitan limestone, 12 from the vadose Capitan, one from the Triassic, one from alluvium, and five from the surface. The total number of replicate data-pairs, whether they represent replicate samplings at different times or replicate analyses of the same sample, was 86. Ten of these data pairs are for samples suspected to be nonrepresentative. A description of the samples, analytical methods, and criteria for judging sample quality is given in detail by Lambert and Harvey (1987). Carbonates from the Magenta (five localities) and Culebra (nine localities) were analyzed for their $\delta^{13}C$ and $\delta^{18}O$ values in a total of 43 replicates (Lambert, 1987; Lambert and Harvey, 1987). Values for $\delta D$ of the water of crystallization in gypsums from selenite veins in the Dewey Lake and veins and alabaster from the Rustler have been measured at 11 horizon-sites representing five different boreholes (20 total replicates). Values for $\delta^{13}C$ and $^{14}C$ (percent-modern-carbon) have been obtained from waters from 16 horizon-sites representing 12 different wells (21 replicates); tritium measurements are available for seven wells (eight replicates). These are described in detail by Lambert (1987). Total uranium concentrations and uranium-isotope activity ratios are available for waters from five Rustler/Salado contacts, nine Culebra locations, two Magenta locations, one potash mine, one rainfall, and one surface spring locality (Lambert and Carter, 1987). Finally, 38

gypsums and anhydrites and 29 carbonates from Dewey Lake veins, Rustler veins and beds, Salado and Castile beds, caliche, and spring deposits have been analyzed for their $^{87}Sr/^{86}Sr$ ratios (Brookins and Lambert, 1988).

Lambert and Harvey (1987) proposed that the same criteria for evaluating the validity of a water sample used in determining a representative solute composition were also applicable to stable-isotope studies. The same criteria described by Robinson (1988) for judging the representativeness of the major solute composition of a water sample, however, are not applicable to certain trace isotope studies, such as radiocarbon. Many of the water samples used in the radiocarbon studies reported by Lambert (1987) and summarized here were collected according to the same criteria for major solutes. However, despite evaluation by such criteria, 12 of the 16 radiocarbon samples were found to be mixtures of native dissolved carbon and contaminant modern carbon introduced during the development of the sampling boreholes.

Other trace isotopes in groundwaters, such as uranium, have required still different sampling criteria. Barr et al. (1979) reported the correlative changes in total dissolved uranium and $^{234}U/^{238}U$ activity ratio with total iron. Lambert and Carter (1984) illustrated the effects of introduced contaminants on the uranium-isotope composition of water from a flowing well. It is tentatively concluded that preferred sampling criteria for $^{234}U/^{238}U$ studies are similar to those for metallic trace elements. The transient changes in such elements (e.g., iron) during a sampling period are discussed by Robinson (1988).

# 1.4 RESULTS OF GEOCHEMICAL STUDIES

## 1.4.1 Major/Minor Element Ratios and Correlations

In simple hydrologic and hydrochemical systems, spatial trends in element concentrations and ratios can be used to suggest flow directions and to delineate potential sites of recharge or interaquifer leakage. Average concentrations of major and minor elements in Culebra

waters were calculated from data sets obtained from the Sandia National Laboratories (SNL), IT Corporation, USGS, and New Mexico Environmental Evaluation Group (EEG) sampling and analysis programs. These average values are given in Table 2-2. Figure 1-8 shows contours of sodium concentration over the study area. Actual values for each well are also given. Contour placement is controlled by several factors, including the selected contour interval, smoothing factors, and radius of influence of the data points. The location of each contour is influenced by several data points; therefore, there may be discrepancies between the placement of contour lines and the concentrations at some well locations. The contours for sodium are similar to those for chloride, total dissolved solids (TDS) and fluid density.

The spatial trends in interelement correlations were examined by contouring ratios of Br/Cl, Na/Cl, Na/K, Sr/Ca, and other minor/major solute ratios. Results of these calculations are given in Chapter 2. The important features that emerge from these plots are given below:

- The Na/Cl molar ratio in the southern portion of the site is higher than would be produced by simple dissolution of halite, suggesting the potential contribution by dissolution of Na-silicates in this area.

- The K/Na weight ratios, Mg/Ca molar ratios, and Na and Sr concentrations are anomalously high at WIPP-27 and WIPP-29, suggesting that contamination by potash refining operations is important at these locations. Contours for the K/Na weight ratio are shown in Figure 1-9. Names for the wells indicated in Figure 1-9 are given in Figure 1-8.

- Element ratios and concentrations of several elements are anomalous at P-14 when compared to water compositions at the surrounding wells. Concentrations of Ca, Sr, and I are anomalously high, and the concentration of $SO_4$ is anomalously low at this site.

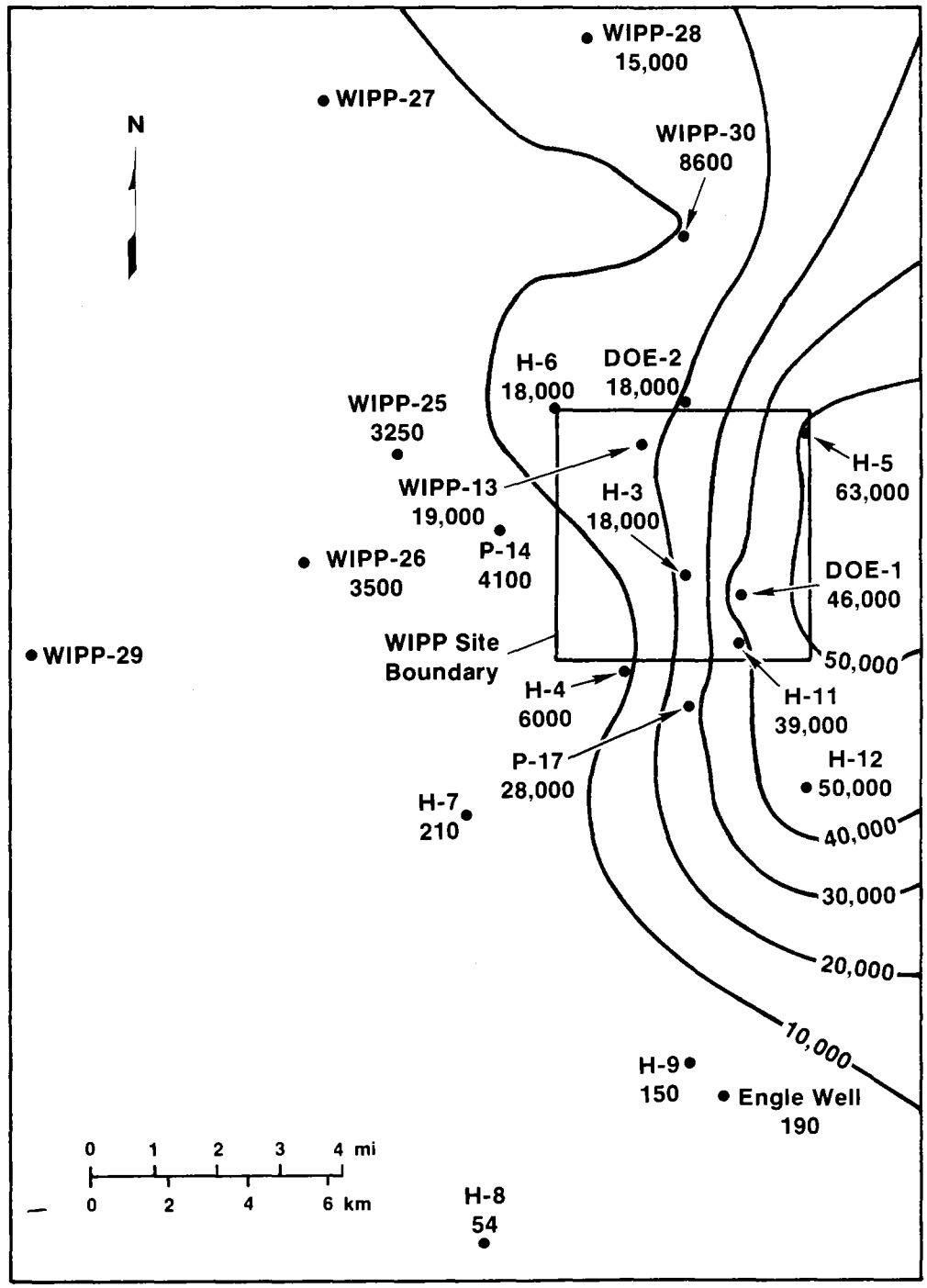


Figure 1-8. Contours of sodium concentration (mg/L) in study area. The WIPP Site boundary is indicated for reference (from Siegel et al., Chapter 2).

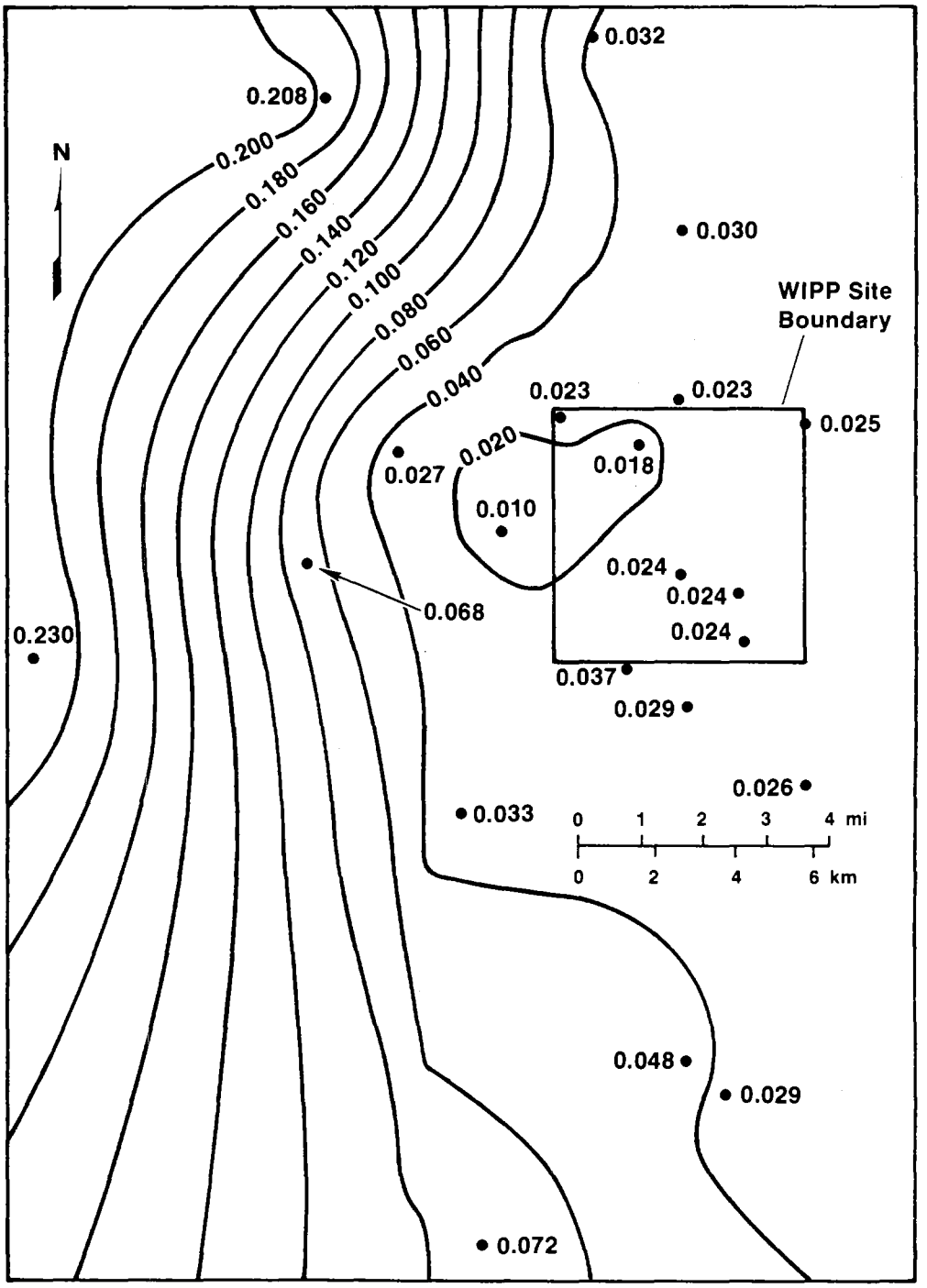


Figure 1-9. Contours of ratios of K/Na concentrations in study area (from Siegel et al., Chapter 2).

- The Cl/Br ratio is highest in Nash Draw, intermediate through the center of the WIPP Site, and lowest in P-14 and H-4.

### 1.4.2 Definition of Hydrochemical Facies of Culebra Groundwater Based on Relative Proportions of Major Solutes

Based on the major solute compositions presented in Table 2-2, four hydrochemical facies are delineated in Figures 1-10, 1-11, 1-12, and 1-13. Compositions of waters at locations indicated by solid circles in Figure 1-10 are described in Figure 1-13. Compositions of several other wells (see Chapter 4) indicated by open circles were not included in the original data set used to define the facies, but their compositions are consistent with the facies borders. The facies borders indicated in Figure 1-13 are located by reference to the wells, whereas the boundaries of the halite dissolution zones are located by reference to control points (Snyder, 1985) plotted by Lappin (1988, Figure 4.1.2).

Zone A contains a saline (about 3.0 molal) NaCl brine with a Mg/Ca molar ratio between 1.2 and 2.0. This water is found in the eastern third of the site; the zone is roughly coincident with the region of low transmissivity. On the western side of the zone, halite in the Rustler has been found only in the unnamed lower member; in the eastern portion of the zone, halite has been observed throughout the Rustler (see Figure 1-13).

Zone B contains a dilute $CaSO_4$-rich water (ionic strength $<0.1$ m) in the southern part of the site. Mg/Ca molar ratios are uniformly low (0.4-0.5). This zone is coincident with a high-transmissivity region; halite is not found in the Rustler in this zone.

Zone C contains waters of variable composition with low-to-moderate ionic strength (0.3 to 1.6 m) in the western part of the WIPP Site and the eastern side of Nash Draw. Mg/Ca molar ratios range from 0.5 to 1.2. This zone is coincident with a region of variable transmissivity. In the eastern part of this zone, halite is present in the lower member of the Rustler; on the western side of the zone, halite is not observed in the formation. The most

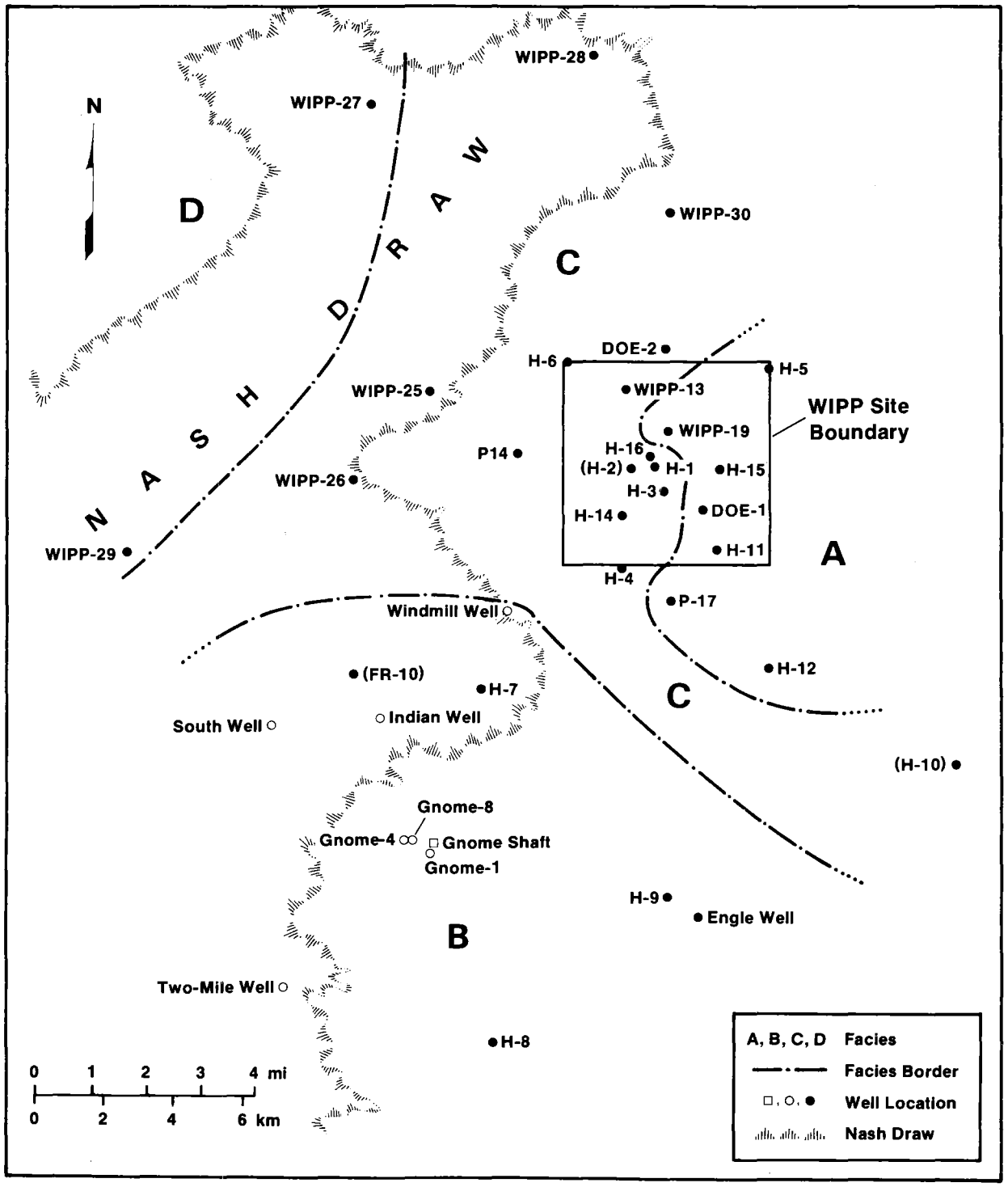


Figure 1-10. Hydrochemical facies of the Culebra dolomite (from Siegel et al., Chapter 2).

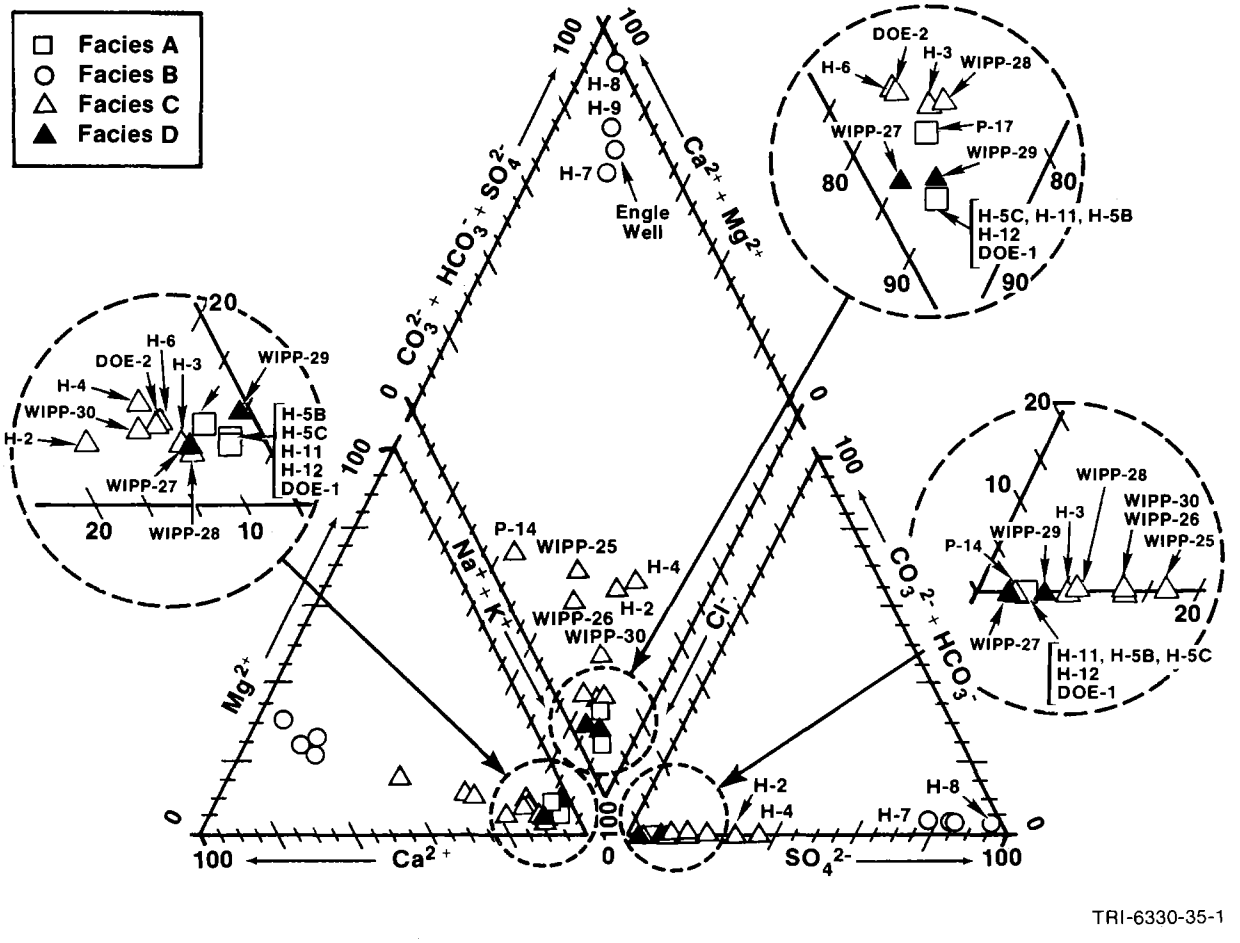


Figure 1-11. Trilinear diagram for Culebra groundwaters (from Siegel et al., Chapter 2).

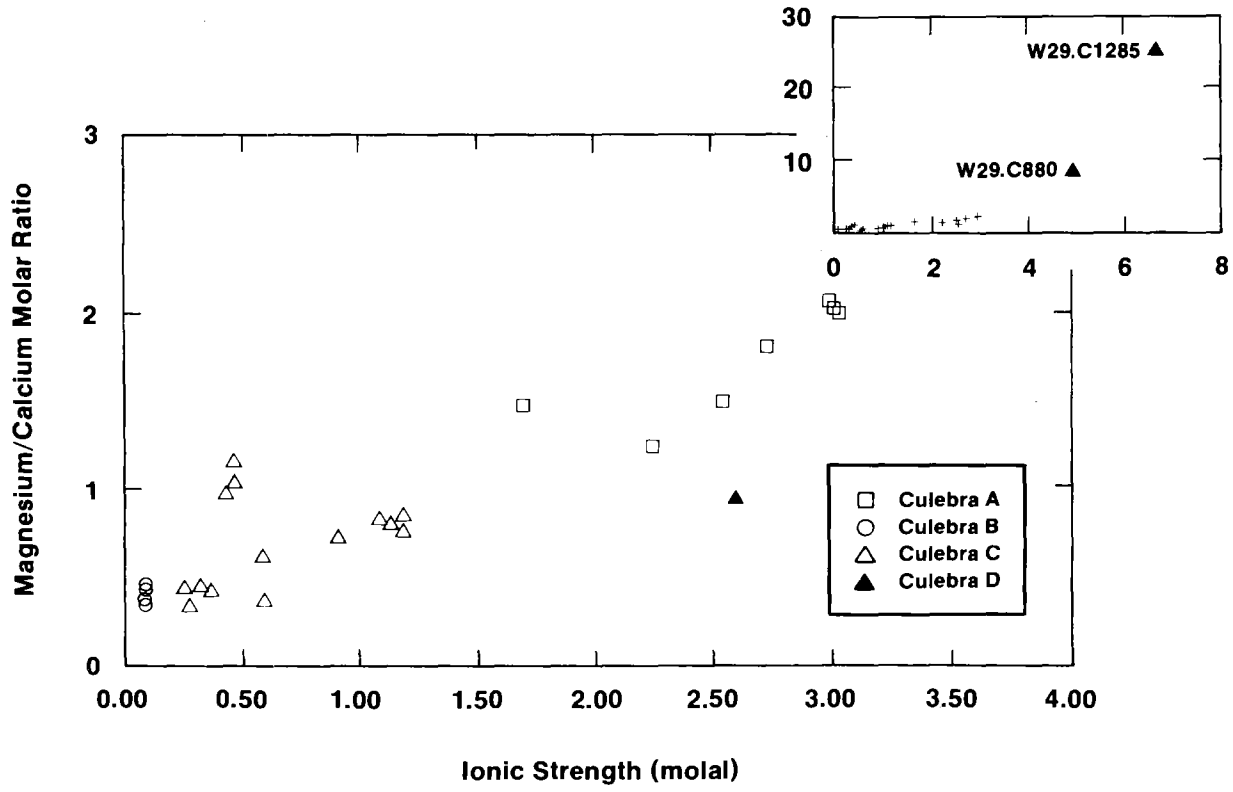


TRI-6344-97-0

Figure 1-12. Relationship between Mg/Ca molar ratio and ionic strength (molal) for Culebra groundwater samples in different hydrochemical facies (from Siegel et al., Chapter 2).

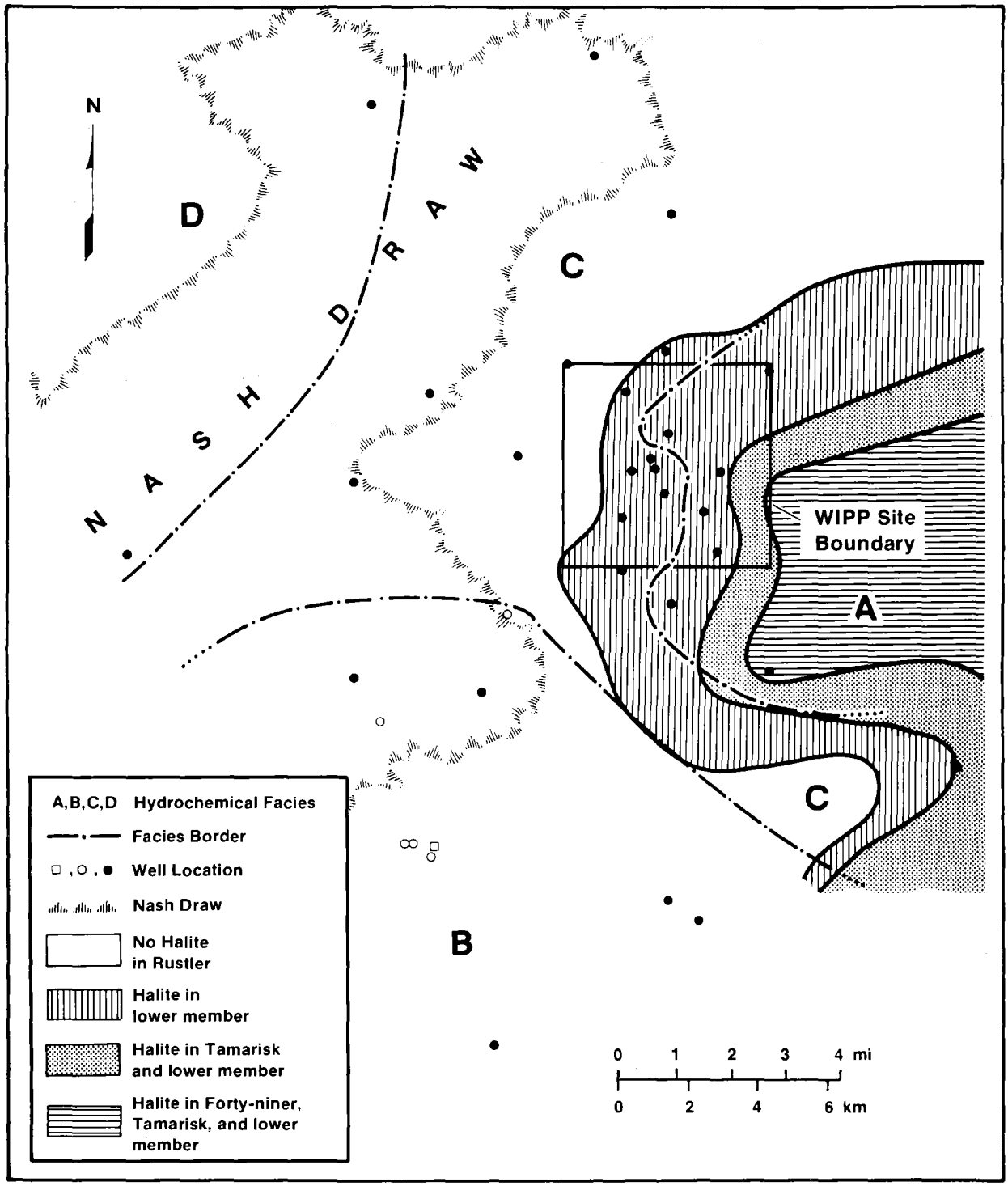


TRI-6344-551-0

Figure 1-13. Relationship between occurrence of halite in the Rustler and hydrochemical facies of the Culebra dolomite.

saline (NaCl-rich) water is found in the eastern edge of the zone, close to core locations where halite is observed in the Tamarisk Member.

Zone D, a fourth zone comprising wells WIPP-27 and WIPP-29, can be defined based on inferred contamination related to potash refining operations in the area. Waters from these wells have anomalously high salinities (3-6 m) and K/Na weight ratios (0.22) compared to other wells at the site (0.01-0.09). At WIPP-29, the composition of the Culebra water has changed over the course of a 7-year monitoring period. The Mg/Ca molar ratio at WIPP-29 is anomalously high, ranging from 10 to 30 during the monitoring period.

The chemical characteristics of each of the facies are described by the Piper (trilinear) diagram shown in Figure 1-11. This plot summarizes relationships between the major solutes in the Na-K-Mg-Ca-Cl-$SO_4$-$CO_3$ system. The diagram shows the relative proportions of the ions on an equivalents/liter basis. Relative proportions of cations and anions are displayed separately in the triangular plots in the bottom half of the figure. In the rhombus in the upper portion of the diagram, the ratio of divalent to monovalent cations and the ratio of chloride to sulfate + carbonate + bicarbonate are shown.

Compositions of Culebra waters from Zone A have nearly identical ionic proportions and plot on the same location in the graph near the Na-Cl corner. They are distinguished from waters in Zone C by their higher Mg/Ca ratio and ionic strengths (see Figure 1-12). Dilute groundwater from Zone B plot near the Ca-$SO_4$ corner and water from Zone C cover a wide area in the plot. Waters from Zone D have similar ionic proportions to those of Zone A and are distinguished primarily on the basis of salinity and K/Na ratio, parameters that are not shown in Figure 1-11.

### 1.4.3 Principal Component Analysis of Rustler Groundwater Compositions

In the previous section, hydrochemical facies for Culebra groundwaters were defined using the relative proportions of the concentrations of seven major solutes. These solute ratios

can be represented by a trilinear plot as shown in Figure 1-11. To show relationships among the 17 independent chemical variables presented in Table 2-2, the method of principal component analysis (PCA) was used. This method summarizes the relationships among the variables and shows how these relationships differ for each water composition.

The principal components or factors identified from PCA can be thought of as hypothetical compositional end members (Q-mode PCA) or can be used to express the relationships among the compositions in terms of a small number of independent underlying correlations (R-mode PCA). This information can be used to refine the definition of hydrochemical facies and to suggest the nature of chemical reactions that control groundwater composition.

In R-mode PCA, several kinds of correlations are possible. For example, two cations that are dissolved from the source mineral will be positively correlated, whereas elements whose concentrations are inversely related by a solubility product will be negatively correlated. Appendix 2B explains the basic concepts and vocabulary of PCA. The origins of the factor-loading matrices and factor-score matrices, the significance of factor rotations, examples of interelement correlations and their possible geochemical interpretations, and the need for data transformations are explained. Section 2.3.3 describes the application of this technique to waters from the Culebra dolomite and related rock units. The following section is a summary of that work.

Two data sets were used in the analysis. Population 1 included data for Ca, Mg, K, Na, Cl, $SO_4$, B, Li, $SiO_2$, Br, Sr, alkalinity, and pH from 22 samples from the Culebra. Population 2 included data from wells for which analyses of the above elements plus Fe, Mn, F, and I were available (20 samples from the Culebra, Magenta, Dewey Lake, and Bell Canyon units). In most respects, the results for the two populations were similar.

### 1.4.3.1 Unrotated Principal Components

R-mode PCA was carried out using the PCA programs in SAS (Statistical Analysis System Institute, 1982). Three principal components (factors) account for approximately 96% of the total variance of population 1 and are shown in Figure 1-14. Factor loadings are listed in Table 2-7. Factor 1 accounts for approximately 67% of the total variance of the data set. It is characterized by high positive correlations (loadings) for all of the variables except pH, bicarbonate alkalinity, and silica. The factor accounts for most of the variance of sodium and chloride, and it is likely that this factor represents addition of solutes by dissolution of evaporite minerals. For this reason, the factor is referred to as the "salinity factor" in this report.

Factor 2 accounts for approximately 18% of the variance of the data set. It is characterized by large loadings for pH, bicarbonate alkalinity, and silica and boron concentrations. This combination of elements may reflect sorption and silicate and carbonate diagenesis. It is referred to as the "silicate/bicarbonate factor" in this report.

Factor 3 accounts for approximately 11% of the total variance and exhibits high positive loadings for calcium and strontium and a high negative loading for sulfate. This element association probably reflects dissolution/precipitation of gypsum and is referred to as the "sulfate factor" in this report.

### 1.4.3.2 Rotated Principal Components

As discussed in Appendix 2B, several alternative orientations of the principal component axes may be equally efficient in describing the variance in the data set. The unrotated principal components described in the previous section were compared to those obtained from varimax, equamax, and quartimax rotational schemes to determine if any element associations were common. It was found that the factor-loading matrices from all rotational schemes contained the same key element associations described above for the unrotated components. The loading matrices differed primarily in the relative loadings of

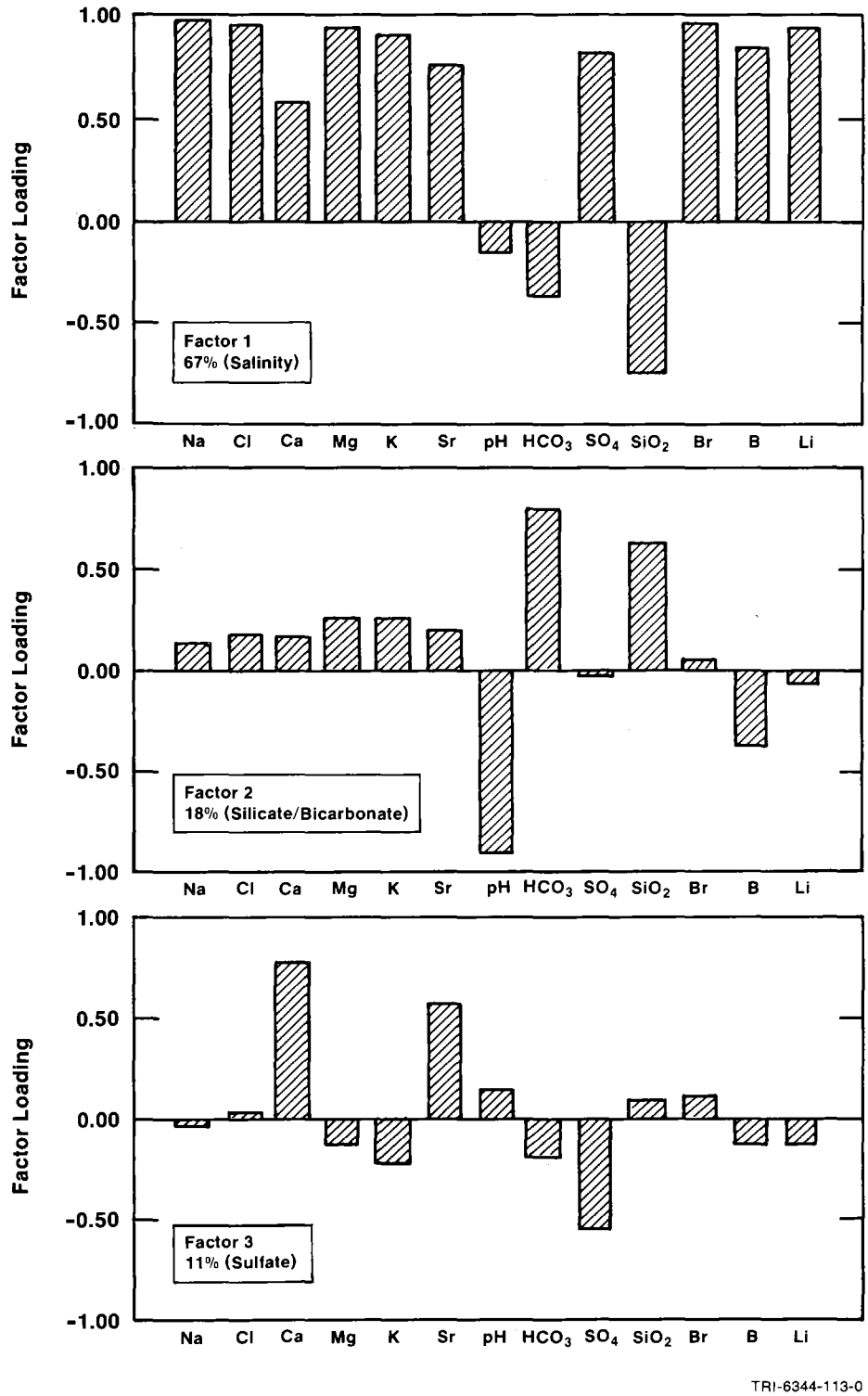


Figure 1-14. Unrotated R-mode factor loadings for factors 1, 2, and 3 for Culebra groundwaters (population 1).

other elements and the variance explained by the salinity, silicate/bicarbonate, and sulfate factors.

The compositions of the samples in terms of the factors are described by the factor scores. Relationships between varimax factor scores for the salinity and sulfate factors are plotted in Figure 1-15, which also indicates hydrochemical facies of each well. Factor scores are listed in Table 2C-2. Figure 1-15 shows that the first two principal components can be used to delineate the same groups of wells identified in Figures 1-10 through 1-12. Thus, the definition of hydrochemical facies based on the proportions of major solutes is supported by correlations among the major and minor elements examined in this study.

#### 1.4.3.3 R-mode Factors Obtained after Partialling Out Total Dissolved Solids

The three major factors obtained from the R-mode analysis described above are strongly affected by halite dissolution. Solutes are added directly from the halite, or indirectly because the solubilities of sulfate and carbonate phases increase as the ionic strength increases (see Section 1.4.5). A second R-mode PCA examined interelement correlations independent of the effects of halite dissolution. In this analysis, the principal components of the partial correlation matrix with respect to TDS concentration were extracted. A more detailed description of the procedure is in Appendix 2B.

Five factors accounted for 99% of the variance that remains after the TDS were partialled out. In Figure 1-16, the variables with the highest loadings for each factor are identified. Factor loadings are plotted only for elements that have important geochemical significance or that strongly influence the orientation of the factors (loading $>0.23$). The complete factor-loading matrix is found in Table 2-8. Factor 1B is dominated by the negative correlation of Ca and Sr with sulfate and is suggestive of dissolution/coprecipitation of Sr and Ca in a sulfate phase such as gypsum or anhydrite. It accounts for 67% of the total variance of Ca, 35% of the total variance of Sr, and 24% of the total variance of sulfate. This factor is similar to the sulfate factor (3) described previously. Factors 2B, 4B, and 5B are similar to the silicate factor (2) described previously and contain all or portions of two negatively

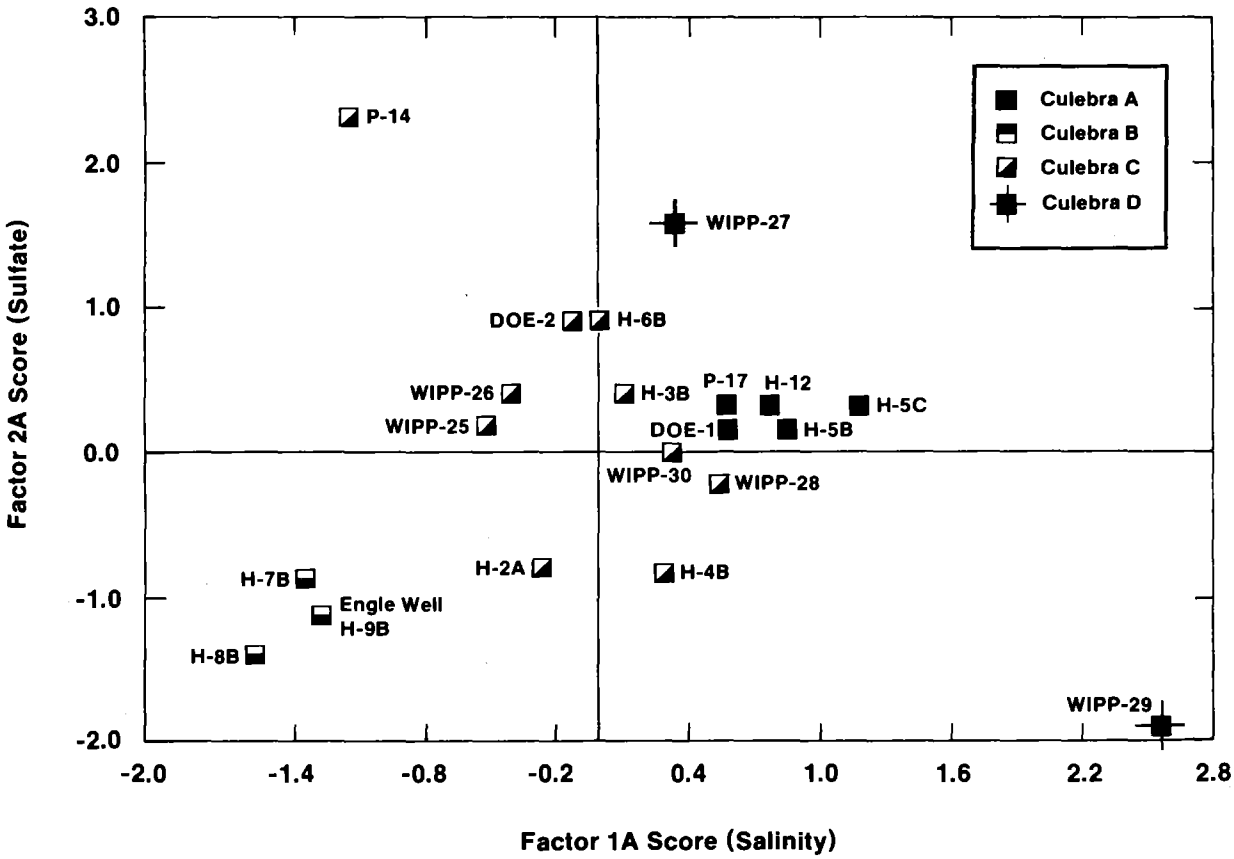


Figure 1-15. Relationship between varimax R-mode factor scores for factors 1A and 2A for Culebra groundwaters (population 1).

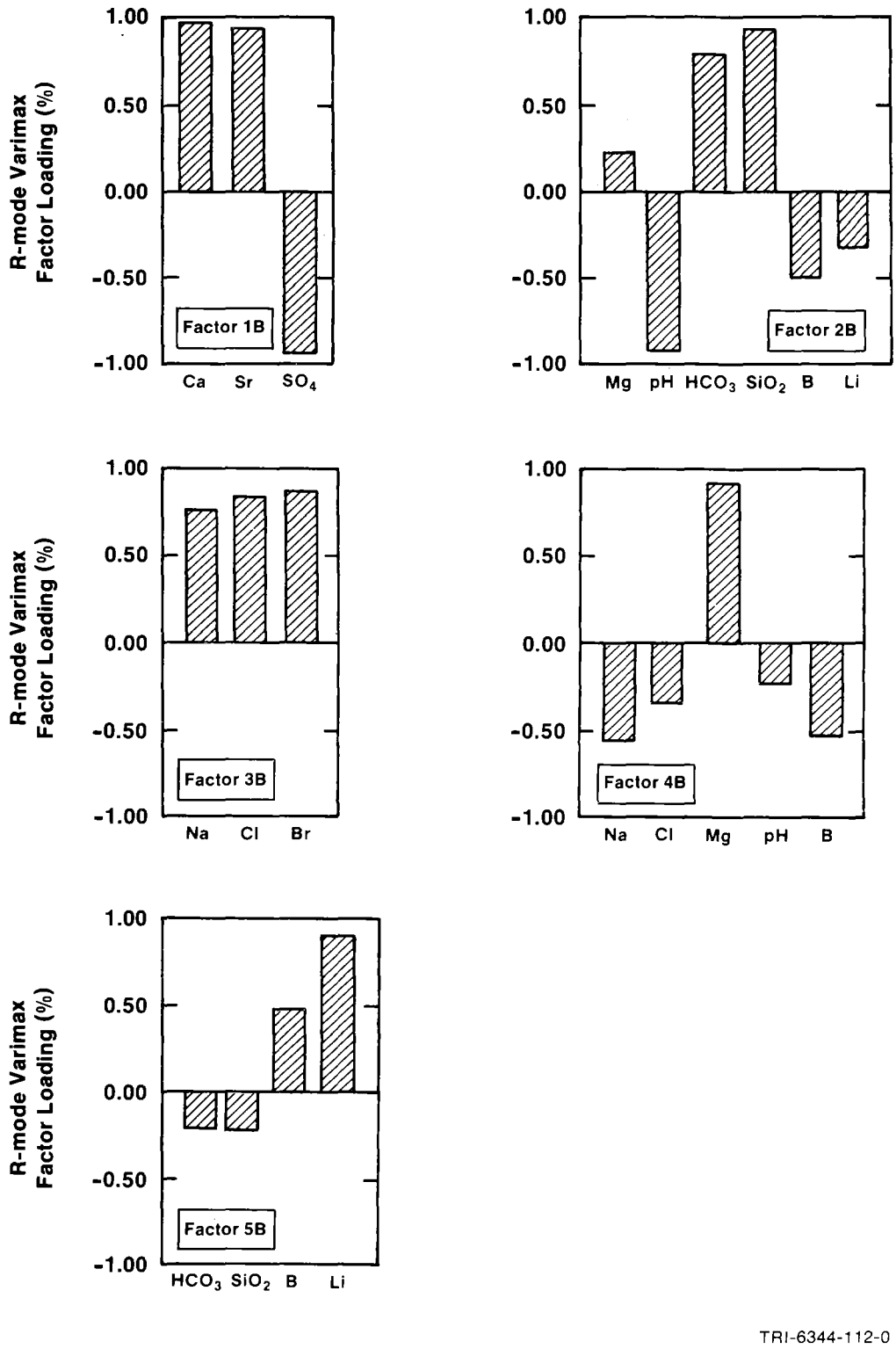


Figure 1-16. Varimax R-mode factor loadings of key elements for factors 1B, 2B, 3B, 4B, and 5B obtained from partial-correlation matrix with respect to TDS for Culebra groundwaters (population 1).

correlated groups of variables. One group involves the correlation of Mg, K, bicarbonate alkalinity, and silica; the other group contains pH, B, and Li. This pattern of element associations may be due to a combination of processes including sorption, ion exchange, carbonate diagenesis and silicate diagenesis and is discussed in more detail in Section 2.4.3.

In another factor extracted from population 2, variance in Mg was associated with a large amount of the variance of F and $SO_4$. As discussed in Chapter 2, this factor may indicate the presence of sellaite ($MgF_2$) contained in anhydrite. Descriptions of the other factors and representation of the compositions of the water samples in terms of the factors are also in Chapter 2.

The correlations of the major elements described by the PCAs confirm the definition of hydrochemical facies described in previous sections. The correlations of the minor elements, as revealed by the PCA, provide insight into the identity of the minerals that control the concentrations of Sr, F, Si, B, and Li. The calculations suggest that Sr is present in sulfates, that F is present as $MgF_2$ in anhydrite, and that concentrations of Si, B, and Li are affected by reactions involving clay minerals.

### 1.4.4 Classification of Rustler Groundwaters by Normative Salt Assemblages

Bodine et al. (Chapter 4) suggest that recasting the chemical composition of a water into a "salt norm" is a useful diagnostic tool for inferring possible origins of the water's solutes. The normative salt assemblage (or "salt norm") is the quantitative equilibrium assemblage of salts that would precipitate from a natural water if it were evaporated to dryness under ideal equilibrium conditions at 25°C and atmospheric pressure. The normative assemblage yields a diagnostic chemical-mineralogical characterization of the water that indicates the nature of possible water/rock interactions in subsurface environments and may contribute in determining the water chemistry's evolutionary path.

The SNORM computer code (Bodine and Jones, 1986) calculates salt norms based on the Gibbs Phase Rule, free energy data, and observed low-temperature mineral associations. Bodine et al. (Chapter 4) applied SNORM to the data set described above that was obtained from their independent evaluation of water chemistry data from the Rustler Formation. Based on these calculations, they identify four end-member norms in brines collected from the WIPP Site:

- Type 1 brines contain normative alkaline-earth chloride salts and low Cl/Br (<300) ratios; these are termed "primitive-diagenetic" norms and may result when connate waters are involved in dolomitization

- Type 2 dilute solutions contain normative alkali-bearing carbonates that suggest dissolution of detrital silicates through carbonic acid hydrolysis in a weathering/recharge zone

- Type 3 dilute sulfate-rich solutions are produced when surface-derived (fresh) waters dissolve anhydrite or gypsum and little else

- Type 4 saline halite-rich brines are produced when surface-derived (fresh) waters dissolve anhydrite or gypsum and halite in the Rustler and upper Salado.

In Chapter 4, Bodine et al. show that the compositions of most waters in the Rustler Formation can be produced by mixing of the above four end-member brines, types 1 and 4 being the most common. The fluid produced by the dehydration of gypsum may also be a component of some well waters. Note, however, that most waters of the four types considered by Bodine et al. for which $\delta^{18}O$ and $\delta D$ values are available have diagnostically meteoric stable-isotope characteristics (Lambert and Harvey, 1987; Lambert, Chapter 5).

In the Culebra member, water (which may or may not be representative of fluid native to the formation) sampled from P-18 contains the highest proportion of primitive-diagenetic brine. In the Rustler/Salado contact zone, wells in the center of the WIPP Site (H-5 and

H-6) contain the highest proportions of the "primitive"-norm-type fluids. Water from WIPP-15 in the Gatuña Formation is dominantly type 2; dissolution of an anhydrite-rich rock by this water would produce waters like H-7 or H-1, which have strong type 3 signatures. Examples of waters with a significant component of type 4 water include H-5 and DOE-1. According to Bodine et al. in Chapter 4, in both the Culebra and the Rustler/Salado contact zones, the relative proportion of recharge water to primitive-diagenetic water increases to the north, west, and south of the WIPP Site.

### 1.4.5 Calculations of Mineral Saturation Indices for Culebra Waters

Mineral saturation indices may provide insight into the nature of chemical processes that control solute concentrations in groundwaters. Saturation indices in Culebra waters have been calculated for minerals commonly observed in the Ochoan Series (see Table 1-3). The computer code PHRQPITZ (Plummer et al., 1988), which uses the Pitzer model for ion-interactions, was utilized for these calculations. All water samples are saturated with respect to gypsum, undersaturated with respect to halite, and with the exception of WIPP-29 in Zone D, all samples are undersaturated with respect to anhydrite. Dolomite and calcite saturation indices are variable, indicating both undersaturation and supersaturation with respect to the carbonates. The relationships between saturation indices and ionic strength for several minerals are shown in Figures 1-17, 1-18, and 1-19.

As discussed by Siegel et al. in Chapter 2, the relationships among the saturation indices, pH, and calculated $pCO_2$ suggest that the loss of $CO_2$ gas from the water during sample collection may be responsible for part of the apparent supersaturation of the carbonates. Other potential sources of error in the calculations of carbonate equilibria include uncertainties in the pH measurements due to the use of an activity scale inappropriate for saline Na-Cl brines, errors in laboratory measurements of major solute compositions, and the choice of an inappropriate value for the Gibbs free energy of formation for dolomite to calculate the saturation indices.

## Table 1-3. Saturation Indices for Common Evaporite Minerals Calculated by PHRQPITZ

| Well | Date | Lab | Ionic Strength (molal) | pH | $^{a}H_2O$ | Charge[1] Balance Error | Saturation Indices[2] | | | | | | log $pCO_2$ |
|---|---|---|---|---|---|---|---|---|---|---|---|---|---|
| | | | | | | | Anh | Cal | Dol | Gyp | Hal | Mag | |
| Culebra: | | | | | | | | | | | | | |
| DOE-1 | 4/85 | UNC | 2.53 | 7.10 | 0.923 | 9.05E-03 | -0.12 | -0.34 | -0.13 | 0.03 | -1.26 | -0.62 | -2.60 |
| DOE-2 | 3/85 | UNC | 1.19 | 7.00 | 0.968 | -6.52E-02 | -0.18 | -0.21 | -0.14 | 0.01 | -2.03 | -0.77 | -2.33 |
| ENGLE | 3/85 | UNC | 0.09 | 7.40 | 0.999 | 1.00E-03 | -0.22 | 0.22 | 0.38 | 0.00 | -6.02 | -0.68 | -2.44 |
| H-2A | 4/86 | UNC | 0.27 | 8.00 | 0.994 | -4.33E-03 | -0.25 | 0.45 | 0.78 | -0.04 | -3.49 | -0.52 | -3.38 |
| H-3B3 | 2/85 | UNC | 1.08 | 7.40 | 0.971 | -2.53E-03 | -0.20 | -0.08 | 0.12 | 0.00 | -2.11 | -0.65 | -2.86 |
| H-3B3 | 6/84 | UNC | 1.08 | 7.40 | 0.972 | -2.56E-02 | -0.15 | -0.02 | 0.23 | 0.04 | -2.13 | -0.59 | -2.83 |
| H-4B | 5/81 | UNC | 0.455 | 8.00 | 0.991 | -1.49E-02 | -0.17 | 0.36 | 1.07 | 0.04 | -3.13 | -0.13 | -3.35 |
| H-4B | 7/85 | UNC | 0.42 | 7.70 | 0.991 | 4.14E-03 | -0.20 | 0.07 | 0.46 | 0.01 | -3.17 | -0.45 | -3.04 |
| H-4C | 8/84 | UNC | 0.45 | 7.80 | 0.991 | 4.82E-03 | -0.20 | 0.19 | 0.77 | 0.01 | -3.12 | -0.26 | -3.11 |
| H-5B | 6/81 | UNC | 2.993 | 7.90 | 0.906 | -1.18E-01 | -0.10 | 0.71 | 2.12 | 0.04 | -1.08 | 0.57 | -3.21 |
| H-5B | 8/85 | UNC | 2.97 | 7.40 | 0.908 | 8.46E-02 | -0.11 | -0.02 | 0.68 | 0.03 | -1.09 | -0.15 | -2.86 |
| H-5C | 10/81 | UNC | 3.002 | 7.90 | 0.906 | -1.20E-01 | -0.08 | 0.75 | 2.20 | 0.05 | -1.08 | 0.61 | -3.17 |
| H-6B | 5/81 | UNC | 1.178 | 7.00 | 0.969 | 2.24E-04 | -0.15 | -0.04 | 0.16 | 0.05 | -2.05 | -0.64 | -2.16 |
| H-6B | 9/85 | UNC | 1.13 | 6.90 | 0.970 | -1.28E-02 | -0.20 | -0.16 | -0.07 | -0.01 | -2.08 | -0.75 | -2.07 |
| H-7B1 | 3/86 | UNC | 0.089 | 7.20 | 0.999 | -4.09E-04 | -0.23 | 0.07 | 0.01 | -0.01 | -5.86 | -0.90 | -2.20 |
| H-8B | 1/86 | UNC | 0.083 | 7.60 | 0.999 | -1.97E-04 | -0.23 | 0.33 | 0.66 | -0.01 | -7.45 | -0.52 | -2.70 |
| H-9B | 11/85 | UNC | 0.087 | 7.40 | 0.999 | 3.70E-04 | -0.22 | 0.24 | 0.37 | 0.00 | -6.23 | -0.71 | -2.43 |

## Table 1-3. Saturation Indices for Common Evaporite Minerals Calculated by PHRQPITZ (Continued)

| Well | Date | Lab | Ionic Strength (molal) | pH | $^{a}H_2O$ | Charge[1] Balance Error | Saturation Indices[2] | | | | | | log $pCO_2$ |
|---|---|---|---|---|---|---|---|---|---|---|---|---|---|
| | | | | | | | Anh | Cal | Dol | Gyp | Hal | Mag | |
| H-11B3 | 6/85 | UNC | 2.23 | 7.20 | 0.934 | -3.60E-02 | -0.13 | -0.17 | 0.12 | 0.03 | -1.39 | -0.54 | -2.63 |
| H-12 | 8/85 | UNC | 2.72 | 7.20 | 0.916 | 4.42E-02 | -0.12 | -0.15 | 0.34 | 0.02 | -1.18 | -0.35 | -2.61 |
| P-14 | 2/86 | UNC | 0.582 | 6.80 | 0.988 | -9.06E-03 | -0.15 | 0.14 | 0.18 | 0.05 | -3.01 | -0.81 | -1.81 |
| P-17 | 3/86 | UNC | 1.67 | 7.50 | 0.953 | -3.61E-02 | -0.18 | 0.10 | 0.73 | 0.00 | -1.70 | -0.22 | -2.90 |
| WIPP-25 | 8/80 | UNC | 0.26 | 6.90 | 0.995 | 3.21E-03 | -0.24 | 0.03 | 0.04 | -0.03 | -3.56 | -0.84 | -1.69 |
| WIPP-26 | 8/80 | UNC | 0.329 | 6.90 | 0.993 | -5.12E-03 | -0.18 | -0.04 | -0.10 | 0.03 | -3.36 | -0.91 | -1.86 |
| WIPP-26 | 8/80 | G | 0.330 | 6.90 | 0.993 | -3.71E-02 | -0.23 | 0.09 | 0.14 | -0.02 | -3.32 | -0.79 | -1.84 |
| WIPP-26 | 11/85 | UNC | 0.371 | 7.10 | 0.992 | -9.29E-03 | -0.20 | 0.10 | 0.18 | 0.02 | -3.22 | -0.77 | -2.14 |
| WIPP-27 | 9/80 | UNC | 2.573 | 6.30 | 0.922 | -7.62E-02 | -0.12 | -0.38 | -0.40 | 0.03 | -1.29 | -0.87 | -1.33 |
| WIPP-28 | 9/80 | UNC | 0.903 | 6.50 | 0.976 | -2.42E-02 | -0.26 | 0.16 | 0.53 | -0.07 | -2.27 | -0.48 | -0.76 |
| WIPP-29 | 8/80 | UNC | 4.908 | 6.10 | 0.840 | -2.06E-01 | 0.02 | -0.72 | 0.01 | 0.09 | -0.61 | -0.21 | -0.87 |
| WIPP-29 | 8/80 | G | 4.472 | 6.10 | 0.853 | -2.74E-01 | -0.15 | -0.45 | 0.61 | -0.07 | -0.64 | 0.21 | -1.10 |
| WIPP-29 | 12/85 | UNC | 6.57 | 5.90 | 0.773 | -2.07D-01 | -0.01 | -1.25 | -0.56 | -0.01 | -0.20 | -0.16 | -0.75 |
| WIPP-30 | 9/80 | UNC | 0.582 | 8.80 | 0.986 | -2.50E-02 | -0.18 | 1.12 | 2.37 | 0.02 | -2.73 | 0.41 | -4.41 |

## Table 1-3. Saturation Indices for Common Evaporite Minerals Calculated by PHRQPITZ (Continued)

| Well | Date | Lab | Ionic Strength (molal) | pH | $^{a}H_2O$ | Charge[1] Balance Error | Saturation Indices[2] | | | | | | log $pCO_2$ |
|---|---|---|---|---|---|---|---|---|---|---|---|---|---|
| | | | | | | | Anh | Cal | Dol | Gyp | Hal | Mag | |
| Magenta: | | | | | | | | | | | | | |
| H-3B1 | 7/85 | UNC | 0.20 | 8.00 | 0.997 | -2.79E-03 | -0.16 | 0.52 | 1.02 | 0.06 | -4.04 | -0.34 | -3.47 |
| Dewey Lake: | | | | | | | | | | | | | |
| TWIN-P | 1/86 | UNC | 0.011 | 7.70 | 0.999 | 4.89E-04 | -1.88 | 0.37 | 0.67 | -1.66 | -7.52 | -0.54 | -2.39 |
| Bell Canyon: | | | | | | | | | | | | | |
| DOE-2 | 7/85 | UNC | 2.95 | 6.60 | 0.907 | 8.68E-03 | -0.13 | -0.17 | -0.40 | 0.00 | -1.09 | -1.07 | -1.96 |

1. Charge balance error (CBE in equivalents per kilogram of water) is calculated as: CBE (eq/kg $H_2O$) = Σ cations (eq/kg $H_2O$) - Σ anions (eq/kg $H_2O$)
2. Mineral names: Anh = anhydrite; Cal = calicite; Dol = dolomite; Gyp = gypsum; Hal = halite; Mag = magnesite.

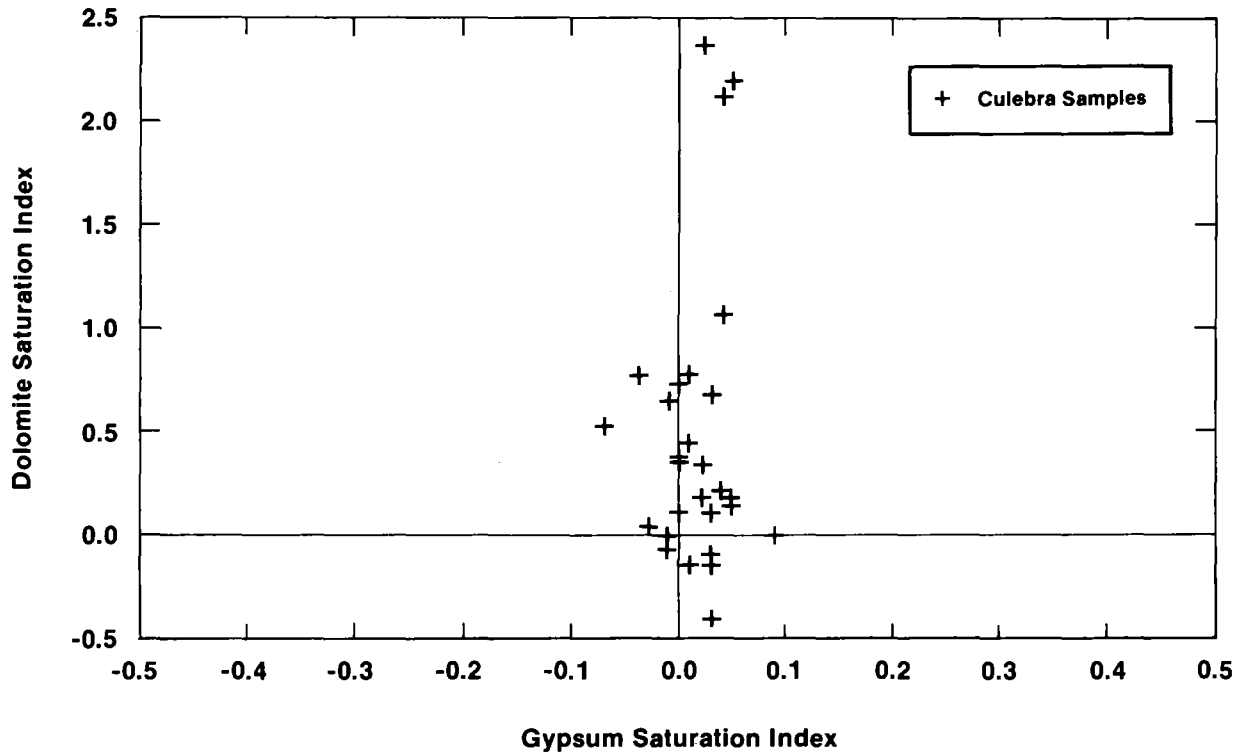


Figure 1-17. Relationship between gypsum and dolomite saturation indices in Culebra groundwater samples (from Siegel et al., Chapter 2).

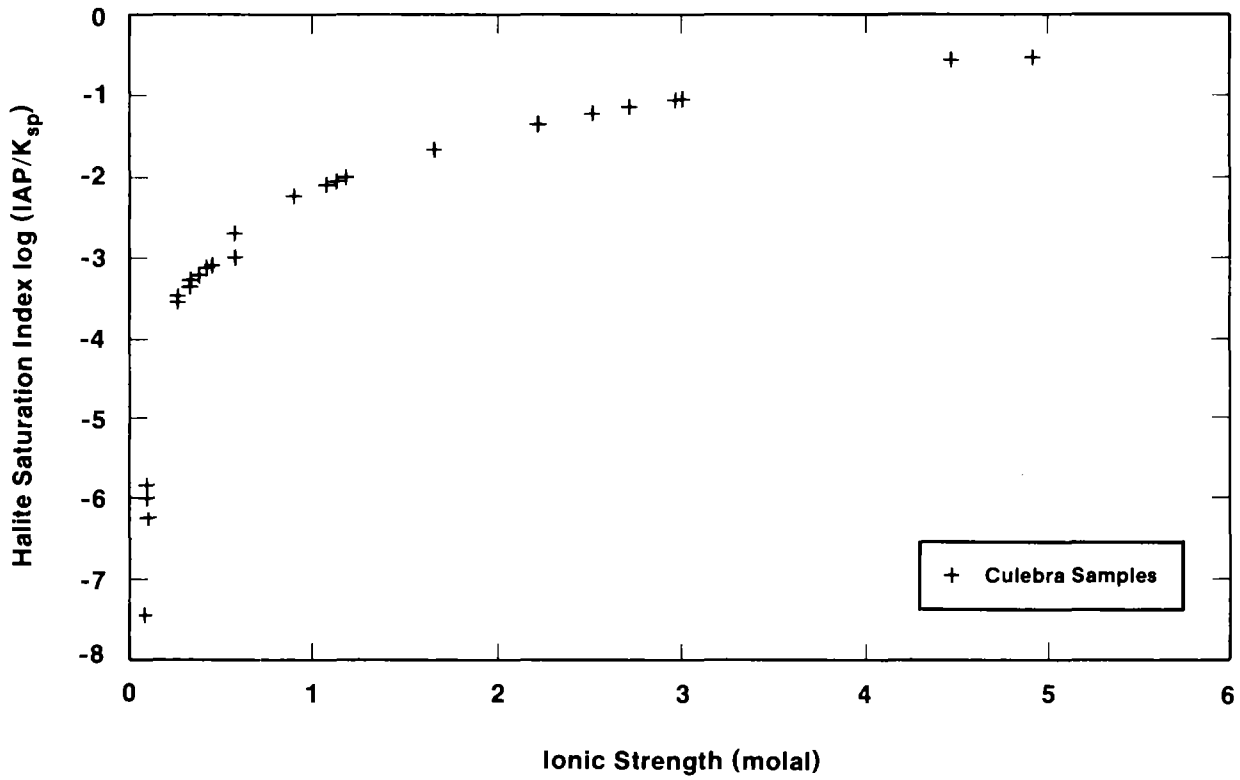


Figure 1-18. Relationship between halite saturation indices and ionic strengths of Culebra groundwater samples (from Siegel et al., Chapter 2).

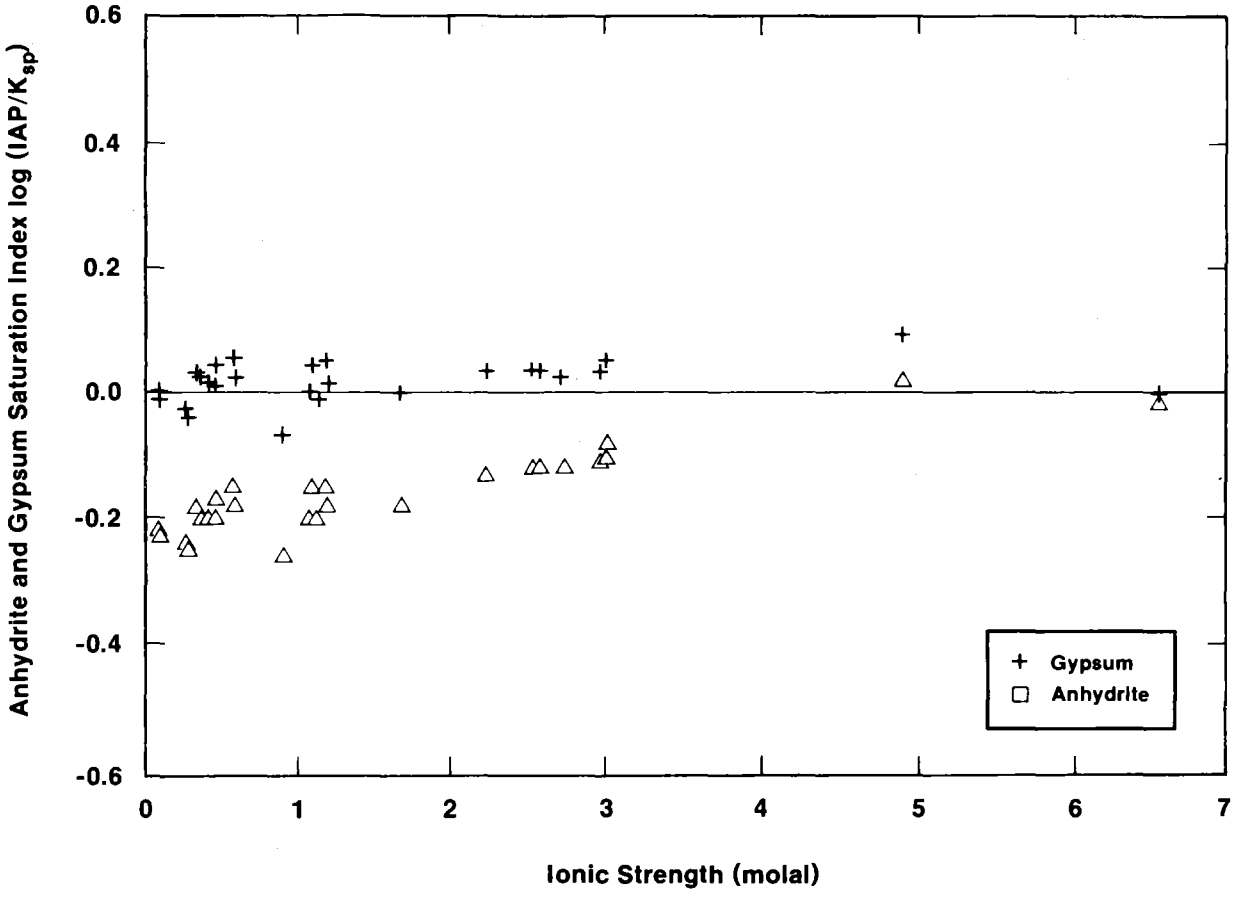


Figure 1-19. Relationship between anhydrite and gypsum saturation indices (states) and ionic strengths of Culebra groundwater samples (from Siegel et al., Chapter 2).

The degree of carbonate mineral saturation independent of the effects due to $CO_2$ outgassing can be determined by examining the value of the saturation index (SI) expression:

$$2\,SI_{calcite} - SI_{dolomite}.$$

The value of this expression is independent of the uncertainty in the carbonate ion activity and equals zero when the solution is saturated with respect to both calcite and dolomite.

Figure 1-20 shows that the value of the saturation index expression for the Culebra waters decreases as a function of ionic strength. This means that once the effects of the $CO_2$ outgassing are corrected for, many of these waters are either supersaturated with respect to dolomite and/or undersaturated with respect to calcite. The degree of disequilibrium increases with ionic strength.

### 1.4.6 Partial Equilibrium Model for Major Solutes

In Chapter 2, Siegel et al. suggest that the solute relationships described in the preceding sections might be indicative of a partial equilibrium system. In a partial equilibrium system, solution/mineral equilibria shift nearly reversibly in response to an irreversible process (Helgeson, 1968; Plummer, 1984). Increase of salinity in Culebra waters due to dissolution of evaporite salts in adjacent rock units is an irreversible chemical reaction process affecting the water chemistry. The increase in salinity changes the apparent solubilities of carbonates and sulfates. As shown in Figure 1-21, the solubilities of dolomite, calcite, and gypsum increase with salinity up to 3 molal ionic strength and then decrease. Thus, even if the saturation indices for these minerals are near zero, the waters may still be capable of dissolving significant amounts of these phases in response to salinity increase.

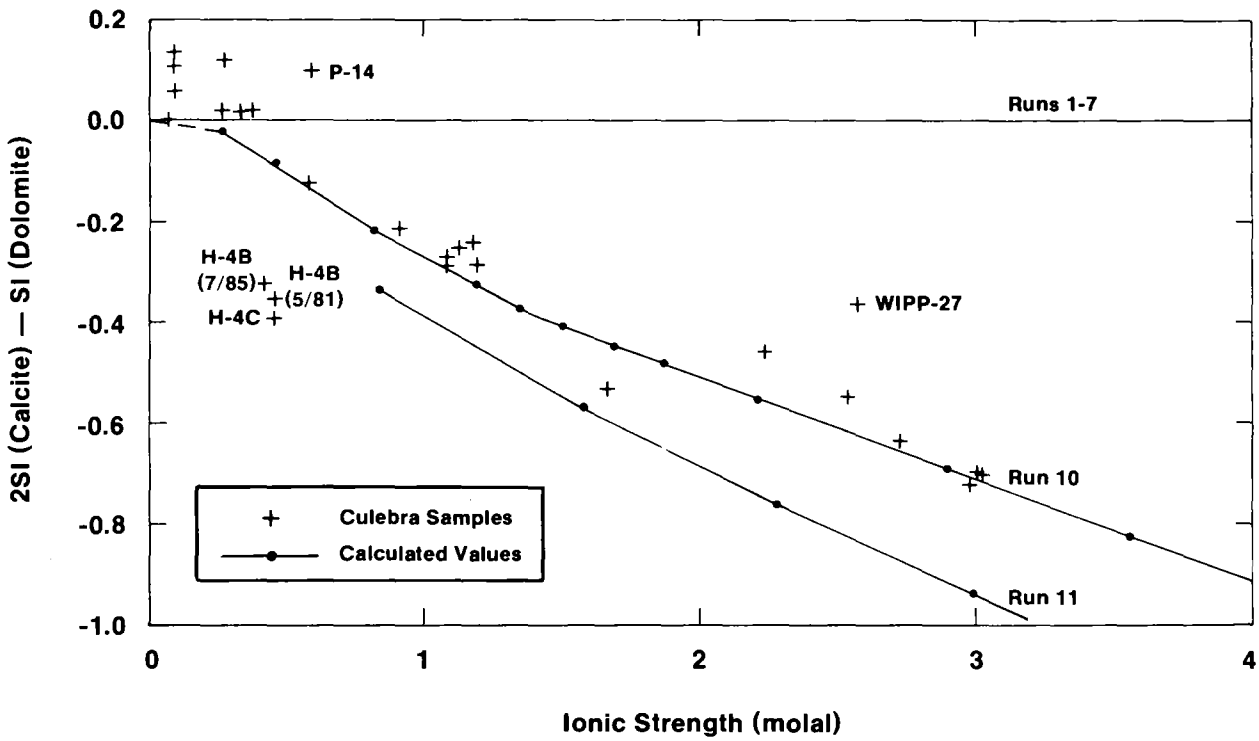


Figure 1-20. Relationship between saturated index expression ($2SI_{calcite}$ - $SI_{dolomite}$) and ionic strengths for Culebra groundwaters. Compositions of hypothetical solutions calculated by reaction-path simulations described in Section 2.4.2.2 are indicated by solid lines (from Siegel et al., Chapter 2).

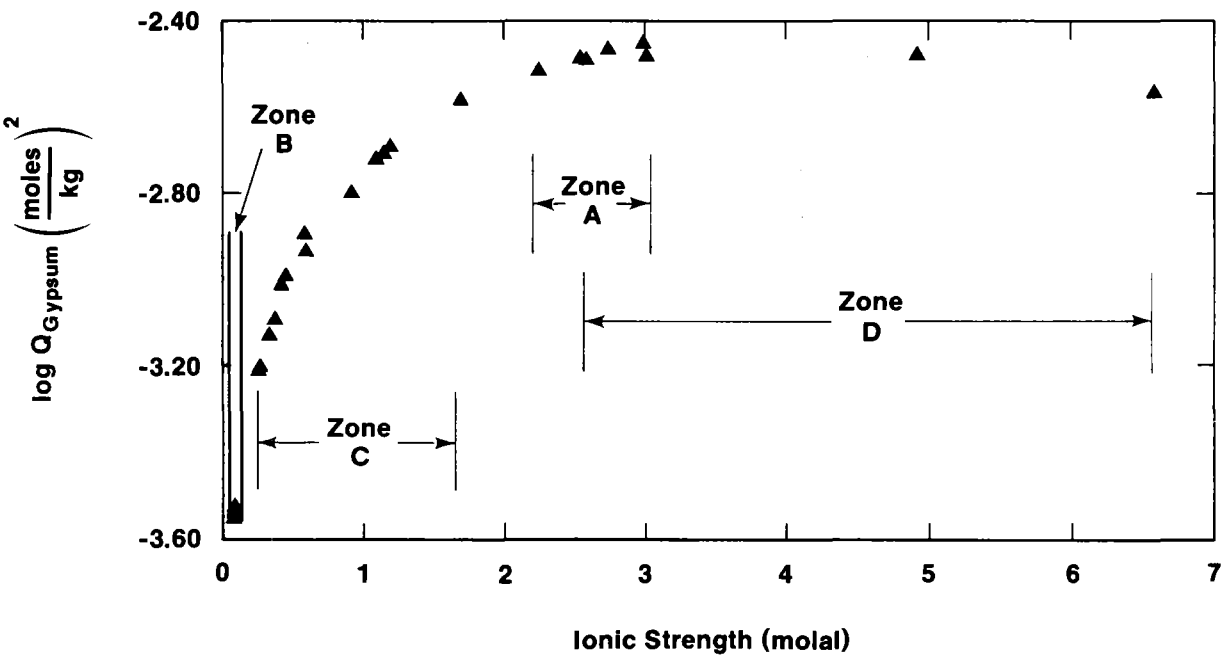


Figure 1-21. Relationship between apparent solubility product logQ for gypsum and ionic strength in Culebra water samples. LogQ is calculated from the thermodynamic solubility constant logK and the activity coefficients of the reactants ($\log Q = \log K - \log\gamma_{Ca^{2+}} - \log\gamma_{SO_4^{2-}} - 2\log a_{H_2O}$).

In Section 2.4.2.2, Siegel et al. use the PHRQPITZ code (Plummer et al., 1988) to evaluate a partial equilibrium model for precipitation/dissolution of gypsum, calcite, and dolomite in the Culebra. The PHRQPITZ code was used to calculate the compositions of waters that would be produced by several hypothetical reaction paths. Parametric simulations were carried out to determine the effect of certain assumptions about chemical reaction rates, sources of solutes, and initial conditions on the groundwater compositions. Figures 1-22 and 1-23 compare the changes in concentrations of major solutes along two hypothetical reaction paths with compositions of waters in the Culebra. Both runs assume equilibrium is maintained with respect to calcite and gypsum, while halite plus accessory evaporite salts are added to solution. The solutions are closed with respect to atmospheric $CO_2$, and initial $pCO_2$ is $10^{-2}$atmosphere. For Figure 1-22, reaction progress is indicated by ionic strength. For Run 1, dolomite saturation is maintained (SI = 0), while pure halite is added to the hypothetical solution. For Run 10, dolomite does not react with solution (variable saturation index), while halite and leonite plus $MgCl_2$ are added. Mg/Ca molar ratios of Culebra groundwaters are plotted for comparison. Values for WIPP-29 are not plotted. For Figure 1-23, reaction progress is indicated by moles of chloride added. Sulfate concentrations of Culebra groundwaters are plotted for comparison.

Run 1 assumes a simple partial equilibrium model in which pure NaCl is added to the solution while the groundwaters are maintained at equilibrium with respect to calcite, dolomite, and gypsum. The concentrations of Ca, Mg, $SO_4$, and $CO_3$ change due to the changes in the solubilities of calcite, dolomite, and gypsum described above. The system is closed with respect to $CO_2$ gas exchange; the initial partial pressure of $CO_2$ is $10^{-2}$ atmospheres. As the reaction proceeds, dedolomitization (dissolution of dolomite and precipitation of calcite) and dissolution of gypsum occur. Figures 1-22 and 1-23 show that Run 1 does not reproduce the compositions of Culebra waters. This simple model provides a good fit to many of the observed calcium concentrations; however, concentrations of Mg and $SO_4$ are considerably below the predicted values.

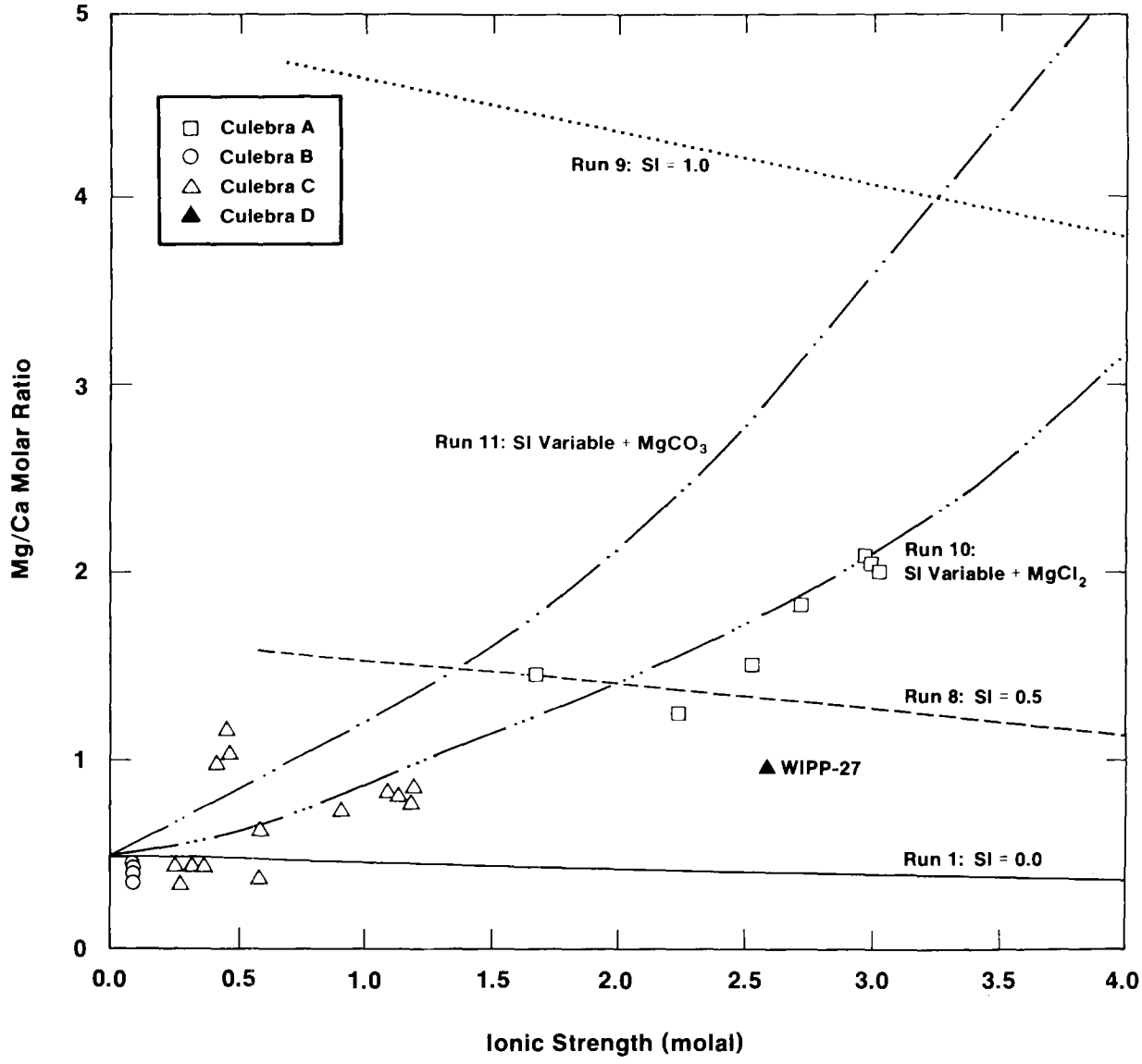


TRI-6344-98-0

Figure 1-22. Change in Mg/Ca molar ratio as a function of reaction progress, types of added salts, and dolomite saturation index for simulated evolution of Culebra groundwaters.

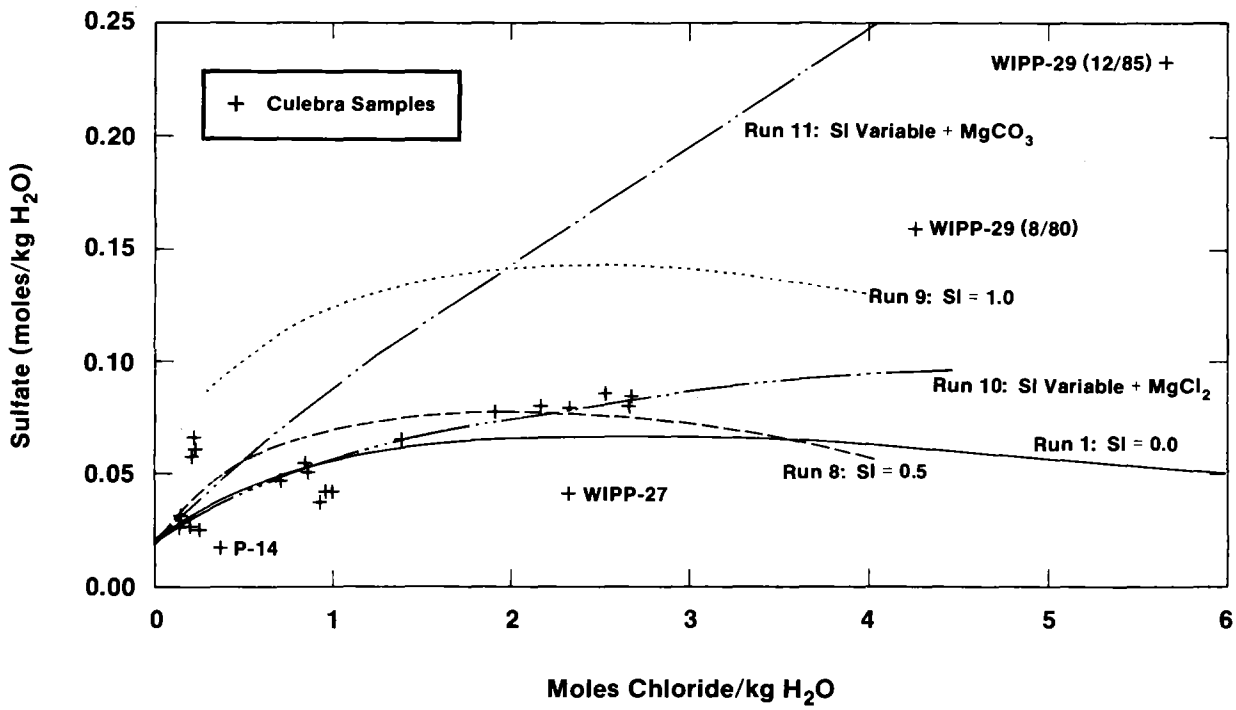


Figure 1-23. Change in sulfate concentration as a function of reaction progress, types of added salts, and dolomite saturation index for simulated evolution of Culebra groundwater compositions.

In Run 10, saturation with dolomite was not maintained. The starting solution was produced by equilibrating distilled water with calcite, dolomite, and gypsum at an initial $pCO_2$ of $10^{-2}$ atmosphere. The system was then closed to $pCO_2$ gas, and addition of Na, Cl, K, Mg, and $SO_4$ by congruent dissolution of halite and incongruent dissolution of polyhalite and carnallite was simulated. Carnallite dissolves incongruently to form KCl and a solution containing $Mg^{2+}$ and $Cl^-$. In Run 10, this was simulated by adding $MgCl_2$ to the reaction solution. Incongruent dissolution of polyhalite was simulated by addition of leonite ($K_2Mg(SO_4)\cdot 4H_2O$). The K/Cl ratio of the Culebra waters was used to estimate a reasonable leonite/halite ratio. The $MgCl_2$/halite ratio was then adjusted to fit the observed Mg/Cl ratio of the Culebra waters. Equilibrium between the waters and gypsum and calcite was maintained; as the reaction proceeded both calcite and gypsum dissolved. The saturation index of dolomite was calculated as the reaction progressed, but dolomite was not allowed to dissolve or precipitate.

Figures 1-22 and 1-23 show that Run 10 reproduces the trends of the Ca, Mg, and $SO_2$ concentrations in this suite of Culebra groundwaters. The calculated dolomite saturation indices for Run 10 were used to calculate values of the saturation index expression described previously and are plotted in Figure 1-20. The good correspondence between the theoretical and observed solute concentrations in these figures shows that addition of solutes (Mg, $SO_4$, K, and Cl) to the Culebra from evaporite minerals such as polyhalite and carnallite in a partial equilibrium system is consistent with the observed groundwater compositions if dolomite does not precipitate from supersaturated solutions.

### 1.4.7 Estimation of Oxidation-Reduction Potentials and Occurrence of Organics in the Culebra Groundwaters

Measurements of redox potentials have been made in Culebra waters using Pt electrodes and N, I, As, and Se redox couple data. Apparent Eh values were calculated from the concentrations of the redox couples using the Nernst equation. Sensitivity calculations showed that the calculated Eh values were fairly insensitive to assumptions about activity/concentration relationships, to reasonable uncertainties in the analytical data, and

to errors introduced by uncertainty in the field pH measurements. However, the total concentrations and concentrations of individual members of the couples were very close to the detection limits of the analytical methods used. This meant that in most cases, the existence of redox equilibria or disequilibria could not be established. Descriptions of the sampling procedure, analytical techniques, and calculations are given in Myers et al. (Chapter 6).

The results of the calculations for the most recent WQSP water samples are summarized in Figure 1-24. Arrows indicate upper or lower limits resulting from one member of the pair being present at levels below the detection limit. In these cases, the analyses were used to set an upper or lower bound on the potential for that couple. Redox potentials could be calculated for four wells and two wells, respectively, from the iodine and nitrogen couples. For most of the other wells, an upper or lower bound could be calculated for these couples. Three wells provided data to calculate potentials for the selenium couple, and data from six wells could be used to calculate potentials for the arsenic couple. Lower redox bounds for three additional wells could be calculated for the arsenic couple.

Although redox equilibrium cannot be established for any of these wells, groups of wells that have similar characteristics can be identified. Samples in the first group include waters from the Engle, H-7B, H-8B, and H-9B wells that show a range of calculated redox potentials all of which are greater than approximately 350 mV. This lower bound is defined by the absence of measurable $NH_4^+$. Samples from H-7B, H-8B, and H-9B from earlier WQSP rounds, however, had measurable $NH_4^+$, and thus the lower bound (indicated by the arrows in the figure) may be an artifact of the analytical technique.

Data from a second group consisting of the WIPP-25, WIPP-26, H-12, and P-14 wells may indicate redox disequilibrium. The calculated potentials span wide ranges and in some wells the redox values calculated for the $I^-/IO_3^-$ data lie above upper bounds defined by the nitrogen data or values calculated for the arsenic couple.

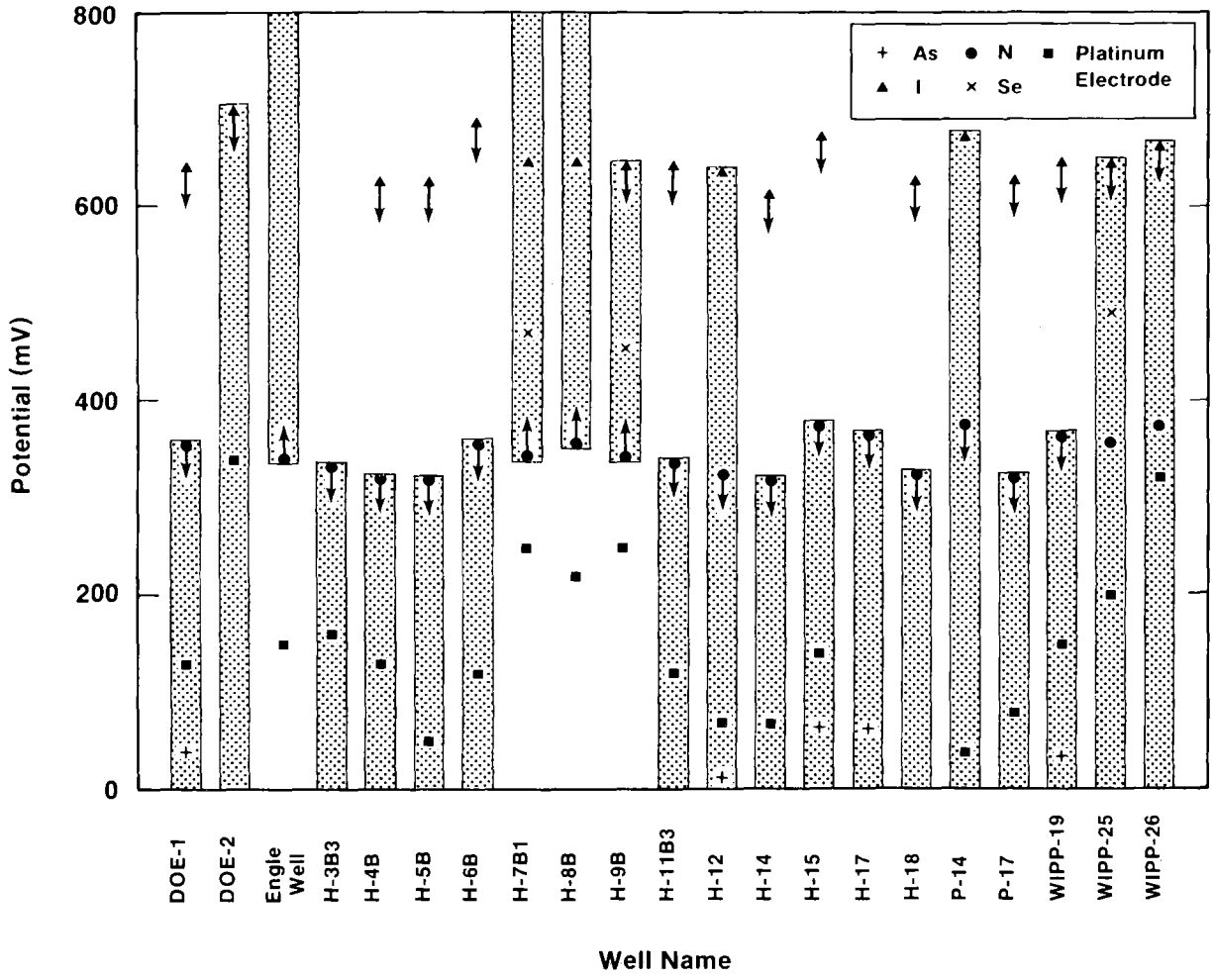


Figure 1-24. Comparison of redox potentials calculated for several different redox couples in waters from Culebra wells.

The final group, consisting of the balance of the wells, has calculated redox values below approximately 350 mV. This upper bound is defined only by the absence of measurable nitrate. Waters from these wells are relatively saline and contain low levels of total nitrogen. If the high salt content of the water has prevented detection of the nitrate, then the "upper bound" may be an artifact of the analytical technique.

In Chapter 6, Myers et al. note that the four wells in the southern part of the study area are distinguished from the other wells by their higher redox potential ranges, lower TDS, and lower halite saturation indices. They conclude that these characteristics suggest that either a hydrologic divide separates them from the other more reduced wells of the north, or that a region of recharge in the southern area provides a source of relatively oxic, low-TDS groundwater to the Culebra.

Observations attesting to the presence of reduced species in some Rustler groundwaters (WIPP-25, WIPP-26, WIPP-28, and WIPP-30) were reported by Lambert and Robinson (1984). These included measurable to less-than-measurable but odoriferous concentrations of hydrogen sulfide, iron slimes, rank (but not $H_2S$) odors, milky-white and black precipitates that developed as water samples stood in bottles under surface conditions, and gaseous effervescence. Some of these observations were only transient over the time of some pump tests. Whether they represent purging of accumulated concentrations of species related to organic chemical reduction or an actual change in redox potential is not known.

There are few data available for oxidation-reduction potentials in the other members of the Rustler Formation. Redox potentials measured by Pt electrodes in wells in Nash Draw were previously shown to be generally higher in the Culebra than at the Rustler/Salado contact (Lambert and Robinson, 1984).

Values of TOC of Culebra samples described by Myers et al. in Chapter 6 range from $< 1$ to 7 mg/L. This range does not include higher values (14-15 mg/L) that are probably

associated with contamination due to drilling or sampling activities. The amount of organic carbon associated with halides (TOX) (Cl, Br, and Cl) was also analyzed and ranged from <0.1 to 9.7 mg/L; however, an observed correlation between TOX and Cl concentration may indicate significant analytical interference. In Chapter 6, Myers et al. conclude that there was no reason to suspect the occurrence of halogenated organics contaminating the Culebra. Other evidence for organic contamination of water samples drawn from the Culebra is based on radiocarbon data and is discussed by Lambert (1987; Chapter 5).

### 1.4.8 Isotopic Studies of Rustler Waters

The isotopic geochemistry of Rustler and related groundwaters is discussed in detail by Lambert in Chapter 5, with a summary of the sources of data (oxygen and hydrogen isotopes, carbon isotopes including radiocarbon, tritium, radiochloride, and uranium concentration and $^{234}U/^{238}U$ activity ratios) and their interpretations. This discussion is in turn a summary of that work, which is drawn from several source documents: Lambert (1978), Lambert (1983), Lambert and Harvey (1987), Lambert (1987), and Lambert and Carter (1987).

Confined Rustler groundwaters near the WIPP and in Nash Draw have isotopic compositions very tightly clustered along the worldwide meteoric field in $\delta D$-$\delta^{18}O$ space (Figure 1-RU). The tightly clustered Rustler data plotting along the meteoric field (heavy solid lines) at more negative $\delta$-values have isotopic compositions that differ from the field of less confined groundwaters having more positive $\delta$-values. Small (up to -10‰) deviations of $\delta$-values from the meteoric field are not considered significant (line a; cf. Allison et al., 1985). WIPP 29 Culebra and Surprise Spring may have evolved by evaporation from a shallow water table, with a $\delta D/\delta^{18}O$ slope of 2 (lines b; cf. Allison, 1982), from water imported from the Ogallala aquifer for use in nearby potash-refining operations, from modern-type water by oxygen-isotope shift (lines c), but probably not from evaporation of confined Rustler-type water (slope = 5; line d; cf. Craig et al., 1963). Groundwaters whose stable-isotope compositions deviate markedly from that of a characteristically meteoric

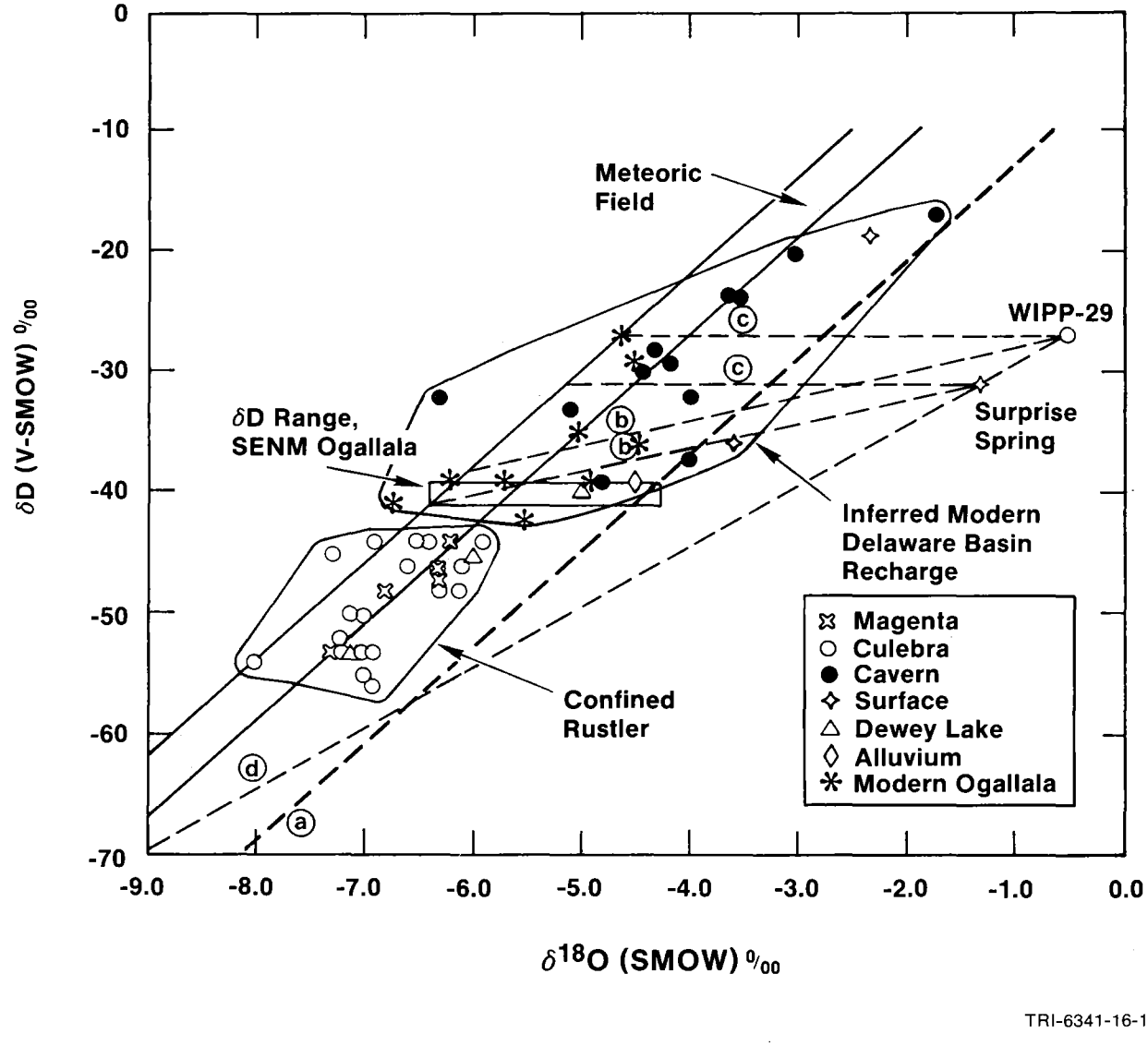


Figure 1-25. Stable-isotope compositions of groundwaters from the Rustler Formation (Figure 5-1, adapted from Lambert and Harvey, 1987).

signature occur at the Rustler/Salado contact in the low-permeability portions of that zone in the central and eastern parts of the WIPP Site (Lambert, Chapter 5) and near the surface in the Culebra and Tamarisk members in the southwest portion of Nash Draw, where hydrologic conditions are not as confining (Figure 1-25). Deviations in waters at the Rustler/Salado contact are attributable to a profound degree of rock/water interaction involving a relatively large rock/water ratio, while the isotopic signatures observed in southwestern Nash Draw can arise from partial evaporation from the vadose zone and the capillary fringe above the water table. Confined meteoric Rustler waters are virtually identical in stable-isotope composition to confined meteoric Capitan waters at the basin margin, indicating recharge of both types of confined waters under similar climatic conditions.

By comparison, vadose Capitan waters from the Carlsbad Caverns system, groundwater from a water table in alluvium, and near-surface accumulations that homogenize seasonal variations in isotopic composition also have meteoric isotopic signatures, but have isotopic compositions more positive in $\delta D$-$\delta^{18}O$ space than confined Rustler and Capitan waters (Lambert and Harvey, 1987). The envelopes of $\delta$-values for these two populations of differing hydrologic character do not overlap (Figure 1-25). The data of Nativ and Smith (1987) reveal that in Ogallala groundwaters underlying the high plains to the east, climatically similar to the Delaware Basin, the only groundwaters containing tritium levels indicative of recent (post-1950) meteoric derivation (>10 tritium units [TU]) all have $\delta D$ values >-42‰ (Figure 1-25), comparable to near-surface unconfined meteoric waters in the Delaware Basin (Figure 1-26). High Plains data for Figure 1-26 are from Nativ and Smith (1987); WIPP data are from Lambert and Harvey (1987) and Lambert (1987). Significantly high tritium concentrations (>10 TU), indicating derivation from a meteoric source since 1950, are restricted largely to groundwaters having $\delta D$ values more positive than about -42‰. Ogallala waters from nearby southeastern New Mexico have $\delta D$ values between -39 and -41‰, corresponding with $\delta D$ values of modern groundwater recharge in the Texas High Plains. Hydrogen-isotope characteristics of groundwaters from the nearby

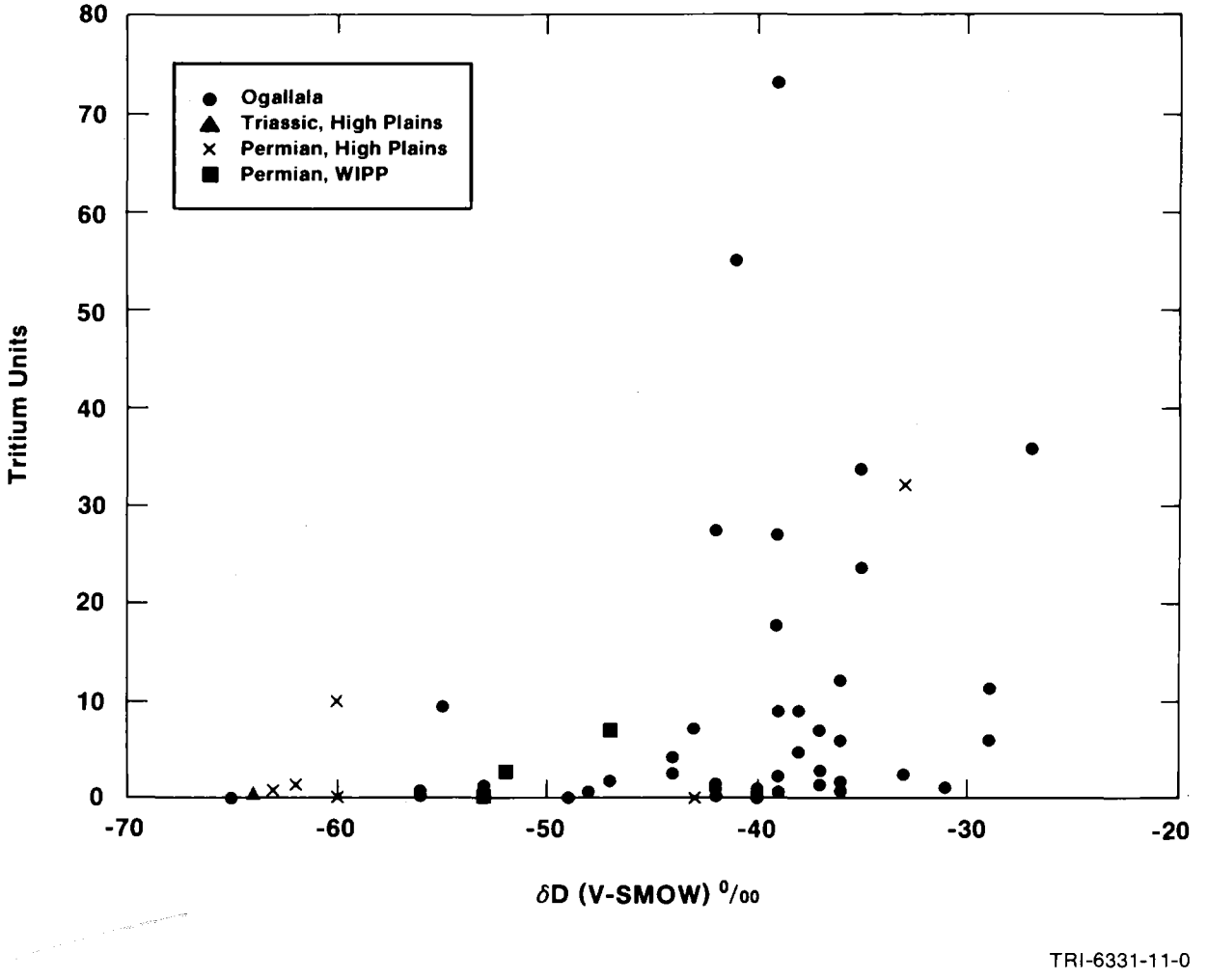


Figure 1-26. Tritium and deuterium concentrations in groundwaters from the Southern High Plains, Texas, and the Delaware Basin, southeastern New Mexico (Figure 5-2, from Lambert and Harvey, 1987).

climatically similar Delaware Basin (WIPP data) are shown for comparison. The isotopic signatures of confined Rustler and Capitan waters are distinct from that of both Ogallala water with discernable modern input and of vadose Capitan and alluvial water. Thus, it is likely that the isotopic compositions of confined Rustler and Capitan groundwaters in the northern Delaware Basin are not characteristic of groundwaters that would be receiving modern meteoric recharge under the present climatic conditions.

Some, but not all, Dewey Lake groundwaters may have a component characteristic of climatic conditions fostering modern surficial recharge (Figure 1-25). Some have stable-isotope compositions comparable to the near-surface occurrences, and some are comparable to confined Rustler groundwaters. Thus, recharge to the Dewey Lake, like recharge to the Ogallala, appears to be variable in both space and time.

Only four out of 16 well-water occurrences gave internally consistent radiocarbon "age" calculations based on the internally consistent interpretive model and assumptions of Evans et al. (1979) for water-bearing carbonate rocks. The model of Evans et al. takes into account dilution of atmospheric carbon by dissolution of carbonate rock, and carbon isotope exchange between water and host rock. The mean of these four is 14,000 years; 95% confidence limits are ± 5,000 years. This is a minimum age estimate. It is not possible to estimate an upper age limit because of the unavoidable possibility of at least small amounts of unmitigable contamination even in these four samples. These tightly clustered ages, given their individual confidence limits, while spread out from north to south across the WIPP Site, do not allow consistent age gradients or travel times to be inferred across the WIPP Site based on differences in radiocarbon ages (Figure 1-27). Ten of the 16 well-water occurrences were complexly contaminated due to unmitigable anthropogenic well-bore effects. The remaining two are ambiguous, but all 16 probably represent three-component mixing, including some contamination. The four dated groundwaters (three Culebra and one Dewey Lake) all have stable-isotope compositions belonging to the more negative population in $\delta D$-$\delta^{18}O$ space (Figure 1-25). Thus, it is inferred that Rustler and Dewey Lake groundwaters in this population have a significant component at least

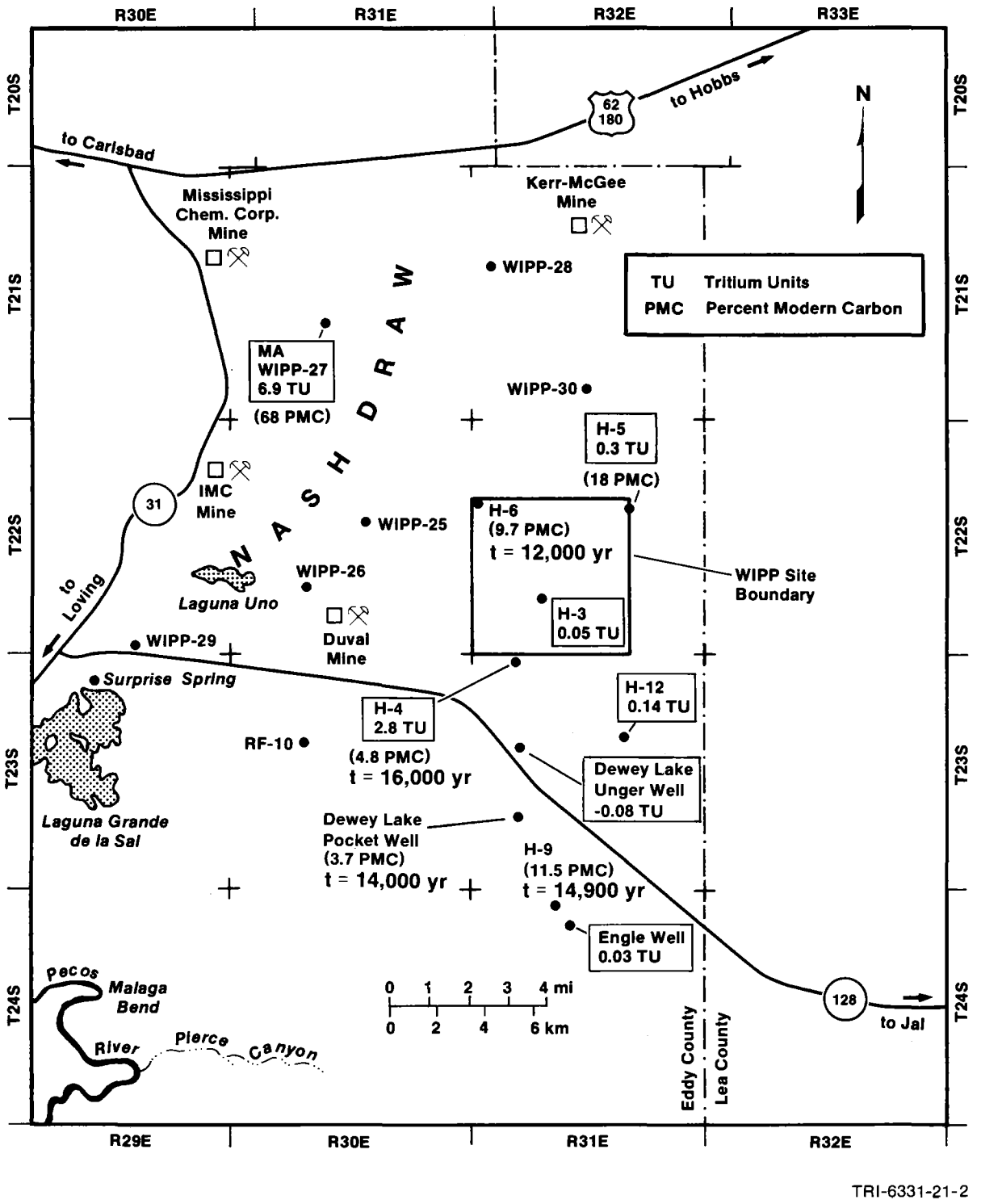


TRI-6331-21-2

Figure 1-27. Tritium and radiocarbon in Rustler and Dewey Lake groundwaters (Figure 5-11, adapted from Lambert and Harvey, 1987).

12,000 radiocarbon years old. All the tritium measurements from the WIPP area, which are associated with the more negative (confined Rustler) isotopic compositions, are <3 TU, indicating little or no contribution from the atmosphere since 1950. Figure 1-27 shows tritium and radiocarbon in Rustler and Dewey Lake groundwaters. Unless otherwise specified as Dewey Lake (DL) or Magenta (MA), measurements in Figure 1-27 (all from Lambert, 1987) apply to water from the Culebra member of the Rustler Formation. The uniformly low (<7 TU) tritium concentrations near the WIPP Site indicate no introduction of an atmospheric component since 1950 (cf. Isaacson et al., 1974). Three Culebra and one Dewey Lake water were amenable to dating by the carbonate-aquifer model of Evans et al. (1979), giving times of isolation from the atmosphere ranging from 12,000 to 16,000 radiocarbon years. These data indicate long residence times or long travel times from recharge areas, but provide no evidence of either modern vertical infiltration or monotonic age gradients indicating north-to-south flow. Three of these data, from water samples also having $\delta D$ analyses, are depicted in Figure 1-26.

The southeastern New Mexico climate more than 10,000 years ago fostered vegetation now found only at higher elevations, as indicated by the packrat-midden studies of Van Devender (1980). Late Pleistocene climate was probably wetter and more conducive to recharge, as indicated by the concordance between the ages of packrat middens and the relatively less contaminated radiocarbon in the Rustler and Dewey Lake groundwaters described above. Fossil fauna (camels, horses, bison) from extinct spring deposits in Nash Draw near the WIPP Site are of similar age and also indicate wetter conditions than at present (Bachman, 1981).

Given the assumptions of the model of Osmond and Cowart (1976) for uranium systematics in confined hydrologic flow systems, generalized flow directions in confined Rustler groundwaters as inferred from $^{234}U/^{238}U$ relationships appear to have involved recharge from a direction with an eastward-flowing component (Figure 1-28). This is not parallel to modern flow directions inferred from potentiometric heads alone (cf. Figure 1-10). A change in flow direction back toward the west (the modern flow direction

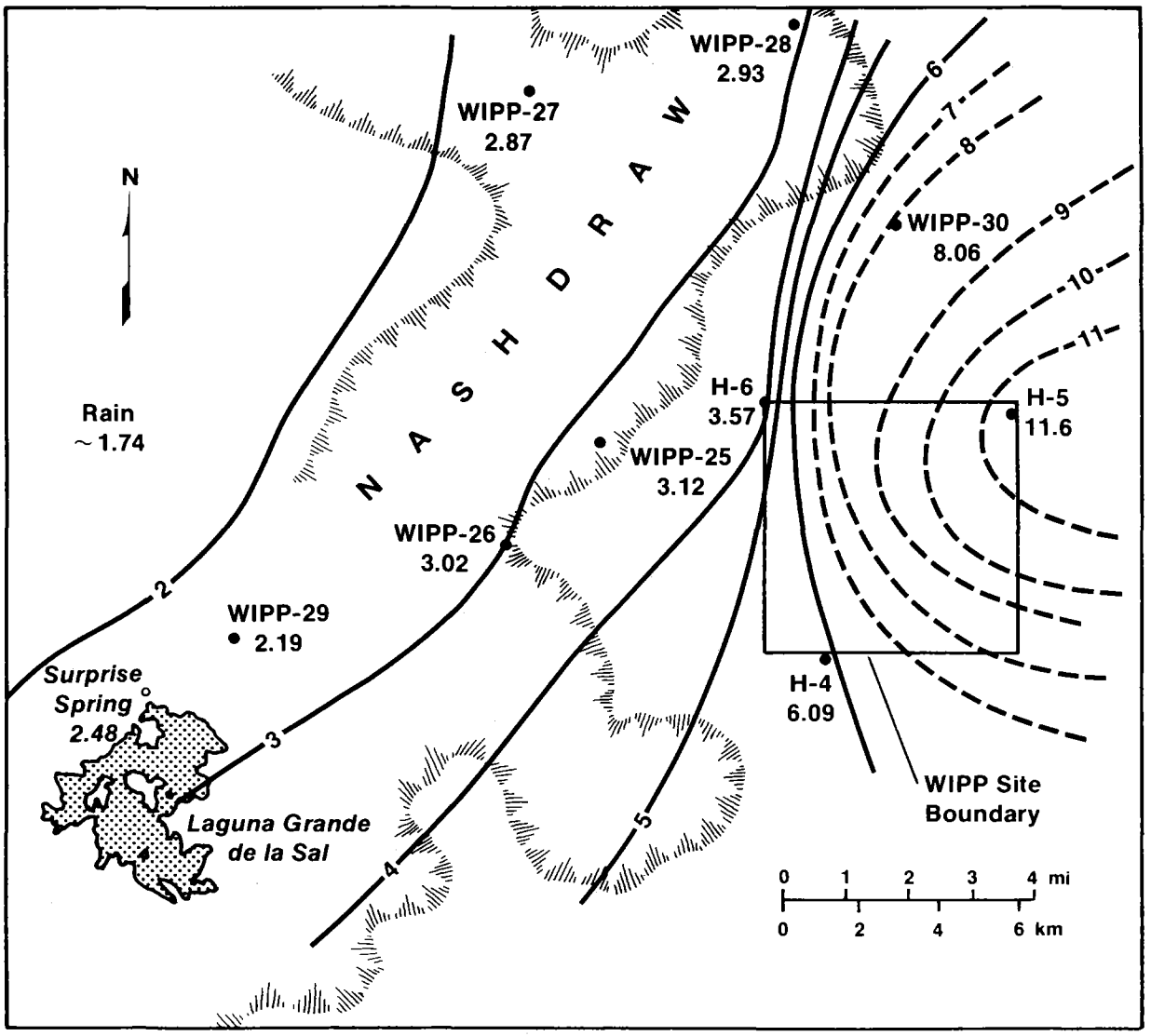


TRI-6331-49-0

Figure 1-28. Contour map of $^{234}U/^{238}U$ activity ratio in groundwater from the Culebra dolomite member of the Rustler Formation (Figure 5-11, from Lambert and Carter, 1987).

indicated for saturated portions of the Magenta; Mercer, 1983) during the past 10,000 to 30,000 years is likely. The activity ratio decreases westward and somewhat southward toward Nash Draw; high activity ratio values typically develop downgradient in hydrologic systems under confined, reducing conditions and are associated with long residence times. Control on contouring east of the WIPP Site is not particularly tight, due to the scarcity of wells suitable for sampling in the eastern low permeability region of the Culebra. Eastward-increasing activity ratio values are interpreted as eastward flow during Pleistocene recharge, and as mimicking an inverse-function of potentiometric head contours during that time. During the time of wetter Pleistocene conditions when the Rustler was being recharged in its outcrops in Nash Draw, the base level there was probably also being lowered by accelerated erosion and dissolution. With the onset of a drier Holocene climate and the cessation of significant recharge, the area whose base level was lowered has probably governed the local hydraulic gradient, resulting in a general southward drainage.

The proposed change in flow direction is consistent with the apparently anomalous data from borehole H-5. It is problematical to obtain either modern or ancient recharge in the vicinity of borehole H-5. In spite of the high potentiometric level there relative to the present downgradient area south and west (a condition commonly interpreted in physical hydrology as indicative of recharge), the water there contains no significant tritium and has the highest $^{234}U/^{238}U$ activity ratio (Lambert, Chapter 5). A high tritium content would be indicative of modern recharge, while a high $^{234}U/^{238}U$ activity ratio would develop in the downgradient, not the upgradient portion of a confined groundwater system, according to the model of Osmond and Cowart (1976). The transmissivity there is also extremely low (Lappin, 1988). Low permeability in the H-5 area may have inhibited subsurface drainage following the cessation of eastward flow to the area, and the high potentiometric level is suspected to be a relic of the paleoflow system.

### 1.4.9 Mineralogical Studies in the Culebra Member

Detailed mineralogical analyses of samples from 12 different locations along three east-west trending traverses have been carried out using a variety of quantitative techniques. Mineralogical and compositional data were obtained from both bulk matrix samples and fractures. The results of this study are in Chapter 3 and briefly summarized below.

Figure 1-29 shows the bulk mineralogy in intact cores of the Culebra along a traverse from Nash Draw (WIPP-29) to the eastern part of the WIPP Site (H-10). The mineralogy of H-7 and H-10 is typical of most cores examined at the site. The dominant mineral is a fairly pure dolomite (Ca/Mg ~ 1.05; FeO ≤0.23%) and comprises about 85% by weight of the bulk rock. Gypsum, calcite, and various clay minerals are observed throughout the Culebra and are distributed heterogeneously both vertically and horizontally. Fractures are observed in all cores and are lined most commonly with clay and gypsum. Clay minerals are present in all samples and comprise approximately 3 to 5% by weight of the bulk mineralogy. They occur as discrete seams along fracture surfaces or are finely dispersed throughout the matrix. The dominant clay minerals are corrensite (an ordered mixed-layer chlorite/smectite), illite, chlorite, and a serpentine-like mineral tentatively identified as amesite. On the regional scale, corrensite is the most abundant mineral observed after dolomite.

Gypsum occurs as a fracture and vug filling; all fracture surfaces examined by XRD showed the presence of nearly pure $CaSO_4 \cdot 2H_2O$. Calcite is present in significant proportions in the top part of WIPP-29 and is interpreted to be of secondary origin (Sewards, et al., Chapter 3). Microprobe analyses of microcrystalline calcite in WIPP-19 show that it is a very low-Mg calcite. Trace amounts of pyrite, magnesite, quartz, and authigenic feldspar have been observed in some cores.

A dark amorphous material is present in abundance in the Culebra samples and has been tentatively identified as organic matter. It is generally associated with clays and often

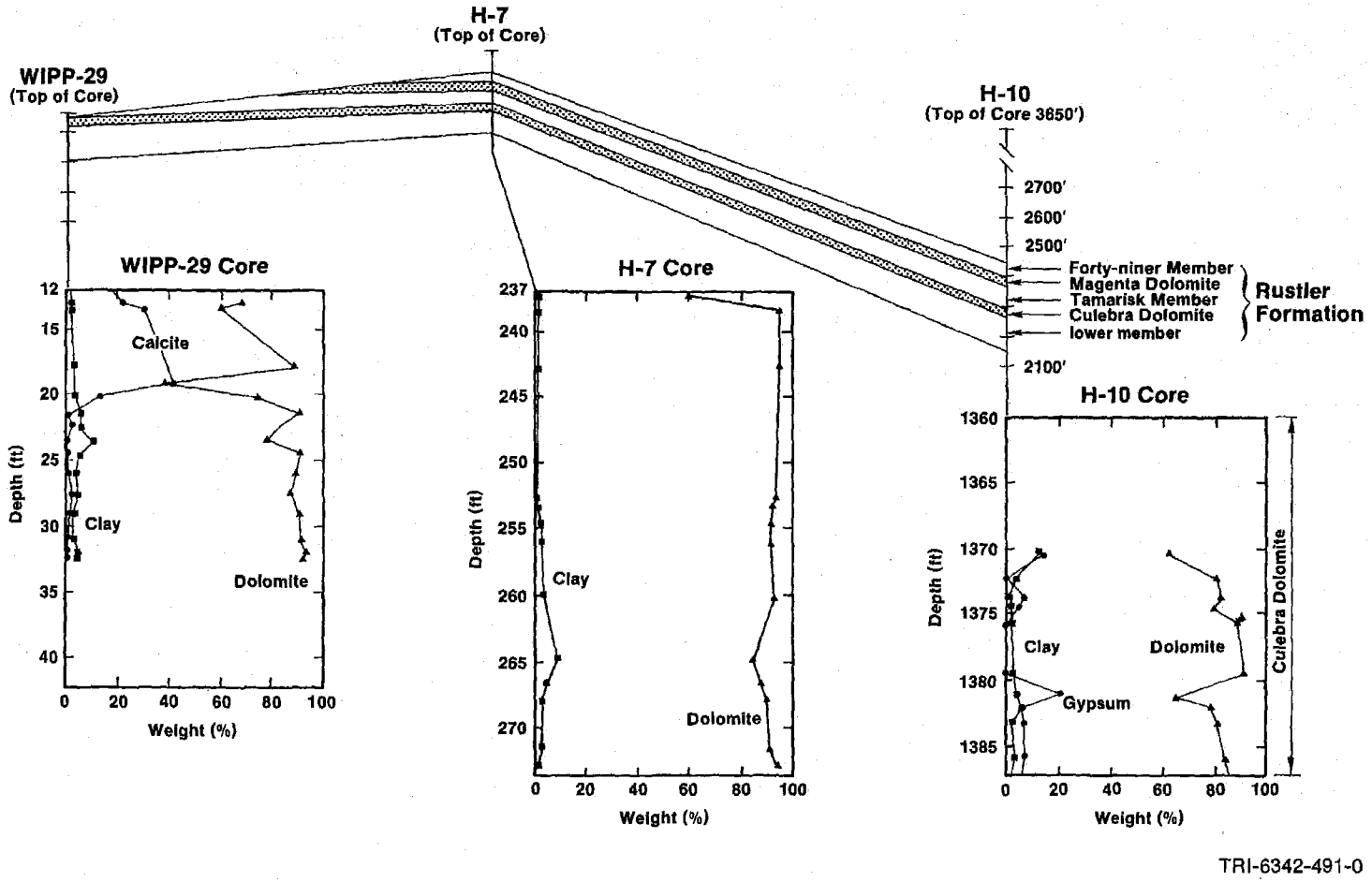


Figure 1-29. Fence diagram showing stratigraphy of the Rustler Formation and mineralogy of the Culebra member (from Sewards et al., Chapter 3).

occurs in algal structures or haloes surrounding vugs whose origin has been attributed to biological activity.

### 1.4.10 Mineral Isotopic Studies

To evaluate further the degree of rock/water interactions in the Culebra and related rocks, supporting data have been collected on the isotopic compositions of rocks and their mineral components. These data include $\delta^{18}O$ and $\delta^{13}C$ values of dolomite and calcite, $\delta D$ values of gypsum, $^{87}Sr/^{86}Sr$ ratios of both carbonates and sulfates, and whole-rock $^{234}U/^{238}U$ activity ratios.

The variations in the $^{234}U/^{238}U$ activity ratio of rock from water-bearing horizons (most rubbled) in the Culebra are minor, generally statistically indistinguishable from the theoretical secular-equilibrium value of unity (Lambert and Carter, 1987). However, water/rock interaction has given rise to significant departures of the activity ratio from unity in coexisting water, which has activity ratio values as high as 11.6 (Figure 1-28).

Despite a conclusively meteoric $\delta^{18}O/\delta D$ signature for confined groundwaters in the Culebra at the WIPP Site and in much of Nash Draw, the carbonate host mineralogy (dominantly dolomite) has generally not recrystallized in the presence of the contained water (Lambert, Chapter 5). However, secondary dolomite dissolution features (such as vugs and etch pits) are commonly developed where the Culebra carries significant amounts of water (Sewards et al., Chapter 3). The only isotopic evidence of carbonate recrystallization in equilibrium with Rustler-type water (Figure 1-30) was found in secondary calcite in a Culebra sample at WIPP-33, a borehole drilled in a collapse feature between the WIPP Site and Nash Draw. This carbonate apparently precipitated in isotopic equilibrium at ambient temperatures, involving a freshwater-type reservoir of carbon. Dolomitic aquifer rock, although partially dissolved to locally enhance the porosity, has an extremely uniform and relatively heavy isotopic composition (mean $\delta^{18}O = +33.4‰$, 95% CL = ±1.0‰, n = 10; mean $\delta^{13}C = +6.1‰$, 95% C = ±1.1‰, n = 10). These values are more consistent with an evaporitic origin than with diagenetic dolomitization of a biogenic limestone precursor

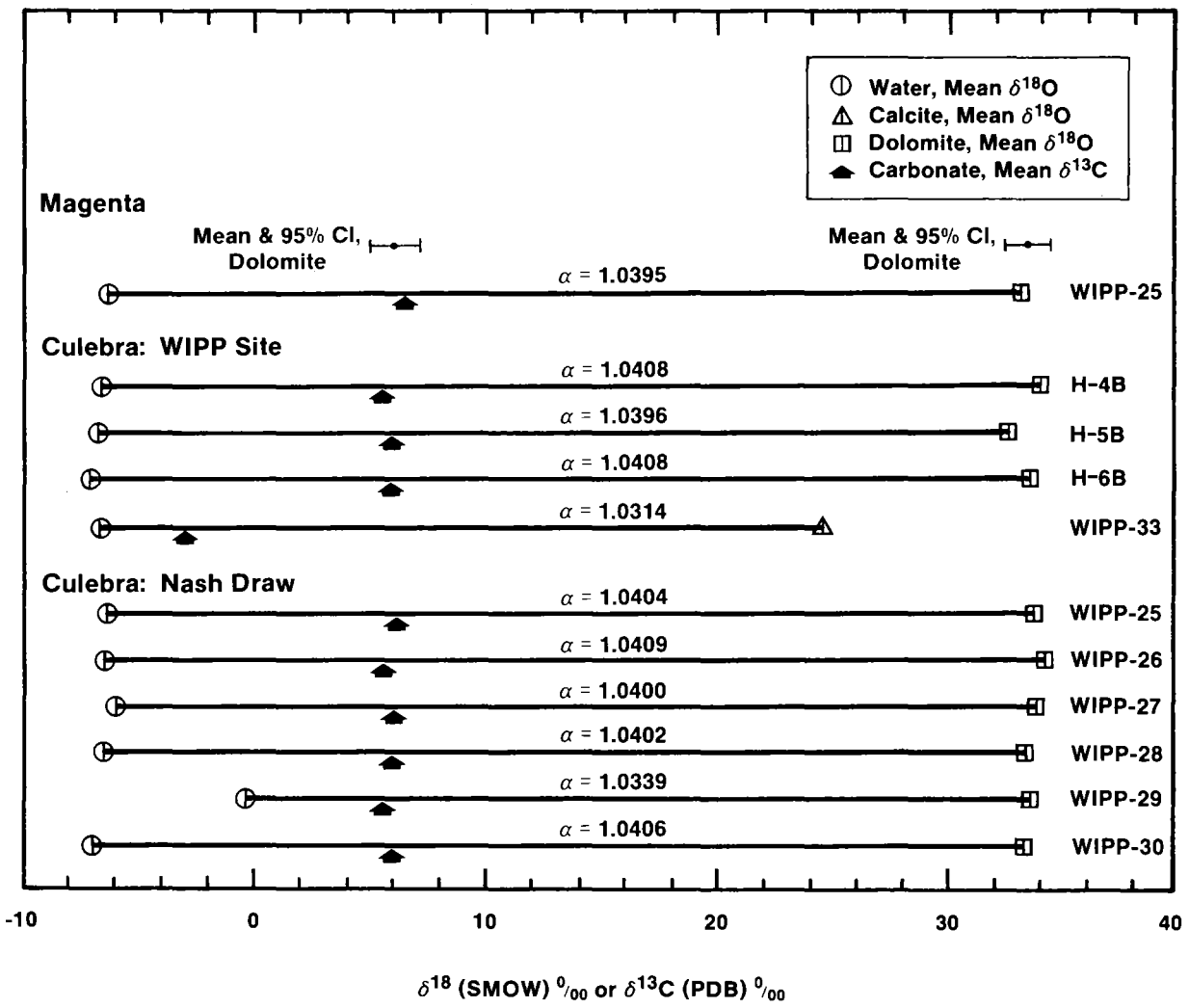


Figure 1-30. $\delta^{18}O$ values for coexisting carbonates and waters in the Rustler Formation (Figure 5-6, from Lambert and Harvey, 1987; Lambert, 1987).

(cf. Parry et al., 1970). Except for WIPP-29 Culebra, which shows both oxygen- and hydrogen-isotope shift, all the waters have a uniform $\delta^{18}O$ value of -6.6 ± 0.8‰. Calculated dolomite/water oxygen-isotope fractionation factors are too high to reflect isotopic equilibrium. Only calcite in the Culebra rubble from WIPP-33 appears to be at isotopic equilibrium with typical meteoric Rustler groundwater at ambient temperature. There is no other indication of carbonate recrystallization (reprecipitation) in the Rustler in isotopic equilibrium with meteoric Rustler groundwater. As discussed in detail by Lambert (1987), the dissolved $HCO_3^-$ is not in $^{13}C/^{12}C$ equilibrium with the host dolomite.

$^{87}Sr/^{86}Sr$ ratios of sulfate and carbonate mineral veins, generally interpreted as the depositional record of fluid flow preferentially concentrated in fractures, are indistinguishable from those of their host rocks throughout the Rustler. This indicates a dominantly internal, not external, source for the mass transport represented by the vein fillings (Brookins and Lambert, 1988; Lambert, Chapter 5). $^{87}Sr/^{86}Sr$ ratios progressively higher in the stratigraphic section reflect a greater contribution of surface-derived cations. Rustler values, exclusive of water-bearing zones (Magenta and Culebra), are little altered by admixture of surface material relative to the tightly clustered Permian Castile/Salado values. Dew Lake veins (calcite and selenite) show a full range of mixing proportions between Rustler-type and surface-type (represented by caliche and gypsite spring deposits) cations. Aside from the Magenta and Culebra, the $^{87}Sr/^{86}Sr$ ratios of the Rustler anhydrites and gypsums ($^{87}Sr/^{86}Sr$ = 0.70694 - 0.70714) are similar to, but slightly greater than those of unaltered anhydrites interbedded with halite and polyhalite in the Salado (Figure 1-31), which have never been in contact with large amounts of meteoric water. This similarity shows that mass transport of sulfate and carbonate from surface-weathered outcrops in the recharge zone has made a limited contribution to the soluble cationic constituent of the Rustler. In contrast, veins in the Dewey Lake Red Beds containing selenite and calcite appear to have a continuum of $^{87}Sr/^{86}Sr$ ratios ($^{87}Sr/^{86}Sr$ = 0.70722 - 0.70861), representing mixing of materials derived from both Ochoan evaporites typical of the Rustler and deeper rocks, and near-surface deposits, such as caliche and gypsite spring deposits (Figure 1-31). These relationships show that the spring deposits were not derived solely and directly from

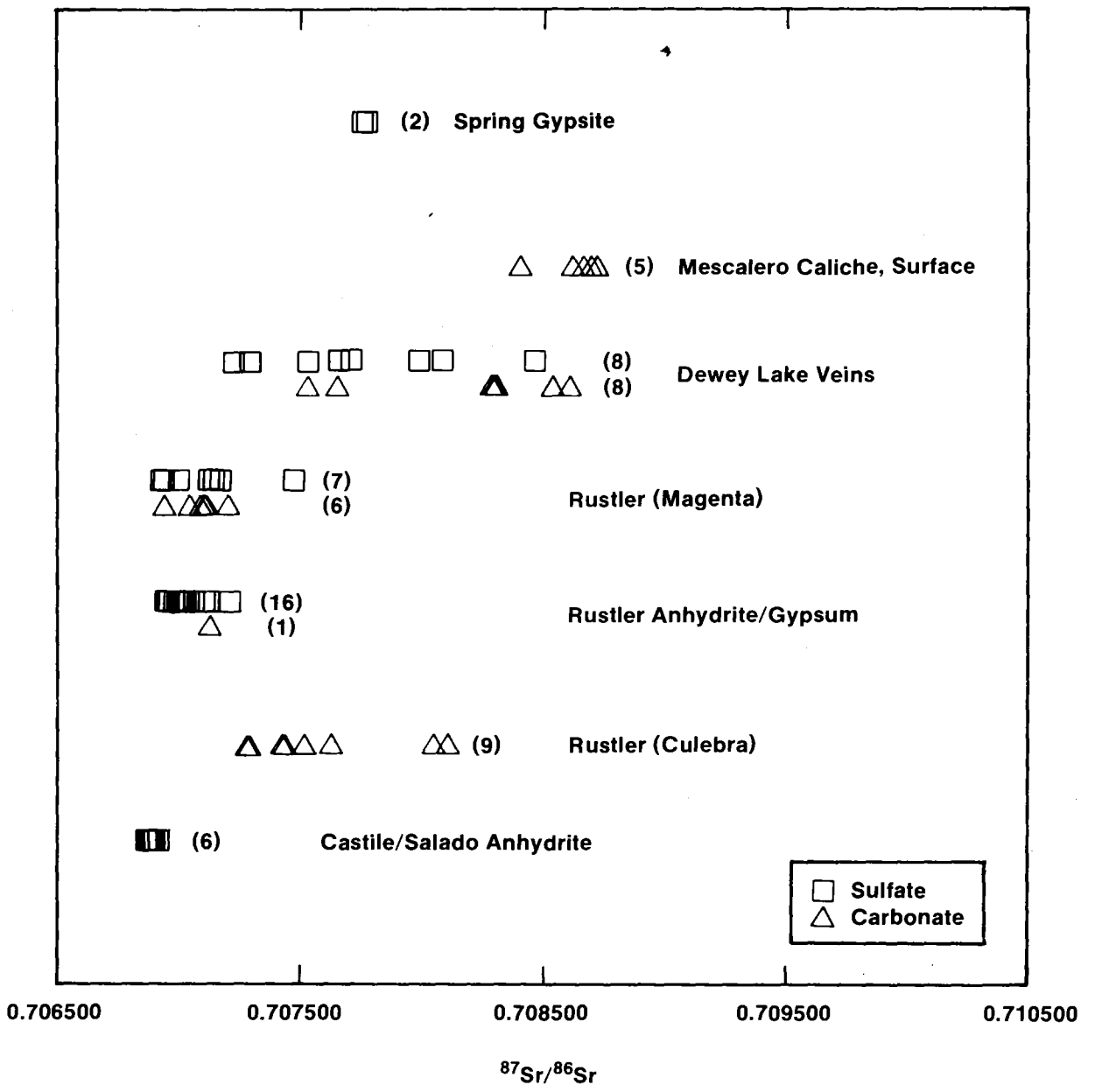


Figure 1-31. $^{87}Sr/^{86}Sr$ ratios in Ochoan and related rocks (Figure 5-17; data from Brookins and Lambert [1988]).

Rustler rock dissolved and mobilized westward in the late Pleistocene (cf. Bachman, 1981), but instead require a dominant component similar to the high-$^{87}Sr$ extreme in Dewey Lake strontium.

Finally, the D/H relationships in gypsums from the Rustler and Dewey Lake Red Beds are characteristic of gypsification of anhydrite (or recrystallization of pre-existing gypsum) in the presence of meteoric water. No gypsum thus far examined bears an isotopic signature that would be expected for primary marine evaporitic sulfate ($\delta D > 0‰$). Although all gypsums examined were meteorically influenced ($\delta D < -40‰$), their $\delta D$ values vary widely. Figure 1-32 plots $\delta D$ values of the water of crystallization in gypsums as a function of depth. Solid lines delineate the range of gypsum compositions expected from recrystallization in the presence of a large amount of Rustler-type meteoric water (extremely high water/rock ratio). Dashed lines bound gypsum $\delta D$ values expected from small amounts of such water completely scavenged during gypsification of anhydrite, and correspond to the $\delta D$ field for confined Rustler waters in Figure 1-25. A few $\delta D$ values are consistent with isotopic equilibrium between their waters of crystallization and large amounts of Rustler-type (Pleistocene) meteoric water. The variations in D/H ratio, both laterally and vertically, attest to differing generations of meteoric water of different isotopic compositions hydrating the sulfate or else differing water/rock ratios with an isotopically uniform reservoir contributing to the crystallographically bound water or some combination of the two. The changes in D/H ratio adjacent to a water-bearing dolomite in WIPP-34 (Figure 1-32) suggest a varying water/rock ratio at that locality, rather than multiple generations of gypsum recrystallization, although throughout the Rustler several discrete episodes may have affected the gypsum.

On a regional basis, there is no correlation of $\delta D$ value with depth, suggesting a non-uniform vertical permeability throughout the Rustler/Dewey Lake section. In a given borehole core, the water/rock ratio inferred from the gypsum D/H ratio is highest, as might be expected, near the brittle, water-bearing zones in the Rustler (i.e., stratabound

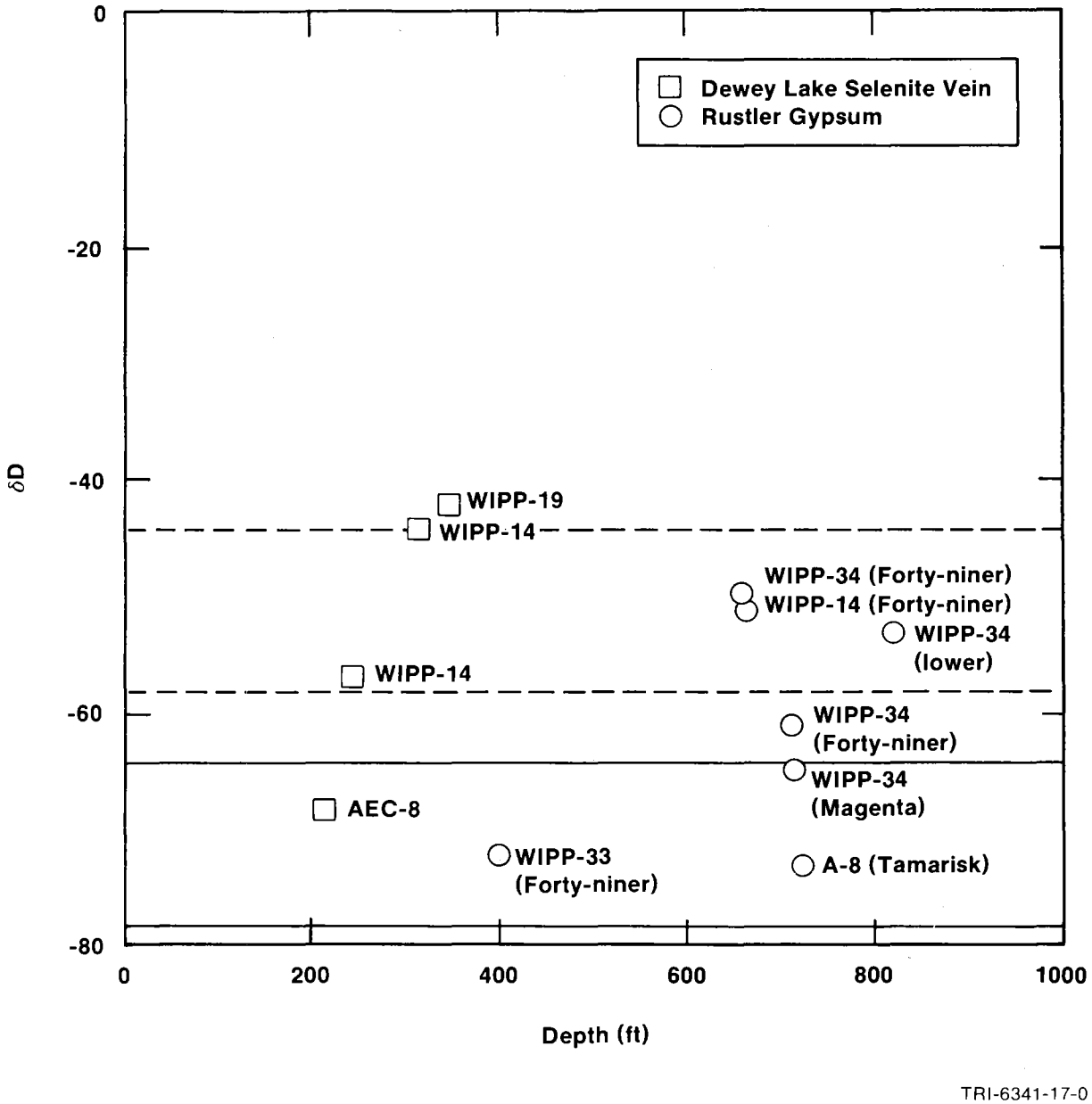


Figure 1-32. δD values of the water of crystallization in gypsums as a function of depth (Figure 19A from Lambert, Chapter 5).

dolomitic layers), but diminishes with distance from such a zone. This shows that recharge has not taken place vertically from the surface. The vertical variations in D/H ratio, together with the minimal surficial component of Sr, suggest that groundwater flow within the Rustler near the WIPP Site is largely stratabound, having been recharged where near-surface exposures of water-bearing units can receive infiltration and subsequently having moved laterally.

# 1.5 DISCUSSION

A primary objective of this study is to determine if the spatial distribution of solutes is consistent with the hydrologic flow directions predicted independently by hydrogeologic studies assuming steady-state confined flow. Ancillary questions concern the time scale on which the Culebra dolomite may be considered confined and the time scale on which the flow within the Culebra may be considered transient.

The observed distribution of solutes in a hydrologic flow field is determined in part by the location and magnitude of solute fluxes from potential sources and to potential sinks. Section 1.5.1 describes a model for the chemical evolution of waters in the Culebra that tentatively identifies the mineralogical sources and sinks for many of the solutes. Resolution of the questions of transience and confined flow is addressed in Section 1.5.2. This involves examination of isotopic ratios and the distribution of diagnostic minerals to differentiate the independent histories of the solutes, water molecules, and mineral phases in the Culebra.

## 1.5.1 Processes Affecting Groundwater Composition

Two common sources of solutes in groundwater are addition of species by mixing with more saline waters and leaching or dissolution of solutes from the rock matrix. An apparent addition of solutes to groundwater will also occur during evaporation. Sinks for solutes include precipitation, coprecipitation, sorption, and ion-exchange; dilution of a concentrated solution by a dilute groundwater will also lead to an apparent loss of solutes.

Table 1-4 lists some of the processes and resulting effects that may have influenced the compositions of groundwater in the Culebra. The relative importance of these processes is discussed in the following sections.

#### 1.5.1.1 Summary of Solute Relationships

The following solute relationships are described in the preceding sections of this chapter and in Chapter 2:

- Increases in the concentrations of Na, Cl, Ca, Mg, K, $SO_4$, Br, B, and Li with ionic strength; this relationship is illustrated by the "salinity factor" described in Section 1.4.3.

- The near-perfect saturation of the solutions with respect to gypsum over the entire range of ionic strength.

- The increase in the Mg/Ca ratio as the ionic strength increases (see Figure 1-12).

- The negative correlation between pH and bicarbonate alkalinity observed after the effects of salt dissolution are factored out. This relationship is most clearly indicated by the silicate/bicarbonate factor described in Section 1.4.3.

- The apparent supersaturation of dolomite; although potential loss of $CO_2$ gas during sampling introduces uncertainty into calculation of saturation indices of individual carbonates, the relationship between saturation indices for calcite and dolomite indicates that the degree of dolomite supersaturation increases with ionic strength (see Figure 1-20).

- The correlation of Mg with $SiO_2$ and the negative correlation of $SiO_2$ with Li and B that is observed after the effects of salt dissolution are factored out. This relationship is also clearly indicated by the silicate/bicarbonate factor.

## Table 1-4. Chemical Processes That May Affect the Solute Compositions of Culebra Groundwaters

| Chemical Process | Potential Effect(s) on Concentrations of Solutes in Culebra Groundwaters |
|---|---|
| Halite dissolution | Increase Na, Cl, Br, Li; decrease Cl/Br; increase solubility of carbonates and sulfates up to 3 molal ionic strength and then decrease solubility causing changes in Ca, Mg, $SO_4$, $CO_3$ |
| Precipitation/dissolution of gypsum | Decrease/increase Ca, $SO_4$ |
| Precipitation/dissolution of calcite and dolomite | Decrease/increase Ca, Mg, $CO_3$ |
| Dolomitization:[1] calcite + Mg → dolomite + Ca | Decrease Mg/Ca ratio |
| Dedolomitization:[1] dissolution of gypsum and dolomite with concurrent precipitation of calcite. | Decrease pH, alkalinity, $SO_4$; must maintain Mg/Ca molar ratio < 1 |
| Sorption/desorption by clays | Loss/gain of Li and B by solution |
| Mixing of connate hypersaline formation water with recharge water that has dissolved gypsum[2] | Increase Mg, Ca, K, Na, Cl; decrease $SO_4$, Cl/Br ratio |
| Incongruent dissolution of polyhalite | Increase Mg, K, $SO_4$; decrease Ca, Cl/Br ratio |
| Dissolution of silicates | Increase Si, Mg, Na |
| Dissolution of anhydrite with sellaite inclusions | Increase Ca, $SO_4$, Mg, F |

1. Process may be important locally, as for example, at WIPP-33.
2. Process discussed in Chapter 4.

In Chapter 2, Siegel et al. suggest that these solute relationships are consistent with the following processes: (1) solutes are added to the Culebra brines by dissolution of evaporite minerals; (2) the solubilities of gypsum and calcite increase as the salinity increases; these minerals dissolve as chemical equilibrium is maintained between them and the groundwater; (3) equilibrium is not maintained between the waters and dolomite; sufficient Mg is added to the waters by dissolution of accessory carnallite or polyhalite so that the degree of dolomite supersaturation increases with ionic strength; and (4) clays within the fractures and rock matrix exert some control on the distribution of Li, B, Mg, and Si via sorption, ion exchange, and dissolution.

### 1.5.1.2 Precipitation and Dissolution of Carbonates, Sulfates, and Evaporite Salts

As discussed in Section 1.4.6, the first three of the above processes might be indicative of a partial equilibrium system in which solution/mineral equilibria shift nearly reversibly in response to increases of salinity due to dissolution of evaporite salts in rock units adjacent to the Culebra. The solubilities of gypsum, calcite, and dolomite increase with salinity up to 3 molal ionic strength and then decrease. Thus, even if the saturation indices for gypsum and calcite are near zero, the waters may still be capable of dissolving significant amounts of these phases as the salinity increases. Reaction path calculations show that addition of solutes (Mg, $SO_3$, K, and Cl) to the Culebra from evaporite minerals such as polyhalite and carnallite in a partial equilibrium system is consistent with the observed groundwater compositions if dolomite does not precipitate from supersaturated solutions.

The results of the reaction path calculations are in qualitative agreement with the SNORM calculations described by Bodine et al. in Chapter 4. In particular, the SNORM calculations show that the saline waters in Zone A all have appreciable $MgCl_2$, $MgSO_4$, and KCl components. This normative signature may be the result of dissolution of the assemblage halite/carnallite/polyhalite or mixing of a primitive brine with halite-dissolution water.

Isotopic studies of minerals and waters provide some support for this model. Stable-isotope compositions of carbonates indicate no recrystallization of dolomite in equilibrium

with the groundwater now found in the Culebra, but local precipitation of calcite, at the expense of dolomite, has apparently occurred in WIPP-33 Culebra. Dissolution of dolomite is possible, but would leave neither a mineralogical nor an isotopic record.

Although the reaction path models predict dissolution of gypsum in response to increases in salinity, reprecipitated gypsum appears to be quite common within the Rustler. The cationic origins of anhydrite and gypsum in the Rustler, including Culebra gypsum, are largely marine, with little contribution from surface weathering sources, as indicated by their $^{87}Sr/^{86}Sr$ ratios (Figure 1-31). Hence, the calcium sulfate was not imported by dissolution in a near-surface weathered recharge zone, but is of local origin. The variations in D/H ratios in the waters of crystallization of Rustler gypsum, however, do attest to recrystallization in the presence of meteoric water. Although most of the dissolved calcium sulfate originated locally within the evaporite section, the solid calcium sulfate hydrated in response to influx of meteoric water (Figure 1-32). Thus, the isotopic data can be reconciled with the results of the reaction path modeling if it assumed that sufficient anhydrite is hydrated to replace the gypsum that dissolves in response to the salinity increase.

### 1.5.1.3 Reactions Involving Silicates

The contribution of solutes from silicates is difficult to establish. In the southern part of the study area (Zone B), the salt norms indicate alkali-carbonate and/or alkali sulfate assemblages, consistent with silicate hydrolysis (Bodine et al., Chapter 4). In addition, the results of the PCAs described by Siegel et al. in Chapter 2 suggest that reactions with clay minerals may exert an observable influence on the water's minor-element chemistry throughout the study area. When the effects of solute addition associated with halite dissolution are factored out prior to the PCA, a Mg-$SiO_2$-alkalinity association is left which is negatively correlated with a pH-B-Li association. As discussed in Chapter 2, these correlations (the silicate/bicarbonate factor) are consistent with several plausible mechanisms, including uptake of Li by vacant octahedral sites in the clay lattice, sorption of

B by surface sites (SOH) of clays (reaction 1), and dissolution of a reactive amorphous Mg-rich layer ($MgSiX_{(am)}$) in corrensite (reaction 2):

$$SOH + B(OH)_4^- + H^+ \rightleftarrows SOH_2^+ B(OH)_4^- \quad [1]$$

$$MgSiX_{(am)} + 2H_2O + 2H^+ \rightarrow Mg^{+2} + H_4SiO_4 \ . \quad [2]$$

The importance of this factor is greatest in the western and southern parts of the site, where dissolution of evaporite salts may have left residues relatively enriched in clays. A survey of the literature provides ample evidence that sorption of boron and lithium and release of magnesium and silica from clays in saline waters is possible (Siegel et al., Chapter 2). However, geochemical and mineralogical evidence either supporting or contradicting this model for the WIPP is ambiguous. The PCA of minor-element data suggests that some degree of silicate hydrolysis has influenced the hydrochemistry throughout the Culebra; however, in more saline waters (Zone C) the normative salts suggestive of silicate hydrolysis are absent (Bodine et al., Chapter 4). This inconsistency may be related to the small data set used in the PCA or due to the masking of the normative signature by subsequent massive dissolution of halite and other readily soluble evaporites.

This controversy might be resolved by a systematic examination of the chemical and isotopic compositions of mineral samples from highly transmissive zones (containing core rubble rather than intact core), examination of the geochronological systematics (e.g., Rb/Sr) of the clays, more rigorous calculations of the extent of mass transfer that could result from ion exchange and sorption, and application of factor analysis to a larger data set of chemical analyses.

## 1.5.2 Consistency Between Solute and Isotope Distributions and Hydrologic Flow

### 1.5.2.1 Steady-State Versus Transient Flow

Ramey (1985) and Chapman (1988) observed that if the Culebra is a confined aquifer at steady state, present-day regional water-flow directions are not consistent with the salinity distribution at the WIPP Site, given the assumption of steady-state confined flow. These observations were based on the compositions of water samples analyzed as of 1983 by the USGS and on data gathered by the New Mexico EEG. The more extensive data set examined in this study confirms these observations. As shown in Figures 1-5, 1-6, and 1-33, Zone B (a facies with low salinity and element ratios inconsistent with halite dissolution) lies downgradient from more saline water in Zone C. Flow within Zone C (but not from Zone C to Zone B) may be consistent with progressive addition of solutes from dissolution of halite in the lower member; however, the lack of a fully coupled flow and transport model does not at this time allow quantitative mass balance calculations to be made along the hydrologic flow paths inferred from physical measurements.

The inconsistencies between the steady-state confined-flow hydrologic model and geochemical interpretations might be reconciled by considering the differences in the time scales reflected by the computed hydrologic flow field, isotope ratios, and spatial distributions of solutes and minerals. Specifically, the assumption of steady-state confined flow may be adequate on the 100-year time scale of hydrologic testing and disturbances related to the construction of the WIPP shafts. However, measurements of modern head potentials, transmissivities, and/or fluid densities do not give any direct indication of time scales on which the system might be transient. In fact, the isotopic data suggest that transient phenomena have taken place over the past 10,000 to 20,000 years in response to climatic change. Similarly, the observation that the Culebra is confined on the time scale of hydrologic testing does not ensure that vertical flux is negligible on a time scale measured in millennia. As discussed below, mineralogical and isotopic data are required to assess the

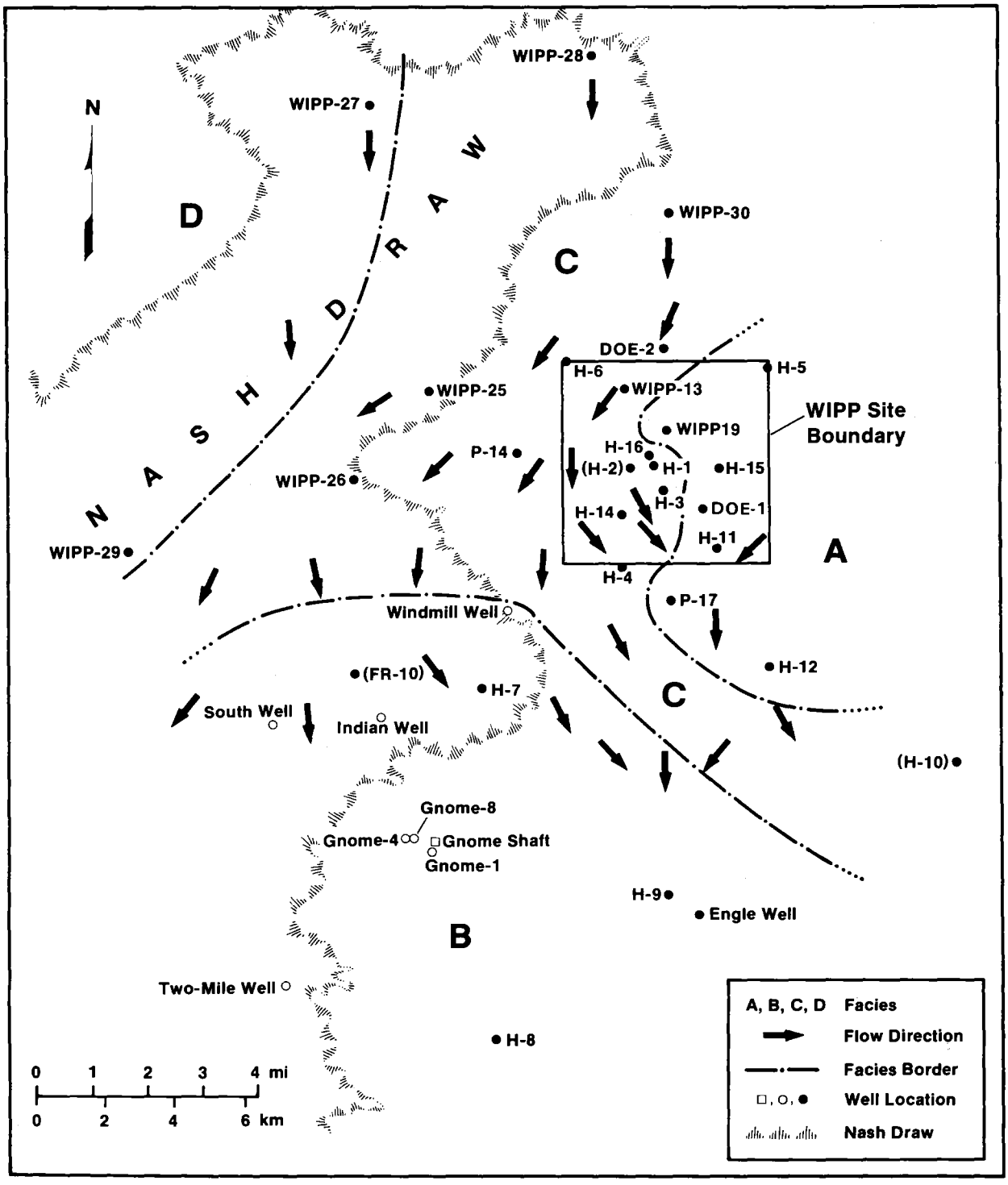


TRI-6331-77-0

Figure 1-33. Relationship between hydrological flow and hydrochemical facies of the Culebra dolomite. Compositions of waters in each zone represented by solid black circles are described in Figure 1-10. Compositions of several other wells (see Chapter 4) indicated by open circles were not included in the original data used to define the facies, but their compositions are consistent with the facies borders.

magnitude of the vertical fluxes of solutes and water into the Culebra over the 10,000-year time period of interest.

In Chapter 5, Lambert suggests that the apparent inconsistency between the steady-state hydrologic model and solute distribution pattern can be explained by a change in flow direction during the last 30,000, or perhaps 12,000 years. As discussed above, the hydrologic balance has changed since the Pleistocene, and groundwater currently flows in a southwesterly direction. Evidence for a change in flow direction consists partly of the available uranium-isotope disequilibrium data. The uranium-isotope disequilibrium model assumes reducing conditions, whereas the Eh values calculated for Culebra waters are interpreted by Myers et al. in Chapter 6 to indicate that oxidizing conditions may prevail at the present. The sensitivity of the uranium isotopic model to the disequilibria must be known before the significance of this possible inconsistency can be assessed. Even if oxidized uranium species predominate in parts of the Culebra at present, reduced species may have been abundant during the development of the observed high $^{234}U/^{238}U$ activity ratios.

#### 1.5.2.2 The Origin of the Southern Low-Salinity Zone

In Chapter 6, Myers et al. suggest that redox conditions in the southern portion of the study area are more oxidizing than in the north. They further suggest that this is indicative of preferential vertical recharge in the south, accounting for dilution of more saline brine apparently flowing from the north. This conclusion is based primarily on the presence of detectable nitrate and lack of detectable ammonium in the south and the presence of detectable ammonium and lack of detectable nitrate to the north. However, as discussed by Robinson in Appendix 6A, these observations may be analytical artifacts related to interference by solutes in the saline brines in the northern and eastern parts of the study area. Moreover, the available radiocarbon model age in the southerly, less saline zone (Zone B, including Engle and H-9 wells), is no younger than in the northerly, more saline zone (Zone C, H-4 and H-6 wells), and thereby argues against dilution by modern vertical recharge in the south. Similarly, model ages are no older in the south, arguing against a

monotonic north-to-south, steady-state flow persisting since the Pleistocene. The one available radiocarbon age from the Dewey Lake Red Beds overlying the Rustler is consistent with this interpretation. The stable isotope characteristics of the Dewey Lake, however, are consistent with the interpretation that waters at least 12,000-16,000 years old and waters representing modern meteoric recharge in the area may be present in this unit.

Steady-state, north-to-south confined flow would not have preserved the lower-salinity zone downgradient from the saline zone (Figure 1-33). The lower-salinity zone could have arisen if the regional flow direction originally had a significant westerly component, as suggested by the generally eastward-increasing $^{234}U/^{238}U$ activity ratios discussed above. Similarities in radiocarbon age in the north and the south are consistent with water recharging both north and south parts of the WIPP area simultaneously from a near-surface Pleistocene infiltration zone in the west-northwest (Figure 1-34), groundwater at one time flowing locally subparallel rather than subnormal to the hydrochemical facies boundary between Zones B and C. Pleistocene recharge from the west-northwest is consistent with the present orientation on the Zone B/C hydrochemical facies boundary, similar radiocarbon ages in Zones B and C, eastward-increasing uranium isotope activity ratio values, and some, but not all, of the calculated modern Darcian flow vectors. This generalized paleoflow pattern during recharge is not consistent with either recharge from due north, or monotonic southward steady-state flow. A likely paleorecharge zone is nearby in surface outcrops of the Rustler Formation to the west in Nash Draw. Although it was once proposed that recharge for water now flowing in the Rustler near the WIPP Site and Nash Draw takes place as far north as Bear Grass Draw (Robinson and Lang, 1938), there is neither need nor geochemical support for such a proposal. In fact, recent work by Hunter (1985) suggests that Rustler flow from Bear Grass Draw southward toward the WIPP area may be intercepted by a major discharge zone in Clayton Basin.

A likely explanation for the less saline waters of Zone B is that at the time of influx of the present generation of Culebra groundwater in late Pleistocene time, Rustler halite was absent adjacent to the Culebra in this area, thus not providing a source of NaCl. This is

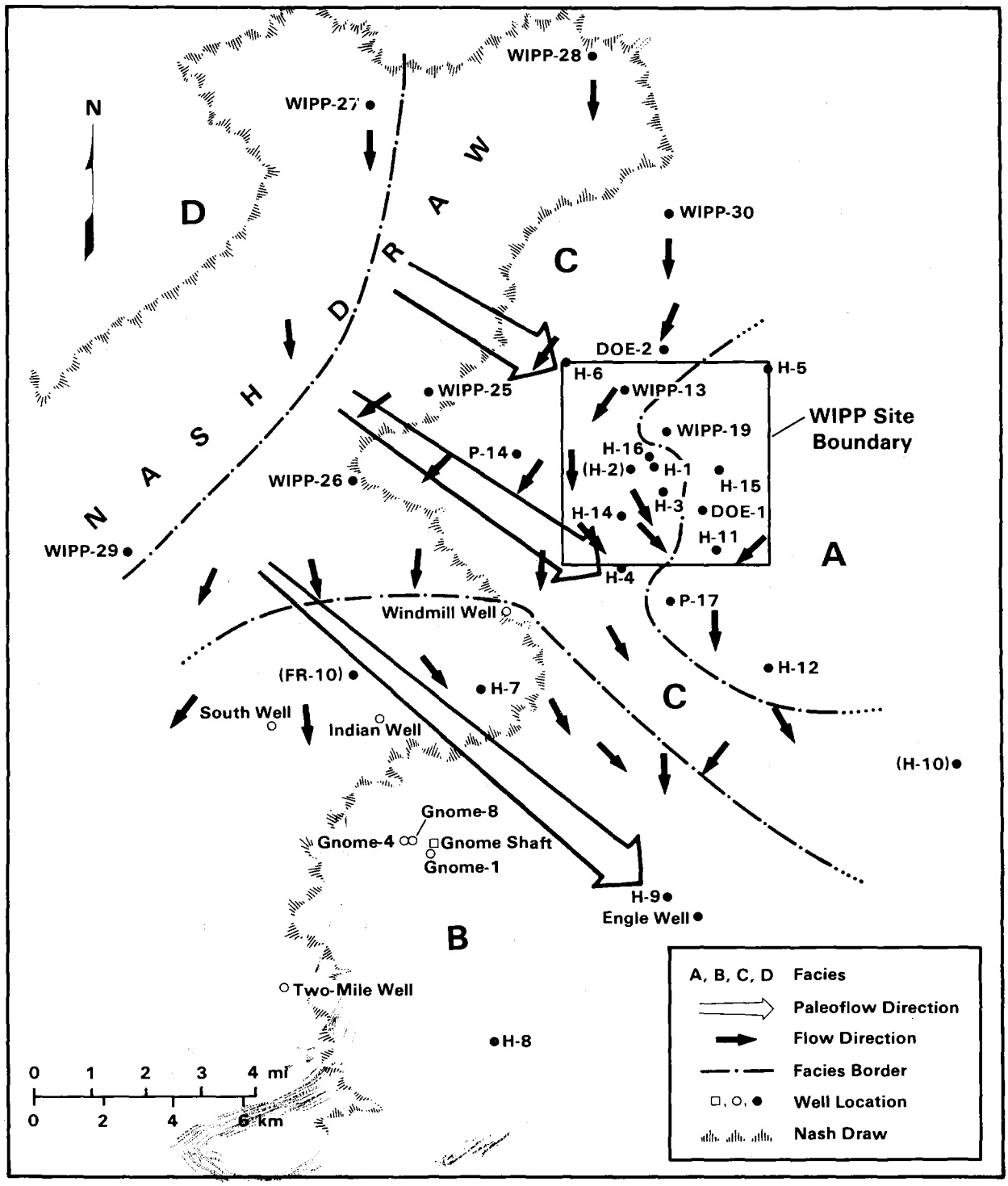


TRI-6330-78-1

Figure 1-34. Paleoflow (late Pleistocene) directions for groundwater in the Culebra member of the Rustler Formation from likely recharge areas on outcrops in Nash Draw. Paleoflow directions are superimposed on hydrochemical facies boundaries and modern flow directions interpreted from numerical modeling of physical hydrology measurements.

consistent with the present-day correlation of halite occurrence in the Rustler and the hydrochemical facies pattern (Figure 1-13). The halite might never have been deposited in the south, or pre-existing halite may have been removed by earlier dissolution during the development of the southeastern lobe of Nash Draw, which is included in Zone B. This dissolution, however, would have taken place in response to an episode of groundwater flow older than the present regime that began as early as 16,000 years ago. This older episode of dissolution could have occurred as early as 600,000 years ago, in a time of wetter climate while Nash Draw was still forming as part of the channel system of the ancestral Pecos River (Bachman, 1980). It is also conceivable that the zone of higher Culebra transmissivity south of the WIPP Site (Lappin, 1988) toward the southeastern lobe of Nash Draw is simply a manifestation of the same processes that have contributed to the widening of Nash Draw. Such processes are apparently responsible for an increasing transmissivity west of the WIPP Site toward the central axis of Nash Draw. By logical extension, it is likely that similar processes have created a "fringe" zone of increased transmissivity for some distance outward in all directions from various parts of Nash Draw (beyond its marginal scarp), including the southeastern lobe.

A karstic fringe zone along a stretch of the ancestral (Tertiary/Pleistocene) Pecos River further south was proposed by Bachman (1984) as a consequence of evaporite dissolution adjacent to the stream channel. There the thickness of the saturated zone approached 1500 ft, in which groundwater lost by upgradient seepage from the stream system dissolved halite throughout the Salado Formation and discharged downgradient. A similar mechanism may have acted on a smaller scale to dissolve evaporites adjacent to the Nash Draw stream system during the Pleistocene, contributing to the development of a marginal zone of enhanced transmissivity locally extending as far east as the WIPP Site. If the water table in the late Pleistocene (at the apparent time of latest Culebra recharge) was at an elevation (about 2977 ft) comparable to that reported for the water table that has arisen from historic potash-brine dumping in Nash Draw (Hunter, 1985), Nash Draw was a possible recharge area for the Culebra, because the base of the Culebra at known points east of Nash Draw is at lower elevations.

### 1.5.2.3 Zonation of Normative Solute Characteristics

The results of Bodine et al. (Chapter 4) suggest that the salt norm distribution is generally consistent with the generalized zonation of solute distributions proposed by Ramey (1985) and further developed by Siegel et al. in Chapter 2. The conceptual model reported by Bodine et al. for Rustler solute distributions involves varying degrees of dilution of primitive-diagenetic brines similar to that found in the low-permeability, halite-rich strata east of the WIPP Site (e.g., P-18 in Zone A; see Figure 1-2). P-14 Culebra water also displays a primitive-diagenetic solute norm. The diluent proposed to have infiltrated from the surface (e.g., recharge fluid) has normative solute characteristics similar to those of waters sampled from the siliciclastic alluvium in WIPP-15 (see Figure 1-2). Hydrolysis of feldspars undergoing weathering in channel deposits of the Gatuña Formation (described by Bachman, 1985) north and west of the WIPP Site is a potential source of solutes bearing a Na-$HCO_3$ or -$SO_4$ normative signature. This alkali-carbonate or -sulfate norm is preserved in Zone B, represented by waters from H-7, -8, and -9 south of the WIPP Site. Fresh waters infiltrating through this weathering zone acquired this solute assemblage, and dissolved halite and anhydrite/gypsum in the Rustler, giving norms characteristic of such dissolution (Zone C). In such dissolution brines, the alkali-carbonate or -sulfate norm may not be preserved. Increasing proportions of recharge water have mixed with the primitive water with increasing distance from P-18 and P-14. Note, however, the anomalous position of the primitive-diagenetic solute norm at P-14, which lies within Zone C rather than Zone A. This suggests that either Zone A-type solutes were at one time more widespread, or that the primitive-diagenetic norm at P-14 is more locally controlled.

The mixing/dilution model of Bodine et al. in Chapter 4 relies heavily on extensive recharge at some time (vertical, lateral, or both), especially in the southern part of the site, to provide the fluids which dilute a pre-existing, perhaps regionally pervasive, primitive-diagenetic signature. The timing of such recharge, however, is unspecified by the model. The isotopic, mineralogic, and hydrologic data discussed in other sections of this report suggest that vertical recharge to the Culebra in the WIPP area and to the east has not occurred for several thousand years.

### 1.5.2.4 The Degree of Hydraulic Versus Geochemical Confinement

Hydrologic testing has revealed that on the time scale of a few months the Culebra is hydrologically confined at all sites that have been sampled, except WIPP-25, WIPP-26, and WIPP-29. Generally, the hydraulic relationships suggest only limited vertical connection between the Culebra and overlying strata. Whereas hydraulic measurements can quantify short-term responses of the hydrologic flow system to transient pressure pulses such as slug- and pump-testing, geochemical measurements are more related to mass transport and rock/water interactions that take place over longer periods, up to several thousand years.

Several geochemical observations are relevant to the degree of confinement of the Culebra waters over long periods of time. First, available radiocarbon ages in the Culebra are in excess of 12,000 to 16,000 years. The three model ages (at H-6, H-4, and H-9) were determined at localities that effectively "bracket" the WIPP Site on the north and south. The lack of a statistically significant difference among these ages, and the lack of a north-south gradient in apparent age suggest either that rates of vertical infiltration at each location have been virtually identical, or that lateral flow times to each location from the surface-recharge area(s) have been virtually identical. Given the significant geological differences in the Culebra environment among the three localities, the first prospect is unlikely. The second prospect is more consistent with the available uranium-isotope and solute data, especially considering the significant differences in solutes among the three sampling localities. Similarly, the absence of a statistically significant vertical gradient in apparent age in the south (14,900 years in the Culebra at H-9 versus 14,000 years in the overlying Dewey Lake at the nearby Pocket well) is inconsistent with a significant degree of modern vertical infiltration there. In any case, groundwater has been isolated from the atmosphere for about the same length of time at all three points in the Culebra.

Second, the preservation of extensive amounts of anhydrite and a varying water/rock ratio during partial gypsification in the nondolomitic Rustler units overlying the Culebra suggest that significant amounts of water have not permeated vertically from the surface to recharge the Culebra where thick beds of overlying anhydrite are preserved. As noted by

Beauheim (1987), at two points the modern Magenta head is higher than that in the overlying Forty-niner, precluding a direct throughgoing connection between the surface and the Culebra in at least parts of the WIPP area at the present time (see Figure 1-7).

Third, strontium isotope data suggest that vertical material transport from the surface to layers underlying the Dewey Lake Red Beds has not been extensive. Even at the localities of suspected vertical solution or fracture channels (e.g., WIPP-14, WIPP-33, and WIPP-34), the $^{87}Sr/^{86}Sr$ ratios in the partially gypsified anhydrites of the Forty-niner and Tamarisk members indicate minimal admixture of surface-type strontium having a high $^{87}Sr/^{86}Sr$ ratio, a moderate amount of such admixture in the Culebra, and extensive admixture in the Dewey Lake. This stratification of strontium constitutes evidence of minimal mass transport across the Rustler/Dewey Lake contact, while allowing lateral transport of some surface-type strontium through the Culebra from its near-surface exposures.

Finally, at certain localities previously suspected to represent karst conduits (e.g., WIPP-14 and WIPP-34) the water/rock ratios in gypsiferous horizons adjacent to the water-bearing dolomites are significantly lower than in the dolomites themselves, as suggested by the D/H ratios of gypsum and of various groundwaters. Such variations in the water/rock ratio are consistent with some water having escaped from the dolomite into adjacent beds (perhaps acquiring some solutes from halite dissolution). These variations are not consistent with water migrating downward into the Culebra, during which water would first pass through a region of low water/rock ratio without having affected the gypsification of overlying anhydrite. If this were a significant mechanism of recharge to the Culebra, the stable-isotope composition of Culebra waters would exhibit a measurable shift away from meteoric values as a result of water/rock interaction in a zone of low water/rock ratio.

## 1.6 SUMMARY

Based on the available data on formation pressures, fluid density distribution, and transmissivities, modern flow within the Culebra at and near the WIPP Site appears to be largely

north-to-south, except in relatively low-transmissivity areas directly affected by either the high-transmissivity zone in the southeastern portion of the WIPP Site or by Nash Draw west of the WIPP Site. The amount of possible vertical flow into and out of the Culebra near the center of the WIPP Site remains indeterminate.

These present-day regional water flow directions are not consistent with the salinity distribution at the WIPP Site, given the assumption of steady-state, confined flow. Zone B, a hydrochemical facies with low salinity and element ratios inconsistent with halite dissolution, lies downgradient from more saline water in Zone C. In addition, the isotopic data presented in this report further indicate that inferences about flow direction and velocity obtained from measurements of modern head potentials and transmissivities may not be applicable to directions and velocities in the past 10,000 years, or in the next 10,000 years--the interval of interest to regulatory agencies governing radioactive-waste repositories.

In Chapter 5, Lambert suggests that this apparent anomaly can be explained by a change in flow direction in the last 30,000, or perhaps 12,000 years. Prior to that time, the recharge direction was dominantly from the west-northwest. In Chapter 4, Bodine et al. suggest that solute distribution is derived by mixing of (perhaps originally widespread) primitive-diagenetic brines now found mostly in the low-permeability, halite-rich strata east of the WIPP Site, with recharge water that has infiltrated from the surface and dissolved halite and anhydrite/gypsum. The isotopic, mineralogic, and hydrologic data discussed in other chapters of this report, however, suggest that vertical material transport into the Culebra in the WIPP area and to the east and south has not occurred to a significant degree for several thousand years (see Chapter 5). The SNORM results are not inconsistent with the isotopic results if the recharge component proposed in Chapter 4 moved from its paleorecharge area (Rustler outcrops in Nash Draw), where it acquired its alkali-carbonate/sulfate signature, thence laterally (stratabound) toward the east-southeast, preserving isotopic indicators of age (radiocarbon) and paleoflow direction (uranium). Such a paleoflow direction from nearby paleorecharge areas could also have resulted in the

preservation of the northwest-southeast orientation of the hydrochemical facies transition zone between Zones B and C.

Waters in the Culebra are undersaturated with respect to halite and anhydrite and saturated with respect to gypsum. Evaluation of water/carbonate (calcite and dolomite) equilibria is hindered by uncertainties in pH related to potential loss of $CO_2$ gas during sample collection. A model for the chemical evolution of water in the Culebra proposed by Siegel et al. in Chapter 2 suggests that dissolution of salt and concomitant changes in mineral solubilities constitute an important irreversible process affecting water chemistry. Na, Cl, Mg, K, and $SO_4$ are added to the Culebra by dissolution of evaporite salts in adjacent strata. Equilibrium is maintained with gypsum and calcite, but dolomite supersaturation increases as the salinity of the water increases. Isotopic studies of minerals and waters provide some support for this model.

Controls on the distribution of minor and trace elements are more problematical. For waters of lower ionic strength, the contribution of solutes from silicates may be more important. The results of the PCA described by Siegel et al. in Chapter 2 suggest that reactions with clay minerals may exert an observable influence on the distribution of $SiO_2$, Mg, Li, and B throughout the entire study area.

# 1.7 REFERENCES

Allison, G. B. 1982. "The Relationship between $^{18}O$ and Deuterium in Water in Sand Columns undergoing Evaporation." *Journal of Hydrology*, Vol. 55:163-169.

Allison, G. B., W. J. Stone, and M. W. Hughes. 1985. "Recharge in Karst and Dune Elements of a Semi-arid Landscape as Indicated by Natural Isotopes and Chloride." *Journal of Hydrology,* Vol. 76:1-25.

Bachman, G. O. 1980. *Regional Geology and Cenozoic History of the Pecos Region, Southeastern New Mexico*. Open File Report 80-1099. Denver, CO: US Geological Survey.

Bachman, G. O. 1981. *Geology of Nash Draw, Eddy County, New Mexico*. Open File Report 81-31. Denver, CO: US Geological Survey.

Bachman, G. O. 1984. *Regional Geology of the Ochoan Evaporites, Northern Part of the Delaware Basin*. Circular 184. Socorro, NM: Bureau of Mines and Mineral Resources.

Bachman, G. O. 1985. *Assessment of Near-Surface Dissolution at and near the Waste Isolation Pilot Plant (WIPP), Southeastern New Mexico*. SAND84-7178. Albuquerque, NM: Sandia National Laboratories.

Barr, G. E., S. J. Lambert, and J. A. Carter. 1979. "Uranium Isotope Disequilibrium in Groundwaters of Southeastern New Mexico and Implications Regarding Age-Dating of Waters." *Proceedings of the International Symposium on Isotope Hydrology*. Vol 2. STI/PUB/493. Vienna, Austria: International Atomic Energy Agency. 645-660.

Beauheim, R. L. 1987. *Interpretations of Single-Well Hydraulic Tests Conducted at and near the Waste Isolation Pilot Plant (WIPP) Site, 1983-1987.* SAND87-0039. Albuquerque, NM: Sandia National Laboratories.

Bodine, M. W., Jr., and B. F. Jones. 1986. *The Salt Norm: A Quantitative Chemical-Mineralogical Characterization of Natural Waters.* Water Resources Investigation Report 86-4086. Reston, VA: US Geological Survey.

Brookins, D. G., and S. J. Lambert. 1987. "K-Ar and Rb-Sr Age Determinations from Clay Minerals and Related Minerals from the WIPP (Waste Isolation Pilot Plant), Southeastern New Mexico." *Isochron/West* No. 49:4-7.

Brookins, D. G., and S. J. Lambert. 1988. "WIPP Site Studies: Secondary Selenite Veins in the Rustler Formation and Dewey Lake Red Beds." *Materials Research Society Symposium Proceedings.* Vol. 112:233-241.

Brookins, D. G., J. K. Register, and H. Krueger. 1980. "Potassium-Argon Dating of Polyhalite in Southeast New Mexico." *Geochimica et Cosmochimica Acta*, Vol. 44:635-637.

Chapman, J. B. 1988. *Chemical and Radiochemical Characteristics of Groundwater in the Culebra Dolomite, Southeastern New Mexico.* EEG-39. Santa Fe, NM: New Mexico Environmental Evaluation Group.

Craig, H., L. I. Gordon, and Y. Horibe. 1963. "Isotopic Exchange Effects in the Evaporation of Water, I: Low-Temperature Experimental Results." *Journal of Geophysical Research*, Vol. 68:5079-5087.

Deer, W. A., R. A. Howie, and J. Zussman. 1962. *Rock-Forming Minerals*. Vol. 3, *Sheet Silicates*. Vol. 4, *Framework Silicates*. Vol. 5, *Non-Silicates*. London: Longman.

Evans, G. V., R. L. Otlet, R. A. Downing, R. A. Monkhouse, and G. Rae. 1979. "Some Problems in the Interpretation of Isotope Measurements in United Kingdom Aquifers." *Proceedings of the International Symposium on Isotope Hydrology*, Vol. 2. STI/PUB 493. Vienna, Austria: International Atomic Energy Agency. 679-706.

Fleischer, M. 1987. *Glossary of Mineral Species*. Tucson, AZ: the Mineralogical Record, Inc.

Haug, A., V. A. Kelly, A. M. LaVenue, and J. F. Pickens. 1987. *Modeling of Ground-Water Flow in the Culebra Dolomite at the Waste Isolation Pilot Plant (WIPP) Site*. SAND86-7167. Albuquerque, NM: Sandia National Laboratories.

Helgeson, H. C. 1968. "Evaluation of Irreversible Reactions in Geochemical Processes Involving Minerals and Aqueous Solutions. I. Thermodynamic Relations." *Geochimica et Cosmochimica Acta*. Vol. 32:853-877.

Hunter, R. L. 1985. *A Regional Water Balance for the Waste Isolation Pilot Plant (WIPP) Site and Surrounding Area*. SAND84-2233. Albuquerque, NM: Sandia National Laboratories.

Isaacson, R. E., L. E. Brownell, R. W. Nelson, and E. L. Roetman. 1974. "Soil-Moisture Transport in Arid Site Vadose Zones." *Proceedings of the International Symposium on Isotope Hydrology:*97-114.

Lambert, S. J. 1978. "Geochemistry of Delaware Basin Groundwaters." *Geology and Mineral Deposits of Ochoan Rocks in Delaware Basin and Adjacent Areas*. Ed. G. S. Austin. Circular 159. Socorro, NM: New Mexico Bureau of Mines and Mineral Resources. 33-38.

Lambert, S. J. 1983. *Dissolution of Evaporites in and Around the Delaware Basin, Southeastern New Mexico and West Texas*. SAND82-0461. Albuquerque, NM: Sandia National Laboratories.

Lambert, S. J. 1987. *Feasibility Study: Applicability of Geochronologic Methods Involving Radiocarbon and Other Nuclides to the Groundwater Hydrology of the Rustler Formation*. SAND86-1054. Albuquerque, NM: Sandia National Laboratories.

Lambert, S. J., and J. A. Carter. 1984. *Uranium-Isotope Disequilibrium in Brine Reservoirs of the Castile Formation, Northern Delaware Basin, Southeastern New Mexico. 1: Principles and Methods*. SAND83-0144. Albuquerque, NM: Sandia National Laboratories.

Lambert, S. J., and J. A. Carter. 1987. *Uranium-Isotope Systematics in Groundwaters of the Rustler Formation, Northern Delaware Basin, Southeastern New Mexico*. SAND87-0388. Albuquerque, NM: Sandia National Laboratories.

Lambert, S. J., and D. M. Harvey. 1987. *Stable-Isotope Geochemistry of Groundwaters in the Delaware Basin of Southeastern New Mexico*. SAND87-0138. Albuquerque, NM: Sandia National Laboratories.

Lambert, S. J., and K. L. Robinson. 1984. *Field Geochemical Studies of Groundwaters in Nash Draw, Southeastern New Mexico*. SAND83-1122. Albuquerque, NM: Sandia National Laboratories.

Lappin, A. R. 1988. *Summary of Site-Characterization Studies Conducted from 1983 Through 1987 at the Waste Isolation Pilot Plant (WIPP) Site, Southeastern New Mexico.* SAND88-0157. Albuquerque, NM: Sandia National Laboratories.

LaVenue, A. M., A. Haug, and V. A. Kelley. 1988. *Numerical Simulation of Ground-Water Flow in the Culebra Dolomite at the Waste Isolation Pilot Plant (WIPP) Site.* SAND88-7002. Albuquerque, NM: Sandia National Laboratories.

Mercer, J. W. 1983. *Geohydrology of the Proposed Waste Isolation Pilot Plant Site, Los Medaños Area, Southeastern New Mexico.* Water Resources Investigation Report 83-4016. Albuquerque, NM: US Geological Survey.

Mercer, J. W. and B. R. Orr. 1979. *Interim Data Report on the Geohydrology of the Proposed Waste Isolation Pilot Plant Site, Southeast New Mexico.* Water Resources Investigation Report 79-98. Albuquerque, NM: US Geological Survey.

Nativ, R., and D. A. Smith. 1987. "Hydrogeology and Geochemistry of the Ogallala Aquifer, Southern High Plains." *Journal of Hydrology*, Vol. 91:217-253.

Osmond, J. K., and J. B. Cowart. 1976. "The Theory and Uses of Natural Uranium Isotopic Variations in Hydrology." *Atomic Energy Review*, Vol. 14:621-679.

Parry, W. T., C. C. Reeves, Jr., and J. W. Leach. 1970. "Oxygen and Carbon Isotope Composition of West Texas Lake Carbonates." *Geochimica et Cosmochimica Acta*, Vol. 34:825-830.

Plummer, L. N. 1984. "Geochemical Modeling: A Comparison of Forward and Inverse Methods." *Proceedings First Canadian/American Conference on Hydrogeology.* Ed. B. Hitchen and E. I. Wallick. Worthington, Ohio: National Water Well Association.

Plummer, L. N., D. L. Parkhurst, G. W. Fleming, and S. A. Dunkle. 1988. "PHRQPITZ - A Computer Program for Geochemical Calculations in Brines." Water Resources Investigation unpublished report. Reston, VA: US Geological Survey.

Powers, D. W., S. J. Lambert, S. E. Shaffer, L. R. Hill, and W. D. Weart, ed. 1978. *Geological Characterization Report, Waste Isolation Pilot Plant (WIPP) Site, Southeastern New Mexico*. SAND78-1596. Albuquerque, NM: Sandia National Laboratories.

Ramey, D. S. 1985. *Chemistry of Rustler Fluids*. EEG-31. Santa Fe, NM: New Mexico Environmental Evaluation Group.

Randall, W. S., M. E. Crawley, and M. L. Lyon. 1988. *Annual Water Quality Data Report for the Waste Isolation Pilot Plant*. DOE-WIPP 88-006. Carlsbad, NM: Waste Isolation Pilot Plant Project Office.

Register, J. K., and D. G. Brookins. 1980. "Rb-Sr Isochron Age of Evaporite Minerals from the Salado Formation (Late Permian), Southeastern New Mexico." *Isochron/West*, No. 29.

Robinson, K. L. 1988. *Analysis of Solutes in Groundwaters from the Rustler Formation at and near the WIPP Site*. SAND86-0917. Albuquerque, NM: Sandia National Laboratories.

Robinson, T. W., and W. B. Lang. 1938. "Geology and Ground-Water Conditions of the Pecos River Valley in the Vicinity of Laguna Grande de la Sal, New Mexico, with Special Reference to the Salt Content of the River Water. *New Mexico State Engineer*. 77-100.

Snyder, R. P. 1985. *Dissolution of Halite and Gypsum, and Hydration of Anhydrite to Gypsum, Rustler Formation, in the Vicinity of the Waste Isolation Pilot Plant, Southeastern New Mexico.* Open File Report 85-229. Denver, CO: US Geological Survey.

Statistical Analysis System Institute. 1982. *SAS User's Guide: Statistics.*

Uhland, D. W., and W. S. Randall. 1986. *Annual Water Quality Data Report.* DOE-WIPP-86-006. Carlsbad, NM: Waste Isolation Pilot Plant Project Office.

Uhland, D. W., W. S. Randall, and R. C. Carrasco. 1987. *Annual Water Quality Data Report, March, 1987.* DOE-WIPP-87-006. Carlsbad, NM: Waste Isolation Pilot Plant Project Office.

United States Department of Energy and the State of New Mexico. 1988. "Agreement for Consultation and Cooperation between Department of Energy and the State of New Mexico on the Waste Isolation Pilot Plant: Updated April 18, 1988." Appendix II:3. On file at the Waste Management and Transportation Library, Sandia National Laboratories, Albuquerque, New Mexico.

Van Devender, T. R. 1980. "Holocene Plant Remains from Rocky Arroyo and Last Chance Canyon, Eddy County, New Mexico." *The Southwestern Naturalist*, Vol. 25:361-372.

# CHAPTER 2:

# SOLUTE RELATIONSHIPS IN GROUNDWATERS FROM THE CULEBRA DOLOMITE AND RELATED ROCKS IN THE WASTE ISOLATION PILOT PLANT AREA, SOUTHEASTERN NEW MEXICO

Malcolm D. Siegel and Karen L. Robinson
Sandia National Laboratories

Jonathan Myers
International Technology Corporation

## ABSTRACT

This chapter summarizes solute concentrations in waters of the Culebra member of the Rustler Formation. The solute relationships are used to delineate hydrochemical facies, to compare flow directions suggested by water chemistry with those indicated by modern hydrologic potentials, and to formulate a hypothesis for the chemical evolution of the Culebra groundwaters. Descriptions of waters from the Magenta dolomite, Rustler/ Salado contact zone, the Dewey Lake Red Beds, and the Bell Canyon Formation are also included.

Four hydrochemical facies have been delineated in the Culebra. Zone A contains saline (about 3.0 m) NaCl brine and is found in the eastern third of the study area, roughly coincident with the region of low transmissivity and the occurrence of halite in several units of the Rustler Formation. Zone B contains a dilute Ca-$SO_4$-rich water (I <0.1 m) in the southern part of the study area and is coincident with a zone of high transmissivity where halite is absent from the Rustler. Zone C contains waters of variable composition and ionic strengths (0.3 to 1.6 m); it extends from the central part of the Waste Isolation Pilot Plant (WIPP) Site (four-mile zone), where halite is present in the unnamed member of the

Rustler, to the eastern side of Nash Draw where no Rustler halite has been found. Zone D contains WIPP-27 and WIPP-29 and is defined on the basis of anomalously high salinities (3-6 m) and K/Na ratios (0.2), probably related to contamination from potash refining operations in the area.

Three factors were extracted by R-mode principal component analysis of major and minor solute data. The first factor is dominated by Na, K, Mg, Br, and Cl. The second most important factor also has a strong Na-Cl influence, but is dominated by Ca, bicarbonate alkalinity, and Sr. It is likely that these two factors represent addition of solutes by the dissolution of halite, gypsum/anhydrite, and carbonates. A third factor showed the interelement correlations independent of effects attributable to halite dissolution. This factor contains two groups of inversely correlated elements: Mg, bicarbonate alkalinity, and $SiO_2$ form one group; and pH, B, and Li form another group. This pattern of element associations might reflect ion exchange, silicate hydrolysis, and carbonate diagenesis.

Saturation indices for minerals commonly observed in the Ochoan Series were calculated with the PHRQPITZ code, which uses the Pitzer model for ion interactions. All water samples are saturated with respect to gypsum. Dolomite and calcite saturation indices generally indicate apparent supersaturation with respect to the carbonates. The Mg/Ca ratios indicate that the degree of supersaturation increases with ionic strength. Potential sources of error in the carbonate data include uncertainties in the pH measurements, loss of $CO_2$ gas from the samples during collection, and uncertainties in the values of the free energy of dolomite used to calculate the saturation indices. All waters are undersaturated with respect to halite, and, with the exception of the Culebra waters from WIPP-29, all samples are undersaturated with respect to anhydrite.

This study confirms earlier observations that solute distribution patterns are not consistent with steady-state hydrologic flow over long (> 10,000 year) time periods. Zone B, a facies with low salinity and element ratios inconsistent with halite dissolution, lies downgradient from more saline water in Zone C.

A model for the chemical evolution of water in the Culebra suggests that as water flowed through the aquifer, it increased in salinity as it dissolved halite, carbonates, and sulfates. Theoretical calculations show that the increase in salinity caused by the dissolution of halite changes the solubilities of carbonates and sulfates; solubilities increase up to 3 molal ionic strength and then decrease. Addition of magnesium by dissolution of carnallite and/or polyhalite and suppression of dolomite precipitation are consistent with the observed Mg/Ca ratios.

# CONTENTS

# CONTENTS (Continued)

# CONTENTS (Continued)

# FIGURES

# FIGURES (Continued)

# FIGURES (Continued)

# TABLES

# CHAPTER 2.0

## 2.1 INTRODUCTION

### 2.1.1 Objectives

This chapter provides a synthesis of solute concentration data available in late 1987 and proposes hypotheses concerning the origin of solutes in groundwaters in the Culebra dolomite of the Rustler Formation. Spatial trends in the concentrations of major solutes in the study area are used to define hydrochemical facies. These facies are then compared to the modern groundwater flow system to determine if flow directions indicated by modern hydraulic head potentials and transmissivities are consistent with flow directions suggested by solute concentrations.

Where relevant, data from the Magenta dolomite, Dewey Lake Red Beds, Rustler/Salado contact zone, and the Bell Canyon Formation are included in this chapter. Data and discussion of the redox potential and isotope geochemistry of Rustler and Dewey Lake groundwaters and a discussion of the mineralogy of the Culebra are found in other chapters of this report.

This synthesis is not intended to be taken as a final comprehensive model of the solute chemistry in the Rustler. Instead, it is a summary of current ideas that may indicate the framework within which some future data collection and modeling activities will be carried out.

### 2.1.2 Study Area and Stratigraphy

Figure 2-1 shows the region of interest for this study, the locations of wells discussed in this chapter, and the site boundary (sometimes called the four-mile zone or the WIPP Site).

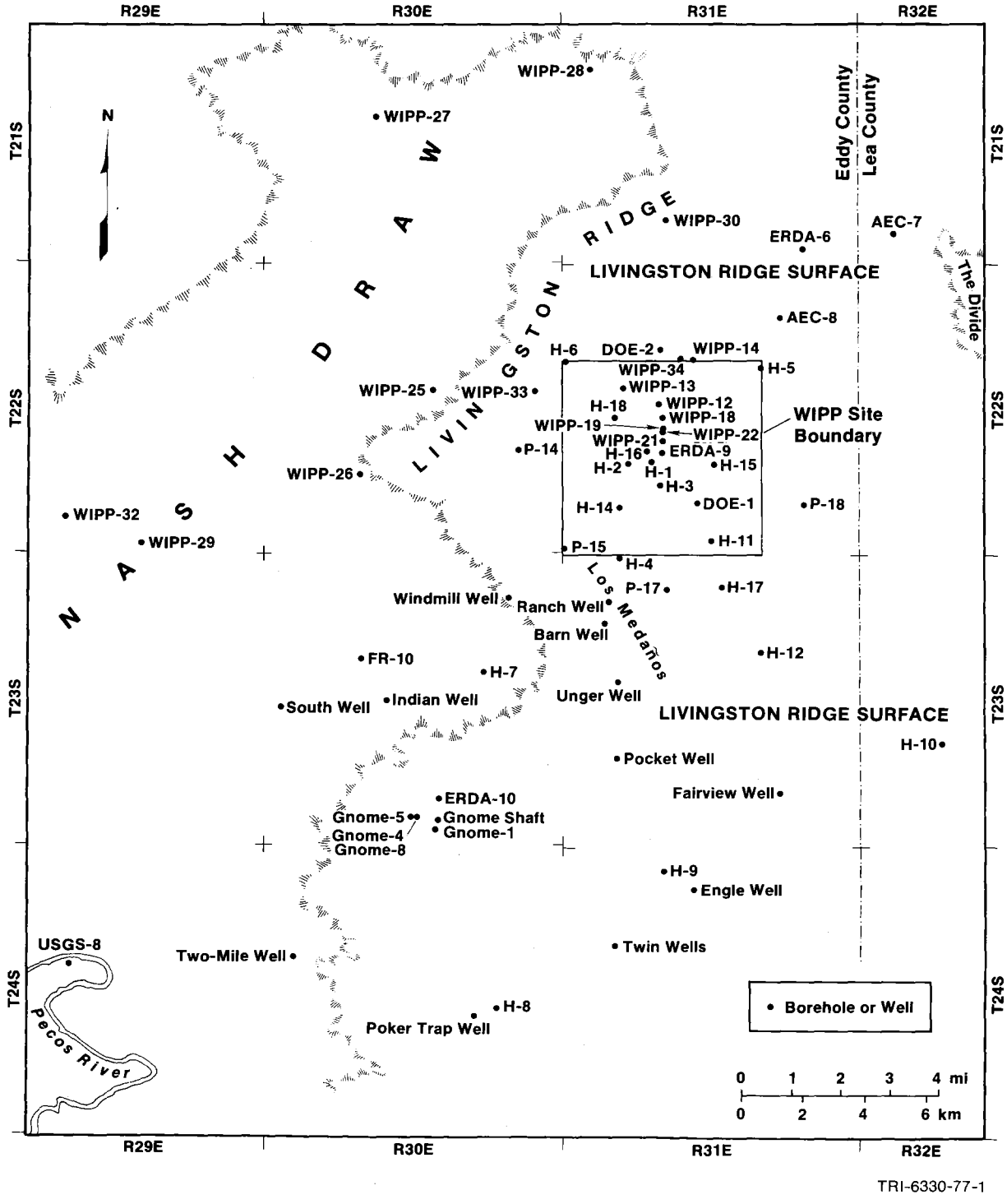


Figure 2-1. Map showing locations of wells in the study area.

The stratigraphy has been well documented (Siegel and Lambert, Chapter 1; Lappin, 1988, and references cited therein) and is not repeated here. In descending order, the units of interest here are the Dewey Lake Red Beds, the Rustler Formation (which contains the Forty-niner, Magenta dolomite, Tamarisk, Culebra dolomite, and unnamed lower members), the Salado Formation, the Castile Formation, and the Bell Canyon Formation.

### 2.1.3 Previous Work

Mercer (1983) provided a summary of geohydrologic and hydrochemical data from the Los Medaños area. The study area included 800 square miles surrounding the WIPP Site. Mercer (1983) summarized the results of previous US Geological Survey (USGS) studies and compiled analyses of major and minor solutes and radiochemical data from the Culebra, Magenta, and Rustler/Salado contact zone collected from 1976 to 1980. Although Mercer did not define any hydrochemical facies zones in the Culebra, he did show a line to the east of which the sum of the potassium plus magnesium concentrations was greater than 100 milliequivalents per liter (Figure 19 of Mercer, 1983). This line approximated the dividing line between regions of higher transmissivity to the west and lower transmissivity to the east. In addition, it coincided roughly with "a line to the east of which halite is present in the Rustler Formation below the Culebra and to the west of which the halite beds have been removed by dissolution" (p. 63, Mercer, 1983). Listings of other relevant reports and sources of data published before 1983 can be found in this report and in Ramey (1985) discussed below.

Ramey (1985) recast the Culebra chemical data from Mercer's report in terms of hydrochemical facies and calculated saturation indices for minerals commonly observed in evaporite deposits. He defined three hydrochemical-facies zones in the Culebra. Ramey's Zone A comprised the eastern quarter of the four-mile zone (Figure 2-1) and extended to the eastern edge of the current study area. It was characterized by a saline (total dissolved solids [TDS] >60,000 mg/L) Na-Cl brine with considerable amounts of Mg and K. Ramey's Zone B lay to the south of the four-mile zone and contained fresher (TDS <3,500 mg/L) Ca-$SO_4$ waters. Ramey's Zone C included the western three-fourths of the

four-mile zone and extended to Nash Draw to the west. Waters in this zone contained Na and Cl as their predominant constituents and showed a wide range of salinities (9,000 mg/L < TDS < 240,000 mg/L).

Ramey observed that the water chemistries in the Culebra did not support the hydrologic flow path proposed by Gonzalez (1983) and Barr et al. (1983). According to these workers, water flows southeast from the center of the site and then westward to Malaga Bend. This would mean that water along the flow path changes from a saline Na-Cl brine to a dilute Ca-$SO_4$ solution along the flow path. No plausible geochemical process has been identified that would cause this transformation in a hydrologically confined aquifer.

For the Culebra samples, Ramey calculated saturation indices for halite (NaCl), anhydrite ($CaSO_4$), gypsum ($CaSO_4 \cdot 2H_2O$), calcite ($CaCO_3$), and dolomite ($CaMg(CO_3)_2$) with the WATEQFC computer code. He found that all Culebra samples were undersaturated with respect to halite and concluded that waters from all parts of the study area had the potential to dissolve additional salt. His calculations indicated that all Culebra waters except those from H-4, H-5, and P-18 were saturated with respect to gypsum, and that, with the exception of WIPP-27 and WIPP-29 to the west, all waters were undersaturated with respect to anhydrite. Saturation indices for carbonates indicated areas of undersaturation and areas of apparent supersaturation.

Ramey suggested that the saturation indices for the saline (>0.5 molal) waters were in error because the WATEQFC code uses an inadequate model for activity coefficients. The code uses the extended Debye-Huckel equation (misidentified by Ramey as the Davies equation) to calculate activity coefficients. The constants used to calculate the activity coefficients by this equation were obtained from mean salt data over a range of approximately 0-3 molar ionic strength (Truesdell and Jones, 1974). Plummer and Parkhurst (1985) provide evidence that this equation accurately estimates the saturation indices of halite, calcite, gypsum, and dolomite in natural waters with ionic strengths of up to 2 molal. However, Møller et al. (1985) and Wolery et al. (1985) show that calculations of solubility

of gypsum in simple Ca-Na-$SO_4$-Cl-$H_2O$ solutions with this equation do not reproduce experimental data satisfactorily. The accuracy of this equation for other minor solutes is generally considered to be poor at moderate to high ionic strengths (>0.2 m) (Phillips et al., 1988).

Meijer et al. (1987) examined the consistency of densities and chemical compositions of water samples collected from the Culebra between 1976 and 1984. They calculated saturation indices for several minerals using a critically-evaluated thermochemical data base and the PHREEQE computer code with a WATEQ-Debye-Huckel equation. They claimed that their calculational method was accurate at ionic strengths up to 3.0 molal (TDS of about 100,000 mg/L), and they suggested that their results were qualitatively similar to those reported by Ramey (1985). Meijer et al. also calculated densities from the chemical analyses and compared them to densities measured in the field. Based on their calculations, they concluded that 11 of the 22 water samples used by Ramey (1985) were not representative Culebra formation waters.

## 2.2 MAJOR, MINOR, AND TRACE SOLUTE DATA

### 2.2.1 Sources of Data

For this work we considered major-, minor-, and trace-solute data from water samples collected by several different agencies and analyzed in different laboratories from 1976 to 1987. Data were obtained from the following sources:

- Sandia National Laboratories (SNL). Samples collected by several different agencies were analyzed by United Nuclear Corporation (UNC) Geotech (formerly Bendix Field Engineering Corporation), Grand Junction, CO. The data, as well as details of methods of sample collection and analytical techniques, are reported in Robinson (1988).

- USGS. Samples collected by the USGS were analyzed by the USGS Central Laboratories (Branch of Analytical Services, Water Resource Division) and reported by Mercer (1983) and Mercer and Orr (1979).

- International Technology (IT) Corporation. Samples collected for the Water Quality Sampling Program (WQSP) were analyzed by the IT Analytical Services (ITAS) laboratory, Murraysville, NJ. The data are given in a series of annual reports (Uhland and Randall, 1986; Uhland, et al., 1987; Randall et al., 1988; and Lyon, 1989).

- New Mexico Environmental Evaluation Group (EEG). The New Mexico Bureau of Mines & Mineral Resources (NMBM&MR) analyzed samples from the WQSP for the EEG (personal communication from Chapman in Robinson, 1988).

Table 2-1 summarizes the different data sets that were consulted in this work.

### 2.2.2 Criteria Used to Evaluate Chemical Data

In some cases, large differences exist between the chemical compositions reported by different laboratories for the same water sample or by the same laboratory for different samples from the same well. Data from UNC, ITAS, the NMBM&MR, and the USGS laboratories collected from 1976 to 1987 were reviewed, and the critical evaluation procedure of Robinson (1988) was used to select those data considered to be most reliable at the time most of the studies in this chapter were being done (late 1987).

Samples, obtained after a lengthy pumping test, have proved to be more reliable than those obtained by bailing or swabbing (Robinson, 1988). During a pumping test, samples can be periodically collected and analyzed for selected parameters in the field. These samples ("serial" samples) are collected at regular intervals until the measured parameters reach a constant value (the "steady-state" value). At this time, "final" samples are collected

## Table 2-1. Sources of Solute Data

| Collection Dates | Program or Collector[1] | Labs[2] | References |
|---|---|---|---|
| 1976-1980 | USGS | USGS | Mercer and Orr, 1979; Mercer, 1983 |
| 1980-1981 | Sandia | UNC | Lambert and Robinson, 1984; Robinson, 1988 |
| 1983-1984 | HGC | UNC | Robinson, 1988 |
| 1985-1987 | WQSP | ITAS, UNC, NMBM&MR | Uhland and Randall, 1986; Uhland et al., 1987; Randall et al., 1988; Robinson, 1988; SNL, unpublished data from UNC |

1. USGS = United States Geological Survey
   WQSP = Water Quality Sampling Program
   HGC = Hydro Geo Chem, Inc., Tucson, AZ (a SNL subcontractor)
2. ITAS = IT Analytical Services, Murraysville, PA
   NMBM&MR = New Mexico Bureau of Mines & Mineral Resources, Socorro, NM
   UNC = UNC Geotech (formerly Bendix Field Engineering Corp.), Grand Junction, CO
   USGS = United States Geological Survey, Central Laboratory

for analysis in various laboratories. For some parameters, such as chloride, the steady-state value is considered representative of the unperturbed groundwater; for other parameters, such as iron, the steady-state value often does not represent the actual concentration in the in-situ groundwater (Robinson, 1988).

During a pumping test, if the concentrations of chloride and divalent cations (calcium plus magnesium) reach steady-state, then the samples are considered representative with respect to concentrations of the major solutes (Cl, $SO_4$, Ca, Mg, Na, and K) and certain minor and trace elements (Br, F, I, B, Li, and Sr). This assumption is based on the observation that at some wells, the same concentrations have been observed in samples collected several years apart using the serial sampling method. However, a steady-state value for a parameter such as iron does not necessarily mean that the sample is not contaminated. For

example, in some wells, the steady-state value for iron varied as the pumping rate changed, suggesting that a process such as corrosion of the well casing was controlling the concentration of iron in the sampled water (Uhland et al., 1987; Robinson, 1988).

We assume that samples are representative of a given location if samples of the same composition have been collected during several different sampling periods several years apart. However, this assumption may not always be valid. Even if reproducible samples (that is, samples with the same solute concentrations) are collected from a well during more than one sampling episode, the samples may still not be representative of unperturbed groundwater. The steady-state concentrations observed during serial-sampling and analyses may actually represent transient conditions. Thus, for example, samples with apparently anomalous solute chemistries such as the Culebra groundwater from P-14 (as discussed in subsequent sections of this chapter) may be extensively contaminated.

## 2.2.3 Results of Evaluation of Data from Culebra Samples

### 2.2.3.1 Major, Minor, and Trace Solute Data

Table 2-2 summarizes the data from the Rustler Formation, the Dewey Lake Red Beds, and the Bell Canyon Formation. The sources in Table 2-1 were consulted for data to estimate the ranges of solute concentrations observed at the wells and to calculate average values for use in element ratio contours described in Section 2.3.1. Analyses reported by UNC Geotech were used in the saturation index calculations and principal component analysis (PCA) discussed in Sections 2.3.4 and 2.3.3, respectively.

Uncertainties in the data are related to several sources including analytical techniques, sampling techniques (contamination introduced by the sampling apparatus or loss of solutes during sampling), and contamination of waters at depth or in the well. The last source of uncertainty is sometimes indicated by a change in the water chemistry over a period of several years.

## Table 2-2. Concentrations of Solutes[1] in Groundwaters from the Rustler Formation, Dewey Lake Red Beds, and Bell Canyon Formation
## Part A: Major Solutes, $pCO_2$, and pH

| Well(s) | Date[2] | Lab[3] | Zone[4] | Na (mg/L) | K (mg/L) | Ca (mg/L) | Mg (mg/L) | $Cl^-$ (mg/L) | $SO_4^{2-}$ (mg/L) | Alkalinity[5] as $HCO_3^-$ (mg/L) | $pCO_2$[6] | pH[5] |
|---|---|---|---|---|---|---|---|---|---|---|---|---|
| DOE-1 | 04/85 | UNC | CuA | 45800 | 1100 | 1730 | 1610 | 73600 | 7350 | 45 | -2.60 | 7.1 |
| DOE-1 | [2] | *avg* | CuA | *46000* | *1100* | *1700* | *1600* | *75000* | *7400* | | | |
| DOE-1 | [2] | rng | CuA | 45000-46000 | [1] | [1] | [1] | 73000-77000 | [1] | 45-46 | | 7.1 |
| DOE-2 | 03/85 | UNC | CuC | 18400 | 410 | 1960 | 1060 | 34600 | 3950 | 67 | -2.33 | 7.0 |
| DOE-2 | [2] | *avg* | CuC | *18000* | *420* | *1900* | *1000* | *33000* | *3700* | | | |
| DOE-2 | [2] | rng | CuC | 17000-19000 | 410-420 | 1900-2000 | 900-1100 | 32000-35000 | 3400-4000 | [1] | | [1] |
| H-2A | 04/86 | UNC | CuC | 3570 | 93.5 | 743 | 167 | 5310 | 2980 | 57 | -3.38 | 8.0 |
| H-3B3 | 06/84 | UNC | CuC | 17400 | 495 | 1550 | 829 | 29500 | 5130 | | -2.83 | 7.4 |
| H-3B3 | 02/85 | UNC | CuC | 18000 | 425 | 1470 | 783 | 30300 | 4820 | 52 | -2.86 | 7.4 |
| H-3B2, H-3B3 | [4] | *avg* | CuC | *18000* | *440* | *1400* | *760* | *29000* | *4800* | | | |
| H-3B2, H-3B3 | [4] | rng | CuC | 17000-19000 | 360-500 | 1200-1600 | 690-830 | 27000-31000 | 4600-5200 | 50-52 | | 7.4 |
| H-4B | 05/81 | UNC | CuC | 6080 | 215 | 700 | 455 | 7980 | 6230 | 71 | -3.35 | 8.0 |
| H-4C | 08/84 | UNC | CuC | 6150 | 222 | 698 | 505 | 7950 | 5700 | 75 | -3.11 | 7.8 |
| H-4B | 07/85 | UNC | CuC | 5850 | 210 | 691 | 427 | 7480 | 5520 | 69 | -3.04 | 7.7 |
| H-4B, H-4C | [4] | *avg* | CuC | *6000* | *220* | *690* | *450* | *7700* | *5700* | | | |
| H-4B, H-4C | [4] | rng | CuC | 5800-6200 | 180-260 | 690-700 | 400-510 | 7400-8000 | 5500-6300 | 68-75 | | 7.6-8.0 |
| H-5B | 06/81 | UNC | CuA | 52400 | 1290 | 1710 | 2140 | 89500 | 7360 | 80 | -3.21 | 7.9 |
| H-5C | 10/81 | UNC | CuA | 52300 | 1300 | 1720 | 2150 | 89500 | 7570 | 86 | -3.17 | 7.9 |
| H-5B | 08/85 | UNC | CuA | 54100 | 1350 | 1700 | 2170 | 85400 | 7840 | 50 | -2.86 | 7.4 |
| H-5B, H-5C | [4] | *avg* | CuA | *53000* | *1300* | *1700* | *2200* | *87000* | *7600* | | | |
| H-5B, H-5C | [4] | rng | CuA | 52000-55000 | 1200-1400 | 1700-1800 | 2100-2200 | 84000-90000 | 7300-7900 | | | |

**Table 2-2. Concentrations of Solutes[1] in Groundwaters from the Rustler Formation, Dewey Lake Red Beds, and Bell Canyon Formation**
**Part A: Major Solutes, $pCO_2$, and pH (Continued)**

| Well(s) | Date[2] | Lab[3] | Zone[4] | Na (mg/L) | K (mg/L) | Ca (mg/L) | Mg (mg/L) | $Cl^-$ (mg/L) | $SO_4^{2-}$ (mg/L) | Alkalinity[5] as $HCO_3^-$ (mg/L) | $pCO_2$[6] | pH[5] |
|---|---|---|---|---|---|---|---|---|---|---|---|---|
| H-6B | 05/81 | UNC | CuC | 18600 | 450 | 2150 | 1080 | 33000 | 3980 | 96 | -2.16 | 7.0 |
| H-6B | 09/85 | UNC | CuC | 18000 | 375 | 2040 | 1040 | 32300 | 3570 | 94 | -2.07 | 6.9 |
| H-6B | [3] | *avg* | CuC | *18000* | *420* | *2000* | *1100* | *33000* | *3600* | | | |
| H-6B | [3] | rng | CuC | 17000-19000 | 370-450 | 1900-2200 | 1000-1200 | 32000-34000 | 3300-4000 | 90-96 | | 6.9-7.2 |
| H-7B1 | 03/86 | UNC | CuB | 207 | 7.0 | 587 | 130 | 320 | 1850 | 120 | -2.20 | 7.3 |
| H-7B1 | [3] | *avg* | CuB | *210* | *7.0* | *570* | *130* | *320* | *1800* | | | |
| H-7B1 | [3] | rng | CuB | 200-210 | 7.0 | 540-590 | 130 | 300-350 | 1700-1900 | 120 | | 7.3-7.4 |
| H-8B | 01/86 | UNC | CuB | 55.1 | 3.83 | 548 | 157 | 30.5 | 1950 | 96 | -2.70 | 7.3 |
| H-8B | [2] | *avg* | CuB | *54* | *3.9* | *540* | *170* | *32* | *1800* | | | |
| H-8B | [2] | rng | CuB | 51-56 | 3.7-4.1 | 520-550 | 150-180 | 30-33 | 1600-2000 | 93-96 | | 7.2-7.3 |
| H-9B | 11/85 | UNC | CuB | 146 | 6.85 | 590 | 137 | 194 | 1900 | 110 | -2.43 | 7.4 |
| H-9B | [2] | *avg* | CuB | *150* | *7.2* | *580* | *150* | *190* | *1800* | | | |
| H-9B | [2] | rng | CuB | 140-150 | 6.8-7.6 | 560-620 | 130-170 | 170-200 | 1700-1900 | 110 | | 7.3-7.4 |
| H-11B3 | 06/85 | UNC | CuA | 40400 | 943 | 1700 | 1320 | 65900 | 7180 | 54 | -2.63 | 7.2 |
| H-11B3 | [2] | *avg* | CuA | *39000* | *940* | *1600* | *1300* | *66000* | *7200* | | | |
| H-11B3 | [2] | rng | CuA | 37000-41000 | [1] | 1500-1700 | 1300-1400 | 65000-67000 | [1] | 54-55 | | 7.2-7.3 |
| H-12 | 08/85 | UNC | CuA | 49200 | 1270 | 1760 | 1980 | 79000 | 7210 | 53 | -2.61 | 7.2 |
| H-12 | [2] | *avg* | CuA | *50000* | *1300* | *1800* | *2000* | *80000* | *7200* | | | |
| H-12 | [2] | rng | CuA | 49000-51000 | [1] | 1700-1900 | 1900-2000 | 78000-80000 | [1] | 53-62 | | 7.2 |

## Table 2-2. Concentrations of Solutes[1] in Groundwaters from the Rustler Formation, Dewey Lake Red Beds, and Bell Canyon Formation
## Part A: Major Solutes, $pCO_2$, and pH (Continued)

| Well(s) | Date[2] | Lab[3] | Zone[4] | Na (mg/L) | K (mg/L) | Ca (mg/L) | Mg (mg/L) | $Cl^-$ (mg/L) | $SO_4^{2-}$ (mg/L) | Alkalinity[5] as $HCO_3^-$ (mg/L) | $pCO_2$[6] | pH[5] |
|---|---|---|---|---|---|---|---|---|---|---|---|---|
| P-14 | 02/86 | UNC | CuC | 4360 | 37.9 | 3520 | 840 | 14500 | 1590 | 110 | -1.81 | 6.8 |
| P-14 | [2] | *avg* | CuC | *4100* | *41* | *3700* | *800* | *14000* | *1600* | | | |
| P-14 | [2] | rng | CuC | 3700-4400 | 37-45 | 3500-3900 | 760-840 | 13000-15000 | 1500-1700 | 100-110 | | 6.8-6.9 |
| P-17 | 03/86 | UNC | CuC | 28300 | 782 | 1620 | 1460 | 48200 | 6020 | 64 | -2.90 | 7.5 |
| P-17 | [2] | *avg* | CuC | *28000* | *820* | *1600* | *1500* | *49000* | *6000* | | | |
| P-17 | [2] | rng | CuC | 28000-29000 | 780-880 | 1500-1700 | 1400-1600 | 48000-51000 | 5900-6100 | 61-64 | | 7.5 |
| WIPP-13 | 02/87 | *avg* | CuC | *19000* | *340* | - | - | *36000* | *4500* | *~120* | | *~6.6* |
| WIPP-25 | 08/80 | UNC | CuC | 3160 | 73.5 | 905 | 260 | 5250 | 2500 | 210 | -1.69 | 6.9 |
| WIPP-25 | 08/80 | *avg* | CuC | *3200* | *74* | *900* | *260* | *5200* | *2500* | | | |
| WIPP-25 | 08/80 | rng | CuC | [1] | [1] | [1] | [1] | 5200-5300 | [1] | [1] | | [1] |
| WIPP-25 | 02/86 | UNC | CuC | 3180 | 102 | 1140 | 315 | 6320 | 2380 | 130 | | 7.2 |
| WIPP-25 | 02/86 | *avg* | CuC | *3300* | *100* | *1100* | *330* | *6200* | *2400* | | | |
| WIPP-25 | 02/86 | rng | CuC | 3100-3400 | 100-110 | 1100-1200 | 310-340 | 6200-6400 | 2300-2400 | [1] | | [1] |
| WIPP-26 | 08/80 | UNC | CuC | 3620 | 170 | 1240 | 355 | 7200 | 2480 | 140 | -1.86 | 6.9 |
| WIPP-26 | 08/80 | *avg* | CuC | *3600* | *170* | *1200* | *360* | *7000* | *2500* | | | |
| WIPP-26 | 08/80 | rng | CuC | [1] | [1] | [1] | [1] | 6900-7200 | [1] | [1] | | 6.9 |

## Table 2-2. Concentrations of Solutes[1] in Groundwaters from the Rustler Formation, Dewey Lake Red Beds, and Bell Canyon Formation
## Part A: Major Solutes, $pCO_2$, and pH (Continued)

| Well(s) | Date[2] | Lab[3] | Zone[4] | Na (mg/L) | K (mg/L) | Ca (mg/L) | Mg (mg/L) | $Cl^-$ (mg/L) | $SO_4^{2-}$ (mg/L) | Alkalinity[5] as $HCO_3^-$ (mg/L) | $pCO_2$[6] | pH[5] |
|---|---|---|---|---|---|---|---|---|---|---|---|---|
| WIPP-26 | 11/85 | UNC | CuC | 4220 | 343 | 1340 | 380 | 8770 | 2420 | 120 | -2.14 | 7.1 |
| WIPP-26 | 11/85 | *avg* | CuC | *4100* | *350* | *1300* | *390* | *8600* | *2400* | | | |
| WIPP-26 | 11/85 | rng | CuC | 3800-4300 | 340-360 | 1200-1400 | 370-430 | 8400-8800 | 2300-2500 | [1] | | [1] |
| WIPP-27 | 09/80 | UNC | CuD | 39200 | 8060 | 3210 | 1900 | 78500 | 3830 | 120 | -1.33 | 6.4 |
| WIPP-27 | [2] | *avg* | CuD | *39000* | *8100* | *3200* | *2000* | *78000* | *3900* | | | |
| WIPP-27 | [2] | rng | CuD | 39000-40000 | [1] | 3100-3300 | 1900-2000 | 77000-79000 | 3800-3900 | [1] | | 6.4 |
| WIPP-28 | 09/80 | UNC | CuC | 15200 | 485 | 1180 | 555 | 24800 | 4380 | | -.076 | 6.5 |
| WIPP-28 | 09/80 | *avg* | CuC | *15000* | *480* | *1200* | *560* | *24000* | *4400* | | | |
| WIPP-28 | 09/80 | rng | CuC | [1] | [1] | [1] | [1] | 24000-25000 | [1] | | | |
| WIPP-29 | 08/80 | UNC | CuD | 71400 | 15600 | 950 | 5480 | 138000 | 14000 | 210 | -0.87 | 6.1 |
| WIPP-29 | 08/80 | *avg* | CuD | *71000* | *16000* | *880* | *5600* | *140000* | *14000* | | | |
| WIPP-29 | 08/80 | rng | CuD | [1] | [1] | 810-950 | 5400-5700 | 130000-140000 | 13000-14000 | [1] | | 6.1 |
| WIPP-29 | 12/85 | UNC | CuD | 94900 | 23300 | 413 | 6500 | 179000 | 20000 | 160 | -0.75 | 5.9 |
| WIPP-29 | 12/85 | *avg* | CuD | *92000* | *22000* | *410* | *6400* | *180000* | *18000* | | | |
| WIPP-29 | 12/85 | rng | CuD | 90000-95000 | 20000-24000 | [1] | 6300-6500 | 179000-180000 | 17000-20000 | [1] | | [1] |
| WIPP-30 | 09/80 | UNC | CuC | 8570 | 255 | 1140 | 460 | 14600 | 4120 | 40 $HCO_3^-$ | -4.41 | 8.8 |
| WIPP-30 | 09/80 | *avg* | CuC | *8600* | *260* | *1100* | *460* | *15000* | *4100* | & 17 $CO_3^{2-}$ | | |
| WIPP-30 | 09/80 | rng | CuC | [1] | [1] | [1] | [1] | 14000-15000 | [1] | [1] | | [1] |

## Table 2-2. Concentrations of Solutes[1] in Groundwaters from the Rustler Formation, Dewey Lake Red Beds, and Bell Canyon Formation
## Part A: Major Solutes, $pCO_2$, and pH (Continued)

| Well(s) | Date[2] | Lab[3] | Zone[4] | Na (mg/L) | K (mg/L) | Ca (mg/L) | Mg (mg/L) | $Cl^-$ (mg/L) | $SO_4^{2-}$ (mg/L) | Alkalinity[5] as $HCO_3^-$ (mg/L) | $pCO_2$[6] | pH[5] |
|---|---|---|---|---|---|---|---|---|---|---|---|---|
| Engle | 03/85 | UNC | CuB | 200 | 5.60 | 588 | 152 | 231 | 1990 | 110 | -2.44 | 7.4 |
| Engle | 03/85 | *avg* | CuB | *190* | *5.5* | *580* | *140* | *230* | *1900* | | | |
| Engle | 03/85 | rng | CuB | 180-200 | 5.4-5.6 | 570-590 | 130-160 | 220-240 | 1800-2000 | [1] | | [1] |
| H-3B1 | 07/85 | UNC | Mag | 1520 | 34.5 | 1000 | 292 | 3360 | 2310 | 47 | | 8.0 |
| H-3B1 | [3] | rng | Mag | 1500-1600 | 34-36 | 1000 | 270-300 | 3300-3400 | 2200-2400 | 45-47 | | 7.7-8.0 |
| H-4C | 11/86 | UNC | Mag | 7110 | 85.1 | 651 | 411 | 8460 | 7100 | 70 | | 8.4 |
| H-4C | [2] | rng | Mag | 7100-7300 | 85-99 | 610-660 | 390-420 | 8400-8500 | [1] | 70-85 | | 8.1-8.4 |
| H-5C | 10/86 | UNC | Mag | 1480 | 33.6 | 550 | 173 | 1070 | 3620 | 56 | | 8.0 |
| H-5C | 10/86 | rng | Mag | 1400-1500 | [1] | [1] | 170-190 | 1000-1100 | [1] | [1] | | [1] |
| H-6C | 10/86 | UNC | Mag | 642 | 16.6 | 546 | 160 | 428 | 2700 | 51 | | 7.7 |
| H-6C | 10/86 | rng | Mag | [1] | [1] | [1] | 160-170 | 420-430 | 2400-2700 | [1] | | [1] |
| WIPP-25 | 09/80 | UNC | Mag | 2910 | 71.5 | 905 | 260 | 5250 | 2490 | 180 | | 6.9 |
| WIPP-27 | 09/80 | UNC | Mag | 43200 | 8090 | 3660 | 2100 | 85200 | 3410 | 210 | | 6.4 |
| WIPP-25 | 07/80 | UNC | R/S | 123000 | 3330 | 560 | 3260 | 192000 | 12400 | 130 | | 7.4 |
| WIPP-26 | 07/80 | UNC | R/S | 68600 | 1200 | 1420 | 1660 | 108000 | 7480 | 270 | | 7.7 |

**Table 2-2. Concentrations of Solutes[1] in Groundwaters from the Rustler Formation, Dewey Lake Red Beds, and Bell Canyon Formation**
**Part A: Major Solutes, $pCO_2$, and pH (Continued)**

| Well(s) | Date[2] | Lab[3] | Zone[4] | Na (mg/L) | K (mg/L) | Ca (mg/L) | Mg (mg/L) | $Cl^-$ (mg/L) | $SO_4^{2-}$ (mg/L) | Alkalinity[5] as $HCO_3^-$ (mg/L) | $pCO_2$[6] | pH[5] |
|---|---|---|---|---|---|---|---|---|---|---|---|---|
| WIPP-28 | 07/80 | UNC | R/S | 97100 | 4300 | 605 | 3400 | 155000 | 16700 | 170 | | 7.0 |
| WIPP-29 | 07/80 | UNC | R/S | 36100 | 1480 | 1080 | 2320 | 58000 | 12000 | 200 | | 7.2 |
| WIPP-30 | 07/80 | UNC | R/S | 121000 | 2180 | 955 | 2770 | 192000 | 7390 | 620 | | 7.5 |
| Ranch | 06/86 | UNC | DL | 200 | 4.0 | 420 | 202 | 418 | 1100 | 220 | | 7.0 |
| Ranch | 06/86 | rng | DL | 180-200 | 3.6-4.0 | [1] | 190-210 | 390-420 | 920-1100 | [1] | | [1] |
| Twin-Pasture | 01/86 | UNC | DL | 25.4 | 3.85 | 80.4 | 22.5 | 44.1 | 75.1 | 230 | | 7.8 |
| Twin-Pasture | 01/86 | rng | DL | 24-26 | 3.7-4.3 | 80-81 | 22-25 | 44-47 | 70-76 | [1] | | [1] |
| DOE-2 | 07/85 | UNC | BC | 49600 | 885 | 5910 | 1330 | 89700 | 2020 | 48 | | 6.8 |
| DOE-2 | 07/85 | rng | BC | [1] | [1] | [1] | [1] | 89000-90000 | [1] | (lab) | | [1] |

## Table 2-2. Concentrations of Solutes[1] in Groundwaters from the Rustler Formation, Dewey Lake Red Beds, and Bell Canyon Formation
## Part B: Minor and Trace Solutes, TDS, and Ionic Strength

| Well(s) | Date[2] | Lab[3] | Zone[4] | TDS[7] (mg/L) | IS[6] (molal) | $Br^-$ (mg/L) | $F^-$ (mg/L) | $I^-$ (mg/L) | B (mg/L) | Li (mg/L) | Sr (mg/L) | Silica as $SiO_2$ (mg/L) | Fe (mg/L) | Mn (mg/L) |
|---|---|---|---|---|---|---|---|---|---|---|---|---|---|---|
| DOE-1 | 04/85 | UNC | CuA | 131200 | 2.53 | 56 | | | 37 | 0.64 | 26 | 8.4 | 0.28 | |
| DOE-1 | [2] | *avg* | CuA | | | *60* | *1.2* | | *36* | *0.64* | *21* | | | |
| DOE-1 | [2] | rng | CuA | | | 56-64 | 1.0-1.7 | | 35-37 | [1] | 16-26 | 8-24 | | |
| DOE-2 | 03/85 | UNC | CuC | 60400 | 1.19 | 34 | 1.7 | 0.22 | 16 | 0.47 | 38 | 17 | 0.036 | 0.30 |
| DOE-2 | [2] | *avg* | CuC | | | *35* | *1.6* | *0.22* | *18* | *0.47* | *29* | | | |
| DOE-2 | [2] | rng | CuC | | | 34-36 | 1.2-2.2 | [1] | 14-24 | [1] | 22-38 | 17-24 | | |
| H-2A | 04/86 | UNC | CuC | 12900 | 0.27 | 5.6 | 2.2 | 0.081 | 10 | 0.22 | 9.5 | 13 | 1.1 | 0.055 |
| H-3B3 | 06/84 | UNC | CuC | 55000 | 1.08 | 29 | 2.1 | 0.13 | 30 | 0.53 | 23 | 9.8 | 0.57 | 0.13 |
| H-3B3 | 02/85 | UNC | CuC | 55800 | 1.08 | 26 | 1.9 | 0.14 | 26 | 0.40 | 30 | 11 | 0.20 | 0.12 |
| H-3B2, H-3B3 | [4] | *avg* | CuC | | | *31* | *1.8* | *0.14* | *28* | *0.41* | *25* | | | |
| H-3B2, H-3B3 | [4] | rng | CuC | | | 26-39 | 1.5-2.1 | 0.13-0.14 | 21-34 | 0.30-0.53 | 23-30 | 9-20 | | |
| H-4B | 05/81 | UNC | CuC | 21700 | 0.46 | 42 | | | 18 | 0.39 | 14 | 11 | | |
| H-4C | 08/84 | UNC | CuC | 21200 | 0.45 | 48 | 2.1 | 0.23 | 20 | 0.49 | 18 | 13 | 2.2 | 0.20 |
| H-4B | 07/85 | UNC | CuC | 20200 | 0.42 | 43 | 2.7 | | 14 | 0.40 | 14 | 14 | 0.32 | 0.11 |
| H-4B, H-4C | [4] | *avg* | CuC | | | *44* | *2.2* | *0.23* | *18* | *0.42* | *15* | | | |
| H-4B, H-4C | [4] | rng | CuC | | | 43-48 | 1.7-2.7 | [1] | 14-23 | 0.39-0.49 | 13-18 | 11-30 | | |
| H-5B | 06/81 | UNC | CuA | 154400 | 2.99 | 62 | | | 33 | 0.77 | 32 | 6.2 | | |
| H-5C | 10/81 | UNC | CuA | 154500 | 3.00 | 64 | | | 35 | 0.77 | 31 | 5.8 | | |
| H-5B | 08/85 | UNC | CuA | 152600 | 2.97 | 49 | 2.0 | 0.19 | 34 | 0.81 | 29 | 7.1 | 2.9 | 0.29 |
| H-5B, H-5C | [4] | *avg* | CuA | | | *58* | *1.3* | *0.19* | *33* | *0.78* | *31* | | | |
| H-5B, H-5C | [4] | rng | CuA | | | 49-64 | 0.8-2.0 | [1] | 29-35 | 0.77-0.81 | 29-32 | 5-36 | | |

**Table 2-2. Concentrations of Solutes[1] in Groundwaters from the Rustler Formation, Dewey Lake Red Beds, and Bell Canyon Formation**
**Part B: Minor and Trace Solutes, TDS, and Ionic Strength (Continued)**

| Well(s) | Date[2] | Lab[3] | Zone[4] | TDS[7] (mg/L) | IS[6] (molal) | $Br^-$ (mg/L) | $F^-$ (mg/L) | $I^-$ (mg/L) | B (mg/L) | Li (mg/L) | Sr (mg/L) | Silica as $SiO_2$ (mg/L)[2] | Fe (mg/L) | Mn (mg/L) |
|---|---|---|---|---|---|---|---|---|---|---|---|---|---|---|
| H-6B | 05/81 | UNC | CuC | 59300 | 1.18 | 34 | | | 11 | 0.44 | 32 | 20 | | |
| H-6B | 09/85 | UNC | CuC | 57400 | 1.13 | 34 | 1.9 | 0.096 | 10 | 0.45 | 30 | 18 | 0.094 | 0.13 |
| H-6B | [3] | *avg* | CuC | | | *34* | *1.6* | *0.096* | *9.5* | *0.44* | *28* | | | |
| H-6B | [3] | rng | CuC | | | 34-35 | 1.3-1.9 | [1] | 7-11 | 0.44-0.45 | 24-32 | 18-43 | | |
| H-7B1 | 03/86 | UNC | CuB | 3220 | 0.089 | 0.57 | 1.5 | 0.052 | 0.76 | 0.10 | 8.5 | 47 | 0.056 | 0.050 |
| H-7B1 | [3] | *avg* | CuB | | | *0.57* | *1.4* | *0.052* | *0.77* | *0.11* | *7.7* | | | |
| H-7B1 | [3] | rng | CuB | | | [1] | 1.2-1.5 | [1] | 0.74-0.80 | 0.10-0.12 | 5.8-8.7 | 47-92 | | |
| H-8B | 01/86 | UNC | CuB | 2830 | 0.083 | 0.085 | 2.5 | 0.14 | 0.48 | 0.12 | 6.9 | 29 | 0.036 | 0.021 |
| H-8B | [2] | *avg* | CuB | | | *0.085* | *2.4* | *0.14* | *0.49* | *0.12* | *6.7* | | | |
| H-8B | [2] | rng | CuB | | | [1] | 2.1-2.5 | [1] | 0.48-0.50 | 0.12 | 5.9-7.4 | 29-56 | | |
| H-9B | 11/85 | UNC | CuB | 3080 | 0.087 | 0.24 | 3.3 | 0.11 | 0.63 | 0.18 | 7.5 | 27 | 0.032 | 0.015 |
| H-9B | [2] | *avg* | CuB | | | *0.24* | *3.0* | *0.11* | *0.66* | *0.18* | *7.2* | | | |
| H-9B | [2] | rng | CuB | | | [1] | 2.6-3.3 | [1] | 0.63-0.70 | 0.17-0.18 | 7.0-7.5 | 27-39 | | |
| H-11B3 | 06/85 | UNC | CuA | 117400 | 2.23 | 47 | | | 32 | 0.62 | 25 | | 0.14 | 0.22 |
| H-11B3 | [2] | *avg* | CuA | | | *48* | *1.3* | | *31* | *0.50* | *20* | | | |
| H-11B3 | [2] | rng | CuA | | | 47-48 | 1.0-1.6 | | 30-32 | 0.38-0.62 | 18-25 | 25-32 | | |
| H-12 | 08/85 | UNC | CuA | 140500 | 2.72 | 76 | | | 39 | 1.2 | 31 | 7.2 | 0.22 | 0.087 |
| H-12 | [2] | *avg* | CuA | | | *76* | *1.5* | | *38* | *0.85* | *29* | | | |
| H-12 | [2] | rng | CuA | | | 76-77 | 1.1-2.3 | | 35-39 | 0.61-1.2 | 18-38 | 7-96 | | |
| P-14 | 02/86 | UNC | CuC | 24900 | 0.58 | 72 | 1.7 | 0.42 | 0.72 | 0.28 | 51 | 30 | 2.0 | 0.18 |
| P-14 | [2] | *avg* | CuC | | | *72* | *1.5* | *0.42* | *0.72* | *0.28* | *50* | | | |
| P-14 | [2] | rng | CuC | | | [1] | 1.2-1.7 | [1] | [1] | [1] | 48-51 | 30-69 | | |

## Table 2-2. Concentrations of Solutes[1] in Groundwaters from the Rustler Formation, Dewey Lake Red Beds, and Bell Canyon Formation
## Part B: Minor and Trace Solutes, TDS, and Ionic Strength (Continued)

| Well(s) | Date[2] | Lab[3] | Zone[4] | TDS[7] (mg/L) | IS[6] (molal) | $Br^-$ (mg/L) | $F^-$ (mg/L) | $I^-$ (mg/L) | B (mg/L) | Li (mg/L) | Sr (mg/L) | Silica as $SiO_2$ (mg/L)[2] | Fe (mg/L) | Mn (mg/L) |
|---|---|---|---|---|---|---|---|---|---|---|---|---|---|---|
| P-17 | 03/86 | **UNC** | CuC | 86500 | 1.67 | 72 | 1.9 | 0.18 | 38 | 0.87 | 29 | 8.5 | 4.0 | 0.87 |
| P-17 | [2] | *avg* | CuC | | | *70* | *1.6* | *0.18* | *35* | *0.87* | *31* | | | |
| P-17 | [2] | rng | CuC | | | 69-72 | 1.2-1.9 | [1] | 32-38 | [1] | 28-36 | 0-8.5 | | |
| WIPP-13 | 02/87 | *avg* | CuC | | | *39* | *1.4* | | *11* | *0.35* | *25* | | | |
| WIPP-25 | 08/80 | **UNC** | CuC | 12100 | 0.26 | 2.6 | | | 1.5 | 0.20 | 12 | 34 | | |
| WIPP-25 | 08/80 | *avg* | CuC | | | *2.6* | | | *1.5* | *0.20* | *12* | | | |
| WIPP-25 | 08/80 | rng | CuC | | | [1] | | | [1] | [1] | [1] | [1] | | |
| WIPP-25 | 02/86 | **UNC** | CuC | 13600 | | 3.4 | 1.7 | 0.042 | 1.7 | 0.22 | 17 | 33 | 0.50 | 0.11 |
| WIPP-25 | 02/86 | *avg* | CuC | | | *3.8* | *1.6* | *0.042* | *1.7* | *0.22* | *17* | | | |
| WIPP-25 | 02/86 | rng | CuC | | | 3.4-4.2 | 1.6-1.7 | [1] | 1.7 | [1] | [1] | 33-67 | | |
| WIPP-26 | 08/80 | **UNC** | CuC | 15100 | 0.33 | 3.2 | | | 1.4 | 0.24 | 17 | 33 | | |
| WIPP-26 | 08/80 | *avg* | CuC | | | *3.2* | | | *1.4* | *0.24* | *17* | | | |
| WIPP-26 | 08/80 | rng | CuC | | | [1] | | | [1] | [1] | [1] | [1] | | |
| WIPP-26 | 11/85 | **UNC** | CuC | 17600 | 0.37 | 3.9 | 1.7 | 0.070 | 1.6 | 0.23 | 20 | 35 | 0.026 | <0.01 |
| WIPP-26 | 11/85 | *avg* | CuC | | | *3.9* | *1.5* | *0.070* | *1.6* | *0.23* | *18* | | | |
| WIPP-26 | 11/85 | rng | CuC | | | [1] | 1.3-1.7 | [1] | [1] | [1] | 17-20 | 35-65 | | |
| WIPP-27 | 09/80 | **UNC** | CuD | 134700 | 2.57 | 28 | | | 2.3 | 0.33 | 51 | 23 | | |
| WIPP-27 | [2] | *avg* | CuD | | | *28* | | | *2.1* | *0.33* | *51* | | | |
| WIPP-27 | [2] | rng | CuD | | | [1] | | | 1.9-2.3 | [1] | [1] | 13-23 | | |

**Table 2-2. Concentrations of Solutes[1] in Groundwaters from the Rustler Formation, Dewey Lake Red Beds, and Bell Canyon Formation**
**Part B: Minor and Trace Solutes, TDS, and Ionic Strength (Continued)**

| Well(s) | Date[2] | Lab[3] | Zone[4] | TDS[7] (mg/L) | IS[6] (molal) | $Br^-$ (mg/L) | $F^-$ (mg/L) | $I^-$ (mg/L) | B (mg/L) | Li (mg/L) | Sr (mg/L) | Silica as $SiO_2$ (mg/L)[2] | Fe (mg/L) | Mn (mg/L) |
|---|---|---|---|---|---|---|---|---|---|---|---|---|---|---|
| WIPP-28 | 09/80 | UNC | CuC | 46600 | 0.90 | 7.2 | | | 5.8 | 0.30 | 16 | 36 | | |
| WIPP-28 | 09/80 | *avg* | CuC | | | *7.2* | | | *5.8* | *0.30* | *16* | | | |
| WIPP-28 | 09/80 | rng | CuC | | | [1] | | | [1] | [1] | [1] | [1] | | |
| WIPP-29 | 08/80 | UNC | CuD | 245400 | 4.91 | 45 | | | 4.4 | 0.78 | 29 | 22 | | |
| WIPP-29 | 08/80 | *avg* | CuD | | | *45* | | | *4.4* | *0.78* | *29* | | | |
| WIPP-29 | 08/80 | rng | CuD | | | [1] | | | [1] | [1] | [1] | [1] | | |
| WIPP-29 | 12/85 | UNC | CuD | 324100 | 6.57 | 61 | 4.6 | 0.38 | 5.2 | 0.70 | 13 | 15 | 1.1 | 1.7 |
| WIPP-29 | 12/85 | *avg* | CuD | | | *61* | | *0.38* | *5.5* | *0.70* | *11* | | | |
| WIPP-29 | 12/85 | rng | CuD | | | [1] | 0.9-4.6 | [1] | 5.2-5.8 | [1] | 9-13 | 15-110 | | |
| WIPP-30 | 09/80 | UNC | CuC | 29100 | 0.58 | 10 | | | 6.1 | 0.27 | 18 | 6.5 | | |
| WIPP-30 | 09/80 | *avg* | CuC | | | *10* | | | *6.1* | *0.27* | *18* | | | |
| WIPP-30 | 09/80 | rng | CuC | | | [1] | | | [1] | [1] | [1] | [1] | | |
| Engle | 03/85 | UNC | CuB | 3270 | 0.09 | 0.27 | 2.8 | 0.12 | 0.97 | 0.17 | 8.4 | 29 | 0.59 | 0.060 |
| Engle | 03/85 | *avg* | CuB | | | *0.27* | *2.8* | *0.12* | *0.87* | *0.17* | *7.7* | | | |
| Engle | 03/85 | rng | CuB | | | [1] | 2.8-2.9 | [1] | 0.77-0.97 | [1] | 7.0-8.5 | 29-54 | | |
| H-3B1 | 07/85 | UNC | Mag | 8560 | | 5.8 | 2.4 | 1.2 | 2.0 | 0.32 | 17 | 10 | 0.11 | 0.028 |
| H-3B1 | [3] | rng | Mag | | | 5.8-6.0 | 1.8-2.6 | 1.2-2.0 | 2.0-4.5 | 0.32 | 13-18 | 10-26 | | |

## Table 2-2. Concentrations of Solutes[1] in Groundwaters from the Rustler Formation, Dewey Lake Red Beds, and Bell Canyon Formation
## Part B: Minor and Trace Solutes, TDS, and Ionic Strength (Continued)

| Well(s) | Date[2] | Lab[3] | Zone[4] | TDS[7] (mg/L) | IS[6] (molal) | $Br^-$ (mg/L) | $F^-$ (mg/L) | $I^-$ (mg/L) | B (mg/L) | Li (mg/L) | Sr (mg/L) | Silica as $SiO_2$ (mg/L)[2] | Fe (mg/L) | Mn (mg/L) |
|---|---|---|---|---|---|---|---|---|---|---|---|---|---|---|
| H-4C | 11/86 | UNC | Mag | 23900 | | 5.9 | 2.4 | 0.31 | 12 | 0.46 | 12 | 9.1 | 0.71 | 0.29 |
| H-4C | [2] | rng | Mag | | | 5.9-7.5 | 2.2-2.6 | [1] | 11-12 | 0.41-0.46 | 12-14 | 9-26 | | |
| H-5C | 10/86 | UNC | Mag | 6980 | | 0.93 | 2.5 | 0.31 | 11 | 0.20 | 10 | 11 | 1.5 | 0.020 |
| H-5C | 10/86 | rng | Mag | | | [1] | 2.5 | [1] | 10-11 | 0.20 | 8-10 | 11-26 | | |
| H-6C | 10/86 | UNC | Mag | 4540 | | 2.3 | 1.5 | 0.086 | 2.2 | 0.21 | 9.8 | 11 | 0.26 | 0.010 |
| H-6C | 10/86 | rng | Mag | | | 1.0-2.3 | 1.5-1.7 | [1] | 2.2-2.4 | 0.19-0.21 | 7.1-9.8 | 11-28 | | |
| WIPP-25 | 09/80 | UNC | Mag | 11900 | | 2.5 | | | 1.5 | 0.20 | 12 | 33 | | |
| WIPP-27 | 09/80 | UNC | Mag | 145700 | | 28 | | | 2.3 | 0.34 | 59 | 30 | | |
| WIPP-25 | 07/80 | UNC | R/S | 334400 | | 51 | | | 41 | 1.6 | 11 | 4.0 | | |
| WIPP-26 | 07/80 | UNC | R/S | 188400 | | 19 | | | 32 | 1.2 | 27 | 6.2 | | |
| WIPP-28 | 07/80 | UNC | R/S | 277100 | | 29 | | | 46 | 1.8 | 12 | 7.8 | | |
| WIPP-29 | 07/80 | UNC | R/S | 111000 | | 12 | | | 20 | 1.3 | 21 | 15 | | |
| WIPP-30 | 07/80 | UNC | R/S | 325900 | | 78 | | | 82 | 0.72 | 18 | 5.5 | | |
| Ranch | 06/86 | UNC | DL | 2520 | | 2.3 | 0.82 | 0.13 | 0.10 | 0.12 | 5.9 | 52 | 0.024 | <0.01 |
| Ranch | 06/86 | rng | DL | | | 2.3 | 0.8-1.0 | [1] | 0.10-0.19 | [1] | 3.2-5.9 | 52-86 | | |

## Table 2-2. Concentrations of Solutes[1] in Groundwaters from the Rustler Formation, Dewey Lake Red Beds, and Bell Canyon Formation
## Part B: Minor and Trace Solutes, TDS, and Ionic Strength (Continued)

| Well(s) | Date[2] | Lab[3] | Zone[4] | TDS[7] (mg/L) | IS[6] (molal) | $Br^-$ (mg/L) | $F^-$ (mg/L) | $I^-$ (mg/L) | B (mg/L) | Li (mg/L) | Sr (mg/L) | Silica as $SiO_2$ (mg/L)[2] | Fe (mg/L) | Mn (mg/L) |
|---|---|---|---|---|---|---|---|---|---|---|---|---|---|---|
| Twin-Pasture | 01/86 | UNC | DL | 401 | | 0.17 | 0.58 | <0.01 | 0.13 | <0.05 | 1.1 | 47 | <0.01 | <0.01 |
| Twin-Pasture | 01/86 | rng | DL | | | [1] | 0.5-1.4 | [1] | 0.13-0.16 | [1] | 0.6-1.1 | 47-90 | | |
| DOE-2 | 07/85 | UNC | BC | 149500 | | 250 | 1.1 | 6.4 | 54 | 5.8 | 150 | 2.5 | 11 | 28 |
| DOE-2 | 07/85 | rng | BC | | | [1] | 0.4-1.4 | 6.4-7.9 | 54-61 | 2.8-5.8 | 150-300 | 2-30 | | |

1. Solute values from various laboratories have been rounded as follows.
   - Na, K, Ca, Mg, $Cl^-$, $SO_4^{2-}$ from UNC : 3 significant figures
   - all other solutes from UNC, all "avg" values, all alkalinity values : 2 sig. figs.
   - all minimum "rng" values : down to 2 sig. figs.
   - all maximum "rng" values : up to 2 sig. figs.
   - all TDS : to nearest 100 mg/L or to 3 sig. figs. (for TDS<10000)
   - all pH values : to 0.1 pH unit
   - all $pCO_2$ values : to 0.01 unit
   - all ionic-strength values : to 0.01 molal

2. The date on which samples were collected. In the "date" column, a number in square brackets indicates that values in the same row are averages or ranges of data for samples collected on that number of dates.

3. avg: average of one or more values from one or more laboratories. These values were used to calculate element ratios and generate contour plots. Values are shown in *italics*.
   rng: range of values from one or more laboratories. The values give crude estimates of the uncertainties associated with the data. A single value means that all values were identical. A "[1]" means that only one reliable value was available (and is listed in the UNC row).

## Table 2-2. Concentrations of Solutes[1] in Groundwaters from the Rustler Formation, Dewey Lake Red Beds, and Bell Canyon Formation
## Part B: Minor and Trace Solutes, TDS, and Ionic Strength (Continued)

UNC: UNC Geotech (formerly, Bendix Field Engineering Corp.), Grand Junction, CO. These data were used in calculations of saturation indices, in factor-analysis calculations, and to generate Piper diagrams. Values are emboldened.

4. The stratigraphic zone and, within the Culebra, the hydrochemical facies (as defined in this work).
   CuA, CuB, CuC, CuD: Culebra dolomite, hydrochemical facies -- Zone A, Zone B, Zone C, Zone D, respectively.
   Mag: Magenta Dolomite
   R/S: Rustler/Salado contact zone
   DL : Dewey Lake Red Beds
   BC : Bell Canyon Formation

5. Alkalinity values and pH values were measured in the field when the samples were collected. (Exception: alkalinity in the DOE-2 Bell Canyon sample was measured in the laboratory.)

6. $pCO_2$ and ionic strength (IS) were calculated using PHRQPITZ. See the text for details.

7. Concentration of TDS, calculated by summing the concentrations of major solutes.

When available, samples from the WQSP were used in this study. Many of the WQSP samples have been analyzed by up to three different laboratories, and the results are amenable to interlaboratory comparisons. In general, most of the major, minor, and trace solute data from UNC Geotech are considered reliable and are used as reference values. Similarly, most of the data from the NMBM&MR are acceptable. Some of the ITAS data from Round 1 of the WQSP are suspect, based on poor charge balance and lack of agreement with the other laboratories. However, the ITAS data from Rounds 2 and 3 of the WQSP seem to be generally acceptable. Some of the USGS (Central Labs) data, especially some potassium analyses, are also suspect.

The evaluation of minor and trace solute data is preliminary, and the values are not considered as reliable as those for the major elements. For some minor and trace solutes, none of the available data is considered reliable at this time. For example, as discussed above, iron concentrations may be controlled by pipe corrosion; other minor or trace elements that may adsorb onto colloids, such as manganese, are also suspect. Although the silica data are considered in some detail in this work, the silica concentrations may be affected by precipitation of a colloidal Fe-Si floc after sample collection.

Table 2-3 identifies wells in which concentrations of major solutes in Culebra groundwaters have changed during the sampling period (1976 to 1987) and wells from which the samples are otherwise suspect. Changes in the Culebra-water composition at WIPP-29 appear to be related to contamination from nearby potash-refining operations. The causes for the changes in the water chemistry at the other wells are not understood at this time.

#### 2.2.3.2 Alkalinity, pH, and $pCO_2$

There are several potential sources of error associated with characterization of the carbonate systems of these waters. These sources include loss of $CO_2$ gas during sample collection, inaccurate pH measurements due to the high ionic strengths of the brines, and inaccuracies in the alkalinity measurements.

## Table 2-3. Wells in Which Culebra Groundwater Compositions Have Changed with Time or for Which Compositions Are Otherwise Suspect

| Hydropad or Well | Remarks |
|---|---|
| DOE-2 | Alkalinity was 67 mg/L $HCO_3^-$ in 3/85 (WQSP round 1) and was 150 mg/L $HCO_3^-$ in 8/86 (WQSP round 2). The increase occurred because the hole was acidized in 1985 (Saulnier et al., 1987). |
| H-2 | Na and Cl are changing with time, although the other major solutes have remained fairly constant. Field chloride values did not reach steady-state during round 1 of the WQSP, and the chloride value measured during round 2 was lower yet. This change in NaCl is not understood at this time. The representativeness of all samples from the Culebra at H-2 is questioned. |
| H-5 | The alkalinity at H-5B was 80 mg/L $HCO_3^-$ in 6/81 and at H-5C was 86 mg/L in 10/81. In 8/85 (WQSP round 1), the alkalinity at H-5B had decreased to 50 mg/L and it remained the same in 5/86 (WQSP round 2). The decrease is thought to be due to the purging of contaminants. |
| WIPP-25 | Between 8/80 (Sandia sampling program) and 2/86 (WQSP round 1) the concentrations of several solutes, notably Ca and Cl (and to a lesser extent Na and Mg), increased significantly. Between 2/86 (WQSP round 1) and 4/87 (WQSP round 2), these concentrations did not change. Also, between 8/80 and 2/86 the alkalinity decreased from 210 to 130 mg/L $HCO_3^-$; it remained at 130 mg/L in 4/87. The change in major solutes is not understood at this time. The decrease in alkalinity is probably due to the purging of contaminants. |

## Table 2-3. Wells in Which Culebra Groundwater Compositions Have Changed with Time or for Which Compositions Are Otherwise Suspect (Continued)

| Hydropad or Well | Remarks |
|---|---|
| WIPP-26 | Between 8/80 (Sandia sampling program) and 11/85 (WQSP round 1), the concentrations of several solutes, notably Na, K, and Cl (and to a lesser extent Ca and Mg), increased significantly. Between 11/85 (WQSP round 1) and 4/87 (WQSP round 2), the values of the solutes decreased to concentrations similar to or lower than those observed in 1980. Also, between 8/80 and 11/85 the alkalinity decreased slightly from 140 to 120 mg/L $HCO_3^-$; it was 110 mg/L in 4/87 (not significantly different from the 11/85 value). The changes in major solutes are not understood at this time. The slight decrease in alkalinity may be due to the purging of contaminants. |
| WIPP-27 | Although WIPP-27 was sampled only in 1980 (by both the USGS and Sandia), the solute relationships indicate that potash-mining activities have affected the groundwater quality at this location. Thus, there is no reason to believe that the 1980 samples are representative of unperturbed native groundwater at this location. |
| WIPP-28 | WIPP-28 was sampled in 9/80 by Sandia. Although the samples are considered representative with respect to most solutes, the alkalinity value measured in the field is <u>not</u> considered representative. During a four-day pumping test, the alkalinity values decreased slowly but steadily; alkalinity had <u>not</u> reached a steady-state value when final samples were collected and the test was terminated. Therefore, the final alkalinity value of 350 mg/L $HCO_3^-$ is considered an upper limit. |

**Table 2-3. Wells in Which Culebra Groundwater Compositions Have Changed with Time or for Which Compositions Are Otherwise Suspect (Continued)**

| Hydropad or Well | Remarks |
|---|---|
| WIPP-29 | Between 8/80 (Sandia sampling program) and 12/85 (WQSP round 1), the concentrations of several solutes, notably Na, K, Cl, and $SO_4$, increased and the concentration of Ca decreased significantly. Between 12/85 (WQSP round 1) and 3/87 (WQSP round 2), the values of the solutes changed again. Also, between 8/80 and 12/85 the alkalinity decreased from 210 to 160 mg/L $HCO_3^-$; it remained at 160 mg/L in 3/87. The changes in major solutes are attributed to potash-refining activities in the area. The decrease in alkalinity is probably due to the purging of contaminants. |

Loss of $CO_2$ Gas

Effervescence of the water samples during collection has been commonly observed and recorded in field notes from various water sampling programs listed in Table 2-1. The effervescence may be due to the loss of $CO_2$ gas in response to changes in the confining pressure and temperature experienced by the water sample during collection, or it may be due to the release of air introduced into the sample during pumping. If the former process is responsible, then the field pH measurements and calculated $pCO_2$ values may be in error, as discussed in Section 2.3.4.4. Unfortunately, because the presence or absence of effervescence was not always recorded in the field notes, no assessment of the ubiquitousness or importance of this effect can be made at this time.

Inaccurate pH Measurements

The accuracy and precision of pH measurements, independent of the effect of $CO_2$ loss, cannot be assessed at this time because there are insufficient data. The pH is a measure of the activity of a single ion, $H^+$; individual pH values only have meaning in a relative sense with reference to a particular activity scale. Problems associated with the interpretation of pH in saline waters have been summarized by workers interested in the measurement of pH in seawater (Plummer and Sundquist, 1982; Plummer et al., 1988; Bates, 1975; Bates and Culberson, 1977). Potential sources of error include liquid junction potential effects and inconsistencies among the activity scales of the buffer solutions, measured pH, and aqueous chemical speciation model.

Inaccurate Alkalinity Measurements

For the groundwaters discussed in this chapter, alkalinity (the ability of a solution to neutralize a standard acid) is assumed to be due only to bicarbonate and carbonate. The low concentrations of boron, silica, and organic carbon in these waters (cf. Table 2-2; Myers et al., Chapter 6) suggest that errors due to the contribution of noncarbonate species to the total alkalinity are probably not appreciable in these waters. However, this assumption is not correct for all waters of interest to the WIPP Project, such as certain intergranular fluids in the Salado Formation or some brines from the Castile Formation.

Although the accuracy cannot be estimated, the precision of the (bi)carbonate alkalinity determinations is probably plus or minus several mg/L $HCO_3^-$ at the 95% confidence level. The loss of $CO_2$ will not affect the alkalinity appreciably. Field measurements of alkalinity are generally made within several minutes of sample collection and are used as reference values. Results of alkalinity measurements made in laboratories are very close to field values, suggesting little change over periods of weeks to months.

The Culebra groundwater in several wells, however, may have been contaminated with modern organic carbon during the drilling process (cf. Lambert, Chapter 5). These organics were apparently metabolized by bacteria, leading to high alkalinities. For example, the samples from H-5 collected in 1981 were contaminated with modern carbon (Lambert, 1987); by 1985, the alkalinity had dropped by a factor of two. At WIPP-25, the alkalinity was 170 mg/L $HCO_3^-$ in 1980 and dropped to 110 mg/L $HCO_3^-$ by 1986. Thus, even if a measurement is accurate, it may represent a transient value due to recent contamination. If carbon-isotope data are not available, or if the available carbon-isotope data cannot be used to conclusively identify contamination, multiple sets of serial samples must be collected over several years to determine if transient effects are present.

The accuracy of measurements of parameters in the carbonate system is of particular concern for a nuclear-waste repository associated with a dolomite aquifer. Values for the pH, carbonate alkalinity, and $pCO_2$ are used in calculations of saturation indices of dolomite ($CaMg(CO_3)_2$) and calcite ($CaCO_3$) and in calculations of the speciation of actinides such as americium, neptunium, and plutonium for which carbonate complexation may be important (Bidoglio et al., 1985; Bidoglio et al., 1987; Tien et al., 1985). For this reason, the significance of the uncertainties in the pH measurements is discussed in Section 2.3.4.4.

# 2.3 SOLUTE RELATIONSHIPS IN WATERS IN THE RUSTLER FORMATION AND RELATED ROCKS

## 2.3.1 Spatial Distributions of Solutes in Culebra Groundwaters

### 2.3.1.1 Introduction

The spatial distributions of selected elements and elemental ratios in Culebra groundwaters have been examined to understand the geochemical and hydrologic processes occurring within the unit. Average concentrations for 13 solutes and element ratios for several pairs of solutes in water samples from the Culebra in 21 wells were calculated as

described below. The spatial distributions of eight solutes and four element ratios were contoured.

The sets of data examined were described in Section 2.2. The solutes considered were calcium, magnesium, sodium, potassium, chloride, sulfate, bromide, fluoride, iodide, boron, lithium, strontium, and silica. Samples from Well H-2A were excluded from consideration because the representativeness of those samples is questioned (see Table 2-3). Other samples of questionable quality (for example, from WIPP-25 and WIPP-26) were included because changes at those wells have been less drastic.

The average values given in Table 2-2 were calculated using the laboratory (UNC, ITAS, NMBM&MR, and USGS) and field data that the authors considered reliable at the time these spatial-distribution studies were being completed (late 1987). Because more recent WQSP data may indicate that some values rejected as outliers are, in fact, reasonable (within acceptable analytical variation), or that some values that appeared reasonable are, in fact, in error, these average values should not be viewed as "recommended" or even "best available" values. Because the silica results from the UNC and ITAS laboratories differed widely, average concentrations for silica were not calculated; rather, the ITAS data were used for the contouring study. Element ratios for several solute pairs--Na/Cl, K/Na, Mg/Ca, and Cl/Br--were calculated using the average values from Table 2-2.

The spatial distributions of the elements and element ratios were contoured on base maps of the WIPP area using the SURFER software package developed by Golden Software, Inc. The contours are produced in a two-stage process. First, a regularly spaced grid is created from the irregularly spaced input data. Then, the file containing the regularly spaced interpolated values is used as input to the contouring routine. Adjustable parameters include grid size, radius of influence, method of interpolation, smoothing factor, and contour interval. The plots presented below employ a kriging technique to generate the regularly spaced grid (Golden Software, Inc., 1987).

Twenty-one wells were part of this investigation. Data from WIPP-29 and in some cases WIPP-27 were not included in contours drawn in Figures 2-2 through 2-12. Figures 2-13 through 2-16 include the data from WIPP-27 and WIPP-29 and are drawn on a coarser contour interval. In Figures 2-2 to 2-16, the concentration (or ratio) at each well is also given; the concentrations are the "average" values given in Table 2-2. The location of the four-mile zone is indicated for reference. Because the location of each contour is influenced by several data points, there may be discrepancies between the placement of contour lines and the concentrations at some well locations. Descriptions of the spatial distributions of the major solutes, Na/Cl ratios, Cl/Br ratios, silica concentrations, the apparent anomalies at P-14, and the apparent anomalies at WIPP-27 and WIPP-29 are discussed below. Because the concentrations of several solutes (B, Li, F) and the element ratios of several solute pairs (Sr/Ca, several trace-solute/Cl pairs) were either uniform over the site or varied randomly, these solutes and element ratios are not discussed in this section.

### 2.3.1.2 Major Solutes

Regional variations in the concentrations of major solutes have been plotted in Figures 2-2, 2-3, and 2-4, which show contours of the distributions of Na, K, and Mg, respectively. This pattern is also representative of the distributions of Cl, TDS, and fluid density. The patterns show lower concentrations of these dissolved constituents in the southern and southwestern areas (H-7B, H-8B, H-9B, and Engle) compared to higher concentrations in the northern and eastern parts of the study area. Within the four-mile zone, the concentrations of the solutes decrease from east to west. The distribution of Mg/Ca weight ratios (Figure 2-5) shows a similar pattern; the ratio increases from approximately 0.3 in the south and west to a value of 1.3 in the eastern part of the region.

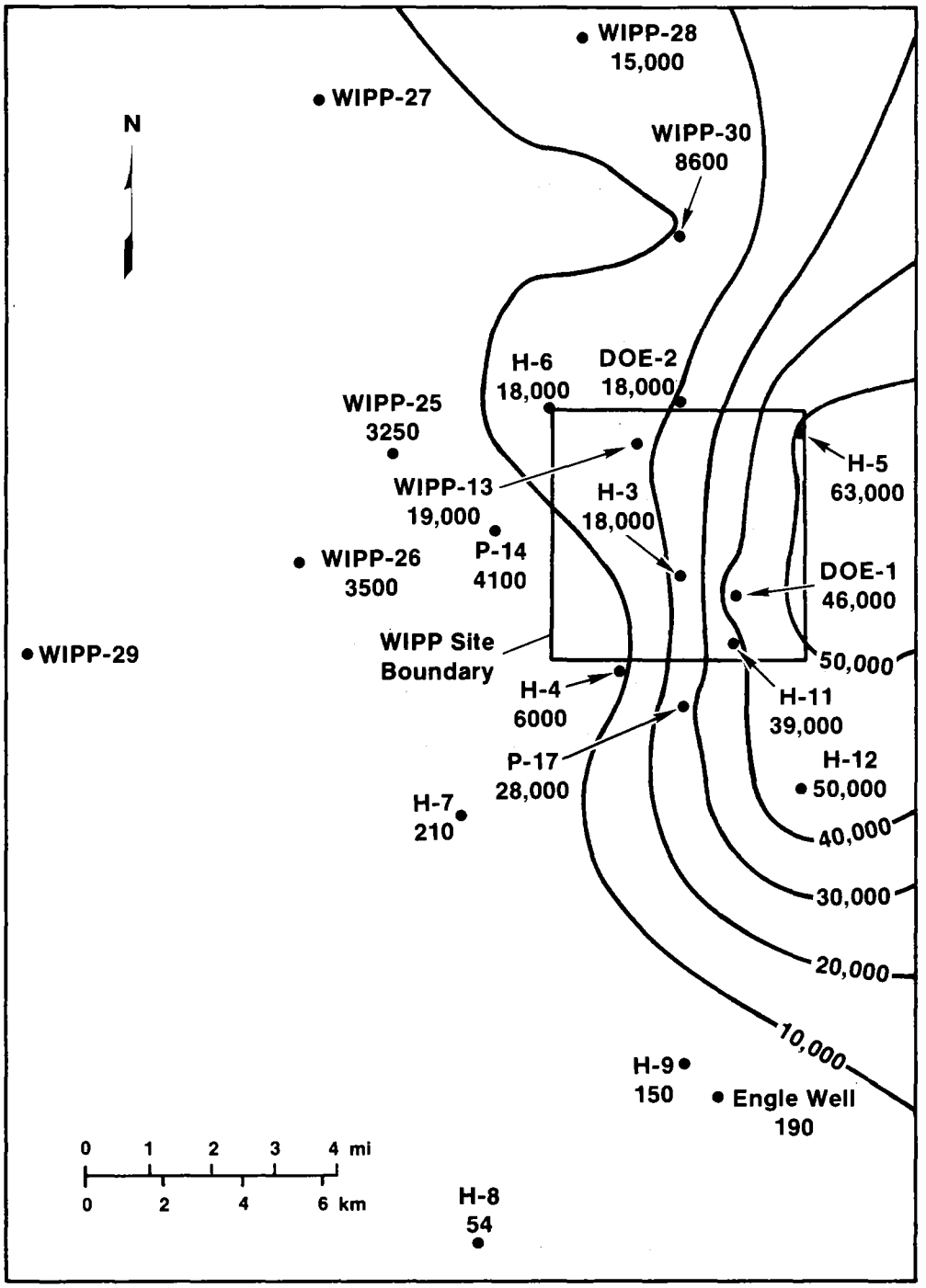


Figure 2-2. Contour plot of sodium concentrations (mg/L) in Culebra groundwaters.

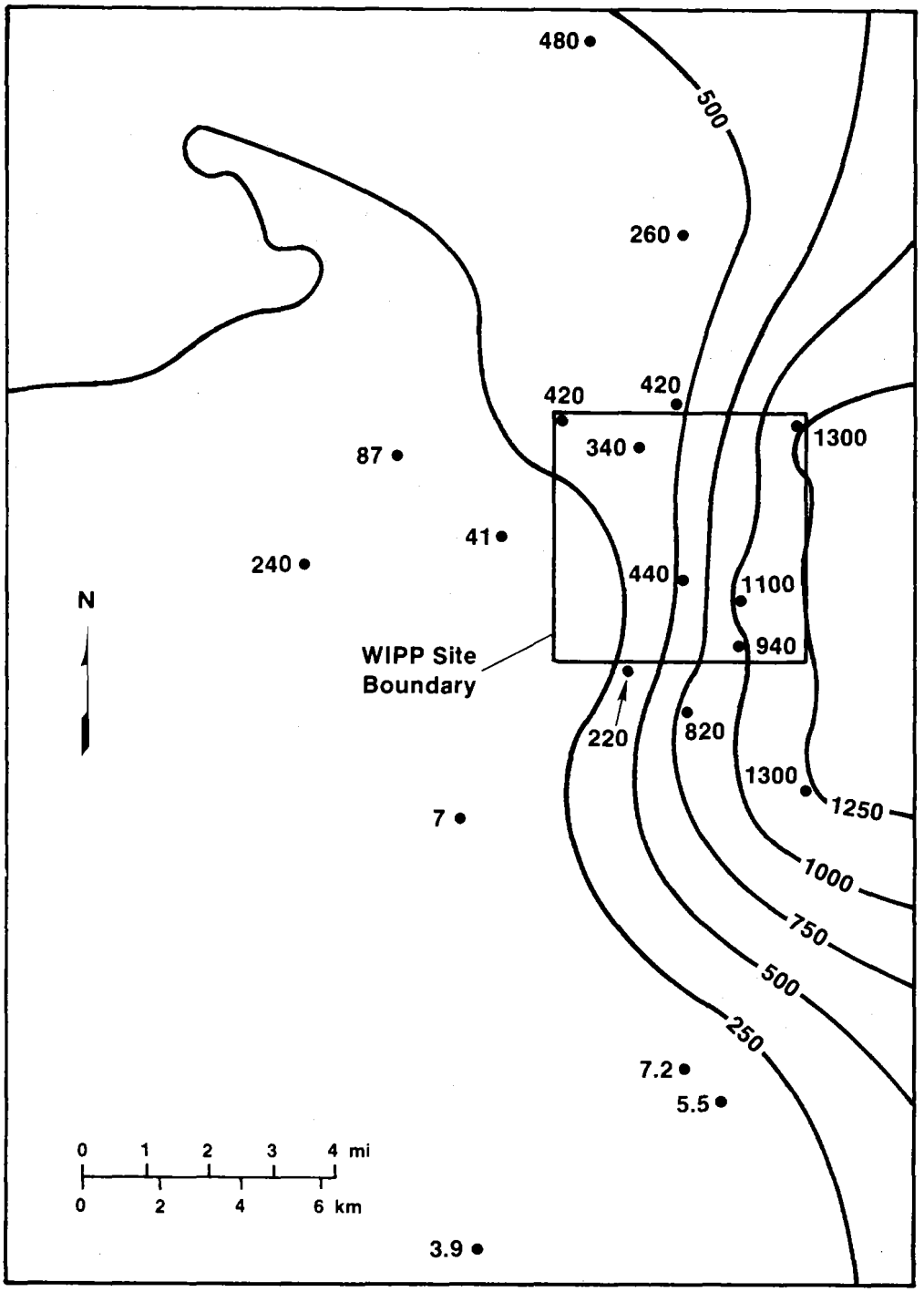


Figure 2-3. Contour plot of potassium concentrations (mg/L) in Culebra groundwaters.

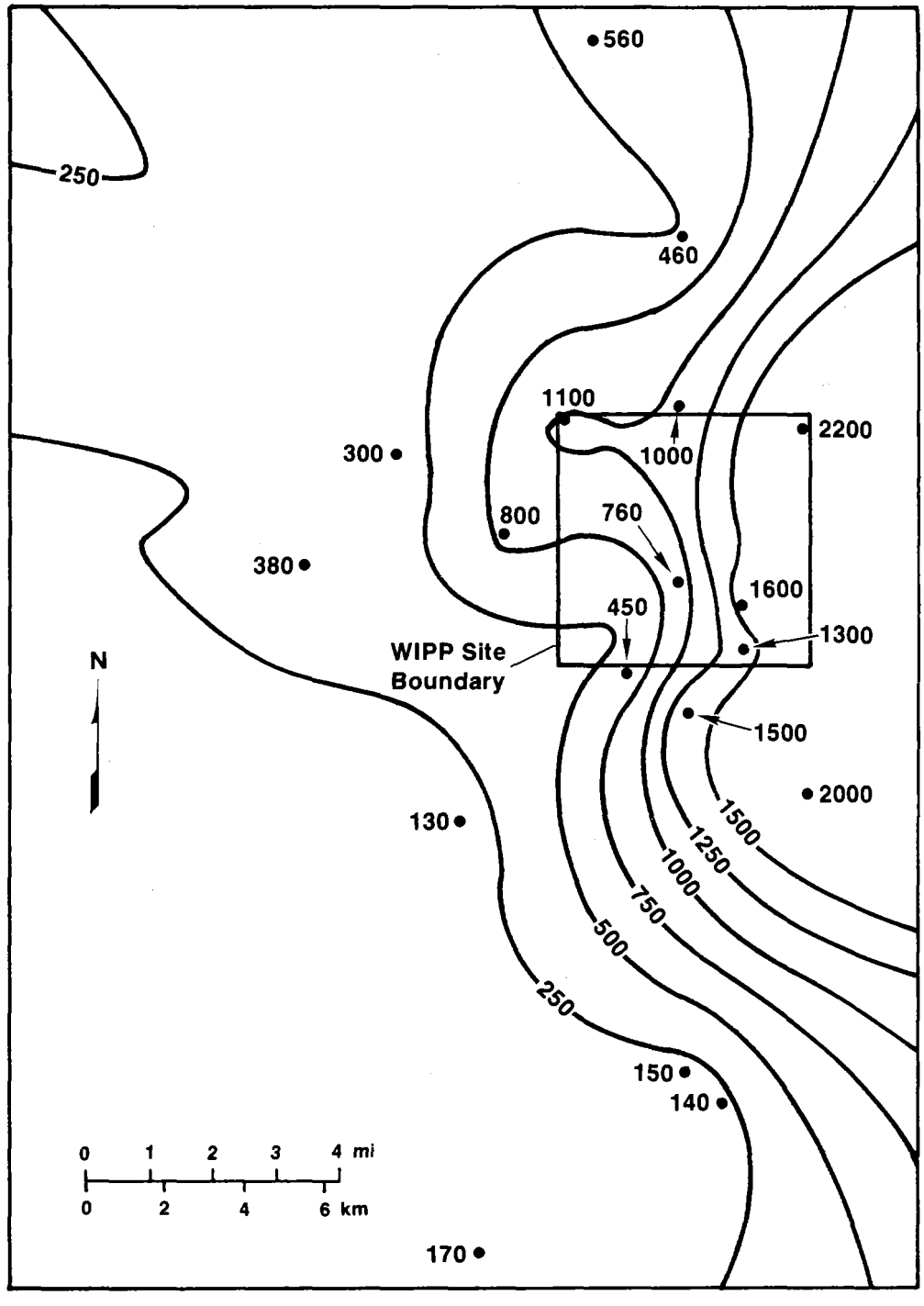


Figure 2-4. Contour plot of magnesium concentrations (mg/L) in Culebra groundwaters.

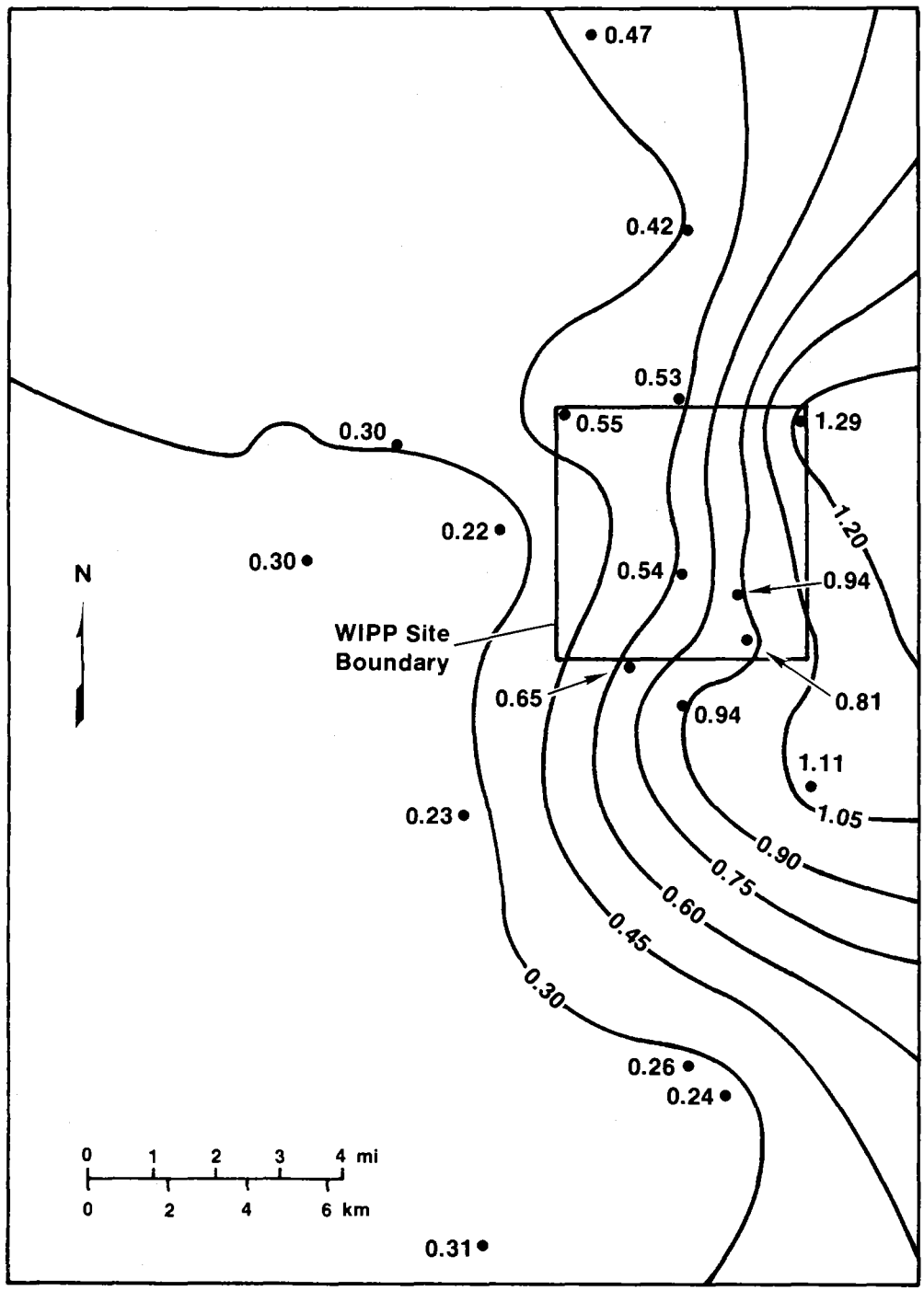


Figure 2-5. Contour plot of Mg/Ca weight ratios ([mg/L]/[mg/L]) in Culebra groundwaters.

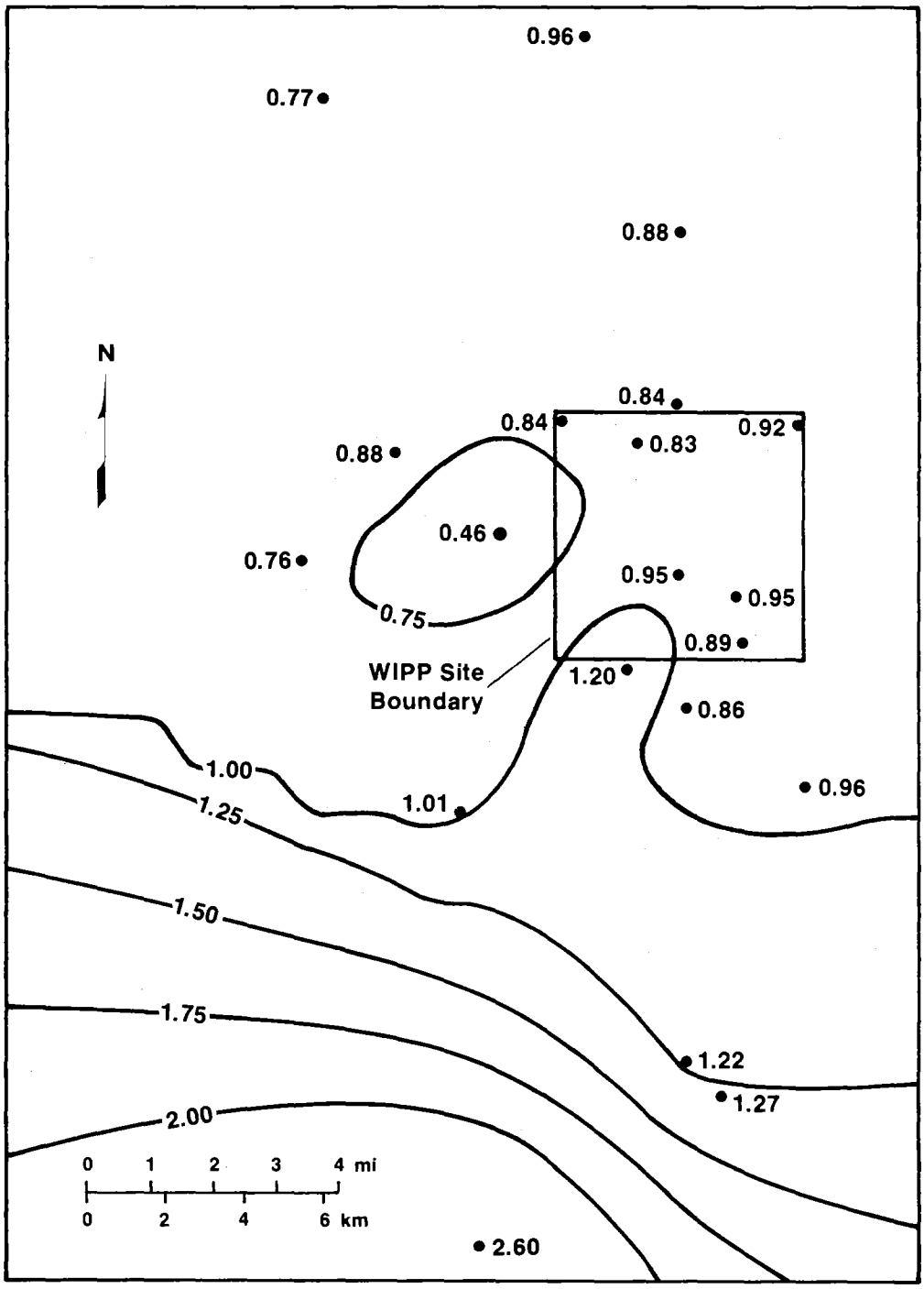


Figure 2-6. Contour plot of Na/Cl molar ratios ([mol/L]/[mol/L]) in Culebra groundwaters.

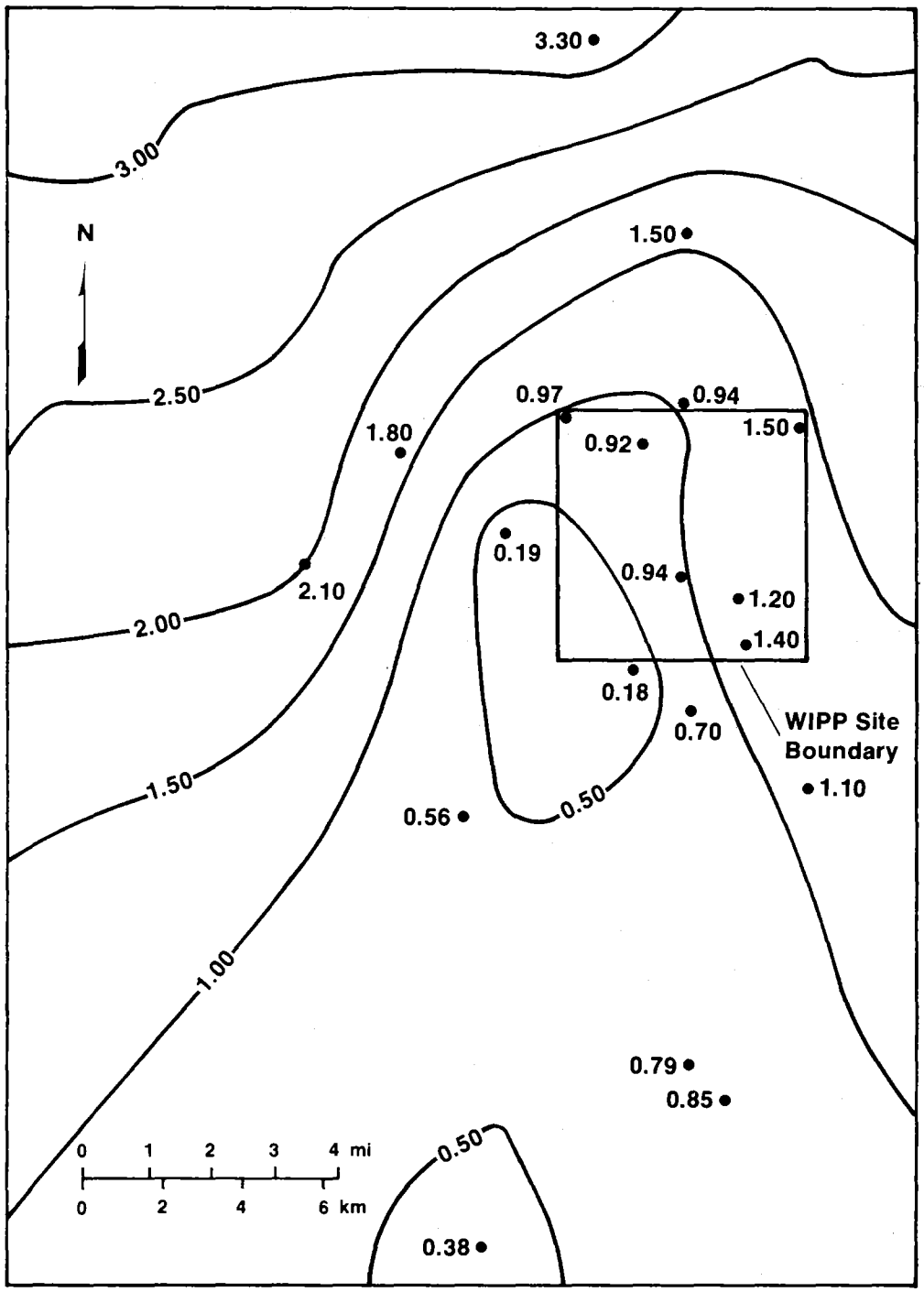


Figure 2-7. Contour plot of Cl/Br weight ratios ([g/L]/[mg/L]) in Culebra groundwaters.

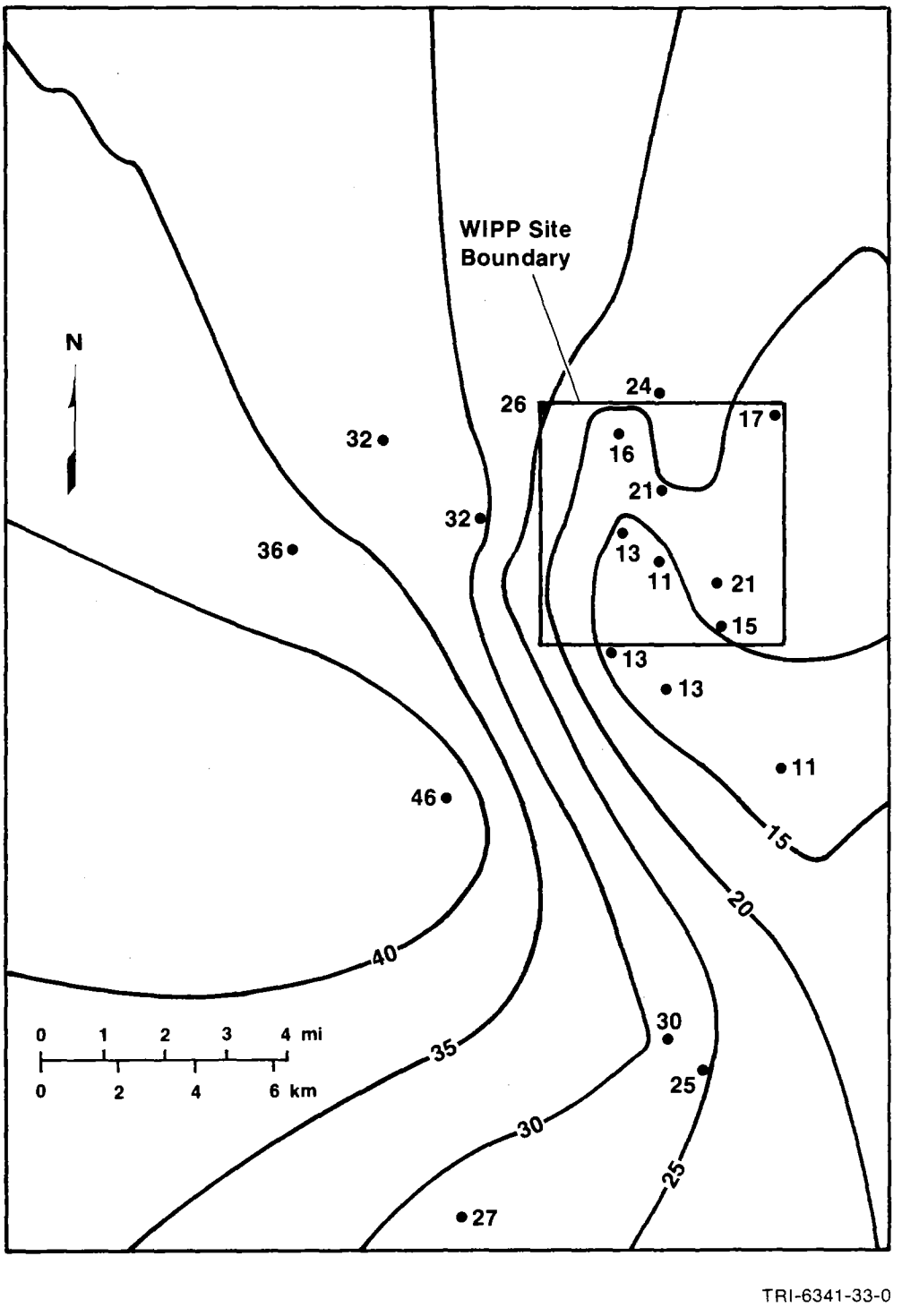


Figure 2-8. Contour plot of silica concentrations (mg/L as $SiO_2$) in Culebra groundwaters.

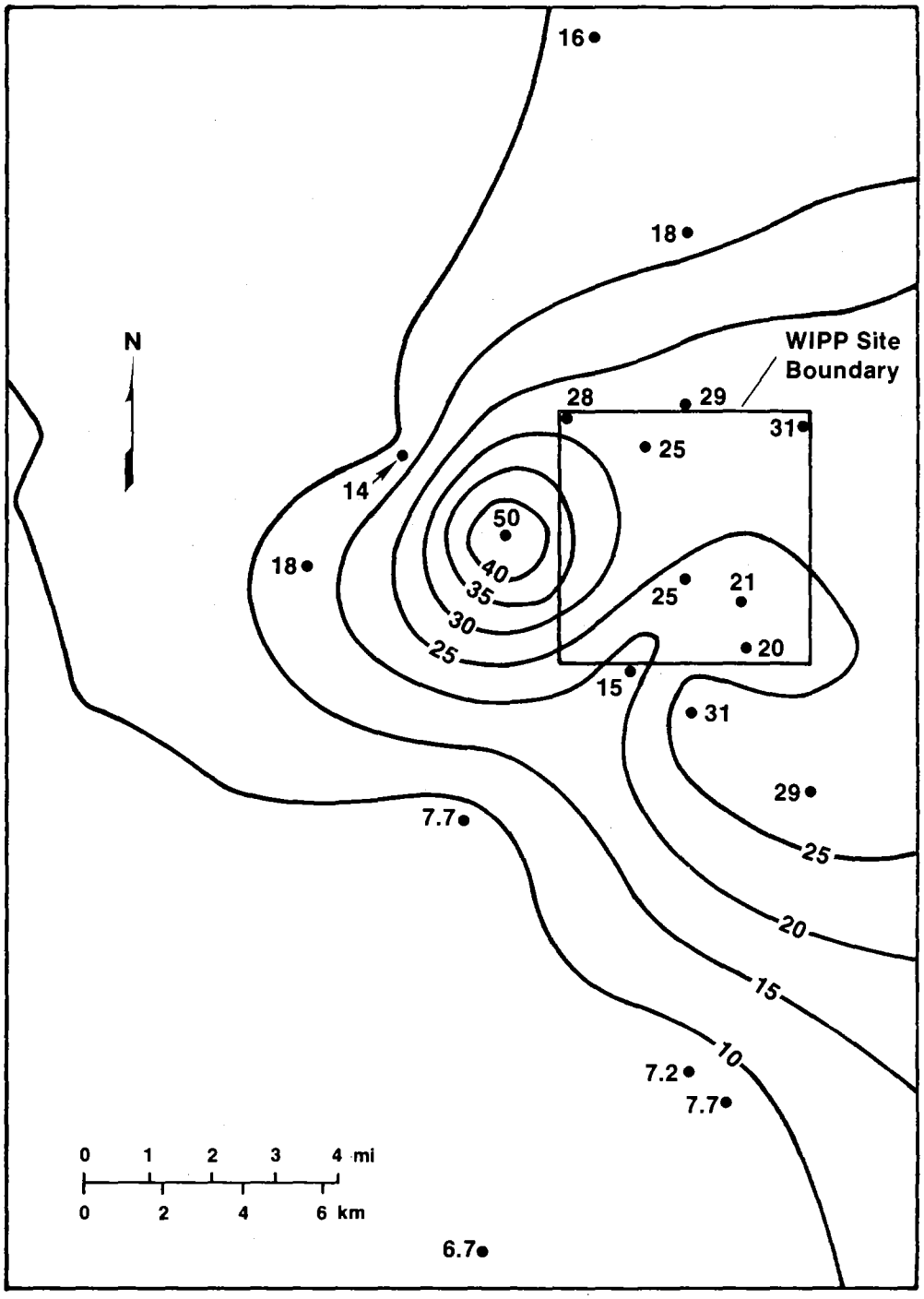


Figure 2-9. Contour plot of strontium concentrations (mg/L) in Culebra groundwaters.

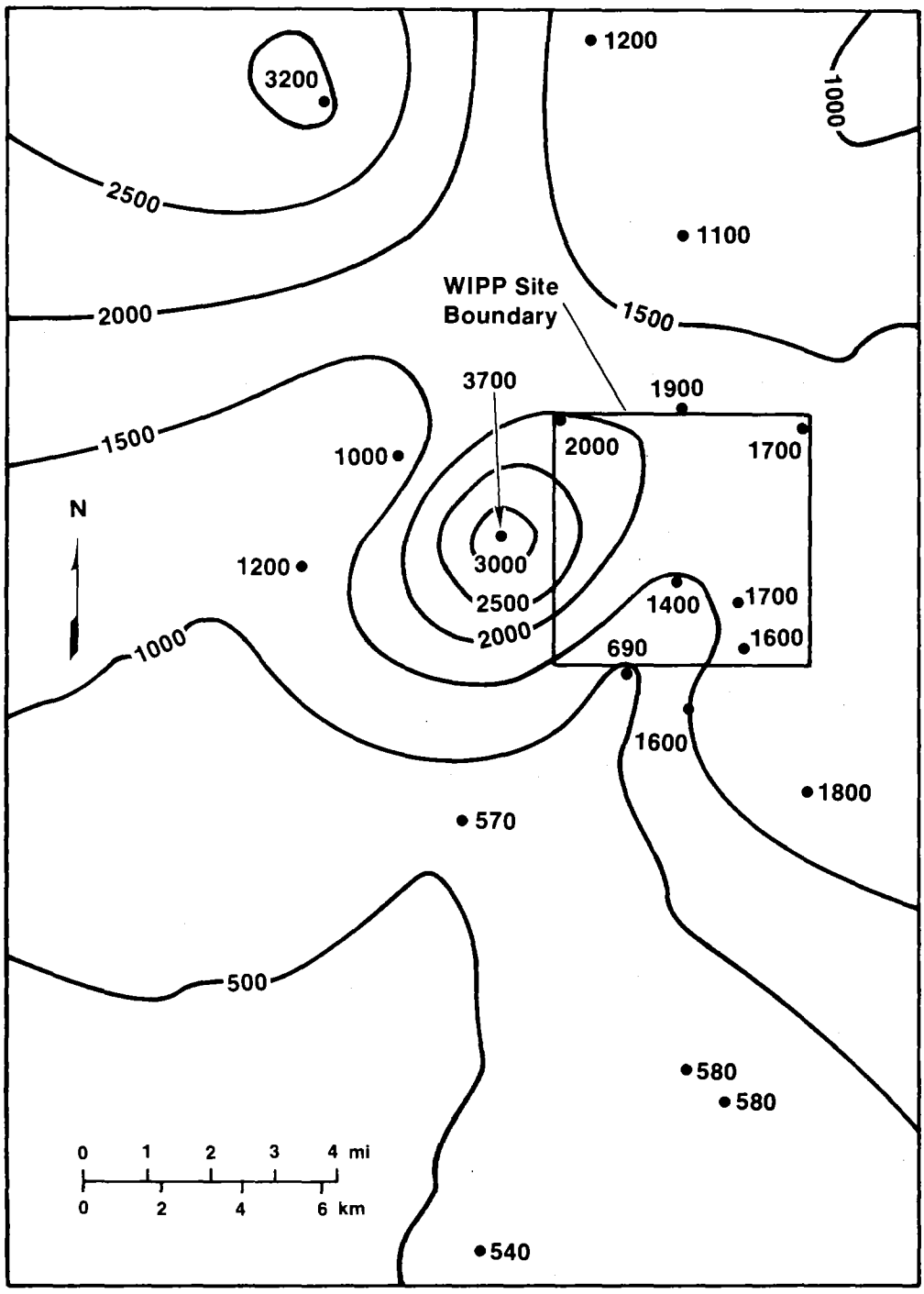


Figure 2-10. Contour plot of calcium concentrations (mg/L) in Culebra groundwaters.

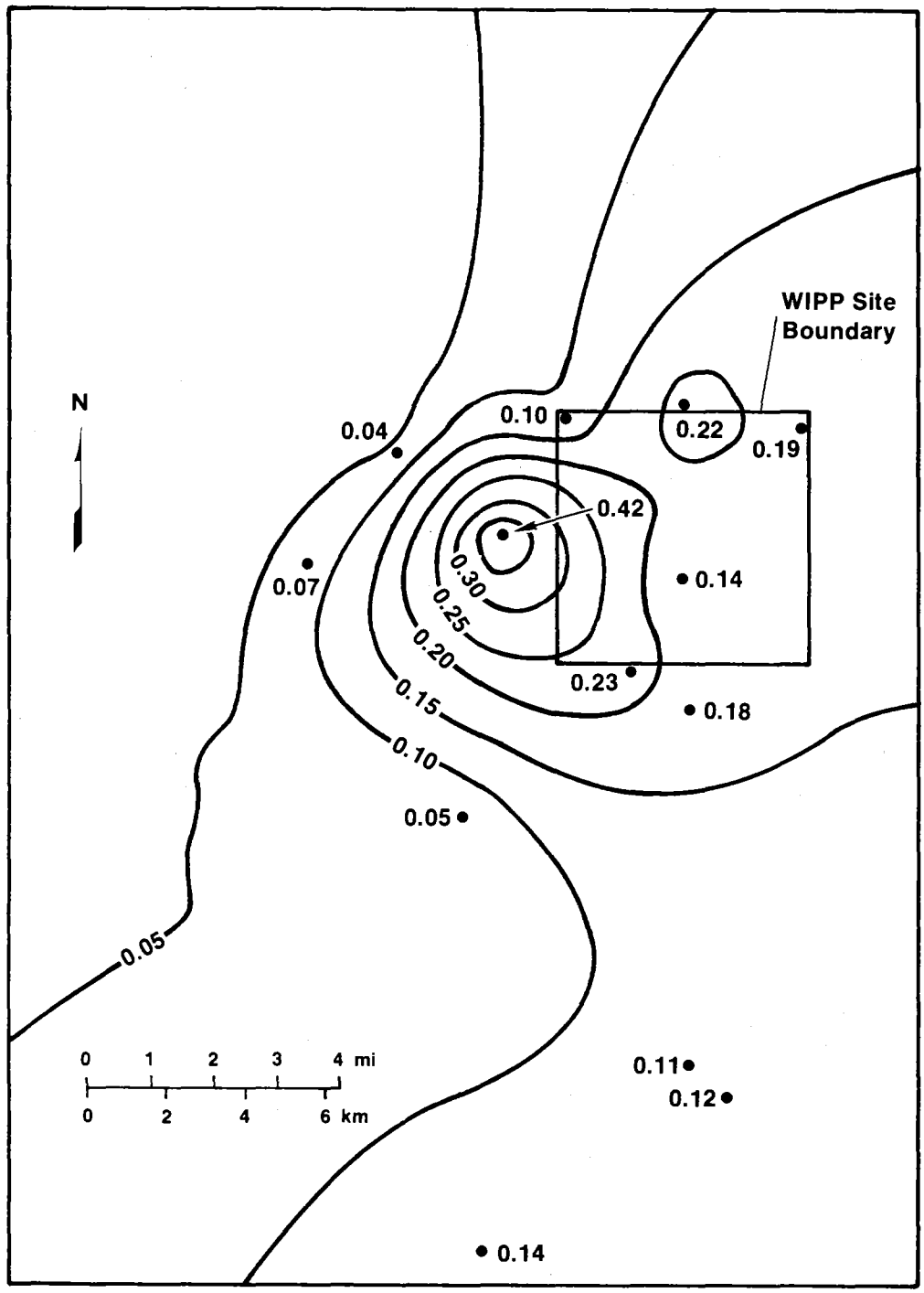


Figure 2-11. Contour plot of iodide concentrations (mg/L) in Culebra groundwaters.

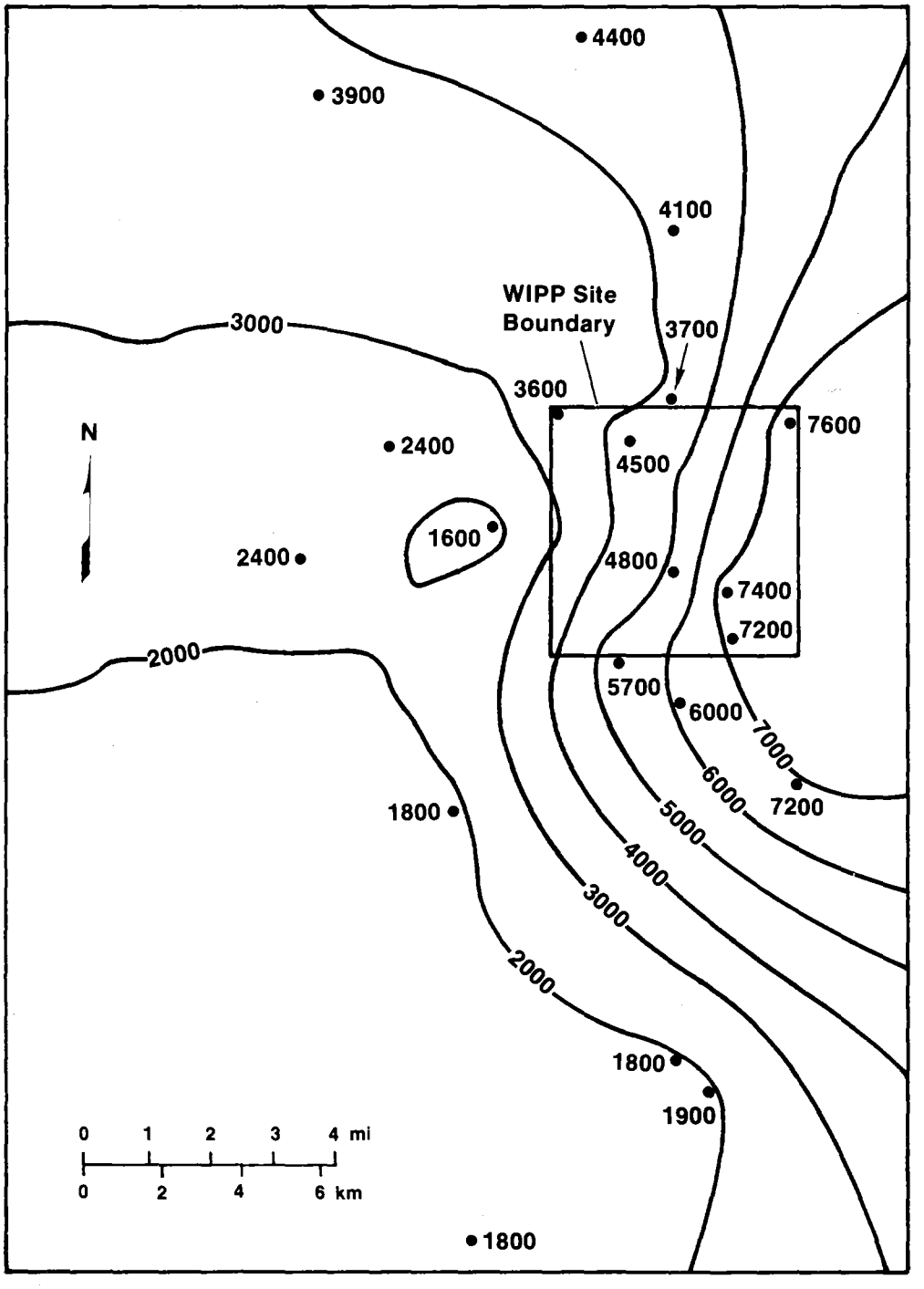


Figure 2-12. Contour plot of sulfate concentrations (mg/L) in Culebra groundwaters.

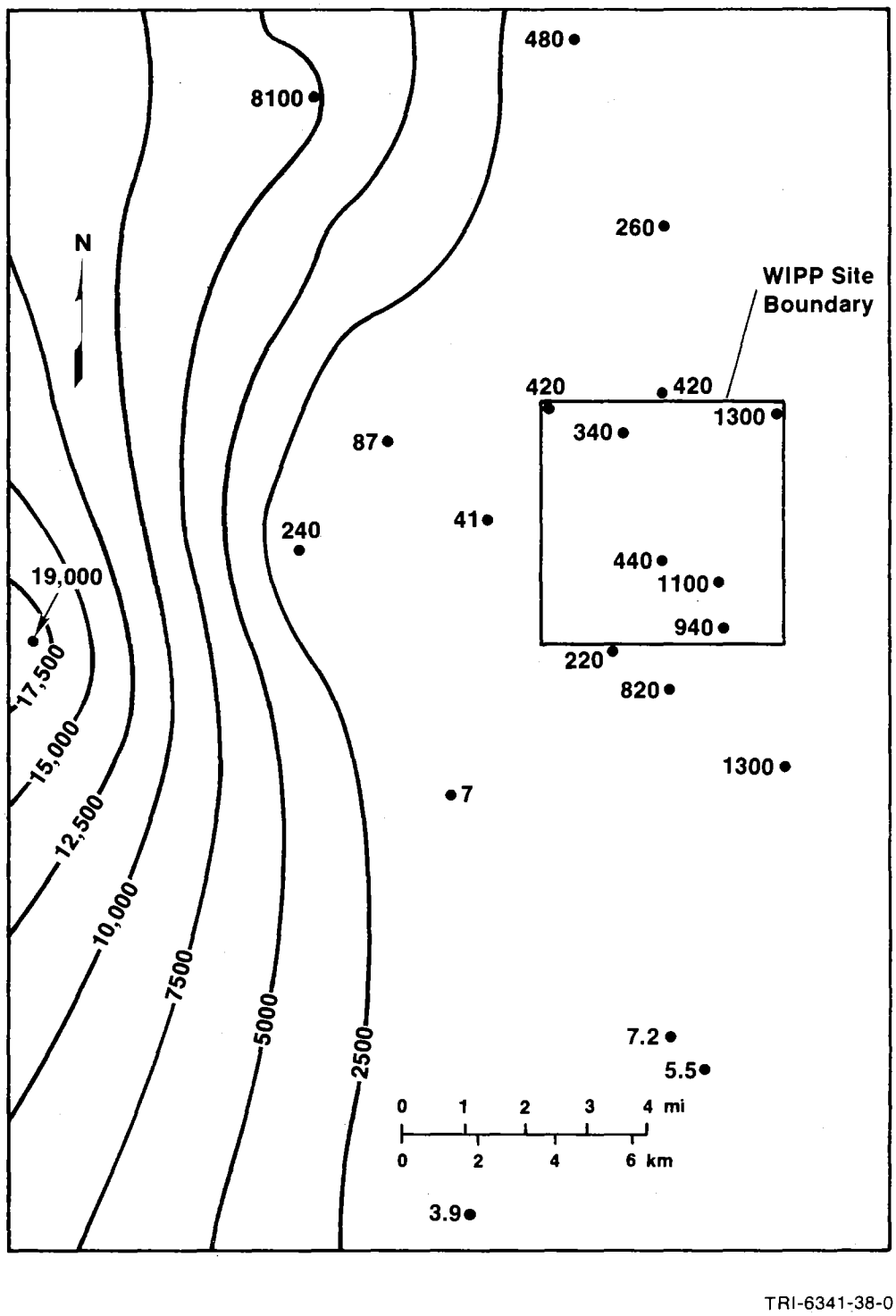


Figure 2-13. Contour plot of potassium concentrations (mg/L) in Culebra groundwaters including samples from WIPP-27 and WIPP-29.

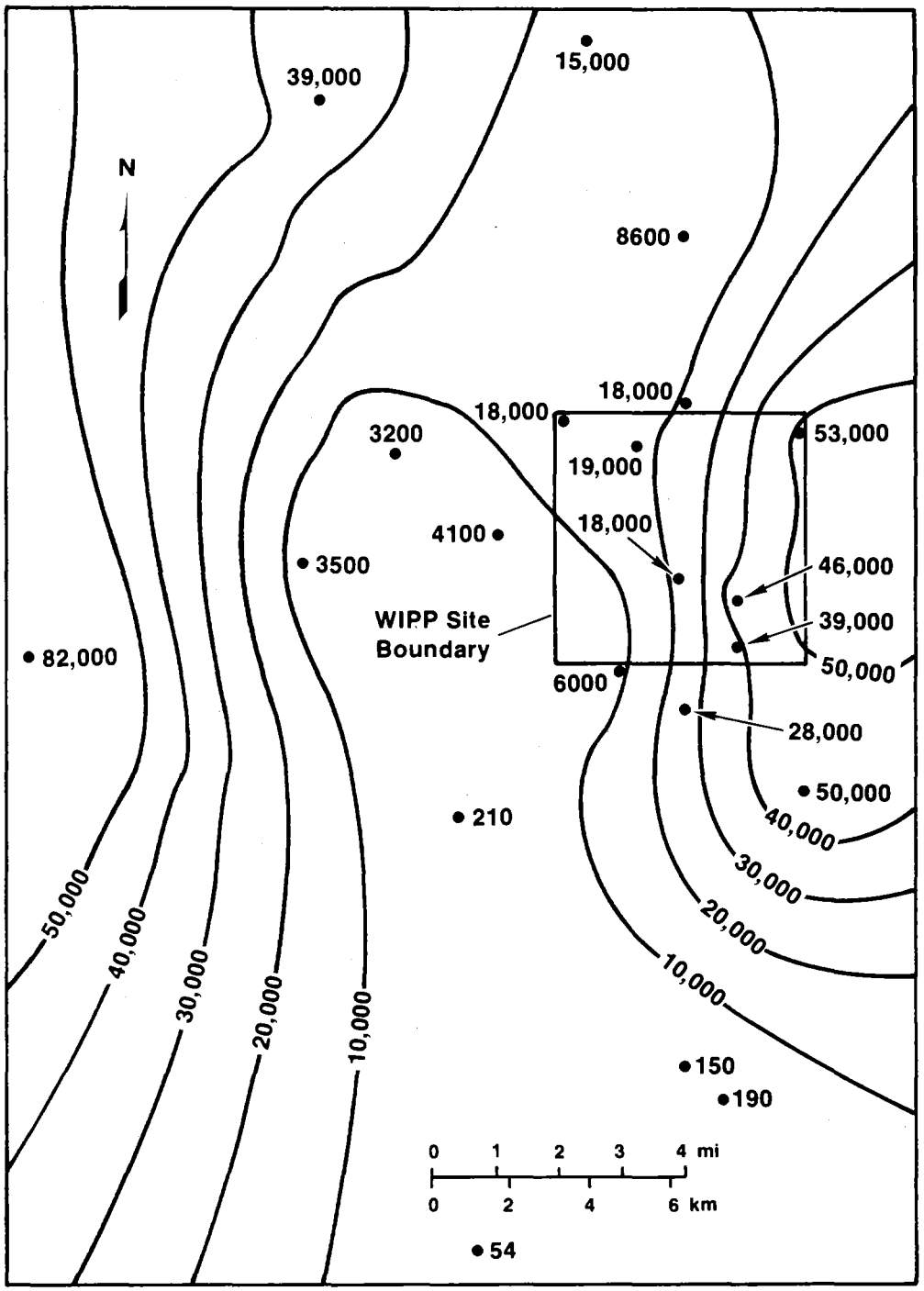


Figure 2-14. Contour plot of sodium concentrations (mg/L) in Culebra groundwaters including samples from WIPP-27 and WIPP-29.

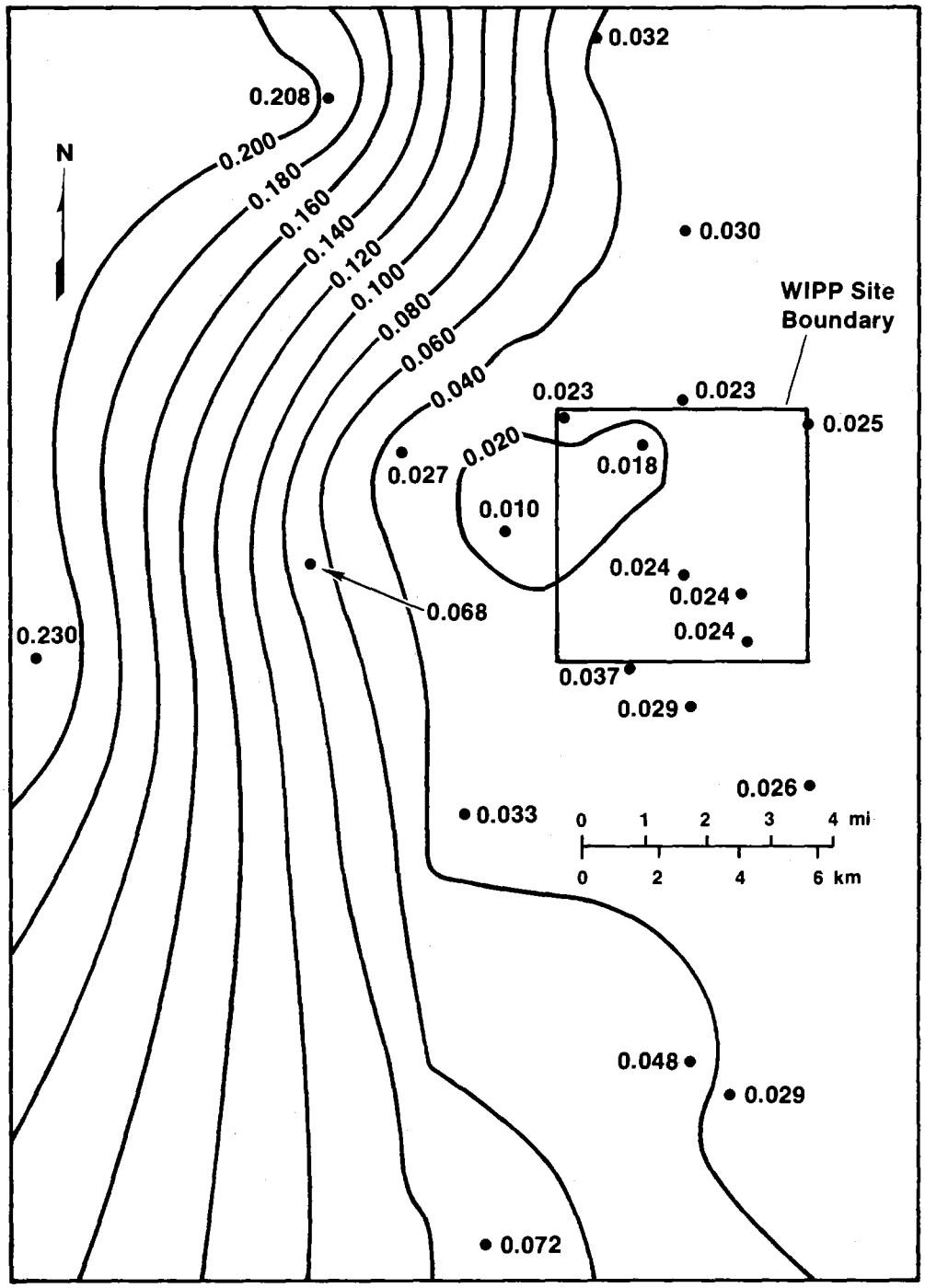


Figure 2-15. Contour plot of K/Na weight ratios ([mg/L]/[mg/L]) in Culebra groundwaters including samples from WIPP-27 and WIPP-29.

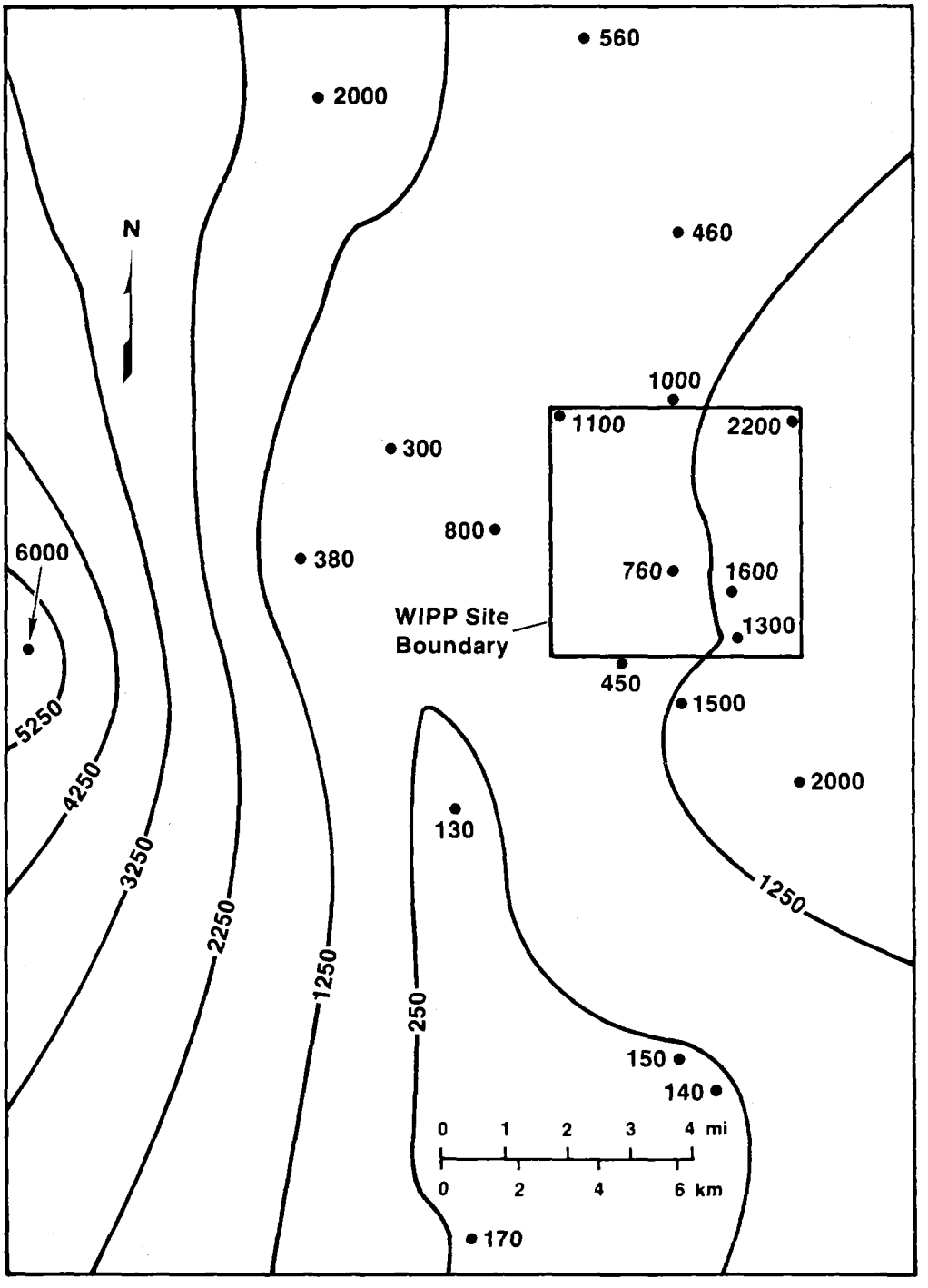


Figure 2-16. Contour plot of magnesium concentrations (mg/L) in Culebra groundwaters including samples from WIPP-27 and WIPP-29.

#### 2.3.1.3 Na/Cl Ratio

The distribution of Na/Cl molar ratios is shown in Figure 2-6. The ratios are very close to unity in the northern and central areas (with the exception of P-14), increase in the south to values of 1.20 and 1.28 at H-9B and Engle, and reach a maximum of 2.56 at H-8B. If dissolution of halite is the main source of the Na and Cl, the Na/Cl molar ratio should be close to 1.0 in solution. The elevated ratios in the southern area indicate a contribution of Na from an additional source, such as the weathering of Na-bearing feldspars or clays. However, the absolute concentrations of Na and Cl are considerably lower in the southern area. Thus, there may also be small contributions of Na from nonhalite sources in the north and central areas that are effectively overwhelmed by the contributions from halite dissolution, creating a Na/Cl ratio close to unity.

#### 2.3.1.4 Distribution of Cl/Br Ratios

The distribution of Cl/Br weight ratios ([g/L]/[mg/L]) is shown in Figure 2-7. The values range from 3.30 at WIPP-28 to 0.37 at H-8B, with the exception of P-14 and H-4B, which have values of 0.20 and 0.18, respectively. The Cl/Br weight ratio in seawater is about 0.30. As seawater evaporates, this ratio rises slightly (0.33 at the onset of halite precipitation; Sonnenfeld, 1984, p. 229) and then decreases in the remaining brine due to the limited incorporation of Br in the halite lattice (Braitsch, 1971). The ratio is further increased at the onset of the precipitation of late-stage minerals such as carnallite, kainite, bischofite, and sylvite, which incorporate more Br into their lattices than halite does. Castile brines from ERDA-6 have average Cl/Br weight ratios of 0.19 (Popielak et al., 1983), and analyses of brine samples collected from the floor of the WIPP Facility have Cl/Br ratios of 0.12 (Stein and Krumhansl, 1986). The fact that the Cl/Br ratios at P-14 and H-4B are lower than seawater may indicate that the wells were contaminated. Alternatively, if the Cl/Br ratios at these wells are reliable, this may suggest that the Br and Cl at these wells originated either from residual concentrated seawater (such as fluid inclusions) or from the dissolution of late-stage evaporite minerals that have lower Cl/Br ratios than halite.

### 2.3.1.5 Distribution of Silica

The distribution of silica is shown in Figure 2-8. Silica values reported by ITAS were used in this figure; these values differ from values reported by UNC (see Table 2-2). As discussed previously, the silica concentrations may be affected by precipitation of a Fe-Si floc after sample collection. The values range from 11 to 46 mg/L $SiO_2$ and are highest in the south and west and decrease toward the east. This silica distribution pattern is roughly the inverse of the general salinity distribution pattern (Figures 2-2, 2-3, and 2-4). Possible controls on the distribution of silica are discussed in Section 2.4.3.2.

### 2.3.1.6 Solute Concentrations and Ratios at P-14

As discussed in Section 2.2, the possibility that the samples from P-14 are contaminated cannot be ruled out; several isoconcentration plots indicate apparently anomalous concentrations and element ratios at P-14. Plots of the distributions of Sr, Ca, and I (Figures 2-9, 2-10, and 2-11) show an elevation of these elements at P-14, which in each case is nearly 2 times higher than the next highest observed value. However, the increased Sr and Ca concentrations in the vicinity of P-14 could be caused by variations in compositions of carbonate and sulfate minerals. The P-14 sample is also depleted in sulfate, as shown in Figure 2-12. The lowest concentrations of sulfate were measured at P-14 (1,600 mg/L), suggesting that Ca and Sr concentrations are currently controlled by equilibria with sulfate minerals.

The anomalously low Cl/Br ratio (0.200 [g/L]/[mg/L]) at P-14 (discussed above) is accompanied by an unusually low Na/Cl molar ratio of 0.46, which is approximately half the value at most of the other wells (Figure 2-6). This low value suggests a major contribution of Cl from some nonhalite source. One such source may be the leakage of high-Mg or high-Ca brine from underlying stratigraphic zones, such as the Rustler/Salado contact. The Ca and Mg concentrations will eventually be buffered by reactions with sulfates and carbonates, but the Cl will remain in solution, depressing the Na/Cl ratio.

#### 2.3.1.7 Solute Concentrations and Ratios at WIPP-27 and WIPP-29

WIPP-27 and WIPP-29 represent anomalies with respect to K and to a lesser extent Na and Mg. Figures 2-13 through 2-16 show the distributions of K, Na, K/Na, and Mg including WIPP-27 and WIPP-29. The anomalies are probably caused by contamination from potash-mining wastes introduced into the Culebra near the eastern edge of Nash Draw. Although both K and Na are elevated at these two wells, the distribution of K/Na ratios (Figure 2-15) clearly indicates a relative enrichment of K by nearly an order of magnitude.

### 2.3.2 Definition of Hydrochemical Facies Based on Relative Proportions of Major Solutes

#### 2.3.2.1 Definition of Hydrochemical Facies in the Culebra Dolomite

Based on the major solute compositions given in Table 2-2, four hydrochemical facies have been delineated and are shown in Figure 2-17. Compositions of waters from several other locations (indicated by open circles, open squares, or parentheses around the well name) were not included in the original data set used to define the facies, but their compositions are consistent with the facies boundaries. Compositions of waters in each zone are described in Figure 2-18.

**Zone A** (DOE-1, H-5, H-11, H-12, P-17) contains saline (~2 to 3 molal) NaCl brines with Mg/Ca molar ratios of about 1.2 to 2 (cf. Figure 2-19). This water is found in the eastern third of the study area; the zone coincides roughly with the region of low transmissivity, although at some of the wells (e.g., DOE-1 and H-11B3) the transmissivities are greater than 1 $ft^2$/day. On the western side of the zone, halite in the Rustler has been found only in the lower unnamed member; in the eastern portion of the zone, halite has been observed above and below the Culebra.

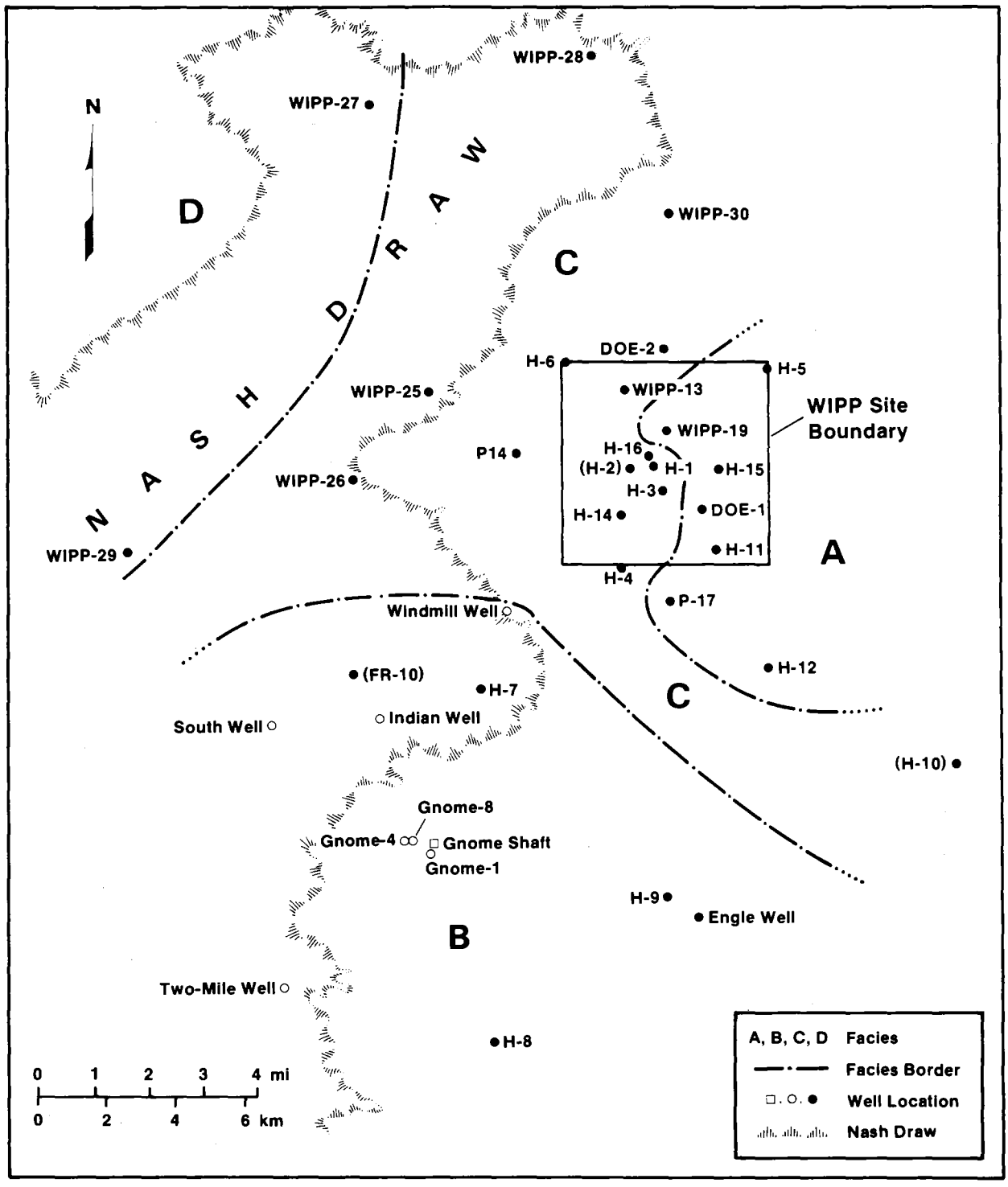


TRI-6331-78-1

Figure 2-17. Hydrochemical facies of the Culebra dolomite.

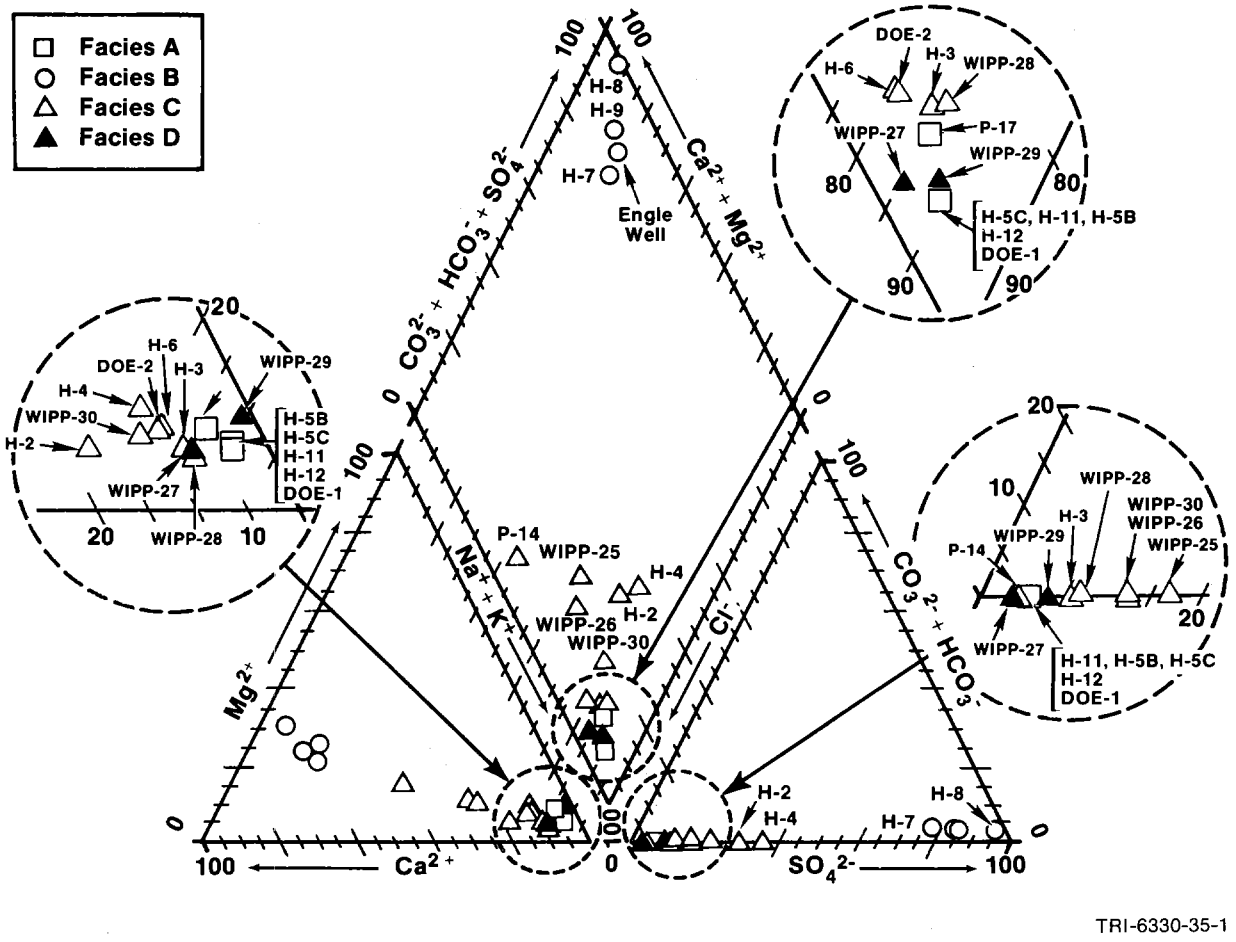


Figure 2-18. Trilinear diagram showing compositions of Culebra groundwaters.

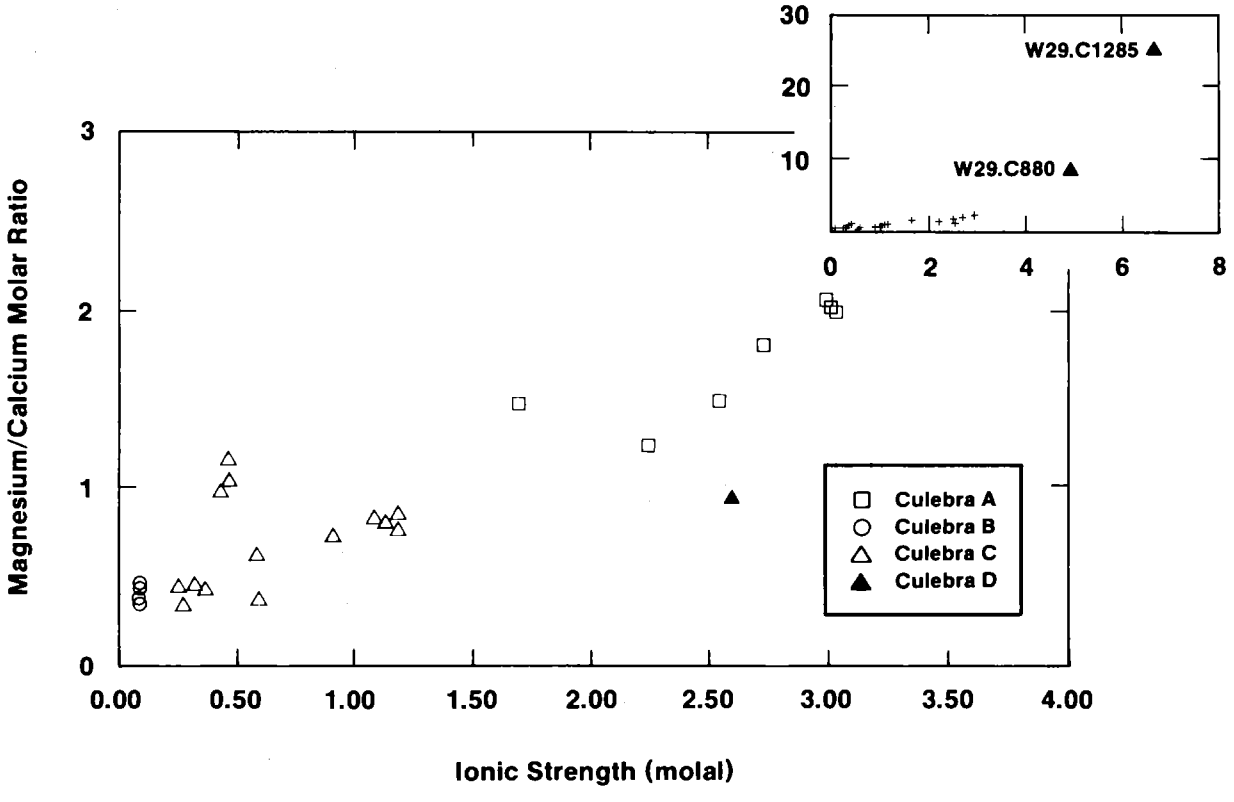


Figure 2-19. Relationship between Mg/Ca molar ratios and ionic strengths of Culebra groundwaters.

**Zone B** (H-7, H-8, H-9, Engle) contains relatively dilute $CaSO_4$-rich groundwater (ionic strength <0.1 m). This water is found in the southern part of the study area. This zone coincides with a region of high transmissivity; halite is not found in the Rustler in this zone. Chemical data from Bodine et al. (Chapter 4) suggest that several stock wells (Windmill, Indian, South, and Two-Mile) and the Gnome (USGS) wells are also part of this zone.

**Zone C** contains waters of variable composition with low to moderate ionic strength (0.3 to 1.6 m). These waters occur in the western part of the WIPP Site and the eastern side of Nash Draw. Mg/Ca molar ratios of the fresher waters in this zone (I <1.25 m) range from about 0.3 to about 1.2. This zone coincides with a region of generally high transmissivity (except wells WIPP-30, H-1, H-2, H-4, H-14, and H-16). In the eastern part of this zone, halite is present in the lower unnamed member of the Rustler; on the western side of the zone, halite is not observed in the formation. The most saline (Na-Cl rich) water is found in the eastern edge of the zone, close to borehole locations where halite is observed in the Tamarisk member.

**Zone D** (WIPP-27, WIPP-29) is defined based on inferred contamination related to potash-refining operations in the area. The Culebra groundwaters from these wells have anomalously high salinities (3-7 m) and K/Na weight ratios (0.2) compared to other wells in the study area (salinities <3 m; K/Na weight ratios 0.01 to 0.09). At WIPP-29, the composition of the Culebra water has changed over the course of a 7-year monitoring period.

Many of the chemical characteristics of the facies are illustrated by the Piper (trilinear) diagram shown in Figure 2-18. This plot summarizes relationships between the major solutes in the Na-K-Mg-Ca-Cl-$SO_4$-$CO_3$ system. The diagram shows the relative proportions of the ions on an equivalents/liter basis. Relative proportions of cations and anions are displayed separately in the triangular plots in the bottom half of the figure. In the

rhombus in the upper portion of the diagram, the ratio of divalent to monovalent cations and the ratio of chloride to the sum of sulfate + carbonate + bicarbonate are shown.

Groundwater samples from each well in Zone A have nearly identical ionic proportions and plot very near the Na-Cl corner of the trilinear diagram. They are distinguished from Zone-C groundwaters primarily on the basis of Mg/Ca ratio and ionic strength (see Figure 2-19). Waters from Zone C cover a wide area in the diagram, whereas the relatively fresh waters from Zone B plot near the Ca-$SO_4$ corner of the diagram. Waters in Zone D have similar ionic proportions to those of Zone A and are distinguished primarily on the basis of the K/Na ratio (see Figure 2-15).

#### 2.3.2.2 Solute Proportions for Other Groundwater Samples

Appendix 2D discusses the major solute compositions of selected samples from the Rustler/Salado contact zone, the Magenta dolomite, the Dewey Lake Red Beds, and the Bell Canyon Formation. There are insufficient data for meaningful isoconcentration or element ratio contours. No hydrogeochemical facies have been defined for these stratigraphic horizons because of the small number of analyses. Additional descriptions of solute relationships in these waters are found in the discussion of factor analysis in Section 2.3.3 and in Appendix 2D.

### 2.3.3 Principal Component Analysis of Water Chemistry Data

In the previous section, hydrochemical facies for Culebra groundwaters were defined using the relative proportions of the concentrations of seven major solutes. These solute ratios can be represented by a trilinear plot as shown in Figure 2-18. To show relationships among the 17 independent chemical variables presented in Table 2-2, PCA was used. This method summarizes the relationships among the variables and shows how these relationships differ for each water composition. This information can be used to refine the definitions of the hydrochemical facies and to suggest the nature of chemical reactions that control groundwater composition. This section contains a brief introduction to the

principles of PCA and then describes the application of this technique to waters from the Culebra dolomite and related rock units.

#### 2.3.3.1 Introduction to Principal Component Analysis

PCA is a method of multivariate statistics that can be used to examine the relationships in complex data sets. It can be used in two ways: (1) to express the relationships among a large number of variables in terms of correlations with a smaller number of underlying components or factors; or (2) to describe the characteristics of a sample suite by defining hypothetical end members of the population.

When the objective of the analysis is to find correlations among variables, R-mode analysis is employed; when the similarities among samples are examined, Q-mode analysis is used.

Appendix 2B explains the basic concepts and vocabulary of PCA. The origins of the factor-loading matrices and factor-score matrices, the significance of factor rotations, and the need for data transformations are explained. A detailed explanation of the mathematical principles that underly the technique is not required to understand this section and is beyond the scope of this work. Similarly, a review of previous applications of PCA in geochemical studies is not included here. References to works that contain excellent discussions of the theory and applications of PCA can be found in Appendix 2B.

In this report, the terms "factor" and "principal component" are used interchangeably. However, as discussed in Appendix 2B, the analysis presented below is, in the strictest sense, a PCA and not a classical factor analysis.

#### 2.3.3.2 Sample Populations Examined by Principal Component Analysis

Table 2-4 describes the two sample populations that were examined using PCA. Population 1 contains 21 water samples from the Culebra dolomite of the Rustler Formation. Where multiple samples from the same well are available, the most recent sample was used. Where data from both UNC and other laboratories were available, data

## Table 2-4. Populations Used in Principal Component Analysis

| Pop. | Wells | Variables used in PCA |
|---|---|---|
| 1 | Culebra: DOE-1, DOE-2, H-2A, H-3B3, H-4B, H-5B, H-5C, H-6B, H-7B1, H-8B, H-9B, H-12, P-14, P-17, WIPP-25, WIPP-26, WIPP-27, WIPP-28, WIPP-29, WIPP-30, Engle | Ca, Mg, K, Na, Cl, $SO_4$, B, Li, $SiO_2$, Br, Sr, $HCO_3$, pH |
| 2 | Dewey Lake: Ranch, Twin-Pasture | Ca, Mg, K, Na, Cl, $SO_4$, B, Li, $SiO_2$, Br, Sr, $HCO_3$, pH, |
| | Magenta: H-3B1, H-4C, H-5C, H-6C | Fe, Mn, F, I |
| | Culebra: DOE-2, H-2A, H-3B3, H-5B, H-6B, H-7B1, H-8B, H-9B, P-14, P-17, WIPP-26, WIPP-29, Engle | |
| | Bell Canyon: DOE-2 | |

from the UNC laboratory were used. The reasons for these choices are discussed in Section 2.2. Factor analysis of population 1 is discussed in detail in the following sections and in Appendix 2C.

Population 2 contains 20 groundwater samples from the Dewey Lake Red Beds, Magenta dolomite, Culebra dolomite, and Bell Canyon Formation. The objective in selecting analyses for this data set was to include as many different solutes as possible. For this reason, several Culebra samples from population 1 that lack minor and trace-element data (Mn, Fe, I) were not included. The interelement correlations involving these additional solutes are described in Section 2.3.3.6. Additional information about factor analysis of population 2 is found in Appendix 2D.

### 2.3.3.3 Q-mode Analysis of Culebra Water Samples

A Q-mode PCA was carried out on population 1 to determine if the data set was homogeneous and therefore amenable to R-mode analysis. The factor analysis programs of SAS (Statistical Analysis System Institute, 1982) were used to extract the principal components. The data set consisted of the logarithms of the raw concentrations; all principal components (factors) that accounted for at least 1% of the total variance were extracted.

Both the unrotated and varimax solutions were examined; the former was more interpretable and was retained for further discussion. The results of the unrotated analysis are presented in Table 2-5 and Figures 2-20 and 2-21. Table 2-5 shows the factor loading matrix; it can be seen that two principal components account for nearly all of the variance. The communalities of all samples are at least 0.93, indicating that combinations of these factors accurately reconstruct the compositions of most of the water samples.

The "Factor A" and "Factor B" columns of Table 2-5 describe the similarity between each sample and principal components A and B, respectively. The rows across the table show the composition of each sample in terms of the components. Figure 2-20 provides a graphical representation of Table 2-5 and describes the water compositions in terms of the two principal components. Figure 2-21 is a graphical representation of the Q-mode factor-score matrix and describes the components in terms of the chemical variables.

The first principal component (factor A) accounts for 96% of the variance of the population (Table 2-5). Most of the samples are similar to this factor (that is, they have factor loadings close to unity), which represents a grand average of all the compositions. H-6 is closest in composition to this hypothetical entity. A few water samples deviate considerably from this grand average composition. The second principal component (factor B) describes this deviation; it accounts for 4% of the variance. WIPP-29 and H-8 are the extrema of this principal component.

## Table 2-5. Unrotated Q-mode Factor Loadings of Culebra Groundwaters (Population 1)

| Well | Coll. Date | Facies[1] | Factor A | Factor B | Communality ($h_i^2$) |
|---|---|---|---|---|---|
| DOE-1 | 4/85 | A | 0.98 | -0.19 | 0.994 |
| H-5C | 10/81 | A | 0.98 | -0.15 | 0.990 |
| H-5B | 8/85 | A | 0.98 | -0.18 | 0.993 |
| H-12 | 8/85 | A | 0.98 | -0.19 | 0.992 |
| P-17 | 3/86 | A | 0.98 | -0.13 | 0.989 |
| H-7B1 | 3/86 | B | 0.94 | 0.33 | 0.998 |
| H-8B | 1/86 | B | 0.90 | 0.43 | 0.990 |
| H-9B | 11/85 | B | 0.93 | 0.35 | 0.997 |
| ENGLE | 3/85 | B | 0.94 | 0.34 | 0.998 |
| DOE-2 | 3/85 | C | 0.99 | -0.09 | 0.996 |
| H-2A | 4/86 | C | 0.99 | 0.08 | 0.985 |
| H-3B3 | 2/85 | C | 0.99 | -0.08 | 0.992 |
| H-4B | 7/85 | C | 0.99 | 0.00 | 0.981 |
| H-6B | 9/85 | C | 0.99 | -0.09 | 0.997 |
| P-14 | 2/86 | C | 0.97 | 0.04 | 0.936 |
| WIPP-25 | 2/86 | C | 0.99 | 0.10 | 0.994 |
| WIPP-26 | 11/85 | C | 0.99 | 0.05 | 0.987 |
| WIPP-28 | 9/80 | C | 0.98 | -0.04 | 0.974 |
| WIPP-30 | 9/80 | C | 0.99 | 0.03 | 0.985 |
| WIPP-27 | 9/80 | D | 0.95 | -0.20 | 0.956 |
| WIPP-29 | 12/85 | D | 0.90 | -0.34 | 0.939 |

Amount and Percent of Variance Explained by Each Factor

| Factor A | Factor B |
|---|---|
| 19.778 | 0.888 |
| 96% | 4% |

1. Hydrochemical facies in the Culebra, as defined in Section 2.3.2.1.

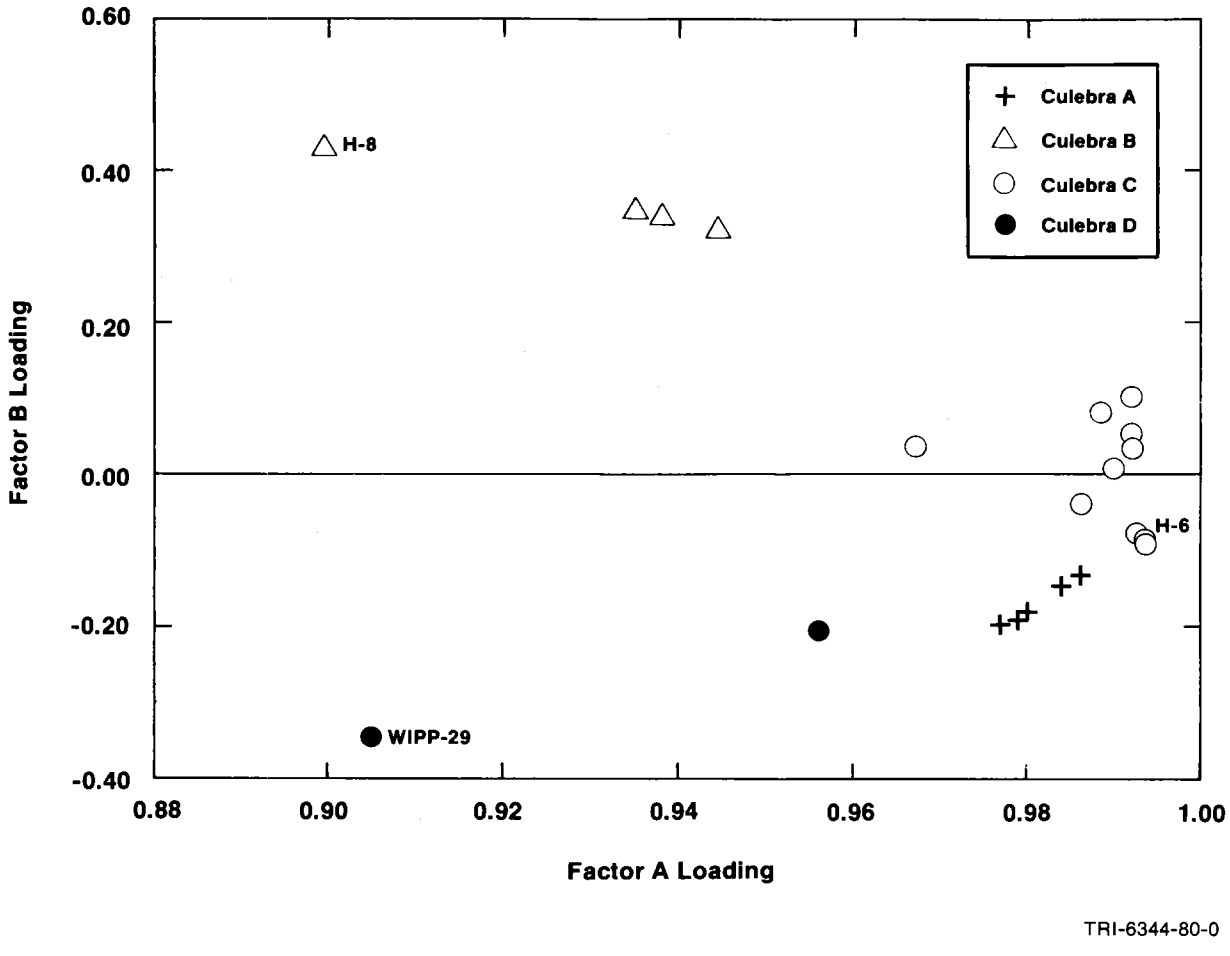


Figure 2-20. Relationship between unrotated Q-mode factor loadings for factors A and B of Culebra groundwaters (population 1).

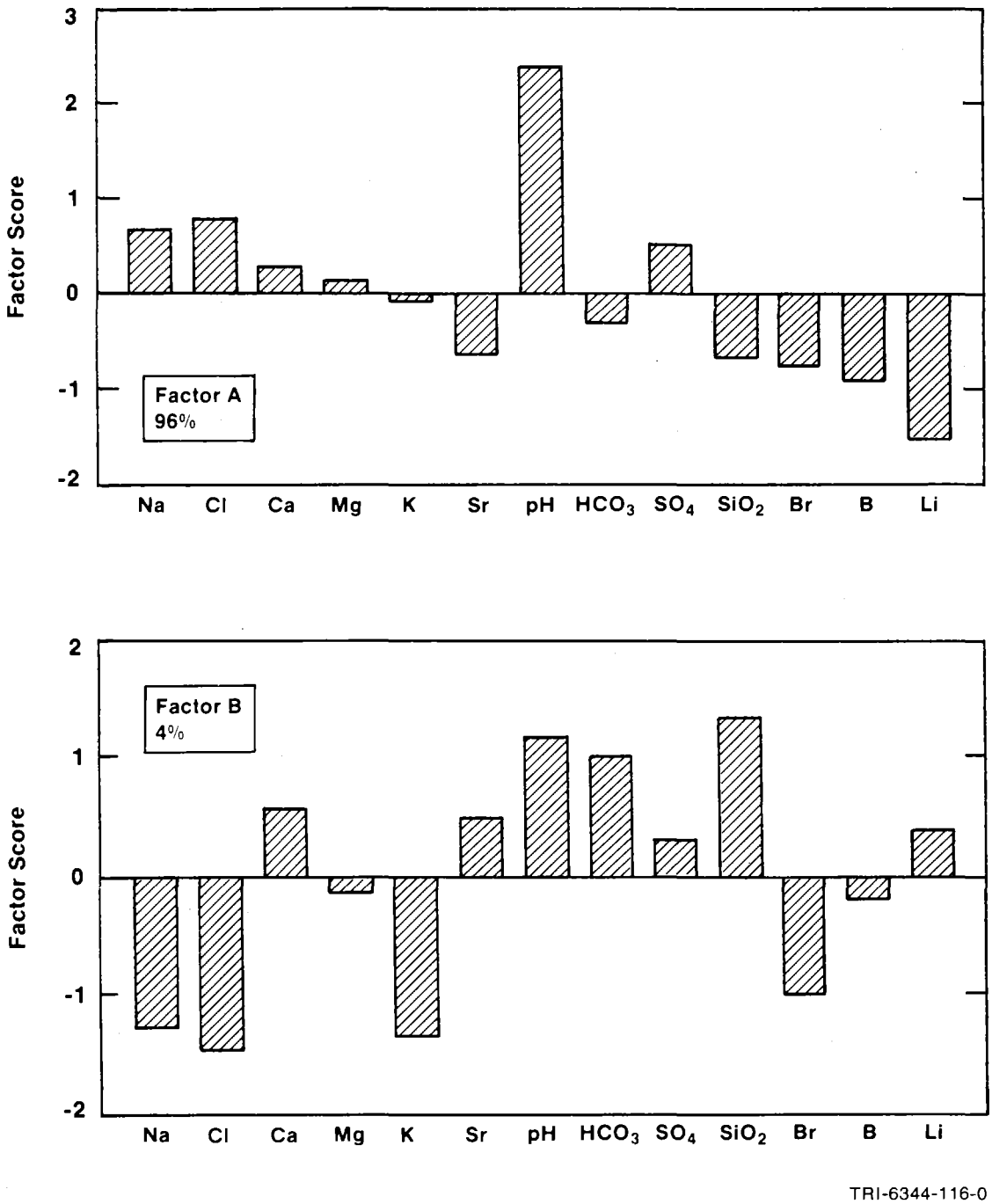


Figure 2-21. Unrotated Q-mode factor scores for factors A and B of Culebra groundwaters (population 1).

In general, as discussed in Appendix 2B, if two or three Q-mode principal components account for most of the sample variance, the population can be considered homogeneous enough for R-mode analysis (Hitchon et al., 1971; Klovan, 1975; Drever, 1982). The results, shown in Table 2-5, indicate that population 1 is homogeneous and therefore amenable to R-mode analysis.

#### 2.3.3.4 R-mode Principal Component Analysis of Culebra Water Samples

##### *2.3.3.4.1 FACTOR LOADINGS*

R-mode PCA was carried out on population 1 using the factor-analysis programs in SAS. The common logarithms of the raw chemical data were calculated; the resulting distributions of the transformed variables were close to normal. The correlation matrix of the transformed data is shown in Table 2-6.

The factor-loading matrix of the principal components extracted from the correlation matrix is described in Table 2-7. Three factors account for approximately 96% of the total variance of the sample population; these three factors are shown in Figure 2-22.

Factor 1 accounts for approximately 67% of the total variance of the data set. It is characterized by high positive loadings for all of the variables except pH, bicarbonate alkalinity, and silica. The factor accounts for most of the variance of sodium and chloride. For this reason, the factor is referred to as the "salinity factor" in this report.

Factor 2 accounts for approximately 18% of the variance of the data set. It is characterized by large loadings for pH, bicarbonate alkalinity, and silica and boron concentrations. It is referred to as the "silicate/bicarbonate factor" in this report.

## Table 2-6. Correlation Matrix for Solute Data[1] in Culebra Groundwaters (Population 1)

| | Ca | Mg | K | Na | Cl | $SO_4$ | B |
|---|---|---|---|---|---|---|---|
| Ca | 1.000 | 0.492 | 0.414 | 0.568 | 0.606 | 0.042 | 0.361 |
| Mg | 0.492 | 1.000 | 0.905 | 0.906 | 0.893 | 0.835 | 0.638 |
| K | 0.414 | 0.905 | 1.000 | 0.945 | 0.930 | 0.847 | 0.663 |
| Na | 0.568 | 0.906 | 0.945 | 1.000 | 0.993 | 0.810 | 0.797 |
| Cl | 0.606 | 0.893 | 0.930 | 0.993 | 1.000 | 0.759 | 0.753 |
| $SO_4$ | 0.042 | 0.835 | 0.847 | 0.810 | 0.759 | 1.000 | 0.755 |
| B | 0.361 | 0.638 | 0.663 | 0.797 | 0.753 | 0.755 | 1.000 |
| Li | 0.456 | 0.882 | 0.801 | 0.886 | 0.859 | 0.839 | 0.864 |
| $SiO_2$ | -0.259 | -0.583 | -0.544 | -0.649 | -0.601 | -0.703 | -0.842 |
| Br | 0.638 | 0.853 | 0.819 | 0.934 | 0.944 | 0.695 | 0.763 |
| Sr | 0.940 | 0.712 | 0.624 | 0.750 | 0.780 | 0.310 | 0.508 |
| pH | -0.118 | -0.412 | -0.351 | -0.223 | -0.239 | -0.187 | 0.187 |
| $HCO_3$ | -0.221 | -0.155 | -0.095 | -0.229 | -0.198 | -0.226 | -0.577 |

| | Li | $SiO_2$ | Br | Sr | pH | $HCO_3$ |
|---|---|---|---|---|---|---|
| Ca | 0.456 | -0.259 | 0.638 | 0.940 | -0.118 | -0.221 |
| Mg | 0.882 | -0.583 | 0.853 | 0.712 | -0.412 | -0.155 |
| K | 0.801 | -0.544 | 0.819 | 0.624 | -0.351 | -0.095 |
| Na | 0.886 | -0.649 | 0.934 | 0.750 | -0.223 | -0.229 |
| Cl | 0.859 | -0.601 | 0.944 | 0.780 | -0.239 | -0.198 |
| $SO_4$ | 0.839 | -0.703 | 0.695 | 0.310 | -0.187 | -0.226 |
| B | 0.864 | -0.842 | 0.763 | 0.508 | 0.187 | -0.577 |
| Li | 1.000 | -0.778 | 0.864 | 0.647 | -0.123 | -0.397 |
| $SiO_2$ | -0.778 | 1.000 | -0.633 | -0.396 | -0.422 | 0.729 |
| Br | 0.864 | -0.633 | 1.000 | 0.816 | -0.153 | -0.329 |
| Sr | 0.647 | -0.396 | 0.816 | 1.000 | -0.202 | -0.266 |
| pH | -0.123 | -0.442 | -0.153 | -0.202 | 1.000 | -0.572 |
| $HCO_3$ | -0.397 | 0.729 | -0.329 | -0.266 | -0.572 | 1.000 |

1. The data are the natural logarithms of the solute concentrations in mg/L (except for pH).

## Table 2-7. Unrotated R-mode Factor Loadings for Culebra Groundwaters (Population 1)

| Element | Factor 1 | Factor 2 | Factor 3 | Factor 4 | Factor 5 | Communality ($h_i^2$) |
|---|---|---|---|---|---|---|
| Ca | 0.590 | 0.177 | 0.773 | 0.017 | 0.005 | 0.979 |
| Mg | 0.922 | 0.255 | -0.128 | -0.146 | -0.160 | 0.980 |
| K | 0.901 | 0.251 | -0.212 | 0.107 | -0.144 | 0.953 |
| Na | 0.976 | 0.125 | -0.039 | 0.135 | 0.010 | 0.990 |
| Cl | 0.962 | 0.168 | 0.019 | 0.159 | 0.001 | 0.981 |
| $SO_4$ | 0.818 | -0.031 | -0.564 | -0.030 | -0.042 | 0.992 |
| B | 0.848 | -0.385 | -0.106 | 0.048 | 0.320 | 0.985 |
| Li | 0.944 | -0.081 | -0.123 | -0.116 | 0.120 | 0.942 |
| $SiO_2$ | -0.748 | 0.616 | 0.115 | -0.001 | 0.132 | 0.971 |
| Br | 0.947 | 0.059 | 0.126 | 0.055 | 0.052 | 0.924 |
| Sr | 0.778 | 0.198 | 0.582 | -0.038 | -0.044 | 0.988 |
| pH | -0.145 | -0.903 | 0.162 | 0.344 | -0.100 | 0.993 |
| $HCO_3$ | -0.379 | 0.799 | -0.208 | 0.360 | 0.049 | 0.960 |

Amount and Percent of Variance Explained by Each Factor

| Factor 1 | Factor 2 | Factor 3 | Factor 4 | Factor 5 |
|---|---|---|---|---|
| 8.4033 | 2.2385 | 1.4456 | 0.3470 | 0.2006 |
| 67% | 18% | 11% | 3% | 2% |

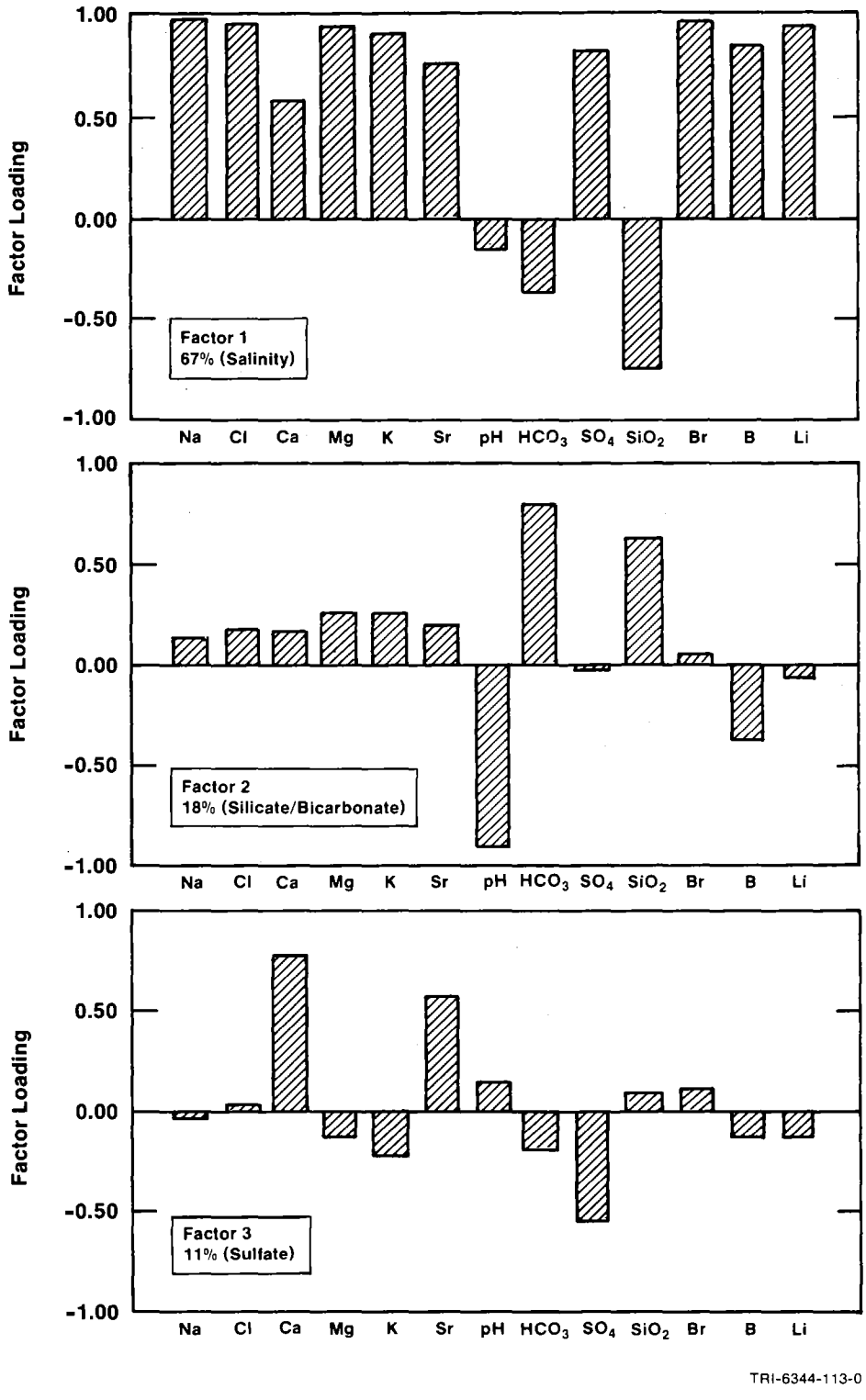


Figure 2-22. Unrotated R-mode factor loadings for factors 1, 2, and 3 of Culebra groundwaters (population 1).

Factor 3 accounts for approximately 11% of the total variance and exhibits high positive loadings for calcium and strontium. It also exhibits a high negative loading for sulfate and is referred to as the "sulfate factor " in this report.

As discussed in Appendix 2B, the factor loadings and scores of the unrotated principal components are strongly influenced by the requirement that the first principal component account for the highest possible amount of variance. As discussed in the appendix, this mathematical constraint may obscure the true relationships among the variables. Other orientations or rotations of the factor axes are possible and are equally mathematically correct in describing the variance of the data set. For this reason, the SAS factor-analysis factor-rotation subroutines were used to examine other factor structures. The mathematical basis for the different rotations is discussed clearly in Nie et al. (1975).

Factor loadings obtained from varimax, equamax, and quartimax rotational schemes were examined to determine if any element associations were common to alternative orientations of the factor axes. It was found that the factor-loading matrices from all rotational schemes contained the same key element associations described above for the unrotated components. The loading matrices differed primarily in the relative loadings of other elements and the variance explained by the salinity, silicate/bicarbonate, and sulfate factors. These differences and similarities are illustrated by examining the results of the varimax rotation discussed in the following section.

#### *2.3.3.4.2 VARIMAX FACTOR LOADINGS*

As discussed in Appendix 2B, the varimax rotation is most commonly used in analysis of hydrochemical and mineralogical data. This rotation is based on numerical criteria that seek to simplify the columns of the factor-loading matrix. This means that in the "ideal" varimax factor-loading matrix, every factor is important for as few elements as possible.

The first three varimax factors are described in Figure 2-23; they are similar to the three unrotated factors shown in Figure 2-22. By convention, the factor loadings are scaled in

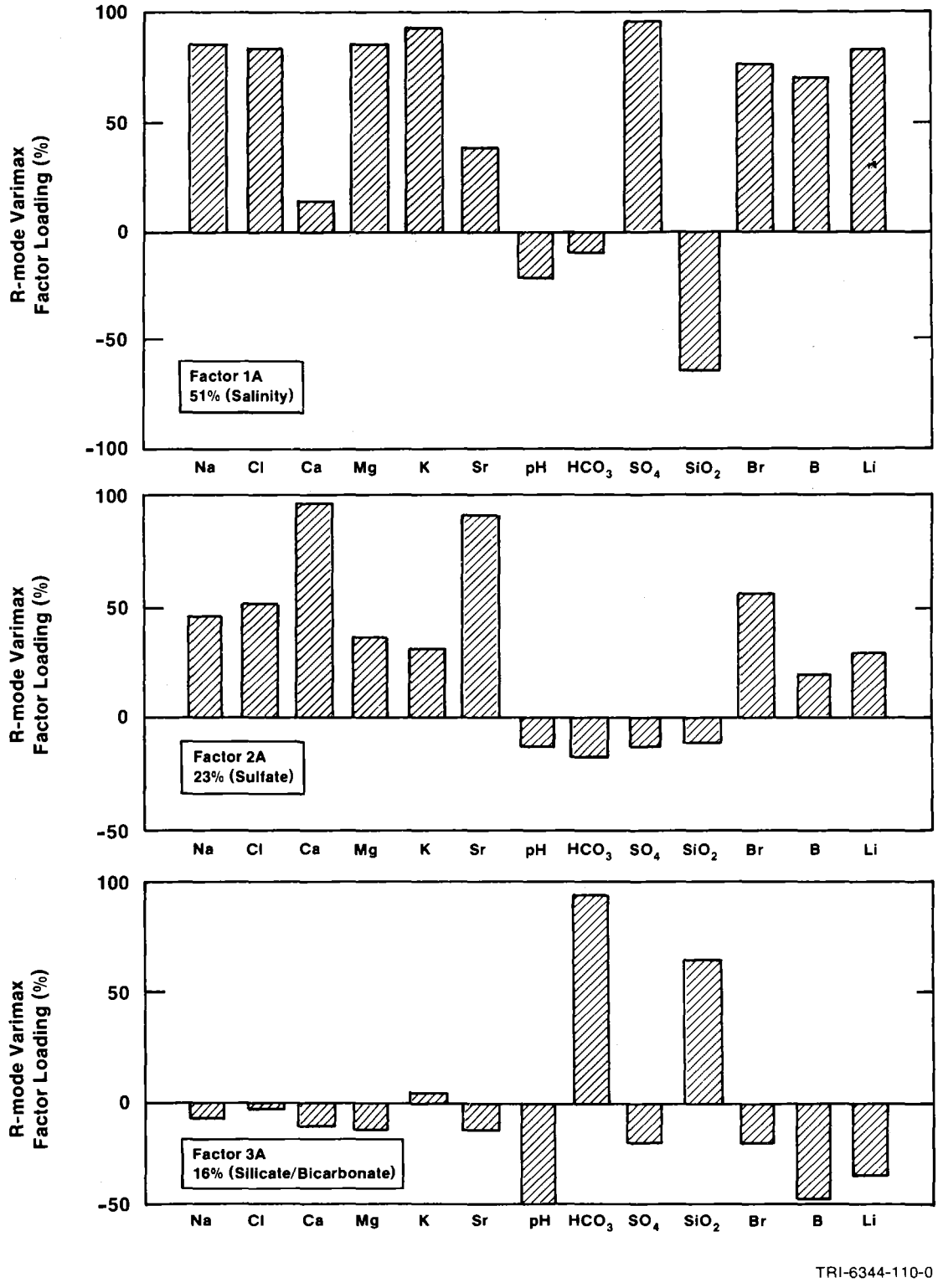


Figure 2-23. Varimax R-mode factor loading for factors 1A, 2A, and 3A of Culebra groundwaters (population 1).

units of percent after rotation, whereas the the unrotated factor loadings are scaled in fractional units. Factors are assigned numbers in order of decreasing variance, also by convention.

Factor 1A contains the same elemental associations as factor 1, the salinity factor, but accounts for slightly less variance. Factor 2A contains the same calcium-strontium correlation as factor 3, the sulfate factor, but is less influenced by sulfate concentration. The varimax factor is more strongly affected by the concentrations of elements such as sodium and bromine and accounts for more variance than its unrotated counterpart. Factor 3A is very similar to factor 2, the silicate/bicarbonate factor. It is more strongly influenced by elements such as sodium and chlorine and explains more variance than the unrotated factor.

More details of the varimax factor loadings and scores are given in Appendix 2C. Because of the similarity of the factors obtained from the different rotations, the discussion of the factor-score matrix that follows is relevant to all four rotations examined. In this discussion, the water sample compositions are compared in terms of the relative importances of the key elemental associations described above as the "salinity," "sulfate," and "silicate/bicarbonate" factors.

#### *2.3.3.4.3 VARIMAX FACTOR SCORES*

The compositions of the samples in terms of the factors are described by the factor scores. Relationships between varimax factor scores for the three most important factors are presented as bivariate plots in Figures 2-24 and 2-25. Scores for the salinity and sulfate factors are plotted in Figure 2-24. This figure shows that the first two principal components can be used to delineate the same groups of wells identified in Figures 2-17 through 2-19. Thus, the definition of hydrochemical facies, based on the proportions of major solutes, is supported by correlations among the major and minor elements examined in this study.

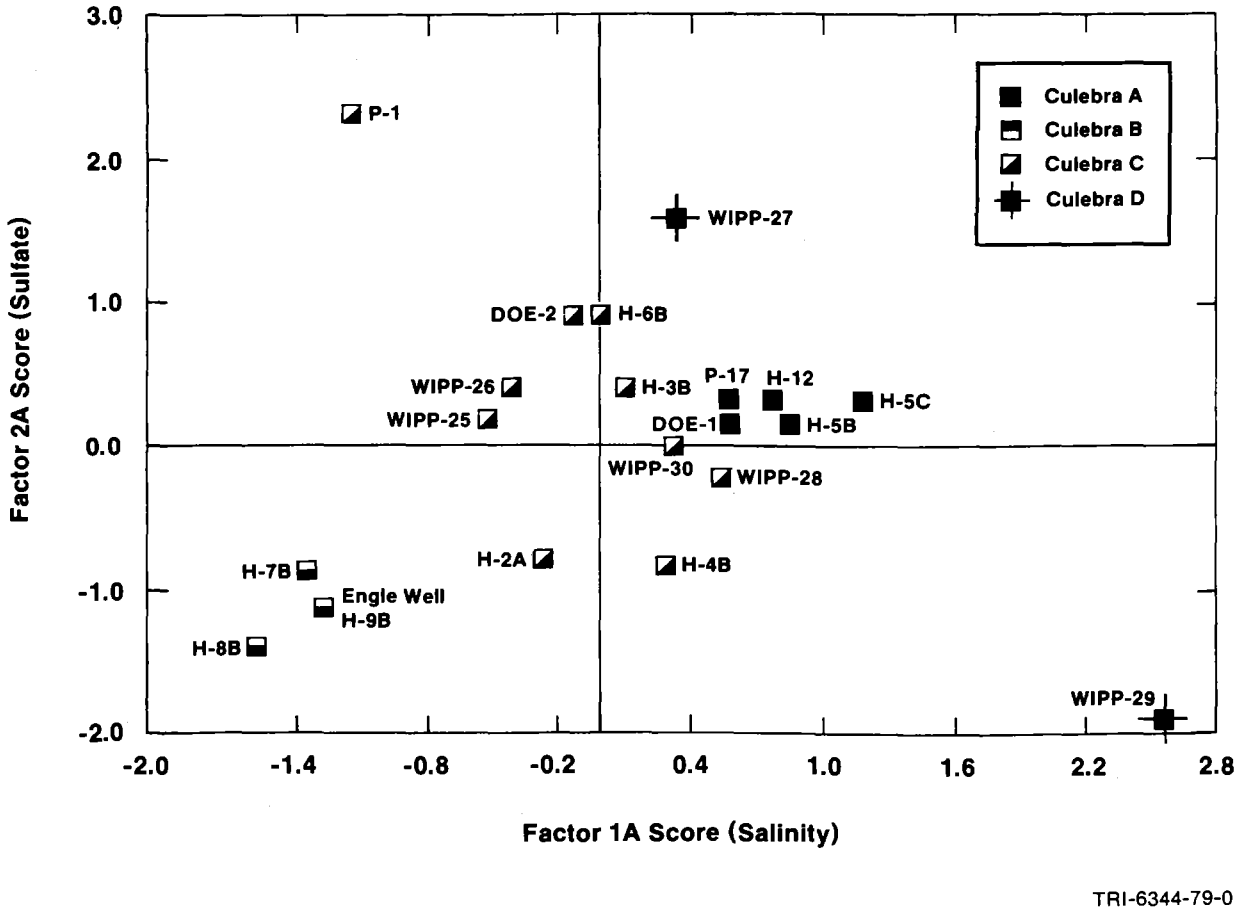


Figure 2-24. Relationship between varimax R-mode factor scores for factors 1A and 2A of Culebra groundwaters (population 1).

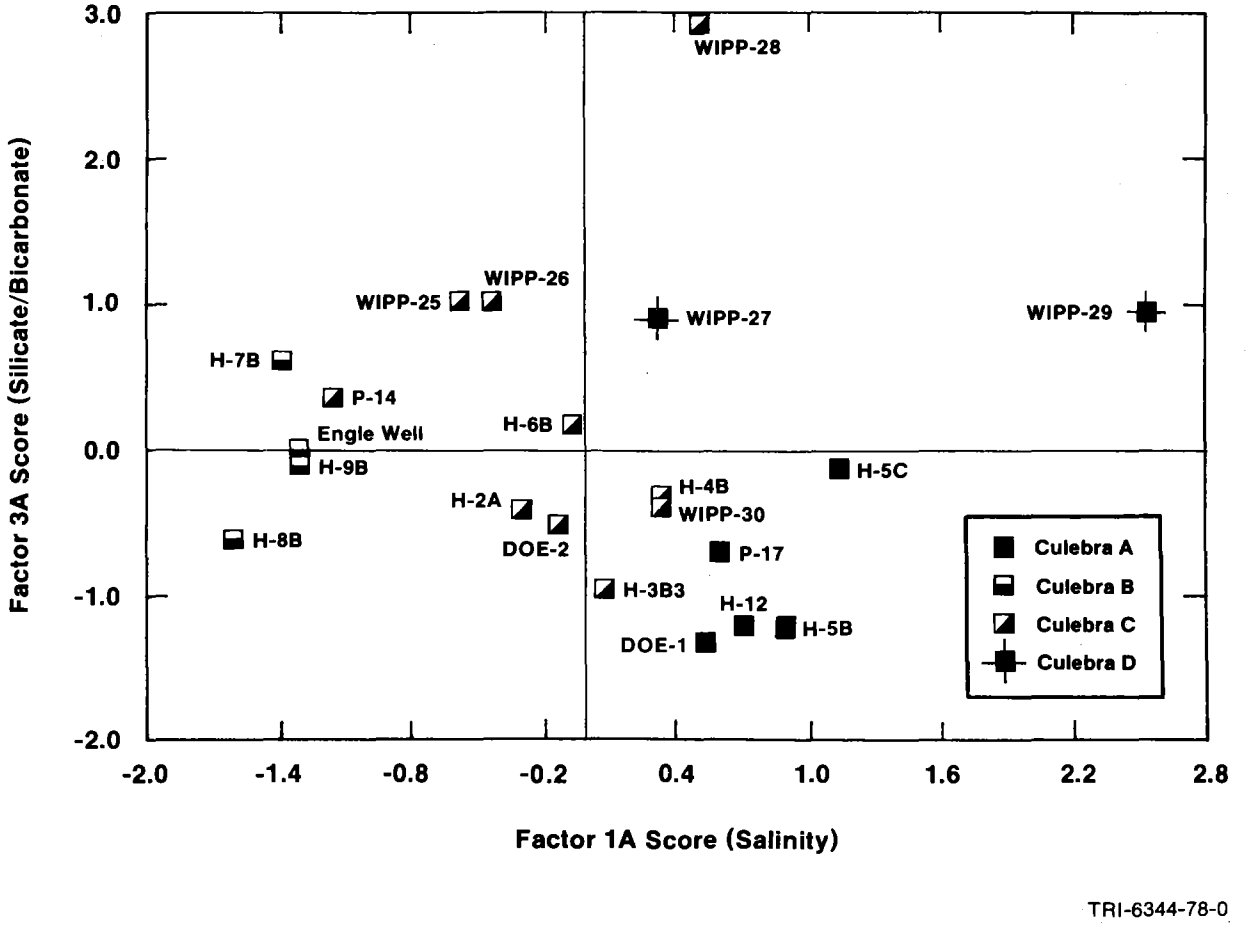


Figure 2-25. Relationship between varimax R-mode factor scores for factors 1A and 3A of Culebra groundwaters (population 1).

Scores for the salinity factor (1A) are lowest for wells in Zone B and are highest for WIPP-29 (Zone D) and for wells in Zone A. In Zone C, the scores for the salinity factor are intermediate; within the zone, the scores are lowest for P-14 and increase radially to the east, west, and north. The contours for the scores of salinity factor are similar to those for sodium concentration (Figure 2-14). This supports the suggestion that this factor is dominated by the effects of halite dissolution. The scores of the salinity factor (1A) are plotted and contoured in Figure 2C-3 in Appendix 2C.

P-14 has the highest score for the sulfate factor (2A). As discussed in Section 2.3.1, the concentrations of several elements in P-14 are anomalous, perhaps because of contamination. Ca, Sr, I, and Br exhibit local highs in their element contours; $SO_4$ and the Na/Cl ratio are anomalously low. The lowest (most negative) score for this factor is exhibited by WIPP-29; this well also has an anomalously high concentration of $SO_4$. The scores for the sulfate factor (2A) are plotted and contoured in Figure 2C-5 in Appendix 2C.

Figure 2-25 shows the scores of the salinity (1A) and silicate/bicarbonate (3A) factors for each well. The scores for the silicate/bicarbonate factor show little relationship to the hydrochemical facies, although there is a general increase in the value of the score from west to east. WIPP-28 has the highest score and is anomalous compared to wells surrounding it. The bicarbonate concentration at WIPP-28 is also anomalously high because of contamination (see Table 2-3, Section 2.2) and dominates the score for this well. Contours of the spatial distribution of scores for the silicate factor are not plotted; the pattern is similar to that of $SiO_2$ presented in Figure 2-8.

### 2.3.3.5 R-mode Factors Obtained After Partialling Out Total Dissolved Solids

#### *2.3.3.5.1 OBJECTIVES AND PROCEDURE*

The three major factors obtained from the R-mode analysis described above are strongly affected by halite dissolution. Solutes are added directly from the halite or indirectly because the solubilities of sulfate and carbonate phases increase as the ionic strength increases (see Section 2.4.2). A second R-mode PCA was carried out to examine interelement correlations independent of the effects of halite dissolution. The analysis was carried out as follows. First, regression equations for each of the chemical variables as a function of the TDS were obtained. Next, the partial correlation matrix with respect to TDS was obtained by calculating the correlations between the residuals from the regression equations. Finally, the eigenvectors of the partial correlation matrix were extracted to give the principal components. A detailed description of the procedure can be found in Appendix 2B.

This PCA was carried out on the variance in the population that is not correlated with variation in the TDS. The amount of this residual variance for each variable is shown in the last column of Table 2-8. After accounting for the correlation with TDS, very little of the variance of Na, Mg, K, and Cl remains. In contrast, a significant portion of the variation in the concentrations of Ca, Sr, B, and $SiO_2$, the pH, and the alkalinity cannot be correlated with the TDS. The results of this analysis are summarized in the following section; a more detailed discussion of the analysis is found in Appendix 2C.

#### *2.3.3.5.2 DESCRIPTION OF FACTORS*

Five factors account for 99% of the variance that remains after the TDS is partialled out. The varimax factor-loading matrix for the five factors is shown in Table 2-8. In Figure 2-26, the variables with the highest loadings for each factor are identified. Table 2-9 recasts the factor loadings in terms of the percentage of the total variance (including the variance correlated to TDS) of each variable that each factor explains. These percentages of the

**Table 2-8. Varimax R-mode Factor Loadings (Percent) Obtained from Partial-Correlation Matrix with Respect to TDS of Culebra Groundwaters (Population 1)**

| Element | Factor 1B | Factor 2B | Factor 3B | Factor 4B | Factor 5B | Communality ($h_i^2$) | Residual Variance[1] |
|---|---|---|---|---|---|---|---|
| Na | 12 | -10 | 76 | -58 | 4 | 98.7 | 4% |
| Cl | 28 | 3 | 84 | -36 | - 4 | 96.1 | 7% |
| Ca | 97 | - 1 | 14 | - 8 | - 1 | 99.2 | 71% |
| Mg | - 3 | 23 | -23 | 92 | 10 | 98.1 | 7% |
| K | -30 | 22 | 5 | -13 | -25 | 98.8 | 9% |
| Sr | 94 | - 1 | 25 | 9 | 1 | 97.1 | 39% |
| pH | - 1 | -93 | 19 | -26 | 7 | 98.7 | 91% |
| $HCO_3$ | -11 | 79 | - 4 | 3 | -22 | 97.1 | 96% |
| $SO_4$ | -94 | -18 | -14 | 5 | 17 | 98.2 | 27% |
| $SiO_2$ | 18 | 93 | 4 | 9 | -24 | 99.0 | 58% |
| Br | 27 | -16 | 86 | 8 | 13 | 96.2 | 19% |
| B | -19 | -52 | 14 | -55 | 47 | 97.3 | 43% |
| Li | -12 | -34 | 7 | 7 | 90 | 99.5 | 18% |

## Table 2-8. Varimax R-mode Factor Loadings (Percent) Obtained from Partial-Correlation Matrix with Respect to TDS of Culebra Groundwaters (Population 1) (Continued)

| Amount and Percent of Variance[1] Explained by Each Factor | | | | |
|---|---|---|---|---|
| Factor 1B | Factor 2B | Factor 3B | Factor 4B | Factor 5B |
| 3.071 | 2.903 | 2.251 | 1.737 | 1.265 |
| 27% | 26% | 20% | 16% | 11% |

1. Variance not correlated to TDS; that is, the amount of variance remaining after TDS was partialled out.

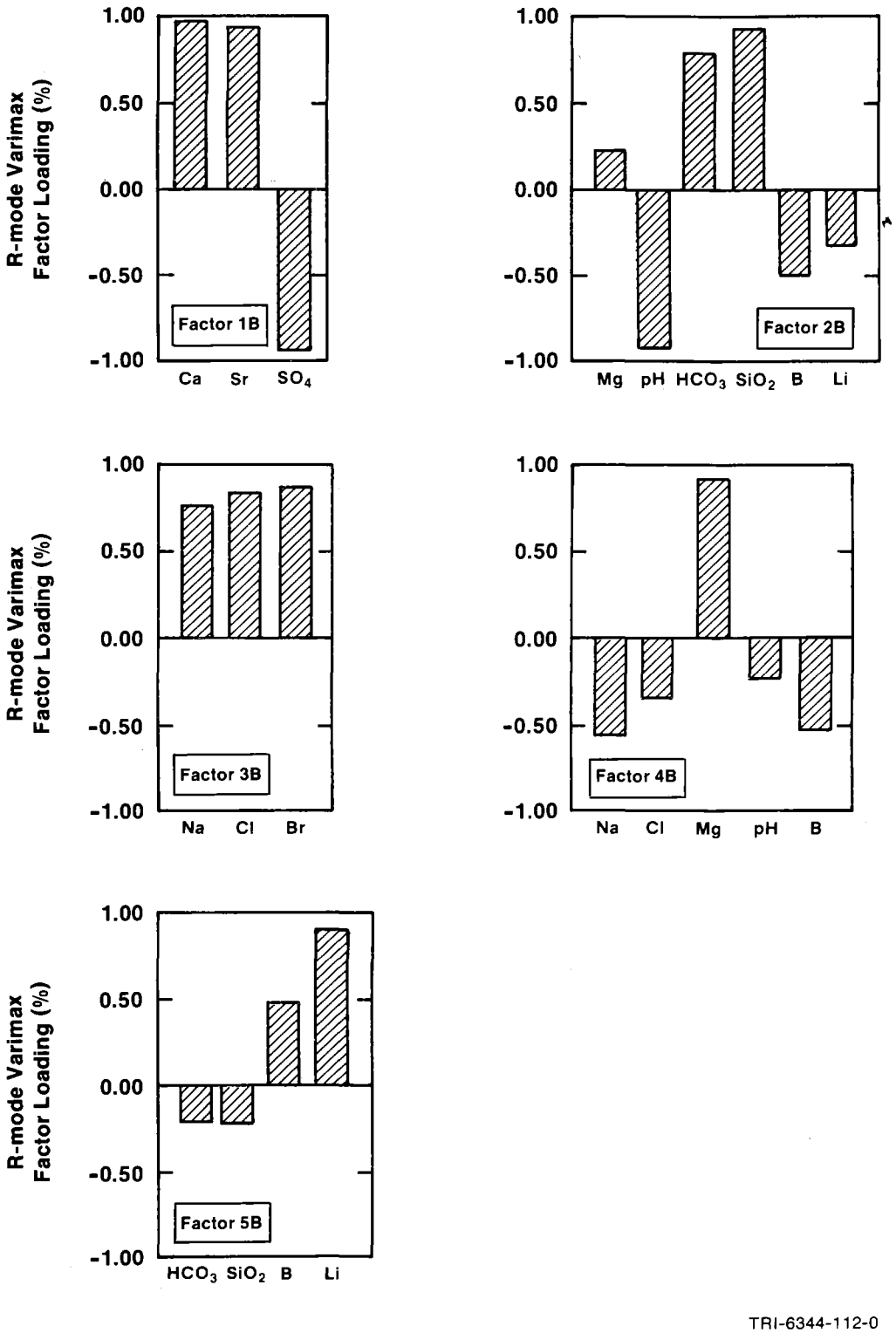


Figure 2-26. Varimax R-mode factor loadings of key (loading >0.23) elements for factors 1B, 2B, 3B, 4B, and 5B obtained from partial-correlation matrix with respect to TDS of Culebra groundwaters (population 1).

**Table 2-9. Percent of Total Variance[1] Explained by Varimax R-mode Factors Obtained from Partial-Correlation Matrix with Respect to TDS of Culebra Groundwaters (Population 1)**

| Element | Factor 1B | Factor 2B | Factor 3B | Factor 4B | Factor 5B | Residual Variance[2] |
|---|---|---|---|---|---|---|
| Na | * | * | * | * | * | 4% |
| Cl | * | * | 5% | * | * | 7% |
| Ca | 67% | * | * | * | * | 71% |
| Mg | * | * | * | 6% | * | 7% |
| K | * | * | * | * | * | 9% |
| Sr | 35% | * | * | * | * | 39% |
| pH | * | -79% | * | -6% | * | 91% |
| $HCO_3$ | * | 60% | * | * | -5% | 96% |
| $SO_4$ | -24% | * | * | * | * | 27% |
| $SiO_2$ | ** | 50% | ** | ** | -3% | 58% |
| Br | * | * | 14% | * | * | 19% |
| B | * | -12% | * | -13% | 10% | 43% |
| Li | * | * | * | * | 15% | 18% |

1. Percent of total variance. Signs indicate type of correlation shown in Table 2-8. An asterisk indicates that the percent variance is <5%; a double asterisk indicates that the percent variance is <3%.
2. Amount of variance that is not correlated with the TDS.

total variance are plotted in Figure 2-27. Figure 2-27 plots variances only for elements for which the factors explain approximately >5% of the total variance.

Factor 1B is dominated by the negative correlation of Ca and Sr with sulfate and is suggestive of dissolution/coprecipitation of Sr and Ca in a sulfate phase such as gypsum or anhydrite. It accounts for 67% of the total variance of Ca, 35% of the total variance of Sr, and 24% of the total variance of sulfate. This factor is similar to the sulfate factors (3 and 2A) described in Section 2.3.3.4. The factor scores are plotted in Figure 2-28. The spatial distribution of the scores is not related to hydrochemical facies; the scores are contoured in

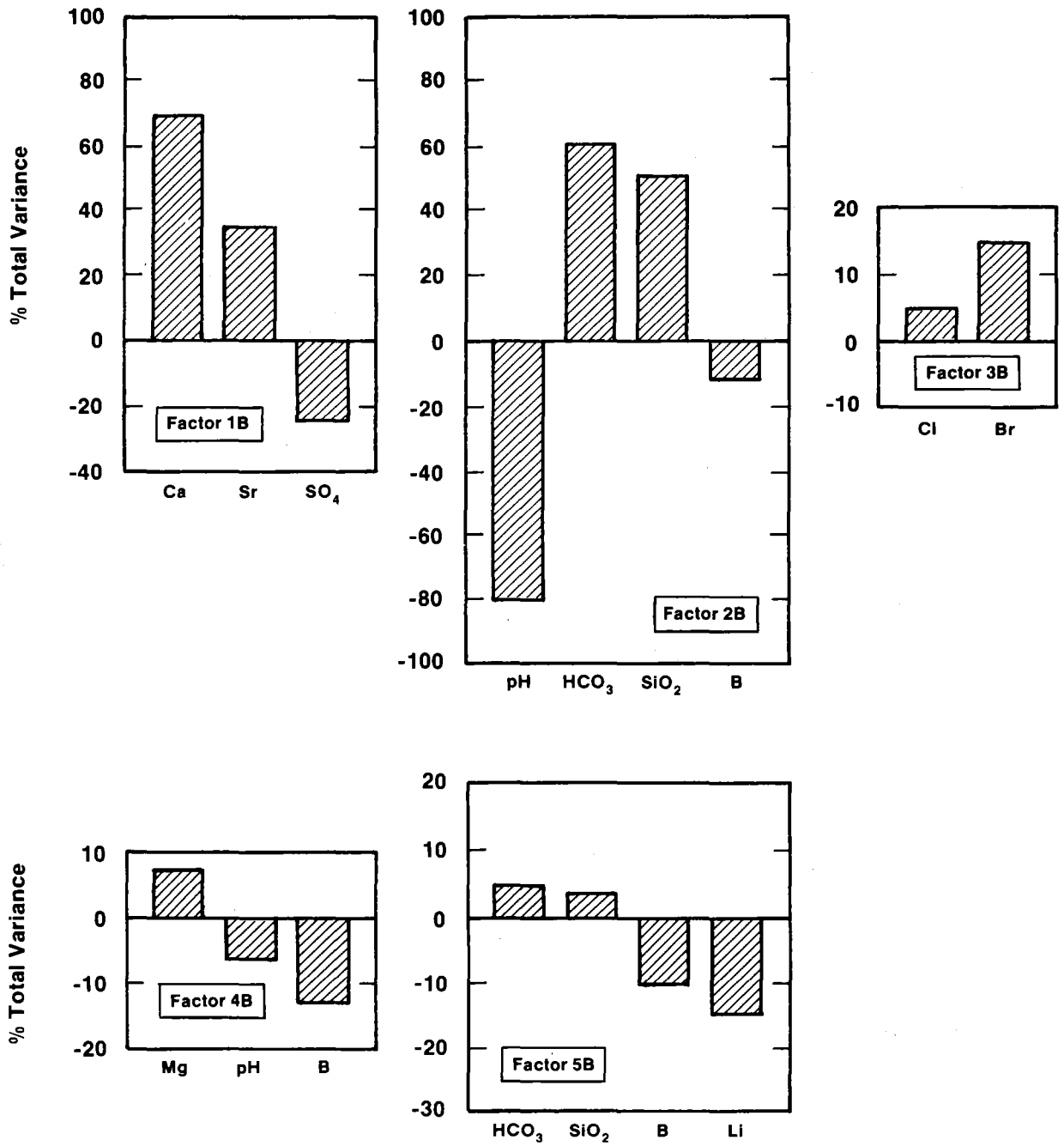


Figure 2-27. Amount of total variance of key elements explained by factors 1B to 5B obtained from the partial-correlation matrix with respect to TDS of Culebra groundwaters (population 1).

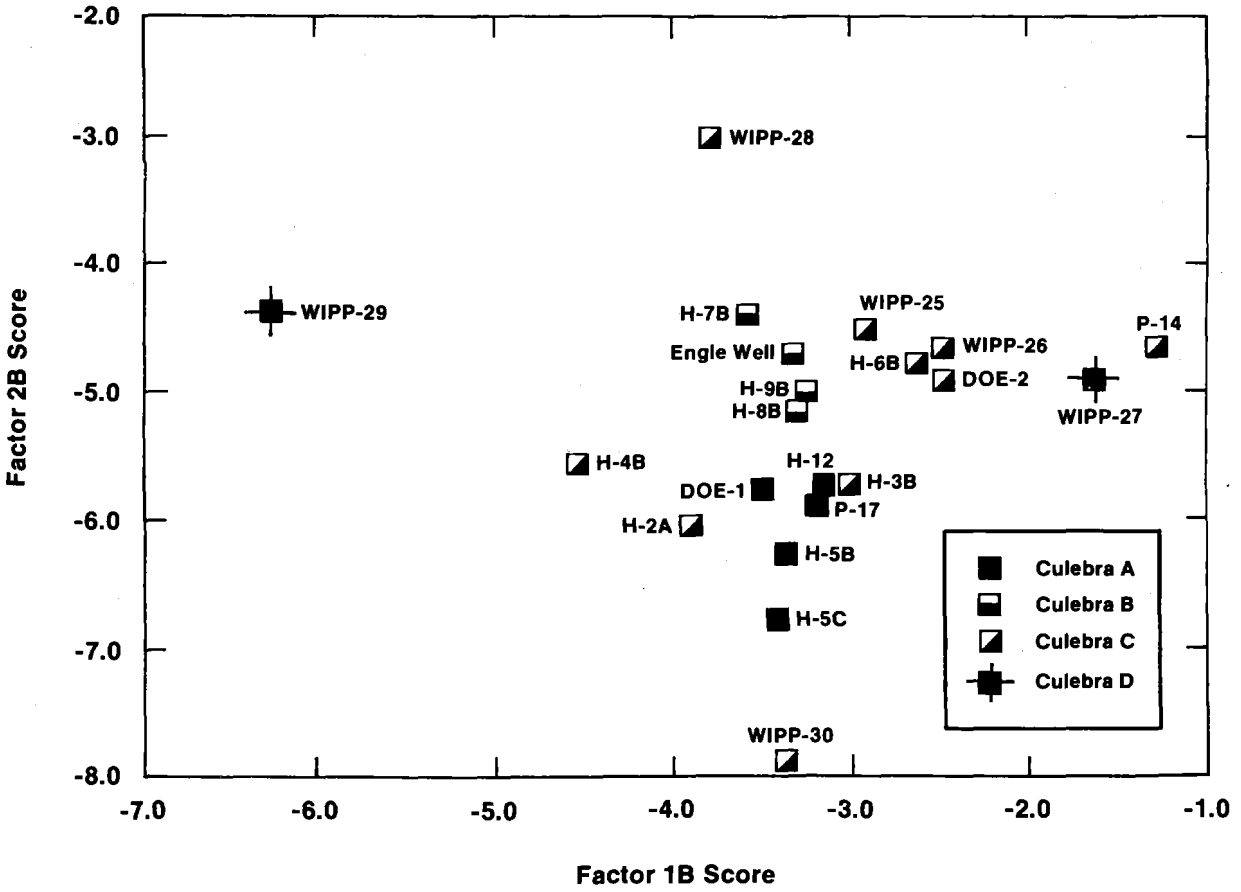


Figure 2-28. Relationship between varimax R-mode factor scores for factors 1B and 2B obtained from the partial-correlation matrix with respect to TDS of Culebra groundwaters (population 1).

Figure 2C-8 in Appendix 2C. Well P-14 has the highest score for this factor; WIPP-29 has the lowest score.

Factors 2B, 4B, and 5B are similar to the silicate factors (2 and 3A) described in Section 2.3.3.4. They contain all or portions of two negatively correlated groups of variables. One group involves the correlation of Mg, K, bicarbonate alkalinity, and silica; the other group contains Na, pH, B, and Li. This pattern of element associations may be due to a combination of processes including sorption, ion exchange, carbonate diagenesis, and silicate diagenesis. The pattern is discussed in more detail in Section 2.4.3.

Figure 2-28 shows that Factor 2B clearly distinguishes hydrochemical facies A from facies B. The extreme values of the factor score, however, are both in Zone C. Both of the extrema, WIPP-30 and WIPP-28, are anomalous with respect to neighboring wells. WIPP-30 exhibits the lowest silica concentration (4 mg/L). WIPP-28 exhibits the highest bicarbonate alkalinity in the population, but is known to be contaminated (Section 2.2). Figure 2-29 shows that on a regional scale, the value of the score increases from east to west. In Section 2.4.3, it is suggested that this trend could be related to a westward increase of the amount of silicates exposed to groundwaters. The increased amounts of silicates are consistent with the greater degree of evaporite dissolution and formation of a residual fraction in the parts of the aquifer in contact with the groundwater.

#### 2.3.3.6 Principal Component Analysis of Culebra, Magenta, Dewey Lake, and Bell Canyon Groundwater Samples

PCA was carried out on a second data set containing water compositions from wells in the Culebra dolomite, Magenta dolomite, Dewey Lake Red Beds, and Bell Canyon Formation. The sample population is designated "population 2" and is described in Table 2-4. The primary purpose of this analysis was to examine the relationships between the major solutes and several minor elements not included in population 1 (which included Culebra data only). Concentrations of iron, manganese, fluoride, and iodide were included in this

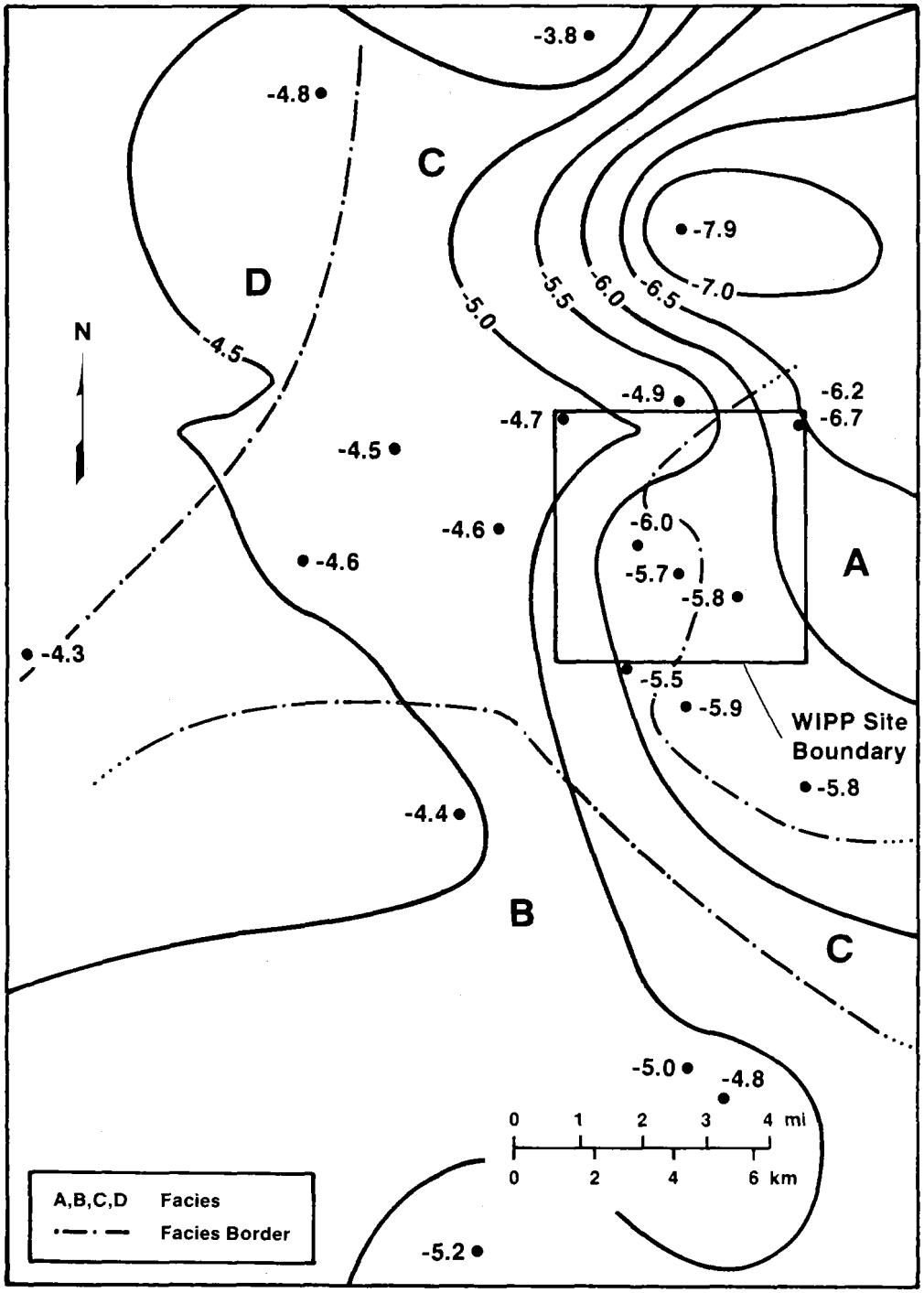


Figure 2-29. Contour plot of varimax R-mode factor scores for factor 2B obtained from the partial-correlation matrix with respect to TDS of Culebra groundwaters (population 1).

data set, in addition to the 13 variables included in the analysis of Culebra data. Only data from the chemical analyses carried out at UNC laboratory and listed in Table 2-2 were used. The results of the analysis pertinent to the primary objective are summarized in this section.

A secondary objective of the analysis of population 2 was to determine if the relationships among chemical variables observed in the Culebra were present in a larger data set drawn from the Rustler and related formations. In Appendix 2D, the solute relationships in population 2 are compared to those of population 1. In addition, the methods of data pretreatment, factor extraction, and rotations, and the factor-loading and score matrices are described in detail in the appendix.

#### *2.3.3.6.1 R-MODE PRINCIPAL COMPONENT ANALYSIS*

The Q-mode analysis, described in Appendix 2D, showed that the data set was homogeneous enough for R-mode analysis. R-mode PCA was carried out on this data set in the same manner that it was carried out with data from the Culebra in the previous section. Seven varimax factors that account for nearly all of the variance (99%) were extracted. The factor loadings are described in Table 2D-5 (Appendix 2D); the five most important factors are shown in Figure 2-30. At least 93% of the variance of each variable could be explained by these factors.

Relationships among major solutes in population 2 are similar to those in population 1. The first three principal components shown in Figure 2-30 account for 67% of the total variance of the sample population. For most elements, they are similar to the salinity, sulfate, and silicate/bicarbonate varimax factors (factors 1A, 2A, and 3A) extracted from the Culebra data set (population 1) and shown in Figure 2-2. The two important exceptions are sulfate and magnesium, discussed below.

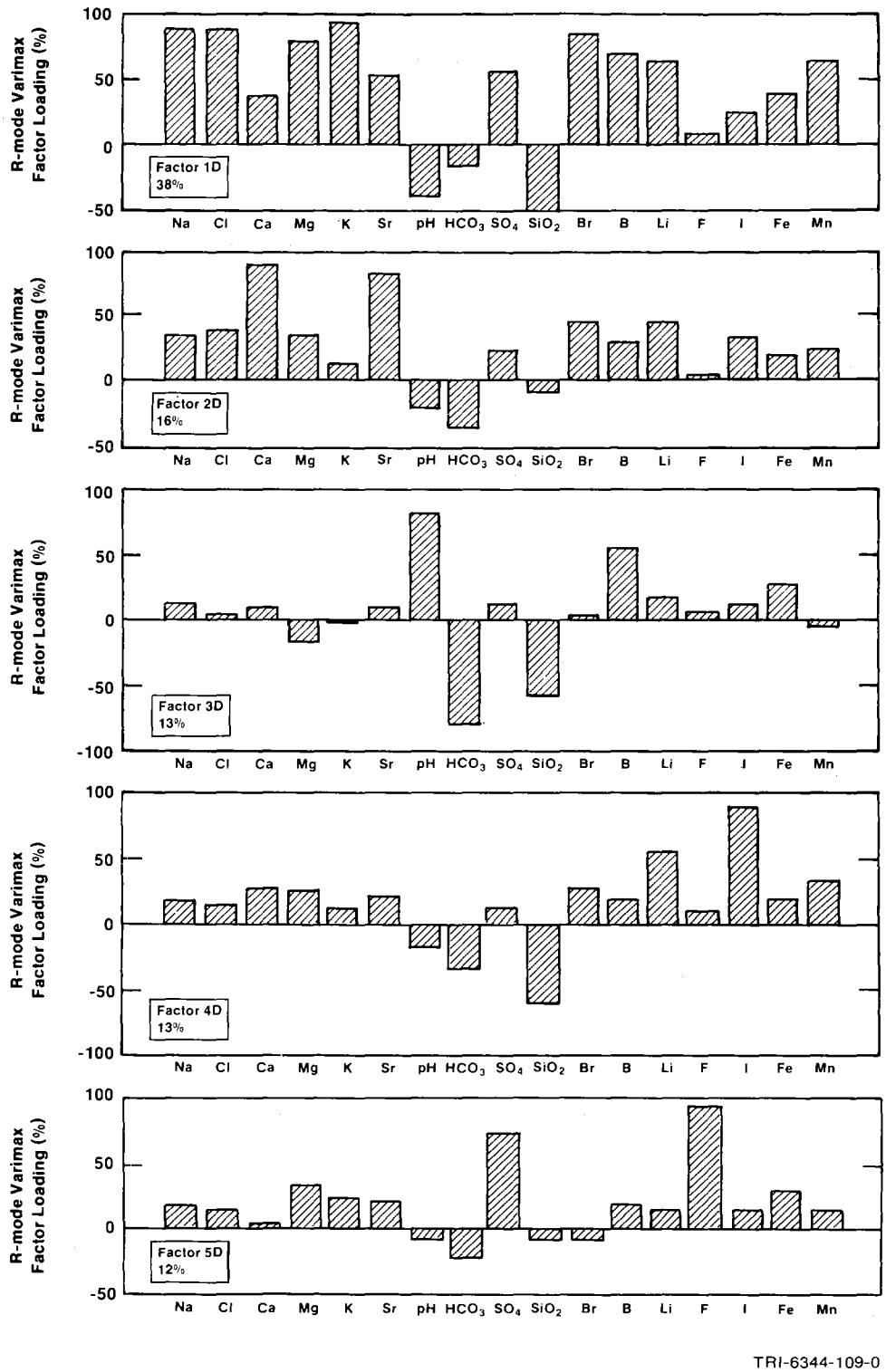


Figure 2-30. Varimax R-mode factor loadings for factors 1D, 2D, 3D, 4D, and 5D of Rustler, Dewey Lake, and Bell Canyon groundwaters (population 2).

The inclusion of data for fluoride concentrations in population 2 affected the factor loadings for sulfate and magnesium in the sulfate and silicate factors. Factor 5D is the most significant factor for both F and $SO_4$ (see Table 2D-5 in Appendix 2D). Fluorine occurs most commonly in fluorite ($CaF_2$) and sellaite ($MgF_2$). Sonnenfeld (1984) notes that typically $MgF_2$ occurs as an accessory mineral associated with anhydrite, whereas $CaF_2$ more commonly occurs with carbonates. The association of F, $SO_4$, and Mg in factor 5D may indicate that $MgF_2$ in anhydrite is the source of fluoride in these waters.

This PCA also allows an examination of the behavior of iodide, iron, and magnanese. Iodide is correlated with Na and Cl and inversely correlated with Si on all factors. Factor 4D of population 2 is dominated by the behaviors of I, Si, and Li and has no counterpart in the Culebra analysis. The geochemical significance of this factor is unclear. Nearly all of the waters in population 2 are enriched in iodide relative to the seawater evaporation curve (cf. Collins, 1975). Potential sources of the excess iodide include dissolution of iodide from evaporite minerals or organic material and desorption from clays. As discussed in Appendix 2D, examination of the factor scores and element ratios suggests that the relative importance of these sources probably varies vertically and horizontally throughout the study area.

Iron loads primarily onto its own principal component, factor 6D; Mn has an appreciable loading onto this factor also (see Table 2D-5). The lack of correlation between Fe and Mn with other major and minor solutes may be due to random errors in sampling or analyses as discussed in Section 2.2. Manganese also loads strongly onto factor 1D and factor 7D; the geochemical significance of these elemental associations is unclear, but might be related to borehole pipe corrosion.

#### *2.3.3.6.2 R-MODE ANALYSIS WITH SALINITY PARTIALLED OUT*

A second R-mode PCA was carried out in which the correlation of each element with the TDS concentration was partialled out. The resulting factor pattern shows the interelement

correlations independent of the effects that may be attributed to halite dissolution. The results are described in Appendix 2D.

## 2.3.4 Saturation Indices for Culebra Groundwaters

### 2.3.4.1 Introduction

Calculations of saturation indices of groundwaters are useful in suggesting the identity of the minerals that may control solute concentrations, in detecting evidence of metastable persistence of mineral phases, and in indicating possible errors in chemical analyses or sampling procedures. Saturation indices for common evaporite minerals for Culebra brine samples are presented in Table 2-10.

The calculations were carried out using the geochemical reaction and speciation code PHRQPITZ (Plummer et al., 1988). This code uses a specific interaction model to calculate activity coefficients in the system Na-Ca-Mg-K-H-OH-$HCO_3$-$CO_3$-$CO_2$-$SO_4$-Cl-$H_2O$. The theory, data, and implementation are based primarily on previous work by Pitzer and coworkers (Pitzer, 1973, 1975; Pitzer and Kim, 1974; Pitzer and Mayorga, 1973, 1974) and Harvie et al. (Harvie and Weare, 1980; Harvie et al., 1984). Estimates of the maximum ionic strength for which the model accurately predicts mineral solubilities range from 6 to 20 molal. For comparison, the Davies equation used in codes such as PHREEQE (Parkhurst et al., 1980) is accurate up to about 0.5 molal.

Given the dissolution of a solid:

$$M_aL_b \rightarrow aM^{m+} + bL^{n-} \qquad \text{(where } a \cdot m = b \cdot n\text{)} \qquad [1]$$

the equilibrium constant is given by:

$$\log K_{sp} = \frac{-\Delta G_R}{2.303\ RT} \qquad [2]$$

## Table 2-10. Mineral Saturation Indices for Culebra Groundwaters

| Well[3] | Date | Density (g/mL) | Temp[4] (°C) | Ionic Str.[1] | pH[5] | $a_{H_2O}$[1] | CBE[1,6] | Saturation Indices[1,2] Anh | Cal | Dol | Gyp | Hal | Mag | log $pCO_2$[1] |
|---|---|---|---|---|---|---|---|---|---|---|---|---|---|---|
| DOE-1 | 4/85 | 1.09 | 22 | 2.53 | 7.10 | 0.923 | 9.05E-03 | -0.12 | -0.34 | -0.13 | 0.03 | -1.26 | -0.62 | -2.60 |
| DOE-2 | 3/85 | 1.04 | 22 | 1.19 | 7.00 | 0.968 | -6.52E-02 | -0.18 | -0.21 | -0.14 | 0.01 | -2.03 | -0.77 | -2.33 |
| ENGLE | 3/85 | 1.00 | 22 | 0.09 | 7.40 | 0.999 | 1.00E-03 | -0.22 | 0.22 | 0.38 | 0.00 | -6.02 | -0.68 | -2.44 |
| H-2A | 4/86 | 1.01 | 22 | 0.27 | 8.00 | 0.994 | -4.33E-03 | -0.25 | 0.45 | 0.78 | -0.04 | -3.49 | -0.52 | -3.38 |
| H-3B3 | 2/85 | 1.04 | 22 | 1.08 | 7.40 | 0.971 | -2.53E-03 | -0.20 | -0.08 | 0.12 | 0.00 | -2.11 | -0.65 | -2.86 |
| H-3B3 | 6/84 | 1.03 | 26 | 1.08 | 7.40 | 0.972 | -2.56E-02 | -0.15 | -0.02 | 0.23 | 0.04 | -2.13 | -0.59 | -2.83 |
| H-4B | 5/81 | 1.01 | 22 | 0.455 | 8.00 | 0.991 | -1.49E-02 | -0.17 | 0.36 | 1.07 | 0.04 | -3.13 | -0.13 | -3.35 |
| H-4B | 7/85 | 1.02 | 22 | 0.42 | 7.70 | 0.991 | 4.14E-03 | -0.20 | 0.07 | 0.46 | 0.01 | -3.17 | -0.45 | -3.04 |
| H-4C | 8/84 | 1.01 | 21 | 0.45 | 7.80 | 0.991 | 4.82E-03 | -0.20 | 0.19 | 0.77 | 0.01 | -3.12 | -0.26 | -3.11 |
| H-5B | 6/81 | 1.10 | 22 | 2.993 | 7.90 | 0.906 | -1.18E-01 | -0.10 | 0.71 | 2.12 | 0.04 | -1.08 | 0.57 | -3.21 |
| H-5B | 8/85 | 1.10 | 22 | 2.97 | 7.40 | 0.908 | 8.46E-02 | -0.11 | -0.02 | 0.68 | 0.03 | -1.09 | -0.15 | -2.86 |
| H-5C | 10/81 | 1.10 | 24 | 3.002 | 7.90 | 0.906 | -1.20E-01 | -0.08 | 0.75 | 2.20 | 0.05 | -1.08 | 0.61 | -3.17 |
| H-6B | 5/81 | 1.04 | 22 | 1.178 | 7.00 | 0.969 | 2.24E-04 | -0.15 | -0.04 | 0.16 | 0.05 | -2.05 | -0.64 | -2.16 |
| H-6B | 9/85 | 1.04 | 22.5 | 1.13 | 6.90 | 0.970 | -1.28E-02 | -0.20 | -0.16 | -0.07 | -0.01 | -2.08 | -0.75 | -2.07 |
| H-7B1 | 3/86 | 1.00 | 22 | 0.089 | 7.20 | 0.999 | -4.09E-04 | -0.23 | 0.07 | 0.01 | -0.01 | -5.86 | -0.90 | -2.20 |
| H-8B | 1/86 | 1.00 | 22 | 0.083 | 7.60 | 0.999 | -1.97E-04 | -0.23 | 0.33 | 0.66 | -0.01 | -7.45 | -0.52 | -2.70 |
| H-9B | 11/85 | 1.00 | 22 | 0.087 | 7.40 | 0.999 | 3.70E-04 | -0.22 | 0.24 | 0.37 | 0.00 | -6.23 | -0.71 | -2.43 |
| H-11B3 | 6/85 | 1.09 | 22.7 | 2.23 | 7.20 | 0.934 | -3.60E-02 | -0.13 | -0.17 | 0.12 | 0.03 | -1.39 | -0.54 | -2.63 |
| H-12 | 8/85 | 1.10 | 24 | 2.72 | 7.20 | 0.916 | 4.42E-02 | -0.12 | -0.15 | 0.34 | 0.02 | -1.18 | -0.35 | -2.61 |
| P-14 | 2/86 | 1.02 | 21.5 | 0.582 | 6.80 | 0.988 | -9.06E-03 | -0.15 | 0.14 | 0.18 | 0.05 | -3.01 | -0.81 | -1.81 |

## Table 2-10. Mineral Saturation Indices for Culebra Groundwaters (Continued)

| Well[3] | Date | Density (g/mL) | Temp[4] (°C) | Ionic Str.[1] | pH[5] | $a_{H_2O}$[1] | CBE[1,6] | Saturation Indices[1,2] Anh | Cal | Dol | Gyp | Hal | Mag | log $pCO_2$[1] |
|---|---|---|---|---|---|---|---|---|---|---|---|---|---|---|
| P-17 | 3/86 | 1.06 | 21.2 | 1.67 | 7.50 | 0.953 | -3.61E-02 | -0.18 | 0.10 | 0.73 | 0.00 | -1.70 | -0.22 | -2.90 |
| WIPP-25 | 8/80 | 1.01 | 23 | 0.26 | 6.90 | 0.995 | 3.21E-03 | -0.24 | 0.03 | 0.04 | -0.03 | -3.56 | -0.84 | -1.69 |
| WIPP-26 | 8/80 | 1.00 | 22 | 0.329 | 6.90 | 0.993 | -5.12E-03 | -0.18 | -0.04 | -0.10 | 0.03 | -3.36 | -0.91 | -1.86 |
| WIPP-26 | 8/80 | 1.01 | 22 | 0.330 | 6.90 | 0.993 | -3.71E-02 | -0.23 | 0.09 | 0.14 | -0.02 | -3.32 | -0.79 | -1.84 |
| WIPP-26 | 11/85 | 1.01 | 22 | 0.371 | 7.10 | 0.992 | -9.29E-03 | -0.20 | 0.10 | 0.18 | 0.02 | -3.22 | -0.77 | -2.14 |
| WIPP-27 | 9/80 | 1.09 | 22 | 2.573 | 6.30 | 0.922 | -7.62E-02 | -0.12 | -0.38 | -0.40 | 0.03 | -1.29 | -0.87 | -1.33 |
| WIPP-28 | 9/80 | 1.03 | 22 | 0.903 | 6.50 | 0.976 | -2.42E-02 | -0.26 | 0.16 | 0.53 | -0.07 | -2.27 | -0.48 | -0.76 |
| WIPP-29 | 8/80 | 1.16 | 20 | 4.908 | 6.10 | 0.840 | -2.06E-01 | 0.02 | -0.72 | 0.01 | 0.09 | -0.61 | -0.21 | -0.87 |
| WIPP-29 | 8/80 | 1.17 | 20 | 4.472 | 6.10 | 0.853 | -2.74E-01 | -0.15 | -0.45 | 0.61 | -0.07 | -0.64 | 0.21 | -1.10 |
| WIPP-29 | 12/85 | 1.22 | 21.5 | 6.57 | 5.90 | 0.773 | -2.07D-01 | -0.01 | -1.25 | -0.56 | -0.01 | -0.20 | -0.16 | -0.75 |
| WIPP-30 | 9/80 | 1.02 | 21 | 0.582 | 8.80 | 0.986 | -2.50E-02 | -0.18 | 1.12 | 2.37 | 0.02 | -2.73 | 0.41 | -4.41 |

1. Unless otherwise indicated, the solute data from UNC Geotech given in Table 2-2 were used in the PHRQPITZ (Plummer et al., 1988) calculations of the ionic strength (molal), the activity of water ($a_{H_2O}$), the charge-balance error, the log $pCO_2$ (atm.), and the saturation indices.
2. Anh = anhydrite; Cal = calcite; Dol = dolomite; Gyp = gypsum; Hal = halite; Mag = magnesite.
3. Samples from WIPP-26 and WIPP-29 were analyzed by the USGS Central Laboratory; the data are given in Mercer (1983).
4. Temperature measured at the wellhead during sampling test and assumed in saturation-index calculations.
5. The pH values used in the PHRQPITZ calculations; a few differ slightly from those given in Table 2.
6. The charge-balance error (CBE in equivalents per kilogram of water) was calculated as: CBE (eq/kg $H_2O$) = Σ cations (eq/kg $H_2O$) - Σ anions (eq/kg $H_2O$)

where $\Delta G_R$ is the free energy of reaction [1] in units of Kcal/mol, R is the gas constant, and T the absolute temperature.

Saturation indices (SI) are calculated as:

$$SI = \log IAP - \log K_{sp} \quad [3]$$

where the IAP is the ion activity product in the solution ($[M^{m+}]^a \cdot [L^{n-}]^b$).

At saturation, the saturation index equals zero; positive and negative values indicate supersaturation and undersaturation, respectively. All of the saturation index calculations in this report used unscaled activity coefficients (Plummer et al., 1988).

#### 2.3.4.2 Saturation Indices of Sulfates

Figure 2-31 illustrates the relationship between ionic strength and the saturation indices of gypsum ($CaSO_4 \cdot 2H_2O$) and anhydrite ($CaSO_4$). All water samples are saturated (SI = 0.00 ± 0.09) with respect to gypsum. This is expected given the common presence of gypsum in the Culebra (Sewards et al., Chapter 3) and the rapid dissolution rates of this mineral under natural conditions (Back et al., 1983).

With the exception of the Culebra samples from WIPP-29 (collected in 9/80 and 12/85 and analyzed by UNC), all samples are undersaturated with respect to anhydrite. Saturation with respect to anhydrite is related to the high ionic strengths of these waters. As discussed previously, the high salinities of these waters are caused by contamination from nearby potash refining operations.

Previous calculations for groundwaters from the Culebra showed nontrivial deviations from gypsum saturation. These may have been due in part to the failure of the ion-pairing

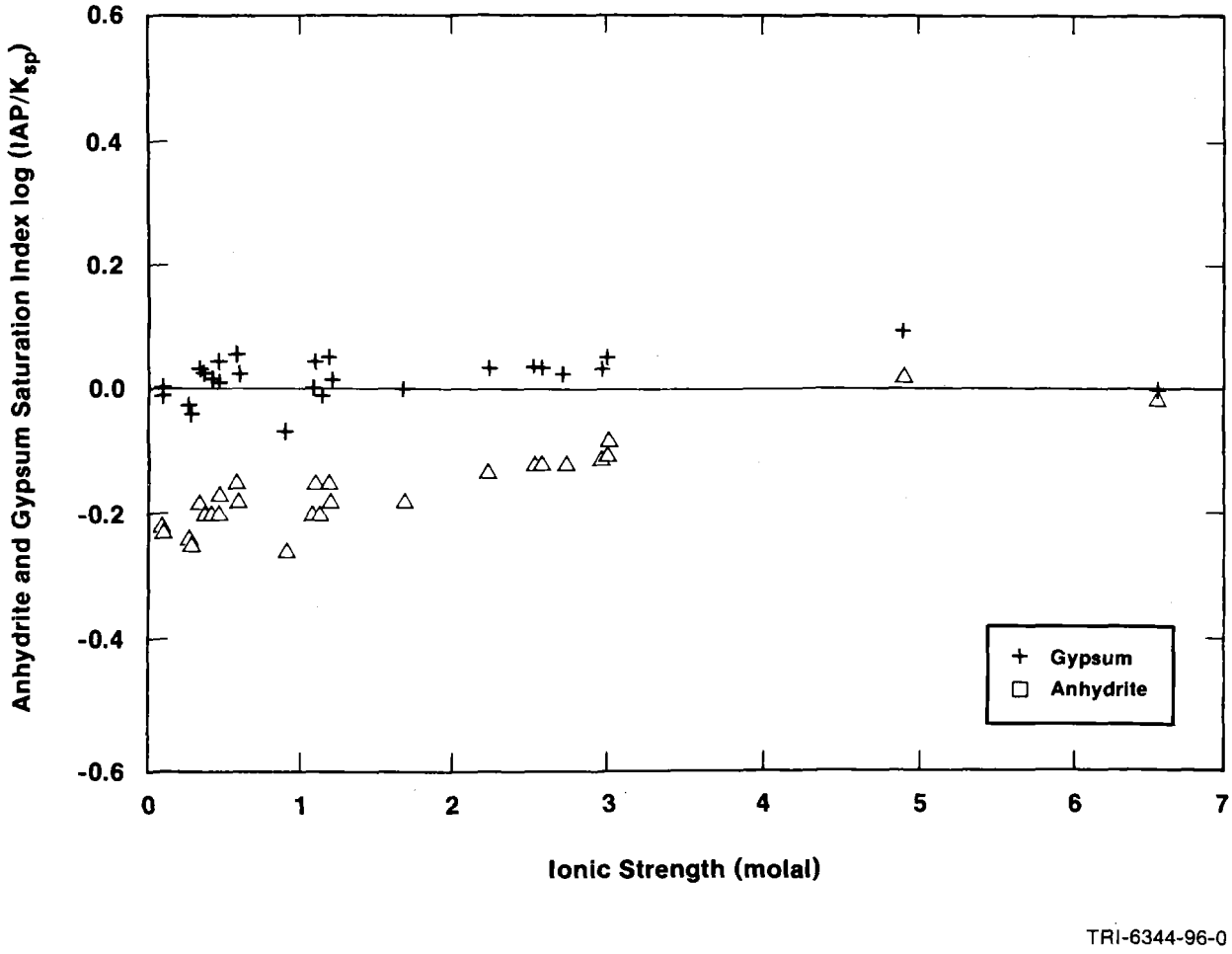


Figure 2-31. Relationship between anhydrite and gypsum saturation indices and ionic strengths of Culebra groundwaters.

chemical model used in WATEQFC and PHREEQE at high ionic strength (Ramey, 1985; Meijer et al., 1987). The calculations presented here show excellent agreement between field observations and predictions based on thermodynamic data.

#### 2.3.4.3 Saturation Indices of Evaporite Salts

Figure 2-32 shows the relationship between ionic strength and the calculated saturation indices for halite. All of the waters analyzed from the Culebra are undersaturated with respect to this mineral. Saturation indices were also calculated for other common evaporite salts (listed in Table 2A-1); all waters were undersaturated with respect to these minerals.

#### 2.3.4.4 Saturation Indices of Carbonates

Figures 2-33 and 2-34 show saturation indices for dolomite and calcite as functions of ionic strength. Many of the samples show appreciable supersaturation or undersaturation with respect to these carbonates. It has been suggested that waters in carbonate aquifers that are older than several hundreds of years should be saturated with these phases (Meijer et al., 1987). Available radiocarbon ages for Culebra waters suggest that they are at least 10,000 years old (Lambert, Chapter 5); thus, the apparent lack of carbonate equilibrium is problematic.

Previous saturation-index calculations for Culebra waters using the PHREEQE and WATEQFC codes also indicated that some samples were supersaturated with respect to the carbonate minerals (Ramey, 1985; Meijer et al., 1987). It was suggested that calculated deviations from saturation were due in part to failures of the aqueous model used in these codes. However, it is unlikely that the supersaturations calculated in Table 2-10 are due to errors in the aqueous model because the Pitzer formulation for the activity coefficients used in PHRQPITZ has been validated against experimental data (Plummer et al., 1988) in chemical systems similar to the Culebra waters. The version of PHRQPITZ used in these calculations does not include speciation of boron. This exclusion introduces a potential

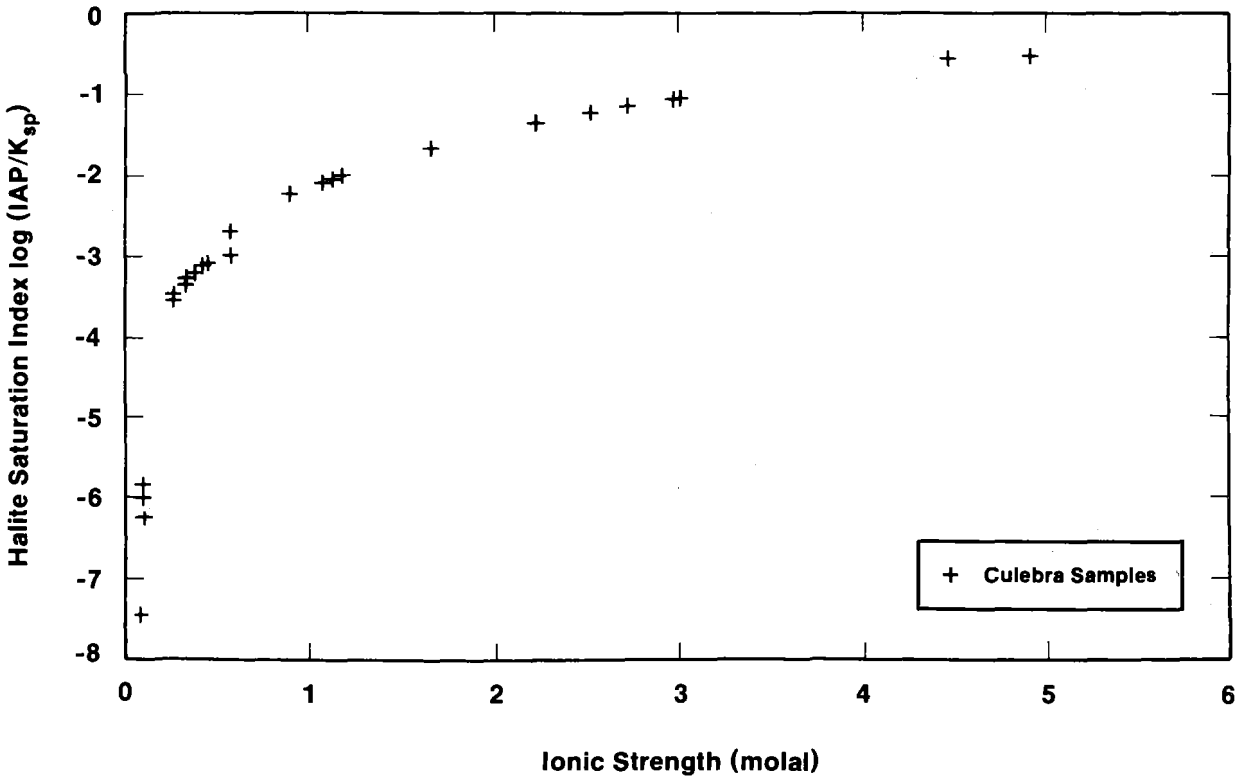


Figure 2-32. Relationship between halite saturation indices and ionic strengths of Culebra groundwaters.

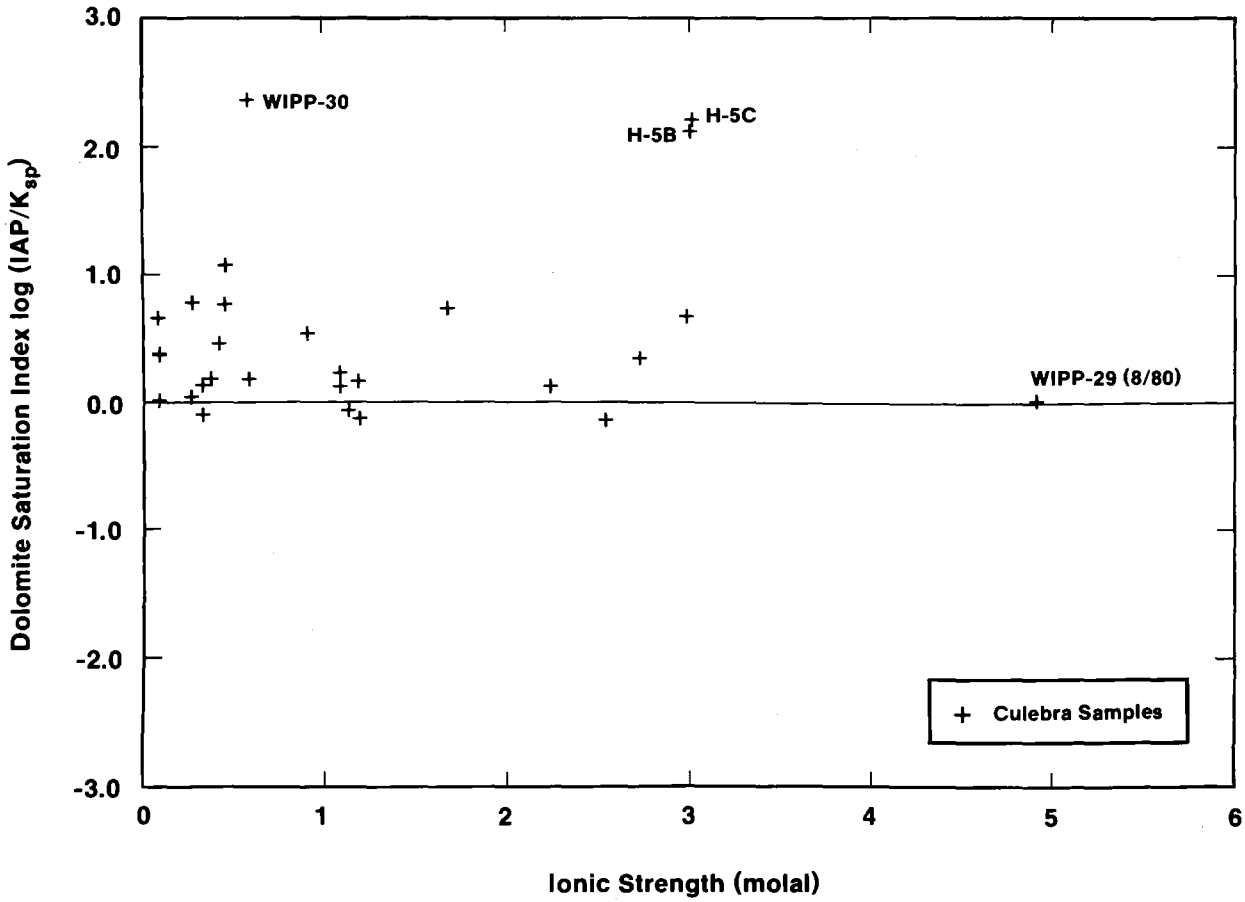


Figure 2-33. Relationship between dolomite saturation indices and ionic strengths of Culebra groundwaters.

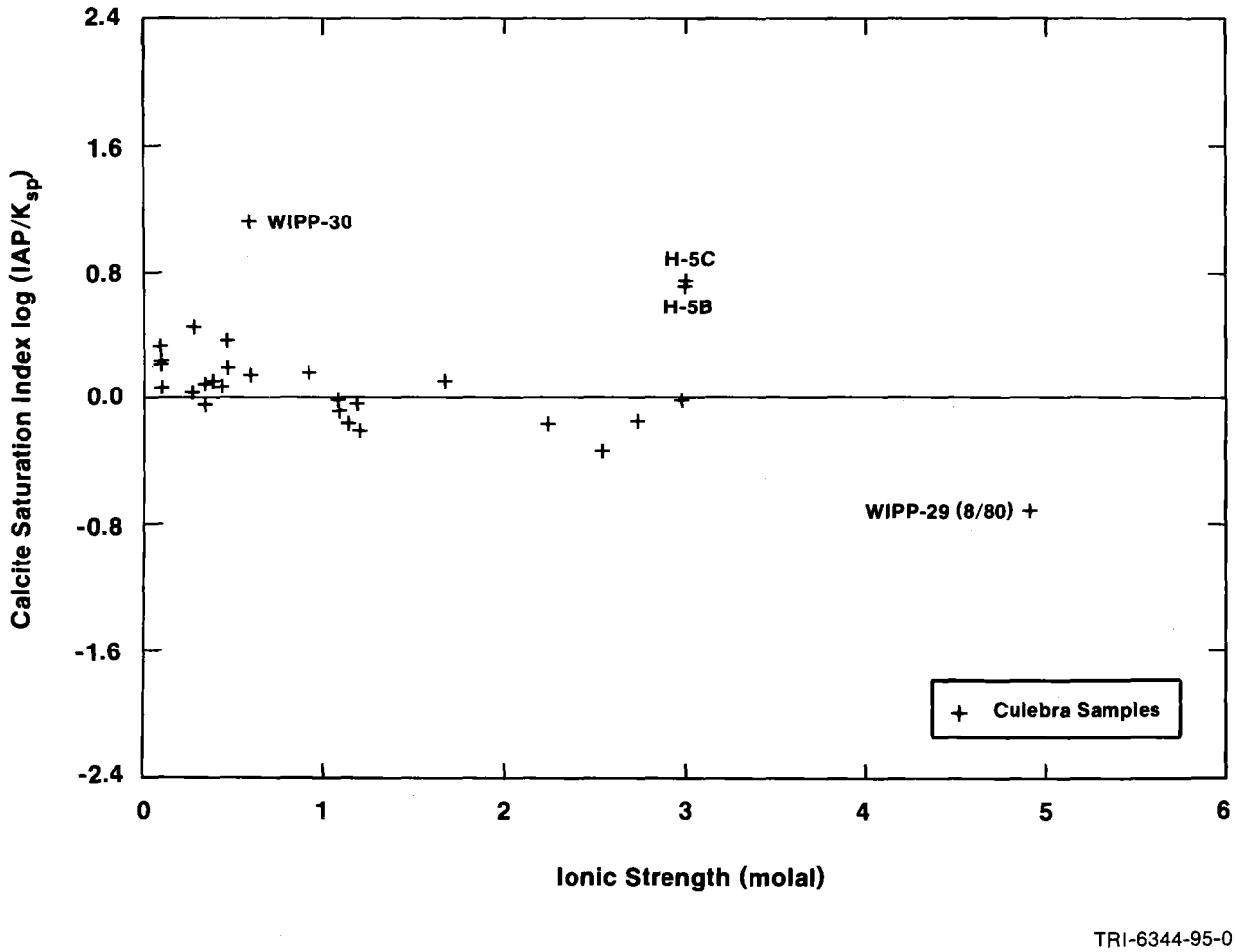


Figure 2-34. Relationship between calcite saturation indices and ionic strengths of Culebra groundwaters.

source of error in the calculated exclusion total inorganic carbon and carbon speciation. As discussed in Section 2.2.3.2, however, the low concentrations of boron in these waters suggest that this error is relatively small. This suggests that the calculated disequilibria may be real or due primarily to other factors such as errors in chemical analysis or sampling.

Errors in analysis of calcium could be responsible for errors in the saturation indices for the carbonates. However, the near-zero values of saturation indices for gypsum reported above and shown in Figure 2-35 suggest that this is not the cause of the calculated super-saturation.

In the following sections, several other possible sources of error are discussed. These include errors associated with pH measurements in brines, uncertainties in the free energies of carbonate solid phases, and $CO_2$ gas loss during sampling.

Finally, evidence that the Culebra waters are actually supersaturated with respect to dolomite and/or calcite is summarized.

#### *2.3.4.4.1 UNCERTAINTY IN pH MEASUREMENTS IN BRINES*

The inconsistency between the activity scales of the measured pH and the computed ion activities can lead to errors in calculated saturation indices. As discussed by Plummer et al. (1988), the activity scales are different because the buffers used to define the pH do not have the same composition as the brine of interest. In addition, due to the liquid-junction potentials, the measured pH is subject to deviations that are not accounted for in the theoretical speciation calculations.

Plummer et al., (1988) show that the magnitude of the error introduced by the use of different activity scales in a speciation calculation can be large, especially for the carbonate system. Plummer et al. (1988, sample problem 1) show that the saturation index for

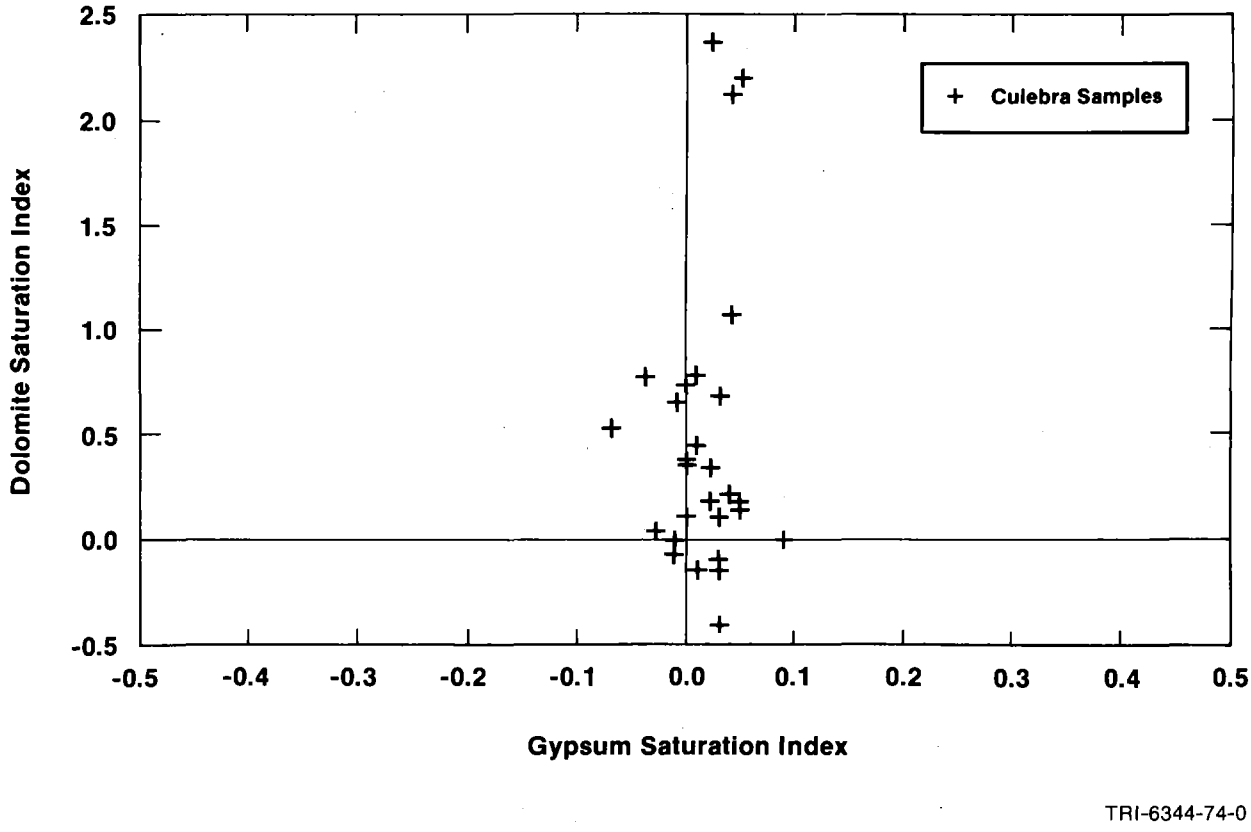


Figure 2-35. Relationship between gypsum and dolomite saturation indices in Culebra groundwaters.

dolomite calculated with two different commonly used scales varies from -1.08 (MacInnes scale) to -0.13 (not adjusted or unscaled) in a Canadian Shield brine sample (ionic strength of 8.5). They also show for the saline brine that the computed total concentration of inorganic carbon and $pCO_2$ varied by 300%, depending on the scale convention used. The error in less saline brines is also significant; individual ion activities in seawater (I = 0.7m) were shown to differ by as much as 10% when calculated with different scales.

In this study, all saturation indices are calculated with unscaled activities. The activity scale error may be responsible for part of the apparent supersaturation in the saturation indices shown in Figures 2-33 and 2-34. Only if the total alkalinity and either total inorganic carbon or $pCO_2$ are measured can the carbonate system be unambiguously defined. With such an approach, the pH is calculated rather than measured and problems associated with the different activity scales are avoided.

#### *2.3.4.4.2 UNCERTAINTY IN THERMODYNAMIC DATA FOR MINERAL PHASES*

Calculations of dolomite saturation indices for Culebra water samples are hindered by lack of reliable values for the free energy of the Culebra dolomite. Studies of carbonates from other areas (Reeder and Wenk, 1979; Reeder, 1981) suggest that nonstoichiometry and disorder may be sources of uncertainty in the Gibbs free energy of formation of the Culebra dolomites. Figure 2-36 compares saturation indices calculated using three different reference values for the free energy of dolomite. Note that these calculations were carried out with the EQ3NR computer code (Wolery, 1983) using the water composition data reported by Uhland and Randall (1986). The thermodynamic data base for EQ3NR contains free energies for disordered (EQ3NR-DIS) and ordered (EQ3NR-ORD) dolomites. Saturation indices calculated with EQ3NR with the free energy for dolomite found in the PHRQPITZ data base are also shown.

Figure 2-36 shows that the uncertainty in the saturation index of dolomite resulting from the choice of the value of free energy is about 1.5 units. This potential error is as large as

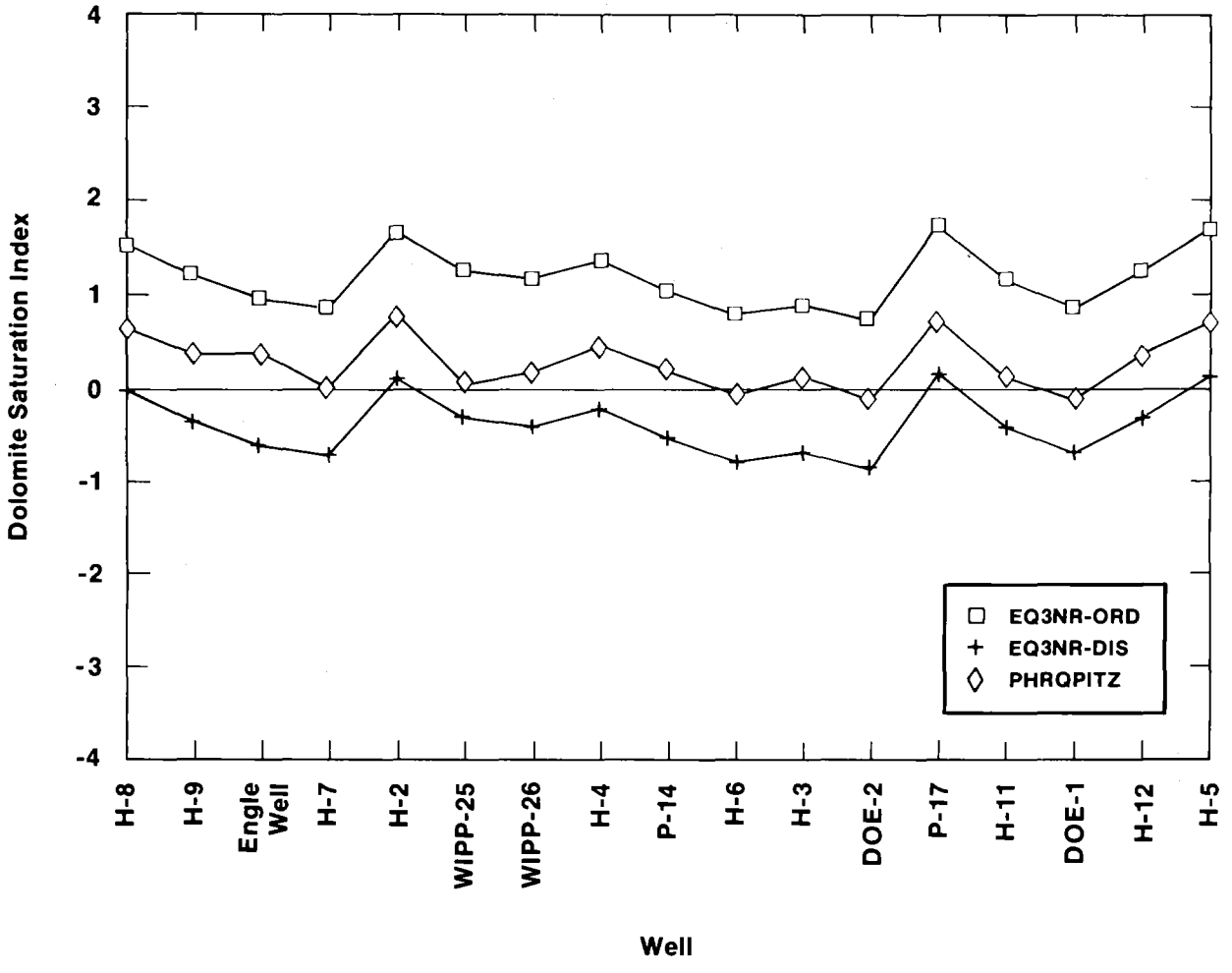


Figure 2-36. Dolomite saturation indices calculated for Culebra groundwaters using alternative values for the $\Delta G_f$ of dolomite. (SI = log [IAP/$K_{sp}$]. EQ3NR-ORD = value for "ordered" dolomite from the data base of EQ3NR [Wolery, 1983]; EQ3-DIS = value for "disordered" dolomite from EQ3NR data base; PHRQPITZ = data for dolomite from PHRQPITZ data base. Wells are arranged in order of increasing ionic strength).

or larger than the degree of supersaturation calculated for most of the samples in Figure 2-33.

#### *2.3.4.4.3 ERRORS RELATED TO LOSS OF $CO_2$ GAS DURING SAMPLING*

In the PHRQPITZ calculations described above, the $pCO_2$ and saturation indices were calculated from the field pH and alkalinity. The relationship in these samples between pH and saturation indices for dolomite and calcite are shown in Figures 2-37 and 2-38.

Changes in pH due to loss of $CO_2$ gas during water sampling result in apparent supersaturation of carbonate minerals; $H^+$ production from oxidation of $Fe^{+2}$ results in apparent undersaturation (Bassett, 1982). For solutions at equilibrium with calcite in the pH range of waters in the Culebra (pH ~6 to 8), the error in the measured pH, ΔpH (where $\Delta pH = pH_{measured} - pH_{equilibrium}$), is equal to the saturation index (i.e., ΔpH = SI) (Pearson et al., 1978). For such waters, plots of saturation index versus pH have slopes of unity and two for calcite and dolomite, respectively.

Bassett (1982) calculated saturation indices for calcite and dolomite for 121 brines from the Permian Wolfcamp carbonates in the Palo Duro, Dalhart, and Anadarko Basins. Many of those water samples are apparently supersaturated with respect to these phases; others are apparently undersaturated. Bassett estimated the $pCO_2$ of the Wolfcamp samples before outgassing using the code AQ/SALT and found that the calculated values were similar to those measured in waters in natural gas reservoirs in the Texas Panhandle. He suggested that these results indicate that $pCO_2$ in both sets of waters were buffered by equilibrium with carbonates but that the Wolfcamp brines lost $CO_2$ during sampling.

Pearson et al. (1978) have estimated the significance of this effect for several dilute calcium-bicarbonate well waters. They calculated the pH from the total inorganic carbon and $pCO_2$ measured in the laboratory and compared it to field pH. They showed that in warm (T = 55°C), weakly-buffered waters (alkalinity = 90-140 mg/L $HCO_3^-$) an error of 1 pH

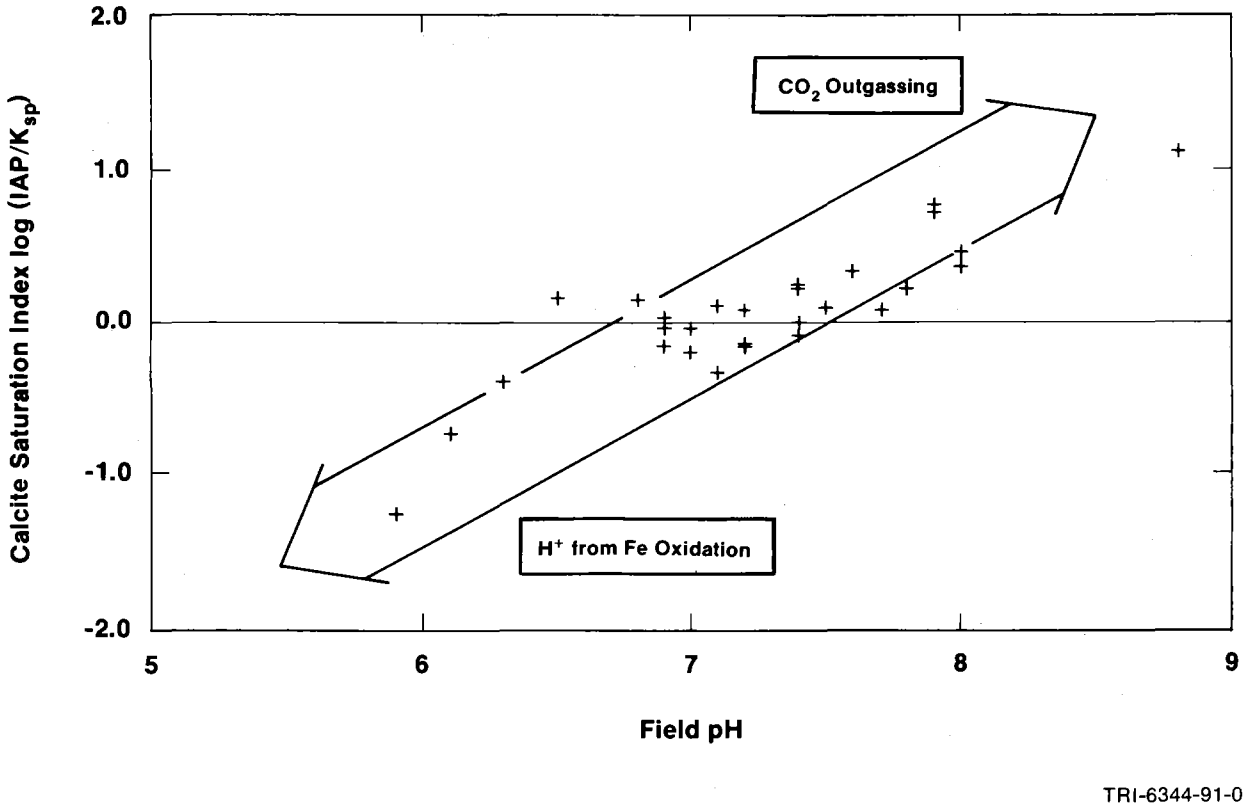


Figure 2-37. Relationship between calcite saturation indices and field pH values for Culebra groundwaters.

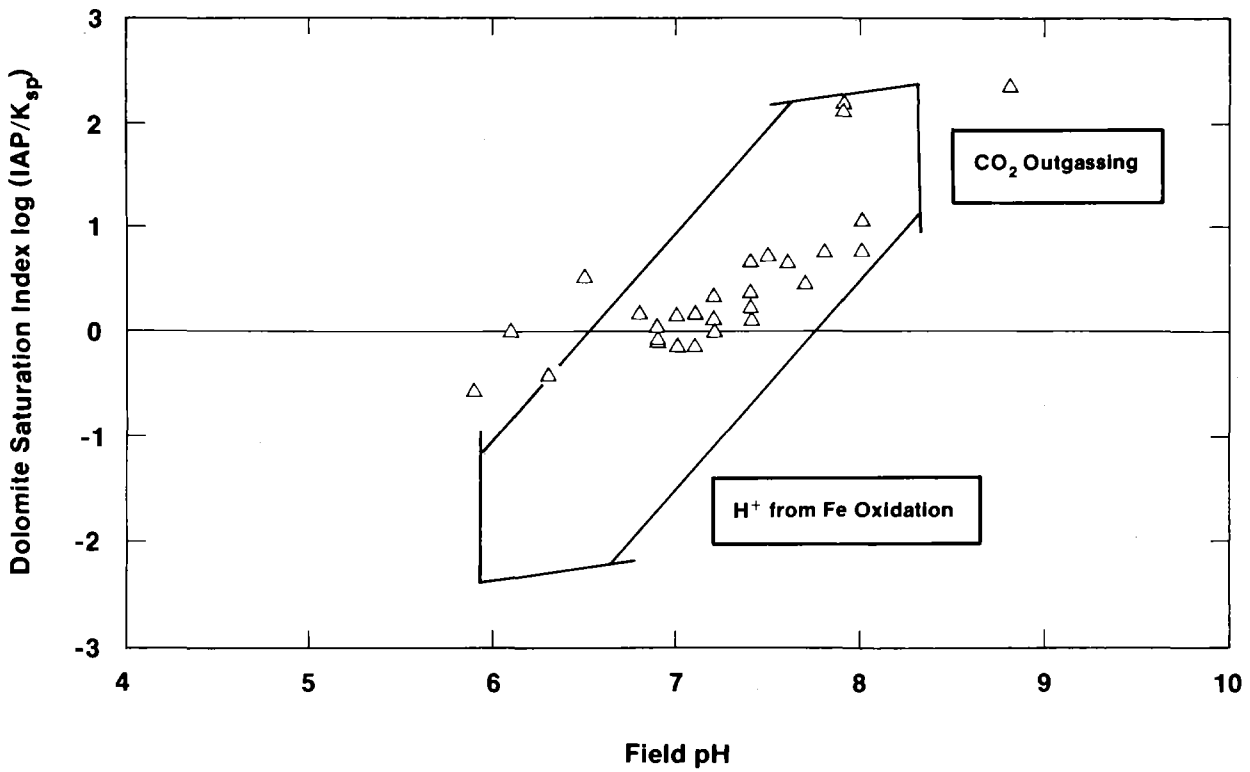


Figure 2-38. Relationship between dolomite saturation indices and field pH for Culebra groundwaters.

unit and 1 log unit in the computed calcite saturation index is possible. In cooler waters, the rates of $CO_2$ loss are lower and the probable error is smaller (about 0.3 pH units).

Many of the data in Figures 2-37 and 2-38 lie along trends that are consistent with the aforementioned mechanisms leading to errors in the field pH. Arrows with slopes of unity and two slopes are superimposed on the data in Figures 2-37 and 2-38, respectively. Most of the plotted points fall between the parallel sides of arrows. There are considerable deviations from these trends, however, and the width of the arrows would have to be very large to accommodate all of the data, suggesting that other processes may also be affecting the saturation indices.

#### *2.3.4.4.4 EVIDENCE OF SUPERSATURATION OF CARBONATE MINERALS*

Meijer et al. (1987) suggest that one can determine the degree of carbonate mineral saturation independent of the effects of $CO_2$ outgassing by examining the value of the saturation index expression:

$$2\,SI_{calcite} - SI_{dolomite} .$$

The value of this expression is independent of the uncertainty in the carbonate ion activity and equals zero when the solution is saturated with respect to both calcite and dolomite. Based on the near zero values of the saturation index expression, Meijer et al. concluded that the waters from the H-3B3 well were saturated with respect to both dolomite and calcite.

Figure 2-39 shows that the value of the saturation index expression for the Culebra waters decreases as a function of ionic strength. This indicates that when the effects of the $CO_2$ outgassing are corrected for, it can be seen that many of these waters are supersaturated with respect to dolomite and/or undersaturated with respect to calcite. The degree of

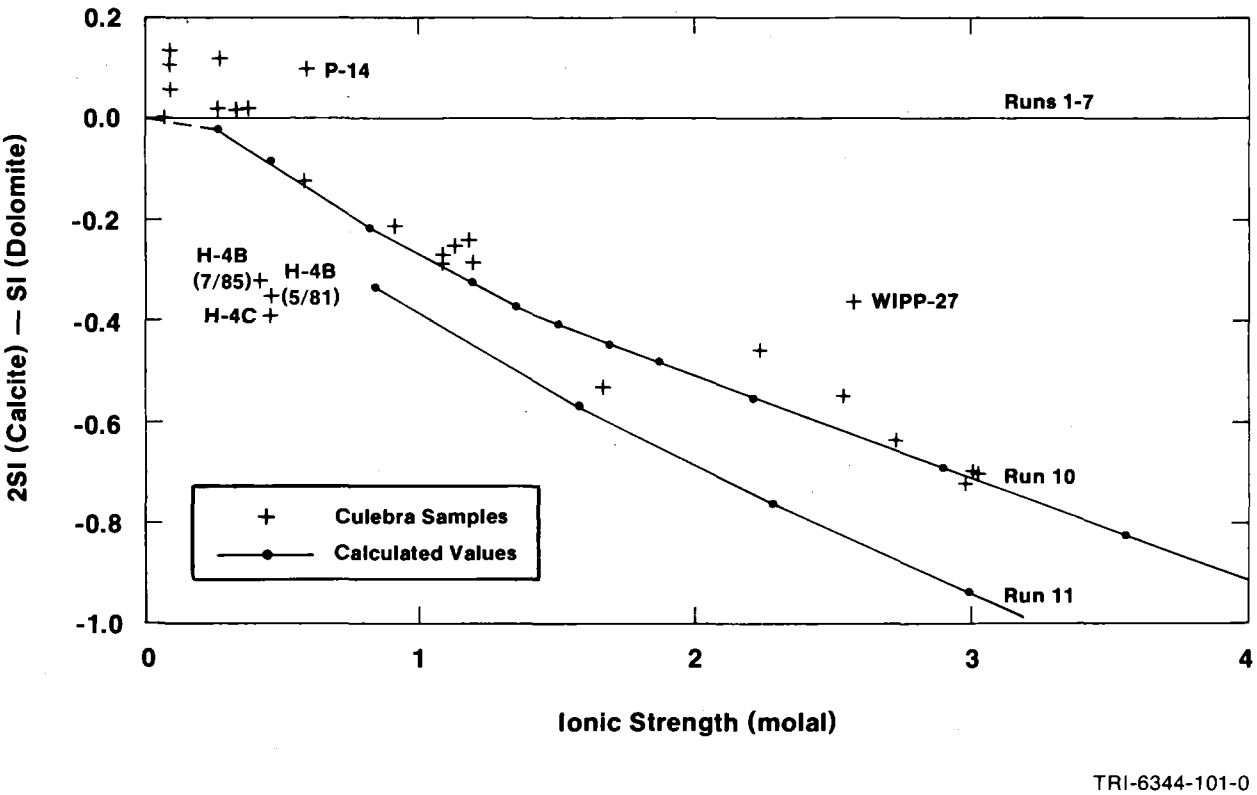


Figure 2-39. Relationship between saturation index expression ($2SI_{calcite}$ - $SI_{dolomite}$) and ionic strengths for Culebra groundwaters.

disequilibrium increases with ionic strength; a chemical model that accounts for this trend is described in the next section.

# 2.4 DISCUSSION: PROCESSES AFFECTING WATER CHEMISTRY

## 2.4.1 Introduction: Summary of Important Solute Relationships

In the previous sections, the complementary techniques of plotting spatial distributions of solutes and element ratios, factor analysis, and thermodynamic models have been used to summarize solute relationships in the Culebra waters. Several of these relationships may provide indications of the chemical processes that affect the groundwater composition.

The following solute relationships were described in the preceding sections:

- Increase in concentrations of Na, Cl, Ca, Mg, K, $SO_4$, Br, B, and Li with ionic strength. This relationship can be seen by examination of the data in Table 2-1 and is illustrated by the "salinity factors" described in Section 1.4.3 and by simple scatterplots such as Figure 2-40, where the total analytical concentrations of calcium and sulfate and the saturation quotient of gypsum and anhydrite are shown as functions of chloride concentration.

- The increase in the Mg/Ca ratio as the ionic strength increases (cf. Figure 2-19).

- The near-perfect saturation of the solutions with respect to gypsum over the entire range of ionic strength. Figure 2-40 shows that while the saturation indices (expressed as $IAP/K_{sp}$) for gypsum and anhydrite are nearly constant over the entire range of chloride the concentration up to 180,000 mg/L, the sum of the concentrations of calcium and sulfate increase nearly continuously. Any local deviation in the trend of increasing calcium concentration is offset by a deviation in sulfate concentration due to the

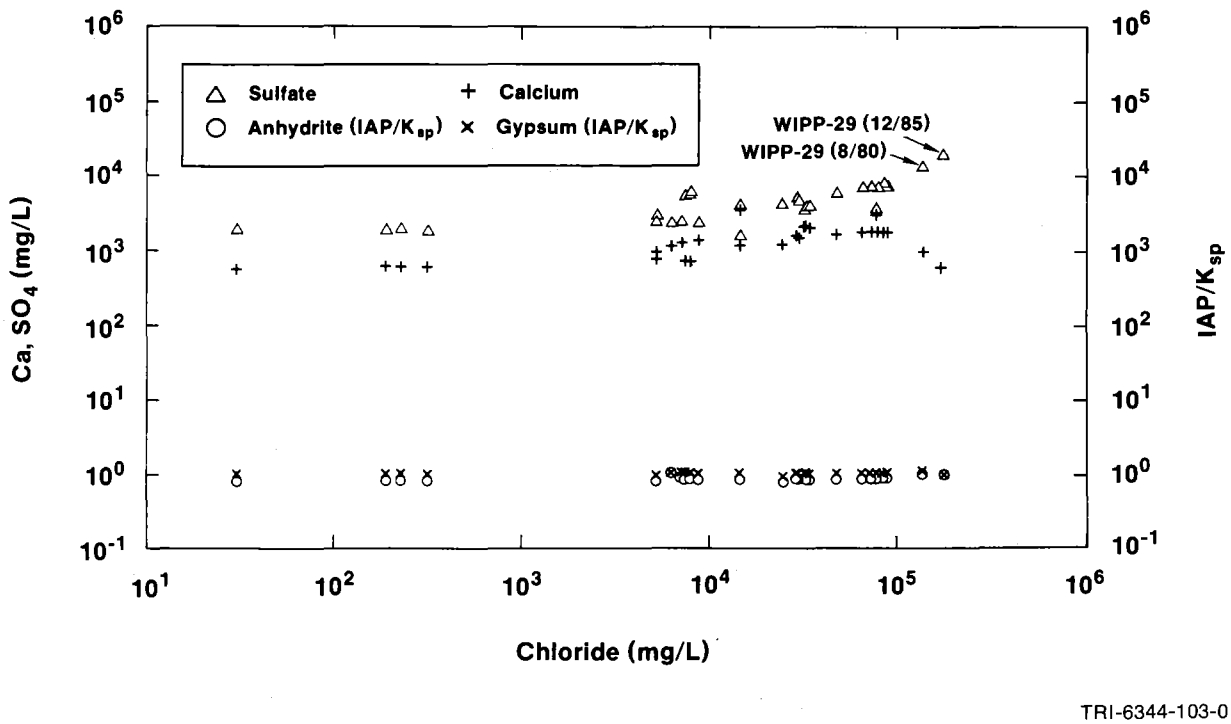


Figure 2-40. Calcium sulfates in Culebra groundwater samples.

saturation control exerted by equilibrium with gypsum. For example, in the two WIPP-29 samples, sulfate concentrations are anomalously high, and calcium concentrations are correspondingly low.

- The apparent supersaturation of dolomite. Outgassing of $CO_2$ during sample collection is a probable source of error in the pH and calculated saturation indices. However, a saturation index expression independent of this uncertainty indicates that the degree of supersaturation increases with ionic strength (cf. Figure 2-39).

- Negative correlation between pH and bicarbonate alkalinity shown in the "silicate/bicarbonate factor" (e.g., factor 2B described in Section 2.3.3.5). This relationship may be an artifact of the $CO_2$ outgassing or may reflect an underlying reaction whose effects are not completely obscured by the the pH shift associated with the $CO_2$ loss.

- An underlying correlation of Mg with $SiO_2$ and negative correlation of both these elements with Li and B observed after the effects of salt dissolution are factored out. This relationship is most clearly indicated by the "silicate/ bicarbonate factor."

In the Rustler Formation, two broad types of chemical processes are likely to affect the water chemistry and produce the above solute relationships: (1) precipitation and dissolution of carbonates, sulfates, halite, and other evaporite salts; and (2) ion exchange and silicate diagenesis involving clays that occur as fracture linings and matrix inclusions.

The purpose of this section is to describe these processes, discuss their probable importance and provide a conceptual framework within which future hydrochemical, mineralogical, and petrographic studies can be conducted. Section 2.4.2 describes the effect of ionic strength on the solubilities of carbonate and sulfate minerals present in the Culebra. The PHRQPITZ code is used to evaluate the effect of reactions involving these minerals and other evaporite salts on groundwater composition. Section 2.4.3 assesses the

effect of reactions involving silicate minerals on the concentrations of several solutes (Si, Li, B, and Mg). Other processes that may affect the groundwater composition are discussed in Section 2.4.4.

## 2.4.2 Precipitation and Dissolution

### 2.4.2.1 Salt Dissolution as an Irreversible Process in Partial Equilibrium Systems

In this study, saturation indices for groundwaters have been used to identify minerals that may control solute concentrations and to determine if the water is capable of dissolving additional rock. However, as Plummer (1984) notes, even if the saturation index of a mineral is zero, this does not indicate whether the mineral is at equilibrium in the system or is continually responding to an irreversible process. In the latter case, the system is said to be at partial equilibrium, and the mineral/water equilibria are shifting along a reaction path driven by the irreversible process. Examples of irreversible processes are temperature and pressure changes, changes in activity coefficients due to changes in salinity that might accompany dissolution of salt, or addition of a component by the exposure of certain minerals (e.g., nodules in a dissolving matrix).

Halite and other evaporite salts are strongly undersaturated in groundwaters in the Culebra dolomite. It is likely that dissolution of halite in strata adjacent to the Culebra acts as an irreversible driving force for changes in water composition. The dissolution of evaporite salts will add solutes directly and will also increase the solubilities of gypsum, calcite, and dolomite as discussed below.

Figure 2-41 shows the relationship between ionic strength and the unscaled activity coefficients for magnesium, calcium, sulfate, and carbonate in the Culebra samples. The unscaled activity coefficients were calculated for the specific composition of each water sample with the PHRQPITZ code (Plummer et al., 1988), according to the formalism described by Pitzer and coworkers (Pitzer, 1973, 1975; Pitzer and Kim, 1974; Pitzer and

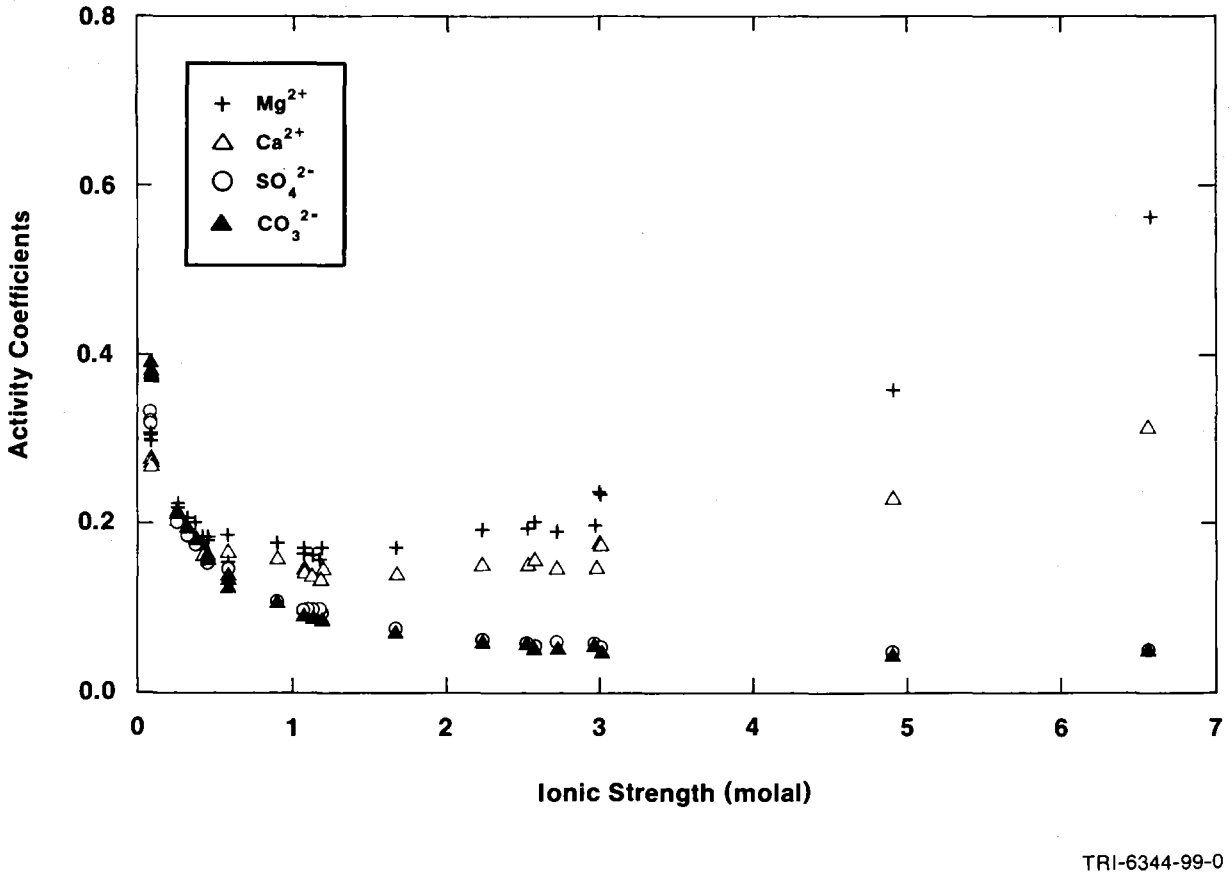


Figure 2-41. Relationships between activity coefficients for magnesium, calcium, sulfate, and carbonate, and ionic strengths of Culebra groundwaters.

Mayorga, 1973, 1974), and using the UNC Geotech data given in Table 2-2. The calculated activity coefficients are functions of the specific interactions in the solutions and the ionic strength.

The relationships between activity coefficient and ionic strength for the anions differ from that of the cations. For these particular water compositions, the activity coefficients of the anions decrease until the ionic strength reaches about 1.0 molal; thereafter, they remain level at about 0.05. The activity coefficients of the cations decrease to minima at an ionic strength of about 1.0 and then increase.

The effect of these changes in activity coefficients on the apparent solubility products of gypsum and dolomite are shown in Figures 2-42 and 2-43. The apparent solubility product for gypsum in each solution was calculated as:

$$\log Q_{gyp} = \log K_{sp(gyp)} - \log(\gamma_{Ca^{2+}} \cdot \gamma_{SO_4^{2-}} \cdot a^2_{H_2O}) \quad [4]$$

where $\log K_{sp(gyp)}$ = the equilibrium solubility product for gypsum at the temperature of interest,

$\gamma_{Ca^{2+}}$ and $\gamma_{SO_4^{2}}$ = the activity coefficents for $Ca^{2+}$ and $SO_4^{2-}$, respectively, in a specific sample, and

$a_{H_2O}$ = activity of water.

Similarly, the apparent solubility product for dolomite in a water sample was calculated as:

$$\log Q_{dol} = \log K_{sp(dol)} - \log(\gamma_{Ca^{2+}} \cdot \gamma_{Mg^{2+}} \cdot \gamma^2_{CO_3^{2-}}) \quad [5]$$

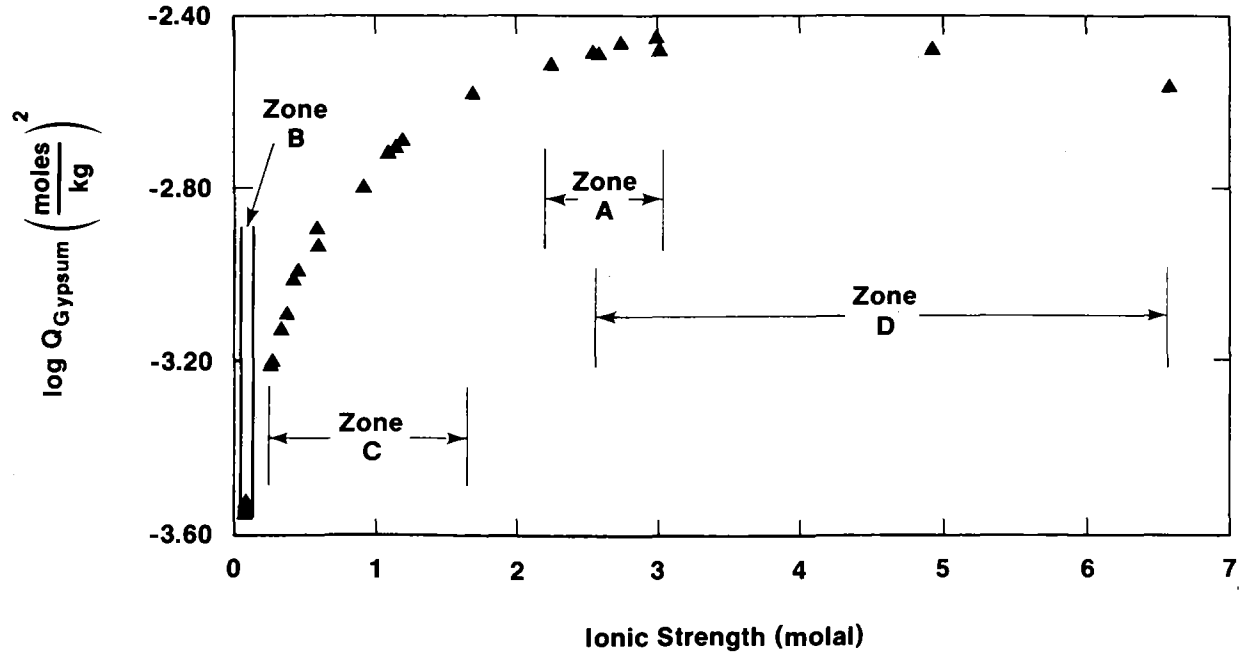


Figure 2-42. Relationship between apparent equilibrium constants for gypsum, log Q, and ionic strengths of Culebra groundwaters.

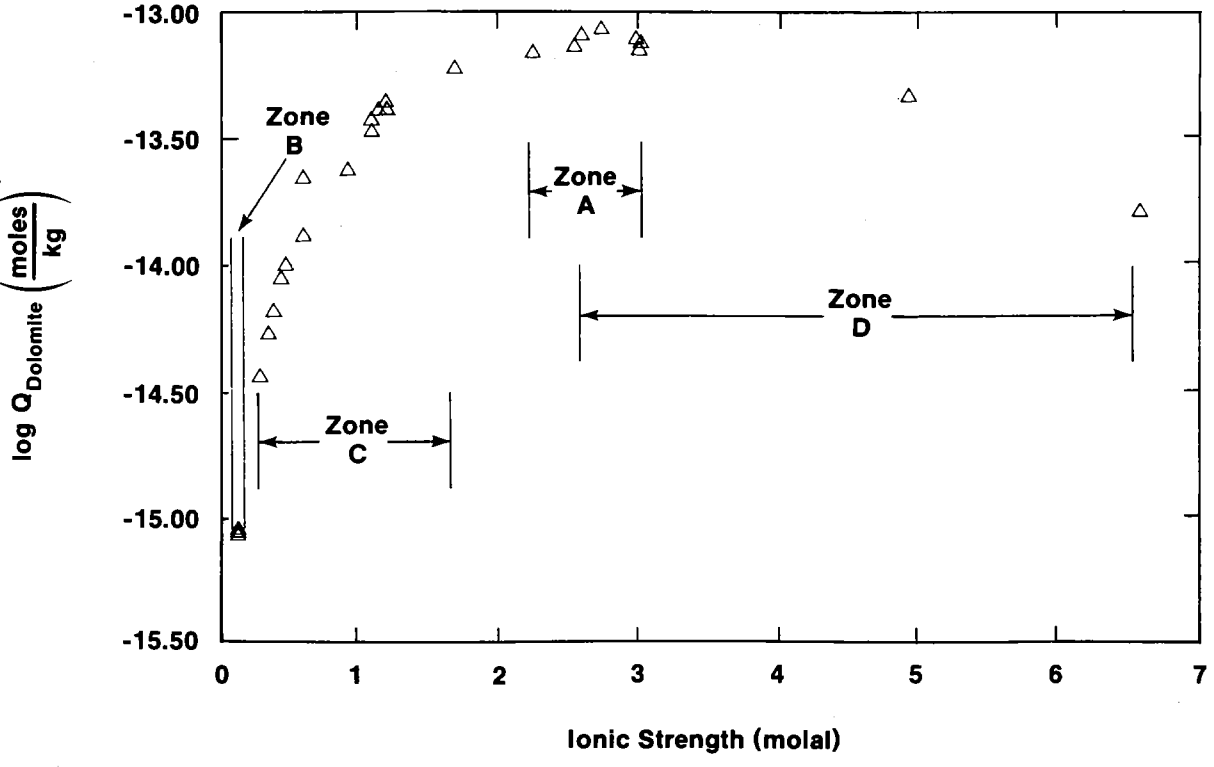


Figure 2-43. Relationship between apparent equilibrium constants for dolomite, log Q, and ionic strengths in Culebra groundwaters.

where $K_{sp(dol)}$ = the equilibrium solubility product for dolomite at the temperature of interest, and

$\gamma_{Mg^{2+}}$ and $\gamma_{CO_3^{2-}}$ = the activity coefficients of $Mg^{2+}$ and $CO_3^{2-}$ in the particular sample.

Dissolution of gypsum, dolomite, and calcite could account for the increase in the concentrations of Mg, Ca, and $SO_4$ as a function of ionic strength. The ability of this process alone to account for the observed solute relationships in the Culebra is examined by the reaction path modeling described in the next section.

#### 2.4.2.2 Reaction Path Models of Culebra Waters

The PHRQPITZ code was used to calculate the compositions of waters that would be produced by several hypothetical reaction paths. A series of parametric simulations was carried out to determine the effect of certain assumptions about chemical reaction rates, sources of solutes, and initial conditions on the groundwater compositions. The simulations are described in Table 2-11. All of the simulations contained two parts.

In the first part, the composition of water (referred to as the "starting solution") in equilibrium with calcite, gypsum, and dolomite at a specified $pCO_2$ was calculated. The initial water assumed in this calculation was distilled water, and therefore the resulting solution (i.e., the "starting solution") consisted only of species containing Ca, Mg, $CO_3$, and $H_2O$.

In the second part of the simulations, the addition of solutes (Na, Cl, Mg, $SO_4$, and K) to the starting solution by dissolution of halite and other evaporite salts was simulated. The progress of the dissolution reaction was specified by adding the halite in successive increments of 0.3 or 0.6 moles until a total of 6 moles of NaCl had been added. In Runs 1 to 4, only halite was added to the starting solution. For Runs 5 to 11, a different dissolution reaction was described by specifying the ratio of NaCl to a particular accessory mineral.

## Table 2-11. Summary of Parameters for Reaction Path Calculations

| Run | $CO_2$ System[1] | log $pCO_2$ (atmos) | Minerals at fixed saturation index (SI)[2,3] | Molar ratio of accessory mineral[4]/halite |
|---|---|---|---|---|
| 1 | closed | -2 | c(0),g(0),d(0) | none |
| 2 | closed | -3.5 | c(0),g(0),d(0) | none |
| 3 | open | -2 | c(0),g(0),d(0) | none |
| 4 | open | -3.5 | c(0),g(0),d(0) | none |
| 5 | closed | -2 | c(0),g(0),d(0) | poly (0.007) |
| 6 | closed | -2 | c(0),g(0),d(0) | mag (0.02)<br>carn (0.014) |
| 7 | closed | -2 | c(0),g(0),d(0) | leon (0.007) |
| 8 | closed | -2 | c(0),g(0),d(0.5) | carn (0.007) |
| 9 | closed | -2 | c(0),g(0),d(1.0) | poly (0.007) |
| 10 | closed | -2 | c(0),g(0) | leon (0.007)<br>$MgCl_2$ (0.025) |
| 11 | closed | -2 | c(0),g(0) | leon (0.007)<br>mag (0.025) |

1. Closed or open to exchange of $CO_2$ with atmosphere.
2. Minerals: c = calcite; g = gypsum; d = dolomite.
3. Saturation index for mineral: log (IAP) - log ($K_{sp}$)(see Section 3.4).
4. Poly = polyhalite; mag = magnesite; carn = carnallite; leon = leonite.

Solutes (Mg, Ca, $CO_2$, and $SO_4$) were added or removed from the solution in amounts needed to maintain saturation levels specified for $CO_2$ gas, calcite, gypsum, and dolomite.

The effect of the following conditions or processes were considered in the various simulations:

- Closed versus open system with respect to $CO_2$ gas
- Identity of accessory evaporite salts used as sources of Mg, K, and $SO_4$
- Degree of saturation of the waters with respect to dolomite.

Table 2-11 summarizes the conditions assumed for the simulations; the results of the calculations are presented in Figures 2-44 to 2-53. In each figure, the concentration of a solute at each reaction step is plotted as a function of the amount of added chloride and compared to the composition of Culebra waters. The types of mass transfers (i.e., precipitation or dissolution) in each simulation are summarized in Table 2-12. The most important results are summarized below.

#### *2.4.2.2.1 EFFECT OF $CO_2$ PARTIAL PRESSURE ON WATER COMPOSITIONS*

Runs 1 to 4 assume the simplest partial equilibrium model in which pure NaCl is added to the solution while the groundwaters are maintained at equilibrium with respect to calcite, dolomite, and gypsum. The concentrations of Ca, Mg, $SO_4$, and $CO_3$ change due to the changes in the solubilities of calcite, dolomite, and gypsum described in Section 2.4.2.1.

The four runs differ only in the assumptions made about the $CO_2$ gas. In Runs 1 and 2, the system is closed with respect to $CO_2$ gas exchange. This means that the sources of the carbonate species in the solutions are the original $CO_2$, dissolved in the recharge and soil water, and carbonate dissolved from the Culebra or adjacent strata.

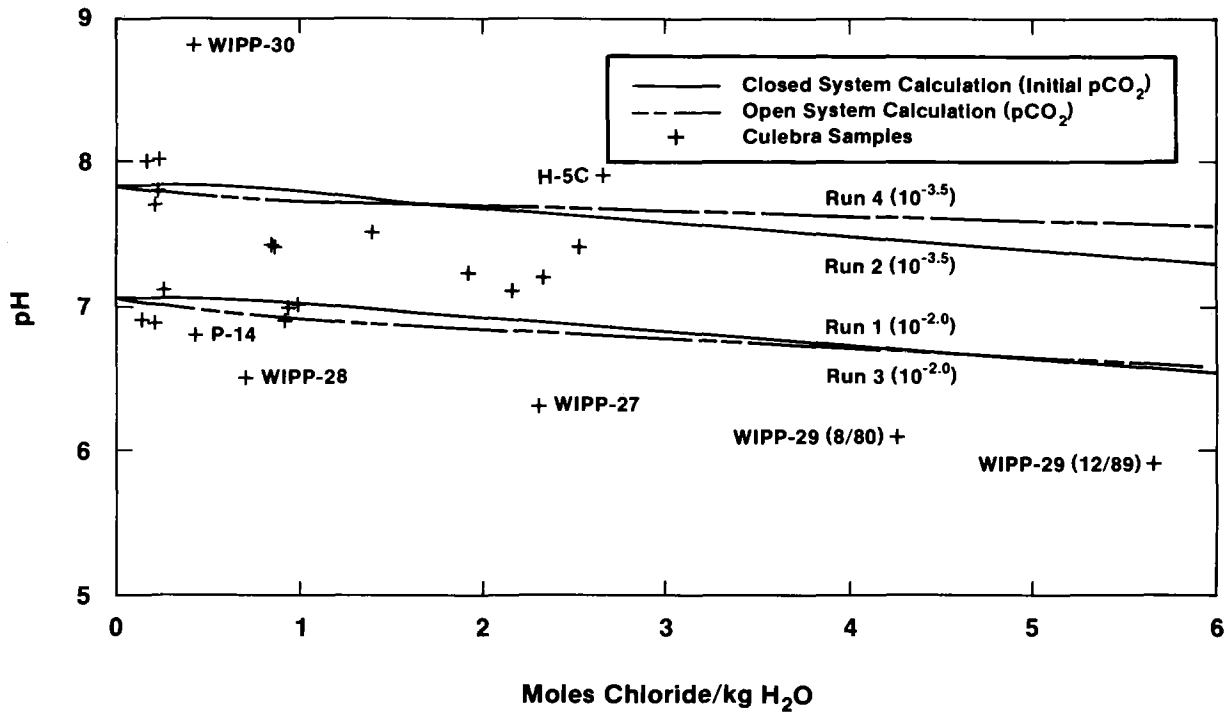


Figure 2-44. Change in pH as a function of reaction progress for simulated evolution of Culebra groundwater compositions.

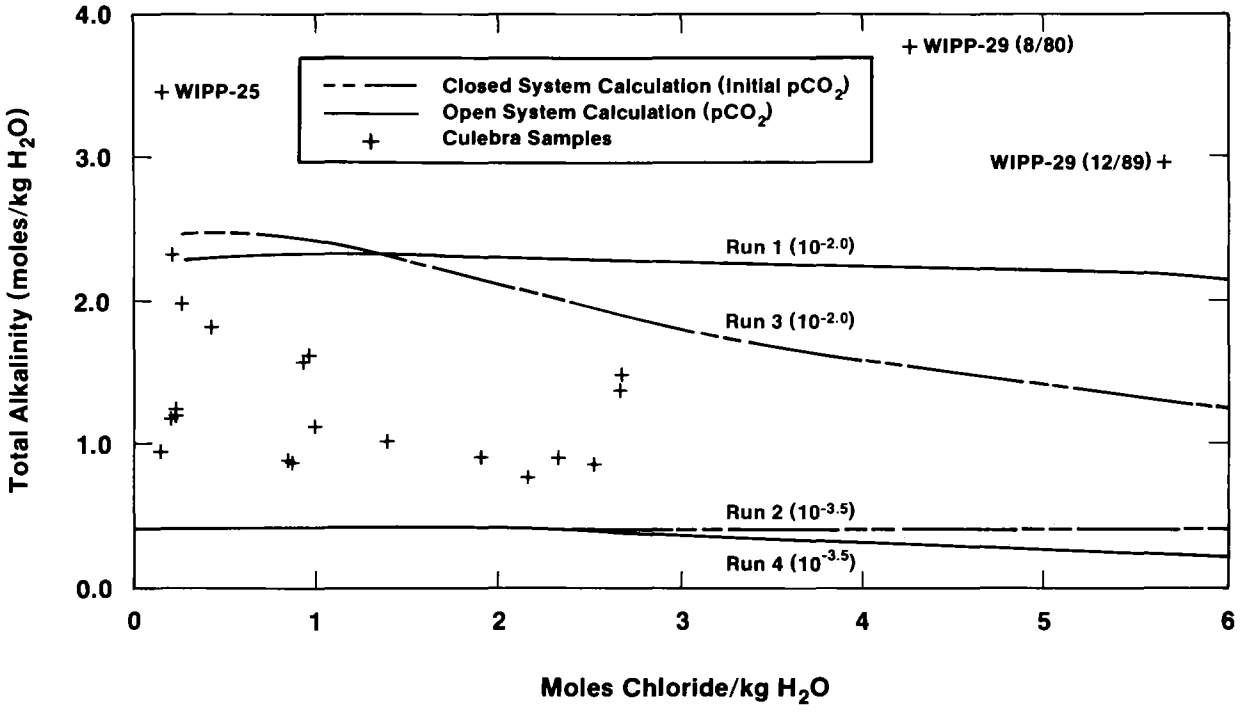


TRI-6344-82-0

Figure 2-45. Change in total alkalinity as a function of reaction progress for simulated evolution of Culebra groundwater compositions.

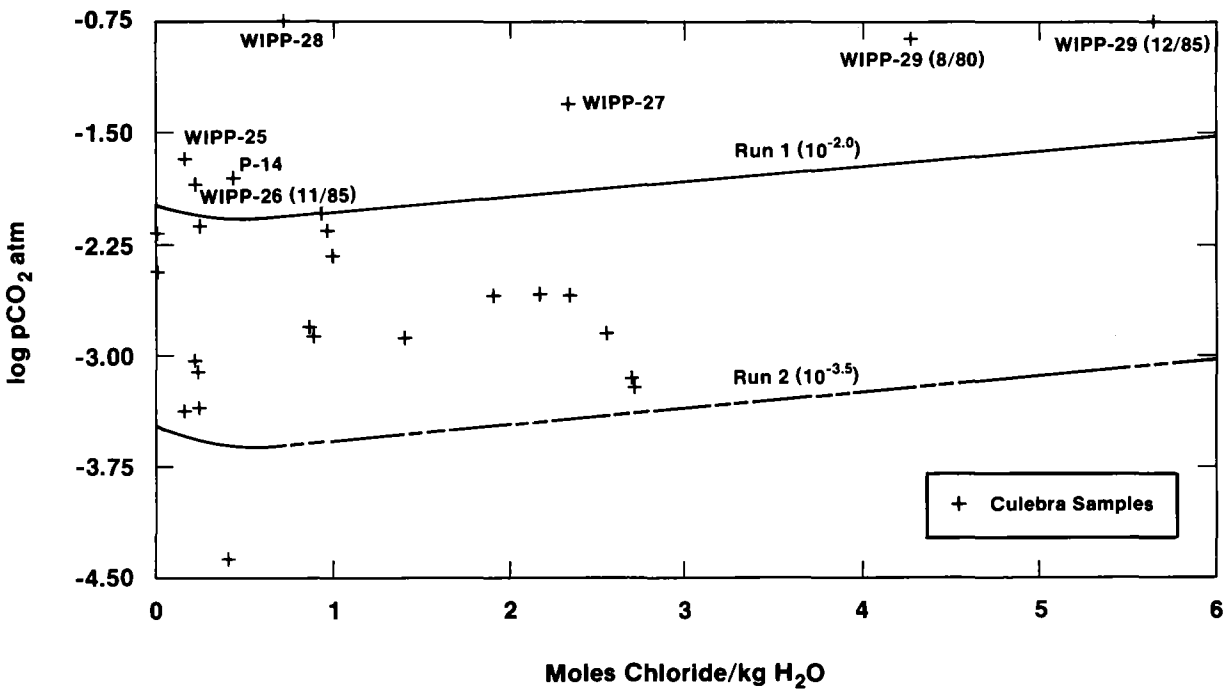


Figure 2-46. Change in $pCO_2$ for systems closed to atmospheric conditions as a function of reaction progress for simulated evolution of Culebra groundwater compositions.

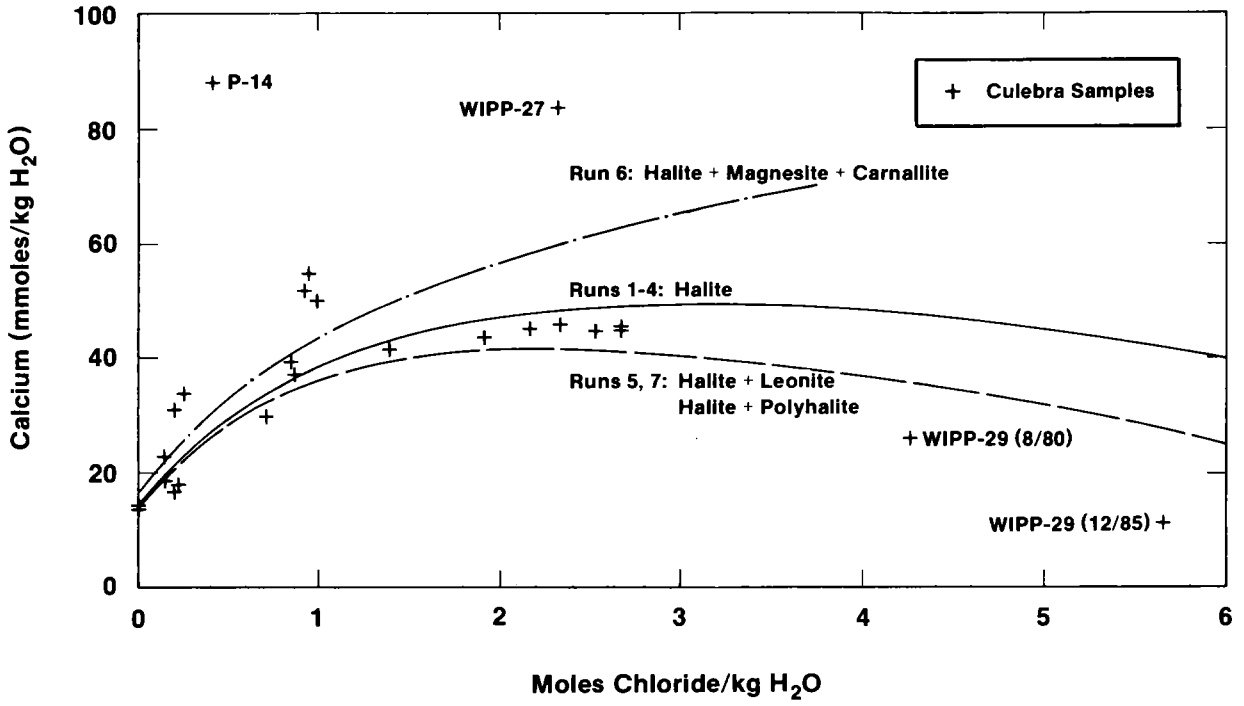


TRI-6344-85-0

Figure 2-47. Change in calcium concentration as a function of reaction progress and types of added salts for simulated evolution of Culebra groundwater compositions.

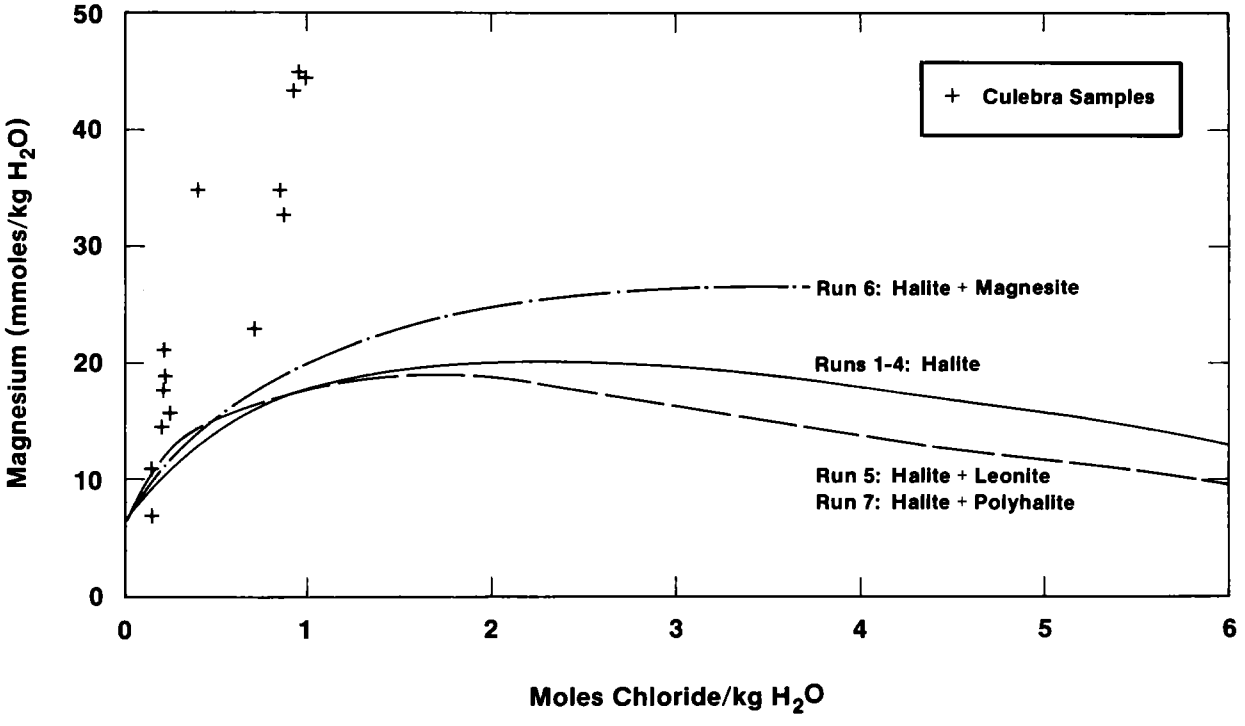


Figure 2-48. Change in magnesium concentration as a function of reaction progress and types of added salts for simulated evolution of Culebra groundwater compositions.

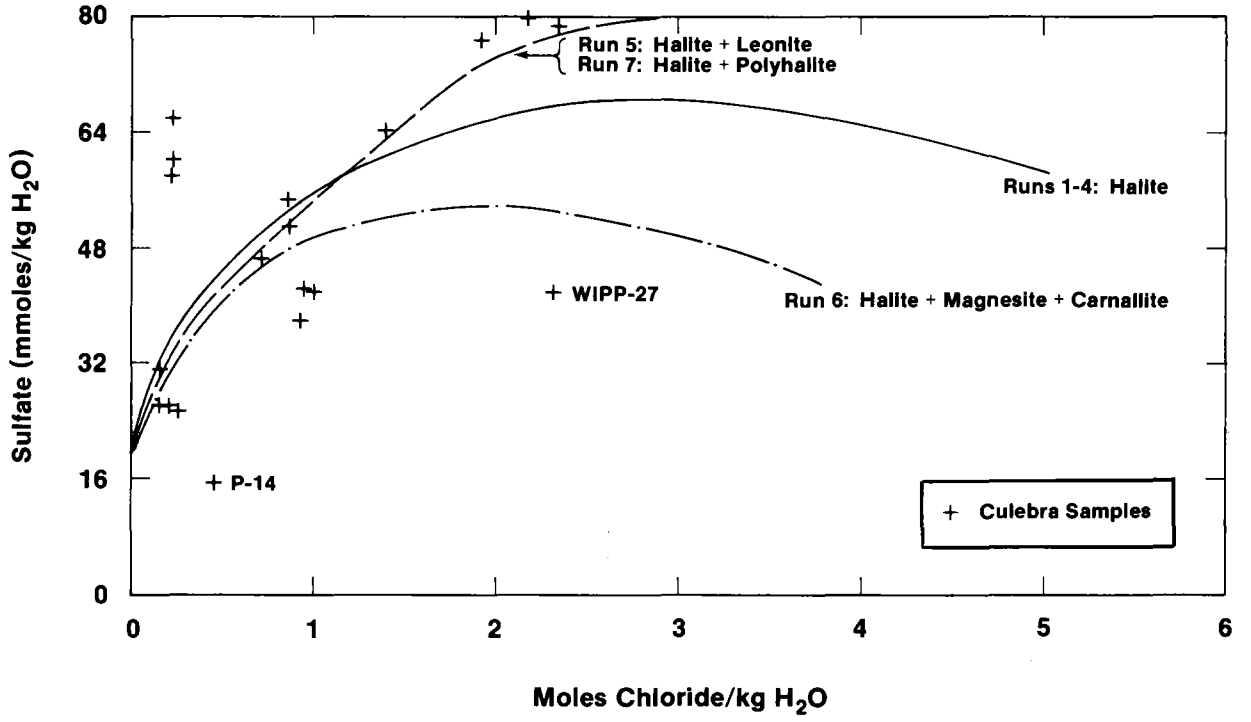


Figure 2-49. Change in sulfate concentration as a function of reaction progress and types of added salts for simulated evolution of Culebra groundwater compositions.

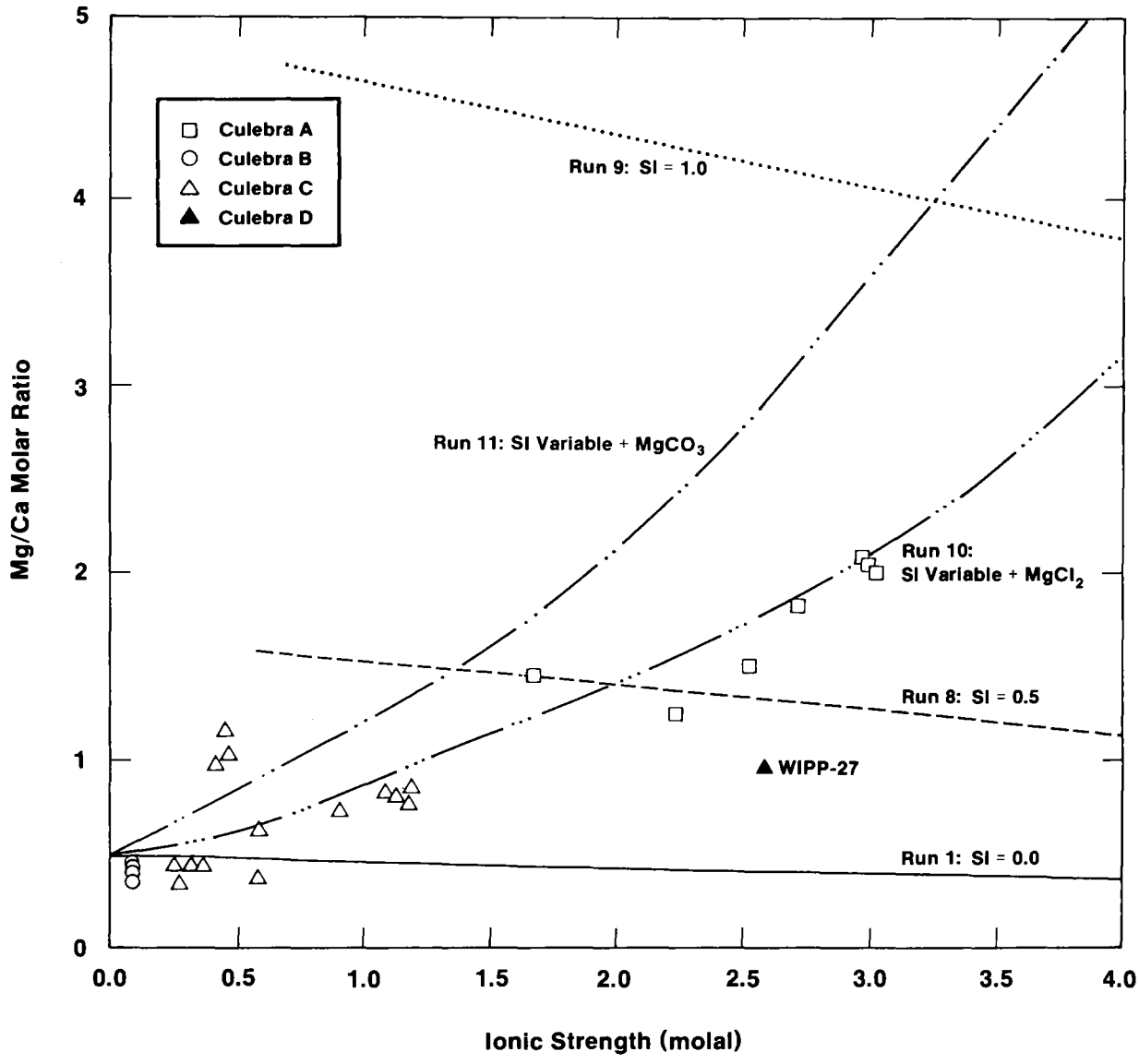


Figure 2-50. Change in Mg/Ca molar ratio as a function of reaction progress, types of added salts, and dolomite saturation index for simulated evolution of Culebra groundwaters.

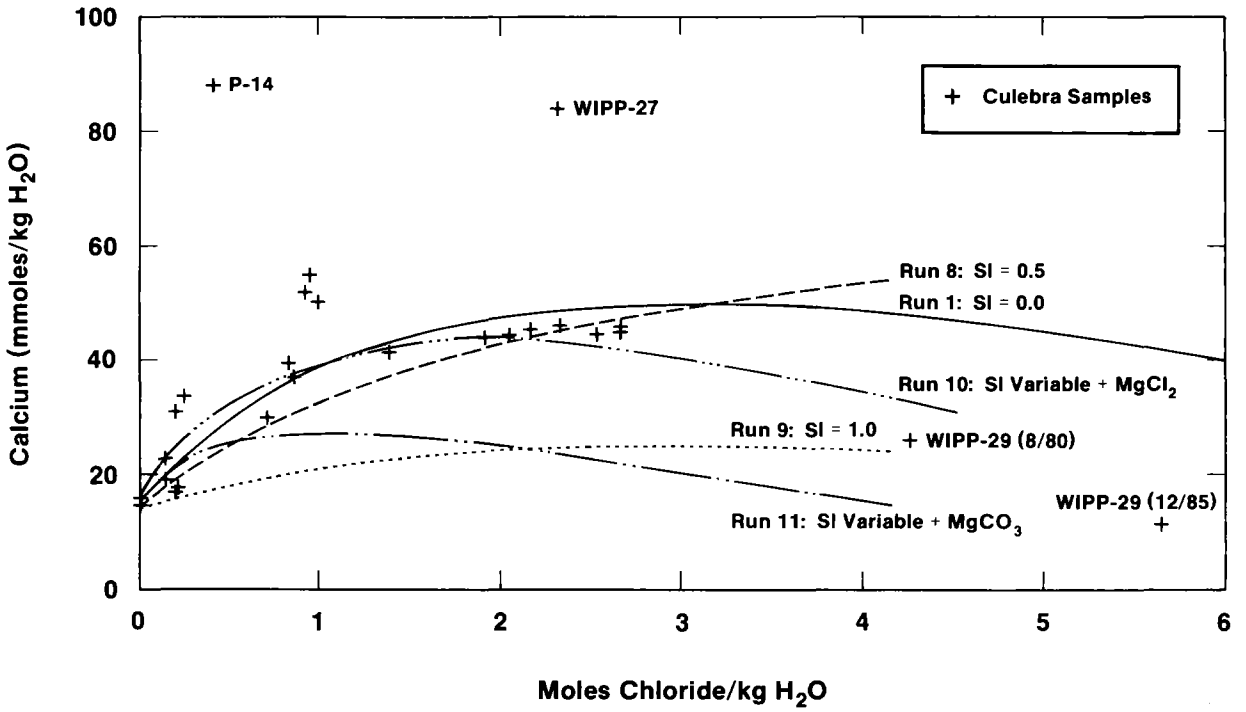


Figure 2-51. Change in calcium concentration as a function of reaction progress, types of added salts, and dolomite saturation index for simulated evolution of Culebra groundwater compositions.

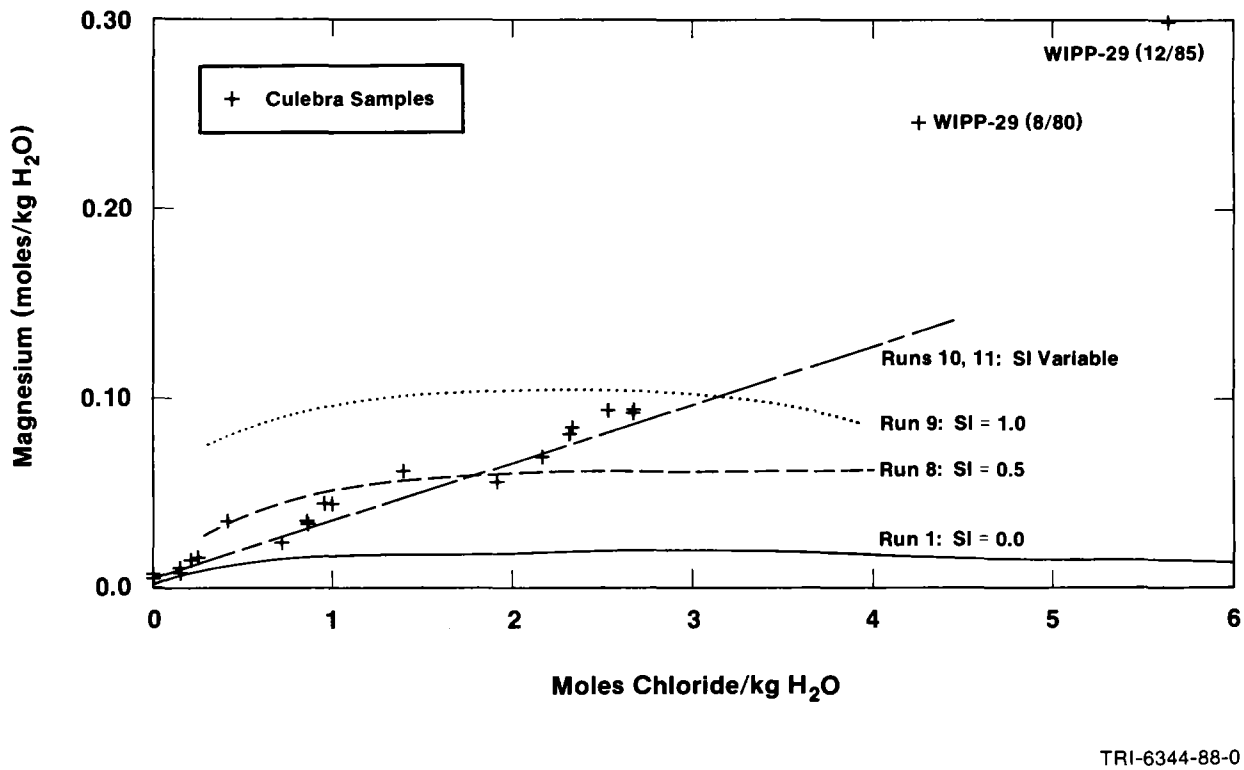


Figure 2-52. Change in magnesium concentration as a function of reaction progress, types of added salts, and dolomite saturation index for simulated evolution of Culebra groundwater compositions.

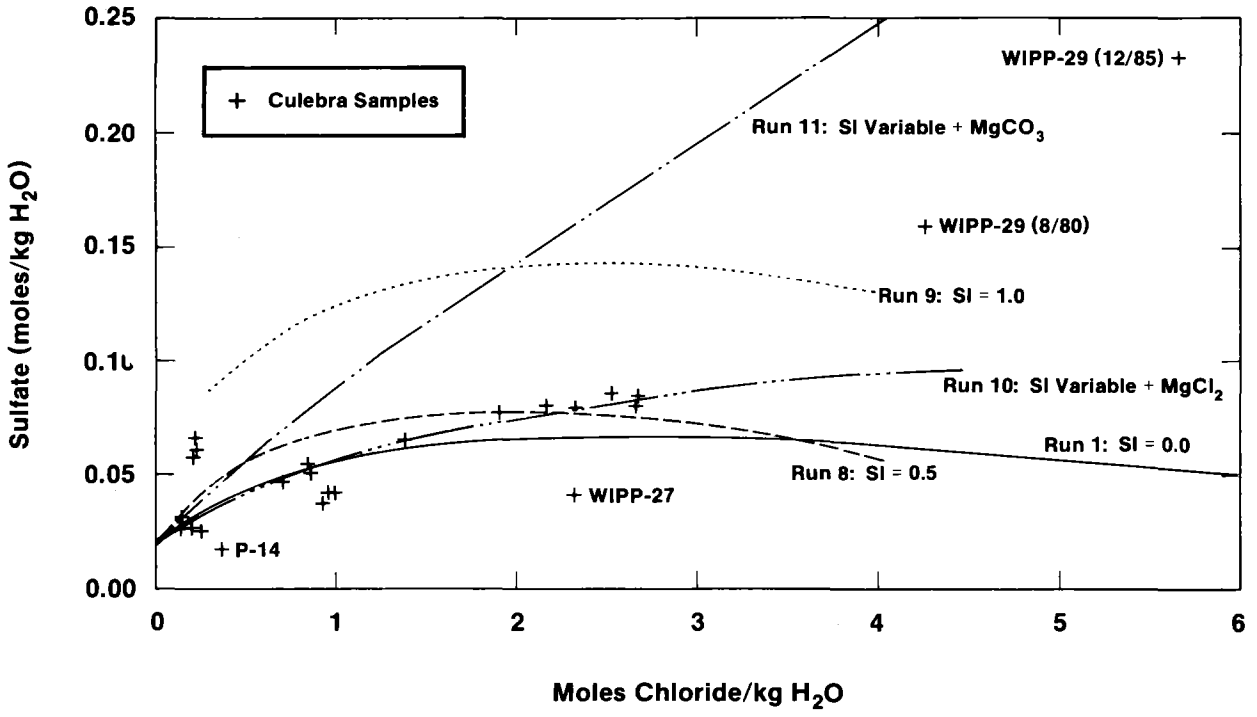


TRI-6344-89-0

Figure 2-53. Change in sulfate concentration as a function of reaction progress, types of added salts, and dolomite saturation index for simulated evolution of Culebra groundwater compositions.

## Table 2-12. Mass Transfers During Reaction Path Calculations[1]

| | Minerals and Gases at Saturation | | | | |
|---|---|---|---|---|---|
| Run | Calcite | Gypsum | Dolomite | $CO_2$ | Cl Range (Molal) |
| 1 | ppt[2] | dis[3] | dis | na[4] | 0.3 - 6 |
| 2 | ppt | dis | dis | na | 0.3 - 6 |
| 3 | ppt | dis | dis | dis | 0.3 - 6 |
| 4 | ppt | dis | dis | dis[5] | 0.3 - 1.5 |
| | ppt | dis | dis | exs[5] | 1.8 - 6 |
| 5 | ppt | dis | dis | na | 0.3 - 1.5 |
| | dis | dis | ppt | na | 1.8 |
| | dis | ppt | ppt | na | 2.1 - 6 |
| 6 | dis | dis | ppt | na | 0.3 - 6 |
| 7 | ppt | dis | dis | na | 0.3 - 1.5 |
| | dis | dis | ppt | na | 1.8 - 4.2 |
| | dis | ppt | ppt | na | 4.5 - 6 |
| 8 | ppt | dis | dis | na | 0.3 - 3.9 |
| | dis | dis | ppt | na | 4.2 - 6 |
| 9 | ppt | dis | dis | na | 0.3 - 3.9 |
| | ppt | ppt | dis | na | 4.2 - 6 |
| 10 | dis | dis | na | na | 0.3 - 6 |
| 11 | ppt | dis | na | na | 0.3 - 6 |

1. The starting solutions for all runs were saturated with respect to calcite, gypsum, dolomite, and $CO_2$ by dissolving gypsum, dolomite, and $CO_2$ and precipitating excess calcite.
2. ppt = mineral precipitates.
3. dis = mineral or gas dissolves.
4. na = reaction not allowed (closed system).
5. exs = gas exsolves.

This closed system assumption is consistent with the models used to interpret the carbon isotope systematics discussed by Lambert (Chapter 5). In Run 1 the initial partial pressure of $CO_2$ is $10^{-2}$ atmospheres; this is a reasonable value for near-surface groundwater in carbonate aquifers that have received $CO_2$ from both the atmosphere and soil organic matter (Drever, 1982). In Run 2, the initial $pCO_2$ is atmospheric ($10^{-3.5}$ atm) corresponding to the case in which there is no $CO_2$ contribution from soil organic matter.

The changes in pH, alkalinity, and $pCO_2$ as a function of added chloride are shown in Figures 2-44 and 2-45. The compositions of the simulated solutions are compared to compositions of Culebra waters in each figure. There is no apparent relationship between the concentrations measured in the Culebra and the theoretical trends predicted by the simple partial equilibrium model. This is consistent with the potential effects of $CO_2$ outgassing, $H^+$ production, and contamination discussed in Section 2.3.4.4.

Figure 2-44 shows that for all simulations the pH decreases as the dissolution reaction proceeds and that the pH is lower for $pCO_2 = 10^{-2.0}$ atmosphere than for $pCO_2 = 10^{-3.5}$ atmosphere. At a given $pCO_2$, the pH of the closed system drops below that of the open system as the reaction progresses. Many of the Culebra samples have pH values that fall outside of the range bound by these simple simulations. This is consistent with the possibility that the pH of many of the Culebra samples rose during sampling due to the loss of $CO_2$ gas or fell due to $H^+$ production during oxidation of ferrous iron from the well casing.

Figure 2-45 shows that the calculated total alkalinity at $pCO_2 = 10^{-3.5}$ atmosphere is a lower limit for measured alkalinities in the Culebra waters. Alkalinities computed for a $pCO_2$ of $10^{-2}$ atmosphere are higher than those measured at all Culebra wells except for WIPP-25, WIPP-28, and WIPP-29. As discussed previously, the value measured for WIPP-28 is not considered representative because the field alkalinity had not reached steady-state when the final samples were collected. Lambert (Chapter 5) reports the presence of significant amounts of modern carbon in WIPP-25 and WIPP-29. Contamination of the wells by organic compounds during drilling and the subsequent production of bicarbonate by

heterotrophic bacteria may be responsible for the anomalously high values of alkalinity. Such contamination may also be responsible for the high $pCO_2$ (Figure 2-46) and low pH in these and other wells.

The changes in concentrations of Ca, Mg, and $SO_4$ as a function of reaction progress for Run 1 are plotted in Figures 2-47 to 2-49. The plots for Runs 2 to 4 are virtually identical to those of Run 1. The figures show that the simple partial equilibrium model provides a good fit to many of the observed calcium concentrations. However, concentrations of Mg and $SO_4$ are considerably below the predicted values.

#### *2.4.2.2.2 EFFECT OF ADDITION OF SOLUTES FROM EVAPORITE SALTS*

Potential sources of additional Mg and $SO_4$ for the Culebra groundwaters are polyhalite ($K_2Ca_2Mg(SO_4)_4 \cdot 2H_2O$), carnallite ($KMgCl_3 \cdot 6H_2O$), and magnesite ($MgCO_3$). All of these minerals have been observed in at least trace amounts in the Rustler. Simulations (Runs 5 and 6) were carried out in which one or more of these salts were added to the solution at constant ratios to halite. The ratios of carnallite and polyhalite to halite were set by the observed K:Cl ratio of Culebra waters. A molar ratio of K/Cl = 0.007 was estimated by examination of scatter plots of K to Cl. The proportion of $MgCO_3$ (magnesite/halite = 0.025) added was determined by the amounts of the other salts and the difference between the observed Mg and the amount calculated in Run 1.

In nature, polyhalite dissolves incongruently to form gypsum plus a solution containing $K^+$, $Mg^{+2}$ and $SO_4^{2-}$. In Run 7, this process was simulated by adding these solutes as leonite ($K_2Mg(SO_4)_2 \cdot 4H_2O$). Because the solutions are saturated with respect to gypsum, congruent (Run 5) and incongruent (Run 7) dissolution of polyhalite produced virtually identical results. Only the amount of gypsum precipitated depended on the method of dissolution in the simple model considered here.

Figures 2-47 to 2-49 show the concentrations of Ca, Mg, and $SO_4$ as a function of reaction progress (indicated by the chloride concentration) for these simulations. In all of these

calculations, saturation was maintained with respect to calcite, gypsum, and dolomite. The system was closed with respect to $CO_2$ gas; the initial $pCO_2$ was $10^{-2}$ atmosphere. None of the theoretical reaction paths reproduce the observed Culebra groundwater compositions. Although the sulfate concentrations are improved at intermediate chloride concentrations by addition of polyhalite/leonite, the magnesium concentrations are not improved.

#### *2.4.2.2.3 EFFECT OF DEGREE OF DOLOMITE SATURATION*

The Mg/Ca ratio of a solution can be specified by specifying the ratio of the saturation indices of dolomite and calcite. A set of reaction path simulations (Runs 8 and 9) was carried out in which halite was added to the starting solution while maintaining saturation with respect to calcite and gypsum and various levels of supersaturation with respect to dolomite (Run 8: SI = 0.5; Run 9: SI = 1.0). Mg, K, $SO_4$, and $CO_3$ were added to the reaction solution by specifying various proportions of polyhalite, carnallite, and magnesite to halite. The results are presented in Figures 2-50 to 2-53.

Figure 2-50 shows that a constant dolomite saturation index leads to a Mg/Ca ratio that decreases slightly as the halite dissolution reaction progresses. Figures 2-51 and 2-52 show that this effect is due to an increase in the calcium concentration and a decrease in the Mg concentration over most of the range of chloride concentration (cf. Runs 1, 8, and 9). This differs from the increase in the Mg/Ca ratio as a function of ionic strength that is observed in the Culebra waters. In addition, the sulfate concentrations calculated with Runs 8 and 9 do not match the concentrations observed in the Culebra either (cf. Figure 2-53).

A final set of simulations (Runs 10 and 11) were run in which saturation with dolomite was not maintained. The starting solution was produced by equilibrating distilled water with calcite, dolomite, and gypsum at an initial $pCO_2$ of $10^{-2}$ atmosphere. The system was then closed to $pCO_2$ gas, and halite plus accessory minerals were added. The saturation index of dolomite was calculated as the reaction progressed, but dolomite was not allowed to dissolve or precipitate.

Run 10 simulated addition of K, Mg, and $SO_4$ by incongruent dissolution of polyhalite and carnallite. Carnallite dissolves incongruently to form KCl and a solution containing $Mg^{2+}$ and $Cl^-$. In Run 10, this was simulated by adding $MgCl_2$ to the reaction solution. Incongruent dissolution of polyhalite was simulated by addition of leonite to the solution. The K:Cl ratio of the Culebra waters was used to estimate a reasonable leonite:halite ratio. The $MgCl_2$:halite ratio was then adjusted to fit the observed Mg:Cl ratio of the Culebra waters. In Run 11, magnesite ($MgCO_3$) was added instead of $MgCl_2$ to adjust the Mg:Cl ratio.

Figures 2-50 through 2-53 show that Run 10 reproduces the trends of the Ca, Mg, and $SO_4$ concentrations in this suite of Culebra groundwaters. The calculated dolomite saturation indices for Run 10 were used to calculate values of the saturation index expression ($2SI_{calcite}$ - $SI_{dolomite}$) described previously and are plotted in Figure 2-39. The good correspondence between the theoretical and observed solute concentrations in these figures show that addition of solutes (Mg, $SO_4$, and K) to the Culebra from evaporite minerals such as polyhalite is consistent with the observed groundwater compositions if dolomite does not precipitate from supersaturated solutions.

#### *2.4.2.2.4 MASS TRANSFER*

Table 2-12 summarizes the nature of mass transfers (dissolution, precipitation, and gas exsolution) that occur during the reaction simulations. For the simplest partial-equilibrium model (Runs 1 through 4) dedolomitization (dissolution of dolomite and precipitation of calcite) and dissolution of gypsum occur over the entire salinity range. In Run 4, which has a constant $pCO_2$ ($10^{-3.5}$ atmosphere), gas begins to exsolve at a chloride concentration of about 1.8 molal. Addition of Mg by dissolution of polyhalite and/or carnallite (Runs 5, 7, and 8) leads to dolomitization (dissolution of calcite and precipitation of dolomite) at intermediate ionic strengths. Dedolomitization occurs over the entire salinity range in a solution maintained at dolomite supersaturation (SI = 1.0, Run 9). If magnesite is added to the solution (Run 6), dolomitization can occur over the entire salinity range. If dolomite precipitation and dissolution are suppressed, addition of K, Mg, and $SO_4$ by incongruent

dissolution of polyhalite and carnallite (as leonite and $MgCl_2$, Run 10) leads to dissolution of calcite and gypsum over the entire reaction path. If magnesite is added instead of $MgCl_2$ (Run 11), calcite precipitates and gypsum dissolves.

The nature of these mass transfers is dependent on the proportions and stoichiometry of the minerals added to the reaction solution, and many plausible combinations exist. Solution compositions during Run 10 are closest to those observed in the Culebra. This simulation predicts dissolution of both calcite and gypsum. However, gypsum and minor calcite have been observed in Culebra fractures (Sewards et al., Chapter 5), and it cannot be stated that these minerals are currently dissolving in the Culebra. In Run 10, if sufficient anhydrite were added to the reaction solution, gypsum would precipitate rather than dissolve.

#### *2.4.2.2.5 COMPARISON OF RESULTS FROM REACTION PATH MODELS AND PRINCIPAL COMPONENT ANALYSIS*

The assumptions of Run 10 are also consistent with the results of the principal component analysis (PCA) described in Section PCA . The slight change in gypsum solubility with ionic strength leads to a moderate positive correlation between Na, Cl, and Ca seen in the salinity factor. This factor accounts for about 35% of the variance of calcium. The equilibrium with gypsum, however, produces a strong negative correlation between Ca and $SO_4$ that is expressed in the sulfate factor and accounts for more than 50% of the variance in calcium. Run 10 assumes that Mg and K are added to the solution along with the halite and are not appreciably controlled by solubility equilibria. This is consistent with the salinity factor, which accounts for more than 80% of both of these elements.

The behavior of sulfate is affected both by addition from salt dissolution and by solubility equilibrium in Run 10. This is consistent with the PCA: the salinity and sulfate factors account for about 60% and 25% of the variance, respectively.

The negative correlation between pH and bicarbonate alkalinity shown in the silicate/bicarbonate factor (e.g., factor 2B) is also consistent with the reactions included in Run 10. For example, a negative correlation could result from dissolution of calcite:

$$CaCO_3 + H^+ \rightarrow Ca^{2+} + HCO_3^- \quad [6]$$

The mass action expression for these reactions can be written as:

$$pH = -\log a_{HCO_3^-} - \log a_{Ca^{2+}} - \log K_6 , \quad [7]$$

where $K_6$ is the equilibrium constant for the reaction described by Equation 6.

Although dolomite was not allowed to dissolve in Run 10 (except in the preparation of the starting solution), the negative correlation between pH and bicarbonate could also reflect dissolution of dolomite in the Culebra:

$$CaMg(CO_3)_2 + 2H^+ \rightarrow Mg^{2+} + Ca^{2+} + 2HCO_3^- \quad [8]$$

with the corresponding mass action expression:

$$2pH = -2\log a_{HCO_3^-} - \log a_{Ca^{2+}} - \log a_{Mg^{2+}} - \log K_8 , \quad [9]$$

where $K_8$ is the equilibrium constant for Equation 8. In a closed chemical system, the inverse relation between pH and alkalinity expressed by either of these equations could show up in a factor such as factor 2B.

The reaction path models described above correspond to a simple hydrologic model in which recharge water enters the Culebra and dissolves dolomite, gypsum, and calcite. As the water migrates within the aquifer, it obtains solutes from fluids that have dissolved

halite and other evaporite salts from adjacent strata. This model is no doubt much simpler than the real system. There is no reason to assume that the ratio of halite to accessory minerals is constant over the entire flow path. It is possible that other combinations of reactants could be added to the "starting solution" to produce the observed trends in the Culebra. Although Run 10 provides the best average fit to the observed Culebra compositions over the entire range of ionic strengths, some of the Culebra waters more closely match the compositions of other runs. Thus, it is likely that each of the water samples in the Culebra has a unique history that does not conform to the simple model described above.

## 2.4.3 Ion Exchange, Sorption, and Silica Diagenesis

### 2.4.3.1 Introduction: Potential Significance of the Silicate/Bicarbonate Factor

The reaction path model described in the previous section includes dissolution and precipitation of chloride, sulfate, and carbonate minerals and accounts for most of the variance of Na, Cl, Ca, $SO_4$, Mg, and K. The model is consistent with the solute relationships expressed by the salinity and sulfate factors from the PCA. In addition, the model is consistent with the negative correlation between pH and bicarbonate that is part of the silicate/bicarbonate factor. This factor also accounts for large portions of the variances of Li, B, and $SiO_2$; however, the variances in the concentrations of these solutes may be related to other processes in addition to salt dissolution or carbonate and sulfate mineral equilibria. For example, factor 2B, obtained from the partial R-mode PCA of Culebra samples (Figure 2-26), shows a moderate Li-B association negatively correlated to a Mg-Si association. The following amounts of the total variance of these elements are explained by the above correlation: $SiO_2$ - 53%; B - 35%; Li - 15%; Mg - 6%.

The relationships among these elements may be partially controlled by reactions involving silicate minerals. Potential processes include release of Si and Mg by dissolution of silica and silicates, and sorption of Li and B by clays.

This hypothesis is supported by the studies of the mineralogy of samples from intact core. Sewards et al. (Chapter 3) report that clays comprise about 3 to 5% by weight of the bulk mineralogy of intact Culebra core samples that have been studied. They occur as discrete seams, as fracture surface coatings, or are finely dispersed throughout the matrix; they are commonly associated with silt-sized quartz. The dominant clay minerals are corrensite (a mixed-layer chlorite/smectite), illite, and serpentine.

Because silica will be released by dissolution of both quartz and clays, the distribution of silica may be controlled by the accessibility of the clays to groundwaters. The extent to which clays react with groundwater is of interest because of their ability to sorb radionuclides. In areas where clays are abundant, both dissolution and ion exchange may affect water chemistry. In Section 2.4.3, relevant laboratory and field data are summarized to assess whether these processes are likely for Culebra groundwaters.

### 2.4.3.2 Dissolution of Clay Minerals and $SiO_2$

#### *2.4.3.2.1 SOLUBILITY OF SILICA IN WIPP GROUNDWATERS*

The distribution of aqueous silica at the WIPP Site may be controlled by saturation with respect to a silica or silicate phase or by the rate of dissolution from a silica-rich rock. The degree of control that saturation with respect to $SiO_2$ polymorphs plays in controlling silica activity may be assessed from Figure 2-54. This figure shows the relationships between the activity of water, the total measured silica concentration for Culebra samples, and the saturation concentrations of $Si(OH)_4^o$ for several silica polymorphs ($SiO_2(s)$). The equilibrium silica concentrations were calculated for the reaction:

$$SiO_2(s) + 2H_2O \rightarrow Si(OH)_4^o \qquad [10]$$

from the relation:

$$[Si(OH)_4^o] = [H_2O]^2 \; K_{10} \qquad [11]$$

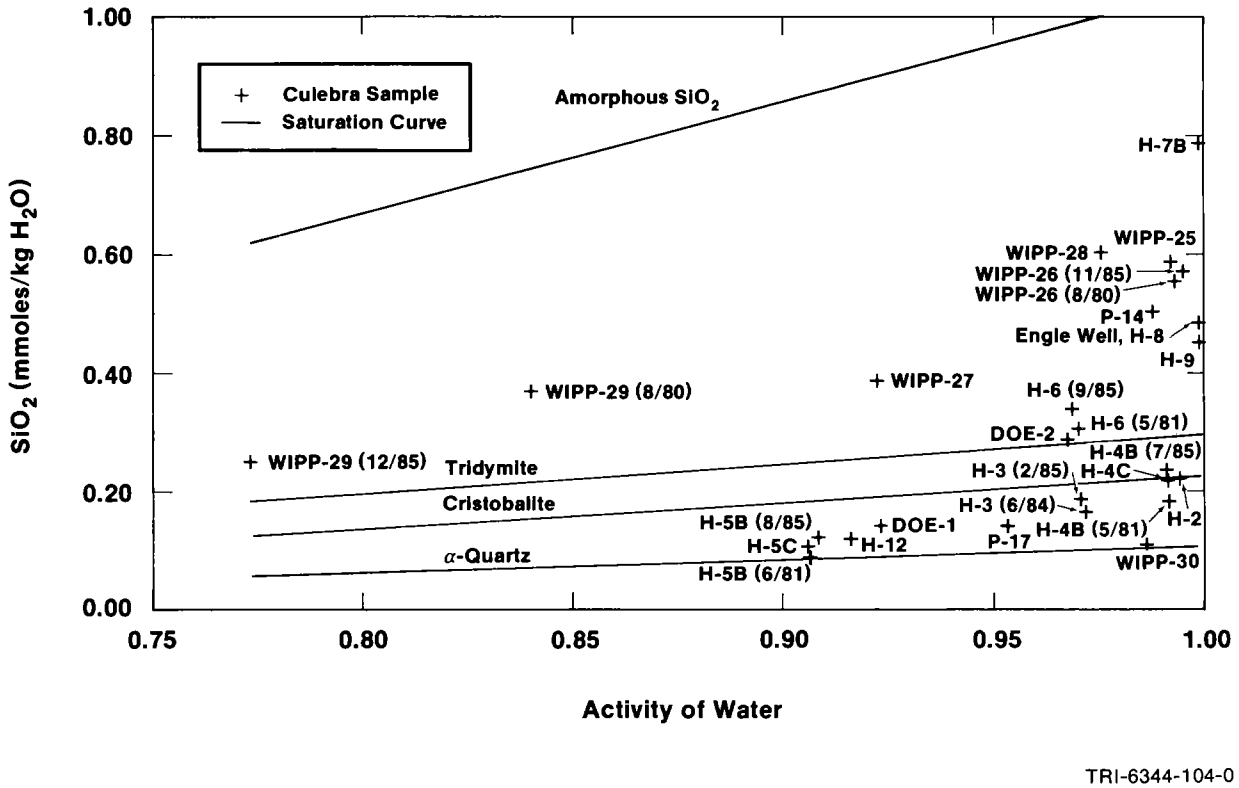


Figure 2-54. Relationship between measured concentrations of aqueous silica (mmoles/L), calculated saturation curves for silica polymorphs, and the activities of water in Culebra groundwaters.

where $K_{10}$ is calculated from the relationship:

$$\Delta G_r = \Delta G_{Si(OH)_4^o} - 2\Delta G_{H_2O} - \Delta G_{SiO_2(s)} = RTlnK_{10} \quad [12]$$

The current version of PHRQPITZ does not have data for any silica species; therefore, two approximations were made in this calculation. First, the contribution of other silica species to the measured silica total has been ignored. This is reasonable because in the pH range of interest (pH 6 to 8) in 0 to 3 M NaCl solutions, $Si(OH)_4^o$ is by far the dominant silica species in solution (cf. Stumm and Morgan, 1981, Figure 9.5). For example, the $Si(OH)_3^-/Si(OH)_4^o$ ratio is $<0.05$ at pH = 8 in 3 M NaCl solution (using thermodynamic data from Phillips et al., 1985). The second assumption was that the activity coefficent of $Si(OH)_4^o$ was equal to unity because it is an uncharged species.

Figure 2-54 shows that the solutions are all undersaturated with respect to amorphous silica. Saline waters in hydrochemical facies Zone A lie close to quartz saturation, and fresh waters from Zone B have silica contents between tridymite and amorphous silica saturation. No pattern is apparent for water samples from Zone C. In general, the silica concentrations do not seem to be related to saturation constraints for the silica polymorphs.

The relationship between the silica concentration and the activity of water might be due to a kinetic effect. Precipitation of $SiO_2$ from solution involves dehydration of $Si(OH)_4^o$. If the rate of this reaction increases with salinity, then equilibrium with alpha quartz might be more rapidly approached by the more saline waters in Zone A and lead to lower concentrations than those of the fresher waters in Zone B. The role of kinetic factors, however, cannot be resolved within the scope of this report.

#### 2.4.3.2.2 SILICA DISSOLUTION AND LEACHING

The spatial pattern of silica concentration contours is different from patterns for elements that are assumed to be dissolved from halite and associated evaporite salts (cf. Figures 2-2 and 2-8). Figure 2-8 shows the concentrations of total silica in Culebra samples analyzed by the ITAS laboratories. The contours illustrate that in general, silica concentrations are highest in the west and decrease to the east. Uncertainties in the silica values were discussed in Section 2.2. The actual range of silica concentrations measured at each site can be found in Table 2-2. In general, UNC Geotech analyses in the eastern section of the site show lower concentrations than the corresponding ITAS values. Use of the UNC Geotech values in Figure 2-8 would reinforce the observed trend of decreasing silica concentrations from west to east.

The lack of solubility control on silica concentration discussed above and the spatial trend shown in Figure 2-8 suggest that the distribution of silica is strongly controlled by the rate of supply of silica to the groundwater (leach-limited). Source rocks in the western part of the site may contain more silica that is accessible to leaching than rocks in the east. This may be due to the greater amount of evaporite dissolution and concomitant concentration of residual detrital silicates in the western and southern parts of the site compared to the eastern section.

#### 2.4.3.2.3 DISSOLUTION OF AUTHIGENIC MIXED-LAYER CLAYS AND THE Mg-$SiO_2$ ASSOCIATION

The correlation of Mg and Si in factor 2B could result from dissolution of a Mg-Si rich phase, possibly a trioctahedral Mg-rich layer in corrensite. The following equation qualitatively illustrates this process:

$$MgSiX_{(am)} + 2H_2O + 2H^+ \rightarrow Mg^{2+} + Si(OH)_4^o \qquad [13]$$

Evidence that an amorphous Mg-rich layer ($MgSiX_{(am)}$) in authigenic mixed-layer clays is more soluble than the Al-Fe-rich smectite layer is found in studies of Salt Lake sediments by Spencer et al. (1985). It is not known if the rate of reaction expressed by equation 13 is rapid enough to affect groundwater chemistry on the time scale of interest to this study (≈10,000 years). The reverse precipitation reaction is probably fast enough to affect the solution composition on this time scale. Jones and Weir (1983) found that sediments in alkaline Lake Albert are ≈2500 years old yet have developed a Mg-rich trioctahedral component in mixed-layer smectite clays.

### 2.4.3.3 Sorption of Lithium and Boron in Saline Water/Clay Systems

#### *2.4.3.3.1 LITHIUM*

Approximately 15% of the variance of lithium is not correlated with ionic strength. Figure 2-55 shows that over most of the ionic strength range, increase in Li concentration is associated with a decrease in the Li/Cl ratio. The depletion of Li relative to Cl in these waters could be due to increasingly lower Li contents of the salt that supplies the Cl, or removal by clays of Li supplied by the salt dissolution.

The importance of the first mechanism is difficult to assess with the available data. A systematic study of the lithium contents in salts adjacent to the Culebra dolomite has not been carried out. In general, in evaporite basins, Li is not taken up appreciably by precipitating salts. Accessory evaporite minerals have different Li contents (e.g., halite, 0.2 ppm; polyhalite, 10 ppm; carnallite, 8 to 9 ppm; sylvite, 16 ppm) (Holser, 1979; Sonnenfeld, 1984). It is possible that the Li/Cl ratio reflects the ratio of accessory salts to halite in dissolving evaporite layers.

The decrease of Li/Cl with increasing Li and Cl concentrations is also consistent with release of Li from clays in relatively fresh Li-poor waters and uptake of Li by clays in saline Li-rich waters. Clays have the highest Li contents of all rock types (up to 120 ppm in shales; Holser, 1979) and can act both as sources and sinks for Li. Evaporitic clays can be sources of Li in oil-field brines (Collins, 1975).

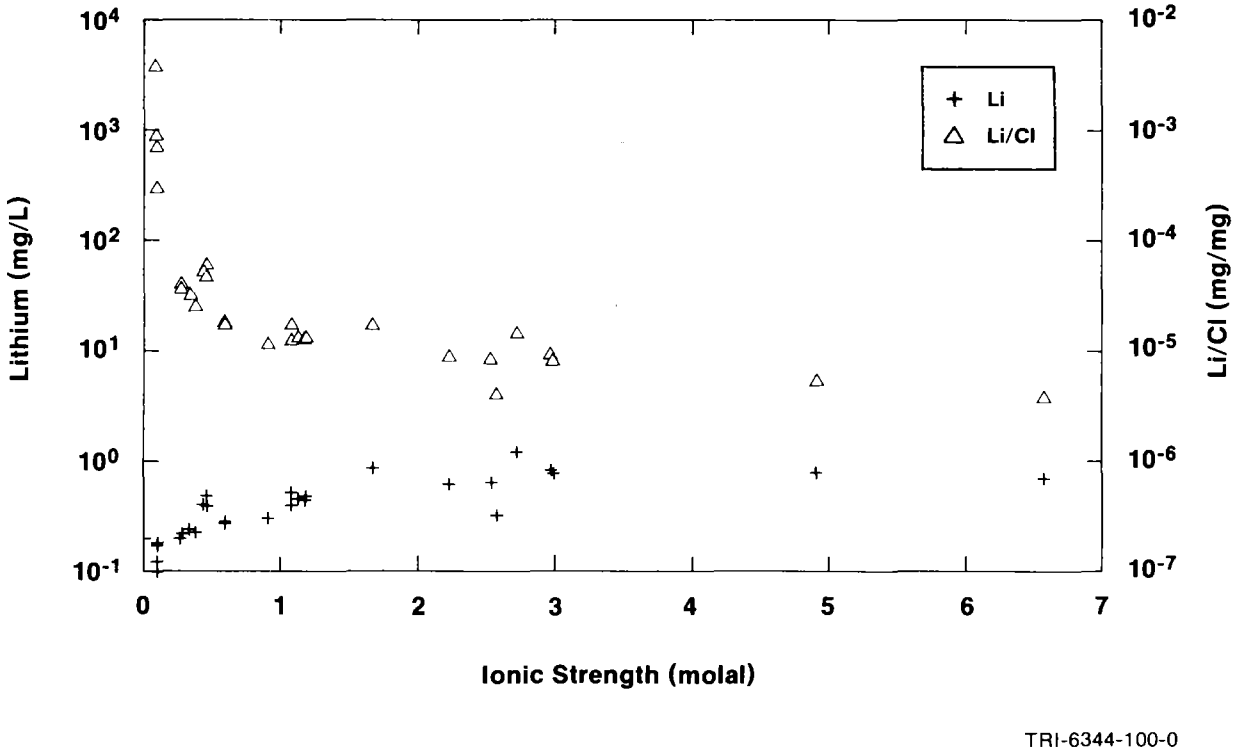


Figure 2-55. Relationship between Li concentrations (mg/L), Li/Cl weight ratios ([mg/L]/[mg/L]), and ionic strengths of Culebra groundwater samples.

The uptake of Li into clays is well documented. Based on a comparison of rates of supply of dissolved Li to the amounts of Li salt in evaporite beds, G. Smith (1976) suggests that 95% of the Li originally supplied to Searles Lake, California was removed by uptake by lake sediments prior to deposition of salt beds. C. Smith (1976) notes that the Li/Cl ratios of Li-rich brines from across the western United States decrease as the Cl content increases, indicating removal or fixation of Li from waters in the vadose zone and surface waters (near surface) during evaporation.

Seyfried et al. (1984) cite ample evidence suggesting that pelagic clays are efficient scavengers of Li from seawater and could remove up to 75% of the total riverine-Li input to the oceans. The uptake of Li by clays may involve substitution (Collins, 1975) or irreversible uptake up by vacant octahedral sites in Al-rich smectites (Schultz, 1969).

The extent of release or uptake of Li by clays could depend on a large number of solution/substrate parameters including surface area, salinity, temperature, and past diagenetic history. It is not possible at this time to formulate a quantitative model for the exchange of Li between clays and Culebra waters. The information provided above, however, suggests that this mechanism is plausible in Culebra waters and may exert some control on the distribution of Li in this aquifer.

#### *2.4.3.3.2 Boron*

About 43% of the variance of B is not correlated with the TDS concentration (Table 2-8). Like Li, B can be either released or sorbed by clays in saline waters. Equation 14 qualitatively illustrates the sorption of borate ion onto a clay surface:

$$SOH + B(OH)_4^- + H^+ \rightarrow SOH_2^+ B(OH)_4^- \quad , \qquad [14]$$

where SOH represents a surface site.

There is abundant field and laboratory evidence that illite and montmorillonite effectively scavenge B from saline solutions such as seawater (Seyfried et al., 1984, and cited references; Harriss, 1969; Goldberg and Glaubig, 1986). In evaporite systems, B is primarily associated with clay minerals and initially substitutes for Al in Si tetrahedra or occupies empty sites in the crystal lattice (Sonnenfeld, 1984; Harder, 1961). During alteration in hypersaline brines when Mg-rich, mixed-layer clays are formed, the original crystal lattice is destroyed and the B is released. The liberated B can form independent minerals or become associated with sulfates such as anhydrite.

A quantitative model for the exchange of B between clays and water in the Culebra cannot be formulated at this time. However, both the negative correlation of B with silica (that is independent of the effects of salt dissolution) and the laboratory and field data discussed above are consistent with the hypothesis that clays in the Culebra could scavenge B from Culebra waters.

#### 2.4.3.4 Determining the Potential Significance of Ion Exchange, Sorption, and Silicate Diagenesis in Culebra Waters: Limitations of Available Information

The role that clay minerals have in affecting the concentration of trace solutes through ion-exchange, sorption, and silicate diagenesis is of particular interest to the WIPP Site characterization studies. Studies of the distribution of minor solutes in waters from the Culebra dolomite may provide some insight into the ability of small amounts of clays in fractures to affect the transport of solutes in general.

The attempt to use the data for B, Si, Mg, and Li to study in-situ ion exchange and sorption onto clays has several limitations. First, it is likely that multiple sources exist for these elements. This problem was addressed by using PCA to distinguish the individual contributions of potential sources that are identified by diagnostic element correlations. The correlations are consistent with the hypothesis that clays remove B and Li from solution and release Mg and silica.

A second limitation in this analysis is the small size of the sample set. The computation of the correlation matrix used in the PCA requires a population with a normal distribution. The small population available hindered the identification of outliers that may exert a disproportionate influence on the orientation of the principal components. This effect may be especially important for minor elements such as B and Li. Because PCAs account for all of the variance in the data set, random variations due to analytical errors may have strongly influenced or dominated the minor factors.

This limitation could be addressed in future studies by carrying out a classical factor analysis of a larger data set. As discussed in Appendix 2B, in classical factor analysis, a proportion of the variance of each variable is assigned to random error and does not influence the orientation of the extracted factors. If the experimental error for each chemical variable could be equated with the unique variance, the disproportionate influence of the analytical imprecision of the trace solute analyses could be reduced.

A final problem is related to the method of PCA itself. This method provides no insights into the identity of the factors, nor does it provide the means to identify meaningless or spurious correlations; additional sources of information are always required. A survey of the literature provides ample evidence that sorption of B and Li and release of Mg and silica from clays in saline waters is possible. However, geochemical and mineralogical evidence supporting or contradicting this model for the WIPP are ambiguous. There are insufficient trace element analyses of clay minerals in the Culebra to allow an independent assessment of the magnitude of the effect of ion exchange on groundwaters at the WIPP. While Sewards et al. (Chapter 3) suggest that the probable high solution-volume/clay ratios in the Culebra indicate that the clays do not significantly affect major solute chemistry, no reliable estimate of the solution/clay ratio is available at this time. Additional analyses of mineral compositions from rock samples and better estimates of the amount of clay that have been in contact with the Culebra fluids are required to test the hypotheses suggested by the PCA.

### 2.4.4 Other Processes

There are several other potential sources of solutes for waters in aquifers in evaporite environments that are discussed briefly here and described in more detail in other chapters of this report. These include:

- Mixing with primitive waters. Waters from fluid inclusions and intergranular fluids are potential sources of solutes which are discussed by Bodine et al. (Chapter 4).

- Mixing with waters from other water-bearing zones or mixing with introduced (contaminant) waters such as process brines, proprietary additives, lubricants, or special treatments in hydrologic testing. These may not always be detectable without knowing the long-term sampling history (over many years) of any single well.

### 2.4.5 Formulation of a Combined Hydrological-Hydrochemical Model for the Chemical Evolution of Waters in the Rustler Formation

One accepted framework for the formulation of a model for the geochemical evolution of a groundwater is a series of mass-balance and reaction path calculations along the hydrologic flow path (Plummer, 1984; Back et al., 1983); such calculations involve using codes like PHRQPITZ and BALANCE (Parkhurst et al., 1982) to simulate the chemical and isotopic reactions that produce a given groundwater composition at the end of a flow path from the composition found at the beginning of the path. Plummer (1984) shows that the data required for these calculations are substantial. The compositions (solutes and isotopes) of waters from wells along a well defined flow path, the textural and compositional data of minerals at the wells, and the equilibrium and rate constants for important reactions are required to produce a well constrained model. Even if these data are available, however, a unique reaction path model is generally not obtainable. Systems with significant fracture flow, systems with hydrochemically undefined vertical mixing, and systems not at hydrological and chemical steady state are not amenable to this kind of modeling.

The available mineralogical, thermodynamic, kinetic, and hydrologic data are not adequate to support a meaningful reaction path calculation along groundwater flow paths at the WIPP Site. Even if additional data are collected, the information summarized in this chapter and in other chapters in this report suggest that the WIPP Site has many attributes that are unfavorable for successful simulation of the chemical evolution of the waters along hydrologic flow paths. As discussed in other sections of this report (cf. Lambert, Chapter 5), there is abundant evidence that the hydrologic flow system is not at steady state. Isotopic, stratigraphic, and geochemical data are consistent with the hypothesis that the direction of groundwater flow changed from a direction with a strong west to east component to one with a dominant north to south component since the late Pleistocene.

# 2.5 SUMMARY AND CONCLUSIONS

The purpose of this chapter is to summarize solute concentration data and to delineate hydrochemical facies in the Culebra Member of the Rustler Formation. These data are used as a basis for hypotheses concerning the chemical evolution of the groundwaters and to show the relationship between patterns of solute distribution and groundwater flow. The composition of waters in the Culebra dolomite is emphasized in this chapter. Preliminary results from work dealing with the Magenta dolomite, the Rustler/Salado contact zone, the Dewey Lake Red Beds, and the Bell Canyon Formation are found in Appendix 2D.

Several kinds of relationships among groundwater chemical variables were examined. These included spatial distributions of element concentrations and ratios (hydrochemical facies and geochemical signatures), interelement correlations expressed by PCA, and mass action (solubility constant) constraints. The methods used, results, and limitations of the analysis are summarized below.

## 2.5.1 Delineation of Hydrochemical Facies in the Culebra

Based on the major solute compositions, four hydrochemical facies have been delineated. Zone A, containing saline (about 3.0 m) NaCl brine with a Mg/Ca molar ratio between 1.2

and 2.0, is found in the eastern third of the study area, roughly coincident with the region of low transmissivity and the occurrence of halite in several units of the Rustler Formation. Zone B, containing a dilute Ca-$SO_4$-rich water (I <0.1 m), is found in the southern part of the study area and coincides with a zone of high transmissivity where halite is absent from the Rustler. Zone C contains waters of variable composition and ionic strengths (0.3 to 1.6 m); Mg/Ca molar ratios range from 0.5 to 1.2. The zone extends from the western part of the four-mile zone where halite is present in the unnamed lower member of the Rustler to the eastern side of Nash Draw where no Rustler halite has been found. Zone D contains WIPP-27 and WIPP-29 and is defined on the basis of anomalously high salinities (3 to 6 m) and K/Na weight ratios (0.2). The composition of the Culebra groundwater at WIPP-29 has changed over the course of a 7-year monitoring period, probably due to contamination from potash-refining operations in the area.

### 2.5.2 Geochemical Signatures as Indicators of Hydrologic Flow Direction

In simple hydrologic systems, spatial trends in element concentrations and ratios (geochemical signatures) can be used to delineate sites of recharge or interaquifer leakage, to provide independent evidence of groundwater flow, and to determine the presence of hydrologic divides. The use of geochemical signatures to delineate groundwater flow direction assumes the following:

- The hydrologic system has been at steady state for at least as long as the residence time of the solutes in the system

- The signature involves elements that are not appreciably removed from solution by chemical processes or do not have multiple sources that supply the solutes at different rates.

In general, those conditions are not present at the WIPP Site. As discussed in Section 2.3.2.1 and by Ramey (1985), the geochemical signatures are inconsistent with the assumption of steady-state hydrologic flow. The regional variation in salinity at the WIPP Site, as shown by the sodium concentration contours in Figure 2-2 and the hydrochemical facies map in Figure 2-1, suggest a southwest-to-northeast groundwater flow direction across the site. The present day flow direction indicated by available hydrologic data (cf. Lappin, 1988) is approximately north to south. Independent isotopic evidence suggests that the flow system has been transient over at least the last 12,000 years and the direction of flow has changed since the late Pleistocene (Lambert, Chapter 5). Paleo-flow directions indicated by $^{234}U/^{238}U$ relationships have a west to east component consistent with the regional variation of most of the solutes.

There is agreement between geochemical signatures and present day flow directions only in limited sections of the WIPP area. Local contours for K, K/Na, Mg, and Na near WIPP-27 and WIPP-29 are consistent with the introduction of wastes from nearby potash refining operations. In the vicinity of the WIPP Site (four-mile zone), the series of wells (H2 → H3 → P-17) may lie along a modern flow path. The salinity of waters sampled from the wells increases along this path. The concordance of flow direction and solute concentration is ambiguous, however, because of uncertainties in the flow direction and in the chemistry of the Culebra water at the H-2 well.

### 2.5.3 Use of Principal Component Analysis to Identify Geochemical Processes Affecting Water Chemistry

Three factors were extracted by R-mode PCA from the major and minor solute data. The first factor (salinity factor) is dominated by Na, K, Mg, Br, and Cl. The second most important factor (sulfate factor) also has a strong Na-Cl influence, but is dominated by Ca, sulfate, bicarbonate alkalinity, and Sr. Geologic data from the site suggest that these two factors represent addition of solutes by the dissolution of halite, gypsum/anhydrite, and carbonates. A third factor (silicate/bicarbonate factor) showed the interelement correlations independent of effects attributable to halite dissolution. This factor contains two

inversely correlated groups of elements: Mg, bicarbonate alkalinity, and $SiO_2$ form one group; and pH, B, and Li form another group. This pattern of element associations might reflect sorption of B and Li by clays, release of Mg and $SiO_2$ by dissolution of authigenic clays, and carbonate diagenesis.

The reification of the principal components in terms of geochemical processes must be done cautiously. The results of the PCA should only be used to suggest possible reactions; independent confirmation must be obtained before the proposed mechanisms are accepted. Other limitations of the PCA presented here are the small size of the data set and the large relative uncertainties in the concentrations of some of the minor and trace solutes.

## 2.5.4 Thermodynamic (Mass Action) Calculations with Solute Concentration Data

### 2.5.4.1 Use of Saturation Index Calculations to Evaluate Chemical Equilibria

Saturation indices of groundwaters can be used to suggest the identity of minerals that control solute concentrations, to detect evidence of the metastable persistence of mineral phases, and to indicate possible errors in chemical analyses, sampling procedures, and chemical speciation models. Waters from the Culebra are saturated with respect to gypsum and undersaturated with respect to halite. Calculated saturation indices for calcite and dolomite indicate saturation for some wells, but many of the waters show apparent supersaturation. The Mg/Ca ratios of the waters are consistent with increasing degrees of dolomite supersaturation with ionic strength.

Uncertainties in the saturation indices must be evaluated on a mineral by mineral basis. Analytical error, errors in calculated activity coefficients, and uncertainties in the equilibrium constants will contribute to the uncertainty in the saturation index. For chemical analyses of Culebra waters, uncertainties in pH will be important for carbonates, and uncertainties in equilibrium constants will be important for phases such as dolomite that exhibit order/disorder.

The uncertainty in the carbonate analyses is especially important for the waters in the dolomite aquifers and can be resolved by modification of sampling techniques in the field. Only if the total alkalinity and either total inorganic carbon or $pCO_2$ are measured can the carbonate system be unambiguously defined. With this approach the pH is calculated rather than measured, and problems associated with loss of $CO_2$ gas and the different activity scales are minimized.

Even if the actual saturation indices of dolomite, calcite, and gypsum are zero, it is likely that these minerals are dissolving in areas where halite dissolution is increasing the ionic strength of the groundwaters over the range of 0 to 3 molal. The Culebra may be a partial-equilibrium system in which the mineral/water equilibria are shifting along a reaction path driven by the irreversible process of halite dissolution. Theoretical calculations show that the increase in salinity caused by the dissolution of halite changes the solubilities of carbonates and sulfates; solubilities increase up to 3 molal ionic strength and then decrease. Additional evidence for the mass transfer could come from petrographic investigations of textural relations in the rock, isotopic data for minerals and aqueous species, and mass balance calculations based on concentration changes along the flow path.

### 2.5.4.2 Reaction Path Modeling

The PHRQPITZ code was used to calculate the compositions of waters that would be produced by several hypothetical reaction paths. A series of parametric simulations was carried out to determine the effects of certain assumptions about chemical reaction rates, sources of solutes, and initial conditions on the groundwater compositions. The results of the reaction path simulations are non-unique; it is possible that fluid compositions can be obtained by several different paths. However, simulations described in Section 2.4.2.2 suggest that equilibrium with dolomite plays a minor role in controlling the chemistry of the more saline Culebra waters in Zones A and C. The relationships between K, Mg, Ca, and $SO_4$ with chloride are consistent with a partial-equilibrium model in which saturation is maintained with respect to calcite and gypsum while these solutes are added to the Culebra by dissolution of halite containing minor amounts of polyhalite and carnallite. Recharge

waters entering the Culebra may initially reach equilibrium with dolomite, but as the ionic strength increases, due to dissolution of halite and the accessory minerals, the solutions become increasingly supersaturated with respect to dolomite.

### 2.5.5 Summary of Chemical Processes Affecting Groundwater Chemistry

Table 2-13 summarizes chemical processes that may affect the chemistry of water samples described in this report. The mixing of connate formation waters with recharge waters is discussed by Bodine et al. (Chapter 4) and cannot be ruled out with the available solute composition data.

## Table 2-13. Chemical Processes That May Affect the Solute Compositions of Culebra Groundwaters

| Chemical Process | Potential Effect(s) on Concentrations of Solutes in Culebra Groundwaters |
|---|---|
| Halite dissolution | increase Na, Cl, Br, Li; increase Cl/Br; increase solubility of carbonates and sulfates up to 3 molal ionic strength and then decrease solubility causing changes in Ca, Mg, $SO_4$, $CO_3$ |
| Precipitation/dissolution of gypsum | decrease/increase Ca, $SO_4$ |
| Precipitation/dissolution of calcite and dolomite | decrease/increase Ca, Mg, $CO_3$ |
| Dolomitization[1]: calcite + Mg → dolomite + Ca | decrease Mg/Ca ratio |
| Dedolomitization[2]: dissolution of gypsum and dolomite with concurrent precipitation of calcite. | decrease pH, alkalinity, $SO_4$; must maintain Mg/Ca molar ratio < 1 |
| Sorption/desorption by clays | loss/gain of Li and B by solution |
| Mixing of connate hypersaline formation water with recharge water that has dissolved gypsum[3] | increase Mg, Ca, K, Na, Cl; decrease $SO_4$, Cl/Br ratio |
| Incongruent dissolution of polyhalite | increase Mg, K, $SO_4$; decrease Ca, Cl/Br ratio |
| Dissolution of silicates | increase Si, Mg, Na |
| Dissolution of anhydrite with sellaite inclusions | increase Ca, $SO_4$, Mg, F |

1. Process may be important locally.
2. Process may be important locally, for example, at WIPP-33.
3. Process discussed by Bodine et al. (Chapter 4).

# 2.6 REFERENCES

Back, W., B. B. Hanshaw, L. N. Plummer, P. H. Rahn, C. T. Rightmire, and M. Rubin. 1983. "Process and Rate of Dedolomitization: Mass Transfer and $^{14}C$ Dating in a Regional Carbonate Aquifer." *Geological Society of America Bulletin*, Vol. 94:1415-1429.

Barr, G. E., W. B. Miller, and D. D. Gonzalez. 1983. *Interim Report on the Modeling of the Regional Hydraulics of the Rustler Formation*. SAND83-0391. Albuquerque, NM: Sandia National Laboratories.

Bassett, R. L. 1982. "Geochemistry and Mass Transfer in Brines from Permian Wolfcamp Carbonates in the Palo Duro, Dalhart, and Anadarko Basins." *Geology and Geohydrology of the Palo Duro Basin, Texas Panhandle: A Report on the Progress of Nuclear Waste Isolation Feasibility Studies (1981)*. Bureau of Economic Geology.

Bates, R. G. 1975. "pH Scales for Sea Water." *The Nature of Seawater*, E. D. Goldberg, ed. Dahlem Workshop Report, Berlin, Abakon: Verlagsgesellschaft.

Bates, R. G., and C. H. Culberson. 1977. "Hydrogen Ions and the Thermodynamic State of Marine Systems." *The Fate of Fossil Fuel $CO_2$ in the Oceans*, N.R. Anderson and A. Malahoff, ed. New York: Plenum Publishing Company.

Bidoglio, G., G. Tanet, and A. Chatt. 1985. "Studies on Neptunium (V) Carbonate Complexes Under Geologic Repository Conditions." *Radiochimica Acta*, Vol. 38:21.

Bidoglio, G., G. Tanet, A. de Plano, and G. P. Lazzari. 1987. "Radionuclide Chemical Species Determination in Waste Management Studies." *Journal of Radioanalytical and Nuclear Chemistry* Articles, Vol. 110, No. 1:91-100.

Bopp, F. III, and R. B. Biggs. 1981. "Metals in Estuarine Sediments: Factor Analysis and its Environmental Significance." *Science*, Vol. 214:441-443.

Braitsch, O. 1971. *Salt Deposits: Their Origin and Composition.* New York: Springer-Verlag.

Collins, A. G. 1975. *Geochemistry of Oil Field Waters.* New York: Elsevier Scientific Publishing Company.

Colton, I. D. and J. G. Morse. 1985. *Water Quality Sampling Plan.* WIPP-DOE-215. Carlsbad, NM: Waste Isolation Pilot Plant Project Office.

Davis, J. C. 1973. *Statistics and Data Analysis in Geology.* New York: John Wiley and Sons, Inc.

Drever, J. I. 1982. *The Geochemistry of Natural Waters.* Englewood Cliffs, NJ: Prentice-Hall, Inc.

Goldberg, S., and R. A. Glaubig. 1986. "Boron Adsorption and Silicon Release by the Clay Minerals Kaolinite, Montmorillonite, and Illite." *Soil Science Society of America Journal*, Vol. 50:1442-1448.

Golden Software, Inc. 1987. *Surfer Version 3.00, Reference Manual.* Golden, CO: Golden Software, Inc.

Gonzalez, D. D. 1983. *Groundwater Flow in the Rustler Formation, Waste Isolation Pilot Plant (WIPP), Southeast New Mexico (SENM).* SAND82-1012. Albuquerque, NM: Sandia National Laboratories.

Gould, S. J. 1981. *The Mismeasure of Man.* New York: W.W. Norton & Company.

Harder, H. 1961. "Einbau von Bor in detritische Tonminerale. Experimente zur Erklarung des Borgehaltes toniger Sediments." *Geochimica et Cosmochimica Acta*, Vol. 21:284-294.

Harriss, R. C. 1969. "Boron Regulation in the Oceans." *Nature*, Vol. 223:290-291.

Harvie, C. E., N. Mϕller, and J. H. Weare. 1984. "The Prediction of Mineral Solubilities in Natural Waters: The Na-K-Mg-Ca-H-Cl-$SO_4$-OH-$HCO_3$-$CO_3$-$CO_2$-$H_2O$ System to High Ionic Strengths at 25°C." *Geochimica et Cosmochimica Acta*, Vol. 48:723-751.

Harvie, C. E., and J. H., Weare. 1980. "The Prediction of Mineral Solubilities in Natural Waters: The Na-K-Mg-Ca-Cl-$SO_4$-$H_2O$ System from Zero to High Concentration at 25°C." *Geochimica et Cosmochimica Acta*, Vol. 44:981-997.

Hem, J. D. 1985. *Study and Interpretation of the Chemical Characteristics of Natural Water.* Water-Supply Paper 2254, Third Edition. Denver, CO: US Geological Survey.

Hitchon, B., G. K. Billings, and J. E. Klovan. 1971. "Geochemistry and Origin of Formation Waters in the Western Canada Sedimentary Basin: III. Factors Controlling Chemical Composition." *Geochimica et Cosmochimica Acta*, Vol. 35:567-598.

Holser, W. T. 1979. "Marine Minerals Chapter 9: Trace Elements and Isotopes in Evaporites" *Mineralogical Society of America Short Course Notes.* R. G. Burns, ed. Vol. 6:295-346. Washington, DC: Mineralogical Society of America.

Jones, B. F., and A. H. Weir. 1983. "Clay Minerals of Lake Albert, An Alkaline, Saline Lake." *Clays and Clay Minerals*, Vol. 31, No. 3:161-172.

Klovan, J. E. 1975. "R- and Q-Mode Factor Analysis." *Concepts in Geostatistics.* McCammon, R., ed. New York: Springer-Verlag.

Lambert, S. J., and K. L., Robinson. 1984. *Field Geochemical Studies of Groundwaters in Nash Draw, Southeastern New Mexico*. SAND83-1122. Albuquerque, NM: Sandia National Laboratories.

Lambert, S. J. 1987. *Feasibility Study: Applicability of Geochronologic Methods Involving Radiocarbon and Other Nuclides to the Groundwater Hydrology of the Rustler Formation, Southeastern New Mexico*. SAND86-1054. Albuquerque, NM: Sandia National Laboratories.

Lappin, A. R. 1988. *Summary of Site-Characterization Studies Conducted From 1983 Through 1987 at the Waste Isolation Pilot Plant (WIPP) Site, Southeastern New Mexico*. SAND88-0157. Albuquerque, NM: Sandia National Laboratories.

Lyon, M. L. 1989. *Annual Water Quality Data Report for the Waste Isolation Pilot Plant*. DOE/WIPP 89-001.

Meijer, A. J., J. L. Lolcama, and F. J. Pearson. 1987. "Appendix E: Consistency of Densities and Chemical Compositions of Water Samples from the Culebra Dolomite." *Modeling of Ground-Water Flow in the Culebra Dolomite at the Waste Isolation Pilot Plant (WIPP) Site: Interim Report*, A. Haug, V. A. Kelly, A. M. LaVenue, and J. F. Pickens, ed. SAND86-7167. Albuquerque, NM: Sandia National Laboratories.

Mercer, J. W. 1983. *Geohydrology of the Proposed Waste Isolation Pilot Plant Site, Los Medaños Area, Southeastern New Mexico*. Water Resources Investigation Report 83-4016. Albuquerque, NM: US Geological Survey.

Mercer, J. W., and B. R. Orr. 1979. *Interim Data Report on the Geohydrology of the Proposed Waste Isolation Pilot Plant Site, Southeast New Mexico*. Water Resources Investigation Report 79-98. Albuquerque, NM: US Geological Survey.

Møller, N., J. H. Weare, and J. Greenberg. 1985. "Prediction of Mineral Solubilities and Diagenesis in Rock/Water Association at High Temperature." *Proceedings of the Conference on the Application of Geochemical Models to High-Level Nuclear Waste Repository Assessment*, G. K. Jacobs and S. K. Whatley, ed. NUREG/CP-0062, ORNL/TM-9585. Oak Ridge, TN: Oak Ridge National Laboratory.

Nie, N. H., C. H. Hull, J. G. Jenkins, K. Steinbrenner, and D. H. Bent. 1975. *SPSS: Statistical Package for the Social Sciences*. 2nd ed. New York: McGraw-Hill, Inc.

Parkhurst, D. L., D. C. Thorstenson, and L. N. Plummer. 1980. *PHREEQE - A Computer Program for Geochemical Calculations*. Water Resources Investigation Report 80-96. Reston, VA: US Geological Survey.

Parkhurst, D. L., L. N. Plummer, and D. C. Thorstenson. 1982. *BALANCE - A Computer Program for Calculation of Chemical Mass Balance*. Water Resources Investigation Report 82-14, NTIS Technical Report PB-82-255902. Reston, VA: US Geological Survey.

Pearson, F. J. Jr., D. W. Fisher, and L. N. Plummer. 1978. "Correction of Ground-Water Chemistry and Carbon Isotope Composition for Effects of $CO_2$ Outgassing." *Geochimica et Cosmochimica Acta*, Vol. 42:1799-1807.

Phillips, S. L., C. A. Phillips, and J. Skeen. 1985. *Hydrolysis, Formation and Ionization Constants at 25°C, and at High Temperature-High Ionic Strength*. LBL-14996. Berkeley, CA: Lawrence Berkeley Laboratory Report.

Phillips, S. L., F. V. Hale, L. F. Silvester, and M. D. Siegel. 1988. *Thermodynamic Tables for Nuclear Waste Isolation, Aqueous Solutions Database*. US Nuclear Regulatory Commision Report. NUREG/CR-4864 Vol. 1 (also LBL-22860 and SAND87-0323).

Pitzer, K. S. 1973. "Thermodynamics of Electrolytes. 1. Theoretical Basis and General Equations." *Journal Physical Chemistry*, Vol. 77:268-277.

Pitzer, K. S. 1975. "Thermodynamics of Electrolytes. 5. Effects of Higher-Order Electrostatic Terms." *Journal Solution Chemistry*, Vol. 4:249-265.

Pitzer, K. S., and J. J. Kim. 1974. "Thermodynamics of Electrolytes. 4. Activity and Osmotic Coefficients for Mixed Electrolytes." *Journal American Chemical Society*, Vol. 96:5701-5707.

Pitzer, K. S., and G. Mayorga. 1973. "Thermodynamics of Electrolytes. 2. Activity and Osmotic Coefficients for Strong Electrolytes with One or Both Ions Univalent." *Journal Physical Chemistry*, Vol. 77:2300-2308.

Pitzer, K. S., and G. Mayorga. 1974. "Thermodynamics of Electrolytes. 3. Activity and Osmotic Coefficients of 2-2 Electrolytes." *Journal Solution Chemistry*, Vol. 3:539-546.

Plummer, L. N., and E. T. Sundquist. 1982. "Total Individual Ion Activity Coefficients of Calcium and Carbonate in Seawater at 25°C and 35% Salinity, and Implications to the Agreement between Apparent and Thermodynamic Constants of Calcite and Aragonite." *Geochimica et Cosmochimica Acta*, Vol. 46:247-258.

Plummer, L. N. 1984. "Geochemical Modeling: A Comparison of Forward and Inverse Methods." *Proceedings First Canadian/American Conference on Hydrogeology*. B. Hitchon and E. I. Wallick, ed. Worthington, OH: National Water Well Association.

Plummer, L. N., and D. L. Parkhurst. 1985. "PHREEQE: Status and Applications" *Proceedings of the Conference on the Application of Geochemical Models to High-Level Nuclear Waste Repository Assessment*, G. K. Jacobs and S. K. Whatley, ed. Oak Ridge National Laboratory, NUREG/CP-0062, ORNL/TM-9585.

Plummer, L. N., D. L. Parkhurst, G. W. Fleming, and S. A. Dunkle. 1988. *PHRQPITZ - A Computer Program for Geochemical Calculations in Brines*. Water Resources Investigation Report 88-4153. Reston, VA: US Geological Survey.

Popielak, R. S., R. L. Beauheim, S. R. Black, W. E. Coons, C. T. Ellingson, and R. L. Olsen. 1983. *Brine Reservoirs in the Castile Formation, Waste Isolation Pilot Plant (WIPP) Project, Southeastern New Mexico*. Waste Isolation Pilot Plant Report TME 3153. Albuquerque, NM: US Department of Energy.

Ramey, D. S. 1985. *Chemistry of Rustler Fluids*. EEG-31. New Mexico Environmental Evaluation Group.

Randall, W. S., M. E. Crawley, and M. L. Lyon. 1988. *Annual Water Quality Data Report for the Waste Isolation Pilot Plant*. DOE-WIPP 88-006. Carlsbad, NM: Waste Isolation Pilot Plant Project Office.

Reeder, R. J. 1981. "Electron Optical Investigation of Sedimentary Dolomites." *Contributions to Mineralogy or Petrology*, Vol. 76:148-157.

Reeder, R. J., and H. R. Wenk. 1979. "Microstructures in Low Temperature Dolomites." *Geophysical Research Letters*, Vol. 6:77-80.

Robinson, K. L. 1988. *Analysis of Solutes in Groundwaters from the Rustler Formation at and near the WIPP Site*. SAND86-0917. Albuquerque, NM: Sandia National Laboratories.

Saulnier, G. J. Jr., G. A. Freeze, and W. A. Stensrud. 1987. *WIPP Hydrology Program, Waste Isolation Pilot Plant, Southeastern New Mexico, Hydrologic Data Report #4*. SAND86-7166. Albuquerque, NM: Sandia National Laboratories.

Schultz, L. G. 1969. "Lithium and Potassium Absorption, Dehydroxylation Temperature, and Structural Water Content of Aluminous Smectites." *Clays and Clay Minerals*, Vol. 17:115-149.

Seyfried, W. E., Jr., D. R. Janecky, and M. L. Mottl. 1984. "Alteration of the Oceanic Crust: Implications for Geochemical Cycles of Lithium and Boron." *Geochimica et Cosmochimica Acta*, Vol. 48:557-569.

Seyhan, E., A. A. van de Griend, and G. B. Engelen. 1985. "Multivariate Analysis and Interpretation of the Hydrogeochemistry of a Dolomite Reef Aquifer, Northern Italy." *Water Resources Research*, Vol. 21, No. 7:1010-1024.

Smith, C. L. 1976. "Use of Lithium and Chloride Concentrations in Ground Water for Lithium Exploration." *Lithium Resources and Requirements by the Year 2000*, J.D. Vine, ed. Professional Paper 1005. Washington, DC: US Geological Survey.

Smith, G. I. 1976. "Origin of Lithium and Other Components in the Searles Lake Evaporites, California." *Lithium Resources and Requirements by the Year 2000*, J. D. Vine, ed. Professional Paper 1005. Washington, DC: US Geological Survey.

Sonnenfeld, P. 1984. *Brines and Evaporites*. New York: Academic Press, Inc.

Spencer, R. J., H. P. Eugster, and B. F. Jones. 1985. "Geochemistry of Great Salt Lake, Utah II: Pleistocene-Holocene Evolution." *Geochimica et Cosmochimica Acta*, Vol. 49:739-747.

Statistical Analysis System Institute. 1982. *SAS User's Guide: Statistics*.

Stein, C. L., and J. L. Krumhansl. 1986. *Chemistry of Brines in Salt from the Waste Isolation Pilot Plant (WIPP), Southeastern New Mexico: A Preliminary Investigation.* SAND85-0897. Albuquerque, NM: Sandia National Laboratories.

Stumm, W., and J. J. Morgan. 1981. *Aquatic Chemistry: An Introduction Emphasizing Chemical Equilibria in Natural Waters.* 2nd ed. New York: John Wiley and Sons.

Tien, P. L., M. D. Siegel, C. D. Updegraff, K. K. Wahi, and R. V. Guzowski. 1985. *Repository Site Data Report for Unsaturated Tuff, Yucca Mountain, Nevada.* SAND84-2668 (also NUREG/CR-4110). Albuquerque, NM: Sandia National Laboratories.

Truesdell, A. H., and B. F. Jones. 1974. "WATEQ: A Computer Program for Calculating Chemical Equilibria of Natural Waters." *US Geological Survey Journal of Research,* Vol. 2:233-248.

Uhland, D. W., and W. S. Randall. 1986. *Annual Water Quality Data Report.* DOE-WIPP-86-006. Carlsbad, NM: Waste Isolation Pilot Plant Project Office.

Uhland, D. W., W. S. Randall, and R. C. Carrasco. 1987. *Annual Water Quality Data Report, March, 1987.* DOE-WIPP-87-006. Carlsbad, NM: Waste Isolation Pilot Plant Project Office.

Wolery, T. J. 1983. *EQ3NR, A Computer Program for Geochemical Aqueous Speciation-Solubility Calculations: User's Guide and Documentation.* UCRL-53414. Livermore, CA: Lawrence Livermore National Laboratory.

Wolery, T. J., D. J. Isherwood, K. J. Jackson, J. M. Delany, and I. Puigdomenech. 1985. "EQ3/6: Status and Applications." *Proceedings of the Conference on the Application of Geochemical Models to High-Level Nuclear Waste Repository Assessment*, G. K. Jacobs and S. K. Whatley, ed. NUREG/CP-0062, ORNL/TM-9585. Oak Ridge, TN: Oak Ridge National Laboratory.

# APPENDIX 2A. MINERALS INCLUDED IN SATURATION INDEX CALCULATIONS WITH PHRQPITZ

As discussed in Section 2.3.4, the code PHRQPITZ (Plummer et al., 1988) was used to calculate saturation indices for many minerals found in evaporite environments. The minerals and their formulas are listed in Table 2A.1.

## Table 2A.1. Chemical Formulas of Minerals Included in Saturation-Index Calculations with PHRQPITZ

| Mineral (synonym) | Formula |
|---|---|
| Anhydrite | $CaSO_4$ |
| Aragonite | $CaCO_3$ |
| Arcanite | $K_2SO_4$ |
| Bischofite | $MgCl_2 \cdot 6H_2O$ |
| Bloedite | $Na_2Mg(SO_4)_2 \cdot 4H_2O$ |
| Brucite | $Mg(OH)_2$ |
| Burkeite | $Na_6CO_3(SO_4)_2$ |
| Calcite | $CaCO_3$ |
| Carnallite | $KMgCl_3 \cdot 6H_2O$ |
| Dolomite | $CaMg(CO_3)_2$ |
| Epsomite | $MgSO_4 \cdot 7H_2O$ |
| Gaylussite | $Na_2Ca(CO_3)_2 \cdot 5H_2O$ |
| Glaserite (Aphthitalite) | $K_3Na(SO_4)_2$ |
| Glauberite | $Na_2Ca(SO_4)_2$ |
| Gypsum | $CaSO_4 \cdot 2H_2O$ |
| Halite | $NaCl$ |
| Hexahydrite | $MgSO_4 \cdot 6H_2O$ |
| Kainite | $KMgClSO_4 \cdot 3H_2O$ |
| Kalicinite | $KHCO_3$ |
| Kieserite | $MgSO_4 \cdot H_2O$ |
| Leonhardtite (Starkeyite) | $MgSO_4 \cdot 4H_2O$ |
| Leonite | $K_2Mg(SO_4)_2 \cdot 4H_2O$ |
| Magnesite | $MgCO_3$ |
| Mirabilite | $Na_2SO_4 \cdot 10H_2O$ |
| Misenite | $K_2SO_4 \cdot 6KHSO_4$ |
| Nahcolite | $NaHCO_3$ |
| Natron | $Na_2CO_3 \cdot 10H_2O$ |
| Nesquehonite | $Mg(HCO_3)(OH) \cdot 2H_2O$ |
| Pentahydrite | $MgSO_4 \cdot 5H_2O$ |
| Pirssonite | $Na_2Ca(CO_3)_2 \cdot 2H_2O$ |

## Table 2A.1. Chemical Formulas of Minerals Included in Saturation-Index Calculations with PHRQPITZ (Continued)

| Mineral (synonym) | Formula |
|---|---|
| Polyhalite | $K_2Ca_2Mg(SO_4)_4 \cdot 2H_2O$ |
| Portlandite | $Ca(OH)_2$ |
| Schoenite (Picromerite) | $K_2Mg(SO_4)_2 \cdot 6H_2O$ |
| Sylvite | KCl |
| Syngenite | $K_2Ca(SO_4)_2 \cdot H_2O$ |
| Trona | $Na_3H(CO_3)_2 \cdot 2H_2O$ |

# APPENDIX 2B. USE OF PRINCIPAL COMPONENT ANALYSIS IN ANALYSIS OF HYDROCHEMICAL DATA: GENERAL PRINCIPLES

## 2B.1 Introduction

### 2B.1.1 Purpose and Background

This appendix will acquaint the reader with the basic concepts and vocabulary of principal component analysis (PCA). A detailed explanation of the mathematical principles that underly the technique is beyond the scope of this work. Similarly, a review of previous applications of PCA in geochemical studies is not included here. Excellent discussions of the theory and applications of PCA can be found in Davis (1973) and Klovan (1975). Applications of PCA in a study similar to the present one can be found in Hitchon et al. (1971). A number of other studies are reviewed by Drever (1982). An enlightening and entertaining explanation of the principles and history of PCA can be found in Gould (1981). The following discussion of the relationship between PCA and correlation coefficients is taken in part from that reference.

### 2B.1.2 Distinction Between Factor Analysis and Principal Component Analysis

The terms "factor" and "principal component" are often used interchangeably in the literature. There are important distinctions between classical PCA and classical factor analysis, however. In the present study, PCA was used exclusively.

In classical PCA, no assumption is made concerning the underlying structure of the data. The technique is primarily a mathematical method of transforming the original variables into another smaller set of variables. Classical factor analysis, on the other hand, requires

an *a priori* model for the underlying structure of the data set. Specifically, it is assumed that part of the variance of each variable is unique and not attributable to the influence of the factors (perhaps due to random error).

In most texts and publications, the strict definitions of factor analysis and PCA are not distinguished. The analysis presented below is a PCA; however, it is equivalent to analyses commonly referred to as "factor analysis" in the literature. In this report, the term "factor" is used interchangeably with the term "principal component" to improve readability and to save space in the data tables.

## 2B.2 Interelement Correlations

PCA is a mathematical method to find the basic structure underlying a large number of bivariate correlations. Understanding the significance of correlations among the concentrations of groundwater solutes is a prerequisite to understanding applications of PCA to water chemistry data. In addition, many of the limitations and potential misuses of PCA can be more easily illustrated by examples from bivariate correlation analysis.

### 2B.2.1 Bivariate Correlations

If the concentrations of two elements in a suite of chemical analyses vary sympathetically, then the concentrations are said to be "correlated." If the concentrations of both elements increase or decrease in concert, then the elements are "positively correlated;" if the increase in the concentration of one element is accompanied by a decrease in another element, then the elements are "negatively correlated." If the values of the two sets of concentrations have been normalized by dividing by the variance of their respective sample distributions, then the strength of the correlation is expressed by "r," the Pearson's product coefficient (often called the correlation coefficient). The value of r ranges from +1 for perfect positive correlation to -1 for a perfect negative correlation; a value of 0 denotes no correlation. The equations used to calculate the covariance and the correlation coefficient

and the assumptions underlying their use can be found in many standard statistics texts (such as Davis, 1973) and will not be presented here.

The fact that two variables are strongly correlated cannot be used to prove that a causal relationship exists between them. Gould (1981) provides a good discussion of the potential pitfalls of overinterpreting the significance of strong correlations. He notes that although some moderate correlations do have an underlying cause (e.g., the correlation between arm length and leg length in children), other strong correlations have no causal connection (e.g., the author's age and the price of gasoline during the 1970's). Similarly, the existence of a correlation between the concentrations of two elements alone does not prove the existence of a particular chemical process relating the elements. The techniques of correlation and PCA must be used in conjunction with other methods, such as thermodynamic or hydrologic modeling. This combination of techniques can be used to suggest alternative models for the chemical processes that have produced an observed groundwater composition.

### 2B.2.2 Examples of Bivariate Correlations Between Concentrations

Meaningful interpretation of observed interelement correlations requires an understanding of the types of chemical processes that are likely to occur in the groundwater system. Examples of correlations that may be produced by different kinds of chemical processes are given below.

1. A positive correlation could reflect a common source for two solutes.

$$CaSO_4 \rightarrow Ca^{2+} + SO_4^{2-} \qquad \text{(B1)}$$

Equation B1 describes the dissolution of anhydrite. The concentrations of calcium and sulfate would be positively correlated in a groundwater that is dissolving anhydrite, if there are no other significant sources of these two elements and if the

water is undersaturated with respect to other minerals containing $Ca^{2+}$ and $SO_4^{2-}$ (e.g., gypsum).

A related example involves substitution of a trace metal (such as strontium) for calcium in the anhydrite. The concentration of the trace metal would be positively correlated with those of calcium and sulfate in waters in which the anhydrite was dissolving.

2. A negative correlation could be due to mineral saturation and a common ion effect.

$$Ca^{2+} + SO_4^{2-} + 2H_2O \leftrightarrow CaSO_4 \cdot 2H_2O \qquad \text{(B2)}$$

$$K_{sp}^{gyp} = a_{Ca^{2+}} \cdot a_{SO_4^{2-}} \cdot a_{H_2O}^2 \qquad \text{(B3)}$$

Equation B2 describes the dissolution/precipitation of gypsum. If a groundwater is in equilibrium with gypsum, then the concentrations of calcium and sulfate will be related via the solubility product of gypsum, defined in Equation B3. If the concentration of one ion increases due to contributions from another source, then the concentration of the other ion will decrease (common ion effect), resulting in a negative correlation between the calcium and the sulfate.

3. Correlations can result from coupled chemical reactions.

$$CaMg(CO_3)_2 + 2H_2O + 2CO_2 \rightarrow Ca^{2+} + Mg^{2+} + 4HCO_3^- \qquad \text{(B4)}$$

$$CaSO_4 \cdot 2H_2O \rightarrow Ca^{2+} + SO_4^{2-} + 2H_2O \qquad \text{(B5)}$$

$$Ca^{2+} + HCO_3^- \rightarrow CaCO_3 + H^+ \qquad \text{(B6)}$$

Equations B4 through B6 represent a set of chemical reactions that occur during dedolomitization of carbonate aquifers (Back et al., 1983). In the rock, the net result of these reactions is the dissolution of dolomite and gypsum and the precipitation of calcite. In the groundwater, the net result is the decrease of pH and the increase in the concentrations of magnesium and sulfate as the reactions proceed. Thus, in a system in which dedolomitization is occurring along the hydrologic flow path, a negative correlation between pH and sulfate and magnesium could be observed.

# 2B.3 Principal Component Analysis

## 2B.3.1 Correlations Among Many Variables and the Goal of Principal Component Analysis

When relationships among many variables are important, a matrix of correlations between all possible pairs of variables can be constructed. Table 2B-1 is a correlation matrix for six major solutes in groundwaters at the WIPP Site. The matrix lists correlation coefficients describing the correlation between the elements identified in the corresponding row and column. PCA can be used to describe the information given by the bivariate correlations in the correlation matrix in terms of a smaller number of variables called principal components or factors.

The techniques and meaning of PCA can be understood more easily by using a geometric representation of correlation matrices as presented by Gould (1981). The set of variables in the correlation matrix is represented by a set of unit vectors radiating from a common origin. In six-dimensional space, the correlation coefficient between a pair of variables is equal to the cosine of the angle between their respective vectors. Thus, the vectors of two variables that are perfectly correlated coincide, and the cosine of the angle between them equals 1.00. The vectors of two variables that are completely uncorrelated are orthogonal, and the cosine of the angle between them equals zero. In Figure 2B-1, each variable in Table 2B-1 is represented by a unit vector. In this two-dimensional figure, the

**Table 2B-1. Correlation Matrix for Major-Solute Data[1] in Culebra Groundwaters**

| Variable | Ca | Mg | K | Na | Cl | $SO_4$ |
|---|---|---|---|---|---|---|
| Ca | 1.000 | 0.492 | 0.414 | 0.568 | 0.606 | 0.043 |
| Mg | 0.492 | 1.000 | 0.906 | 0.907 | 0.893 | 0.836 |
| K | 0.414 | 0.906 | 1.000 | 0.946 | 0.930 | 0.847 |
| Na | 0.568 | 0.907 | 0.946 | 1.000 | 0.994 | 0.810 |
| Cl | 0.606 | 0.893 | 0.930 | 0.994 | 1.000 | 0.760 |
| $SO_4$ | 0.043 | 0.836 | 0.847 | 0.810 | 0.760 | 1.000 |

1. The data are the common logarithms of the solute concentrations in mg/L.

angles are distorted from their true values. The figure shows principal components (factors) for a hypothetical unrotated R-mode analysis. The first principal component (or factor, labelled I) lies as close as possible to the largest number of vectors; the second principal component (or factor, labelled II) is orthogonal to the first.

In Figure 2B-1, five of the six variables are highly correlated and their vectors lie within a tight cluster. The extraction of the first principal component from the correlation matrix involves finding an axis that can be used as a grand average of all six vectors. This is equivalent to accounting for as much of the variance of the data set as possible with a single axis. The amount of variance of each variable that a principal component describes (or resolves) is represented by the length of the projection of the variable's vector onto the principal component axis (see Figure 2B-2). This resolving power is called the "loading" of the variable onto the factor and is listed in the factor-loading matrix. The amount of variance of variable A resolved or "explained" by the principal component (or factor, labelled I) is equal to the ratio of the length of OA', the projection of OA onto the axis I, to the length of vector OA. In Figure 2B-2, vector OA lies close to the principal component and has a high loading onto the axis. In contrast, vector OB lies far from the principal component axis I. The principal component I explains little of the variance of variable B, and the loading of this variable onto the principal component is low.

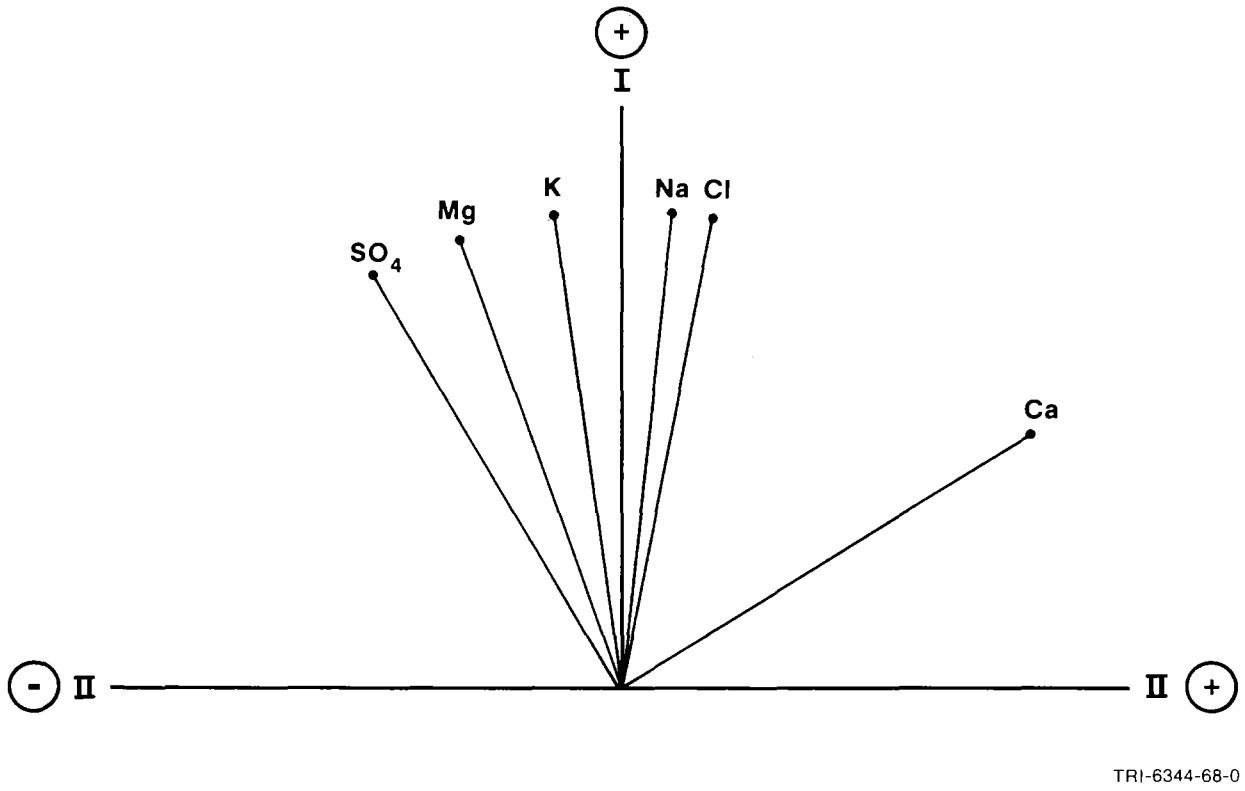


Figure 2B-1. Qualitative geometric representation of correlations among major solute concentrations for Culebra waters samples.

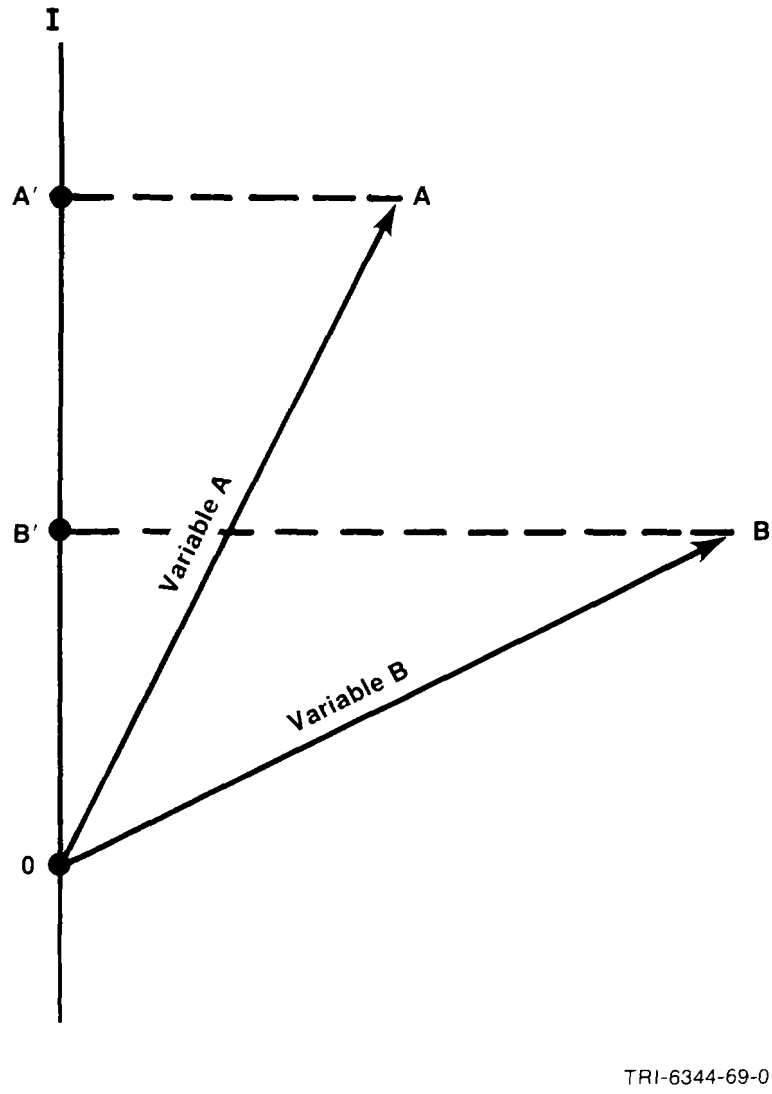


Figure 2B-2. Geometric representation of principal component (factor) loadings.

Mathematically, the principal components are obtained by extracting the eigenvectors of the correlation matrix. The necessary techniques can be found in many texts on linear algebra and will not be described here. In this example, the first principal component for the matrix in Table 2B-1 is shown in Figure 2B-1 and accounts for most of the variance of all the variables. A second principal component is located to account for as much of the remaining variance as possible. In most applications of PCA, all principal components are orthogonal to each other. Each succeeding principal component accounts for smaller and smaller amounts of the variance until either all of the variance in the data set has been accounted for or a predetermined amount of variance is resolved.

The communality, $h_i^2$, for the $i^{th}$ variable (or $i^{th}$ sample) is defined as the amount of variance of the $i^{th}$ variable (or sample) that is accounted for by a set of principal components. It is calculated as:

$$h_i^2 = \sum_j F_{ij}^2$$

where $F_{ij}$ is the loading of the $i^{th}$ normalized variable (or sample) onto the $j^{th}$ principal component.

The fraction of the variance of the $i^{th}$ normalized variable (or sample) explained by the $j^{th}$ principal component is $F_{ij}^2$ (the loading squared).

### 2B.3.2 Distinction Between R- and Q-Mode Principal Component Analysis

PCA can be used to express the relationships among a large number of variables in terms of correlations with a smaller number of underlying components, or to describe the characteristics of a sample suite by defining hypothetical end members of the population.

When the objective of the analysis is to find correlations among variables, R-mode analysis is employed. When the similarities among samples are examined, Q-mode analysis is used.

Figure 2B-1 was used to describe R-mode analysis; the unit vectors refer to individual variables (e.g., solute concentrations) and the cosines of the angles between the vectors equal the correlation coefficients. Figure 2B-3 provides the corresponding graphical representation for Q-mode analysis. Each vector in the figure corresponds to a different well water sample and the cosines of the angles between vectors are the similarity coefficients.

Q-mode analysis of the compositions of some Culebra water samples is described in Section 2.3.3.3. In the analysis, two principal components (factors) were sufficient to explain more than 99% of the total variance. The Q-mode factor-loading matrix is shown in Table 2-5 in Section 2.3.3.3. The two components can be thought of as "hypothetical entities that are completely dissimilar in terms of the proportions of their constituents" (Klovan, 1975, p. 51). Combinations of these components can be used to reconstruct the original water sample compositions. The "Factor A" and "Factor B" columns of Table 2-5 describe the similarity between a component and each sample. The rows of the table show the composition of each sample in terms of the components.

Q-mode analysis is used primarily to evaluate the statistical homogeneity of the sample population. If the data set is homogeneous, then it is amenable to R-mode analysis. A statistical criterion for recognizing homogeneity of a group of samples has not been developed for geological applications of PCA. In previous studies, if two or three Q-mode principal components accounted for most of the variance, then the population was considered homogeneous enough for R-mode analysis (see Hitchon et al., 1971; Klovan, 1975; Drever, 1982).

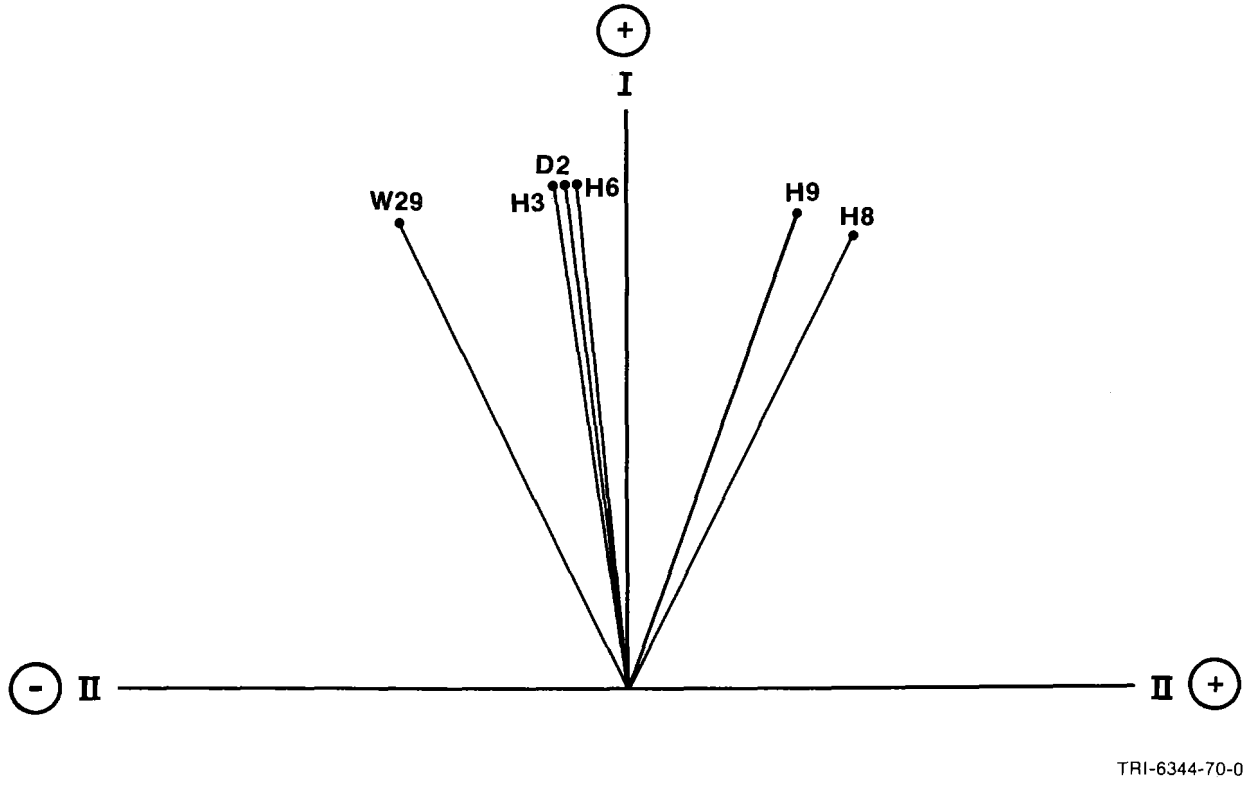


Figure 2B-3. Qualitative geometric representation of a similarity matrix for water sample compositions.

### 2B.3.3 Factor-Loading and Factor-Score Matrices

In R-mode analysis, the eigenvalues and eigenvectors of the correlation matrix are extracted; in Q-mode analysis, the similarity matrix (Klovan, 1975) is examined. The extraction of the eigenvectors in both R-mode and Q-mode analysis "decomposes" the original matrix into a "factor-loading matrix" and a "factor-score matrix:"

- The factor-loading matrix of a Q-mode analysis describes compositions of samples in terms of the Q-mode factors.

- The factor-loading matrix of an R-mode analysis describes the relations among the variables in terms of the R-mode factors.

Figure 2B-4 provides a graphical representation of the first two principal components (factors) of the correlation matrix shown in Table 2B-1 and the vectors shown in Figure 2B-1; it depicts the factor loadings. Factor loadings have values between +1 and -1 if they are expressed as fractions or between 100% and -100% if they are expressed as percents. In R-mode analysis, if the loadings of two variables have the same sign, the variables are positively correlated; if they have opposite signs, they are negatively correlated. If a sample has a high loading in a Q-mode factor-loading matrix, it is similar in composition to the factor. The absolute sign of any particular variable or sample in the factor-loading matrix is unimportant; only the relationships among the variables and samples provide useful information:

- The factor-score matrix from a Q-mode analysis describes the relations among the variables in terms of the Q-mode factors.

- The factor-score matrix from an R-mode analysis describes compositions of samples in terms of the R-mode factors.

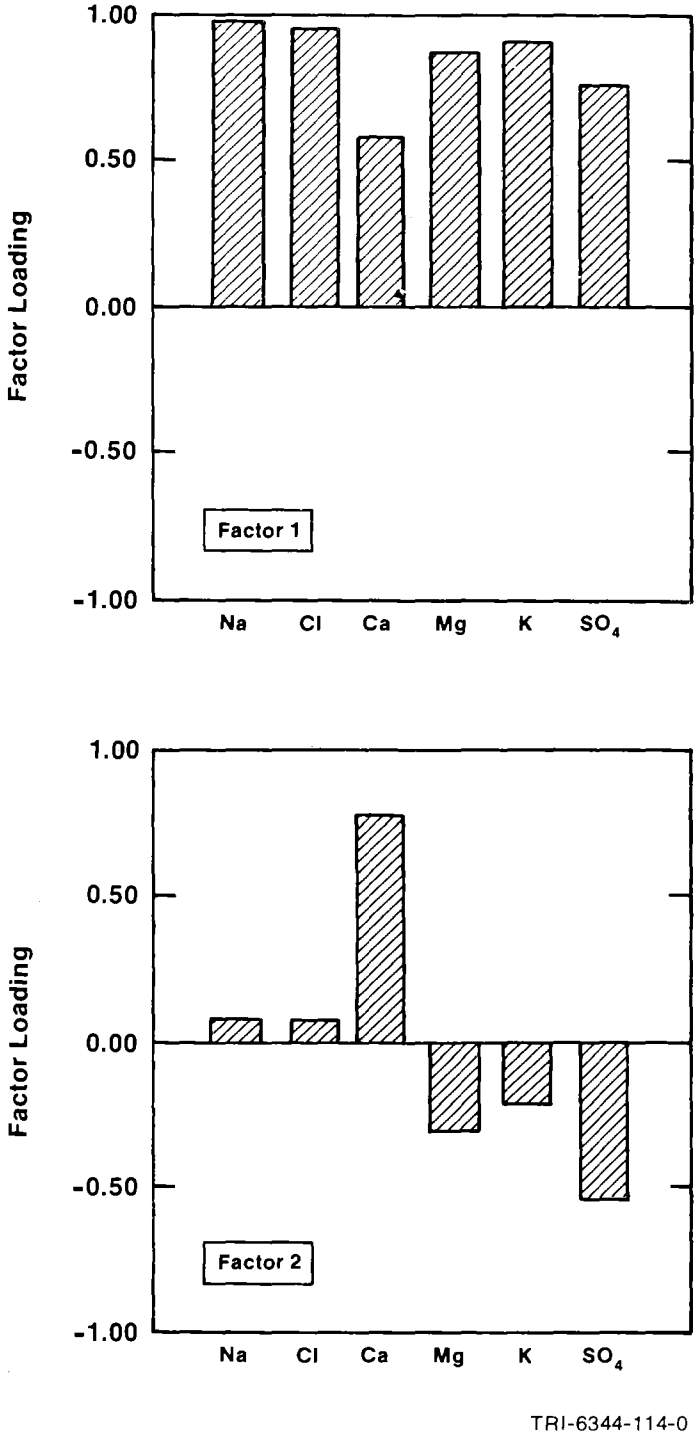


Figure 2B-4. Graphical representation of R-mode principal-component (factor) loadings.

The scales and absolute values of the factor-score matrix are not easily interpreted; the matrix should be examined in terms of the relative relationships between the samples or variables.

# 2B.4 Mathematical Options in PCA

## 2B.4.1 Data Pretreatment

Before the correlation or similarity matrix of the data set is calculated, the raw data may be transformed by arithmetic operations. Commonly used transformations include standardization (Davis, 1973), percent sample and percent range transformations, percent maximum value (Bopp and Biggs, 1981), and logarithmic transformations of raw or percent range/sample/maximum data (Seyhan et al., 1985).

The choice of the type of transformation often involves subjective judgment on the part of the analyst. For example, the solute concentrations could be represented as percents of the range of values or percents of the maximum value in order to prevent the variance of major elements from swamping the patterns of minor element variations.

A basic assumption of PCA is that the principal components are linearly related. A natural log or $\log_{10}$ transformation of water quality analyses may be appropriate since the total dissolved solid (TDS) concentrations of water samples often approximate log-normal distributions (Hitchon et al., 1971). Most of the uses of PCA in hydrochemical facies have factored the raw (untransformed) data; thus, transformation is not always necessary to obtain an interpretable set of principal components. In the present study, the $\log_{10}$ of the concentrations was used to calculate the correlation matrix.

### 2B.4.2 Partialling Out a Variable: PCA of Partial-Correlation Matrices

In some cases, many solutes may be strongly correlated with one or two major solutes, and the relationships among the other variables may be obscured by this effect. In this report, for example, nearly all variables were strongly correlated with the TDS and the sodium and chloride concentrations. To examine the relationships among the other solutes independent of this correlation, the principal components of the partial-correlation matrix with respect to TDS were extracted.

In this work, the effects of TDS were partialled out in the following way.

First, the linear regression equations were solved for each variable as a function of the TDS.

$$\log(Na) = a_1 + b_1 \log(TDS) + e_{Na} \quad \text{(B7a)}$$

$$\log(Ca) = a_2 + b_2 \log(TDS) + e_{Ca} \quad \text{(B7b)}$$

etc.

where $a_1$ and $b_1$ are the linear regression terms (intercept and slope), $e_x$ is an error term, and (x) is the concentration of solute x.

Next, the residuals from each of these equations were calculated:

$$res(Na)_i = \log (Na)_i - \log (\hat{Na})_i \quad \text{(B8a)}$$

$$res(Ca)_i = \log (Ca)_i - \log (\hat{Ca})_i \quad \text{(B8b)}$$

etc.

where i refers to the $i^{th}$ water sample and $(\hat{Na}_i)$, $(\hat{Ca}_i)$, etc., are the predicted values from the regression equations.

Then, the partial correlations with respect to TDS were calculated for all pairs of variables. The partial correlation between any two variables adjusted for the TDS is defined as the simple correlation of their residuals. For example, the partial correlation of Na and Ca adjusted for TDS is:

$$r_{Na,Ca.TDS} = \frac{\Sigma[\,res(Na_i) - \overline{res}(Na)][res(Ca_i) - \overline{res}(Ca)]}{\sqrt{\Sigma[res(Na_i) - \overline{res}(Na)]^2}\ \sqrt{\Sigma[res(Ca_i) - \overline{res}(Ca)]^2}} \qquad \text{(B9)}$$

where $\overline{res}(x)$ is the mean of the residuals for variable x.

The partial correlations with respect to TDS for all pairs of variables were calculated in this way.

Finally, these correlations were gathered into the partial-correlation matrix, and the eigenvectors for this matrix were extracted to obtain the principal components with the TDS partialled out.

The amount of variance of each variable that is explained by these factors can be calculated from $R^2$, the coefficient of determination for the regression equations (B7) above. $R^2$ is defined as the fraction of the variance of a variable explained by the regression expression. For example, the fraction of the variance of Na explained by the regression with TDS is the $R^2$ for Equation B7a. The percent of variance of Na that is not explained by correlation with TDS and that remains after the TDS is partialled out is equal to $1-R^2$ for Equation B7a. Thus, for each variable, $1-R^2$ is the total amount of variance that can be explained or resolved by the principal components extracted from the partial-correlation

matrix. The amount of variance that each of the principal components explains is calculated from the factor loadings as described above.

### 2B.4.3 Rotations

Extraction of the eigenvectors from the correlation or similarity matrix produces components that are constrained in two ways:

- The first principal component must account for the most variance, the second for the most of the remaining variance, and so on.

- The principal components must be orthogonal to one another.

Since the first component will represent a grand mean of all the correlations among variables, its orientation will be strongly influenced by the particular sample population. Therefore, the results of the PCA may not accurately reflect the true nature of the underlying independent components.

For example, in Figure 2B-1, the first principal component (factor) is drawn through the larger data cluster on the left. The loadings of all variables on the first factor are positive, whereas the loadings of some variables on the second factor are negative (Figure 2B-4). Both factors are important for Ca, Mg, K, and $SO_4$. Rotating the factors to coincide with clusters of samples, as shown in Figure 2B-5, "simplifies" the structure for these elements since only one factor is important for each variable. A graphical representation of the rotated factors is shown in Figure 2B-6. The effect of the rotation can be seen by comparing this figure with Figure 2B-4.

Several different rotational schemes exist; all attempt to "simplify" the structure or composition of the terminal (rotated) principal-component (factor) matrix. The rotation can be designed to simplify the complexity of the variables (quartimax rotation), the components (varimax rotation), or both (equimax rotation). In addition, rotations in which the principal

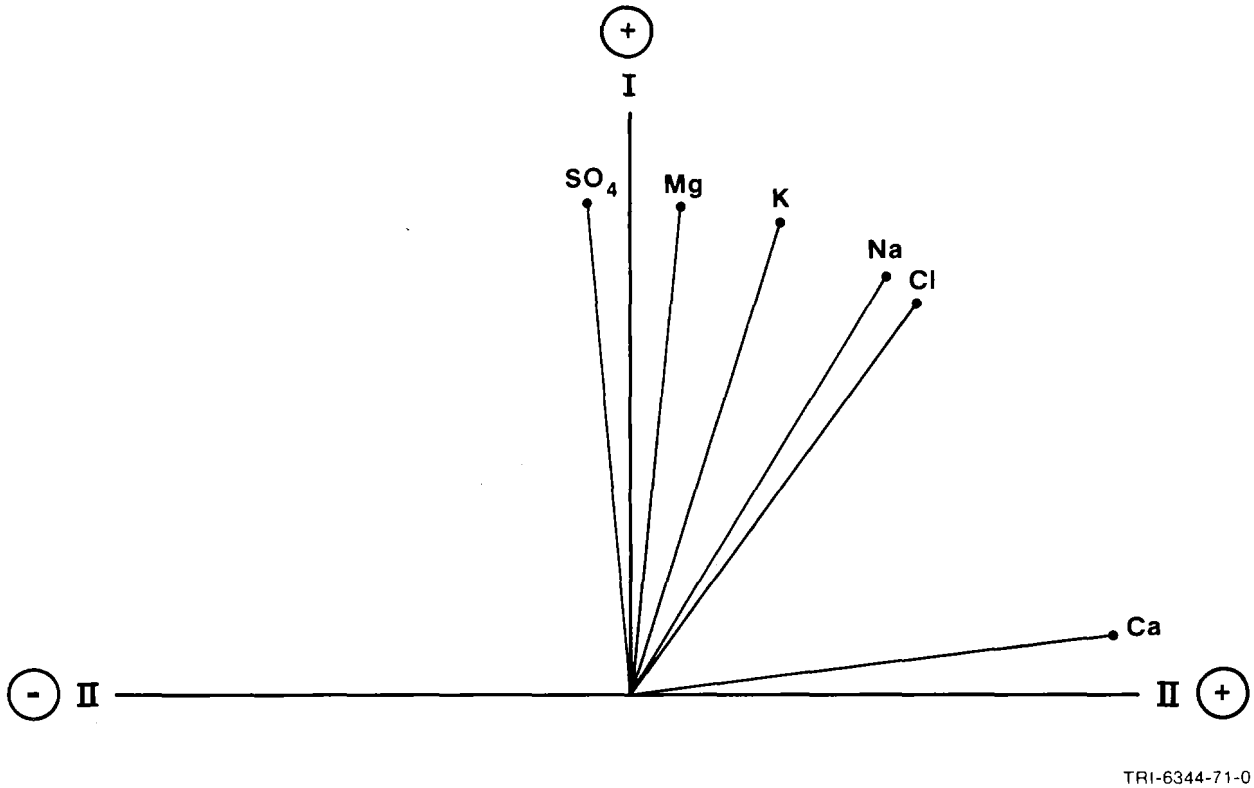


Figure 2B-5. Qualitative geometric representation of rotated principal components (factors).

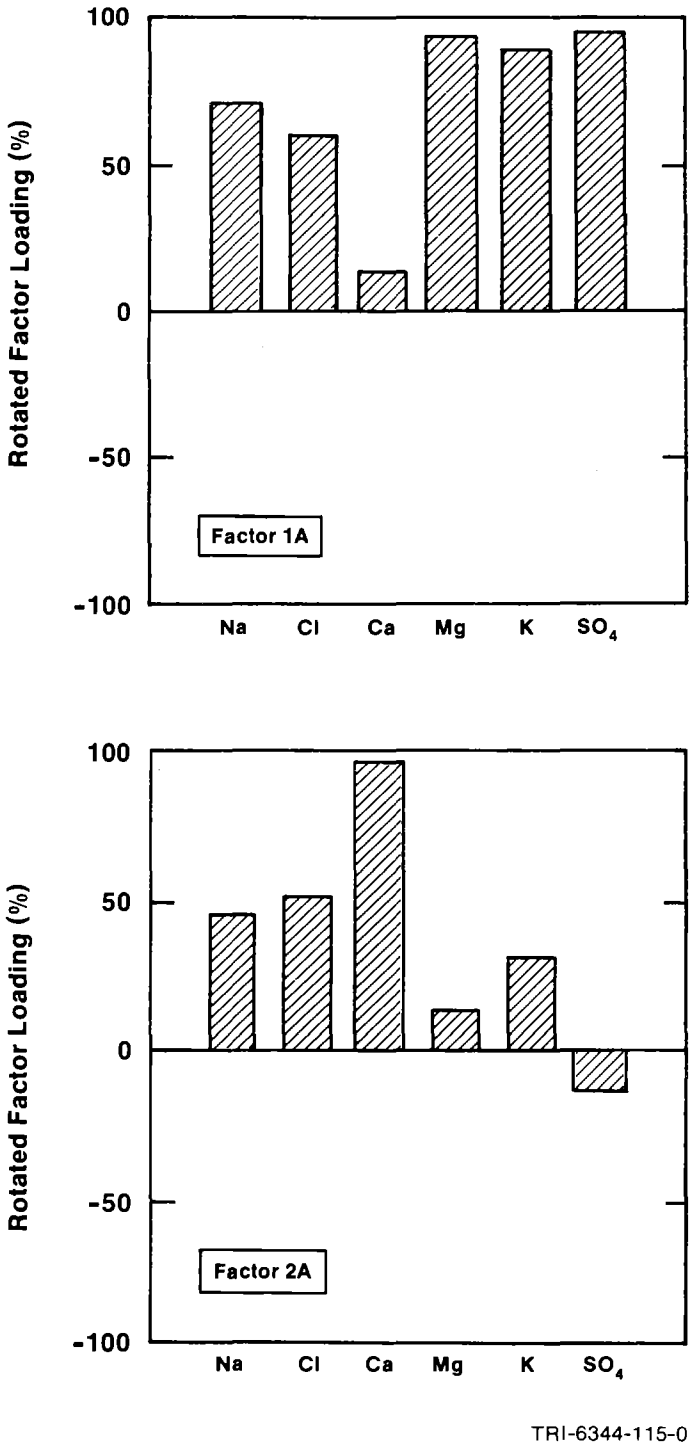


Figure 2B-6. Graphical representation of rotated R-mode principal-component (factor) loadings.

components (factors) are not constrained to be orthogonal (oblique transformations) are also used. Excellent descriptions of the mathematical criteria underlying the rotations used in this study can be found in Nie et al. (1975).

It cannot be said that any particular method of rotation is innately superior to another. All rotations are obtained from the same correlation matrix and therefore explain the same amount of variance. The insights provided by the different rotations are often complementary. In most cases, the choice of the "best" rotation will involve a great deal of subjectivity. PCA can only summarize the relationships among variables; the choice of rotational scheme must be based on the interpretability of the components and requires insight from other sources of information. In geochemical studies these other sources include thermodynamic constraints, geological data, and kinetic models.

# APPENDIX 2C. VARIMAX R-MODE PRINCIPAL COMPONENT ANALYSIS OF CULEBRA WATERS: SUPPLEMENTAL RESULTS

## 2C.1 Introduction

Section 2.3.3 of this chapter summarizes the principal component analysis (PCA) of a data set comprising the chemical compositions of water samples from the Culebra dolomite. An introduction to the methods and objectives of PCA is given in Appendix 2B. Several rotations of the R-mode principal components were examined to assess the robustness of the factor-loading matrix. As discussed in Section 2.3.3, all the matrices contained the same key solute correlations observed in the unrotated principal components. Because the varimax rotation is the rotation most commonly used in the earth sciences, a more detailed PCA was carried out for this rotation. The results of this analysis are described in this appendix.

The data set examined in this analysis is designated as "population 1;" samples are listed in Table 2-4 in Section 2.3.3.2, and the solute data are given in Table 2-2 in Section 2.2.2. Q-mode and R-mode analyses of the data prior to varimax rotation are described in Sections 2.3.3.3 and 2.3.3.4. The interpretation of the factors in terms of geochemical processes is found in Section 2.2.4.

In this appendix, Section 2CVM discusses the varimax R-mode analysis of population 1. Section 2.CV- discusses the varimax R-mode analysis after total dissolved solids (TDS) were partialled out.

# 2C.2 Varimax R-Mode Analysis

## 2C.2.1 Factor Loadings

Five factors accounted for more than 99% of the variance. The factor-loading matrix is shown in Table 2C-1 and the first three factors (1A, 2A, and 3A) are shown in Figure 2C-1. At least 92% of the variance of each chemical variable is explained by the first five factors (that is, the communality, $h_i^2$, was > 0.92 for each variable). The first three factors account for 90% of the total variance of the data set. Because the other factors (4A and 5A) account for less than 10% of the variance, they are not considered further.

Factor 1A

Factor 1A accounts for 51% of the total variance of population 1 and is dominated by the covariance of nearly all the major and minor elements. The association Na-Cl-Br-B-Li may be due to the dissolution of halite and other evaporite salts. The association of K with this assemblage may reflect dissolution of polyhalite associated with halite. The B and Li could also be desorbed from iron oxyhydroxide inclusions in the polyhalite. Factor 1A accounts for 85% of the variance in K, for approximately 70 to 75% of the variance in Na, Cl, and Li, and for approximately 50 to 55% of the variance in B and Br.

The only element that has a significant negative loading on factor 1A is silicon; this factor accounts for 42% of the variance of this element.

Factor 1A also explains 74% of the variance of Mg and 94% of the variance of sulfate. The strong correlation of magnesium and sulfate with the solutes attributed to dissolution of halite and other evaporite salts may reflect dissolution of polyhalite or the increase of gypsum and dolomite solubility with increasing ionic strength as discussed in Section 2.4.

**Table 2C-1. Varimax R-Mode Factor Loadings (Percent) for Culebra Groundwaters (Population 1)**

| Element | Factor 1A | Factor 2A | Factor 3A | Factor 4A | Factor 5A | Communality ($h_i^2$) |
|---|---|---|---|---|---|---|
| Na | 88 | 45 | - 6 | - 1 | 10 | 99.0 |
| Cl | 85 | 50 | - 2 | 0 | 9 | 98.1 |
| Ca | 14 | 97 | - 9 | - 2 | 4 | 97.9 |
| Mg | 86 | 36 | -11 | -29 | -11 | 98.0 |
| K | 92 | 30 | 5 | -10 | - 7 | 95.3 |
| Sr | 39 | 90 | -13 | -10 | 0 | 98.8 |
| pH | -22 | -11 | -49 | 83 | 3 | 99.3 |
| $HCO_3$ | -10 | -15 | 94 | -19 | - 4 | 95.9 |
| $SO_4$ | 97 | -12 | -18 | -10 | 4 | 99.1 |
| $SiO_2$ | -65 | -10 | 65 | -33 | - 1 | 97.1 |
| Br | 75 | 56 | -17 | - 2 | 14 | 92.3 |
| B | 72 | 20 | -45 | 17 | 45 | 98.5 |
| Li | 82 | 30 | -34 | -11 | 21 | 94.2 |

Amount and Percent of Variance Explained by Each Factor

| Factor 1A | Factor 2A | Factor 3A | Factor 4A | Factor 5A |
|---|---|---|---|---|
| 6.418 | 2.936 | 1.981 | 0.996 | 0.304 |
| 51% | 23% | 16% | 8% | 2% |

Factor 2A

Factor 2A accounts for 23% of the variance of population 1. It is qualitatively similar to factor 1A and includes a Na-Cl-Br association that may be indicative of halite dissolution. This factor accounts for only about 20 to 30% of the variance of these variables, however, and whereas factor 1A was dominated by Na and Cl, factor 2A is more strongly influenced by Br.

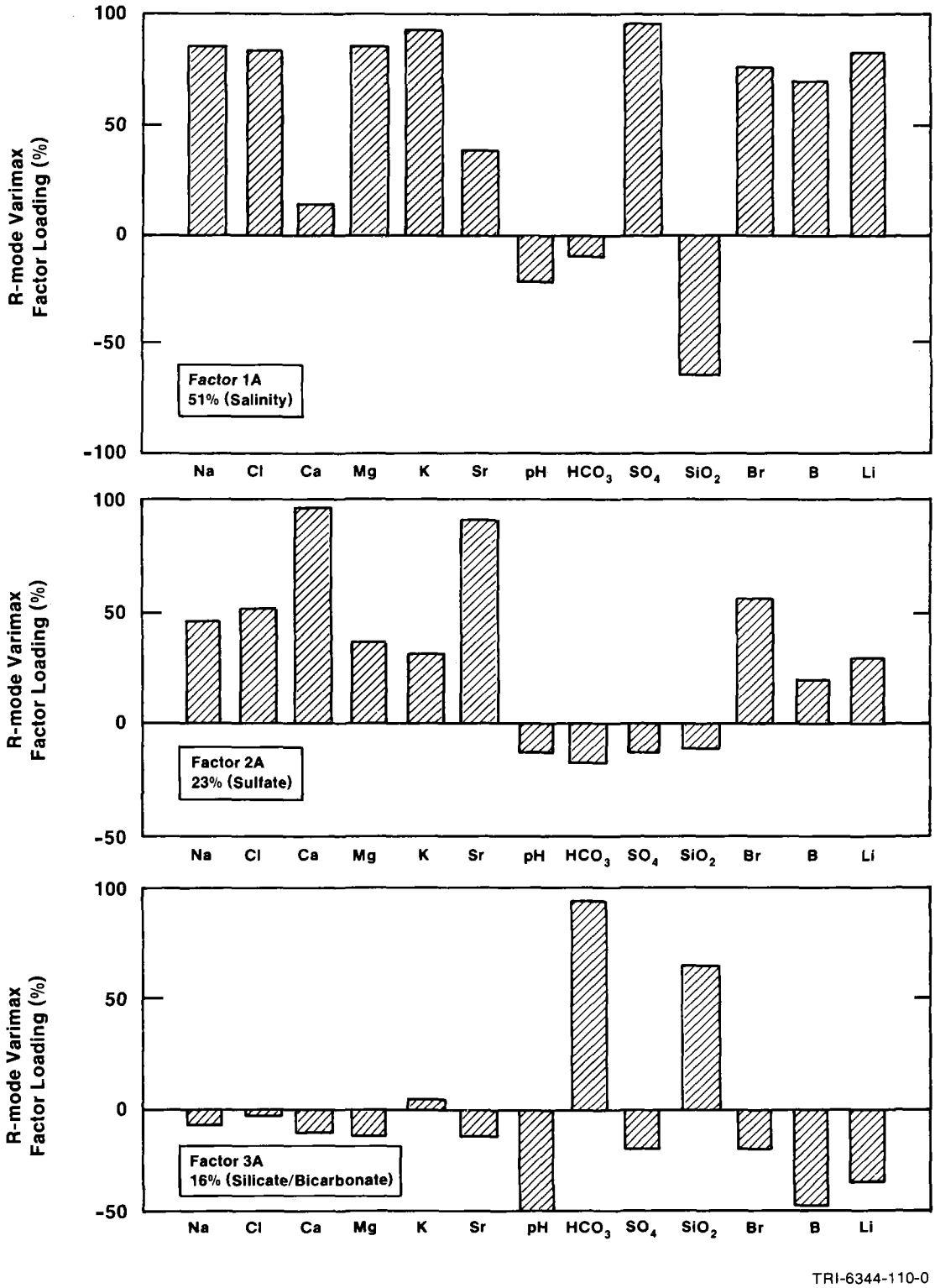


Figure 2C-1. Varimax R-mode factor loadings for factors 1A, 2A, and 3A of Culebra groundwaters (population 1).

Factor 2A is strongly influenced by the variance of Ca and Sr, accounting for 94% and 81% respectively of their variances. The negative correlations of these variables with both bicarbonate and sulfate are consistent with saturation with respect to both calcite and gypsum/anhydrite.

Factor 3A

Factor 3A accounts for approximately 16% of the total variance of population 1. It is dominated by the behavior of bicarbonate alkalinity, $SiO_2$, pH, B, and Li, and it accounts for 88%, 42%, 24%, 20%, and 12%, respectively, of their variances. It accounts for less than 5% of the variance of any of the other variables. The negative correlation between pH and alkalinity probably reflects carbonate equilibria. The relationship between Si, B, and Li may be related to ion exchange and silica diagenesis or desorption from clays as discussed in Section 2.4.

## 2C.2.2 Factor Scores

The compositions of the samples in terms of the three most important factors are described by the factor-score matrix, given in Table 2C-2. The scores are plotted in Figures 2C-2 through 2C-5 and are discussed in this section. Relationships between factor scores for the three most important factors are presented as bivariate plots in Figures 2C-2 and 2C-4. Spatial variation of the scores of factors 1A and 2A are plotted and contoured in Figures 2C-3 and 2C-5.

Factor 1A

Scores for factor 1A are lowest for samples from hydrochemical facies zone B and are highest for the sample from WIPP-29 (zone D) and for samples from zone A (Figure 2C-2). Factor 1A scores for samples from zone C are intermediate in value; within the zone, the scores are lowest for the P-14 sample and increase radially to the east, west, and north (Figure 2C-3).

## Table 2C-2. Varimax R-Mode Factor Scores[1] for Culebra Groundwaters (Population 1)

| Well | Coll. Date | Facies[2] | Factor 1A | Factor 2A | Factor 3A |
|---|---|---|---|---|---|
| DOE-1 | 4/85 | A | 0.59 | 0.22 | -1.33 |
| H-5C | 10/81 | A | 1.16 | 0.34 | -0.06 |
| H-5B | 8/85 | A | 0.84 | 0.23 | -1.20 |
| H-12 | 8/85 | A | 0.76 | 0.30 | -1.25 |
| P-17 | 3/86 | A | 0.61 | 0.32 | -0.73 |
| H-7B1 | 3/86 | B | -1.36 | -0.86 | 0.56 |
| H-8B | 1/86 | B | -1.62 | -1.39 | -0.68 |
| H-9B | 11/85 | B | -1.27 | -1.13 | -0.09 |
| ENGLE | 3/85 | B | -1.27 | -1.07 | -0.05 |
| DOE-2 | 3/85 | C | -0.12 | 0.91 | -0.48 |
| H-2A | 4/86 | C | -0.30 | -0.75 | -0.42 |
| H-3B3 | 2/85 | C | 0.09 | 0.39 | -0.88 |
| H-4B | 7/85 | C | 0.29 | -0.77 | -0.32 |
| H-6B | 9/85 | C | -0.03 | 0.86 | 0.16 |
| P-14 | 2/86 | C | -1.16 | 2.26 | 0.37 |
| WIPP-25 | 2/86 | C | -0.52 | 0.16 | 1.03 |
| WIPP-26 | 11/85 | C | -0.43 | 0.41 | 0.99 |
| WIPP-28 | 9/80 | C | 0.53 | -0.16 | 2.93 |
| WIPP-30 | 9/80 | C | 0.32 | -0.03 | -0.38 |
| WIPP-27 | 9/80 | D | 0.33 | 1.65 | 0.91 |
| WIPP-29 | 12/85 | D | 2.54 | -1.89 | 0.93 |

1. Factors 4A and 5A, which account for less than 10% of the total variance, are not given here or discussed in the text.
2. Hydrochemical facies in the Culebra, as defined in Section 2.3.2.1.

Factor 2A

The P-14 sample has the highest score for factor 2A; the WIPP-29 sample has the lowest score for this factor (Figure 2C-4). The hydrochemical facies zones are not clearly differentiated on the basis of this factor. Samples from zone A have factor scores of approximately 0.3 ± 0.1, whereas samples from zone B have values less than -0.8. Values for samples from zones C and D are quite variable, and no spatial pattern is evident (Figure 2C-5).

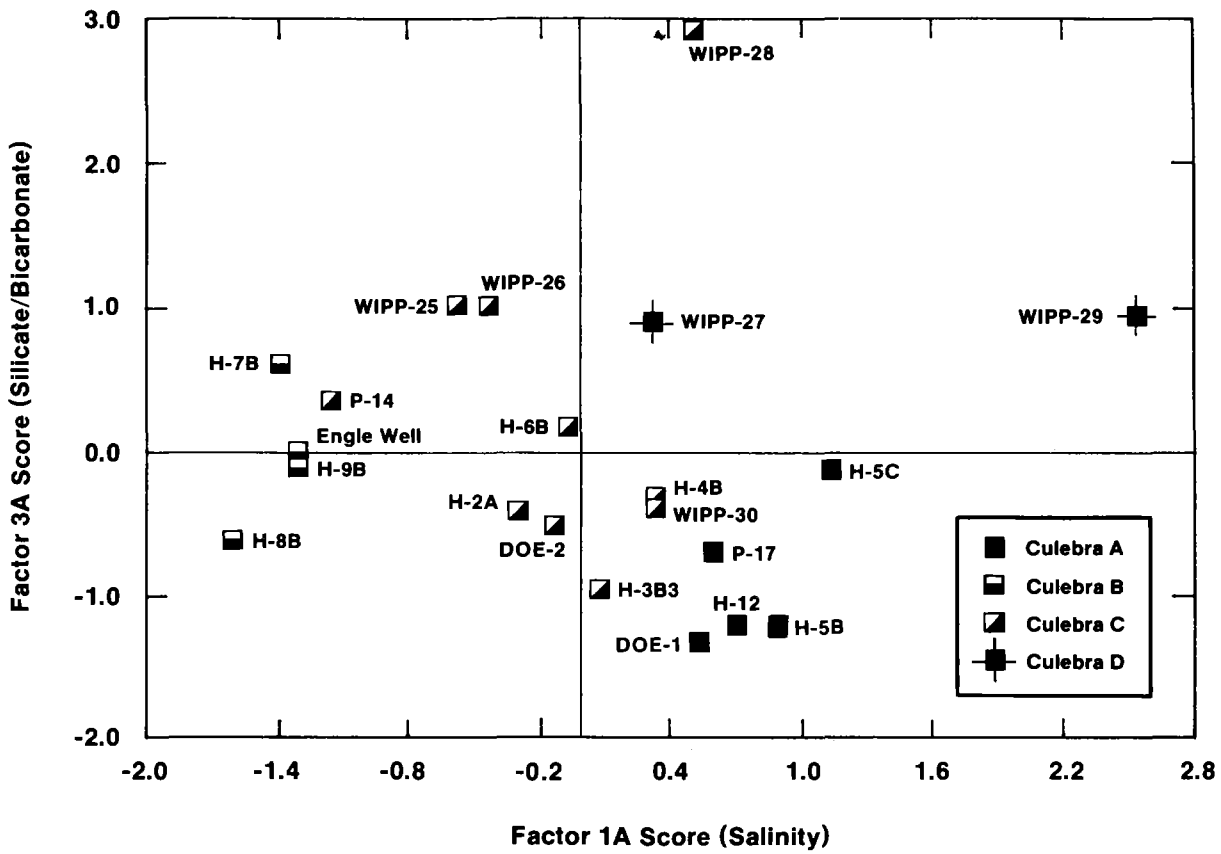


Figure 2C-2. Relationship between varimax R-mode factor scores for factors 1A and 3A of Culebra groundwaters (population 1).

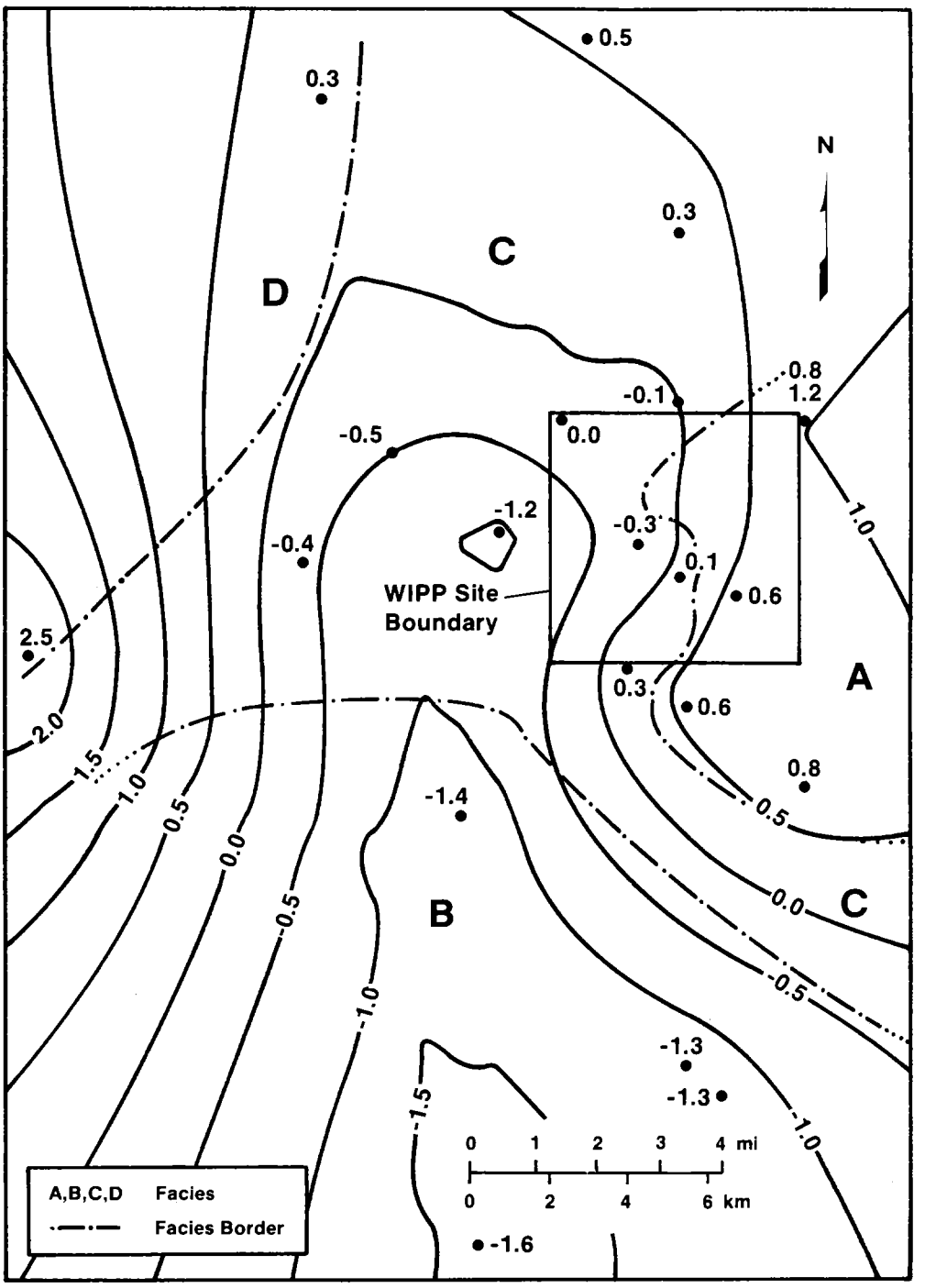


TRI-6341-44-0

Figure 2C-3. Contours of varimax R-mode factor scores for factor 1A of Culebra groundwaters (population 1).

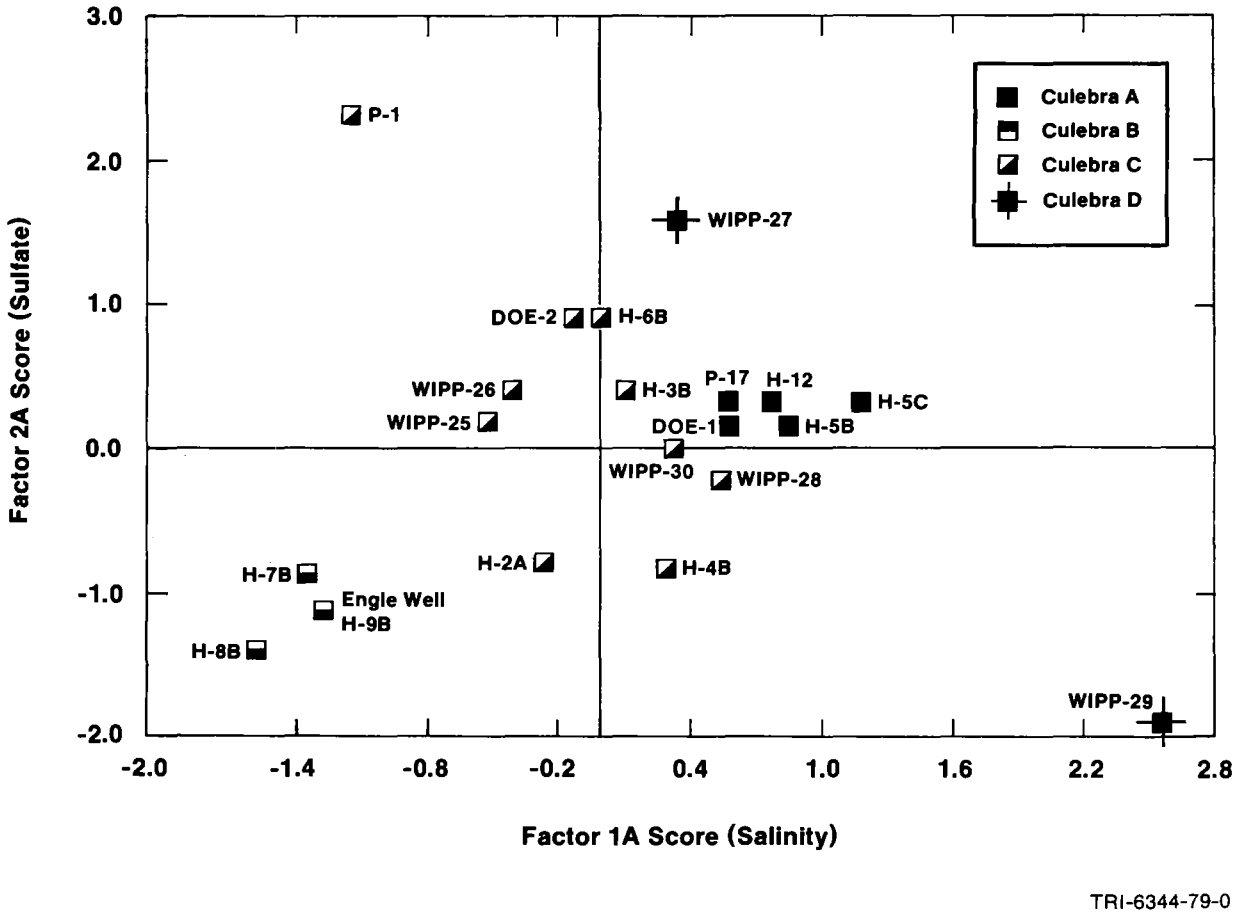


Figure 2C-4. Relationship between varimax R-mode factor scores for factors 1A and 2A of Culebra groundwaters (population 1).

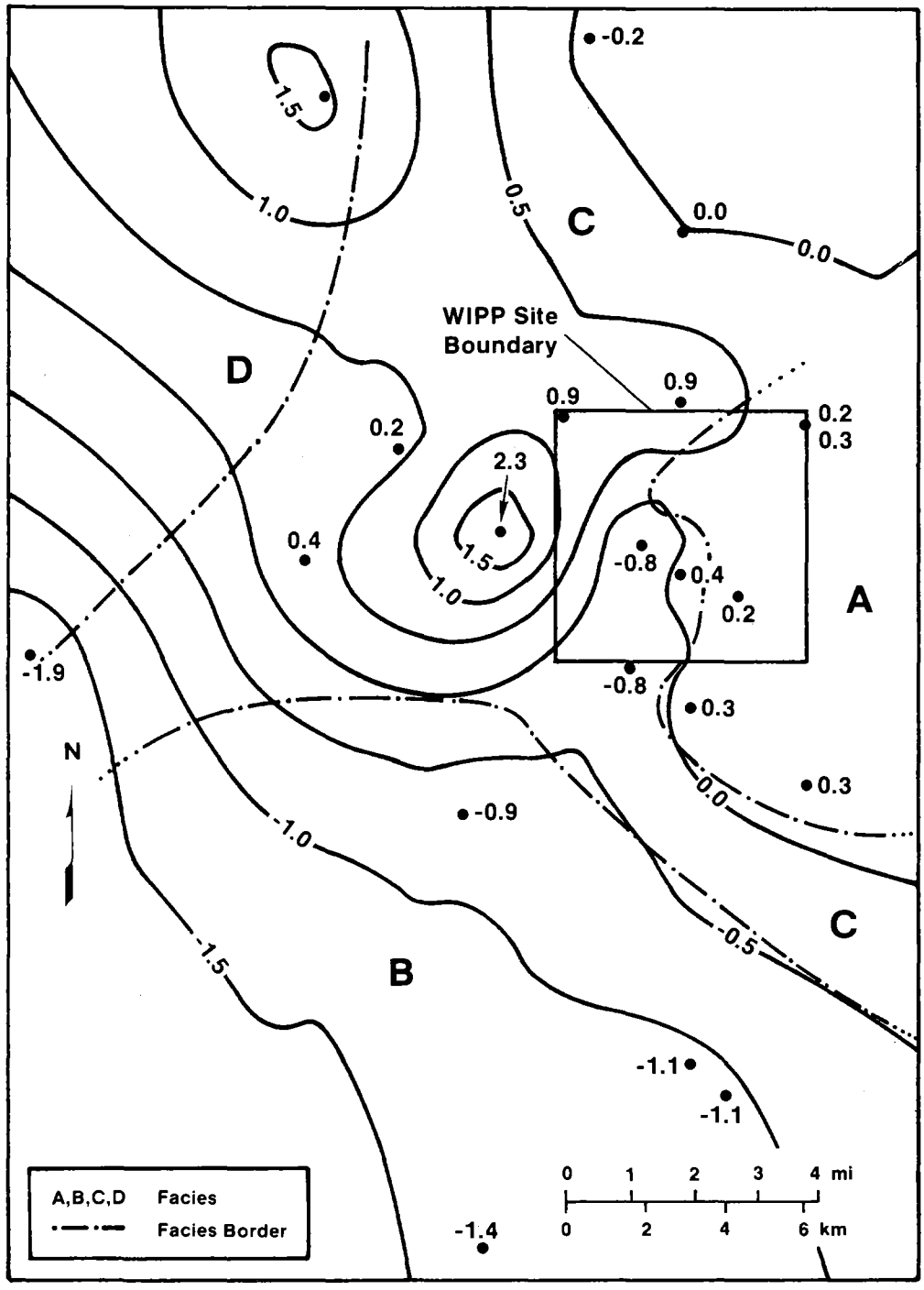


Figure 2C-5. Contours of varimax R-mode factor scores for factor 2A of Culebra groundwaters (population 1).

Factor 3A

The scores for factor 3A show little relationship to the hydrochemical facies (Figure 2C-2), although there is a general increase in the value of the score from west to east. The sample from WIPP-28 has the highest score and is anomalous compared to wells surrounding it; the bicarbonate content of the WIPP-28 sample, however, is known to be high because of contamination (see Section 2.2.2). Contours of the spatial distribution of scores for factor 3A are not plotted; however, the pattern is similar to that of $SiO_2$ presented in Figure 2-8 in Section 2.3.1.5.

# 2C.3 Varimax R-Mode Analysis With Total Dissolved Solids Partialled Out

## 2C.3.1 Objectives and Procedure

The three major factors obtained from the varimax R-mode analysis described above are all dominated by the effects of halite dissolution. Solutes are added directly from the halite or indirectly because the solubilities of sulfate and carbonate phases increase as the ionic strength increases (see Section 2.4.2).

A second varimax R-mode PCA was carried out to examine interelement correlations independent of the effects of halite dissolution. The analysis was carried out as follows. First, regression equations for each of the chemical variables as a function of the TDS were obtained. Next, the partial-correlation matrix with respect to TDS was obtained by calculating the correlations between the residuals from the regression equations. Then, the eigenvectors of the partial correlation matrix were extracted to give the factors. Finally, the varimax criterion was used to rotate the factors. A more detailed description of the procedure is in Appendix 2B.

This PCA is carried out on the variance in the population that is not correlated with variation in the TDS. The amount of this residual variance for each variable is shown in the last column of Table 2C-3. After accounting for the correlation with TDS, very little of the variance of Na, Mg, K, and Cl remains. In contrast, a significant portion of the variation in the concentrations of Ca, Sr, B, and $SiO_2$, the pH, and the alkalinity cannot be correlated with the TDS.

## 2C.3.2 Factor Loadings

Five factors accounted for 99% of the variance that remained after the TDS was partialled out. The factor-loading matrix for the five factors is shown in Table 2C-3. The factor loadings for the two most important factors are shown in Figure 2C-6 and are discussed below. For all five factors, the factor loadings for key elements (elements that have important geochemical significance or strongly influence the orientation of the factors, that is, with loadings >0.23) are discussed in Section 2.3.3.5.

Factor 1B

Factor 1B is dominated by the negative correlation of Ca and Sr with sulfate. It accounts for 67% of the total variance of Ca, 35% of the total variance of Sr, and 24% of the total variance of sulfate. This association is found in the factor 2A described previously and is suggestive of dissolution/coprecipitation of Sr and Ca in a sulfate phase such as gypsum or anhydrite.

Factor 2B

Factor 2B is similar to factor 3A. It shows two negatively correlated groups of variables. One group involves the correlation of Mg, K, bicarbonate alkalinity, and silica; the other group contains Na, pH, B, and Li. This pattern of element associations may be due to sorption onto a mineral surface, ion exchange, or silicate diagenesis. Several possible

## Table 2C-3. Varimax R-Mode Factor Loadings (Percent) Obtained from Partial-Correlation Matrix with Respect to Total Dissolved Solids for Culebra Groundwaters (Population 1)

| Element | Factor 1B | Factor 2B | Factor 3B | Factor 4B | Factor 5B | Communality ($h_i^2$) | Residual Variance[1] |
|---|---|---|---|---|---|---|---|
| Na | 12 | -10 | 76 | -58 | 4 | 98.7 | 4% |
| Cl | 28 | 3 | 84 | -36 | - 4 | 96.1 | 7% |
| Ca | 97 | - 1 | 14 | - 8 | - 1 | 99.2 | 71% |
| Mg | - 3 | 23 | -23 | 92 | 10 | 98.1 | 7% |
| K | -30 | 22 | 5 | -13 | -25 | 98.8 | 9% |
| Sr | 94 | - 1 | 25 | 9 | 1 | 97.1 | 39% |
| pH | - 1 | -93 | 19 | -26 | 7 | 98.7 | 91% |
| $HCO_3$ | -11 | 79 | - 4 | 3 | -22 | 97.1 | 96% |
| $SO_4$ | -94 | -18 | -14 | 5 | 17 | 98.2 | 27% |
| $SiO_2$ | 18 | 93 | 4 | 9 | -24 | 99.0 | 58% |
| Br | 27 | -16 | 86 | 8 | 13 | 96.2 | 19% |
| B | -19 | -52 | 14 | -55 | 47 | 97.3 | 43% |
| Li | -12 | -34 | 7 | 7 | 90 | 99.5 | 18% |

Amount and Percent of Variance[1] Explained by Each Factor

| Factor 1B | Factor 2B | Factor 3B | Factor 4B | Factor 5B |
|---|---|---|---|---|
| 3.071 | 2.903 | 2.251 | 1.737 | 1.265 |
| 27% | 26% | 20% | 16% | 11% |

1. Variance not correlated to TDS; that is, the amount of variance remaining after TDS was partialled out.

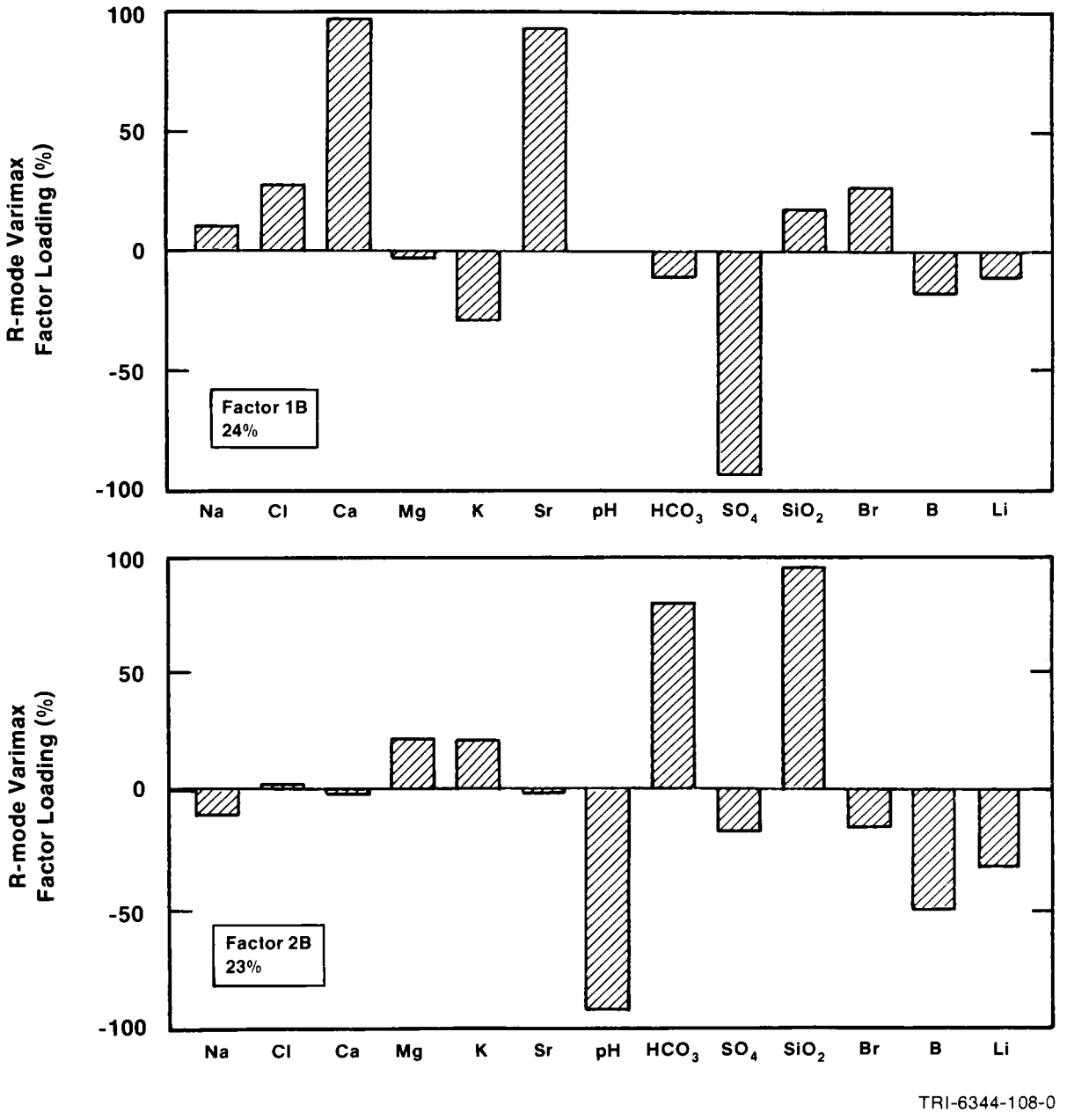


Figure 2C-6. Varimax R-mode factor loadings for factors 1B and 2B obtained from the partial-correlation matrix with respect to TDS of Culebra groundwaters (population 1).

chemical reactions that may cause these interelement correlations are discussed in Section 2.4.

### 2C.3.3 Factor Scores

The compositions of the samples in terms of the two most important factors are described by the factor scores plotted in Figure 2C-7. The spatial distributions of scores for factors 1B and 2B are plotted in Figures 2C-8 and 2C-9, respectively.

Factor 1B

Figure 2C-7 shows that the scores for factor 1B are not related to hydrochemical facies. Scores of this factor in samples from zone A and zone B are very similar; samples from zone C and zone D have the extreme score values.

The sample from P-14 has the highest score for this factor; locally, the values of the score decrease radially from this well (Figure 2C-7). As discussed in Section 2.2.3.1, the concentrations of several elements in the P-14 sample are anomalous, perhaps because of contamination. Ca, Sr, I, and Br exhibit local highs in their element contours; $SO_4$ and the Na/Cl ratio are anomalously low. The lowest (most negative) score for this factor is exhibited by the WIPP-29 sample; this sample has an anomalously high concentration of $SO_4$.

Factor 2B

Figure 2C-7 shows that factor 2B clearly distinguishes hydrochemical facies zone A from zone B. The extreme values of the factor score, however, are both in zone C. Both of the extrema, samples from WIPP-30 and WIPP-28, are anomalous with respect to neighboring wells. The sample from WIPP-30 exhibits the lowest silica concentration (4 mg/L). The sample from WIPP-28 exhibits the highest bicarbonate alkalinity in the population, but is known to be contaminated (Section 2.2.2). Figure 2C-9 shows that on a regional scale, the

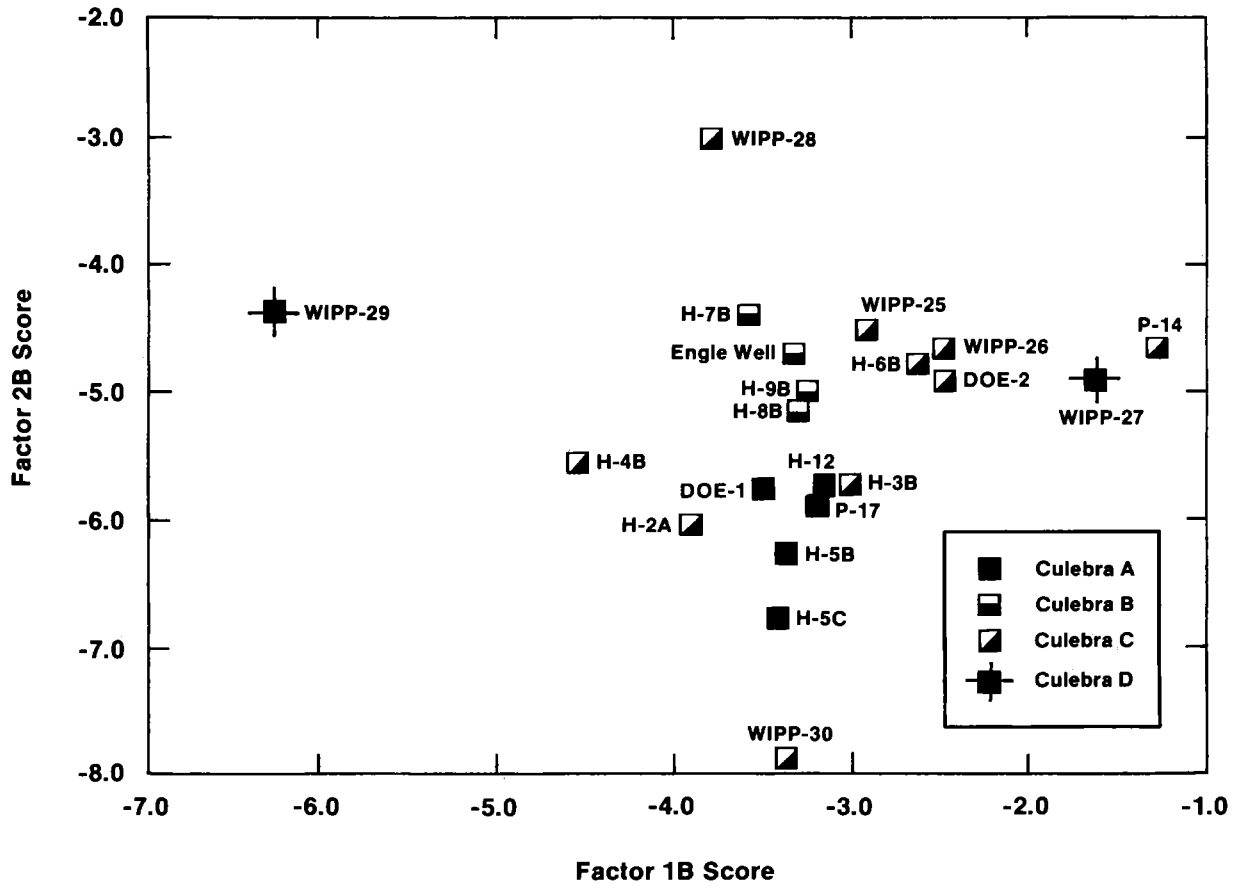


Figure 2C-7. Relationship between varimax R-mode factor scores for factor 1B and factor 2B obtained from the partial-correlation matrix with respect to TDS of Culebra groundwaters (population 1).

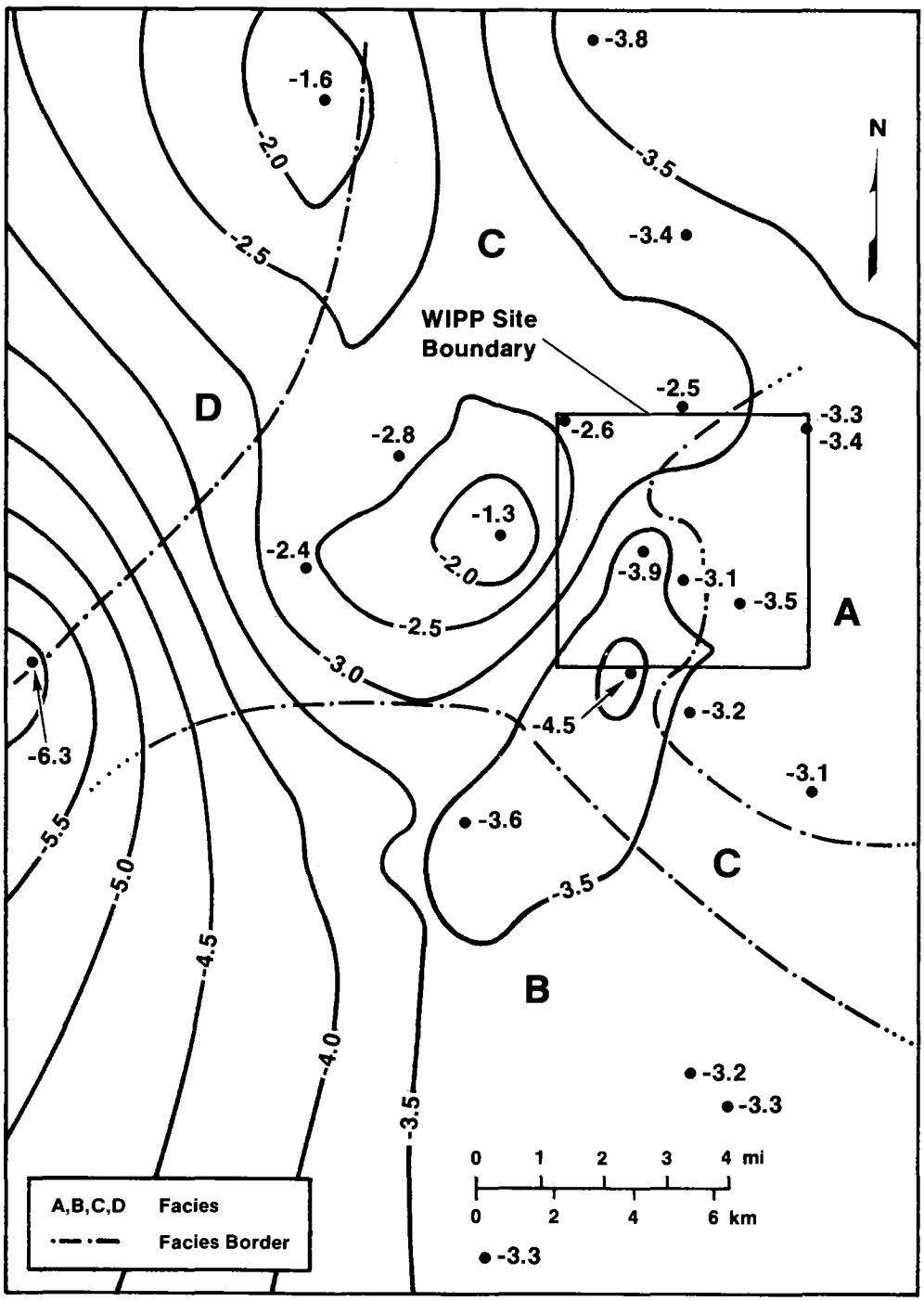


TRI-6341-46-0

Figure 2C-8. Contours of varimax R-mode factor scores for factor 1B obtained from the partial-correlation matrix with respect to TDS of Culebra groundwaters (population 1).

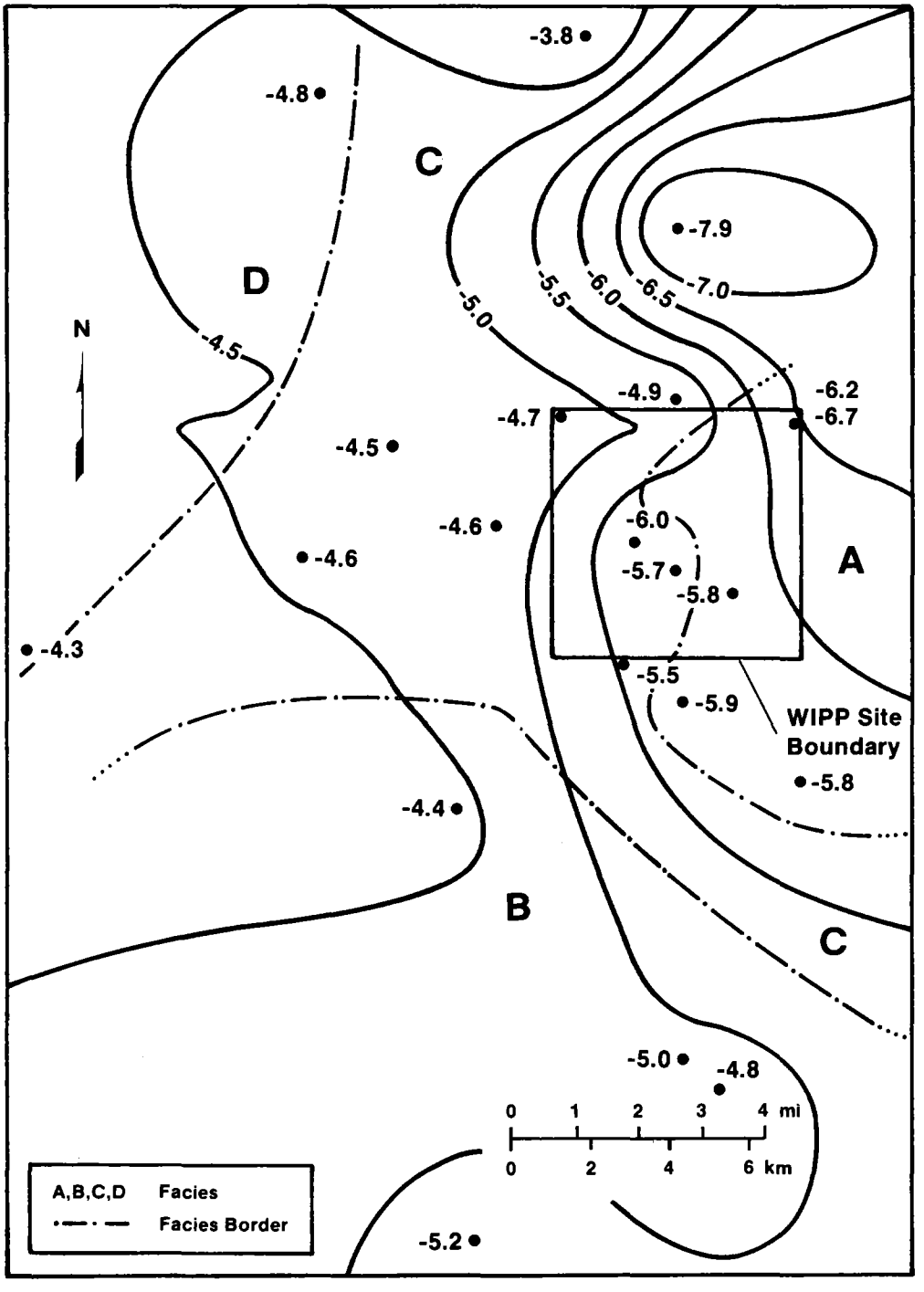


TRI-6341-43-0

Figure 2C-9. Contours of varimax R-mode factor scores for factor 2B obtained from the partial-correlation matrix with respect to TDS of Culebra groundwaters (population 1).

value of the score increases in a east to west direction. In Section 2.4.3, it is suggested that the east to west trend of increasing silica is consistent with an increase in the amount of detrital silicates exposed to groundwaters. The increased amounts of silicates are consistent with the greater degree of evaporite dissolution and formation of a residual fraction in the parts of the aquifer in contact with the groundwater.

# APPENDIX 2D. SUPPLEMENTAL ANALYSIS OF SOLUTE RELATIONSHIPS IN SELECTED WATERS FROM THE CULEBRA AND MAGENTA DOLOMITES, RUSTLER/SALADO CONTACT ZONE, DEWEY LAKE RED BEDS, AND BELL CANYON FORMATION

## 2D.1 Introduction

Although for purposes of computer modeling, the Culebra is considered a confined aquifer (Lappin, 1988), leakage of groundwater into the Culebra from underlying and overlying units cannot be ruled out with the solute data available at this time (Siegel and Lambert, Chapter 1; Bodine et al., Chapter 4). In addition, even if the groundwaters in different units are completely isolated from each other, they may have evolved along similar geochemical reaction paths. Wherever possible, a comparison of water compositions from other units with Culebra waters is useful in obtaining a basic understanding of the water/rock interactions important in this hydrochemical system.

Mercer (1983) and Ramey (1985) have previously summarized water-chemistry data from the Magenta, Rustler/Salado contact zone, and other units.

This appendix documents preliminary analyses of solute relationships in a data set describing samples taken from the Magenta dolomite, the Culebra dolomite, the Rustler/Salado contact zone, the Dewey Lake Red Beds, and the Bell Canyon Formation. Descriptions of the locations, compositions, and histories of the samples are found in Sections 2.1 and 2.2 (see Figure 2-1 and Tables 2-1, 2-2, and 2-3). In this appendix, the solute relationships are examined using methods described in Section 2.3 and in Appendix 2B.

Section 2.D.2 summarizes the relationships among the major solutes using trilinear diagrams. Section 2.D.3 describes a principal component analysis (PCA) of major and minor solute data from the Culebra dolomite, the Magenta dolomite, the Dewey Lake Red Beds, and the Bell Canyon Formation.

# 2D.2 Solute Proportions in Samples from the Rustler Formation, Dewey Lake Red Beds, and Bell Canyon Formation

## 2D.2.1 Trilinear Plot of Solute Data

Figure 2D-1 uses a trilinear (Piper) diagram to compare the compositions of selected samples from the Rustler/Salado contact zone, the Magenta dolomite, and the Dewey Lake Red Beds. This plot summarizes relationships between the major solutes in the Na-K-Mg-Ca-Cl-$SO_4$-$HCO_3$ system. The diagram shows the relative proportions of the ions on an equivalents/liter basis. Relative proportions of cations and anions are displayed separately in the triangular plots in the bottom half of the figure. In the rhombus in the upper portion of the diagram, the ratio of divalent to monovalent cations and the ratio of chloride to the sum of sulfate + bicarbonate + carbonate are shown. Construction of trilinear diagrams is reviewed in Hem (1985).

Figure 2D-1 shows saline waters from the Rustler/Salado contact zone plot near the Na-Cl corner of the trilinear diagram in portions of the areas occupied by hydrochemical facies zone A, zone C, and zone D of the Culebra dolomite (cf. Figure 2-18). Samples from the Magenta dolomite have compositions intermediate between Culebra zones C and B. The Magenta samples from WIPP-25 and H-4C have solute proportions that overlap those found in Culebra zone C. The two samples from the Dewey Lake Red Beds are similar in composition to those from Culebra zone B. No hydrochemical facies have been defined for stratigraphic horizons other than the Culebra because of the small number of analyses.

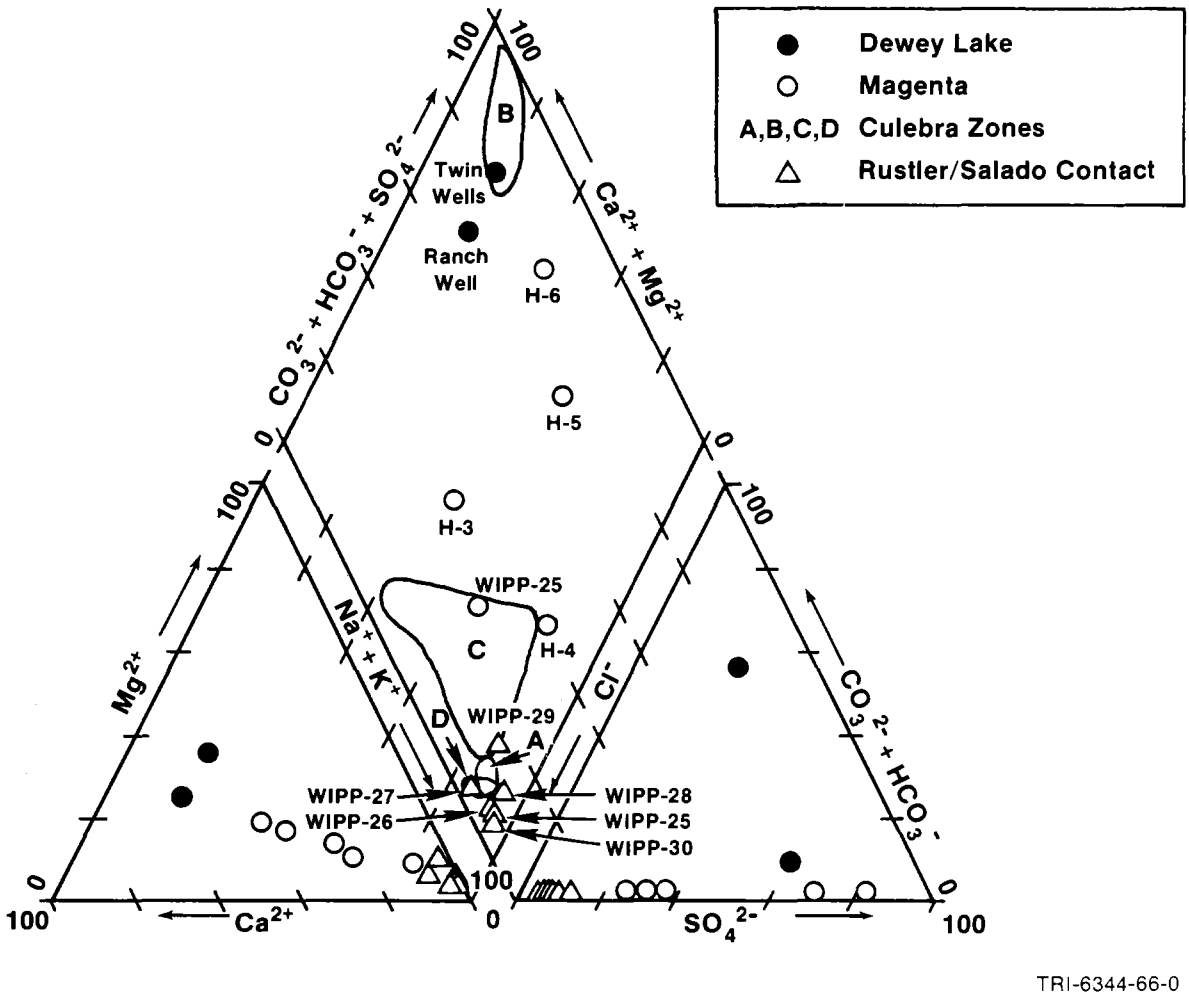


Figure 2D-1. Trilinear diagram showing compositions of groundwaters from the Rustler/Salado contact zone, the Magenta dolomite, and the Dewey Lake Red Beds.

### 2D.2.2 Comparison of Samples from Different Stratigraphic Horizons in the Same Well

Figure 2D-2 is a portion of a trilinear diagram showing the compositions of groundwater samples from locations where two or three stratigraphic horizons in the Rustler were sampled. Table 2D-1 compares the total dissolved solids (TDS) content of the same samples. For the majority of wells, groundwaters in the Magenta are relatively fresher and have higher proportions of Ca and $SO_4$, while groundwaters in the Culebra and at the Rustler/Salado contact are more saline and richer in Na and Cl. In addition, waters from the Rustler/Salado contact zone generally have higher concentrations of TDS than the waters from the Culebra. Notable exceptions to this are samples from the H-4, WIPP-25, WIPP-27, and WIPP-29 hydropads, discussed below.

Samples from the Magenta and Culebra at H-4 have similar TDS concentrations and proportions of major solutes. However, they differ dramatically in bromide and potassium concentrations (cf. Table 2-2).

Samples from the Magenta and Culebra at WIPP-25 are similar in TDS concentrations and proportions of all solutes. This similarity may indicate vertical connection between these two units at WIPP-25.

Samples from the Magenta and Culebra at WIPP-27 have nearly identical TDS and solute proportions. The similarity in composition in the Magenta and Culebra samples may indicate vertical connection between these two units at WIPP-27. The salinity of the Magenta samples at WIPP-27 is anomalously high compared to other Magenta samples. The high TDS and potassium concentrations of the Culebra and Magenta samples from WIPP-27 may be due to contamination from potash-refining operations in the area.

The hydrologic and isotopic evidence suggesting vertical connections between the Magenta and Culebra at WIPP-25 and WIPP-27 are summarized in Siegel and Lambert (Chapter 1).

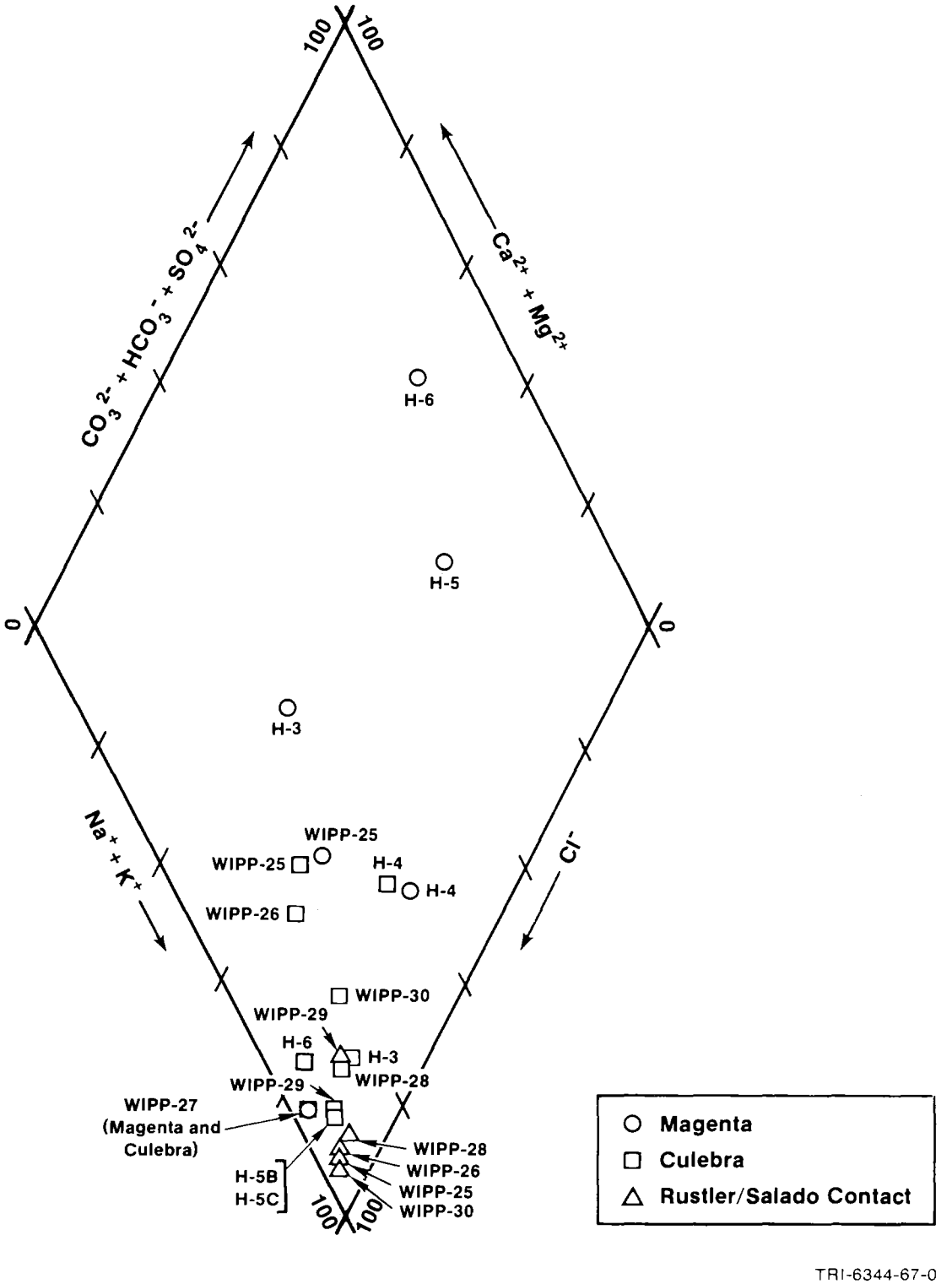


Figure 2D-2. Portion of a trilinear diagram showing compositions of Rustler groundwaters from wells where two or three stratigraphic horizons were sampled.

## Table 2D-1. Concentrations of TDS in Groundwaters from the Rustler Formation, Dewey Lake Red Beds, and Bell Canyon Formation

| Well | Strat. Hor.[1] (Facies) | Coll. Date | TDS (mg/L) |
|---|---|---|---|
| H-3B1 | Mag | 7/85 | 8560 |
| H-3B3 | Cul(C) | 2/85 | 55800 |
| H-4C | Mag | 11/86 | 23900 |
| H-4B | Cul(C) | 7/85 | 20200 |
| H-4C | Cul(C) | 8/84 | 21200 |
| H-5C | Mag | 10/86 | 6980 |
| H-5B | Cul(A) | 8/85 | 152600 |
| H-5C | Cul(A) | 10/81 | 154500 |
| H-6C | Mag | 10/86 | 4540 |
| H-6B | Cul(C) | 9/85 | 57400 |
| DOE-2 | Cul(C) | 3/85 | 60400 |
| DOE-2 | BC | 7/85 | 149500 |
| WIPP-25 | Mag | 9/80 | 11900 |
| WIPP-25 | Cul(C) | 2/86 | 13600 |
| WIPP-25 | R/S | 7/80 | 334400 |
| WIPP-26 | Cul(C) | 11/85 | 17600 |
| WIPP-26 | R/S | 7/80 | 188400 |
| WIPP-27 | Mag | 9/80 | 145700 |
| WIPP-27 | Cul(D) | 9/80 | 134700 |
| WIPP-28 | Cul(C) | 9/80 | 46600 |
| WIPP-28 | R/S | 7/80 | 277100 |
| WIPP-29 | Cul(D) | 12/85 | 324100 |
| WIPP-29 | R/S | 7/80 | 111000 |
| WIPP-30 | Cul(C) | 9/80 | 29100 |
| WIPP-30 | R/S | 7/80 | 325900 |
| RANCH | DL | 6/86 | 2520 |
| TWIN-P | DL | 1/86 | 401 |

1. Stratigraphic horizons: Cul = Culebra dolomite; Mag = Magenta dolomite; BC = Bell Canyon Fm.; DL = Dewey Lake Red Beds.
Facies (in parentheses) are the hydrochemical facies in the Culebra, as defined in Section 2.3.2.1.

At WIPP-29, the Culebra water samples are more saline and have different solute proportions than the samples from the Rustler/Salado contact. This difference indicates a lack of vertical connection between the two strata at this location.

## 2D.3 Principal Component Analysis of Groundwater Samples from the Rustler Formation, Dewey Lake Red Beds, and Bell Canyon Formation

PCA was carried out on a data set composed of samples from wells in the Dewey Lake Red Beds, Magenta and Culebra dolomites, and Bell Canyon Formation. An explanation of the methods and objectives of PCA is found in Appendix 2B. Only data from the UNC Geotech laboratory were used; the common logs ($\log_{10}$) of the raw concentration data were used in the analysis.

The objective in selecting analyses for this PCA was to include as many different elements as possible. For this reason, several Culebra samples that lack reliable minor and trace element data (Mn, Fe, I) were not included. A secondary objective in this PCA was to compare the solute relationships in this more extensive data set to those observed in the data set drawn from the Culebra alone. This PCA is in no way to be considered a comprehensive analysis of water from all water-bearing strata at the WIPP Site. Data from other stratigraphic horizons (the Rustler/Salado contact zone, the Castile Formation, and the Salado Formation) and additional data from the Magenta dolomite, Dewey Lake Red Beds, and Bell Canyon Formation would be required to produce a data set that is truly representative of the full range of solute compositions of water from rocks in the Ochoan. Table 2D-2 compares the data set (population 2) used in this analysis with the data set (population 1) used in the PCA of Culebra samples (described in Section 2.2.3.3).

### 2D.3.1 Q-Mode Principal Component Analysis

Q-mode analysis was carried out to determine if the samples were drawn from a statistically homogeneous population suitable for R-mode PCA. Both unrotated and varimax

## Table 2D-2. Populations Used in Principal Component Analyses

| Population | Wells | Variables used in PCA |
|---|---|---|
| 1 | Culebra: DOE-1, DOE-2, H-2A, H-3B3, H-4B, H-5B, H-5C, H-6B, H-7B1, H-8B, H-9B, H-12, P-14, P-17, WIPP-25, WIPP-26, WIPP-27, WIPP-28, WIPP-29, WIPP-30, Engle | Ca, Mg, K, Na, Cl, $SO_4$, B, Li, $SiO_2$, Br, Sr, $HCO_3$, pH |
| 2 | Dewey Lake: Ranch, Twin-Pasture<br>Magenta: H-3B1, H-4C, H-5C, H-6C<br>Culebra: DOE-2, H-2A, H-3B3, H-5B, H-6B, H-7B1, H-8B, H-9B, P-14, P-17, WIPP-26, WIPP-29, Engle<br>Bell Canyon: DOE-2 | Ca, Mg, K, Na, Cl, $SO_4$, B, Li, $SiO_2$, Br, Sr, $HCO_3$, pH, Fe, Mn, F, I |

solutions were examined. The unrotated factors were the more interpretable and were retained for further discussion.

The factor loadings and scores are shown in Table 2D-3 and Figures 2D-3 and 2D-4. Table 2D-3 shows that two factors account for nearly all of the variance; at least 94% of the composition of all water samples can be mathematically expressed as a linear combination of these two hypothetical end-members. Figure 2D-4 shows the composition of the two factors.

Figure 2D-3 shows the composition of the samples in terms of the factors. Most of the samples are similar to factor 1C (97% of the variance); it represents a grand mean of the compositions. The Culebra sample from WIPP-25 is closest in composition to this factor. Along the factor-1C axis, Na, Cl, Ca, Mg, pH, $SO_4$, and TDS increase, and the

## Table 2D-3. Unrotated Q-Mode Factor Loadings for Rustler, Dewey Lake, and Bell Canyon Groundwaters (Population 2)

| Well | Strat.Hor.[1] (Facies) | Coll. Date | Factor 1C | Factor 2C | Communality ($h_i^2$) |
|---|---|---|---|---|---|
| H-5B | Cul(A) | 8/85 | 0.97 | 0.22 | 0.993 |
| P-17 | Cul(A) | 3/86 | 0.97 | 0.20 | 0.987 |
| H-7B1 | Cul(B) | 3/86 | 0.98 | -0.18 | 0.994 |
| H-8B | Cul(B) | 1/86 | 0.95 | -0.29 | 0.987 |
| H-9B | Cul(B) | 11/85 | 0.97 | -0.22 | 0.994 |
| Engle | Cul(B) | 3/85 | 0.97 | -0.22 | 0.989 |
| DOE-2 | Cul(C) | 3/85 | 0.98 | 0.16 | 0.983 |
| H-2A | Cul(C) | 4/86 | 0.99 | 0.01 | 0.984 |
| H-3B3 | Cul(C) | 2/85 | 0.99 | 0.14 | 0.995 |
| H-6B | Cul(C) | 9/85 | 0.98 | 0.15 | 0.990 |
| P-14 | Cul(C) | 2/86 | 0.98 | 0.06 | 0.956 |
| WIPP-25 | Cul(C) | 2/86 | 0.99 | <0.01 | 0.989 |
| WIPP-26 | Cul(C) | 11/85 | 0.99 | 0.02 | 0.973 |
| WIPP-29 | Cul(D) | 12/85 | 0.91 | 0.33 | 0.947 |
| H-3B1 | Mag | 7/85 | 0.99 | -0.05 | 0.982 |
| H-4C | Mag | 11/86 | 0.99 | 0.01 | 0.982 |
| H-5C | Mag | 10/86 | 0.98 | -0.09 | 0.971 |
| H-6C | Mag | 10/86 | 0.99 | -0.11 | 0.991 |
| RANCH | DL | 6/86 | 0.97 | -0.18 | 0.973 |
| TWIN-P | DL | 1/86 | 0.95 | -0.27 | 0.974 |
| DOE-2 | BC | 7/85 | 0.93 | 0.31 | 0.963 |

Amount and Percent of Variance Explained by Each Factor

| | Factor 1C | Factor 2C |
|---|---|---|
| | 19.886 | 0.713 |
| | 96% | 4% |

1. Stratigraphic horizons: Cul = Culebra dolomite; Mag = Magenta dolomite; BC = Bell Canyon Fm.; DL = Dewey Lake Red Beds.
Facies (in parentheses) are the hydrochemical facies in the Culebra, as defined in Section 2.3.2.1.

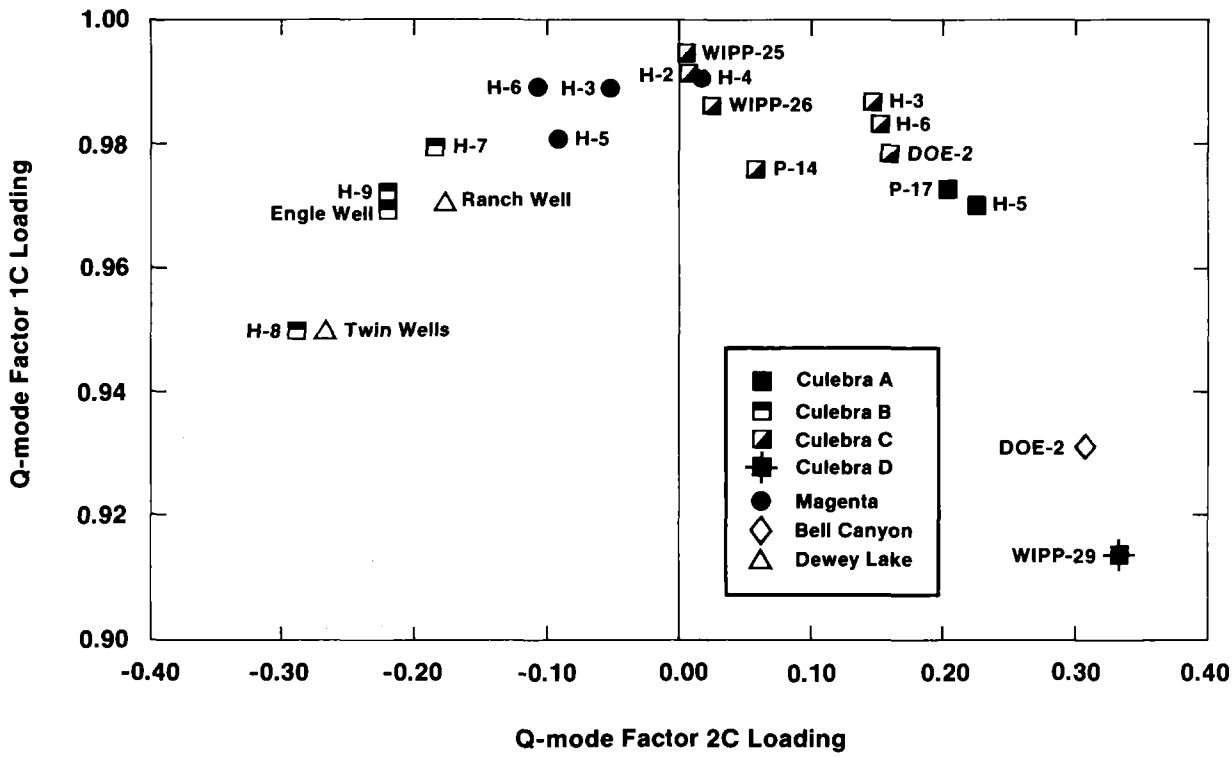


Figure 2D-3. Relationship between unrotated Q-mode factor loadings for factors 1C and 2C of Rustler, Dewey Lake, and Bell Canyon groundwaters (population 2).

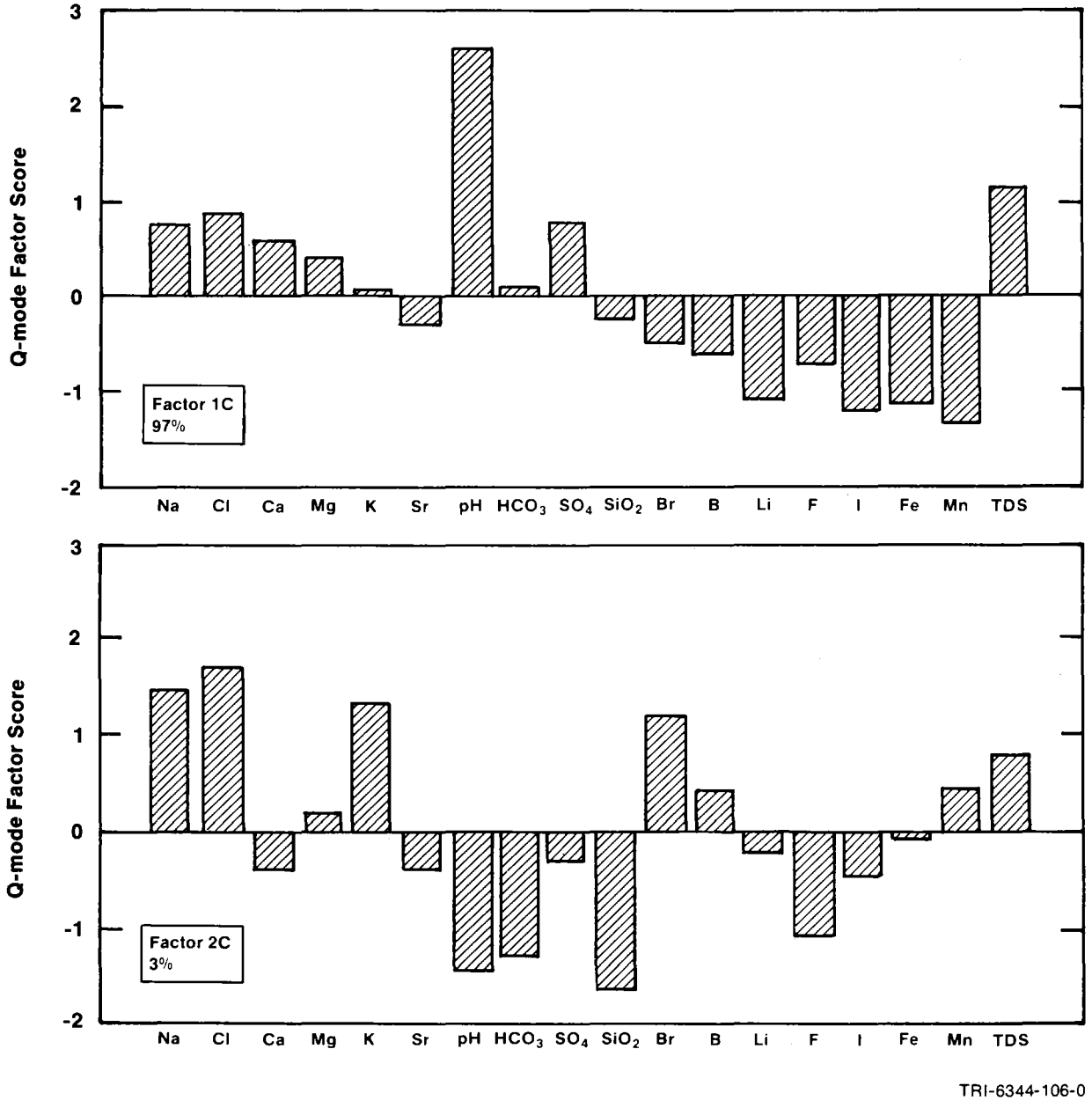


Figure 2D-4. Unrotated Q-mode factor scores for factors 1C and 2C of Rustler, Dewey Lake, and Bell Canyon groundwaters (population 2).

other solutes decrease. The rest of the variation in the sample population can be expressed in terms of factor 2C. Along the factor-2C axis, concentrations of Na, Cl, K, Br, B, Mn, and TDS increase, and the other concentrations decrease. Culebra samples from WIPP-29 and H-8 are the extrema of factor 2C.

Figure 2D-3 also shows that samples from the Dewey Lake are similar to samples from hydrochemical facies zone B of the Culebra. The sample from the Bell Canyon Formation at DOE-2 has the same TDS concentration as the Culebra sample from H-5B (hydrochemical facies zone A); however, Figure 2D-3 shows that it is very different in composition from Culebra samples from zone A.

As discussed in Appendix 2B, a data set is generally considered homogeneous enough for R-mode analysis if two or three Q-mode factors are sufficient to explain all of the population variance. The results shown in Table 2D-3 indicate that population 2 is amenable to R-mode factor analysis.

### 2D.3.2 Varimax R-Mode Principal Component Analysis

R-mode PCA was carried out on the data in population 2 using the SAS program (Statistical Analysis System Institute, 1982). The correlation matrix of the data (the common logs of the concentrations) is given in Table 2D-4 Several rotations of the factors were examined; only the varimax solution is considered in this discussion. Seven varimax factors were extracted; they account for more than 99% of the variance (see Table 2D-5). At least 93% of the variance of each variable could be explained by these factors. The first five factors account for 91% of the variance. The factor loadings for the first five factors are shown in Figure 2D-5; the factor scores for the first two factors are plotted in Figure 2D-6.

## Table 2D-4. Correlation Matrix for Solute Data[1] in Rustler, Dewey Lake, and Bell Canyon Groundwaters (Population 2)

| | Ca | Mg | K | Na | Cl | $SO_4$ | B | Fe | Li |
|---|---|---|---|---|---|---|---|---|---|
| Ca | 1.000 | 0.656 | 0.505 | 0.690 | 0.700 | 0.450 | 0.621 | 0.460 | 0.796 |
| Mg | 0.656 | 1.000 | 0.897 | 0.916 | 0.909 | 0.785 | 0.674 | 0.566 | 0.820 |
| K | 0.505 | 0.897 | 1.000 | 0.947 | 0.934 | 0.703 | 0.761 | 0.509 | 0.753 |
| Na | 0.690 | 0.916 | 0.947 | 1.000 | 0.989 | 0.740 | 0.849 | 0.626 | 0.852 |
| Cl | 0.700 | 0.909 | 0.934 | 0.989 | 1.000 | 0.675 | 0.786 | 0.582 | 0.821 |
| $SO_4$ | 0.450 | 0.785 | 0.703 | 0.740 | 0.675 | 1.000 | 0.679 | 0.634 | 0.665 |
| B | 0.621 | 0.674 | 0.761 | 0.849 | 0.786 | 0.679 | 1.000 | 0.638 | 0.814 |
| Fe | 0.460 | 0.566 | 0.509 | 0.626 | 0.582 | 0.634 | 0.638 | 1.000 | 0.610 |
| Li | 0.796 | 0.820 | 0.753 | 0.852 | 0.821 | 0.665 | 0.814 | 0.610 | 1.000 |
| Mn | 0.595 | 0.811 | 0.750 | 0.799 | 0.784 | 0.609 | 0.727 | 0.662 | 0.819 |
| $SiO_2$ | -0.520 | -0.532 | -0.583 | -0.679 | -0.610 | -0.511 | -0.858 | -0.618 | -0.831 |
| Br | 0.748 | 0.866 | 0.831 | 0.928 | 0.950 | 0.538 | 0.715 | 0.558 | 0.826 |
| F | 0.122 | 0.395 | 0.328 | 0.290 | 0.229 | 0.739 | 0.308 | 0.423 | 0.276 |
| I | 0.628 | 0.561 | 0.399 | 0.521 | 0.503 | 0.441 | 0.499 | 0.454 | 0.799 |
| Sr | 0.957 | 0.791 | 0.644 | 0.808 | 0.809 | 0.629 | 0.694 | 0.538 | 0.810 |
| pH | -0.303 | -0.592 | -0.465 | -0.353 | -0.394 | -0.227 | 0.030 | 0.001 | -0.316 |
| $HCO_3$ | -0.547 | -0.301 | -0.315 | -0.473 | -0.396 | -0.469 | -0.770 | -0.505 | -0.594 |

1. The data are the common logarithms of the solute concentrations in mg/L (except pH).

**Table 2D-4. Correlation Matrix for Solute Data[1] in Rustler, Dewey Lake, and Bell Canyon Groundwaters (Population 2) (Continued)**

| | Mn | $SiO_2$ | Br | F | I | Sr | pH | $HCO_3$ |
|---|---|---|---|---|---|---|---|---|
| Ca | 0.595 | -0.520 | 0.748 | 0.122 | 0.628 | 0.957 | -0.303 | -0.547 |
| Mg | 0.811 | -0.532 | 0.866 | 0.395 | 0.561 | 0.791 | -0.592 | -0.301 |
| K | 0.750 | -0.583 | 0.831 | 0.328 | 0.399 | 0.644 | -0.465 | -0.315 |
| Na | 0.799 | -0.679 | 0.928 | 0.290 | 0.521 | 0.808 | -0.353 | -0.473 |
| Cl | 0.784 | -0.610 | 0.950 | 0.229 | 0.503 | 0.809 | -0.394 | -0.396 |
| $SO_4$ | 0.609 | -0.511 | 0.538 | 0.739 | 0.441 | 0.629 | -0.227 | -0.469 |
| B | 0.727 | -0.858 | 0.715 | 0.308 | 0.499 | 0.694 | 0.030 | -0.770 |
| Fe | 0.662 | -0.618 | 0.558 | 0.423 | 0.454 | 0.538 | 0.001 | -0.505 |
| Li | 0.819 | -0.831 | 0.826 | 0.276 | 0.799 | 0.810 | -0.316 | -0.594 |
| Mn | 1.000 | -0.640 | 0.766 | 0.311 | 0.588 | 0.655 | -0.391 | -0.349 |
| $SiO_2$ | -0.640 | 1.000 | -0.628 | -0.214 | -0.720 | -0.536 | -0.132 | 0.819 |
| Br | 0.766 | -0.628 | 1.000 | 0.042 | 0.576 | 0.821 | -0.410 | -0.406 |
| F | 0.311 | -0.214 | 0.042 | 1.000 | 0.272 | 0.266 | -0.087 | -0.280 |
| I | 0.588 | -0.720 | 0.576 | 0.272 | 1.000 | 0.614 | -0.188 | -0.538 |
| Sr | 0.655 | -0.536 | 0.821 | 0.266 | 0.614 | 1.000 | -0.341 | -0.566 |
| pH | -0.391 | -0.132 | -0.410 | -0.087 | -0.188 | -0.341 | 1.000 | -0.377 |
| $HCO_3$ | -0.349 | 0.819 | -0.406 | -0.280 | -0.538 | -0.566 | -0.377 | 1.000 |

1. The data are the common logarithms of the solute concentrations in mg/L (except pH).

## Table 2D-5. Varimax R-Mode Factor Loadings (Percent) For Rustler, Dewey Lake, and Bell Canyon Groundwaters (Population 2)

| Element | Factor 1D | Factor 2D | Factor 3D | Factor 4D | Factor 5D | Factor 6D | Factor 7D | Communality ($h_i^2$) |
|---|---|---|---|---|---|---|---|---|
| Na | 89 | 31 | 11 | 18 | 18 | 17 | 8 | 99.5 |
| Cl | 89 | 34 | 4 | 16 | 11 | 17 | 3 | 98.2 |
| Ca | 37 | 86 | 8 | 28 | 3 | 11 | 10 | 98.8 |
| Mg | 80 | 32 | -18 | 27 | 32 | 15 | 8 | 97.1 |
| K | 94 | 11 | - 1 | 13 | 23 | 5 | 13 | 97.6 |
| Sr | 51 | 79 | 8 | 22 | 18 | 13 | 2 | 99.4 |
| pH | -40 | -22 | 81 | -14 | - 9 | 12 | -16 | 93.2 |
| $HCO_3$ | -19 | -37 | -79 | -31 | -21 | - 5 | - 8 | 95.1 |
| $SO_4$ | 55 | 20 | 12 | 14 | 73 | 18 | 0 | 93.6 |
| $SiO_2$ | -48 | -11 | -58 | -57 | - 8 | -16 | -22 | 98.1 |
| Br | 82 | 41 | 1 | 28 | - 9 | 22 | 0 | 97.6 |
| B | 67 | 27 | 54 | 18 | 20 | 13 | 30 | 98.2 |
| Li | 61 | 41 | 15 | 55 | 16 | 14 | 24 | 96.1 |
| F | 7 | 2 | 4 | 9 | 97 | 11 | 6 | 96.2 |
| I | 22 | 31 | 9 | 89 | 15 | 12 | 2 | 98.3 |
| Fe | 36 | 18 | 24 | 19 | 29 | 80 | 9 | 97.8 |
| Mn | 61 | 22 | - 5 | 33 | 17 | 36 | 52 | 95.9 |

## Table 2D-5. Varimax R-Mode Factor Loadings (Percent) For Rustler, Dewey Lake, and Bell Canyon Groundwaters (Population 2) (Continued)

| | Amount and Percent of Variance Explained by Each Factor | | | | | |
|---|---|---|---|---|---|---|
| Factor 1D | Factor 2D | Factor 3D | Factor 4D | Factor 5D | Factor 6D | Factor 7D |
| 6.242 | 2.523 | 2.073 | 2.089 | 1.970 | 1.058 | 0.552 |
| 38% | 15% | 13% | 13% | 12% | 6% | 3% |

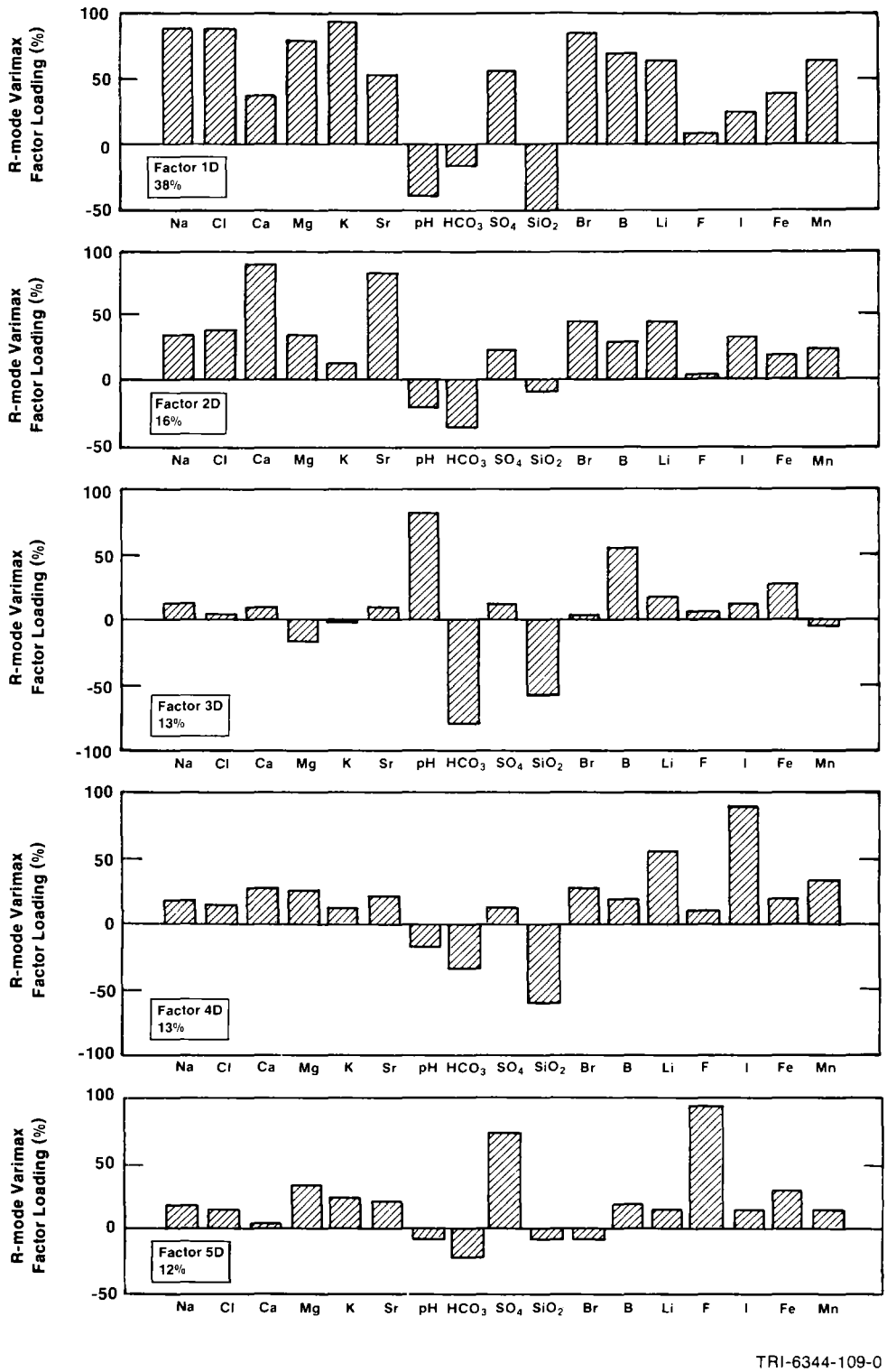


Figure 2D-5. Varimax R-mode factor loadings for factors 1D, 2D, 3D, 4D, and 5D of Rustler, Dewey Lake, and Bell Canyon groundwaters (population 2).

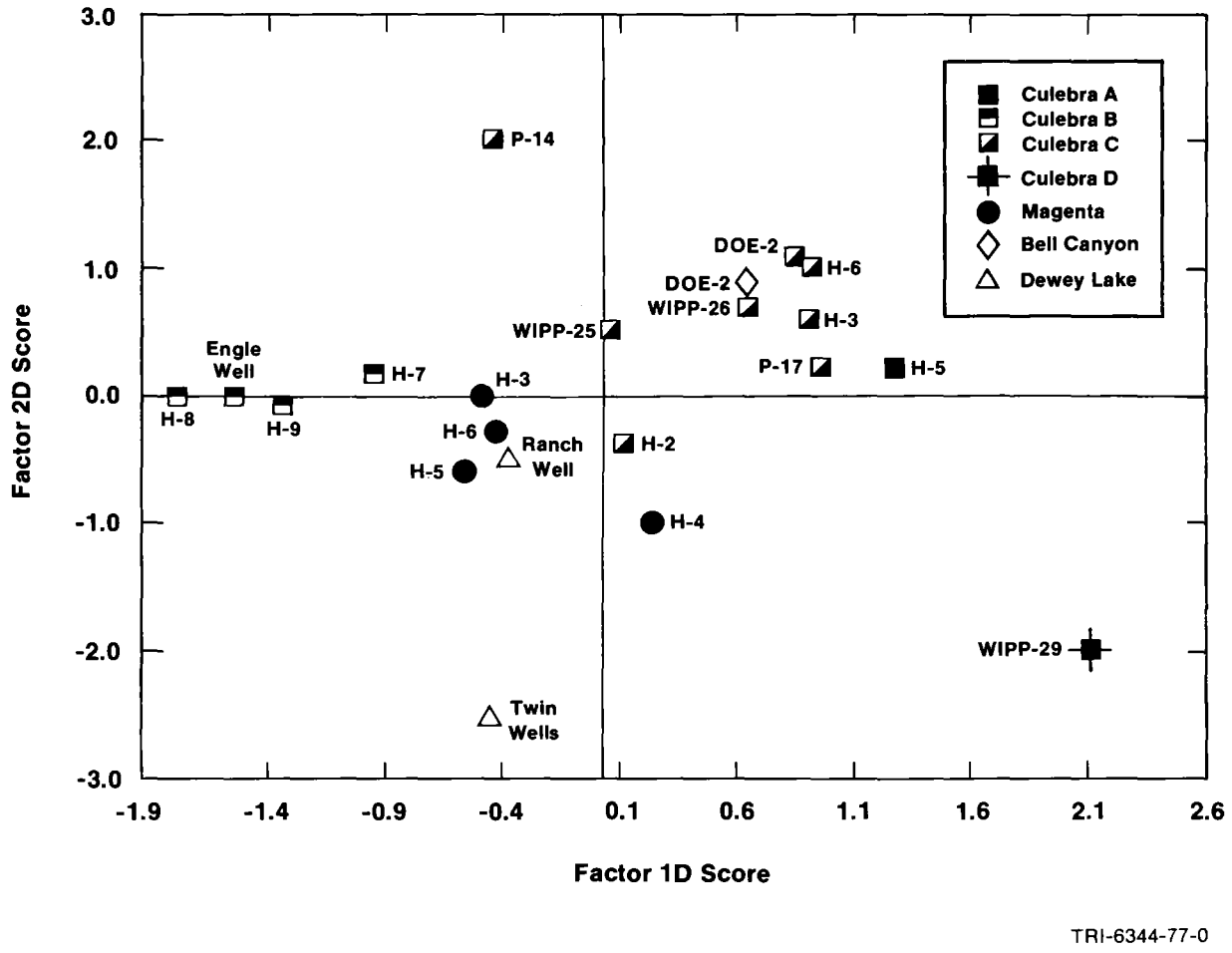


Figure 2D-6. Relationship between varimax R-mode factor scores for factors 1D and 2D of Rustler, Dewey Lake, and Bell Canyon groundwaters (population 2).

"Salinity," "Sulfate," and "Silicate/Bicarbonate" Factors

Most of the chemical variability of the sample population can be correlated with the variance in the concentrations of Na and Cl. Factor 1D, the most important factor produced by the R-mode analysis, is dominated by Na, K, Mg, Br, and Cl. All solutes except for $SiO_2$, alkalinity, and pH exhibit positive correlations with this factor. Factor 1D is similar to the salinity factor (factor 1A) of population 1 described in Section 2.3.3.4.

The second most important factor, factor 2D, also has a strong Na-Cl influence, but is most strongly influenced by Ca, bicarbonate alkalinity, and Sr. It is similar to the sulfate factor (factor 2A) of population 1. As discussed in Section 2.3.3.4 for the Culebra analysis, several sources of data from the site suggest that these salinity and sulfate factors represent addition of solutes by the dissolution of halite, gypsum, anhydrite, and carbonates.

Factor 3D is similar to the silicate/bicarbonate factor (factor 3A) of population 1. It is strongly influenced by the concentrations of Si, B, Li, and bicarbonate and by the pH. However, the loading of Mg in this factor is different from that in the Culebra factor 3A.

Additional Elements

This R-mode analysis allows an examination of the behavior of several elements that were not included in population 1. Factor 4D of population 2 (see Table 2D-5) is dominated by the behaviors of I, Si, and Li and has no counterpart in the Culebra analysis. The geochemical significance of this factor is unclear. Iodide is concentrated in residual brines and in formation waters. The iodide concentration of the waters in population 2 ranges from a level approximately equal to that of seawater (0.05 mg/L in Culebra samples from H-7B) to 6.4 mg/L in the Bell Canyon sample from DOE-2. Nearly all of the waters are generally enriched in iodide relative to the seawater evaporation curve (cf. Collins, 1975). Potential sources of the excess iodide include dissolution of iodide from evaporite minerals or organic material and desorption from clays.

Iodide is correlated with Na and Cl and inversely correlated with Si on all factors extracted in the R-mode analysis. If high silica contents are assumed to be indicative of effects related to clay diagenesis, then this may indicate that the desorption from clays is not a significant source of iodine. In the Magenta and in hydrochemical facies zone A, zone C, and zone D of the Culebra, the main source of the iodide is probably halite and associated evaporite salts. The high I/Cl ratios and low Cl concentrations in the samples from the Dewey Lake and hydrochemical facies zone B of the Culebra, however, do not support a salt source for the iodide in that area.

Factor 5D is the most significant factor for both F and $SO_4$ (see Table 2D-5). Fluorine occurs most commonly in fluorite ($CaF_2$) and sellaite ($MgF_2$). Sonnenfeld (1984) notes that typically, $MgF_2$ occurs as an accessory mineral associated with anhydrite, whereas $CaF_2$ more commonly occurs with carbonates. The association of F, $SO_4$, and Mg in factor 5D may indicate that $MgF_2$ in anhydrite or gypsum is the source of fluorine in these waters.

Iron loads primarily onto its own principal component, factor 6D; Mn has an appreciable loading onto this factor also (see Table 2D-5). The lack of correlation between Fe and Mn with other major and minor solutes may be due to random errors in sampling or analyses as discussed in Section 2.2. Manganese also loads strongly onto factor 1D and factor 7D; the geochemical significance of these elemental associations is unclear, but might be related to corrosion of well casing in the borehole.

### 2D.3.3 Varimax R-Mode Principal Component Analysis With Total Dissolved Solids Partialled Out

A second set of R-mode PCAs was carried out in which the correlation of each element with the TDS concentration was partialled out; the method is described in Appendix B. The resulting factor pattern shows the interelement correlations independent of the effects that may be attributed to halite dissolution.

The factor-loading matrix is shown in Table 2D-6. The first three factors account for 57% of the variance left after the TDS concentration is partialled out (see Figure 2D-7). The results are similar to those obtained from the analysis of the population 1.

The primary factor (factor 1E) contains two groups of inversely correlated elements. Mg, bicarbonate alkalinity, and $SiO_2$ form one group; and Na, pH, B, and Li form another group. All of these chemical variables are known to be related with dissolution or ion-exchange reactions involving clays (see Section 2.4.3). This pattern of element associations might reflect clay diagenesis or silicate hydrolysis.

The second factor (factor 2E) shows a Ca-Sr-$HCO_3$-$SO_4$ association indicative of coprecipitation of Sr and Ca in sulfates and carbonates. Sulfate and fluorine dominate factor 3E and may reflect the occurrence of accessory $MgF_2$ in $CaSO_4$ as discussed previously.

**Table 2D-6. Varimax R-Mode Factor Loadings (Percent) Obtained from Partial-Correlation Matrix with Respect to Total Dissolved Solids for Rustler, Dewey Lake, and Bell Canyon Groundwaters (Population 2)**

| Element | Factor 1E | Factor 2E | Factor 3E | Factor 4E | Factor 5E | Factor 6E | Factor 7E | Factor 8E | Factor 9E | Communality ($h_i^2$) |
|---|---|---|---|---|---|---|---|---|---|---|
| Ca | 8 | 94 | -18 | 3 | 20 | - 2 | - 1 | -14 | 8 | 99.5 |
| Mg | -82 | 0.1 | 11 | -26 | 5 | - 9 | 5 | 37 | -21 | 95.3 |
| K | - 2 | -77 | - 5 | 23 | -25 | -24 | -15 | -43 | - 2 | 96.5 |
| Na | 42 | - 9 | -19 | 83 | -10 | -20 | 11 | - 2 | 7 | 97.5 |
| Cl | 1 | 4 | -32 | 92 | -12 | - 6 | - 3 | - 8 | - 3 | 98.6 |
| $SO_4$ | 8 | - 3 | 86 | -16 | - 2 | -18 | 19 | 34 | 13 | 96.5 |
| B | 97 | 3 | 3 | 0.3 | 4 | 6 | 7 | - 3 | 9 | 95.1 |
| Fe | 23 | 7 | 20 | 7 | 8 | 20 | 92 | 3 | - 0.3 | 99.4 |
| Li | 28 | 30 | -12 | -13 | 82 | 12 | 5 | - 3 | 31 | 98.0 |
| Mn | 3 | - 3 | - 8 | -16 | 16 | 94 | 18 | 1 | 1 | 98.0 |
| $SiO_2$ | -74 | 9 | 12 | 8 | -61 | - 2 | -19 | - 3 | 5 | 98.9 |
| Br | - 8 | 24 | -70 | 55 | 18 | - 1 | 11 | 17 | -17 | 95.5 |
| F | - 1 | - 4 | 93 | -21 | 3 | 3 | 12 | -11 | -19 | 97.4 |
| I | 3 | 25 | 5 | - 5 | 92 | 12 | 2 | 5 | -18 | 96.1 |
| Sr | 4 | 97 | - 1 | 11 | 9 | -12 | 1 | 0.2 | - 8 | 97.9 |
| pH | 85 | 1 | 18 | 30 | 5 | 2 | 14 | 24 | - 5 | 92.9 |
| $HCO_3$ | -82 | -31 | -10 | 8 | -29 | 17 | -13 | - 6 | 21 | 97.1 |

## Table 2D-6. Varimax R-Mode Factor Loadings (Percent) Obtained from Partial-Correlation Matrix with Respect to Total Dissolved Solids for Rustler, Dewey Lake, and Bell Canyon Groundwaters (Population 2) (Continued)

| Amount and Percent of Variance Explained by Each Factor | | | | | | | | |
|---|---|---|---|---|---|---|---|---|
| Factor 1E | Factor 2E | Factor 3E | Factor 4E | Factor 5E | Factor 6E | Factor 7E | Factor 8E | Factor 9E |
| 3.887 | 2.751 | 2.398 | 2.190 | 2.177 | 1.141 | 1.059 | 0.570 | 0.328 |
| 24% | 17% | 15% | 13% | 13% | 7% | 6% | 3% | 2% |

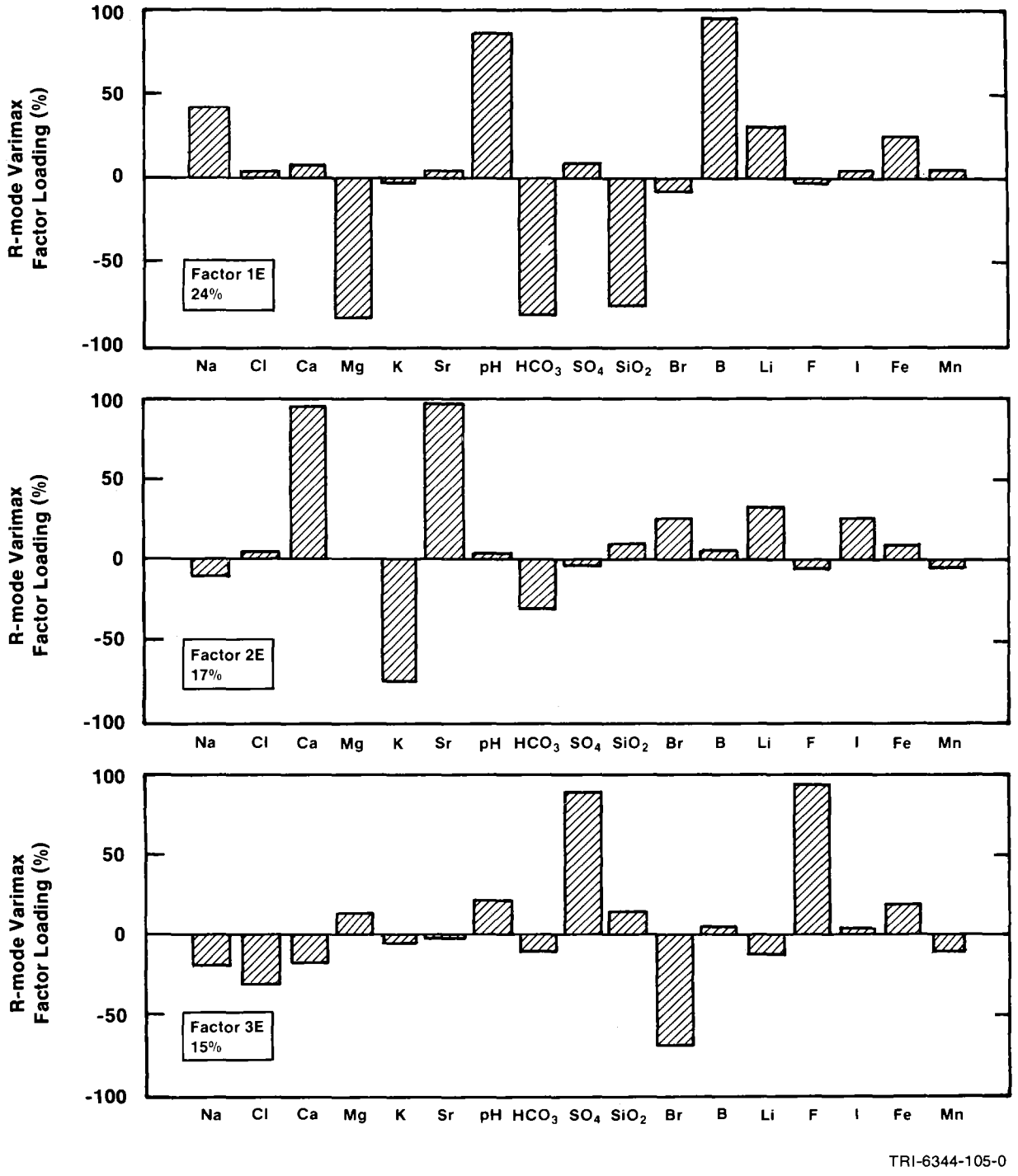


Figure 2D-7. Varimax R-mode factor loadings for factors 1E, 2E, and 3E obtained from partial-correlation matrix with respect to TDS of Rustler, Dewey Lake, and Bell Canyon groundwaters (population 2).

# CHAPTER 3:

# MINERALOGY OF THE CULEBRA DOLOMITE

Terry Sewards, Michael L. Williams, and Klaus Keil
University of New Mexico

Steven J. Lambert and Carol L. Stein
Sandia National Laboratories

## ABSTRACT

Samples from twelve cores containing the Culebra dolomite member of the Rustler Formation were selected for detailed mineralogical analysis as part of the characterization of hydrogeochemical facies within this formation. One hundred and sixteen samples were analyzed by semiquantitative x-ray diffraction, x-ray fluorescence, and optical microscopy. These samples, and the cores from which they were taken, were selected to represent the Culebra dolomite both vertically through the stratigraphic section and laterally over a distance of several kilometers, but locally high fracture densities in zones likely to carry groundwater may have inhibited sampling of fluid-rich zones. The primary mineral constituent of the Culebra is dolomite, with subsidiary calcite, gypsum, anhydrite, quartz, and clays. On the average, dolomite constitutes 85 to 90 weight percent of the samples examined. Total gypsum plus dolomite is generally a constant, although relative amounts of these phases are variable. Clays are present in all samples, comprising approximately 3 to 5 weight percent of the total bulk mineralogy. Clays occur either finely dispersed throughout the dolomite, frequently in association with organic matter, or as discrete clay seams or laminae. X-ray diffraction analyses of clay mineral separates show the major clay species to be illite, corrensite, chlorite, and a serpentine-like mineral tentatively identified as amesite. The latter three minerals are consistent with previous workers' conclusions regarding the neoformation of Mg-rich clay phases in evaporitic environments. Culebra

mineralogies can partially dissolve to yield some of the solutes in Culebra groundwaters. However, sources of the dissolved sodium chloride are not readily available within the unit, and are better sought in adjacent strata that are likely to contain halite.

# CONTENTS

# FIGURES



# PLATES



# TABLES

# CHAPTER 3.0

## 3.1 INTRODUCTION

This chapter characterizes the mineralogy of the Culebra member of the Rustler Formation based on studies of samples from cores from 12 boreholes surrounding the Waste Isolation Pilot Plant (WIPP) repository. Since the Rustler Formation contains both evaporite lithologies and meteorically derived groundwater, the detailed mineralogy of water-bearing units such as the Culebra is relevant to identifying potential sources of solutes in the Rustler groundwaters.

The stratigraphy of the Rustler Formation, showing the position of the Culebra dolomite, is illustrated in Figure 3-1. Some horizons in the Culebra dolomite member have a high fracture porosity (Ferrall and Gibbons, 1979; Haug et al., 1987). This unit is considered to be the most probable conduit of radionuclides to the accessible environment in the event of a low-pressure breach in the repository.

This investigation had four main goals: (1) to investigate both the lateral and vertical variation of the mineralogy of the Culebra unit to the extent possible, given the poor core recovery in many parts of the Culebra; (2) to obtain accurate modal compositions of the samples selected; (3) to characterize fracture surfaces in particular detail, for evidence that these surfaces may have been water-bearing; and (4) to identify potential sources of major and minor solutes in Culebra groundwaters. Analytical methods employed to achieve these goals include x-ray diffraction (XRD) analysis, x-ray fluorescence (XRF) spectroscopic analysis, electron microprobe (EMX) elemental analysis, analytical electron (AEM) microscopy, and optical microscopy.

Rock samples used in this study were taken from cores of ten different boreholes in the vicinity of the WIPP Site: H-3, H-6, H-7, H-10, H-11, WIPP-12, WIPP-19, WIPP-25, WIPP-26, and WIPP-29 (Figure 3-2). In addition, a preliminary study conducted by

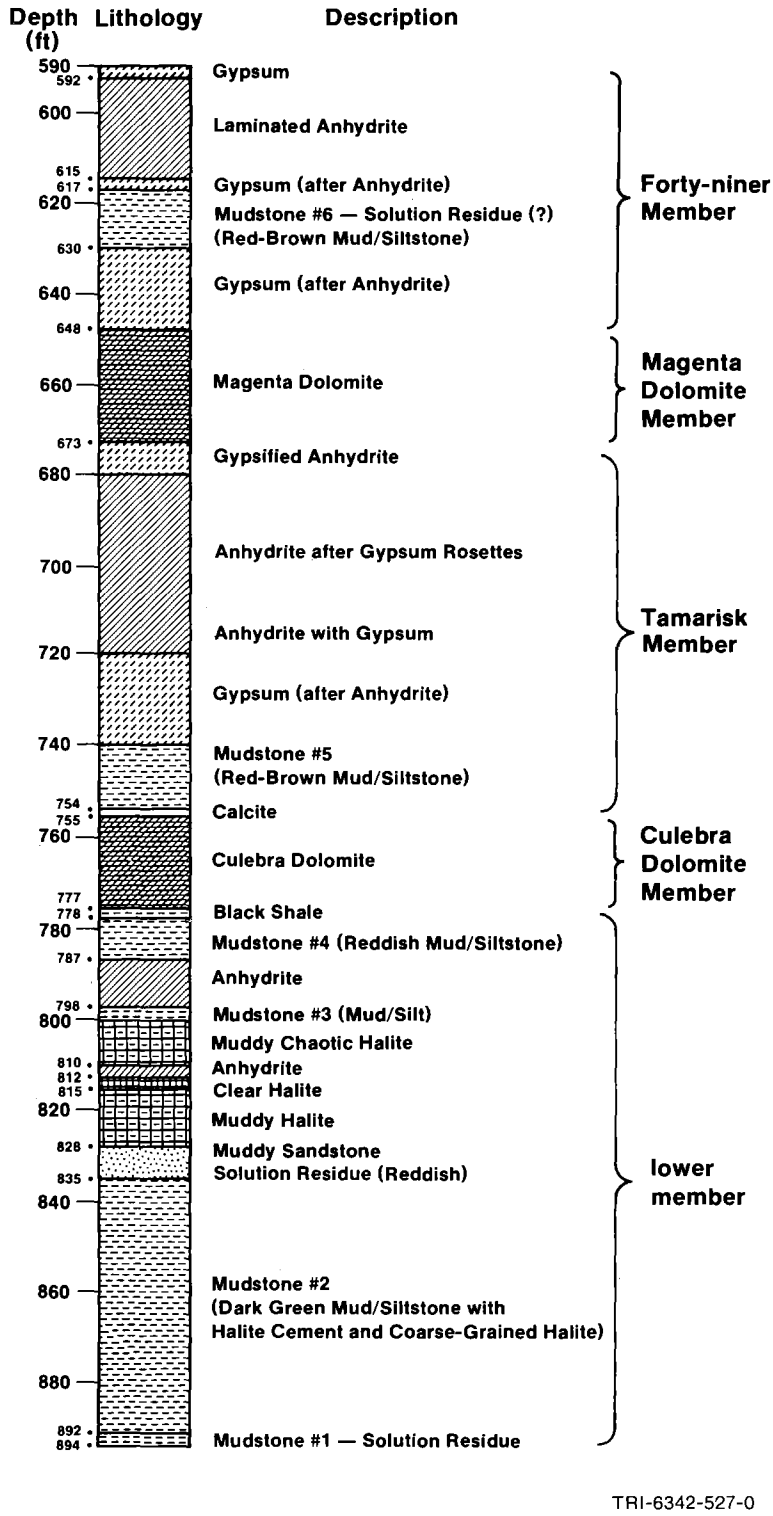


Figure 3-1. Stratigraphic section of Rustler Formation, WIPP-19 core. Lithologic log modified from Ferrall and Gibbons (1979).

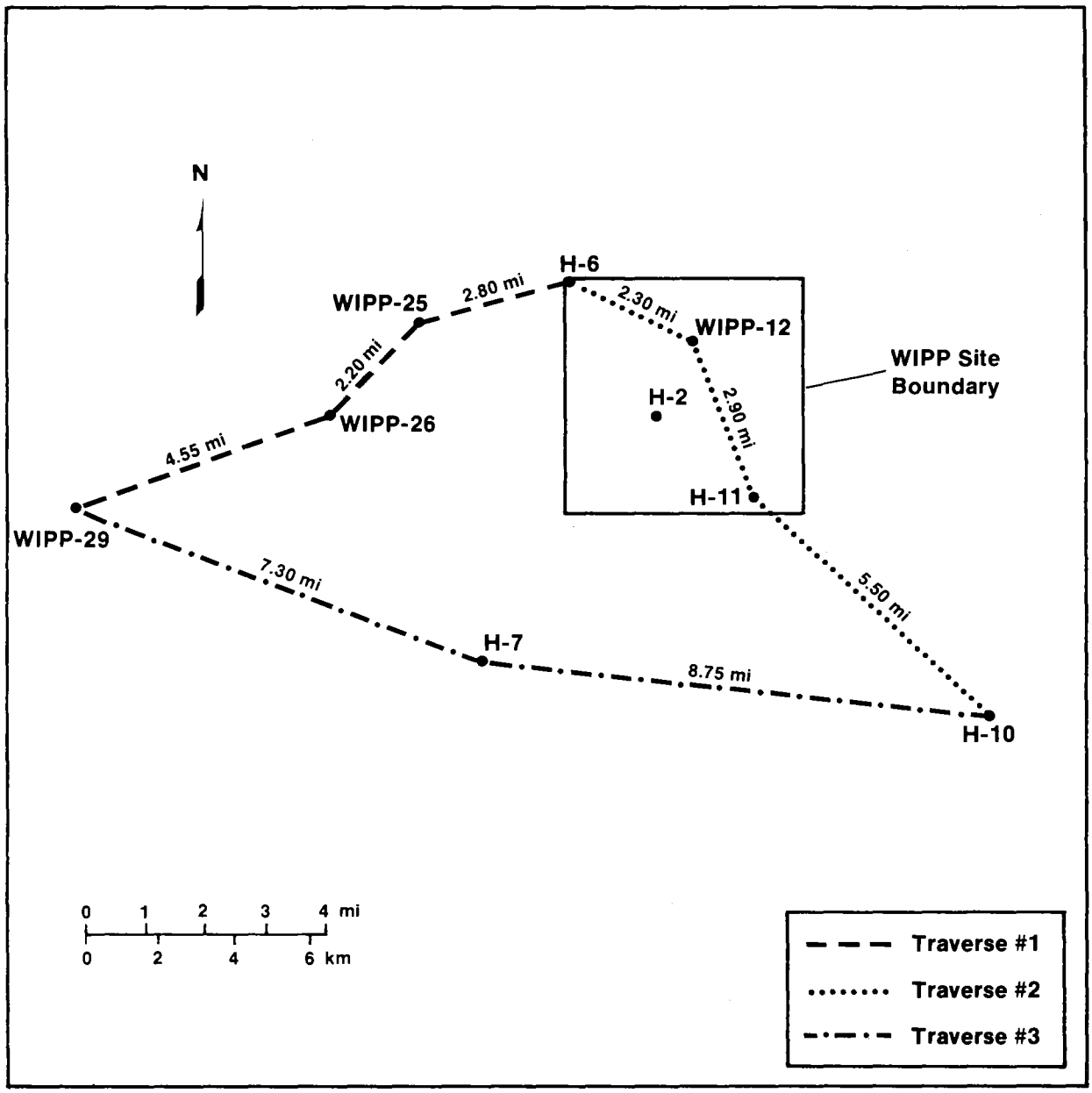


Figure 3-2. Map of WIPP Site and vicinity showing locations of cores used in this study.

Core Laboratories, Inc. (Harville, 1986) examined samples of Culebra dolomite taken from cores H-2, H-3, H-4, and H-6. With the exception of the material selected for the Core Laboratories study (chosen for physical properties measurements), the samples described here were chosen by visual inspection to provide three different types of information. First, maximum spatial coverage of the Culebra was attempted. Second, lithologic boundaries such as contacts between dolomite and mudstone, dolomite and gypsum, etc. were sampled for general mineralogical characterization as well as for evidence that such contacts may have been active pathways for fluid transport. Third, textural features, such as fractures, vugs, and clay seams, were sampled to allow analysis of potential water-bearing surfaces.

The degree to which these three kinds of information can be obtained from core is limited. In some boreholes, core recovery was incomplete, allowing only partial coverage of the dolomite unit. In many cases, the abundant fracturing giving rise to fragmentation of core and subsequent poor recovery is also responsible for the locally high hydraulic conductivity of the unit (Mercer, 1983). This is particularly true of the boreholes in and near Nash Draw, where the Rustler Formation has been disrupted by postdepositional hydration and dissolution (Snyder, 1985; Bachman, 1987). This has probably affected boreholes WIPP-25, WIPP-26, WIPP-29, H-7, and H-11 to varying degrees. It is likely that borehole coring selectively biases against recovery of Culebra samples most likely to be carrying groundwater.

Most samples in this preliminary mineralogical survey of the Rustler were taken from zones in which core recovery was more complete. Those samples are less likely to contain water. Where the integrity of the recovered core was poor (i.e., rubbled), fewer samples were taken. Additional sampling would be required to characterize the highly fractured zones, which are more likely to contain water. Due to the centimeter-to-centimeter lithologic variability of the Culebra (Holt and Powers, 1988), the degree to which the rock characteristics can be interpolated between vertically adjacent samples of analyzed core in the same borehole, or between laterally adjacent (stratigraphically equivalent) samples in different boreholes, is highly variable.

Samples were analyzed by XRF to determine their compositions and by XRD to determine the minerals present. Mineral modes for the 101 samples that were analyzed by XRF for the constituent oxides were calculated based on the compositional data. Details of the mineralogical studies summarized herein are given by Sewards, Williams, and Keil (1991).

## 3.2 MINERAL DISTRIBUTION

### 3.2.1 General Observations

To illustrate the vertical and horizontal variations of the major minerals in the cores examined in this study, three fence diagrams of the Rustler Formation (Figures 3-3A, 3-3B, and 3-3C), highlighting its component members, were prepared based on the three traverses indicated in Figure 3-2. In each fence diagram, the major minerals in each section of Culebra core are plotted beneath the location of the borehole.

Several conclusions can be drawn from these fence diagrams. First, clay is present in all the cores, averaging around 3 to 5 weight percent of the total. Second, the typical dolomite content of these samples is 85 to 90 weight percent, with the remainder usually consisting of quartz, clay, and gypsum. Third, the relative proportions of gypsum and dolomite may be variable, but these variations do not appear to influence the clay content. Fourth, several clay-rich seams are present in the Culebra.

### 3.2.2 Calcite

The top of the Culebra in borehole WIPP-29 is ≈12 ft below the ground surface; samples from the top of the Culebra contain abundant calcite. Why calcite is more abundant near the top of the core is not known, but the reason may be related to near-surface processes. Calcite was also found in the WIPP-19 core (Sewards, Glenn, and Keil, 1991) at the top of the Culebra unit. Small amounts of calcite may be present throughout the Culebra, principally close to fractures that may have been water-bearing. A highly fractured

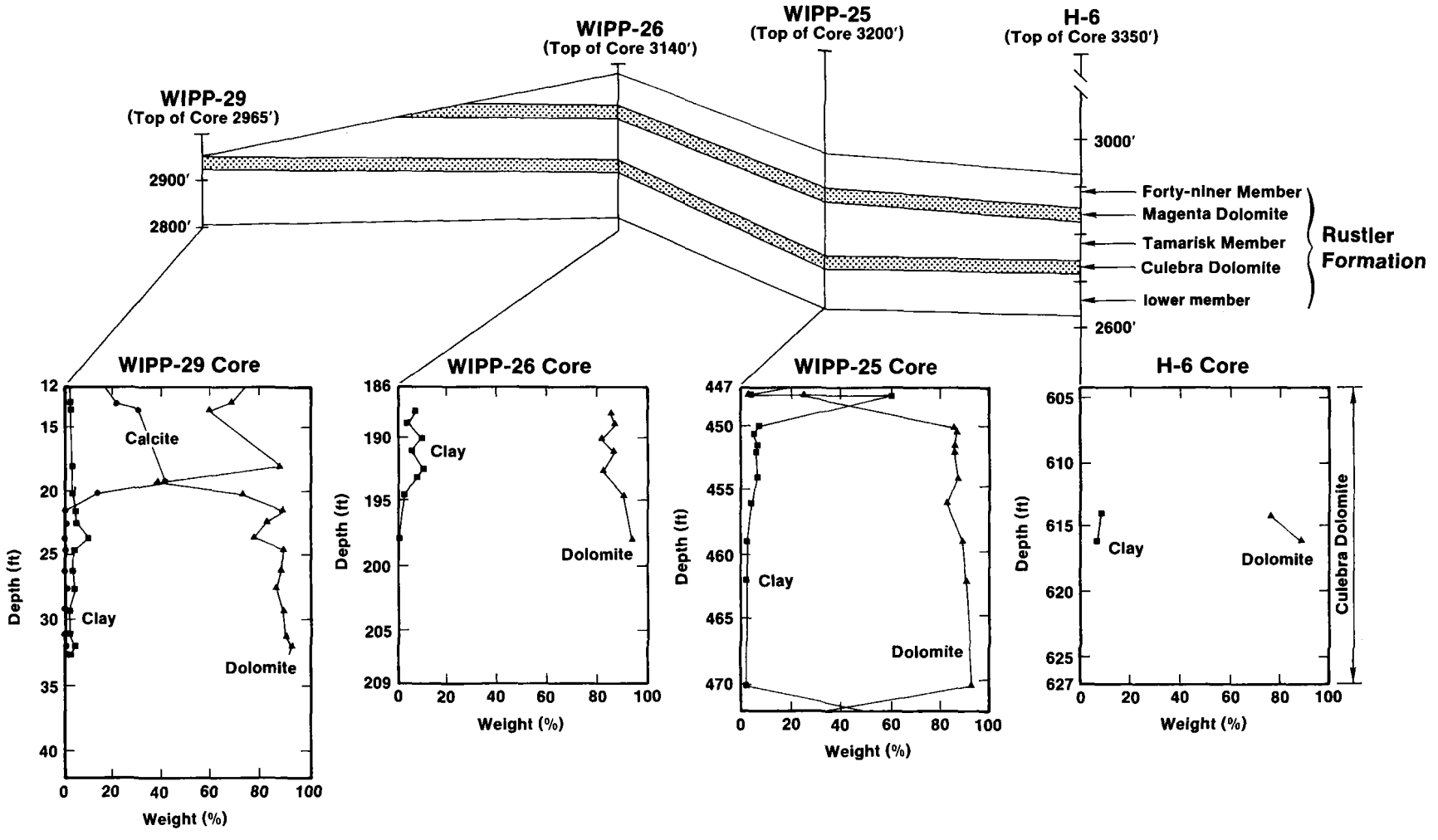


Figure 3-3. Fence diagrams showing stratigraphy of the Rustler Formation and mineralogy of the Culebra member. A. Traverse No. 1; boreholes WIPP-29, WIPP-26, WIPP-25, and H-6.

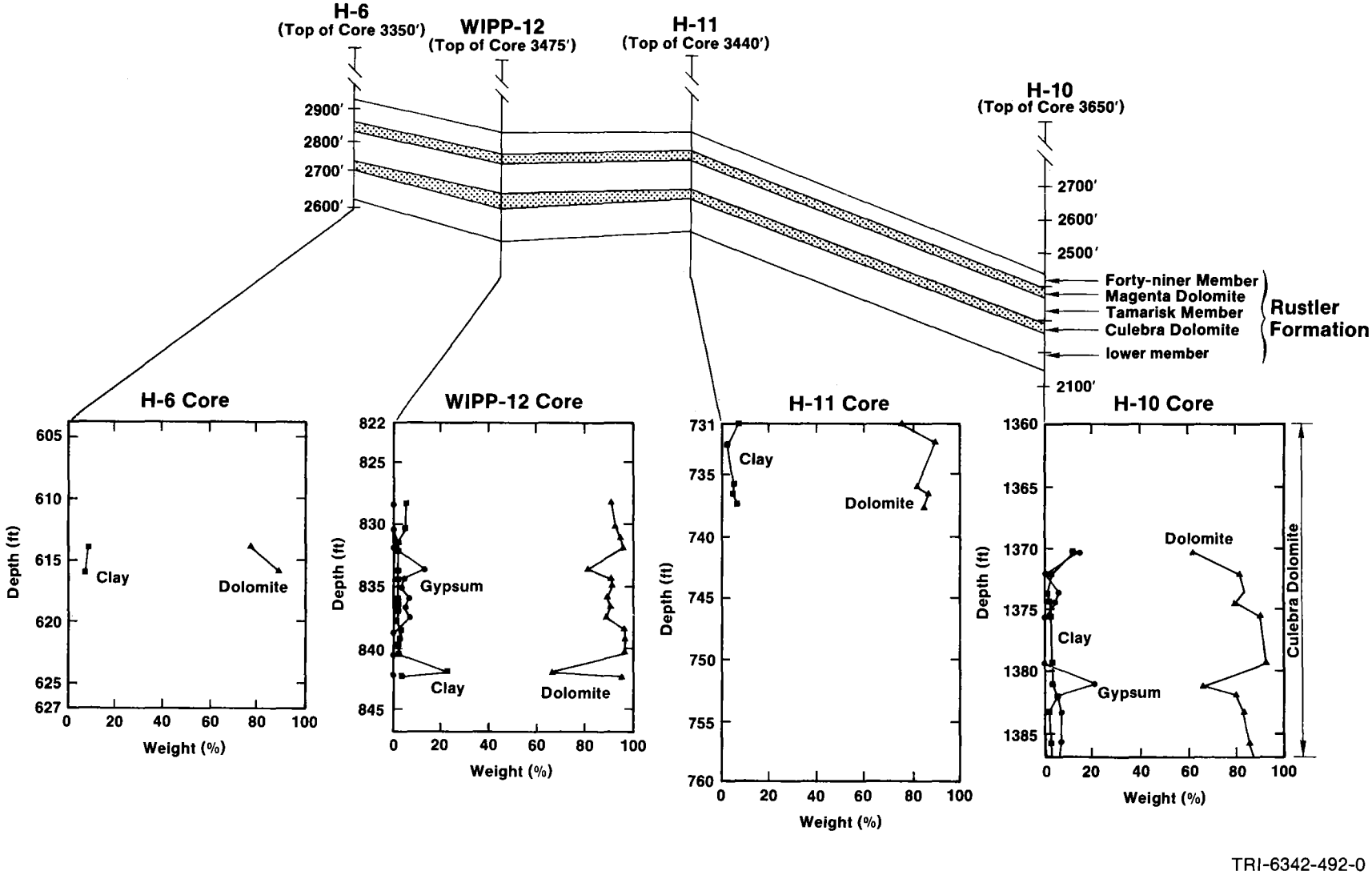


B. Traverse No. 2; boreholes H-6, WIPP-12, H-11, and H-10.

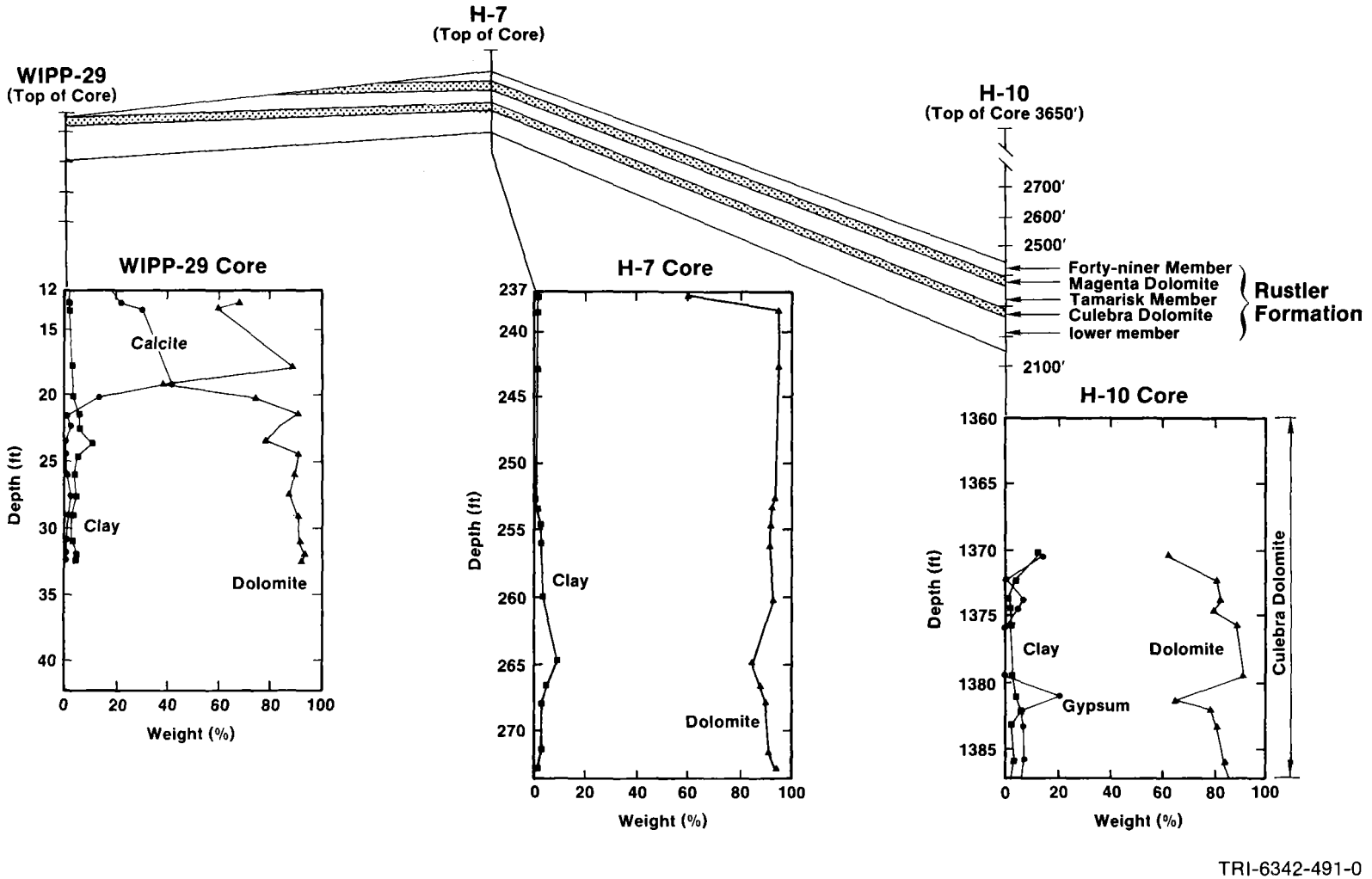


C. Traverse No. 3; boreholes WIPP-29, H-7, and H-10.

sample from the Magenta member, higher up in the Rustler Formation, in WIPP-33 consists of 8 weight percent calcite, and no dolomite (Lambert and Harvey, 1987).

### 3.2.3 Gypsum

Quantitative mineralogical analysis of this selection of cores indicates that gypsum is most abundant (on the order of 5 weight percent of the bulk) in the Culebra cores from boreholes H-10 and WIPP-12. There appear to be two gypsum-rich zones at similar stratigraphic horizons in these two boreholes, at depths of approximately 833 and 842 ft in WIPP-12 and at 1373 and 1382 ft in H-10 (Figure 3-3B). According to core descriptions (Mercer et al., 1987; SNL and USGS, 1980a, 1980b), similar zones of gypsum-filled fractures occur at similar horizons in DOE-2, WIPP-30, and WIPP-19. Incomplete sampling of the H-6 and H-11 cores, which lie in the vicinity of the aforementioned boreholes, prevents more widespread areal confirmation of this trend. Gypsum is a very minor component in the remaining selected and analyzed cores, all of which lie to the south and west of H-10 and WIPP-12.

### 3.2.4 Halite

Halite appeared in the x-ray diffractograms of several of the Culebra samples in this study. Also, dissolution of water-soluble material during the preparation of some samples for clay-mineral determinations resulted in some mass loss, which was tentatively attributed to halite by Sewards, Glenn, and Keil (1991) and Sewards, Williams, and Keil (1991). The presence of minor and trace halite in diffractograms of untreated powdered rock is not surprising, because cores were typically taken using NaCl-saturated brine as a circulating medium to minimize dissolution in halite-bearing horizons of the Rustler. These occurrences of halite in the Culebra probably represent contamination by the residue of drilling brine.

Mass loss attributed to halite (in the two Culebra samples from WIPP-19) is more problematical. The cause of the mass loss, whether by actual dissolution of one or more

phases or due to spillage of material during processing, has not been conclusively identified. The undersaturation of virtually all Culebra groundwater occurrences with respect to NaCl (Siegel et al., Chapter 2) is not consistent with the natural occurrence of halite in the Culebra. This is especially problematical where Rustler halite adjacent to the Culebra is rare, and where the Culebra produces more copious quantities of groundwater. Pending further investigation, the presence of halite in water-producing localities in the Culebra is not considered a natural occurrence.

## 3.3 TEXTURAL FEATURES

Most of the observations in the following section are based on samples from a single drill core, WIPP-12. This core yielded many relatively massive samples that illustrate the range of mineralogical and textural characteristics typical of a vertical section through the intact portions of the Culebra member. Attention was primarily focused on features in the Culebra member that might control or preserve a record of its permeability and reactivity to past, present, and future through-flowing fluids. Intact cores, however, may not represent many horizons of preferential development of permeability, and hence the original characteristics of those horizons may not be observable in any core that has carried appreciable amounts of water.

The following discussion will summarize the detailed observations of textural features. The first part will discuss the mineralogical and textural characteristics of intact massive dolomite. The subsequent parts will focus on the nature and distribution of vugs, holes, and fractures within the Culebra.

### 3.3.1 Textures in Massive Dolomitic Rock

Intact Culebra core samples consist of domains or layers of relatively pure, massive dolomite separated by domains or layers of quartz and clay-rich dolomite. The thickness and relative purity of the layers are extremely variable. Clay-rich layers range from discontinuous lenses, less than 1 mm thick, to continuous laminae, several centimeters in

thickness. Clay-rich layers typically contain approximately 5 to 20 weight percent quartz and clay, whereas massive dolomite typically contains less than 3 weight percent quartz and clay. Both quartz/clay-rich and massive dolomite layers are permeated to varying degrees by fractures and vugs, as discussed later in this section.

Thin (<1 mm) reddish-brown stringers and lenses were frequently observed in the Culebra thin sections examined in this study. This material was typically associated with clays and less commonly with euhedral dolomite rhombs. Neither XRD, scanning electron microscope/energy dispersive x-ray (SEM/EDAX), or reflected-light microscopy indicated a distinct mineralogy for this material. Samples containing this material frequently exhibit unusually bright "charging" during SEM examination; this effect is probably due to volatilization of carbonaceous material under the electron beam. This material has been tentatively identified as organic matter.

Massive dolomite domains in the Culebra are characterized by nearly equigranular mosaics of dolomite crystals. Grain size is typically 5 m, but varies from 2 to 20 $\mu$m. Individual grain boundaries are generally not visible in transmitted light because of the fine grain size and the high birefringence of the dolomite crystals. Scanning electron microscope images of dolomite reveal that grains are commonly subhedral rhombs with impurities (clay, organic matter) concentrated on the boundaries (Plate 3-1). Even massive dolomite domains contain isolated local pods and lenses of clay minerals. Coarse mica phases are also present and include muscovite, biotite, and iron-rich and iron-poor chlorite.

### 3.3.2 Vugs

Vugs are present within most samples of the Culebra core. They can be divided into two broad classes and a number of subclasses. Small vugs (<0.5 mm) are associated with the clean massive dolomite domains and are probably formed during a secondary recrystallization of the primary, more organic-rich dolomite. These micro-vugs are extremely clean, containing no associated phases or halos. Larger vugs (1 mm to 1 cm) are extremely

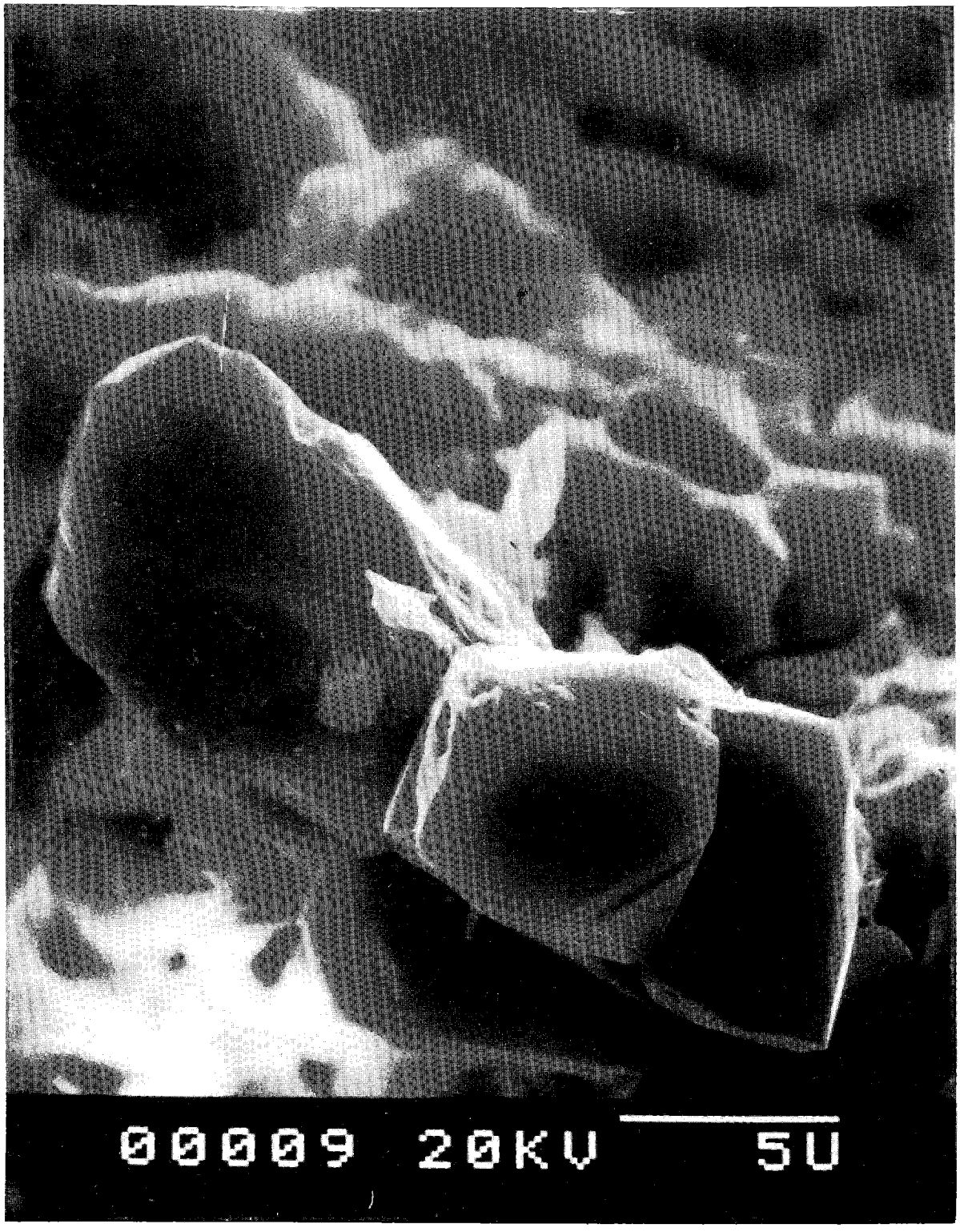


Plate 3-1. Scanning electron microscope image of dolomite showing subhedral rhombs (Sample R7, WIPP-19 borehole, 850 ft depth).

heterogeneous in appearance. These vugs are generally associated with fractures and quartz/clay-rich layers in the Culebra samples. They occur most commonly near the intersections of fractures and quartz/clay-rich horizons, but they are relatively common near fractures or quartz/clay layers alone.

Vugs of the second broad class may be either empty or partially or completely filled with a secondary precipitate. Three types of vug-fillings have been identified in these samples: a mixture of impure dolomite and organic matter, clean dolomite, and gypsum.

Several mechanisms may contribute to the origin, enlargement, and filling of vugs. If they are primary, they may represent the locations of spherical nodules that have since dissolved. The coalescence of vugs to form a spongy "boneyard"-like structure, such as in the Culebra core from WIPP-29, suggests that some vugs are enlarged by dolomite dissolution. If vugs are dissolutional in origin, the association of vugs with clay-rich layers suggests enhanced dissolution in which the clay-rich layers may be zones of increased permeability.

Another vug-forming process can be inferred from a careful examination of vuggy sections of samples from core H-3B3 in thin sections and by SEM. In plane light microscopy, under low magnification (40 x), many of the vugs in the buff-colored dolomite appeared to be surrounded by dark "halos." These halos have the following characteristics:

- A much finer-grained dolomite than that seen in the surrounding lighter-colored matrix, which is also composed of fine-grained dolomite but with a distinctly larger grain size.

- An abundance of tiny black specks in the "halos" in the fine-grained dolomite (observed at 630 x magnification), probably organic carbon (based on their apparent volatilization upon exposure to the electron beam during scanning electron microscopy).

- Amorphous yellowish-brown material, possibly organic matter.

- Silt-size quartz grains present in greater abundance than in the surrounding matrix dolomite, as well as fragments of potassium feldspar, hematite, and rare glauconite.

The visual appearance of these features as seen under the microscope and their textural and mineralogical composition (finer grain size, presence of detrital components, organic matter, and the observation of glauconite) suggest that the origin of the vugs may be related to biological activity such as burrowing, perhaps accompanied by microbial activity such as sulfate reduction.

### 3.3.3 Fractures

Virtually all recovered Culebra core samples display fractures to some extent (Plate 3-2). A wide variety of fracture types and fracture fillings can occur, even within a single sample. Fractures range from narrow, almost imperceptible structures, defined by subtle halos or selvages, to broad gypsum-filled structures. Certain horizons within the Culebra, as noted previously, have been completely rubbled by fracturing; such fractures have probably been an important pathway for exposure of the dolomite to a variety of fluids. The following is a summary of the most common varieties of fracture types observed in the Culebra dolomite.

- Gypsum-filled fractures: These are relatively continuous fractures that are completely or partly filled by gypsum. They typically have little or no edge effects or selvages but may have minor concentrations of clay minerals along the fracture walls. Gypsum-filled fractures typically occur at relatively high angles to bedding and are usually associated with gypsum-filled vugs and cavities.

- Clay-lined fractures: These fractures are defined by narrow concentrations of brown/black clay-rich material with little or no open space along the fracture. They display extremely irregular, convoluted shapes somewhat similar to carbonate stylolites. Several of these features cut, terminate against, or grade into gypsum-filled fractures, and some appear to have been subsequently filled by gypsum. They are generally not associated with selvages, halos, or other edge effects.

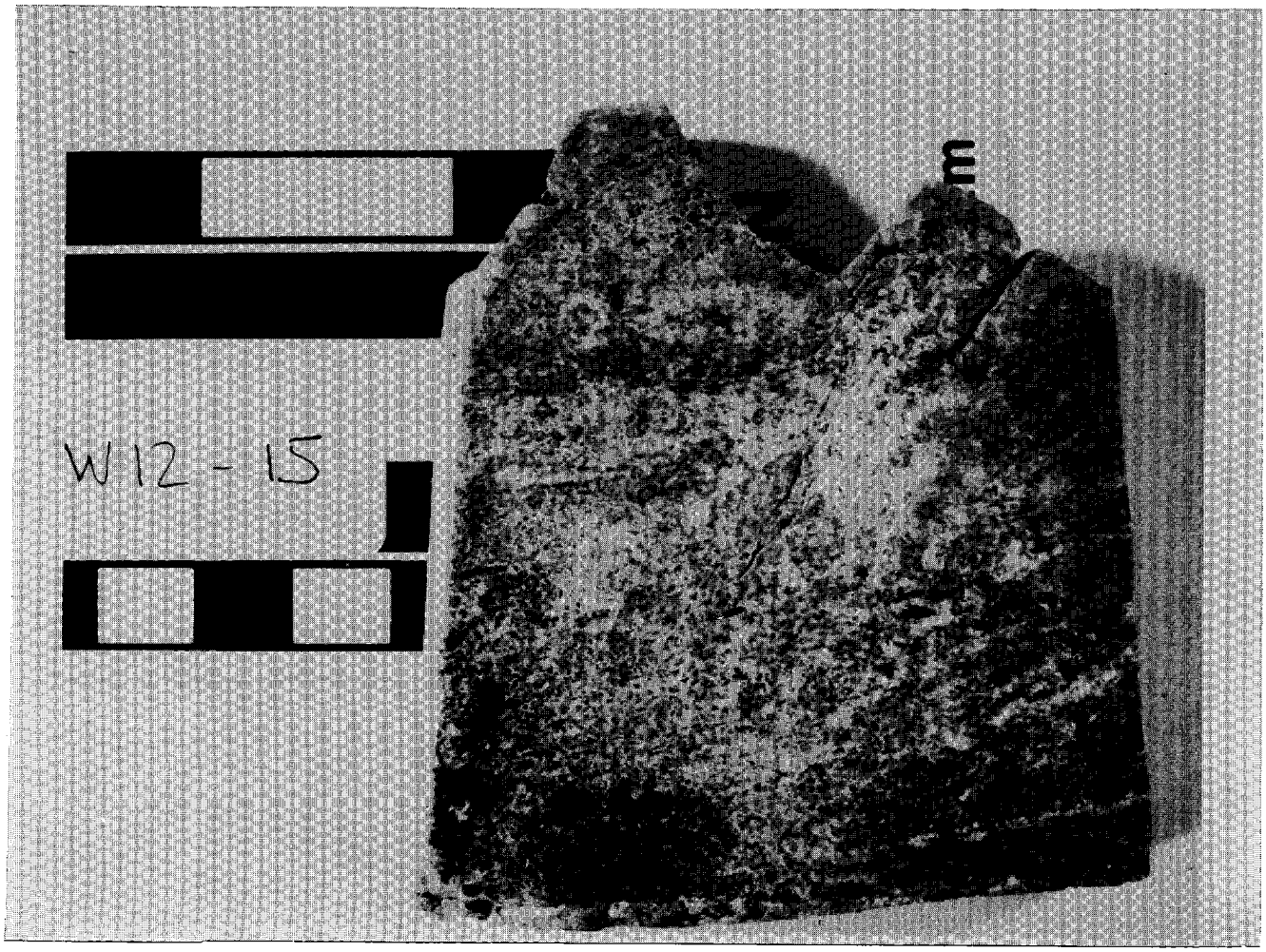


Plate 3-2. Culebra dolomite showing typical association of fractures and vugs in intact core (sample W12-15, WIPP-12 borehole, 840.6 ft depth).

- "Healed" fractures: These fractures appear as a string of tiny holes within clean dolomite, giving the appearance that an original fracture has been healed by precipitation of secondary dolomite. These are typically associated with empty vugs along their length. Of all fracture types, these are characterized by the most pronounced edge effects. They are surrounded by zones of coarser, clean dolomite (that possibly represents secondary, reprecipitated dolomite), which are, in turn, surrounded by halos of dark (possible organic-rich) material.

- Fractures along clay-rich layers: Most of the relatively thick (1 to 2 cm) clay-rich layers in the Culebra member are associated to some degree with fractures. These fractures are irregular, almost anastomosing, in shape, and they occur at somewhat irregular intervals along the clay-rich layer. In many cases, the fractures are associated with the darkest, most clay-rich parts of the quartz-clay layers. Although some of these fractures may have formed during drilling and thin-section preparation, others show evidence of having locally accumulated gypsum, clay, or clean dolomite and are, therefore, a significant feature in the dolomite. These fractures are important because they suggest that fluids may have been preferentially channeled through clay-rich regions in the dolomite and, thus, may have an increased opportunity to interact with the clay minerals.

- Open (possibly fluid-bearing) fractures: Obviously the most important type of fractures in the Culebra member are open fractures that show evidence of fluid transport (Plates 3-3 and 3-4). These fractures are not visible in thin section, since the core sections are invariably broken along their surfaces. XRD analyses of powders obtained from scraping the fracture surfaces show that they are lined with powdery dolomite and calcite, clay, quartz, and gypsum, in varying proportions. It is not possible to estimate the width of these open fractures in situ, as the adjoining core sections separate on extraction from the drill casing.


Plate 3-3. Culebra dolomite showing fracture developed across core axis. Note outer edge of core, circular in cross section. Core commonly separates along such fractures upon extraction from the core barrel (sample W12-12; WIPP-12 borehole, 838.6 ft depth).

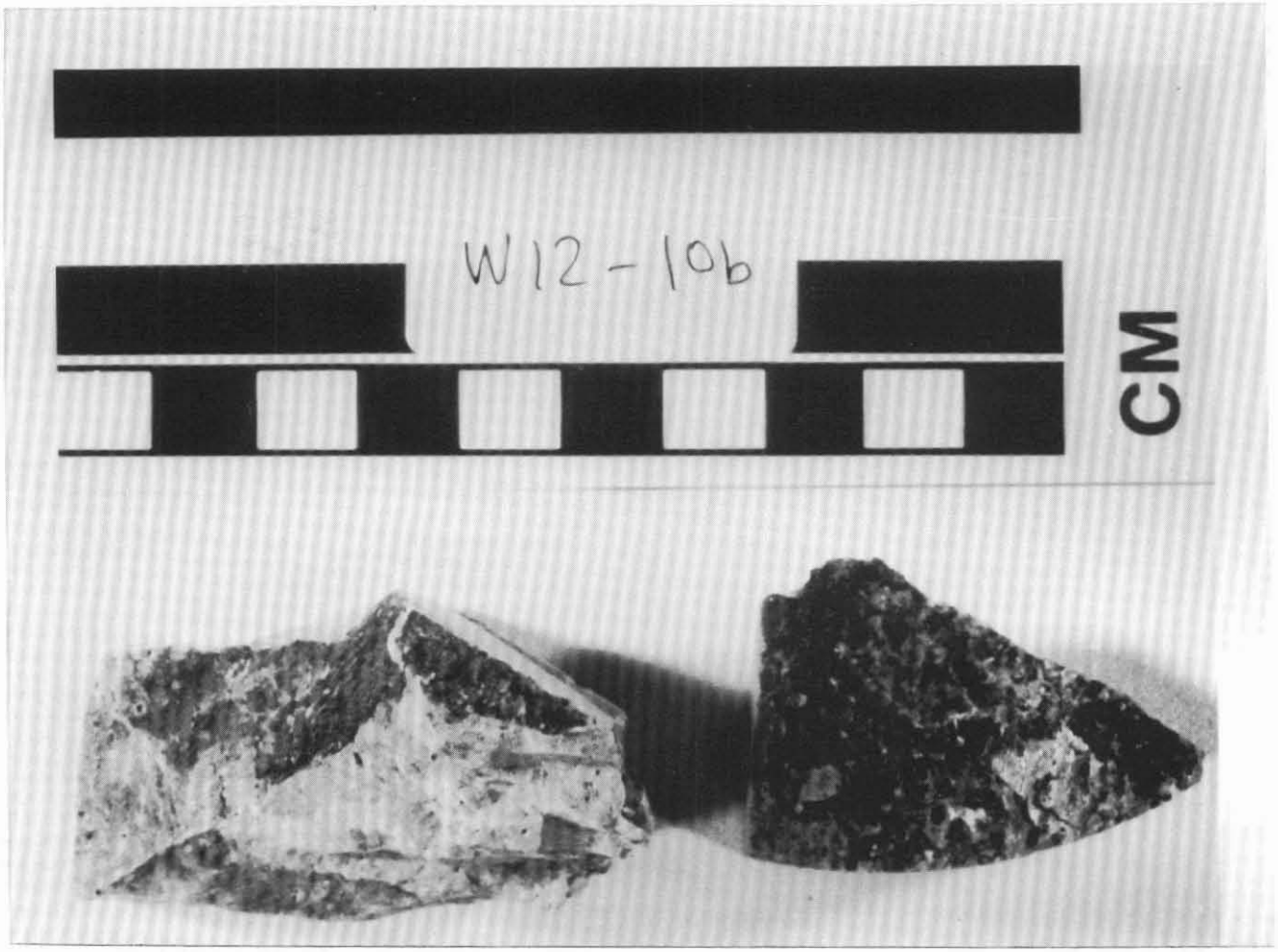


Plate 3-4. Fragments of core separated by natural fractures. Such fragments commonly contain fine-grained powdery mineralization on fracture surfaces. Extremely high local fracture density results in complete rubblization of core recovered from the core barrel (sample W12-10b, WIPP-12 borehole, 837 ft depth).

Many Culebra core samples contain several fracture types within a relatively small area. Within a single thin section, for example, gypsum-filled fractures, clay-rich fractures, and open fractures typically exhibit cross-cutting relationships.

# 3.4 MINERAL COMPOSITION

## 3.4.1 Dolomite

The composition of dolomite in six different samples, five from the WIPP-12 core and one from the H-6B core, was obtained by EMX. The iron content in all samples examined is quite low, the maximum being 0.23% FeO. The calcium-to-magnesium ratios for these samples, for six non-evaporite dolomites, and for four other evaporite dolomites (Goldsmith and Graf, 1958) are plotted in Figure 3-4. Analyses 1 through 10 are from Goldsmith and Graf (1958); Culebra samples (analyses 11 through 16) are from Sewards, Williams, and Keil (1991). This figure shows that the Culebra dolomite compositions have a Ca/Mg ratio of about 1.05, intermediate between that of other evaporite dolomites (usually less than 1.0) and that of non-evaporite dolomites (usually above 1.1).

It should be noted that the Ca/Mg ratios from Goldsmith and Graf (1958) were determined by XRD, rather than EMX analysis. The determination of Ca/Mg ratios in dolomite by electron microprobe analysis is highly accurate. However, this technique involves the examination of a very small sample area, on the order of only a few thousand unit cells. Therefore the precision of this method may be variable and may depend on the number of points analyzed on any one sample, among other factors. The XRD technique for Ca/Mg analysis of dolomites examines a much larger number of crystallites in any given sample; thus, the analytical statistics (precision) are better than the microprobe determination, but the accuracy is not as good. Additional details are given by Sewards, Williams, and Keil (1991).

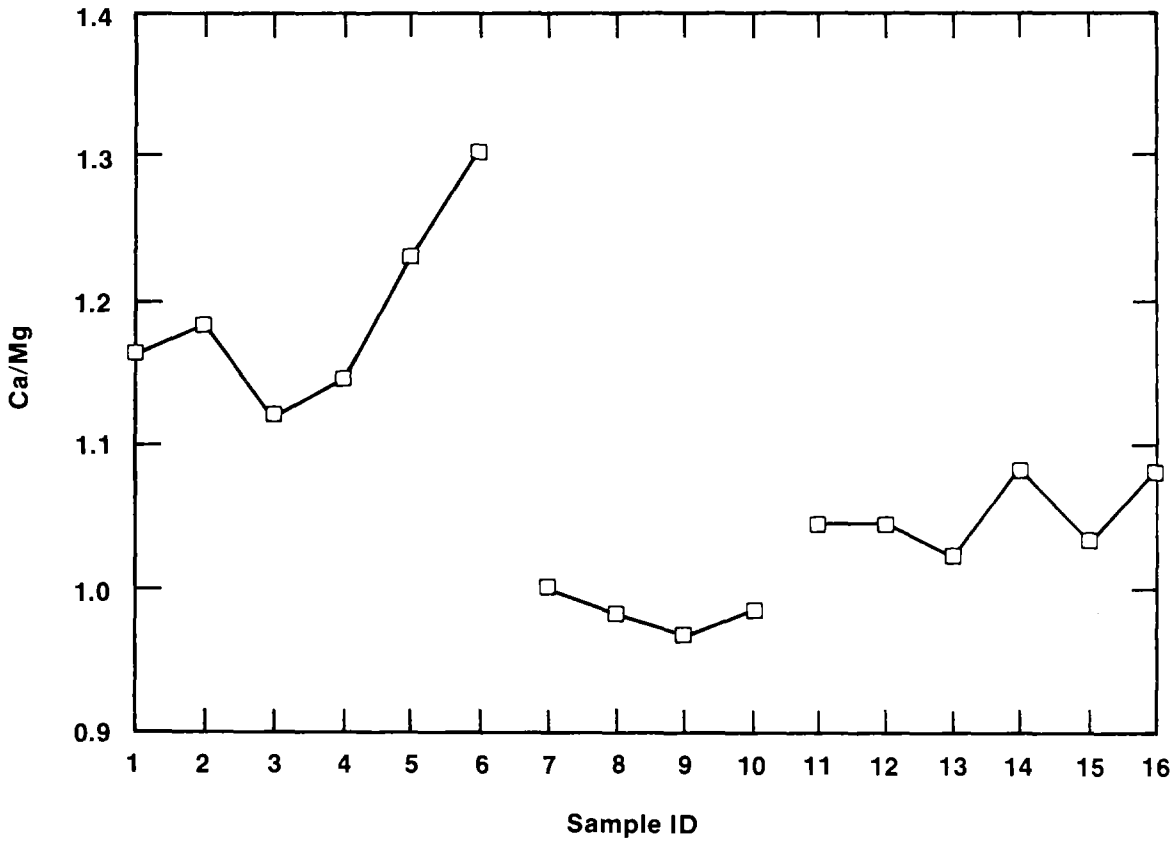


| | | |
|---|---|---|
| 1 | G-1322 | Galena Platteville Formations, Ordovician, Oglesby, Illinois |
| 2 | G-1331 | Edgewood Dolomite, Silurian, Pike County, Illinois |
| 3 | G-1181 | Cogollo Formation, Cretaceous, Venezuela |
| 4 | G-379 | Inglis Member, Moodys Branch Formation, Upper Eocene, Levy County, Florida |
| 5 | G-1055 | Avon Park Formation, Middle Eocene, Levy County, Florida |
| 6 | G-1138 | Funafuti (Pacific Island Core) Depth 840 Feet |
| 7 | G-1387 | Anhydrite-Dolomite Rock, Permian, Yorkshire |
| 8 | G-1187 | Salina Formation, Silurian, Michigan |
| 9 | G-1121 | Evaporite Sequence, Saskatchewan |
| 10 | G-1374 | Edwards Formation, Early Cretaceous, New Mexico |
| 11 | WIPP-12 | #1 |
| 12 | WIPP-12 | #2 |
| 13 | WIPP-12 | #9 |
| 14 | WIPP-12 | #12 |
| 15 | WIPP-12 | #16 |
| 16 | H-6B | #4 |

TRI-6342-478-0

Figure 3-4. Ca:Mg ratios for various dolomites.

Microprobe analyses show the presence of an average of 0.004 atoms of Fe per dolomite cell. The Ca/Mg ratios and Fe content imply that the dolomite structure is disordered, i.e., there is not a strict alternation of calcium and magnesium layers along the c axis of the structure. Disorder in a crystal structure affects thermodynamic parameters such as the Gibbs free energy of formation, enthalpy, and entropy of formation (Carpenter, 1985; Landau and Lifshitz, 1958; de Fontaine, 1979). Reeder and Wenk (1979) and Reeder (1981) have shown that low-temperature calcian dolomites commonly show exsolution features when examined under the transmission electron microscope, suggesting the presence of two phases. Reeder (1981) suggests that one of the two phases present may be a stoichiometric dolomite, while the second is disordered and calcium rich. As discussed in Siegel et al. (Chapter 2), calculations of dolomite saturation indices for Culebra water samples are hindered by lack of reliable values for the free energy of the Culebra dolomite. Non-stoichiometry and disorder of dolomite in the Culebra would contribute to uncertainties in the Gibbs free energy of formation.

### 3.4.2 Calcite and Gypsum

EMX analyses of samples from the WIPP-19 core (Sewards, Glenn, and Keil, 1991) show that calcite found at the top of the Culebra is nearly pure, with less than 1% total MgO + FeO. Similarly, numerous analyses of gypsum from various samples in this study show that it is pure $CaSO_4 \cdot 2H_2O$; all other elements measured were below detection limits.

### 3.4.3 Clay Mineralogy

Clay fraction (<2 $\mu$m) separates were obtained from three samples and analyzed by XRD using oriented mounts to identify the clay minerals present and to determine the modes of each clay mineral. The XRD analyses showed that the clay minerals present were corrensite (ordered mixed-layer chlorite/smectite), illite, serpentine, and chlorite. The most abundant mineral was corrensite, usually constituting approximately 50 weight percent of the total clay fraction, followed by illite. Serpentine and chlorite were relatively minor components.

AEM was used to examine the textural relationships between the different clay minerals. Illite, serpentine, and chlorite were easily imaged and showed the typical morphologies of these minerals. These phases have well-ordered basal periodicities and good crystalline structure for up to 400 Å in the basal direction. Energy dispersive spectrometer spectra of these phases confirm the clay mineral identification made on the basis of XRD analyses. In general, corrensite expanded layers are very difficult to image because of rapid damage rates and poor diffraction contrast. Nevertheless, examples of image contrast consistent with intercalated corrensite were obtained (Plate 3-5). Regular alteration of 14 Å and 18 Å layers is typically restricted to two or three repeats, and in some instances, the variable extent of layer expansion due to intercalated laurylamine hydrochloride (the reagent used in the expansion technique) is readily seen. The presence of these very thin, or "fundamental" particles is evidence that interparticle diffraction may be responsible for the XRD peaks for corrensite (Nadeau et al., 1984).

The fact that corrensite is the dominant phase in the Culebra samples is important. Corrensite has a high cation exchange capacity (CEC) and high surface area (Grim, 1968), so it may be able to sorb radionuclides very efficiently. Although the clay minerals of only three Culebra samples (a clay-poor dolomite and a clay-rich dolomite from WIPP-12, and a shaly horizon from H-6B) were investigated in detail (Table 3-1), the semi-quantitative modal analyses of Sewards, Glenn, and Keil (1991) are comparable and show that mixed-layer chlorite/smectite is the dominant clay phase throughout the Rustler Formation in WIPP-19. It is reasonable to suggest that mixed-layer chlorite/smectite is also the most common clay phase in the Culebra. This result is not surprising, as corrensite forms from a smectite precursor, which is frequently an abundant product of weathering (Blatt, 1982).

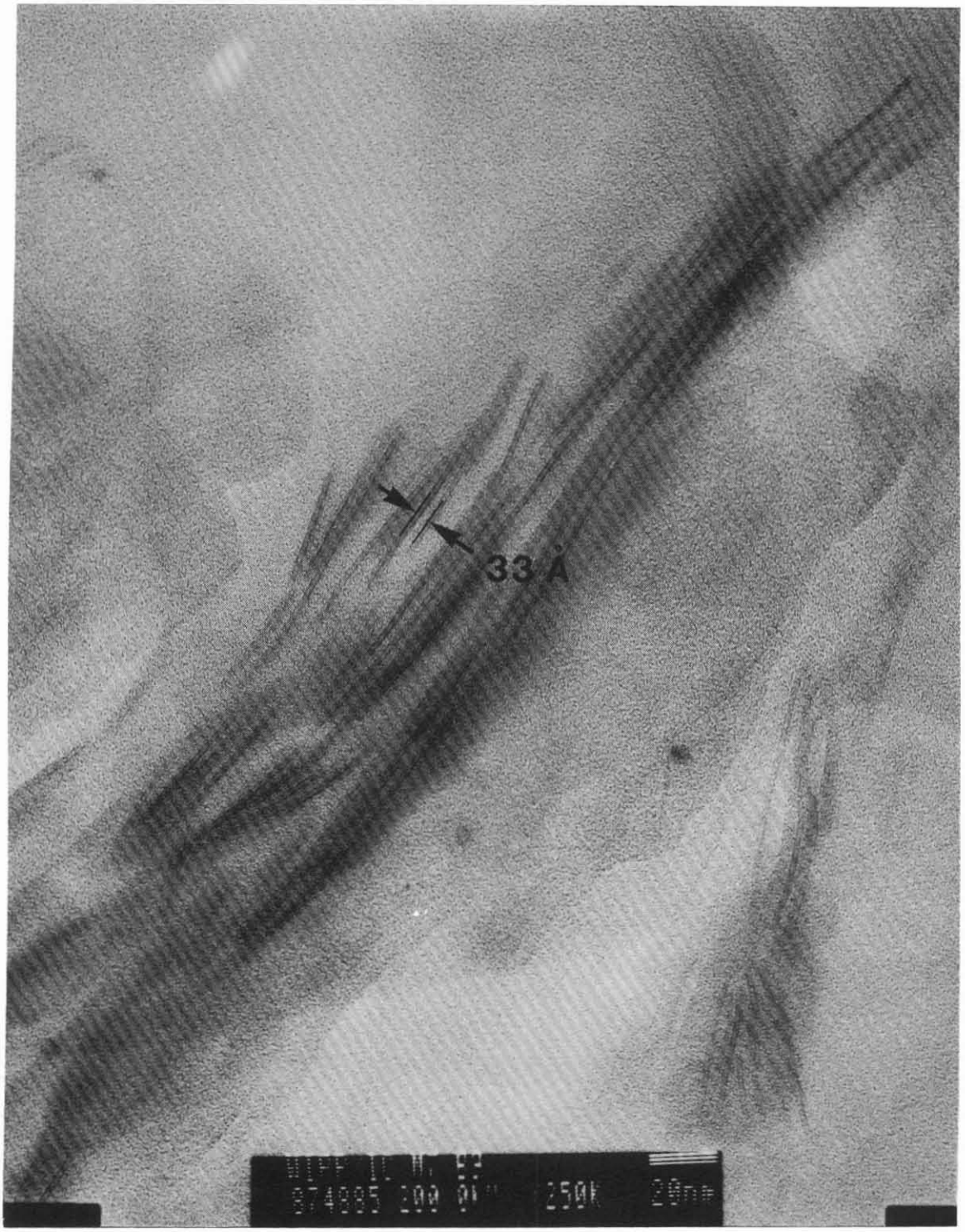


Plate 3-5. Corrensite structure revealed by analytical electron microscopy (sample H6B-3, H-6 borehole, 631 ft depth).

**Table 3-1. Clay Mineral Modal Analysis--Culebra Member**

| Sample | Corrensite | Serpentine | Illite | Chlorite |
|---|---|---|---|---|
| W-12 #3 | 58% | 3% | 34% | 5% |
| W-12 #16 | 62% | 3% | 32% | 3% |
| H6B #3 | 49% | 28% | 18% | 5% |

There is, however, a discrepancy between the results of the quantitative XRD analysis and the results of the AEM investigation of the H-6B sample. In that sample, the XRD results show that the sample contains approximately 50% corrensite. When imaging was attempted on the AEM, it was extremely difficult to find any corrensite at all; the dominant phases appeared to be serpentine, illite, and chlorite. Klimentidis and Mackinnon (1986) have noted a similar discrepancy while attempting to image mixed-layer clay minerals.

# 3.5 DIAGENETIC INTERPRETATION

## 3.5.1 Carbonates

As shown in Figure 3-4, the Ca/Mg values for Culebra dolomites range from approximately 1.05 to 1.09, slightly higher than the values taken from the literature for other evaporite dolomites and slightly lower than the Ca/Mg ratios for non-evaporite dolomites. If we assume that the present-day Culebra represents postdepositional dolomitization of originally calcitic sediments, this observation may reflect a diagenetic brine composition with a Ca/Mg ratio atypical of an evaporite environment. However, isotopic evidence (Lambert and Harvey, 1987) is not consistent with a hypothesis of later dolomitization of primary calcite, but is more consistent with evaporitic dolomite formation (Parry et al., 1970). The Ca/Mg content of the brine responsible for the Ca/Mg ratios in the Culebra dolomites may have resulted from postdepositional mixing with nonmarine (fluvial) higher-Ca water in the Delaware Basin. Alternatively, the higher Ca/Mg ratios in Culebra

dolomites may reflect a tendency for $Mg^{2+}$ in dolomitization brines to be preferentially incorporated in detrital clay minerals and authigenic Mg-rich clay species (Bodine, 1978; 1983).

### 3.5.2 Sulfates

The sulfate minerals found in the Culebra samples examined in this study are gypsum, anhydrite, and bassanite ($CaSO_4 \cdot \frac{1}{2}H_2O$). EMX elemental analysis of gypsum in these samples indicates that it is almost pure $CaSO_4 \cdot 2H_2O$; all other elements were below detection limits.

Mineralogical and textural evidence from all samples examined here suggests that gypsum formation is predominantly, if not exclusively, secondary. Harville (1986) reports the occurrence of secondary gypsum as detrital clasts, identified by their parallel orientation to bedding. Much more commonly (as, for example, in observations of thin sections from WIPP-19 and H-3 samples), gypsum occurs as acicular, bladed, or sheaf-like crystals randomly oriented with respect to bedding; this mode of occurrence strongly suggests replacement of anhydrite by gypsum. Also, all gypsums studied by Lambert (Chapter 5) have characteristically meteoric, not marine, $\delta D$ values.

Whether the anhydrite occurred as a primary phase is problematical. The petrographic evidence necessary to resolve this question, mainly regarding structural deformation on a microscopic scale caused by the large volume change between gypsum and anhydrite, was beyond the scope of the present study. The occurrence of secondary gypsum, frequently as selenite, filling veins, vugs, and fractures in the dolomite, is commonly observed. In the thin section study of WIPP-19 and H-3 samples, not only was the replacement of anhydrite by gypsum frequently observed; but occasionally this secondary gypsum was, in turn, partially inverted to anhydrite, possibly as a consequence of burial depth, temperature increase, and/or increasing ionic strength of diagenetic solutions.

Gypsum was also observed (in WIPP-19 and H-3 thin sections) to be partially replaced by magnesite crystallites; the presence of inferred remnant algal material in these sediments suggests the former presence of an indigenous microbial population and an environment that may have supported bacterial sulfate reduction. The presence of pyrite in Culebra samples (as observed by Harville, 1986) from H-3, H-4, and H-6 suggests that pyrite-bearing horizons in the Culebra have not been exposed to water recharged from the atmosphere, especially under the present hydrologic regime, whereas other Culebra horizons contain such water. This attests to the nonuniform permeability of the Culebra.

The presence of bassanite ($CaSO_4 \cdot \frac{1}{2}H_2O$), observed by Harville (1986) in samples from H-2, H-3, and H-4, is problematical. "Hemihydrate, $CaSO_4 \cdot \frac{1}{2}H_2O$, as a mineral (bassanite) in salt deposits is dubious. It is clear from laboratory experiments that hemihydrate plays an important role and in a fine crystalline form it may be mistaken for anhydrite" (Braitsch, 1971). Furthermore, "the hemihydrate ... exist[s] only metastably. Thus under equilibrium conditions the reaction [governing the transition from gypsum to anhydrite by dehydration] occurs without the formation of intermediate compounds" (Deer et al., 1962). The possibility that metastable hemihydrate of calcium sulfate may have formed as an artifact of thin section preparation cannot be dismissed. Clearly, however, both the sulfate and carbonate mineralogical components of Culebra samples illustrate a complex diagenetic history.

### 3.5.3 Clays and Clay Mineral Genesis

The origin of the clay mineral species now found in the Culebra dolomite is of importance because clay minerals are very sensitive to changes in their environment. In particular, fluids that come into contact with them can cause them to change both their structure and composition. Palmer (1981; also see Bodine, 1985) concluded that the detrital clay mineral assemblage that was deposited in the Permian Delaware and related basins included dioctahedral smectite, mixed-layer illite/smectite, illite, kaolinite, and clay chlorite. These clay minerals reacted with the various brines and pore fluids in contact with them to form the species that we now observe. The generalized mechanisms of clay-mineral alteration in

evaporite environments, inferred by Palmer and possibly relevant to the Rustler, are summarized below.

Because the interlayer space of illite is fixed with potassium ions, this phase is relatively stable, especially at low temperatures. However, in a very magnesium-rich environment that is clearly out of the illite stability field, illite crystallites may react with the pore fluid that surrounds them, especially on a time scale of millions of years. The extent to which this reaction occurs is dependent on illite particle size and degree of crystallinity. In general, because the CEC of illite is approximately an order of magnitude less than for the smectite-type clays, it is probable that at least some portion of the observed illites is little changed from those that were deposited in Permian times.

Dioctahedral smectite, a far more reactive phase than illite, undergoes a more radical transformation. The pore fluids in the original sediments constituted an "infinite reservoir" (relative to the volume of clay present) for magnesium, if the pore fluid had evolved from near-normal seawater evaporation. This magnesium replaced aluminum in the original smectite octahedral layers, while aluminum replaced silicon in the tetrahedral layers. Concurrently, brucite hydroxide layers were deposited in some of the interlayer spaces. The result is a mixed-layer chlorite/ smectite; if the ratio of chlorite to smectite layers is 1:1 and the stacking sequence is ordered, the product is corrensite.

Mixed-layer illite/smectite would undergo a similar transformation. The smectite layers not fixed by potassium would take up magnesium from the interstitial fluid. Some of the interlayer spaces would accept brucite hydroxide layers, while the illite layers would remain essentially unchanged. The result would be a mixed layer illite/smectite/chlorite, with diffractograms very similar to that of mixed-layer chlorite/smectite, provided the percentage of illite layers is small. Therefore, it is not possible, based on XRD analysis alone, to determine the presence of mixed-layer illite/smectite/chlorite.

Serpentine may be formed by direct transformation from kaolinite; magnesium replaces some of the aluminum in the octahedral layer, while aluminum replaces some of the silicon in the tetrahedral layer, in order to maintain the charge balance. The result is a serpentine with a composition similar to that of amesite.

Given the presence of authigenic quartz and potassium feldspar in Rustler Formation samples, plus textural evidence from lattice fringe images obtained on the AEM, these reactions apparently occurred layer by layer (Bethke and Altaner, 1986). Tetrahedral and octahedral layers were not destroyed. Their composition is altered, but the bulk volume of clay remains essentially constant. It is reasonable to suppose that this general mechanism is largely responsible for the composition of the clay species now observed in the Culebra.

However, the nature and extent of reactions between present-day Culebra waters and clay minerals remains to be examined. Again, lack of abundant data precludes writing explicit reactions, as knowledge of the initial conditions (original detrital clay species) is limited at best. Data on clay species from H-6B versus WIPP-12 show considerable variation in relative amounts of corrensite, serpentine, chlorite, and illite. The paucity of such data renders a regional-scale extrapolation impossible, but these data suggest that the distribution and relative amounts of clay species are variable on a regional scale.

The present Culebra water probably has not participated in the mechanism in which Mg uptake fills octahedral sites in a clay structure to yield the observed mineralogy. While this type of reaction may satisfactorily explain the observed mineralogy (Mg-silicates and authigenic quartz), the kinetics are necessarily very slow, on the order of tens of millions of years. The Pleistocene age of Culebra water (Lambert, Chapter 5) is much shorter than the time required for such reactions. Cation exchange is a more probable mechanism, because it involves appropriately faster reaction kinetics.

Whereas cation exchange between Rustler clay minerals and Culebra fluids may have been in part responsible for the observed clay assemblages, it is highly improbable that the

mechanism of cation exchange would have significantly influenced the observed major-solute ($Na^+$, $K^+$, $Ca^{2+}$, $Mg^{2+}$, $Cl^-$, $SO_4^{2-}$) chemistry of the present-day Culebra water. Two observations are consistent with this hypothesis. First, the observed Culebra fluid compositions assumed to be in contact with these clays contain significant yet highly variable (unbuffered) amounts of Mg and K in brines ranging from 0.1 M to 3 M NaCl (Siegel et al., Chapter 2). Second, the volume of fluid is inferred to be large relative to the mass of minerals containing exchangeable constituents accessible to the groundwater (Lambert, Chapter 5). However, ion exchange involving clay minerals may exert more significant control on the concentrations of the minor elements.

## 3.6 TIMING OF DIAGENETIC EVENTS

During the time of deposition of the Upper Ochoan units, the Delaware Basin was probably a broad, flat topographic depression that received periodic influxes of fresh water. One indication of this occurs in observable exposures, such as the outcrops of the collapsed Culebra (Bachman, 1980) along the Pecos River and in largely intact sections in the WIPP shafts (Holt and Powers, 1988). The presence of stromatolite-like structures in such localities suggests that at least a portion of the Culebra unit may have existed originally as a reefal deposit and therefore developed within the upper part of the photic zone. Thus, the depth of the Delaware Basin at this time probably did not exceed ~10 m. The present-day Rustler mineralogy, which includes gypsum/anhydrite, halite, and dolomite, is a typical marine evaporite suite and indicates evaporation from a closed basin. The periodic addition of fresh water (either fresh seawater or as fluvial input) into the Delaware Basin during Rustler time is suggested by the lack of a well-developed suite of soluble bittern salts or potash mineralization. Potassium and magnesium evaporite minerals would have been removed by periodic contact with solutions undersaturated with such minerals, although polyhalite has been found in the Rustler (Snyder, 1985). Also, addition of water from external sources probably concentrated detrital clay residues by dissolution of underlying sediments and imported clastics. These clay residues and accumulations are visible

now as thin stringers, laminae, or discrete seams within the dolomite as well as in other Rustler units.

A comprehensive discussion of the paragenesis or absolute timing of the dolomite mineralization relative to an original Culebra precursor such as calcite is not within the scope of this study. It is sufficient to note that this event required a solution high in $Mg^{2+}$, a condition easily satisfied in a shallow basin undergoing rapid evaporation. At the same time, the concurrent concentration of $Ca^{2+}$ and $SO_4^{2-}$ resulted in the precipitation of gypsum, largely depleting the solution in $Ca^{2+}$. The texture, structure, and mineralogy of the vugs in Culebra dolomite indicate the possibility that at least some portion of them formed early in the diagenetic sequence and may have been filled at approximately the same time.

Because the gypsum-anhydrite transition occurs at relatively low temperatures and pressures, it is possible that many cycles of replacement of one by the other occurred. Thin section descriptions of Culebra samples contain many examples of anhydrite pseudomorphs after gypsum and gypsum replacement of anhydrite. Moreover, many microscale examples of gypsum and/or anhydrite replacing dolomite have also been noted, which may be taken as further evidence that dolomitization preceded formation or remobilization of some of the calcium sulfates.

Subsequently, gypsum dissolution and reprecipitation may have occurred numerous times; it is not possible to discriminate between episodes simply by petrographic observation of textural relations. Possibly these episodes could be distinguished by detailed isotopic analyses (Lambert, Chapter 5). The reaction kinetics of gypsum formation are relatively rapid and occur readily at surface temperatures and atmospheric pressure. While it is reasonable to infer from textural information that some of the sulfate precipitation (as noted above) must have been early, it is also highly likely that much of it (such as fracture fillings) is postdepositional.

The increasing $Mg^{2+}$ content in a concentrated-seawater brine also apparently reacted with the clay residues. Illite, the most common continental detritus, is still identifiable in Culebra samples. In addition, it appears that other members of the dioctahedral suite (kaolinite, smectite) altered to Mg-enriched phases, primarily serpentine and mixed-layer chlorite/smectite (corrensite). Although it is not possible to write explicit reactions to explain the clay mineral alteration sequence, it appears that the silicate reactions resulted in the release of free silica, aluminum, and potassium. Evidence for clay reactions proceeding in this direction is provided by the occurrence of euhedral authigenic quartz and potassium feldspar. No direct evidence is available to establish the time that clay alteration began early in the diagenetic history of the Culebra. However, the kinetics of silicate alteration at low temperatures and pressures are sufficiently slow that the reactions described in preceding sections--i.e., uptake of $Mg^{2+}$ by detrital clays, formation of Mg-rich clay phases, and precipitation of authigenic quartz and feldspar--must have taken place over many millions of years. Given that the minimum age of isolation from the atmosphere of Rustler waters is ~12,000 years (Lambert, Chapter 5), it is not likely that $Mg^{2+}$-exchange between rock and water involved the water presently found in the Culebra, nor are such reactions likely to have influenced the presently observed Culebra major-solute geochemistry (Siegel et al., Chapter 2).

## 3.7 SUMMARY

The Culebra member of the Rustler Formation is mineralogically and texturally heterogeneous, both vertically and horizontally. The predominant mineral is dolomite, but clay, quartz, gypsum, and calcite are geologically significant, although in some cases minor, constituents of the unit. Trace minerals include phyllosilicates of low-temperature metamorphic/metasomatic origin, halite (possibly a residue of drilling brine), feldspar, and (locally) pyrite.

Dolomite in the samples examined in this study forms an equigranular microcrystalline mosaic, in which individual grains are subhedral rhombs, typically 5 $\mu$m in equivalent

diameter, but varying from 2 to 20 $\mu$m. Dolomite compositions have an average calcium to magnesium ratio of 1.05 and an average of 0.004 atoms of iron per unit cell. The origin of the dolomite may be the result of early-stage dolomitization of chemically sedimented calcite deposited in shallow waters, but an evaporitic origin is more consistent with the stable-isotope data. Algal mats probably formed what is now interstitial organic matter that is mixed with clay. The dolomite content of samples examined in this study ranges from a few percent to nearly 99% of the total. The majority of these samples had 80% or more dolomite. The sample selection may have been biased in favor of intact core whose depth was precisely known and biased against horizons of poorer core recovery that are more likely to have contained water.

The next most abundant constituent of the Culebra is clay. Because it is concentrated along textural features, particularly the surfaces of open fractures (i.e., surfaces of core separation) and vugs, it may be particularly important to the characterization of solute transport within the unit. Clay abundances range from less than 1% to nearly 60% of bulk samples, the latter representing clay-rich, dolomite-poor horizons. Within the "massive" (intact, less fractured) samples, there are domains parallel to bedding that alternate between clay-rich and clay-poor compositions; these domains give the massive dolomite samples a laminated appearance. Organic matter is intimately associated with the clay in all the samples and gives the mixture a dark brown to black color.

The clay mineral assemblage includes four minerals: corrensite (ordered mixed-layer chlorite/smectite), illite, serpentine, and chlorite. Corrensite is the dominant clay mineral, usually constituting about 50% of the clay assemblage; illite is the next most abundant constituent, and serpentine and chlorite are relatively minor components. Because of its high CEC, the corrensite is particularly important. Corrensite might be an effective sorbent of radionuclide cations in the event of a breach in the WIPP Facility. The remaining clay minerals have much lower CECs.

Gypsum is present largely as a vein- and vug-filling cement. It is probably almost entirely of secondary origin, the product of the gypsification of the anhydrite in the Tamarisk member overlying the Culebra and the remobilization of the resulting gypsum into the Culebra. Such local-scale remobilization is consistent with the gypsum D/H ratios (Lambert, Chapter 5). Surfaces of open fractures examined by XRD show the presence of gypsum, and fluids moving through the unit are probably saturated with gypsum. This is consistent with the calculated gypsum saturation indices for Culebra waters (Siegel et al., Chapter 2). Except for one sample in the WIPP-12 core, gypsum rarely exceeds 10% of the bulk in these samples; it is typically much less than that in intact core, but may have been greater in horizons of higher permeability and poorer core recovery. EMX elemental analysis of gypsum in the Culebra samples shows that it is almost pure $CaSO_2 \cdot 2H_2O$; all other elements that might have been present were below detection levels.

Calcite is abundant in the WIPP-29 core, where it is a major component of the top part of the core. Calcite there is interpreted to be of secondary and possibly in part surficial origin, produced to some degree by dedolomitization of dolomite by calcium-rich (possibly gypsum-saturated) waters of meteoric origin. Thin layers of calcite in samples from the WIPP-19 core are microcrystalline; the crystals form a mosaic pattern that is very similar in appearance to the micritic dolomite of adjacent horizons in the same borehole. EMX analyses of a sample from the WIPP-19 core show that calcite is nearly pure $CaCO_3$ with less than 1% total MgO + FeO.

Two texturally important features of samples from the Culebra are vugs and fractures. Vugs appear to have been formed by dissolution, and some are filled with secondary gypsum, dolomite, and clay, although those connected with open fractures usually remain empty. The most important type of fracture in these samples is that bearing evidence of fluid movement along its surfaces. The surfaces of these fractures are coated with clay, powdery dolomite, calcite, and gypsum. The minerals on these surfaces might interact directly with radionuclide-bearing brines in the event of a low-pressure breach in the WIPP Facility.

# 3.8 CONCLUSIONS

Analyses of samples from 12 cores through the Culebra member of the Rustler Formation show the primary constituents to be dolomite, calcite, gypsum, anhydrite, quartz, and clays. The dolomite is disordered, as inferred from a Ca/Mg ratio of approximately 1.05, as well as trace amounts of Fe. Both the calcite and gypsum are relatively pure phases, containing insignificant quantities of Mg and Fe; their compositions and modes of occurrence suggest that these phases are secondary in origin. Textural evidence, from thin-section studies, shows that the gypsum-anhydrite transition occurred numerous times throughout the Culebra diagenetic history, possibly in response to varying burial depth, temperature, and/or ionic strength of interstitial solutions.

Clay minerals constitute typically 3 to 5 weight percent of the bulk sample mineralogy. Species present are (in approximate order of decreasing abundance) corrensite, illite, serpentine, and chlorite. Other workers have explained this Mg-enriched clay mineral suite as the product of diagenetic reactions between detrital clays and concentrated brines that occurred relatively early in the burial history of the Delaware Basin. The paucity of data on clay mineral species and distribution do not permit a comprehensive discussion of the potential effects of ongoing diagenetic reactions between the observed Culebra brines and clays. The most probable mechanisms involved in clay alteration are substitution into octahedral sites and cation exchange. The first has relatively slow reaction kinetics. Due to the relatively young (Pleistocene) age of the waters now in contact with this suite of clays and the relatively small volume ratio of reactive clays to brines, it seems improbable that the clay mineral assemblage observed in the portion of the Culebra examined in this study exerts a significant influence on major solutes in the present-day Culebra water compositions. However, the kinetics of cation exchange and the mineral/water ratios may be consistent with control of some minor solutes by the clays.

Variations in the NaCl content of Culebra groundwaters were probably derived from halite-bearing strata adjacent to the Culebra. Dolomite and gypsum in the Culebra can, however, have partially dissolved to account for some of the solutes.

# 3.9 REFERENCES

Bachman, G. O. 1980. *Regional Geology and Cenozoic History of Pecos Region, Southeastern New Mexico*. Open File Report 80-1099. Denver, CO: US Geological Survey.

Bachman, G. O. 1987. *Karst in Evaporites in Southeastern New Mexico*. SAND86-7078. Albuquerque, NM: Sandia National Laboratories.

Bethke, C. M., and S. P. Altaner. 1986. "Layer-by-layer Mechanism of Smectite Illitization and Application of a New Rate Law." *Clays and Clay Minerals*, Vol. 34:136-145.

Blatt, H. 1982. *Sedimentary Petrology*. San Francisco: W. H. Freeman and Co.

Bodine, M. W., Jr. 1978. "Clay Mineral Assemblages from Drill Cores of Ochoan Evaporites, Eddy County, New Mexico." *Geology and Mineral Deposits of Ochoan Rocks in Delaware Basin and Adjacent Areas.* New Mexico Bureau of Mines and Mineral Resources, Circ. 159:21-31.

Bodine, M. W., Jr. 1983. "Trioctahedral Clay Mineral Assemblages in Paleozoic Marine Evaporite Rocks." *Sixth International Symposium on Salt*, Vol. I:267-284.

Bodine, M. W., Jr. 1985. "Clay Mineralogy of Insoluble Residues of Marine Evaporites." *Society of Mining Engineers of AIME, Process Mineralogy V: Application to the Mineral Industries.*

Braitsch, O. 1971. *Salt Deposits, Their Origin and Composition*. Berlin-Heidelberg: Springer-Verlag.

Carpenter, M. A. 1985. "Order-Disorder Transformations in Mineral Solid Solutions." *Reviews in Mineralogy*, Vol. 14:428.

Deer, W. A., R. A. Howie, and J. Zussman. 1962. *Rock-Forming Minerals, Volume 5: Non-Silicates*. London: Longman.

De Fontaine, D. 1979. "Configurational Thermodynamics of Solid Solutions." *Solid State Physics*, Vol. 34:73-274.

Ferrall, C. C., and J. F. Gibbons. 1979. *Core Study of the Rustler Formation Over the WIPP Site*. SAND79-7110. Albuquerque, NM: Sandia National Laboratories.

Goldsmith, J. R., and D. L. Graf. 1958. "Structural and Compositional Variations in Some Natural Dolomites." *Journal of Geology*, Vol. 66:678-693.

Grim, R. E. 1968. *Clay Mineralogy*. New York: McGraw-Hill Book Company.

Harville, D. G. 1986. *Petrographic Analysis of Fourteen Samples from Permian-Age Rustler Formation (Culebra Member) from Wells H2b, H3b2, H3b3, H4b, and H6b, WIPP Site, Eddy Co., New Mexico*. Report to INTERA Technologies, Inc. for Sandia National Laboratories.

Haug, A., V. A. Kelley, A. M. LaVenue, and J. F. Pickens. 1987. *Modeling of Ground-Water Flow in the Culebra Dolomite at the Waste Isolation Pilot Plant (WIPP) Site*. SAND86-7167. Albuquerque, NM: Sandia National Laboratories.

Holt, R., and D. W. Powers. 1988. *Facies Variability and Post-Depositional Alteration within the Rustler Formation in the Vicinity of the Waste Isolation Pilot Plant, Southeastern New Mexico*. DOE/WIPP-88-004. Carlsbad, NM: Waste Isolation Pilot Plant Project Office.

Klimentidis, R. E., and I. D. R. Mackinnon. 1986. "High Resolution Imaging of Ordered Mixed-Layer Clays." *Clays and Clay Minerals*, Vol. 34:155-164.

Lambert, S. J., and D. M. Harvey. 1987. *Stable-Isotope Geochemistry of Groundwaters in the Delaware Basin of Southeastern New Mexico*. SAND87-0138. Albuquerque, NM: Sandia National Laboratories.

Landau, L. D., and E. M. Lifshitz. 1958. *Statistical Physics*. Reading, MA: Addison Wesley.

Mercer, J. W. 1983. *Geohydrology of the Proposed Waste Isolation Pilot Plant Site, Los Medaños Area, Southeastern New Mexico*. Water Resources Investigation Report 83-4016. Albuquerque, NM: US Geological Survey.

Mercer, J. W., R. L. Beauheim, R. P. Snyder, and G. M. Fairer. 1987. *Basic Data Report for Drilling and Hydrologic Testing of Drillhole DOE-2 at the Waste Isolation Pilot Plant (WIPP) Site*. SAND86-0611. Albuquerque, NM: Sandia National Laboratories.

Nadeau, P. H., J. M. Tait, W. J. McHardy, and M. J. Wilson. 1984. "Interstratified XRD Characteristics of Physical Mixtures of Elementary Clay Particles." *Clay Minerals*, Vol. 19:67-76.

Palmer, D. P. 1981. "Clay Mineralogy of Permian Sabkha Sequences, Palo Duro Basin, Texas." University of Texas at Austin: unpubublished M.S. thesis.

Parry, W. T., C. C. Reeves, Jr., and J. W. Leach. 1970. "Oxygen and Carbon Isotope Composition of West Texas Lake Carbonates." *Geochimica et Cosmochimica Acta*, Vol 34: 825-830.

Reeder, R. J. 1981. "Electron Optical Investigation of Sedimentary Dolomites." *Contributions to Mineralogy and Petrology*, Vol. 76:148-157.

Reeder, R. J., and H. R. Wenk. 1979. "Microstructures in Low-Temperature Dolomites." *Geophysical Research Letters*, Vol. 6:77-80.

SNL (Sandia National Laboratories) and USGS (US Geological Survey). 1980a. *Basic Data Report for Drillhole WIPP 19 (Waste Isolation Pilot Plant - WIPP)*. SAND79-0276. Albuquerque, NM: Sandia National Laboratories.

SNL (Sandia National Laboratories) and USGS (US Geological Survey). 1980b. *Basic Data Report for Drillhole WIPP 30 (Waste Isolation Pilot Plant - WIPP)*. SAND79-0284. Albuquerque, NM: Sandia National Laboratories.

Sewards, T., R. Glenn, and K. Keil. 1991. *Mineralogy of the Rustler Formation in the WIPP-19 Core*. SAND87-7036. Albuquerque, NM: Sandia National Laboratories.

Sewards, T., M. L. Williams, and K. Keil. 1991. *Mineralogy of the Culebra Dolomite Member of the Rustler Formation*. SAND90-7008. Albuquerque, NM: Sandia National Laboratories.

Snyder, R. P. 1985. *Dissolution of Halite and Gypsum, and Hydration of Anhydrite to Gypsum, Rustler Formation, in the Vicinity of the Waste Isolation Pilot Plant, Southeastern New Mexico*. Open File Report 85-229. Denver, CO: US Geological Survey.

# CHAPTER 4:

# NORMATIVE ANALYSIS OF GROUNDWATERS FROM THE RUSTLER FORMATION ASSOCIATED WITH THE WASTE ISOLATION PILOT PLANT, SOUTHEASTERN NEW MEXICO

Marc W. Bodine, Jr. and Blair F. Jones
US Geological Survey

Steven J. Lambert
Sandia National Laboratories

## ABSTRACT

Salt norms, the quantitative idealized equilibrium mineral assemblages that crystallize when a natural water solution is evaporated to dryness at 25°C and 1 bar pressure under atmospheric partial pressure of carbon dioxide, have been calculated using the computer code SNORM for 124 groundwater sample analyses from the three principal water-bearing zones of the Ochoan (Permian) Rustler Formation, and for four analyses from overlying strata at and near the Waste Isolation Pilot Plant (WIPP). Interpretation of the norms indicates Rustler solutes range from primitive connate and diagenetic to recharge meteoric types. The recharge waters have norms reflecting hydrolysis of framework silicate minerals in the surficial weathering environment, pervasive anhydrite re-solution in the Rustler Formation throughout the region, and, as inferred in part from Cl/Br ratios, little to extensive re-solution of Rustler or Salado Formation halite. The distribution of redissolved halite in the fluids, for the most part, is consistent with the boundaries of halite occurrences observed in the three evaporite-bearing intervals of the Rustler Formation. Characteristics of the salt norms indicate: (1) strong primitive-diagenetic signatures in the solutes within small, apparently isolated areas of the Culebra and Magenta members overlain by halite-free strata of exceedingly low transmissivity; (2) extensive incursion of recharge waters into

the Rustler-Salado contact, Culebra, and Magenta zones within most areas of overlying halite absence in the Rustler Formation; and (3) areal distribution of norms and consequent inferences about the origins of solutes that are not consistent with steady-state groundwater flow having a single dominant flow direction.

# CONTENTS

# FIGURES

# TABLES

# CHAPTER 4.0

## 4.1 INTRODUCTION

The groundwaters in the Rustler Formation above the WIPP Facility exhibit a wide range of compositions, origins, and flow regimes that have been investigated by a variety of techniques. We propose that recasting the chemical composition of a water into a "salt norm" (Bodine and Jones, 1986) is a useful diagnostic tool in this effort. The salt norm is the hypothetical equilibrium assemblage of mineral salts at surficial conditions that is quantitatively equivalent to the solute concentrations in the water. The salt norm can be envisioned as the hypothetical assemblage of salts that would have precipitated from the evaporated water sample and would be in equilibrium with the last vestige of remaining water. The normative assemblage yields a diagnostic chemical-mineralogical characterization of the water, aids in the interpretation of the possible (but not necessarily unique) origins of the solutes of the water, is indicative of the character of water-rock interaction in subsurface environments, and may contribute in determining the evolutionary path of the water chemistry.

In this report, we review the calculation of the salt norm and the criteria for its interpretation. We present salt norms for selected analyses of groundwaters from the Rustler Formation and from overlying strata from the WIPP region and discuss their use in characterizing the waters and suggesting mechanisms for their origin and evolution.

## 4.2 THE SALT NORM

### 4.2.1 The Normative Concept

Presenting the dissolved constituents of a water as neutral salt abundances is not new. In the nineteenth century it was the accepted practice to report water compositions in terms of abundances of simple salts. As Hem (1970) pointed out, this practice predated acceptance of the Arrhenius concept of dissociated ions, and although it also attempted to

express water compositions in terms of the salts produced upon evaporation, it was actually more closely related to classical gravimetric analytical procedures with minimal regard to salt speciation and association. It is not surprising, then, that this form of expressing water composition diminished in the twentieth century with only occasional use for specific purposes in the more recent literature such as forming assemblages of simple salts (see, for example, Rankama and Sahama, 1950, p. 318) or attempts at forming reasonable associations of mineral salts (Lambert, 1978).

The striking differences in salt mineral assemblages in marine and nonmarine evaporite deposits are clearly indicative of both lithologic origin and subsequent geochemical evolution for the dissolved constituents (Eugster and Jones, 1979; Eugster et al., 1980). Thus, it appears informative to reconstruct solute content of a natural water into the equilibrium salt assemblage that would result if the water evaporated to dryness under earth surface conditions.

The salt norm is analogous to the CIPW norm (Cross et al., 1902) which is an idealized equilibrium assemblage of igneous minerals that is calculated from the chemical composition of the rock. The CIPW norm has proved useful in igneous petrology not only for characterizing and classifying igneous rocks, but also for providing invaluable quantitative data for rigorous interpretation of the origin and evolution of an igneous complex. We suggest similar advantages for the salt norm in characterizing natural waters and interpreting their chemical evolution, although not with the same degree of rigor. Characterization of a water composition as a salt norm is more detailed and more suggestive of solute origin and subsequent interaction than major cation-anion predominance, which is the most commonly used system of hydrochemical classification (cf. Collins, 1975). The normative characteristic of a water stands by itself as an indicator. Comparisons of norms from adjacent water samples, however, do not necessarily suggest evolutionary paths that relate the origins of those adjacent waters to one another.

### 4.2.2 Calculation of the Salt Norm

The salt norm is calculated with the computer program SNORM (Bodine and Jones, 1986); this summary will be limited to the program's major features. The program computes the norm by quantitatively assigning up to 18 solutes (Table 4-1) into the equilibrium assemblage of salts obtained from a list of 63 normative salts (Table 4-2). SNORM computes the normative assemblage directly from the solute matrix without proceeding along a succession of reaction paths. The salt norm characterizes the composition of a natural water and indirectly suggests a solute source and chemical evolution of the water. No direct information on specific reaction paths or extent of mineral saturation for an individual water sample is given by SNORM.

**Table 4-1. Solutes in Water Analyses Assigned to Normative Salts**

| | CATIONS | | ANIONS | |
|---|---|---|---|---|
| Major | | | | |
| | $Mg^{2+}$ | $Na^{+}$ | $Cl^{-}$ | $HCO_3^{-}$ |
| | $Ca^{2+}$ | $K^{+}$ | $SO_4^{2-}$ | $CO_3^{2-}$ |
| Minor | | | | |
| | $Li^{+}$ | $Sr^{2+}$ | $F^{-}$ | $NO_3^{-}$ |
| | $NH_4^{+}$ | $Ba^{2+}$ | $Br^{-}$ | B |
| | | | $I^{-}$ | $PO_4^{3-}$ |

## Table 4-2. Chemical Formulas of the Normative Salts

| | |
|---|---|
| Ammonia niter | $NH_4NO_3$ |
| Anhydrite (D[1]) | $CaSO_4$ |
| Antarcticite (D) | $CaCl_2 \cdot 6H_2O$ |
| Aphthitalite (D) | $K_3Na(SO_4)_2$ |
| Arcanite (D,X[2]) | $K_2SO_4$ |
| Barite | $BaSO_4$ |
| Bischofite (D) | $MgCl_2 \cdot 6H_2O$ |
| Bloedite (D) | $Na_2Mg(SO_4)_2 \cdot 4H_2O$ |
| Borax | $Na_2B_4O_7 \cdot 10H_2O$ |
| Burkeite (D) | $Na_6CO_3(SO_4)_2$ |
| Calcite (D) | $CaCO_3$ |
| Carnallite(D) | $KMgCl_3 \cdot 6H_2O$ |
| Celestite | $SrSO_4$ |
| Dolomite (D) | $CaMg(CO_3)_2$ |
| Epsomite (D) | $MgSO_4 \cdot 7H_2O$ |
| Fluorapatite | $Ca_5(PO_4)_3F$ |
| Fluorite | $CaF_2$ |
| Glauberite (D) | $Na_2Ca(SO_4)_2$ |
| Gypsum | $CaSO_4 \cdot 2H_2O$ |
| Halite (D) | $NaCl$ |
| Hydroxyapatite | $Ca_5(PO_4)_3OH$ |
| Inderite | $Mg_2B_6O_{11} \cdot 15H_2O$ |
| Inyoite | $Ca_2B_6O_{11} \cdot 13H_2O$ |
| Kainite (D) | $KMgClSO_4 \cdot 3H_2O$ |
| Kalicinite (D,X) | $KHCO_3$ |
| Kieserite (D) | $MgSO_4 \cdot H_2O$ |
| Leonite (D) | $K_2Mg(SO_4)_2 \cdot 4H_2O$ |
| Magnesite (D) | $MgCO_3$ |
| Mascagnite | $(NH_4)_2SO_4$ |
| Mirabilite | $Na_2SO_4 \cdot 10H_2O$ |
| Niter | $KNO_3$ |
| Nitrobarite | $Ba(NO_3)_2$ |
| Nitrocalcite | $Ca(NO_3)_2 \cdot 4H_2O$ |

## Table 4-2. Chemical Formulas of the Normative Salts (Continued)

| | |
|---|---|
| Nitromagnesite | $Mg(NO_3)_2 \cdot 6H_2O$ |
| Picromerite (D,X) | $K_2Mg(SO_4)_2 \cdot 6H_2O$ |
| Pirssonite (D,X) | $Na_2Ca(CO_3)_2 \cdot 2H_2O$ |
| Polyhalite (D) | $K_2Ca_2Mg(SO_4)_4 \cdot 2H_2O$ |
| Salammoniac | $NH_4Cl$ |
| Sellaite | $MgF_2$ |
| Soda niter | $NaNO_3$ |
| Strontianite | $SrCO_3$ |
| Sylvite (D) | $KCl$ |
| Syngenite (D) | $K_2Ca(SO_4)_2 \cdot H_2O$ |
| Tachyhydrite (D) | $Mg_2CaCl_6 \cdot 12H_2O$ |
| Teschemacherite | $NH_4HCO_3$ |
| Thenardite (D) | $Na_2SO_4$ |
| Trona (D) | $Na_3H(CO_3)_2 \cdot 2H_2O$ |
| Ulexite | $NaCaB_5O_9 \cdot 8H_2O$ |
| Villiaumite | $NaF$ |
| Wagnerite | $Mg_2PO_4F$ |
| Witherite | $BaCO_3$ |
| - | $BaCl_2 \cdot H_2O$ |
| - | $BaCl_2 \cdot 2H_2O$ |
| - | $LiCl \cdot H_2O$ |
| - | $Li_2CO_3$ |
| - | $LiF$ |
| - | $LiNO_3 \cdot 3H_2O$ |
| - | $Li_2SO_4 \cdot H_2O$ |
| - | $Mg_3(PO_4)_2$ |
| - | $Na_3PO_4$ |
| - | $SrCl_2 \cdot 2H_2O$ |
| - | $SrCl_2 \cdot 6H_2O$ |
| - | $Sr(NO_3)_2$ |

1. Diagnostic major cation and anion salt (gypsum and mirabilite omitted because their respective hydration equilibria preclude chloride or nitrate in the water).
2. Diagnostic salt not occurring in norms of WIPP groundwater.

#### 4.2.2.1 Solutes

The solutes (Table 4-1) were selected to comply with two criteria: (1) they occur in natural waters in more than negligible (trace) concentrations; and (2) they form normative salt(s) through direct combination with other solutes in the analysis without interacting with the aqueous environment (e.g., no incongruent reactions) or requiring any chemical speciation or charge modification (e.g., no oxidation-reduction or complexation reactions). Thus, neither pH nor redox enter directly into the SNORM calculations. Only boron, which is reported as the element in conventional water analyses, fails to comply with these criteria. In SNORM boron is recast as borate and contributes to the total anion charge of the analysis.

Total cation equivalency must equal total anion equivalency, to assign all solutes to neutral salt species. This criterion is satisfied in SNORM by proportioning all cation and anion concentrations in the analysis to yield neutral charge balance. Minimal deviation of the cation and anion proportion factors from unity is an indication of the completeness and accuracy of the analysis.

#### 4.2.2.2 Normative Salts

SNORM forms the salt norm from a list of 63 permissible normative salts (Table 4-2). Most of the salts occur as minerals and are thermodynamically stable at 25°C, 1 bar total pressure, and atmospheric partial pressure of carbon dioxide ($10^{-3.5}$ bars) at the water activity imposed by the salt assemblage.

After SNORM establishes the maximum number of phases in the assemblage with the Gibbs phase rule, the salt norm is calculated by assigning the solutes to the single assemblage that (1) quantitatively consumes all solutes, and (2) contains no unstable salt associations. The unstable salt associations have been determined with free energy minimization reactions. Where thermodynamic data were lacking, mineral associations in surficial assemblages and analogies with relations in similar equilibria were used to estimate unstable associations.

Some pairs of normative salts (kieserite/epsomite, leonite/picromerite, anhydrite/ gypsum, thenardite/mirabilite) give a choice of hydration states. As explained in Table 4-2, the less hydrated salt in each of the last two pairs (anhydrite and thenardite) is favored because of the presence of the indicator salts that preclude the more hydrated salt in each pair. The presence of chloride salts in virtually all of the waters considered here precludes the occurrence of normative gypsum, even though gypsum might have dissolved in several cases to produce the observed major solute assemblage. Similarly, thenardite is the sodium-sulfate salt favored over mirabilite in chloride-bearing solutions, since mirabilite is stable with solutions having an activity of water $>0.81$, a condition not likely to be obtained in chloride solutions (Bodine and Jones, 1986). For similar reasons, leonite is always favored over picromerite in chloride solutions. Kieserite is the magnesium-sulfate salt favored in assemblages containing normative indicator salts (as defined by Bodine and Jones, 1986) bischofite, carnallite, or nitromagnesite; whereas the absence of these permits epsomite.

### 4.2.3 Interpretation of the Salt Norm

Characterization and interpretation of the salt norm relies almost exclusively on the major cation/major anion salts in the norm (those salts denoted with a "D" in Table 4-2) although salts of minor solutes are included in the calculation. We have elected to express normative salt relative abundances as their anhydrous weight percentages in the salt norm. Anhydrous weight percentage of the normative salt excludes waters of hydration in the salt's formula from the salt's weight in calculating relative abundance. Such normative abundances more closely reflect solute proportions.

Because the salt norm relates water composition to the relative abundances of both cations and anions, one or more of the key salts in the salt norm characterizes water composition more fully than does cation or anion predominance. Thus, designating a water sample as a "tachyhydrite water" is more explicit than designating it as a "chloride-rich water." Even more importantly, the norm, both qualitatively and quantitatively, is suggestive of possible solute sources and the character of water/rock interactions that may have occurred during

the evolution of the water. Although SNORM does not uniquely identify the specific water/rock interactions that have given rise to the observed solutes, the normative mineralogies considered with the mineralogies of host and adjacent rocks can provide clues in the search for these interactions. This is especially relevant in evaporitic environments, where congruent and incongruent dissolution of readily soluble minerals is likely to make important contributions to the solutes. Thus, the use of SNORM, with normative minerals corresponding to known common and less common evaporite minerals, is especially relevant to interpreting solute assemblages in groundwaters associated with the Ochoan evaporites of southeastern New Mexico.

Bodine and Jones (1986) developed categories relating the occurrence of normative salts to candidate solute sources and chemical evolution of the water. Three major categories of solute sources are recognized: a meteoric source in which the waters derive their solutes through surficial weathering processes; a marine source that, with or without modification, reflects a dominant seawater origin for the solutes, whether the solution actually is a seawater relic or a brine containing redissolved marine evaporites; and a diagenetic source in which the solutes reflect a significant degree of rock/water interaction.

#### 4.2.3.1 Meteoric Norms

Norms for meteoric waters characteristically contain alkali-bearing sulfate or carbonate normative salts. Although dissolution of soluble minerals (such as calcite and other carbonates, gypsum, and halite) and rocks composed thereof, anthropogenic contaminants, and aerosols often contribute an appreciable fraction of the solutes in meteoric waters, it is commonly the hydrolysis reactions involved in the weathering of silicate rocks that generate the most diagnostic features in the norms of meteoric waters. Alkali-bearing carbonate salts in the norm can indicate atmospheric carbon dioxide/water interaction forming carbonic acid, and accompanying hydrolysis of silicate minerals. Alternatively, alkali-bearing sulfate salts in the norm can reflect sulfide mineral oxidation forming sulfuric acid with consequent hydrolysis of silicate minerals.

#### 4.2.3.2 Marine Norms

Seawater has a characteristic halite-bischofite-kieserite-carnallite-anhydrite norm. Its single unique diagnostic feature is the magnesium chloride association represented by the bischofite-carnallite pair in the norm. It is difficult to attribute this association ultimately to any other than a marine source, though there may have been subsequent continental recycling (Bodine and Jones, 1986).

Only a few subsurface waters (other than those in the immediate vicinity of a marine source) yield norms quantitatively similar to the seawater norm. This is not unexpected. Mixing, continental cycling, and water/rock interaction, including re-solution of marine evaporite salts, can be expected not only to produce quantitative variations among the seawater normative minerals but to qualitatively modify the normative mineralogy, as in many cases reviewed by Bodine and Jones (1986). For example, a connate marine groundwater mixing with meteoric water bearing normative alkali sulfates can eliminate bischofite and generate sylvite in the norm as magnesium becomes associated with sulfate rather than chloride. The presence of kainite or polyhalite in an otherwise marine-like norm can provide an indication of marine-meteoric water mixing.

Surface brines, which have evolved through fractional precipitation of calcium sulfate, halite, or even the bitter salts, yield norms qualitatively identical to seawater but quantitatively distinct. Subsurface waters from a marine evaporite source are subject to similar modifications as subsurface marine waters; however, elimination of the bischofite or bischofite-carnallite signature from the norm becomes less likely.

#### 4.2.3.3 Diagenetic Norms

The presence of the calcium-bearing chloride minerals tachyhydrite and antarcticite (Table 4-2) in the salt norm is indicative of solute diagenesis. Nearly all such norms in Bodine and Jones (1986) were obtained from subsurface fluids associated with deep sedimentary basins, highly saline strata, or crystalline shield areas, and are most readily interpreted as

evolving through the exchange of magnesium and sodium in solution for calcium in the solid phase. Because of the relatively low solubility of calcium sulfate, the abundance of normative sulfate salts becomes vanishingly small as calcium-bearing chlorides increase.

In carbonate rocks the exchange of magnesium in solution for calcium in the solid phase primarily reflects dolomitization. The extent of the exchange is limited by the Ca/Mg concentration ratio for the calcite-dolomite equilibrium. Although affected by aqueous calcium and magnesium ion activity coefficients, temperature, and mineralogy of the carbonate species, the Ca/Mg ratio, reflected in the norm by the antarcticite-to-tachyhydrite ratio, is not expected to greatly exceed unity due to dolomitization alone.

Alternatively, in silicate rocks sodium and magnesium exchange in solution for calcium in plagioclase and Ca-bearing mafic minerals, respectively. The resultant albitization and chloritization can proceed much farther than exchange accompanying dolomitization, particularly because of the decrease in solubility of magnesium silicate at moderately elevated temperatures.

### 4.2.4 Graphic Representation of the Salt Norm

A simplified representation of the salt norm for graphic display on maps has led to the definition of the "simple-salt assemblage" (Bodine and Jones, 1986). The simple-salt assemblage is constructed by SNORM from the salt norm through separation of each major-ion normative salt into its simple-salt components (all salts with minor solutes are omitted). For example, 1 mole of polyhalite (Table 4-2) in the norm is recast as 2 moles of $CaSO_4$, 1 mole of $K_2SO_4$, and 1 mole of $MgSO_4$. The abundance of each simple salt from its respective normative-salt sources is summed and normalized to its weight and molar percentage in the simple-salt assemblage. Each simple salt is defined with an anion charge of -2 to maintain consistency throughout an array of simple salts; this results in molar units of the alkali chlorides being expressed as $Na_2Cl_2$ and $K_2Cl_2$. Twelve different simple salts are recognized: the carbonates (bicarbonate in normative salts is recast as carbonate), the

sulfates, and the chlorides (chloride includes any bromine and iodine as if in solid solution) of each major cation--calcium, magnesium, potassium, and sodium.

Graphic display of the simple salt abundances is formatted as a rose diagram in which the circle is divided into 12 30-degree segments with each segment representing a specific simple salt (Figure 4-1A). The simple salts are arranged on the diagram with the sulfates occupying the upper third of the circle, the carbonates occupying the lower left third, and the chlorides occupying the lower right third. The three anion groups are separated by radial boundary lines on the rose diagram (Figure 4-1B). The salts in each anion group are sequentially arranged in terms of their respective relative solubilities. For example, calcium sulfate, the least soluble of the sulfates, occupies the rightmost segment in the sulfate area and is followed from right to left by $Mg_2SO_4$, $K_2SO_4$, and $Na_2SO_4$, the most soluble of the sulfates, in the leftmost segment of the sulfate group.

The radius of each segment of the rose is a function of that salt's relative molar or weight abundance in the simple-salt assemblage. Because the more diagnostic salts commonly have low abundance we have adopted equating segment radius to the cube root of the salt's fraction in the assemblage (Figure 4-1B). We recognize that small-to-moderate differences in abundance above 25% will not be readily apparent.

### 4.2.5 Additional Constraints on Salt Norm Interpretations

As mentioned above, solute norm assemblages can provide clues to the origins of solutes by analogy with brine solute assemblages whose origins are understood reasonably well. The normative salt assemblages do not in themselves specify an evolutionary path for the solutes, nor do they give a source for the water molecules. Similarly, the salt norms may not respond to subtle changes in minor constituents (such as bromide) arising from limited degrees of rock/water interaction, if such interaction does not in some way change the relative proportions of the major solutes. Bromide is a particularly important minor

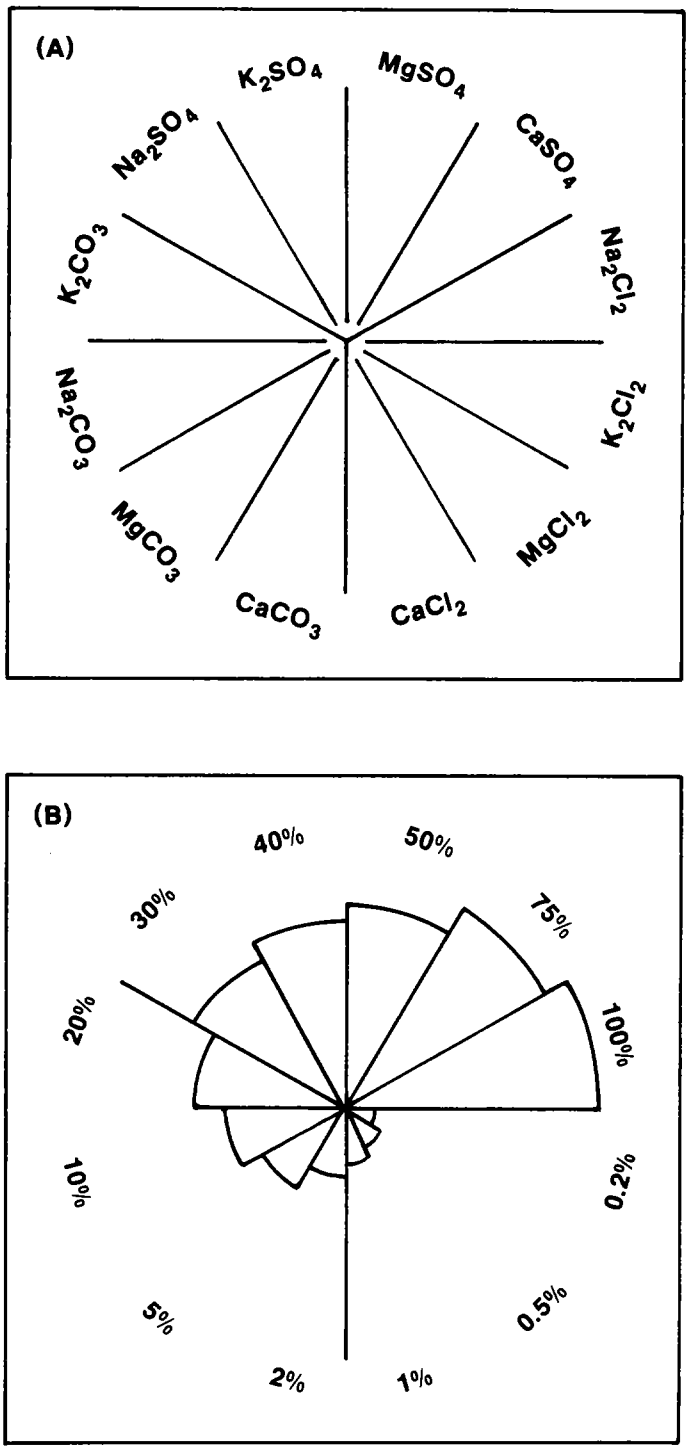


Figure 4-1. The simple-salt rose diagram.
A. Location of simple-salt segments on the rose diagram.
B. Relative scale of segment radii as a function of the cube root of the salt's weight or mole fraction in the assemblage.

constituent. Although bromide is not expressed in normative salts of its own, the Cl/Br ratio is used to further evaluate interpretations based on norms from evaporitic environments. Also, mixing of different reservoirs will result in simple, inert mixing of some solutes, if solubility limits are not exceeded in the mixture. Conversely, precipitation of a mineral phase accompanying mixing may not be directly indicated in the salt norm and must be evaluated by independent solubility computations.

Although some salt norms are considered characteristically "meteoric" or "marine," the source of water molecules (meteoric or marine) is better determined from stable-isotope ratios. Stable-isotope ratios have been reported by Lambert and Harvey (1987) for groundwater occurrences in the Rustler Formation and in other environments in the Delaware Basin. Mixing of reservoirs expected to have distinctly different isotopic compositions will yield a mixture of intermediate isotopic composition, inasmuch as trace isotopes behave ideally; this is not the case for all combinations of major solutes.

Finally, in groundwaters associated with more typical aquifer rock types (dominantly siliceous or calcareous), certain minerals in the salt norms appear unusual. For such occurrences it is necessary to postulate a combination or sequence of water/rock interactions to account for the observed assemblages. But because many of the 63 permissible normative salts are known to appear in ancient and modern evaporite deposits, the appearance of such a mineral in the norm of a Rustler groundwater can be simply indicative of dissolution of an evaporite mineral associated with the Rustler containing similar ionic proportions. For example, the normative assemblage polyhalite-leonite, with or without normative halite, in waters associated with silicate terrain might result from the weathering of mafic minerals and calcic plagioclase, accompanied by sulfuric acid hydrolysis (Bodine and Jones, 1986). However, the normative assemblage halite-polyhalite-leonite in a solution from an evaporite terrain, especially one known to contain polyhalite as does the Rustler Formation, is more likely indicative of the incongruent dissolution of polyhalite, in which a small amount of calcium, all the potassium and magnesium, and half the sulfate dissolve from the polyhalite (Braitsch, 1971). Similarly, the normative assemblage

thenardite-glauberite might indicate sulfuric acid hydrolysis of mafic minerals in a silicate rock, but could simply reflect the incongruent dissolution of glauberite, a mineral known to occur in the Salado and Castile Formations of southeastern New Mexico.

# 4.3 THE WIPP SITE SETTING

## 4.3.1 Relevant Geology

The geology of the Delaware Basin has been studied extensively over the past half century. In addition to the recent geologic investigations of the WIPP Site area, the Delaware Basin has long been a focus of geologic interest because of its abundant fluid hydrocarbon resources and its thick and somewhat unusual marine evaporite succession containing the nation's major potash deposits.

For detailed discussions of geology, stratigraphy, and hydrology of the northern Delaware Basin in general and the WIPP Site in particular, refer to Powers et al. (1978), Mercer (1983), Lambert (1983), and Bachman (1984, 1987).

Three water-bearing zones, areally pervasive to varying degrees, occur in the Rustler Formation: the Rustler/Salado contact zone (generally taken to immediately overlie the uppermost occurrence of halite), the Culebra dolomite member, and the Magenta member. These zones are separated by variable proportions of halite, anhydrite or gypsum, and clastic beds. Halite appears to account for about 50 m (160 ft) or more of the formation's total thickness and, in complete stratigraphic sections or where not removed by dissolution, occurs above and below both the Culebra and Magenta members. The uppermost stratigraphic occurrence of halite in the formation deepens progressively east-to-west; only at the eastern boundary of the WIPP Site is halite present throughout the formation. In the center of the site there is halite only below the Culebra member. No halite occurs in the Rustler Formation at the western site boundary. Except in areas of extreme sulfate dissolution, such as immediately east of the Pecos River or in the Nash Draw area, there appears to be minimal hydrologic connection among any of the three zones (Mercer, 1983).

The basal-Rustler/uppermost-Salado zone at the WIPP Site consists of a clayey dissolution residuum containing fragmental gypsum and some mudstone or siltstone. The residuum thickens markedly to the west and in some exposures along the Pecos River involves the entire Salado Formation section. To the east of the site the residuum grades into and interfingers with its original clayey halite lithology.

## 4.3.2 Water Samples

Our data base consisted of 128 chemical analyses of waters (35 Rustler/Salado contact zone; 62 Culebra; 19 Magenta; 4 supra-Rustler; 8 discharge) from 43 sites representing 76 horizon-site sampling points (21, 33, 13, 4 and 5, respectively). Multiple analyses from the same site and horizon are either replicate data from different investigators for the water sample or data for samples collected at different times, generally according to different sampling criteria.

### 4.3.2.1 Site Locations

Most sites that provided data for this study are wells that were drilled in support of the WIPP Site geologic and hydrologic characterization studies (the DOE, H, P, and WIPP groups of wells; Figure 4-2). A few were drilled in support of the GNOME project, an underground nuclear test, shown in Figure 4-3, and one (USGS-8) was drilled as part of the Malaga Bend Salinity Alleviation project. Figure 4-3 shows GNOME-5, the GNOME shaft, and ERDA-10 for reference. The remainder were drilled for a variety of other purposes, including regional studies of the northern Delaware Basin in support of the WIPP Site studies, petroleum and potash exploration, and development of agricultural or domestic water supplies (Figure 4-4).

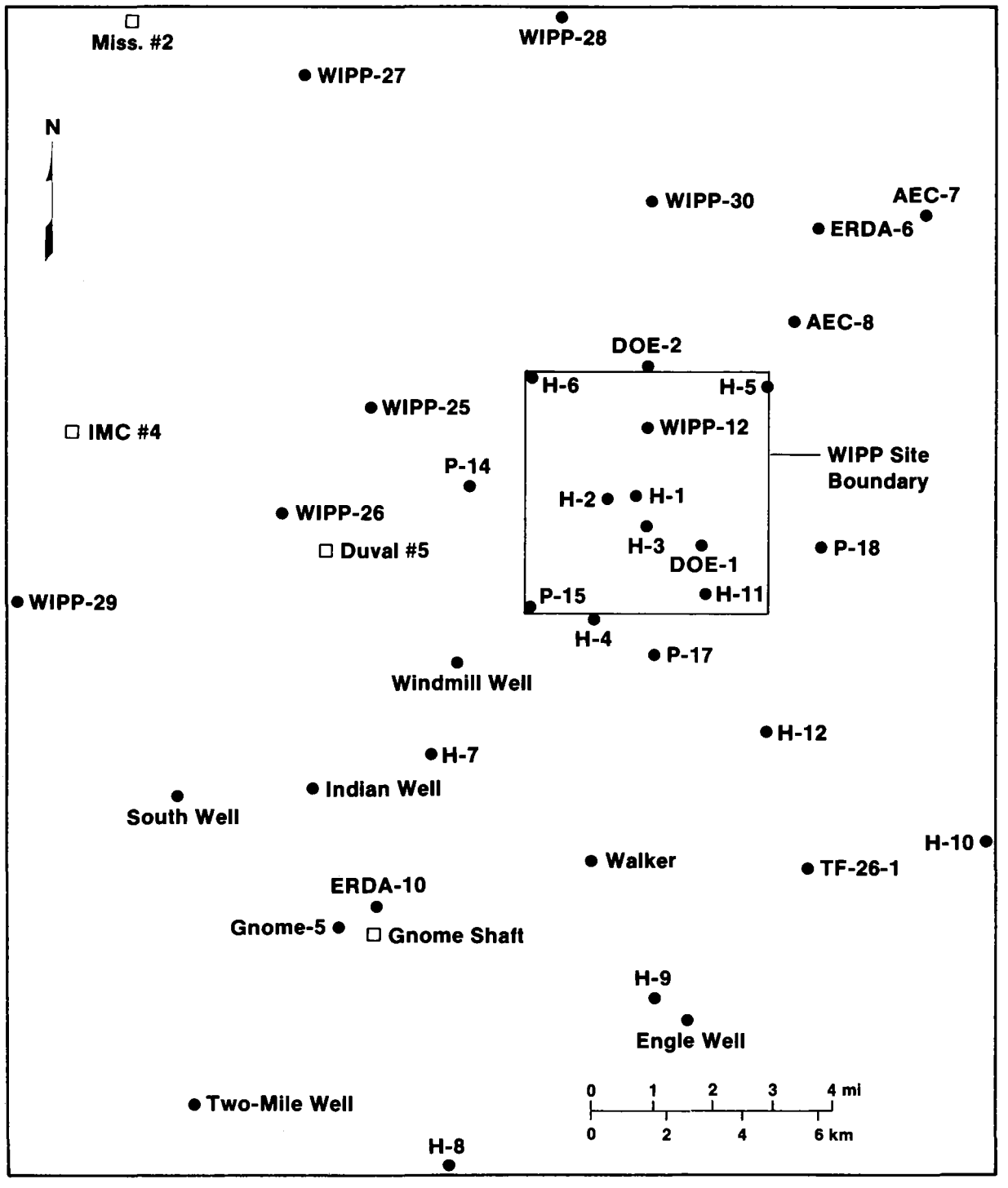


TRI-6341-48-0

Figure 4-2. Water sample locations within and near the WIPP Site (solid circles are well sites and open squares are mine shafts).

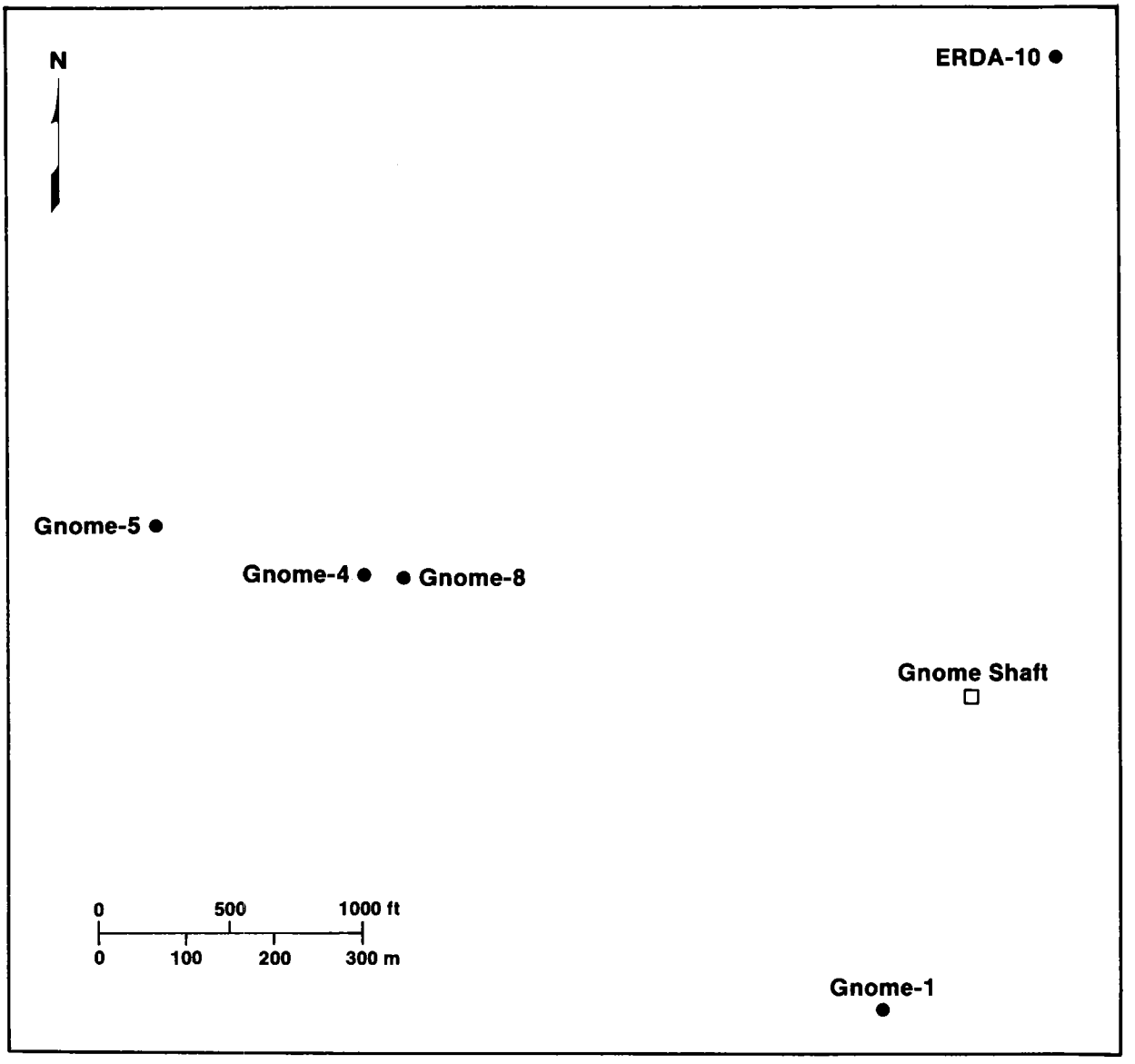


Figure 4-3. Water sample locations in the area of the GNOME site southwest of the WIPP Site (solid circles are well sites and open squares are mine shafts).

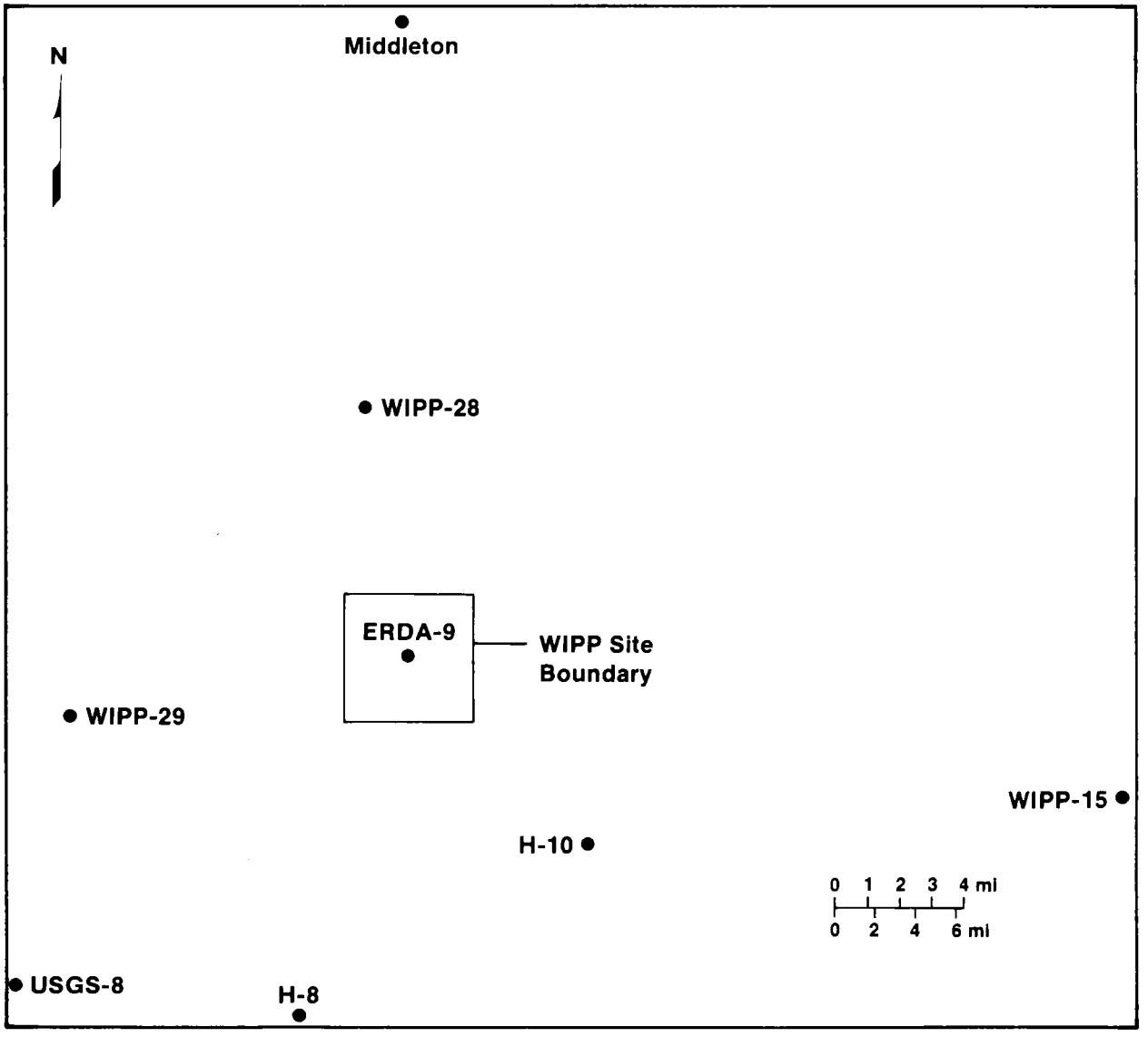


Figure 4-4. Water sample locations at greater distance from the WIPP Site (solid circles are well sites).

#### 4.3.2.2 Chemical Analyses

Analytical data for these waters are from a wide variety of sources. Most have been published in reports concerned with site characterization studies for the WIPP Project. Analyses include those by the Bendix (now United Nuclear) Corporation (Robinson, 1987). Others are from the US Geological Survey (USGS) Water Resources Division either in older Technical Files or more recent data from the Denver Central Laboratory. In addition, 34 analyses by S. L. Rettig (USGS, Reston) are included. Most of Rettig's data represent replicate measurements on waters previously analyzed by the Denver Central Laboratory and reported in Mercer (1983). These analyses by Rettig generally yield improved results and include analytical data for bromine.

## 4.4 RESULTS

Tables 4-3 through 4-7 contain the original analytical data for key chemical analyses and report our SNORM calculations, including salt norms and simple-salt assemblages. The tables are arranged stratigraphically: the Rustler/Salado contact waters (Table 4-3), discharge waters from the Rustler Formation in the Pecos River area (Table 4-4), waters from the Culebra dolomite (Table 4-5) and Magenta dolomite (Table 4-6) in the Rustler Formation, and waters from younger strata (Table 4-7).

Each table identifies the site of sample collection and reports, if known, sample collection date, sample density, and sample pH. The chemical analysis, excluding solutes not forming normative salts, is reported with its source cited. Those analyses that were used in interpretations and for plotting on maps and diagrams with simple-salt rose are also identified in the tables. Other determinations on samples of questionable representativeness are given with their norms for the purposes of discussion. The total dissolved solids (TDS), rounded to three significant figures, is the sum from SNORM of the solutes reported in the analysis and is neither the residue weight after drying nor necessarily the value reported in the cited reference. The Cl/Br ratio is reported in the tables as the weight ratio.

## Table 4-3. Chemical Analysis, Salt Norm (anhydrous weight percent), and Simple Salts (weight percent) of Rustler/Salado Contact Waters

| | Site | | | |
|---|---|---|---|---|
| | H-1[1] | H-2[2] | H-3[3] | H-4[4] |
| Date collected | 2/23/77 | 2/23/77 | 2/23/77 | 3/16/79 |
| pH | 7.2 | 5.9 | 7.6 | - |
| Chemical analysis | mg/L | mg/L | mg/L | mg/L |
| Mg | 30,000. | 25,000. | 25,000. | 27,000. |
| Ca | 13,000. | 9,200. | 18,000. | 8,300. |
| Na | 56,000. | 66,000. | 59,000. | 66,000. |
| K | 17,000. | 9,100. | 14,000. | 8,600. |
| F | - | - | - | 1.7 |
| Cl | 210,000. | 200,000. | 210,000. | 210,000. |
| $NO_3$ | 1.3 | 4.9 | 3.4 | 1.2 |
| $HCO_3$ | 675. | 199. | 467. | 1.0 |
| $SO_4$ | 520. | 1,300. | 370. | 1,400. |
| B | 110. | 150. | 1.9 | 360. |
| TDS | 327,000. | 311,000. | 327,000. | 322,000. |
| Balance (+/-) | 1.006 | 0.989 | 0.990 | 0.959 |
| Salt norm | | | | |
| Dolomite | 0.2 | <0.1 | 0.1 | <0.1 |
| Anhydrite | 0.2 | 0.6 | 0.2 | 0.6 |
| Halite | 43.3 | 54.3 | 46.2 | 53.5 |
| Carnallite | 22.5 | 12.8 | 18.7 | 11.9 |
| Bischofite | 5.0 | 11.5 | - | 16.0 |
| Tachyhydrite | 28.7 | 20.5 | 31.1 | 17.5 |
| Antarcticite | - | - | 3.7 | - |

**Table 4-3. Chemical Analysis, Salt Norm (anhydrous weight percent), and Simple Salts (weight percent) of Rustler/Salado Contact Waters (Continued)**

| | Site | | | |
|---|---|---|---|---|
| | H-1[1] | H-2[2] | H-3[3] | H-4[4] |
| Simple salts | | | | |
| $CaCO_3$ | 0.1 | <0.1 | 0.1 | <0.1 |
| $MgCO_3$ | 0.1 | <0.1 | 0.1 | <0.1 |
| $CaSO_4$ | 0.2 | 0.6 | 0.2 | 0.6 |
| $Na_2Cl_2$ | 43.4 | 54.4 | 46.2 | 53.8 |
| $K_2Cl_2$ | 9.9 | 5.6 | 8.2 | 5.3 |
| $MgCl_2$ | 35.7 | 31.7 | 30.1 | 33.9 |
| $CaCl_2$ | 10.6 | 7.6 | 15.2 | 6.5 |

1. Mercer (1983); salt rose plotted.
2. Mercer (1983); salt rose plotted.
3. Mercer (1983); salt rose plotted.
4. Mercer (1983).

## Table 4-3. Chemical Analysis, Salt Norm (anhydrous weight percent), and Simple Salts (weight percent) of Rustler/Salado Contact Waters (Continued)

| | Site | | | |
|---|---|---|---|---|
| | H-4[5] | H-5[6] | H-5[7] | H-6[8] |
| Date collected | 3/16/79 | 5/16/79 | 5/16/79 | 4/9/79 |
| Density (g/cc) | 1.212 | - | 1.263 | 1.209 |
| pH | 3.00 | - | 4.34 | 2.91 |
| Chemical analysis | mg/kg | mg/L | mg/kg | mg/kg |
| Mg | 20,600. | 82,000. | 63,300. | 16,500. |
| Ca | 7,140. | 2,100. | 1,580. | 3,470. |
| Sr | 229. | - | 26. | 83. |
| Li | 16. | - | 18. | 1.7 |
| Na | 56,400. | 14,000. | 12,400. | 68,800. |
| K | 6,850. | 21,000. | 14,100. | 6,450. |
| Cl | 167,000. | 290,000. | 207,000. | 166,000. |
| Br | 1,355. | - | 3,060. | 907. |
| $HCO_3$ | - | 300. | - | - |
| $SO_4$ | 594. | 2,000. | 1,090. | 1,220. |
| B | 167. | 67. | 194. | 117. |
| TDS | 260,000. | 412,000. | 303,000. | 264,000. |
| Balance (+/-) | 0.995 | 0.972 | 1.052 | 0.993 |
| Cl/Br | 123. | - | 68. | 183. |
| Salt norm | | | | |
| Dolomite | - | 0.1 | - | - |
| Anhydrite | 0.3 | 0.7 | 0.5 | 0.7 |
| Halite | 55.6 | 8.8 | 10.1 | 66.4 |
| Carnallite | 11.5 | 22.6 | 19.6 | 10.7 |
| Bischofite | 12.5 | 65.6 | 67.3 | 13.6 |
| Tachyhydrite | 19.5 | 2.2 | 2.1 | 8.1 |

## Table 4-3. Chemical Analysis, Salt Norm (anhydrous weight percent), and Simple Salts (weight percent) of Rustler/Salado Contact Waters (Continued)

| | Site | | | |
|---|---|---|---|---|
| | H-4[5] | H-5[6] | H-5[7] | H-6[8] |
| Simple salts | | | | |
| $CaCO_3$ | - | <0.1 | - | - |
| $MgCO_3$ | - | <0.1 | - | - |
| $CaSO_4$ | 0.3 | 0.7 | 0.5 | 0.7 |
| $Na_2Cl_2$ | 55.9 | 8.8 | 10.1 | 66.9 |
| $K_2Cl_2$ | 5.1 | 9.9 | 8.7 | 4.7 |
| $MgCl_2$ | 31.5 | 79.7 | 79.9 | 24.7 |
| $CaCl_2$ | 7.2 | 0.8 | 0.8 | 3.0 |

5. Rettig (unpub.); preferred analysis; salt rose plotted.
6. Mercer (1983).
7. Rettig (unpub.); preferred analysis; salt rose plotted.
8. Rettig (unpub.); salt rose plotted.

## Table 4-3. Chemical Analysis, Salt Norm (anhydrous weight percent), and Simple Salts (weight percent) of Rustler/Salado Contact Waters (Continued)

| | Site | | | |
|---|---|---|---|---|
| | H-7[9] | H-7[10] | H-8[11] | H-8[12] |
| Date collected | 3/20/80 | 3/20/80 | 9/6/80 | 9/6/80 |
| Density (g/cc) | 1.048 | 1.047 | - | 1.085 |
| pH | 6.80 | 7.13 | 7.60 | 7.22 |
| Chemical analysis | mg/kg | mg/kg | mg/L | mg/kg |
| Mg | 910. | 788. | 430. | 392. |
| Ca | 2,600. | 2,340. | 1,200. | 1,110. |
| Sr | - | 42. | - | 18. |
| Li | - | 0.3 | - | - |
| Na | 22,000. | 21,500. | 46,000. | 43,700. |
| K | 210. | 164. | 660. | 350. |
| F | 0.8 | - | 0.4 | - |
| Cl | 41,000. | 37,800. | 70,000. | 66,400. |
| Br | - | 12. | - | 8.3 |
| $NO_3$ | 0.1 | - | - | - |
| $HCO_3$ | - | 47. | - | - |
| $SO_4$ | 2,900. | 2,710. | 5,300. | 4,700. |
| B | 3.1 | 25. | 1.3 | 3.4 |
| TDS | 69,600. | 65,400. | 124,000. | 117,000. |
| Balance (+/-) | 0.959 | 0.998 | 1.014 | 1.015 |
| Cl/Br | - | 3,150. | - | 8,000. |
| Salt norm | | | | |
| Dolomite | - | 0.1 | - | - |
| Anhydrite | 5.8 | 5.9 | 1.4 | 2.2 |
| Kieserite | - | - | 0.9 | - |
| Epsomite | - | - | - | 1.1 |
| Polyhalite | - | - | 3.8 | 2.2 |
| Bloedite | - | - | - | 0.3 |
| Halite | 82.5 | 83.6 | 93.8 | 94.3 |
| Carnallite | 1.3 | 1.1 | <0.1 | - |
| Tachyhydrite | 7.1 | 6.5 | - | - |
| Antarcticite | 3.2 | 2.6 | - | - |

## Table 4-3. Chemical Analysis, Salt Norm (anhydrous weight percent), and Simple Salts (weight percent) of Rustler/Salado Contact Waters (Continued)

| | Site | | | |
|---|---|---|---|---|
| | H-7[9] | H-7[10] | H-8[11] | H-8[12] |
| Simple salts | | | | |
| $CaCO_3$ | - | <0.1 | - | - |
| $MgCO_3$ | - | <0.1 | - | - |
| $CaSO_4$ | 5.8 | 5.9 | 3.3 | 3.2 |
| $MgSO_4$ | - | - | 1.7 | 1.6 |
| $K_2SO_4$ | - | - | 1.2 | 0.7 |
| $Na_2SO_4$ | - | - | - | 0.2 |
| $Na_2Cl_2$ | 82.5 | 83.9 | 93.8 | 94.3 |
| $K_2Cl_2$ | 0.6 | 0.5 | <0.1 | - |
| $MgCl_2$ | 5.3 | 4.7 | <0.1 | - |
| $CaCl_2$ | 5.9 | 5.0 | - | - |

9. Mercer (1983).
10. Rettig (unpub.); preferred analysis; salt rose plotted.
11. Mercer (1983).
12. Rettig (unpub.); preferred analysis; salt rose plotted.

## Table 4-3. Chemical Analysis, Salt Norm (anhydrous weight percent), and Simple Salts (weight percent) of Rustler/Salado Contact Waters (Continued)

| | Site | | | |
|---|---|---|---|---|
| | H-9[13] | H-9[14] | H-10[15] | H-10[16] |
| Date collected | 5/20/80 | 5/20/80 | 5/19/80 | 5/19/80 |
| Density (g/cc) | 1.202 | 1.203 | 1.198 | 1.202 |
| pH | 7.0 | 6.21 | 6.3 | 5.74 |
| Chemical analysis | mg/L | mg/kg | mg/L | mg/kg |
| Mg | 870. | 707. | 11,000. | 8,400. |
| Ca | 1,300. | 1,120. | 1,500. | 1,120. |
| Sr | - | 15. | - | 42. |
| Li | - | 3.3 | - | 3.7 |
| Na | 130,000. | 102,000. | 100,000. | 86,500. |
| K | 1,200. | 790. | 4,000. | 2,950. |
| F | 0.1 | - | 0.7 | - |
| Cl | 190,000. | 155,000. | 190,000. | 155,000. |
| Br | - | 79. | - | 832. |
| $NO_3$ | 4.9 | - | 3.7 | - |
| $SO_4$ | 2,600. | 3,990. | 3,300. | 3,830. |
| B | 19. | 20. | 120. | 97. |
| TDS | 326,000. | 264,000. | 310,000. | 259,000. |
| Balance (+/-) | 1.075 | 1.027 | 0.999 | 1.027 |
| Cl/Br | - | 1,960. | - | 186. |
| Salt norm | | | | |
| Anhydrite | 1.2 | 1.2 | 1.5 | 1.4 |
| Kieserite | - | 0.5 | - | 0.6 |
| Polyhalite | - | 0.4 | - | - |
| Halite | 97.0 | 96.8 | 82.0 | 83.7 |
| Carnallite | 1.5 | 1.0 | 5.6 | 4.9 |
| Bischofite | - | - | 10.7 | 9.2 |
| Tachyhydrite | 0.2 | - | - | - |
| Antarcticite | <0.1 | - | - | - |

**Table 4-3. Chemical Analysis, Salt Norm (anhydrous weight percent), and Simple Salts (weight percent) of Rustler/Salado Contact Waters (Continued)**

| | Site | | | |
|---|---|---|---|---|
| | H-9[13] | H-9[14] | H-10[15] | H-10[16] |
| Simple salts | | | | |
| $CaSO_4$ | 1.2 | 1.4 | 1.5 | 1.5 |
| $MgSO_4$ | - | 0.6 | - | 0.6 |
| $K_2SO_4$ | - | 0.1 | - | - |
| $Na_2Cl_2$ | 97.1 | 96.9 | 82.1 | 83.9 |
| $K_2Cl_2$ | 0.7 | 0.5 | 2.5 | 2.1 |
| $MgCl_2$ | 1.0 | 0.6 | 13.9 | 12.0 |
| $CaCl_2$ | 0.1 | - | - | - |

13. Mercer (1983).
14. Rettig (unpub.); preferred analysis; salt rose plotted.
15. Mercer (1983).
16. Rettig (unpub.); preferred analysis; salt rose plotted.

## Table 4-3. Chemical Analysis, Salt Norm (anhydrous weight percent), and Simple Salts (weight percent) of Rustler/Salado Contact Waters (Continued)

| | Site | | | |
|---|---|---|---|---|
| | P-14[17] | P-14[18] | P-15[19] | H-17[20] |
| Date collected | 2/24/77 | 2/4/80 | 4/3/79 | 5/11/79 |
| Density (g/cc) | - | 1.126 | 1.042 | 1.193 |
| pH | 7.2 | 3.55 | 7.98 | 6.36 |
| Chemical analysis | mg/L | mg/kg | mg/kg | mg/kg |
| Mg | 1,200. | 941. | 240. | 29,300. |
| Ca | 570. | 1,190. | 864. | 14,400. |
| Sr | - | 20. | 30. | 380. |
| Li | - | - | - | 1.0 |
| Na | 120,000. | 70,200. | 21,900. | 20,100. |
| K | 1,300. | 1,380. | 1,250. | 9,640. |
| Cl | 180,000. | 111,000. | 34,400. | 152,000. |
| Br | - | - | 28. | 2,725. |
| $NO_3$ | 1.5 | - | - | - |
| $HCO_3$ | 222. | - | 152. | - |
| $SO_4$ | 10,000. | 7,640. | 3,220. | 478. |
| B | 1.7 | 42. | 3.4 | 184. |
| TDS | 313,000. | 192,000. | 62,100. | 229,000. |
| Balance (+/-) | 1.017 | 0.980 | 1.007 | 0.981 |
| Cl/Br | - | - | 1,230. | 56. |
| Salt norm | | | | |
| Magnesite | <0.1 | - | 0.2 | - |
| Anhydrite | - | <0.1 | 2.1 | 0.3 |
| Kieserite | - | 1.1 | - | - |
| Epsomite | 0.1 | - | - | - |
| Polyhalite | 1.3 | 4.2 | 5.4 | - |
| Leonite | 0.9 | - | - | - |
| Bloedite | 2.3 | - | - | - |
| Kainite | - | 0.1 | - | - |
| Halite | 95.4 | 93.9 | 89.4 | 22.7 |
| Sylvite | - | - | 2.1 | - |
| Carnallite | - | 0.4 | 0.7 | 18.6 |
| Bischofite | - | - | - | 11.1 |
| Tachyhydrite | - | - | - | 46.7 |

## Table 4-3. Chemical Analysis, Salt Norm (anhydrous weight percent), and Simple Salts (weight percent) of Rustler/Salado Contact Waters (Continued)

| | Site | | | |
|---|---|---|---|---|
| | P-14[17] | P-14[18] | P-15[19] | H-17[20] |
| Simple salts | | | | |
| $MgCO_3$ | <0.1 | - | 0.2 | - |
| $CaSO_4$ | 0.6 | 2.1 | 4.7 | 0.3 |
| $MgSO_4$ | 1.8 | 2.1 | 1.2 | - |
| $K_2SO_4$ | 0.9 | 1.4 | 1.7 | - |
| $Na_2SO_4$ | 1.2 | - | - | - |
| $Na_2Cl_2$ | 95.4 | 94.0 | 89.5 | 22.8 |
| $K_2Cl_2$ | - | 0.2 | 2.4 | 8.2 |
| $MgCl_2$ | - | 0.2 | 0.4 | 51.4 |
| $CaCl_2$ | - | - | - | 17.3 |

17. Mercer (1983).
18. Rettig (unpub.); preferred sample?; salt rose plotted.
19. Rettig (unpub.); non-representive sample.
20. Rettig (unpub.); salt rose plotted.

## Table 4-3. Chemical Analysis, Salt Norm (anhydrous weight percent), and Simple Salts (weight percent) of Rustler/Salado Contact Waters (Continued)

| | Site | | | |
|---|---|---|---|---|
| | P-18[21] | WIPP-25[22] | WIPP-25[23] | WIPP-26[24] |
| Date collected | 5/20/80 | 3/19/80 | 7/17/80 | 3/18/80 |
| Density (g/cc) | 1.266 | 1.171 | - | 1.078 |
| pH | 5.35 | 7.14 | 7.4 | 8.5 |
| Chemical analysis | mg/kg | mg/kg | mg/L | mg/L |
| Mg | 41,100. | 2,390. | 3,260. | 1,300. |
| Ca | 22,400. | 572. | 560. | 2,700. |
| Sr | 55. | 9.4 | 11.3 | - |
| Li | 8.5 | 0.8 | 1.58 | - |
| Na | 15,200. | 78,600. | 122,800. | 52,000. |
| K | 11,800. | 2,050. | 3,330. | 1,000. |
| Cl | 199,000. | 127,000. | 192,000. | 88,000. |
| Br | 3,120. | 41. | 51. | - |
| $NO_3$ | - | - | - | 0.2 |
| $HCO_3$ | - | 105. | 130. | - |
| $SO_4$ | 197. | 9,380. | 12,400. | 7,600. |
| B | 161. | 40. | 40.9 | 30. |
| TDS | 293,000. | 220,000. | 335,000. | 153,000. |
| Balance (+/-) | 0.974 | 0.980 | 1.009 | 0.957 |
| Cl/Br | 64. | 3,100. | 3,760. | - |
| Salt norm | | | | |
| Magnesite | - | <0.1 | <0.1 | - |
| Anhydrite | 0.1 | - | - | 6.2 |
| Kieserite | - | 2.8 | 1.9 | 0.7 |
| Polyhalite | - | 1.9 | 1.2 | - |
| Kainite | - | 1.4 | 2.8 | - |
| Halite | 13.6 | 92.0 | 92.9 | 88.9 |
| Carnallite | 18.0 | 1.7 | 1.2 | 2.9 |
| Bischofite | 9.5 | - | - | 1.2 |
| Tachyhydrite | 58.5 | - | - | - |

**Table 4-3. Chemical Analysis, Salt Norm (anhydrous weight percent), and Simple Salts (weight percent) of Rustler/Salado Contact Waters (Continued)**

| | Site | | | |
|---|---|---|---|---|
| | P-18[21] | WIPP-25[22] | WIPP-25[23] | WIPP-26[24] |
| Simple salts | | | | |
| $MgCO_3$ | - | <0.1 | <0.1 | - |
| $CaSO_4$ | 0.1 | 0.9 | 0.6 | 6.2 |
| $MgSO_4$ | - | 4.1 | 3.9 | 0.7 |
| $K_2SO_4$ | - | 0.6 | 0.4 | - |
| $Na_2Cl_2$ | 13.6 | 92.1 | 92.9 | 89.0 |
| $K_2Cl_2$ | 7.9 | 1.3 | 1.6 | 1.3 |
| $MgCl_2$ | 56.8 | 1.0 | 0.6 | 2.8 |
| $CaCl_2$ | 21.6 | - | - | - |

21. Rettig (unpub.); non-representative sample; salt rose plotted.
22. Rettig (unpub.); salt rose plotted.
23. Bendix (unpub.); preferred sample.
24. Mercer (1983).

## Table 4-3. Chemical Analysis, Salt Norm (anhydrous weight percent), and Simple Salts (weight percent) of Rustler/Salado Contact Waters (Continued)

| | Site | | | |
|---|---|---|---|---|
| | WIPP-26[25] | WIPP-26[26] | WIPP-27[27] | WIPP-27[28] |
| Date collected | 3/18/80 | 7/23/80 | 5/21/80 | 7/24/80 |
| Density (g/cc) | 1.107 | - | 1.204 | 1.073 |
| pH | 8.03 | 7.7 | 7.43 | 7.31 |
| Chemical analysis | mg/kg | mg/L | mg/kg | mg/kg |
| Mg | 1,170. | 1,660. | 1,040. | 1,680. |
| Ca | 1,310. | 1,410. | 1,160. | 1,070. |
| Sr | 20. | 27. | 10. | 21. |
| Li | 1.0 | 1.15 | 1.2 | 2.0 |
| Na | 50,100. | 68,600. | 102,000. | 32,100. |
| K | 814. | 1,200. | 2,570. | 1,580. |
| Cl | 82,400. | 108,000. | 154,000. | 52,400. |
| Br | 24. | 19.3 | 51. | 16. |
| $HCO_3$ | 123. | 270. | - | - |
| $SO_4$ | 6,730. | 7,480. | 5,190. | 8,670. |
| B | 43. | 31.8 | 13. | 16. |
| TDS | 143,000. | 189,000. | 266,000. | 97,600. |
| Balance (+/-) | 0.957 | 1.004 | 1.043 | 0.982 |
| Cl/Br | 3,430. | 5,600. | 3,020. | 3,280. |
| Salt norm | | | | |
| Magnesite | <0.1 | 0.1 | - | - |
| Anhydrite | 2.6 | 2.1 | 0.1 | 0.6 |
| Kieserite | 2.4 | 2.4 | - | 4.9 |
| Polyhalite | 1.2 | 0.8 | 2.8 | 6.5 |
| Halite | 91.7 | 92.2 | 95.0 | 84.6 |
| Sylvite | - | - | 0.3 | - |
| Carnallite | 1.8 | 2.3 | 1.8 | 3.2 |

## Table 4-3. Chemical Analysis, Salt Norm (anhydrous weight percent), and Simple Salts (weight percent) of Rustler/Salado Contact Waters (Continued)

| | Site | | | |
|---|---|---|---|---|
| | WIPP-26[25] | WIPP-26[26] | WIPP-27[27] | WIPP-27[28] |
| Simple salts | | | | |
| $MgCO_3$ | <0.1 | 0.1 | - | - |
| $CaSO_4$ | 3.2 | 2.5 | 1.4 | 3.8 |
| $MgSO_4$ | 2.7 | 2.5 | 0.6 | 6.3 |
| $K_2SO_4$ | 0.4 | 0.3 | 0.9 | 2.0 |
| $Na_2Cl_2$ | 91.8 | 92.3 | 95.0 | 84.7 |
| $K_2Cl_2$ | 0.8 | 1.0 | 1.1 | 1.4 |
| $MgCl_2$ | 1.0 | 1.3 | 1.0 | 1.8 |

25. Rettig (unpub.).
26. Bendix (unpub.); preferred sample; salt rose plotted.
27. Rettig (unpub.); non-representative sample.
28. Rettig (unpub.); difficult sampling.

## Table 4-3. Chemical Analysis, Salt Norm (anhydrous weight percent), and Simple Salts (weight percent) of Rustler/Salado Contact Waters (Continued)

| | Site | | | |
|---|---|---|---|---|
| | WIPP-28[29] | WIPP-28[30] | WIPP-29[31] | WIPP-29[32] |
| Date collected | 3/20/80 | 7/31/80 | 3/18/80 | 7/24/80 |
| Density (g/cc) | 1.138 | 1.180 | 1.067 | - |
| pH | 6.72 | 7.0 | 6.86 | 7.20 |
| Chemical analysis | mg/kg | mg/L | mg/kg | mg/L |
| Mg | 2,070. | 3,400. | 1,930. | 2,320. |
| Ca | 615. | 605. | 872. | 1,080. |
| Sr | 11. | 11.6 | 17. | 21. |
| Li | 0.9 | 1.82 | 0.9 | 1.34 |
| Na | 65,000 | 97,100. | 29,500. | 36,100. |
| K | 2,070. | 4,300. | 842. | 1,480. |
| Cl | 102,000. | 155,000. | 45,200. | 58,000. |
| Br | 36. | 29. | 12. | 12.5 |
| $HCO_3$ | 260. | 170. | 154. | 200. |
| $SO_4$ | 11,000. | 16,700. | 11,300. | 12,000. |
| B | 54. | 46.2 | 45. | 19.9 |
| TDS | 183,000. | 277,000. | 89,900. | 111,000. |
| Balance (+/-) | 0.990 | 0.983 | 0.995 | 0.981 |
| Cl/Br | 2,830. | 5,340. | 3,770. | 4,640. |
| Salt norm | | | | |
| Magnesite | 0.1 | <0.1 | 0.1 | 0.1 |
| Anhydrite | - | - | <0.1 | <0.1 |
| Kieserite | - | - | - | 7.5 |
| Epsomite | 3.0 | 2.0 | 7.9 | - |
| Polyhalite | 2.4 | 1.6 | 6.8 | 6.9 |
| Leonite | 1.4 | 1.2 | - | - |
| Bloedite | - | - | 2.2 | - |
| Kainite | 2.2 | 5.2 | - | - |
| Halite | 90.8 | 90.0 | 82.7 | 83.6 |
| Carnallite | - | - | - | 1.8 |

## Table 4-3. Chemical Analysis, Salt Norm (anhydrous weight percent), and Simple Salts (weight percent) of Rustler/Salado Contact Waters (Continued)

| | Site | | | |
|---|---|---|---|---|
| | WIPP-28[29] | WIPP-28[30] | WIPP-29[31] | WIPP-29[32] |
| Simple salts | | | | |
| $MgCO_3$ | 0.1 | <0.1 | 0.1 | 0.1 |
| $CaSO_4$ | 1.2 | 0.7 | 3.3 | 3.3 |
| $MgSO_4$ | 5.4 | 6.0 | 10.3 | 9.0 |
| $K_2SO_4$ | 1.6 | 1.2 | 2.1 | 2.1 |
| $Na_2SO_4$ | - | - | 1.2 | - |
| $Na_2Cl_2$ | 91.0 | 90.0 | 82.9 | 83.7 |
| $K_2Cl_2$ | 0.8 | 2.0 | - | 0.8 |
| $MgCl_2$ | - | - | - | 1.0 |

29. Rettig (unpub.); non-representative sample; salt rose plotted.
30. Bendix (unpub.); preferred sample.
31. Rettig (unpub.); non-representative sample; salt rose plotted.
32. Bendix (unpub.); preferred sample.

## Table 4-3. Chemical Analysis, Salt Norm (anhydrous weight percent), and Simple Salts (weight percent) of Rustler/Salado Contact Waters (Continued)

| | Site | | |
|---|---|---|---|
| | WIPP-30[33] | WIPP-30[34] | GNOME-5[35] |
| Date collected | 3/19/80 | 7/17/80 | 1/27/80 |
| Density (g/cc) | 1.200 | - | 1.200 |
| pH | 6.23 | 7.50 | 7.0 |
| Chemical analysis | mg/kg | mg/L | mg/kg |
| Mg | 1,830. | 2,770. | 2,710. |
| Ca | 758. | 955. | 424. |
| Sr | 12. | 18.4 | 33. |
| Li | - | 0.72 | 2.82 |
| Na | 92,500. | 120,600. | 94,700. |
| K | 1,330. | 2,180. | 2,090. |
| F | - | - | 4.2 |
| Cl | 150,000. | 192,000. | 156,000. |
| Br | 72. | 78. | 5.5 |
| $NO_3$ | - | - | 0.4 |
| $HCO_3$ | - | 620. | 18. |
| $SO_4$ | 6,300. | 7,390. | 540. |
| B | 79. | 81.6 | - |
| TDS | 253,000. | 327,000. | 257,000. |
| Balance (+/-) | 0.972 | 0.999 | 1.001 |
| Cl/Br | 2,080. | 2,460. | 28,400. |
| Salt norm | | | |
| Dolomite | - | - | <0.1 |
| Magnesite | - | 0.1 | - |
| Anhydrite | 0.8 | 0.9 | 0.3 |
| Kieserite | 2.0 | 1.9 | - |
| Polyhalite | 0.4 | 0.1 | - |
| Halite | 94.6 | 94.0 | 93.8 |
| Carnallite | 2.1 | 2.8 | 3.5 |
| Bischofite | - | - | 1.8 |
| Tachyhydrite | - | - | 0.6 |

## Table 4-3. Chemical Analysis, Salt Norm (anhydrous weight percent), and Simple Salts (weight percent) of Rustler/Salado Contact Waters (Continued)

| | Site | | |
|---|---|---|---|
| | WIPP-30[33] | WIPP-30[34] | GNOME-5[35] |
| Simple salts | | | |
| $CaCO_3$ | - | - | <0.1 |
| $MgCO_3$ | - | 0.1 | <0.1 |
| $CaSO_4$ | 1.0 | 1.0 | 0.3 |
| $MgSO_4$ | 2.1 | 1.9 | - |
| $K_2SO_4$ | 0.1 | <0.1 | - |
| $Na_2Cl_2$ | 94.7 | 94.1 | 93.8 |
| $K_2Cl_2$ | 0.9 | 1.2 | 1.6 |
| $MgCl_2$ | 1.2 | 1.6 | 4.1 |
| $CaCl_2$ | - | - | 0.2 |

33. Rettig (unpub.); non-representative sample.
34. Bendix (unpub.); preferred sample; salt rose plotted.
35. USGS (unpub. Tech file); salt rose plotted.

Remarks

4. Samples 4 and 5 represent H-4 water collected on the same date. Analysis 5 is preferred because of its better charge balance and because the major solutes agree with results reported by Sandia for another sample collected on the same date (Robinson, 1987).

6. Samples 6 and 7 represent H-5 water collected on the same date. Even though its charge balance is not as good as analysis 6, analysis 7 is preferred because it has a bromide value and because the major solutes agree with results reported by Sandia for another sample collected on the same date (Robinson, 1987). The representativeness of some solute data from H-5 may be questionable due to low productivity leading to incomplete purging.

9. Samples 9 and 10 represent H-7 water collected on the same date. Analysis 10 is preferred, due to its slightly better charge balance and the presence of a bromide value.

11. Samples 11 and 12 represent H-8 water collected on the same date. Analysis 12 is preferred, because it has a bromide value.

## Table 4-3. Chemical Analysis, Salt Norm (anhydrous weight percent), and Simple Salts (weight percent) of Rustler/Salado Contact Waters (Continued)

13. Samples 13 and 14 represent H-9 water collected on the same date. Analysis 14 is preferred, because it has a better charge balance and a bromide value.

15. Samples 15 and 16 represent H-10 water collected on the same date. Analysis 16 is preferred because it has a bromide value, even though its charge balance is not as good as analysis 15.

18. Sample 18 is preferred because the overall salinity is lower, perhaps indicative of purging of introduced drilling brine over a 3-yr period.

19. Probably a nonrepresentative sample; see Lambert and Harvey (1987) for details.

21. Probably a nonrepresentative sample; production rate is 0.5 gallon/day (Mercer and Orr, 1979), not conducive to purging of introduced KCl-enriched drilling brine and/or $CaCl_2$-rich concrete leachate. See Lambert and Harvey (1987) for details.

23. Sample 23 is preferred to 22, even though the salt rose is plotted for 22. 23 was collected according to the criteria of Lambert and Robinson (1984) and is hence deemed more representative. Note that Na and Cl are higher in analysis 23, but the norms are very similar.

26. Sample 26 is preferred to 24 and 25; it was collected according to the criteria of Lambert and Robinson (1984).

28. Neither sample 27 nor 28 is representative. Well ran dry during July 1980 pump test (Lambert and Robinson, 1984). Note profound difference between analyses; the latter sample was taken after 24 hr purging.

30. Sample 30 is preferred over 29, having been collected according to the criteria of Lambert and Robinson (1984), and is hence considered more representative, regardless of the somewhat better charge balance of 29.

32. Preferred over 31 for the same reasons.

34. Preferred over 33 for the same reasons.

## Table 4-4. Chemical Analysis, Salt Norm (anhydrous weight percent), and Simple Salts (weight percent) of Waters Discharged in the Malaga Bend Area (1-5), Laguna Grande de la Sal (6), and Surprise Spring (7-8)

| | Site | | | |
|---|---|---|---|---|
| | USGS-8[1] | USGS-8[2] | USGS-8[3] | ANDERSON[4] |
| Date collected | 2/25/54 | 1/17/64 | 5/1/64 | 4/20/66 |
| Density (g/cc) | 1.207 | 1.209 | 1.214 | 1.214 |
| Chemical analysis | mg/L | mg/L | mg/L | mg/L |
| Mg | 2,020. | 2,750. | 3,540. | 3,790. |
| Ca | 411. | 550. | 436. | 480. |
| Na | 101,000. | 120,000. | 119,000. | 118,000. |
| K | 3,310. | 4,500. | 6,300. | 6,920. |
| Cl | 158,000. | 187,000. | 187,000. | 187,000. |
| $HCO_3$ | 78. | 102. | 146. | 158. |
| $SO_4$ | 10,200. | 13,100. | 15,300. | 17,100. |
| B | - | 15. | 19. | 29. |
| TDS | 275,000. | 328,000. | 332,000. | 334,000. |
| Balance (+/-) | 0.999 | 1.007 | 1.010 | 1.002 |
| Salt norm | | | | |
| Magnesite | <0.1 | <0.1 | <0.1 | <0.1 |
| Epsomite | 0.5 | 0.3 | - | - |
| Polyhalite | 1.1 | 1.2 | 0.9 | 1.0 |
| Leonite | 0.9 | 0.5 | 0.1 | 0.6 |
| Kainite | 4.1 | 5.4 | 8.1 | 8.2 |
| Halite | 93.4 | 92.6 | 90.7 | 89.8 |
| Sylvite | - | - | 0.3 | 0.2 |
| Simple salts | | | | |
| $MgCO_3$ | <0.1 | <0.1 | <0.1 | <0.1 |
| $CaSO_4$ | 0.5 | 0.6 | 0.4 | 0.5 |
| $MgSO_4$ | 3.6 | 4.1 | 5.2 | 5.5 |
| $K_2SO_4$ | 0.8 | 0.6 | 0.3 | 0.7 |
| $Na_2Cl_2$ | 93.4 | 92.6 | 90.7 | 89.9 |
| $K_2Cl_2$ | 1.6 | 2.1 | 3.3 | 3.4 |

1. Kunkler (1980).
2. Kunkler (1980); salt rose plotted.
3. Kunkler (1980).
4. Kunkler (1980); lake surface water.

**Table 4-4. Chemical Analysis, Salt Norm (anhydrous weight percent), and Simple Salts (weight percent) of Waters Discharged in the Malaga Bend Area (1-5), Laguna Grande de la Sal (6), and Surprise Spring (7-8) (Continued)**

| | Site | | | |
|---|---|---|---|---|
| | ANDERSON[5] | GRANDE[6] | SURPRISE[7] | SURPRISE[8] |
| Date collected | 4/20/66 | 9/81 | 1938 | 1975 |
| Density (g/cc) | 1.215 | 1.213 | - | - |
| pH | - | 7.40 | - | - |
| Chemical analysis | mg/L | mg/kg | mg/L | mg/L |
| Mg | 3,820. | 5,610. | 304. | 2,200. |
| Ca | 428. | 376. | 76.6 | 2,000. |
| Sr | - | 24. | 1.0 | 6.0 |
| Li | - | 7.5 | - | 4.0 |
| Na | 118,000. | 87,400. | 1,175. | 14,400. |
| K | 6,930. | 15,700. | 128. | 580. |
| Cl | 187,000. | 157,000. | 3,080. | 30,000. |
| Br | - | 73.2 | - | 16. |
| $HCO_3$ | 164. | - | 150. | 170. |
| $SO_4$ | 16,900. | 12,900. | 2,610. | 3,470. |
| B | 28. | 29. | - | - |
| TDS | 333,000. | 279,000. | 8,210. | 52,900. |
| Balance (+/-) | 1.003 | 0.997 | 0.819 | 1.003 |
| Cl/Br | - | 2,144. | - | 1,875. |
| Salt norm | | | | |
| Dolomite | - | - | - | 0.2 |
| Magnesite | <0.1 | - | 1.2 | - |
| Anhydrite | - | - | 36.7 | 9.3 |
| Kieserite | - | - | 5.3 | - |
| Polyhalite | 0.9 | 1.0 | - | - |
| Leonite | 0.5 | - | - | - |
| Kainite | 8.4 | 8.0 | - | - |
| Halite | 89.9 | 79.7 | 42.1 | 69.2 |
| Sylvite | 0.3 | 4.5 | - | - |
| Carnallite | - | 6.8 | 7.8 | 4.8 |
| Bischofite | - | - | 6.9 | 8.8 |
| Tachyhydrite | - | - | - | 7.4 |

## Table 4-4. Chemical Analysis, Salt Norm (anhydrous weight percent), and Simple Salts (weight percent) of Waters Discharged in the Malaga Bend Area (1-5), Laguna Grande de la Sal (6), and Surprise Spring (7-8) (Continued)

| | Site | | | |
|---|---|---|---|---|
| | ANDERSON[5] | GRANDE[6] | SURPRISE[7] | SURPRISE[8] |
| Simple salts | | | | |
| $CaCO_3$ | - | - | - | 0.1 |
| $MgCO_3$ | <0.1 | - | 1.2 | 0.1 |
| $CaSO_4$ | 0.4 | 0.5 | 36.7 | 9.3 |
| $MgSO_4$ | 5.6 | 5.1 | 5.3 | - |
| $K_2SO_4$ | 0.6 | 0.3 | - | - |
| $Na_2Cl_2$ | 89.9 | 79.8 | 42.1 | 69.4 |
| $K_2Cl_2$ | 3.5 | 10.5 | 3.4 | 2.1 |
| $MgCl_2$ | - | 3.8 | 11.2 | 16.2 |
| $CaCl_2$ | - | - | - | 2.7 |

5. Kunkler (1980); lake water at 10-foot depth.
6. Rettig (unpub.).
7. USGS (unpub.).
8. USGS (unpub.); compare with analysis of Lambert (1983).

Remarks

8. Compare the following analysis of Surprise Spring reported by Lambert (1983), of a sample collected in 1977, analyzed by Sandia National Laboratories (mg/L):

| | |
|---|---|
| Mg | 2000 |
| Ca | 2420 |
| Sr | 60 |
| Li | 4 |
| Na | 14400 |
| K | 580 |
| Cl | 30000 |
| Br | 16 |
| $HCO_3$ | 170 |
| $SO_4$ | 3470 |

## Table 4-5. Chemical Analysis, Salt Norm (anhydrous weight percent), and Simple Salts (weight percent) of Culebra Waters

| | Site | | | |
|---|---|---|---|---|
| | H-1[1] | H-2[2] | H-2[3] | H-3[4] |
| Date collected | 6/2/76 | 2/22/77 | 4/21/86 | 3/17/77 |
| Density (g/cc) | - | - | 1.009 | - |
| pH | 7.6 | 8.4 | 8.0 | 7.4 |
| Chemical analysis | mg/L | mg/L | mg/L | mg/L |
| Mg | 280. | 160. | 167. | 670. |
| Ca | 780. | 690. | 743. | 1,500. |
| Sr | - | - | 9.54 | - |
| Li | - | - | 0.225 | - |
| Na | 9,400. | 2,100. | 3,570. | 19,000. |
| K | 190. | 91. | 93.5 | 630. |
| F | 5.1 | 2.0 | 2.24 | 0.5 |
| Cl | 12,000. | 2,800. | 5,310. | 29,600. |
| Br | - | - | 5.6 | - |
| I | - | - | 0.081 | - |
| $NO_3$ | - | 0.04 | - | 0.3 |
| $HCO_3$ | 105. | 59. | 60. | 115. |
| $CO_3$ | - | 5.0 | - | - |
| $SO_4$ | 7,400. | 3,000. | 2,980. | 5,700. |
| B | 2.4 | 9.5 | 10.4 | 20. |
| TDS | 30,200. | 8,920. | 13,000. | 57,200. |
| Balance (+/-) | 0.962 | 0.987 | 0.977 | 1.017 |
| Cl/Br | - | - | 948. | - |
| Salt norm | | | | |
| Magnesite | 0.2 | 0.5 | 0.3 | 0.1 |
| Anhydrite | - | 19.9 | 17.2 | 6.8 |
| Kieserite | - | - | - | 3.0 |
| Epsomite | - | - | 0.4 | - |
| Polyhalite | - | 7.5 | 5.3 | 4.3 |
| Bloedite | 9.4 | 14.3 | 9.1 | - |
| Glauberite | 18.4 | 5.7 | - | - |
| Aphthitalite | 1.8 | - | - | - |
| Thenardite | 5.2 | - | - | - |
| Halite | 64.8 | 51.6 | 67.1 | 83.5 |
| Carnallite | - | - | - | 2.2 |

## Table 4-5. Chemical Analysis, Salt Norm (anhydrous weight percent), and Simple Salts (weight percent) of Culebra Waters (Continued)

| | Site | | | |
|---|---|---|---|---|
| | H-1[1] | H-2[2] | H-2[3] | H-3[4] |
| Simple salts | | | | |
| $MgCO_3$ | 0.2 | 0.5 | 0.3 | 0.1 |
| $CaSO_4$ | 9.0 | 26.4 | 19.9 | 8.8 |
| $MgSO_4$ | 4.3 | 8.2 | 5.7 | 3.9 |
| $K_2SO_4$ | 1.4 | 2.3 | 1.6 | 1.3 |
| $Na_2SO_4$ | 20.2 | 10.7 | 5.0 | - |
| $Na_2Cl_2$ | 64.8 | 51.8 | 67.5 | 83.7 |
| $K_2Cl_2$ | - | - | - | 1.0 |
| $MgCl_2$ | - | - | - | 1.2 |

1. Mercer (1983); salt rose plotted.
2. Mercer (1983).
3. Bendix (unpub.); salt rose plotted.
4. Mercer (1983).

## Table 4-5. Chemical Analysis, Salt Norm (anhydrous weight percent), and Simple Salts (weight percent) of Culebra Waters (Continued)

| | Site | | | |
|---|---|---|---|---|
| | H-3[5] | H-3[6] | H-4[7] | H-4[8] |
| Date collected | 6/11/84 | 2/4/85 | 12/14/78 | 5/29/81 |
| Density (g/cc) | 1.035 | - | - | 1.010 |
| pH | 7.4 | 7.4 | 7.6 | 8.0 |
| Chemical analysis | mg/L | mg/L | mg/L | mg/L |
| Mg | 829. | 783. | 430. | 455. |
| Ca | 1,550. | 1,470. | 180. | 700. |
| Sr | 22.6 | 30.5 | - | 14. |
| Li | 0.53 | 0.4 | - | 0.39 |
| Na | 17,400. | 18,000. | 5,800. | 6,080. |
| K | 495. | 425. | 180. | 215. |
| F | 2.09 | 1.94 | 1.9 | - |
| Cl | 29,500. | 30,300. | 7,500. | 7,980. |
| Br | 28.8 | 25.8 | - | 41.5 |
| I | 0.133 | 0.138 | - | - |
| $NO_3$ | - | - | 0.09 | - |
| $HCO_3$ | 52.0 | 52.0 | 59. | 71. |
| $SO_4$ | 5,130. | 4,820. | 4,000. | 6,230. |
| B | 30. | 26.3 | 19. | 17.9 |
| TDS | 55,000. | 55,900. | 18,200. | 21,800. |
| Balance (+/-) | 0.973 | 0.974 | 1.015 | 0.959 |
| Cl/Br | 1,020. | 1,170. | - | 192. |
| Salt norm | | | | |
| Magnesite | 0.1 | 0.1 | 0.2 | 0.2 |
| Anhydrite | 9.7 | 9.1 | - | 2.0 |
| Kieserite | 2.9 | 2.6 | - | - |
| Polyhalite | - | - | 0.5 | 7.3 |
| Syngenite | - | - | 3.6 | - |
| Bloedite | - | - | 24.3 | 19.0 |
| Glauberite | - | - | 2.5 | 11.2 |
| Halite | 81.8 | 83.2 | 68.3 | 59.6 |
| Carnallite | 4.0 | 3.4 | - | - |
| Bischofite | 1.3 | 1.4 | - | - |

## Table 4-5. Chemical Analysis, Salt Norm (anhydrous weight percent), and Simple Salts (weight percent) of Culebra Waters (Continued)

| | Site | | | |
|---|---|---|---|---|
| | H-3[5] | H-3[6] | H-4[7] | H-4[8] |
| Simple salts | | | | |
| $MgCO_3$ | 0.1 | 0.6 | 0.2 | 0.2 |
| $CaSO_4$ | 9.8 | 9.1 | 3.1 | 11.1 |
| $MgSO_4$ | 2.9 | 2.6 | 11.3 | 10.4 |
| $K_2SO_4$ | - | - | 2.2 | 2.3 |
| $Na_2SO_4$ | - | - | 14.5 | 16.1 |
| $Na_2Cl_2$ | 82.0 | 83.4 | 68.7 | 60.0 |
| $K_2Cl_2$ | 1.8 | 1.5 | - | - |
| $MgCl_2$ | 3.5 | 3.3 | - | - |

5. Bendix (unpub.); sample is representative; salt rose plotted.
6. Bendix (unpub.); sample is representative.
7. Mercer (1983).
8. Bendix (unpub.).

## Table 4-5. Chemical Analysis, Salt Norm (anhydrous weight percent), and Simple Salts (weight percent) of Culebra Waters (Continued)

| | Site | | | |
|---|---|---|---|---|
| | H-4[9] | H-4[10] | H-5[11] | H-5[12] |
| Date collected | 8/10/84 | 7/20/85 | 12/19/78 | 6/1/81 |
| Density (g/cc) | 1.010 | 1.015 | - | 1.100 |
| pH | 7.8 | 7.7 | 6.8 | 7.9 |
| Chemical analysis | mg/L | mg/L | mg/L | mg/L |
| Mg | 505. | 427. | 1,900. | 2,140. |
| Ca | 698. | 691. | 360. | 1,710. |
| Sr | 17.8 | 14.3 | - | 31.6 |
| Li | 0.49 | 0.40 | - | 0.77 |
| Na | 6,150. | 5,850. | 53,000. | 52,400. |
| K | 222. | 210. | 1,400. | 1,290. |
| F | 2.13 | - | 1.4 | - |
| Cl | 7,950. | 7,480. | 86,000. | 89,500. |
| Br | 47.7 | 42.6 | - | 62.5 |
| I | 0.226 | - | - | - |
| $NO_3$ | - | - | 0.04 | - |
| $HCO_3$ | 75. | 70. | 41. | 80. |
| $SO_4$ | 5,700. | 5,520. | 810. | 7,360. |
| B | 19.8 | 14.1 | 36. | 33.2 |
| TDS | 21,400. | 20,300. | 144,000. | 155,000. |
| Balance (+/-) | 1.014 | 1.007 | 1.029 | 0.963 |
| Cl/Br | 167. | 176. | - | 1,430. |
| Salt norm | | | | |
| Dolomite | - | - | <0.1 | - |
| Magnesite | 0.2 | 0.2 | - | <0.1 |
| Anhydrite | 5.5 | 3.3 | 0.8 | 3.0 |
| Kieserite | - | - | - | 2.5 |
| Polyhalite | 7.5 | 7.5 | - | - |
| Bloedite | 21.0 | 18.4 | - | - |
| Glauberite | 3.5 | 9.1 | - | - |
| Halite | 61.7 | 61.0 | 92.2 | 88.4 |
| Carnallite | - | - | 4.2 | 3.7 |
| Bischofite | - | - | 2.7 | 1.4 |

## Table 4-5. Chemical Analysis, Salt Norm (anhydrous weight percent), and Simple Salts (weight percent) of Culebra Waters (Continued)

| | Site | | | |
|---|---|---|---|---|
| | H-4[9] | H-4[10] | H-5[11] | H-5[12] |
| Simple salts | | | | |
| $CaCO_3$ | - | - | <0.1 | - |
| $MgCO_3$ | 0.2 | 0.2 | <0.1 | <0.1 |
| $CaSO_4$ | 10.8 | 11.4 | 0.8 | 3.9 |
| $MgSO_4$ | 11.3 | 10.1 | - | 2.5 |
| $K_2SO_4$ | 2.3 | 2.3 | - | - |
| $Na_2SO_4$ | 13.2 | 14.7 | - | - |
| $Na_2Cl_2$ | 62.1 | 61.3 | 92.3 | 88.5 |
| $K_2Cl_2$ | - | - | 1.8 | 1.6 |
| $MgCl_2$ | - | - | 5.0 | 3.5 |

9. Bendix (unpub.).
10. Bendix (unpub.); preferred sample; salt rose plotted.
11. Mercer (1983).
12. Bendix (unpub.).

## Table 4-5. Chemical Analysis, Salt Norm (anhydrous weight percent), and Simple Salts (weight percent) of Culebra Waters (Continued)

| | Site | | | |
|---|---|---|---|---|
| | H-5[13] | H-5[14] | H-6[15] | H-6[16] |
| Date collected | 10/15/81 | 8/27/85 | 12/20/78 | 5/2/81 |
| Density (g/cc) | 1.100 | 1.104 | - | 1.040 |
| pH | 7.9 | 7.4 | 7.3 | 7.0 |
| Chemical analysis | mg/L | mg/L | mg/L | mg/L |
| Mg | 2,150. | 2,170. | 970. | 1,080. |
| Ca | 1,720. | 1,700. | 1,200. | 2,150. |
| Sr | 31.3 | 29.3 | - | 32.0 |
| Li | 0.77 | 0.81 | - | 0.44 |
| Na | 52,300. | 54,100. | 18,000. | 18,600. |
| K | 1,300. | 1,350. | 500. | 450. |
| F | - | 1.95 | 1.5 | - |
| Cl | 89,500. | 85,400. | 28,000. | 33,000. |
| Br | 64. | 48.6 | - | 34.3 |
| I | - | 0.191 | - | - |
| $NO_3$ | - | - | 0.09 | - |
| $HCO_3$ | 86. | 49. | - | 96. |
| $SO_4$ | 7,570 | 7,840. | 3,800. | 3,980. |
| B | 35.2 | 33.7 | 9.5 | 10.9 |
| TDS | 155,000. | 153,000. | 52,500. | 59,400. |
| Balance (+/-) | 0.958 | 1.030 | 1.076 | 1.001 |
| Cl/Br | 1,400. | 1,760. | - | 962. |
| Salt norm | | | | |
| Dolomite | - | - | - | 0.1 |
| Magnesite | <0.1 | <0.1 | - | - |
| Anhydrite | 3.9 | 3.7 | 7.4 | 9.5 |
| Kieserite | 2.6 | 3.2 | 2.8 | - |
| Halite | 88.3 | 88.4 | 83.3 | 79.6 |
| Carnallite | 3.8 | 3.8 | 4.0 | 3.3 |
| Bischofite | 1.4 | 0.7 | 2.5 | 1.6 |
| Tachyhydrite | - | - | - | 5.8 |

## Table 4-5. Chemical Analysis, Salt Norm (anhydrous weight percent), and Simple Salts (weight percent) of Culebra Waters (Continued)

| | Site | | | |
|---|---|---|---|---|
| | H-5[13] | H-5[14] | H-6[15] | H-6[16] |
| Simple salts | | | | |
| $CaCO_3$ | - | - | - | 0.1 |
| $MgCO_3$ | <0.1 | <0.1 | - | 0.1 |
| $CaSO_4$ | 3.9 | 3.7 | 7.4 | 9.5 |
| $MgSO_4$ | 2.6 | 3.2 | 2.8 | - |
| $Na_2Cl_2$ | 88.4 | 88.6 | 83.4 | 79.7 |
| $K_2Cl_2$ | 1.7 | 1.7 | 1.7 | 1.5 |
| $MgCl_2$ | 3.5 | 2.9 | 4.7 | 7.1 |
| $CaCl_2$ | - | - | - | 2.1 |

13. Bendix (unpub.).
14. Bendix (unpub.); preferred sample; salt rose plotted.
15. Mercer (1983).
16. Bendix (unpub.).

## Table 4-5. Chemical Analysis, Salt Norm (anhydrous weight percent), and Simple Salts (weight percent) of Culebra Waters (Continued)

| | Site | | | |
|---|---|---|---|---|
| | H-6[17] | H-7[18] | H-7[19] | H-7[20] |
| Date collected | 9/15/85 | 3/20/80 | 3/20/80 | 3/26/86 |
| Density (g/cc) | 1.042 | 1.001 | 1.000 | 1.001 |
| pH | 6.9 | 7.0 | 7.65 | 7.2 |
| Chemical analysis | mg/L | mg/L | mg/kg | mg/L |
| Mg | 1,040. | 130. | 130. | 130. |
| Ca | 2,040. | 590. | 530. | 587. |
| Sr | 30.4 | - | 12. | 8.51 |
| Li | 0.45 | - | 0.1 | 0.1 |
| Na | 18,000. | 210. | 238. | 207. |
| K | 375. | 1.4 | 11. | 7.0 |
| F | 1.9 | 1.4 | - | 1.51 |
| Cl | 32,330. | 350. | 337. | 320. |
| Br | 34.0 | - | 0.76 | 0.57 |
| I | 0.096 | - | - | 0.053 |
| $NO_3$ | - | 1.8 | - | - |
| $HCO_3$ | 94. | - | 130. | 120. |
| $SO_4$ | 3,570. | 1,900. | 1,960. | 1,850. |
| B | 10.4 | 0.78 | 1.9 | 0.755 |
| TDS | 58,000. | 3,190. | 3,350. | 3,230. |
| Balance (+/-) | 0.992 | 0.995 | 0.915 | 0.995 |
| Cl/Br | 951. | - | 443. | 561. |
| Salt norm | | | | |
| Dolomite | 0.1 | - | - | - |
| Magnesite | - | - | 2.7 | 2.6 |
| Anhydrite | 8.8 | 63.1 | 57.1 | 62.3 |
| Kieserite | - | 18.8 | - | - |
| Epsomite | - | - | 13.0 | 16.0 |
| Polyhalite | - | - | 2.6 | 1.6 |
| Bloedite | - | - | 7.1 | 0.1 |
| Halite | 80.0 | 16.8 | 16.4 | 16.6 |
| Carnallite | 2.9 | 0.2 | - | - |
| Bischofite | 1.0 | 0.9 | - | - |
| Tachyhydrite | 7.0 | - | - | - |

## Table 4-5. Chemical Analysis, Salt Norm (anhydrous weight percent), and Simple Salts (weight percent) of Culebra Waters (Continued)

| | Site | | | |
|---|---|---|---|---|
| | H-6[17] | H-7[18] | H-7[19] | H-7[20] |
| Simple salts | | | | |
| $CaCO_3$ | 0.1 | - | - | - |
| $MgCO_3$ | 0.1 | - | 2.7 | 2.6 |
| $CaSO_4$ | 8.8 | 63.3 | 59.0 | 63.6 |
| $MgSO_4$ | - | 18.8 | 17.0 | 16.5 |
| $K_2SO_4$ | - | - | 0.8 | 0.5 |
| $Na_2SO_4$ | - | - | 3.9 | 0.1 |
| $Na_2Cl_2$ | 80.2 | 16.9 | 16.6 | 16.7 |
| $K_2Cl_2$ | 1.3 | 0.1 | - | - |
| $MgCl_2$ | 7.1 | 1.0 | - | - |
| $CaCl_2$ | 2.6 | - | - | - |

17. Bendix (unpub.); salt rose plotted.
18. Mercer (1983).
19. Rettig (unpub.).
20. Bendix (unpub.); preferred analysis; salt rose plotted.

## Table 4-5. Chemical Analysis, Salt Norm (anhydrous weight percent), and Simple Salts (weight percent) of Culebra Waters (Continued)

| | Site | | | |
|---|---|---|---|---|
| | H-8[21] | H-8[22] | H-8[23] | H-9[24] |
| Date collected | 2/11/80 | 2/11/80 | 1/22/86 | 2/5/80 |
| Density (g/cc) | 1.000 | 1.000 | 1.002 | 1.000 |
| pH | 7.3 | 7.61 | 7.6 | 7.57 |
| Chemical analysis | mg/L | mg/kg | mg/L | mg/kg |
| Mg | 170. | 150. | 157. | 150. |
| Ca | 570. | 530. | 548. | 580. |
| Sr | - | 7.0 | 6.92 | 11. |
| Li | - | 0.1 | 0.115 | 0.2 |
| Na | 82. | 81. | 55.1 | 220. |
| K | 4.7 | 4.3 | 3.83 | 8. |
| F | 2.4 | - | 2.45 | - |
| Cl | 57. | 60. | 30.5 | 327. |
| Br | - | 0.18 | 0.085 | 0.58 |
| I | - | - | 0.145 | - |
| $NO_3$ | 4.2 | - | - | - |
| $HCO_3$ | - | 76. | 95. | 110. |
| $SO_4$ | 2,000. | 2,050. | 1,950. | 2,070. |
| B | 0.58 | 0.89 | 0.485 | 1.1 |
| TDS | 2,890. | 2,960. | 2,850. | 3,480. |
| Balance (+/-) | 1.061 | 0.933 | 0.994 | 0.947 |
| Cl/Br | - | 333. | 359. | 564. |
| Salt norm | | | | |
| Magnesite | - | 1.8 | 2.4 | 2.2 |
| Anhydrite | 63.9 | 64.3 | 66.2 | 58.9 |
| Epsomite | 23.7 | 19.7 | 20.6 | 17.4 |
| Polyhalite | 0.5 | 1.1 | 1.0 | 1.8 |
| Bloedite | 8.1 | 9.28 | 7.2 | 3.3 |
| Halite | 3.3 | 3.3 | 1.8 | 15.5 |

## Table 4-5. Chemical Analysis, Salt Norm (anhydrous weight percent), and Simple Salts (weight percent) of Culebra Waters (Continued)

| | Site | | | |
|---|---|---|---|---|
| | H-8[21] | H-8[22] | H-8[23] | H-9[24] |
| Simple salts | | | | |
| $MgCO_3$ | - | 1.8 | 2.4 | 2.2 |
| $CaSO_4$ | 64.5 | 65.3 | 67.2 | 60.3 |
| $MgSO_4$ | 27.7 | 24.3 | 24.4 | 19.5 |
| $K_2SO_4$ | 0.1 | 0.3 | 0.3 | 0.5 |
| $Na_2SO_4$ | 4.4 | 5.0 | 4.0 | 1.8 |
| $Na_2Cl_2$ | 3.3 | 3.4 | 1.8 | 15.7 |

21. Mercer (1983).
22. Rettig (unpub.).
23. Bendix (unpub.); preferred sample; salt rose plotted.
24. Rettig (unpub.).

## Table 4-5. Chemical Analysis, Salt Norm (anhydrous weight percent), and Simple Salts (weight percent) of Culebra Waters (Continued)

| | Site | | | |
|---|---|---|---|---|
| | H-9[25] | H-10[26] | H-11[27] | H-12[28] |
| Date collected | 11/14/85 | 3/21/80 | 6/3/85 | 8/8/85 |
| Density (g/cc) | 1.002 | 1.044 | 1.090 | 1.096 |
| pH | 7.4 | 8.01 | 7.2 | 7.2 |
| Chemical analysis | mg/L | mg/kg | mg/L | mg/L |
| Mg | 137. | 785. | 1,320. | 1,980. |
| Ca | 590. | 1,580. | 1,700. | 1,760. |
| Sr | 7.5 | 19. | 24.7 | 30.6 |
| Li | 0.175 | 0.6 | 0.615 | 1.15 |
| Na | 146. | 20,600. | 40,400. | 49,200. |
| K | 6.85 | 479. | 943. | 1,270. |
| F | 3.31 | - | - | - |
| Cl | 194. | 33,600. | 65,900. | 79,000. |
| Br | .24 | 12. | 47.4 | 76. |
| I | 0.11 | - | - | - |
| $HCO_3$ | 110. | 50. | 55. | 53. |
| $SO_4$ | 1,903. | 4,950. | 7,180. | 7,210. |
| B | 0.63 | 29. | 31.7 | 39.3 |
| TDS | 3,100. | 62,100. | 118,000. | 141,000. |
| Balance (+/-) | 1.007 | 0.999 | 0.983 | 1.018 |
| Cl/Br | 808. | 2,800. | 1,390. | 1,040. |
| Salt norm | | | | |
| Magnesite | 2.5 | 0.1 | <0.1 | <0.1 |
| Anhydrite | 64.7 | 8.6 | 4.8 | 4.2 |
| Kieserite | - | 2.3 | 3.1 | 2.7 |
| Epsomite | 16.2 | - | - | - |
| Polyhalite | 1.6 | - | 0.3 | - |
| Bloedite | 3.6 | - | - | - |
| Halite | 10.5 | 84.3 | 88.3 | 88.0 |
| Carnallite | - | 3.4 | 3.3 | 3.9 |
| Bischofite | - | 1.1 | - | 1.0 |

## Table 4-5. Chemical Analysis, Salt Norm (anhydrous weight percent), and Simple Salts (weight percent) of Culebra Waters (Continued)

| | Site | | | |
|---|---|---|---|---|
| | H-9[25] | H-10[26] | H-11[27] | H-12[28] |
| Simple salts | | | | |
| $MgCO_3$ | 2.5 | 0.1 | <0.1 | 0.3 |
| $CaSO_4$ | 66.1 | 8.7 | 5.0 | 4.2 |
| $MgSO_4$ | 18.3 | 2.3 | 3.1 | 2.7 |
| $K_2SO_4$ | 0.5 | - | 0.1 | - |
| $Na_2SO_4$ | 2.0 | - | - | - |
| $Na_2Cl_2$ | 10.6 | 84.6 | 88.4 | 88.1 |
| $K_2Cl_2$ | - | 1.5 | 1.5 | 1.7 |
| $MgCl_2$ | - | 3.0 | 1.9 | 3.2 |

25. Bendix (unpub.); preferred sample; salt rose plotted.
26. Rettig (unpub.); salt rose plotted.
27. Bendix (unpub.); salt rose plotted.
28. Bendix (unpub.); salt rose plotted.

## Table 4-5. Chemical Analysis, Salt Norm (anhydrous weight percent), and Simple Salts (weight percent) of Culebra Waters (Continued)

| | Site | | | |
|---|---|---|---|---|
| | ENGLE[29] | P-14[30] | P-14[31] | P-15[32] |
| Date collected | 3/5/85 | 3/14/77 | 2/26/86 | 5/10/77 |
| Density (g/cc) | - | - | 1.019 | - |
| pH | 7.4 | 6.0 | 6.8 | - |
| Chemical analysis | mg/L | mg/L | mg/L | mg/L |
| Mg | 152. | 760. | 840. | 63. |
| Ca | 588. | 3,100. | 3,510. | 770. |
| Sr | 8.36 | - | 50.8 | - |
| Li | 0.17 | - | 0.275 | - |
| Na | 200. | 7,600. | 4,360. | 6,900. |
| K | 5.6 | 600. | 37.9 | 1,700. |
| F | 2.8 | 0.9 | 1.69 | 1.2 |
| Cl | 231. | 20,000. | 14,470. | 11,000. |
| Br | 0.27 | - | 72. | - |
| I | 0.116 | - | 0.415 | - |
| $NO_3$ | - | 0.04 | - | 0.2 |
| $HCO_3$ | 110. | 357. | 110. | 63. |
| $CO_3$ | - | - | - | 24. |
| $SO_4$ | 1,990. | 1,400. | 1,590. | 3,200. |
| B | 0.97 | 0.7 | 0.72 | 4.7 |
| TDS | 3,290. | 33,800. | 25,000. | 23,700. |
| Balance (+/-) | 1.019 | 0.940 | 0.983 | 1.022 |
| Cl/Br | 856. | - | 201. | - |
| Salt norm | | | | |
| Dolomite | - | 0.8 | 0.3 | - |
| Magnesite | 2.4 | - | - | 0.3 |
| Anhydrite | 60.3 | 5.8 | 9.0 | 2.4 |
| Epsomite | 15.1 | - | - | - |
| Polyhalite | 1.2 | - | - | 3.8 |
| Syngenite | - | - | - | 15.1 |
| Bloedite | 8.2 | - | - | - |
| Halite | 11.8 | 59.7 | 45.0 | 73.0 |
| Sylvite | - | - | - | 5.3 |
| Carnallite | - | 8.1 | 0.7 | - |
| Tachyhydrite | - | 6.8 | 20.3 | - |
| Antarcticite | - | 18.9 | 24.4 | - |

## Table 4-5. Chemical Analysis, Salt Norm (anhydrous weight percent), and Simple Salts (weight percent) of Culebra Waters (Continued)

| | Site | | | |
|---|---|---|---|---|
| | ENGEL[29] | P-14[30] | P-14[31] | P-15[32] |
| Simple salts | | | | |
| $CaCO_3$ | - | 0.4 | 0.2 | - |
| $MgCO_3$ | 2.4 | 0.4 | 0.2 | 0.3 |
| $CaSO_4$ | 61.4 | 5.8 | 9.0 | 10.9 |
| $MgSO_4$ | 19.4 | - | - | 0.8 |
| $K_2SO_4$ | 0.4 | - | - | 9.7 |
| $Na_2SO_4$ | 4.5 | - | - | - |
| $Na_2Cl_2$ | 11.9 | 59.7 | 45.1 | 73.1 |
| $K_2Cl_2$ | - | 3.5 | 0.3 | 5.3 |
| $MgCl_2$ | - | 8.8 | 13.2 | - |
| $CaCl_2$ | - | 21.4 | 32.0 | - |

29. Bendix (unpub.).
30. Mercer (1983).
31. Bendix (unpub.); preferred sample; salt rose plotted.
32. Mercer (1983).

## Table 4-5. Chemical Analysis, Salt Norm (anhydrous weight percent), and Simple Salts (weight percent) of Culebra Waters (Continued)

| | Site | | | |
|---|---|---|---|---|
| | P-17[33] | P-17[34] | P-18[35] | WIPP-25[36] |
| Date collected | 5/10/77 | 3/17/86 | 5/10/77 | 8/14/80 |
| Density (g/cc) | - | 1.065 | - | 1.014 |
| pH | 7.4 | 7.5 | 7.2 | 7.3 |
| Chemical analysis | mg/L | mg/L | mg/L | mg/L |
| Mg | 1,600. | 1,460. | 16,000. | 250. |
| Ca | 1,700. | 1,620. | 5,600. | 920. |
| Sr | - | 29.1 | - | - |
| Li | - | 0.87 | - | - |
| Na | 30,000. | 28,300. | 9,200. | 5,100. |
| K | 120. | 782. | 6,200. | 0.9 |
| F | 1.5 | 1.87 | 1.2 | 1.4 |
| Cl | 54,000. | 48,200. | 80,000. | 8,300. |
| Br | - | 71.5 | - | - |
| I | - | 0.175 | - | - |
| $NO_3$ | 0.3 | - | 3.6 | 3.0 |
| $HCO_3$ | 77. | 61. | 310. | - |
| $SO_4$ | 5,000. | 6,020. | 980. | 2,400. |
| B | 1.7 | 37.5 | 100. | 1.9 |
| TDS | 92,500. | 86,600. | 118,000. | 17,000. |
| Balance (+/-) | 0.936 | 0.978 | 0.942 | 1.014 |
| Cl/Br | - | 674. | - | - |
| Salt norm | | | | |
| Dolomite | - | - | 0.2 | - |
| Magnesite | 0.1 | <0.1 | - | - |
| Anhydrite | 6.5 | 6.5 | 1.2 | 18.2 |
| Kieserite | 0.9 | 2.9 | - | 1.7 |
| Halite | 86.0 | 84.4 | 20.6 | 75.7 |
| Carnallite | 0.6 | 4.0 | 23.7 | <0.1 |
| Bischofite | 6.0 | 2.0 | 20.6 | 4.3 |
| Tachyhydrite | - | - | 33.4 | - |

## Table 4-5. Chemical Analysis, Salt Norm (anhydrous weight percent), and Simple Salts (weight percent) of Culebra Waters (Continued)

| | Site | | | |
|---|---|---|---|---|
| | P-17[33] | P-17[34] | P-18[35] | WIPP-25[36] |
| Simple salts | | | | |
| $CaCO_3$ | - | - | 0.1 | - |
| $MgCO_3$ | 0.1 | <0.1 | 0.1 | - |
| $CaSO_4$ | 6.5 | 6.5 | 1.2 | 18.3 |
| $MgSO_4$ | 0.9 | 2.9 | - | 1.7 |
| $Na_2Cl_2$ | 86.0 | 84.6 | 20.6 | 75.7 |
| $K_2Cl_2$ | 0.3 | 1.8 | 10.4 | <0.1 |
| $MgCl_2$ | 6.3 | 4.3 | 55.2 | 4.3 |
| $CaCl_2$ | - | - | 12.3 | - |

33. Mercer (1983); nonrepresentative sample.
34. Bendix (unpub.); preferred sample; salt rose plotted.
35. Mercer (1983); nonrepresentative sample; salt rose plotted.
36. Mercer (1983).

## Table 4-5. Chemical Analysis, Salt Norm (anhydrous weight percent), and Simple Salts (weight percent) of Culebra Waters (Continued)

| | Site | | | |
|---|---|---|---|---|
| | WIPP-25[37] | WIPP-25[38] | WIPP-25[39] | WIPP-26[40] |
| Date collected | 8/14/80 | 8/20/80 | 2/12/86 | 8/18/80 |
| Density (g/cc) | 1.011 | 1.010 | 1.010 | 1.009 |
| pH | 7.11 | 6.9 | 7.2 | 7.34 |
| Chemical analysis | mg/kg | mg/L | mg/L | mg/kg |
| Mg | 247. | 260. | 315. | 362. |
| Ca | 890. | 905. | 1,140. | 1,190. |
| Sr | 12. | 12. | 16.6 | 19. |
| Li | 0.2 | 0.2 | 0.22 | 0.2 |
| Na | 5,300. | 3,160. | 3,180. | 3,770. |
| K | 69. | 73.5 | 102. | 149. |
| F | - | - | 1.68 | - |
| Cl | 8,020. | 5,250. | 6,320. | 7,260. |
| Br | 2.4 | 2.6 | 3.35 | 3.0 |
| I | - | - | 0.042 | - |
| $HCO_3$ | - | 210. | 130. | - |
| $SO_4$ | 2,570. | 2,500. | 2,380. | 2,380. |
| B | 1.8 | 1.52 | 1.67 | 1.8 |
| TDS | 17,100. | 12,400. | 13,600. | 15,100. |
| Balance (+/-) | 1.063 | 1.013 | 0.974 | 1.012 |
| Cl/Br | 3,340. | 2,020. | 1,890. | 2,420. |
| Salt norm | | | | |
| Dolomite | - | - | 0.7 | - |
| Magnesite | - | 1.2 | - | - |
| Anhydrite | 17.0 | 24.9 | 24.7 | 22.4 |
| Kieserite | 4.1 | 3.5 | - | - |
| Halite | 75.8 | 65.0 | 60.8 | 62.8 |
| Carnallite | 1.7 | 2.6 | 3.3 | 4.2 |
| Bischofite | 1.2 | 2.6 | 1.7 | - |
| Tachyhydrite | - | - | 8.4 | 9.0 |
| Antarcticite | - | - | - | 1.2 |

## Table 4-5. Chemical Analysis, Salt Norm (anhydrous weight percent), and Simple Salts (weight percent) of Culebra Waters (Continued)

| | Site | | | |
|---|---|---|---|---|
| | WIPP-25[37] | WIPP-25[38] | WIPP-25[39] | WIPP-26[40] |
| Simple salts | | | | |
| $CaCO_3$ | - | - | 0.4 | - |
| $MgCO_3$ | - | 1.2 | 0.3 | - |
| $CaSO_4$ | 17.0 | 24.9 | 24.8 | 22.4 |
| $MgSO_4$ | 4.1 | 3.5 | - | - |
| $Na_2Cl_2$ | 75.9 | 65.1 | 61.0 | 63.0 |
| $K_2Cl_2$ | 0.7 | 1.1 | 1.5 | 1.9 |
| $MgCl_2$ | 2.2 | 4.1 | 8.9 | 9.3 |
| $CaCl_2$ | - | - | 3.1 | 3.3 |

37. Rettig (unpub.).
38. Bendix (unpub.); preferred sample; salt rose plotted.
39. Bendix (unpub.).
40. Rettig (unpub.); salt rose plotted.

## Table 4-5. Chemical Analysis, Salt Norm (anhydrous weight percent), and Simple Salts (weight percent) of Culebra Waters (Continued)

| | Site | | | |
|---|---|---|---|---|
| | WIPP-26[41] | WIPP-26[42] | WIPP-27[43] | WIPP-27[44] |
| Date collected | 8/24/80 | 11/25/85 | 8/22/80 | 9/3/80 |
| Density (g/cc) | 1.005 | 1.012 | 1.092 | 1.090 |
| pH | 6.9 | 7.1 | 6.63 | 6.3 |
| Chemical analysis | mg/L | mg/L | mg/kg | mg/L |
| Mg | 355. | 380. | 1,740. | 1,900. |
| Ca | 1,240. | 1,340. | 2,700. | 3,210. |
| Sr | 16.8 | 19.5 | 44. | 50.9 |
| Li | 0.24 | 0.23 | - | 0.33 |
| Na | 3,620. | 4,220. | 38,500. | 39,200. |
| K | 170. | 343. | 7,140. | 8,060. |
| F | - | 1.73 | - | - |
| Cl | 7,200. | 8,770. | 73,300. | 78,500. |
| Br | 3.2 | 3.9 | 27. | 28.3 |
| I | - | 0.070 | - | - |
| $HCO_3$ | 140. | 120. | - | 120. |
| $SO_4$ | 2,480. | 2,420. | 3,300. | 3,830. |
| B | 1.45 | 1.65 | 2.1 | 2.3 |
| TDS | 15,200. | 17,600. | 127,000. | 135,000. |
| Balance (+/-) | 0.985 | 0.970 | 1.000 | 0.971 |
| Cl/Br | 2,250. | 2,250. | 2,710. | 2,770. |
| Salt norm | | | | |
| Calcite | - | - | - | 0.1 |
| Dolomite | 0.7 | 0.5 | - | - |
| Anhydrite | 23.1 | 19.3 | 3.7 | 4.0 |
| Halite | 61.3 | 62.3 | 77.2 | 75.3 |
| Sylvite | - | - | 6.5 | 7.2 |
| Carnallite | 4.9 | 8.7 | 9.6 | 10.0 |
| Tachyhydrite | 9.7 | 5.6 | - | - |
| Antarcticite | <0.1 | 3.4 | 2.9 | 3.4 |

## Table 4-5. Chemical Analysis, Salt Norm (anhydrous weight percent), and Simple Salts (weight percent) of Culebra Waters (Continued)

| | Site | | | |
|---|---|---|---|---|
| | WIPP-26[41] | WIPP-26[42] | WIPP-27[43] | WIPP-27[44] |
| Simple salts | | | | |
| $CaCO_3$ | 0.4 | 0.3 | - | 0.1 |
| $MgCO_3$ | 0.3 | 0.2 | - | - |
| $CaSO_4$ | 23.1 | 19.4 | 3.7 | 4.0 |
| $Na_2Cl_2$ | 61.5 | 62.5 | 77.3 | 75.3 |
| $K_2Cl_2$ | 2.2 | 3.8 | 10.8 | 11.6 |
| $MgCl_2$ | 8.9 | 8.40 | 5.4 | 5.6 |
| $CaCl_2$ | 3.6 | 5.4 | 2.9 | 3.4 |

41. Bendix (unpub.); preferred 1980 sample.
42. Bendix (unpub.).
43. Rettig (unpub.).
44. Bendix (unpub.); preferred sample; affected by potash inwash.

## Table 4-5. Chemical Analysis, Salt Norm (anhydrous weight percent), and Simple Salts (weight percent) of Culebra Waters (Continued)

| | Site | | | |
|---|---|---|---|---|
| | WIPP-28[45] | WIPP-28[46] | WIPP-29[47] | WIPP-27[48] |
| Date collected | 8/21/80 | 9/11/80 | 8/20/80 | 8/28/80 |
| Density (g/cc) | 1.041 | 1.030 | 1.174 | 1.160 |
| pH | 6.80 | 6.5 | 6.88 | 6.1 |
| Chemical analysis | mg/kg | mg/L | mg/kg | mg/L |
| Mg | 624. | 555. | 3,750. | 5,480. |
| Ca | 1,130. | 1,180. | 698. | 950. |
| Sr | 17. | 15.5 | 20. | 28.8 |
| Li | - | 0.3 | 1.0 | 0.78 |
| Na | 19,900. | 15,200. | 67,600. | 71,400. |
| K | 346. | 485. | 12,700. | 15,600. |
| Cl | 32,400. | 24,800. | 123,000. | 138,000. |
| Br | 1.0 | 7.2 | 44. | 45. |
| $HCO_3$ | - | - | - | 210. |
| $SO_4$ | 3,360. | 4,380. | 11,200. | 14,000. |
| B | 2.9 | 5.83 | - | 4.4 |
| TDS | 57,800. | 46,600. | 219,000. | 246,000. |
| Balance (+/-) | 0.999 | 0.984 | 0.975 | 0.956 |
| Cl/Br | 32,400. | 3,440. | 2,800. | 3,070. |
| Salt norm | | | | |
| Magnesite | - | - | - | 0.1 |
| Anhydrite | 6.6 | 7.7 | - | - |
| Kieserite | 1.4 | 3.1 | - | - |
| Polyhalite | - | 2.0 | 2.3 | 2.8 |
| Kainite | - | - | 7.1 | 7.8 |
| Halite | 87.6 | 83.7 | 79.7 | 76.0 |
| Sylvite | - | - | 5.6 | 5.1 |
| Carnallite | 2.6 | 3.3 | 5.3 | 8.6 |
| Bischofite | 1.7 | - | - | - |

## Table 4-5. Chemical Analysis, Salt Norm (anhydrous weight percent), and Simple Salts (weight percent) of Culebra Waters (Continued)

| | Site | | | |
|---|---|---|---|---|
| | WIPP-28[45] | WIPP-28[46] | WIPP-29[47] | WIPP-27[48] |
| Simple salts | | | | |
| $MgCO_3$ | - | - | - | 0.1 |
| $CaSO_4$ | 6.7 | 8.7 | 1.1 | 1.4 |
| $MgSO_4$ | 1.4 | 3.5 | 4.9 | 5.2 |
| $K_2SO_4$ | - | 0.6 | 0.7 | 0.9 |
| $Na_2Cl_2$ | 87.7 | 83.8 | 79.7 | 76.0 |
| $K_2Cl_2$ | 1.1 | 1.5 | 10.6 | 11.7 |
| $MgCl_2$ | 3.1 | 1.9 | 3.0 | 4.8 |

45. Rettig (unpub.).
46. Bendix (unpub.); preferred sample; salt rose plotted.
47. Rettig (unpub.).
48. Bendix (unpub.); preferred 1980 sample; affected by potash.

## Table 4-5. Chemical Analysis, Salt Norm (anhydrous weight percent), and Simple Salts (weight percent) of Culebra Waters (Continued)

| | Site | | | |
|---|---|---|---|---|
| | WIPP-29[49] | WIPP-30[50] | WIPP-30[51] | GNOME SH[52] |
| Date collected | 12/14/85 | 8/13/80 | 9/6/80 | 12/10/60 |
| Density (g/cc) | 1.216 | 1.070 | 1.020 | - |
| pH | 5.9 | 6.36 | 8.8 | 7.7 |
| Chemical analysis | mg/L | mg/kg | mg/L | mg/kg |
| Mg | 6,500 | 804. | 460. | 153. |
| Ca | 413. | 1,010. | 1,140. | 597. |
| Sr | 12.8 | 15. | 17.9 | - |
| Li | 0.7 | - | 0.27 | - |
| Na | 94,900. | 35,500. | 8,570. | 555. |
| K | 23,300. | 888. | 255. | 17. |
| F | 4.59 | - | - | 1.9 |
| Cl | 178,800. | 56,500. | 14,600. | 828. |
| Br | 61. | 30. | 10.5 | - |
| I | 0.385 | - | - | - |
| $NO_3$ | - | - | - | 11. |
| $HCO_3$ | 160. | - | 40. | 106. |
| $CO_3$ | - | - | 17. | - |
| $SO_4$ | 20,000. | 5,050. | 4,120. | 2,040. |
| $PO_4$ | - | - | - | 12. |
| B | 5.17 | 18. | 6.09 | - |
| TDS | 324,000. | 99,800. | 29,200. | 4,320. |
| Balance (+/-) | 0.967 | 0.991 | 0.950 | 0.981 |
| Cl/Br | 2,930. | 1,880. | 1,390. | - |
| Salt norm | | | | |
| Magnesite | <0.1 | - | 0.2 | 1.7 |
| Anhydrite | - | 1.9 | 13.5 | 47.3 |
| Kieserite | - | 1.9 | 5.0 | - |
| Epsomite | - | - | - | 12.7 |
| Polyhalite | 0.9 | 3.2 | 0.3 | 1.8 |
| Bloedite | - | - | - | 3.8 |
| Kainite | 11.1 | - | - | - |
| Halite | 76.0 | 90.9 | 77.0 | 31.8 |
| Sylvite | 7.6 | - | - | - |
| Carnallite | 4.3 | 2.0 | 3.7 | - |

## Table 4-5. Chemical Analysis, Salt Norm (anhydrous weight percent), and Simple Salts (weight percent) of Culebra Waters (Continued)

| | Site | | | |
|---|---|---|---|---|
| | WIPP-29[49] | WIPP-30[50] | WIPP-30[51] | GNOME SH[52] |
| Simple salts | | | | |
| $MgCO_3$ | <0.1 | - | 0.2 | 1.7 |
| $CaSO_4$ | 0.4 | 3.5 | 13.7 | 48.6 |
| $MgSO_4$ | 7.0 | 2.6 | 5.1 | 15.0 |
| $K_2SO_4$ | 0.3 | 1.0 | 0.1 | 0.5 |
| $Na_2SO_4$ | - | - | - | 2.1 |
| $Na_2Cl_2$ | 76.0 | 91.0 | 77.2 | 32.1 |
| $K_2Cl_2$ | 13.8 | 0.9 | 1.6 | - |
| $MgCl_2$ | 2.4 | 1.1 | 2.1 | - |

49. Bendix (unpub.).
50. Rettig (unpub.); contaminated sample; salt rose plotted.
51. Bendix (unpub.); preferred sample.
52. USGS (unpub. Tech file).

## Table 4-5. Chemical Analysis, Salt Norm (anhydrous weight percent), and Simple Salts (weight percent) of Culebra Waters (Continued)

| | Site | | | |
|---|---|---|---|---|
| | GNOME-1[53] | GNOME-4[54] | GNOME-8[55] | INDIAN[56] |
| Date collected | 8/18/60 | 12/5/61 | 1/27/63 | 1/22/63 |
| pH | 7.6 | 7.5 | 7.1 | 7.6 |
| Chemical analysis | mg/kg | mg/kg | mg/kg | mg/kg |
| Mg | 146. | 134. | 155. | 169. |
| Ca | 608. | 644. | 624. | 624. |
| Sr | - | 8.8 | 1.0 | 1.1 |
| Li | - | 0.1 | 0.25 | 0.27 |
| Na | 520. | 640. | 630. | 315. |
| K | 11. | 16. | 27. | 8.6 |
| F | 0.3 | 1.0 | 2.4 | 2.1 |
| Cl | 770. | 948. | 1,190. | 533. |
| $NO_3$ | 7.8 | 10. | 7.6 | 4.2 |
| $HCO_3$ | 114. | 114. | 108. | 193. |
| $SO_4$ | 1,960. | 1,950. | 2,050. | 1,950. |
| $PO_4$ | - | 0.8 | - | - |
| TDS | 4,140. | 4,470. | 4,800. | 3,810. |
| Balance (+/-) | 1.011 | 1.031 | 0.923 | 1.005 |
| Salt norm | | | | |
| Magnesite | 1.9 | 1.8 | 1.5 | 3.6 |
| Anhydrite | 49.7 | 47.9 | 47.1 | 56.9 |
| Kieserite | - | - | 10.7 | 15.1 |
| Epsomite | 13.6 | 11.4 | - | - |
| Polyhalite | 1.1 | 1.5 | - | - |
| Bloedite | 2.1 | 0.8 | - | - |
| Halite | 31.2 | 35.8 | 35.6 | 21.5 |
| Carnallite | - | - | 2.6 | 1.0 |
| Bischofite | - | - | 1.6 | 0.9 |

## Table 4-5. Chemical Analysis, Salt Norm (anhydrous weight percent), and Simple Salts (weight percent) of Culebra Waters (Continued)

| | Site | | | |
|---|---|---|---|---|
| | GNOME-1[53] | GNOME-4[54] | GNOME-8[55] | INDIAN[56] |
| Simple salts | | | | |
| $MgCO_3$ | 2.0 | 1.8 | 1.6 | 3.6 |
| $CaSO_4$ | 50.4 | 49.0 | 47.5 | 57.4 |
| $MgSO_4$ | 14.8 | 12.2 | 10.8 | 15.3 |
| $K_2SO_4$ | 0.3 | 0.5 | - | - |
| $Na_2SO_4$ | 1.2 | 0.4 | - | - |
| $Na_2Cl_2$ | 31.3 | 36.1 | 35.9 | 21.7 |
| $K_2Cl_2$ | - | - | 1.2 | 0.4 |
| $MgCl_2$ | - | - | 3.1 | 1.5 |

53. USGS (unpub. Tech file); salt rose plotted.
54. USGS (unpub. Tech file).
55. USGS (unpub. Tech file).
56. USGS (unpub. Tech file); salt rose plotted.

## Table 4-5. Chemical Analysis, Salt Norm (anhydrous weight percent), and Simple Salts (weight percent) of Culebra Waters (Continued)

| | Site | | | |
|---|---|---|---|---|
| | DOE-1[57] | DOE-1[58] | TWO-MILE[59] | WINDMILL[60] |
| Date collected | 4/24/85 | 3/11/85 | 8/8/62 | 9/14/61 |
| Density (g/cc) | 1.090 | 1.040 | - | - |
| pH | 7.1 | 7.0 | 6.7 | 8.0 |
| Chemical analysis | mg/L | mg/L | mg/kg | mg/kg |
| Mg | 1,610. | 1,060. | 177. | 139. |
| Ca | 1,730. | 1,960. | 630. | 564. |
| Sr | 26.2 | 37.7 | 14. | - |
| Li | 0.635 | 0.47 | 0.32 | - |
| Na | 45,800. | 18,400. | 1,410. | 525. |
| K | 1,100. | 410. | 25. | 23. |
| F | - | 1.69 | 2.0 | - |
| Cl | 73,600 | 34,600. | 2,200. | 515. |
| Br | 56. | 33.5 | - | - |
| I | - | 0.225 | - | - |
| $NO_3$ | - | - | 2.5 | - |
| $HCO_3$ | 45. | 67. | 66. | 108. |
| $SO_4$ | 7,350. | 3,950. | 2,200. | 2,290. |
| B | 36.6 | 15.6 | - | - |
| TDS | 131,000. | 60,500. | 6,730. | 4,160. |
| Balance (+/-) | 1.004 | 0.940 | 0.933 | 0.985 |
| Cl/Br | 1,310. | 1,030. | - | - |
| Salt norm | | | | |
| Dolomite | - | 0.1 | - | - |
| Magnesite | <0.1 | - | 0.7 | 1.8 |
| Anhydrite | 4.5 | 9.0 | 31.1 | 45.2 |
| Kieserite | 3.0 | - | 11.5 | - |
| Epsomite | - | - | - | 0.8 |
| Polyhalite | - | - | 2.1 | 4.1 |
| Bloedite | - | - | - | 27.5 |
| Halite | 88.4 | 80.4 | 53.8 | 20.6 |
| Carnallite | 3.6 | 3.1 | 0.3 | - |
| Bischofite | 0.2 | 2.3 | - | - |
| Tachyhydrite | - | 4.9 | - | - |

## Table 4-5. Chemical Analysis, Salt Norm (anhydrous weight percent), and Simple Salts (weight percent) of Culebra Waters (Continued)

| | Site | | | |
|---|---|---|---|---|
| | DOE-1[57] | DOE-1[58] | TWO-MILE[59] | WINDMILL[60] |
| Simple salts | | | | |
| $CaCO_3$ | - | <0.1 | - | - |
| $MgCO_3$ | <0.1 | <0.1 | 0.7 | 1.8 |
| $CaSO_4$ | 4.5 | 9.1 | 32.3 | 47.1 |
| $MgSO_4$ | 3.1 | - | 12.0 | 14.3 |
| $K_2SO_4$ | - | - | 0.7 | 1.3 |
| $Na_2SO_4$ | - | - | - | 14.9 |
| $Na_2Cl_2$ | 88.6 | 80.6 | 54.1 | 20.6 |
| $K_2Cl_2$ | 1.6 | 1.4 | 0.1 | - |
| $MgCl_2$ | 2.3 | 7.1 | 0.1 | - |
| $CaCl_2$ | - | 1.8 | - | - |

57. Bendix (unpub.); salt rose plotted.
58. Bendix (unpub.).
59. USGS (unpub. Tech file); salt rose plotted.
60. USGS (unpub. Tech file); salt rose plotted.

## Table 4-5. Chemical Analysis, Salt Norm (anhydrous weight percent), and Simple Salts (weight percent) of Culebra Waters (Continued)

| | Site | |
|---|---|---|
| | WINDMILL[61] | SOUTH[62] |
| Date collected | 8/8/62 | 8/8/62 |
| pH | 6.8 | 7.4 |
| Chemical analysis | mg/kg | mg/kg |
| Mg | 138. | 90. |
| Ca | 580. | 589. |
| Sr | 10. | 10. |
| Li | 0.32 | 0.2 |
| Na | 500. | 24. |
| K | 28. | 4.8 |
| F | 3.0 | 1.4 |
| Cl | 588. | 18. |
| $NO_3$ | 2.6 | 9.0 |
| $HCO_3$ | 113. | 196. |
| $SO_4$ | 2,080. | 1,660. |
| TDS | 4,040. | 2,600. |
| Balance (+/-) | 1.018 | 0.993 |
| Salt norm | | |
| Magnesite | 2.0 | 5.4 |
| Anhydrite | 46.6 | 80.4 |
| Epsomite | 5.6 | 8.8 |
| Polyhalite | 4.7 | - |
| Bloedite | 15.8 | 2.7 |
| Halite | 24.5 | 1.2 |
| Simple salts | | |
| $MgCO_3$ | 2.0 | 5.5 |
| $CaSO_4$ | 49.2 | 81.6 |
| $MgSO_4$ | 14.0 | 10.2 |
| $K_2SO_4$ | 1.5 | - |
| $Na_2SO_4$ | 8.7 | 1.5 |
| $Na_2Cl_2$ | 24.7 | 1.2 |

61. USGS (unpub. Tech file).
62. USGS (unpub. Tech file); salt rose plotted.

## Table 4-5. Chemical Analysis, Salt Norm (anhydrous weight percent), and Simple Salts (weight percent) of Culebra Waters (Continued)

Remarks

1. Tentatively considered a representative sample. For an account of mixing and contamination involving a later sample (3/17/77), see Lambert and Harvey (1987).

3. Sampling strategy of 3 is preferred over that of 2 because of collection according to the criteria of Colton and Morse (1985), although field-measured chloride never achieved steady-state. This well has been subjected to a prolonged recirculating tracer test, and sample 2 may better represent pre-test conditions if it actually consists of formation fluid. It is not possible to determine if either represents a defensible H2 Culebra sample given the present state of knowledge.

4, 5, 6. Note little significant change in major or minor solutes over 9-yr period.

7, 8, 9, 10. Note little significant change in most major and minor solutes over 8-yr period; sample 10 is preferred because it was taken according to the criteria of Colton and Morse (1985).

11, 12, 13, 14. Note little significant change in most major and minor solutes over 8-yr period; sample 14 is preferred because it was taken according to the criteria of Colton and Morse (1985).

15, 16, 17. Note little significant change in most major and minor solutes over 8-yr period; sample 17 is preferred because it was taken according to the criteria of Colton and Morse (1985).

18, 19, 20. Note little significant change in most major and minor solutes over 8-yr period; sample 20 is preferred because it was taken according to the criteria of Colton and Morse (1985).

21, 22, 23. Note little significant change in most major and minor solutes over 8-yr period; sample 23 is preferred because it was taken according to the criteria of Colton and Morse (1985). Note significant relative decrease of Na and Cl in 23, even though initially low in 21 and 22.

24, 25. Note little significant change in most major and minor solutes over 8-yr period; sample 25 is preferred because it was taken according to the criteria of Colton and Morse (1985). Note significant relative decrease of Na and Cl in 25, even though initially low in 24.

## Table 4-5. Chemical Analysis, Salt Norm (anhydrous weight percent), and Simple Salts (weight percent) of Culebra Waters (Continued)

29. Also called "Ingle Well" by Cooper and Glanzman (1971).

31. Preferred over 30, because it was taken according to the criteria of Colton and Morse (1985). Note decrease in Na and Cl, probably due to prolonged purging of process brine introduced during well development.

32. Tentatively considered a representative sample. A sample from a later episode (4/11/79) was believed to be contaminated. See Lambert and Harvey (1987) for details.

34. Preferred over 33, because it was taken according to the criteria of Colton and Morse (1985). Note decrease in Na and Cl, probably due to prolonged purging of process brine introduced during well development. Sample 33 was believed by Mercer and Orr (1977) to be contaminated in part with higher-salinity fluid from the underlying Rustler/Salado contact zone, by means of a packer leak.

35. Probably a non-representative sample; production rate was 0.5 gallon/day (Mercer and Orr, 1979), not conducive to purging of introduced KCl-enriched drilling brine and/or $CaCl_2$-rich concrete leachate. See Lambert and Harvey (1987) for details.

36, 37, 38, 39. Sample 38 is preferred, having been collected according to the criteria of Lambert and Robinson (1984). Note little significant change in most major and minor solutes (sample 39).

40, 41, 42. Samples 41 and 42 are preferred, because they were collected according to the criteria of Lambert and Robinson (1984) and Colton and Morse (1985), respectively. Note increase in many major solutes over a 6-yr period. This is not due to inwash of potash-tailings; this locality lies significantly upslope from all such known facilities.

43, 44. Sample 44 is preferred, since it was collected according to the criteria of Lambert and Robinson (1984), although both have been influenced by inwash from a nearby potash-refining operation.

45, 46. Sample 46 is preferred, since it was collected according to the criteria of Lambert and Robinson (1984).

47, 48, 49. Samples 48 and 49 are preferred, because they were collected according to the criteria of Lambert and Robinson (1984) and Colton and Morse (1985), respectively. Note increase in many major solutes over a 6-yr period. This may be due to inwash of potash-tailings; this locality lies just downslope from such a facility. The Culebra lies only 12 ft below the surface here, and its water has been isotopically affected by near-surface processes as well. See Lambert and Harvey (1987) and Lambert and Carter (1987) for details.

## Table 4-5. Chemical Analysis, Salt Norm (anhydrous weight percent), and Simple Salts (weight percent) of Culebra Waters (Continued)

50. A sample known to be contaminated. This solute analysis is intermediate between that of a later Culebra sample (51) and that of an earlier Rustler/Salado contact zone sample (Table 3, #34) at this same locality. Following the wellbore test that provided sample #50, the packer intended to isolate the Culebra from the Rustler/Salado during the Culebra test was found to be missing its shear plug, thus allowing admixing of higher-salinity fluid from the underlying Rustler/Salado zone into the Culebra sample. See Lambert and Robinson (1984) for details.

51. Sample preferred over 50, because it was taken after the repair of the packer leak, and was collected according to the criteria of Lambert and Robinson (1984).

52. Gnome Shaft.

60, 61. "Little Windmill Well" of Cooper and Glanzman (1971); also known as "Mobley #3" of Lambert and Harvey (1987).

62. Also known as "Mobley" of Lambert and Harvey (1987).

## Table 4-6. Chemical Analysis, Salt Norm (anhydrous weight percent), and Simple Salts (weight percent) of Magenta Waters

| | Site | | | |
|---|---|---|---|---|
| | H-1[1] | H-2[2] | H-3[3] | H-3[4] |
| Date collected | 6/4/76 | 2/22/77 | 5/10/77 | 7/1/85 |
| Density (g/cc) | - | - | - | 1.006 |
| pH | 7.4 | 8.6 | 8.0 | 8.0 |
| Chemical analysis | mg/L | mg/ml | mg/L | mg/L |
| Mg | 270. | 170. | 480. | 292. |
| Ca | 890. | 820. | 1,200. | 1,000. |
| Sr | - | - | - | 17.3 |
| Li | - | - | - | 0.32 |
| Na | 5,700. | 2,700. | 9,300. | 1,520. |
| K | 70. | 81. | 250. | 34.5 |
| F | 2.8 | - | 1.8 | 2.43 |
| Cl | 8,000. | 4,100. | 15,000. | 3,360. |
| Br | - | - | - | 5.85 |
| I | - | - | - | 1.2 |
| $NO_3$ | - | 0.2 | 0.4 | - |
| $HCO_3$ | 92. | 74. | 51. | 46. |
| $SO_4$ | 3,900. | 2,400. | 3,400. | 2,310. |
| B | 2.2 | 0.22 | 13. | 2.05 |
| TDS | 18,900. | 10,400. | 29,700. | 8,590. |
| Balance (+/-) | 1.025 | 1.045 | 1.030 | 0.982 |
| Cl/Br | - | - | - | 574. |
| Salt norm | | | | |
| Dolomite | - | - | - | 0.4 |
| Magnesite | 0.3 | 0.5 | 0.1 | - |
| Anhydrite | 14.5 | 25.1 | 13.5 | 38.0 |
| Kieserite | - | 5.4 | 2.6 | - |
| Epsomite | 0.6 | - | - | - |
| Polyhalite | 2.7 | 2.5 | - | - |
| Bloedite | 11.4 | - | - | - |
| Halite | 70.5 | 64.7 | 78.1 | 45.6 |
| Carnallite | - | 1.8 | 3.6 | 1.8 |
| Bischofite | - | - | 1.9 | 10.0 |
| Tachyhydrite | - | - | - | 3.6 |

## Table 4-6. Chemical Analysis, Salt Norm (anhydrous weight percent), and Simple Salts (weight percent) of Magenta Waters (Continued)

| | Site | | | |
|---|---|---|---|---|
| | H-1[1] | H-2[2] | H-3[3] | H-3[4] |
| Simple salts | | | | |
| $CaCO_3$ | - | - | - | 0.2 |
| $MgCO_3$ | 0.3 | 0.5 | 0.1 | 0.2 |
| $CaSO_4$ | 15.8 | 26.3 | 13.5 | 38.2 |
| $MgSO_4$ | 6.4 | 5.9 | 2.6 | - |
| $K_2SO_4$ | 0.8 | 0.8 | - | - |
| $Na_2SO_4$ | 6.2 | - | - | - |
| $Na_2Cl_2$ | 70.5 | 64.7 | 78.3 | 45.9 |
| $K_2Cl_2$ | - | 0.8 | 1.6 | 0.8 |
| $MgCl_2$ | - | 1.0 | 3.9 | 13.4 |
| $CaCl_2$ | - | - | - | 1.4 |

1. Mercer (1983); salt rose plotted.
2. Mercer (1983); salt rose plotted.
3. Mercer (1983).
4. Bendix (unpub.); preferred sample; salt rose plotted.

## Table 4-6. Chemical Analysis, Salt Norm (anhydrous weight percent), and Simple Salts (weight percent) of Magenta Waters (Continued)

| | Site | | | |
|---|---|---|---|---|
| | H-4[5] | H-5[6] | H-6[7] | H-8[8] |
| Date collected | 12/14/78 | 12/14/78 | 12/20/78 | 2/12/80 |
| Density (g/cc) | - | - | - | 1.006 |
| pH | 8.0 | 7.8 | 7.3 | 9.3 |
| Chemical analysis | mg/L | mg/L | mg/L | mg/L |
| Mg | 410. | 170. | 160. | 17. |
| Ca | 210. | 240. | 520. | 870. |
| Na | 7,000. | 1,500. | 1,100. | 2,400. |
| K | 130. | 53. | 46. | 84. |
| F | 2.5 | 2.8 | 1.4 | 0.7 |
| Cl | 7,500. | 880. | 1,200. | 3,500. |
| $NO_3$ | 0.04 | 0.04 | 0.1 | 0.3 |
| $HCO_3$ | 63. | 50. | 51. | - |
| $SO_4$ | 7,000. | 3,200. | 2,700. | 2,100. |
| B | 13. | 11. | 2.5 | 3.1 |
| TDS | 22,300. | 6,110. | 5,780. | 8,980. |
| Balance (+/-) | 0.980 | 0.996 | 0.967 | 1.061 |
| Salt norm | | | | |
| Magnesite | 0.2 | 0.6 | 0.6 | - |
| Anhydrite | - | - | 23.6 | 29.3 |
| Polyhalite | - | - | 5.9 | 4.1 |
| Syngenite | - | - | - | 0.6 |
| Bloedite | 19.4 | 28.0 | 25.9 | - |
| Glauberite | 6.6 | 27.3 | 9.8 | - |
| Aphthitalite | 1.7 | 2.5 | - | - |
| Thenardite | 16.9 | 17.0 | - | - |
| Halite | 55.0 | 23.7 | 34.0 | 65.4 |
| Sylvite | - | - | - | 0.3 |

## Table 4-6. Chemical Analysis, Salt Norm (anhydrous weight percent), and Simple Salts (weight percent) of Magenta Waters (Continued)

| | Site | | | |
|---|---|---|---|---|
| | H-4[5] | H-5[6] | H-6[7] | H-8[8] |
| Simple salts | | | | |
| $MgCO_3$ | 0.2 | 0.6 | 0.6 | - |
| $CaSO_4$ | 3.3 | 13.5 | 31.3 | 31.7 |
| $MgSO_4$ | 8.9 | 13.0 | 13.2 | 0.9 |
| $K_2SO_4$ | 1.3 | 2.0 | 1.8 | 1.6 |
| $Na_2SO_4$ | 31.2 | 47.1 | 19.0 | - |
| $Na_2Cl_2$ | 55.1 | 23.9 | 34.1 | 65.5 |
| $K_2Cl_2$ | - | - | - | 0.3 |

5. Mercer (1983); salt rose plotted.
6. Mercer (1983); salt rose plotted.
7. Mercer (1983); salt rose plotted.
8. Mercer (1983).

## Table 4-6. Chemical Analysis, Salt Norm (anhydrous weight percent), and Simple Salts (weight percent) of Magenta Waters (Continued)

| | Site | | | |
|---|---|---|---|---|
| | H-8[9] | H-9[10] | H-9[11] | H-10[12] |
| Date collected | 2/12/80 | 2/5/78 | 2/5/80 | 3/21/80 |
| Density (g/cc) | 1.004 | 1.003 | 1.000 | 1.171 |
| pH | 7.8 | 8.5 | 7.2 | 4.70 |
| Chemical analysis | mg/kg | mg/L | mg/kg | mg/kg |
| Mg | 15. | 170. | 170. | 2,130. |
| Ca | 845. | 550. | 535. | 2,310. |
| Sr | 20. | - | 15. | 38. |
| Li | 0.2 | - | 0.3 | 5. |
| Na | 2,300. | 800. | 800. | 78,600. |
| K | 75. | 28. | 26. | 307. |
| F | - | 1.8 | - | - |
| Cl | 3,520. | 750. | 750. | 136,000. |
| Br | 0.82 | - | 2.5 | 158. |
| $NO_3$ | - | 0.09 | - | - |
| $HCO_3$ | 34. | - | 42. | - |
| $SO_4$ | 2,490. | 2,700. | 2,760. | 2,680. |
| B | 6.9 | 2.6 | 2.5 | 22. |
| TDS | 9,310. | 5,000. | 5,100. | 222,000. |
| Balance (+/-) | 0.959 | 0.992 | 0.963 | 0.955 |
| Cl/Br | 4,290. | - | 300. | 861. |
| Salt norm | | | | |
| Magnesite | 0.3 | - | 0.6 | - |
| Anhydrite | 26.0 | 34.6 | 32.4 | 1.7 |
| Polyhalite | 2.2 | 4.1 | 3.8 | - |
| Syngenite | 2.1 | - | - | - |
| Bloedite | - | 34.7 | 33.5 | - |
| Glauberite | 7.2 | 1.7 | 4.8 | - |
| Halite | 61.4 | 24.6 | 24.1 | 92.5 |
| Carnallite | - | - | - | 0.6 |
| Bischofite | - | - | - | 0.8 |
| Tachyhydrite | - | - | - | 4.2 |

## Table 4-6. Chemical Analysis, Salt Norm (anhydrous weight percent), and Simple Salts (weight percent) of Magenta Waters (Continued)

| | Site | | | |
|---|---|---|---|---|
| | H-8[9] | H-9[10] | H-9[11] | H-10[12] |
| Simple salts | | | | |
| $MgCO_3$ | 0.3 | - | 0.6 | - |
| $CaSO_4$ | 31.8 | 37.6 | 36.9 | 1.7 |
| $MgSO_4$ | 0.5 | 16.8 | 16.3 | - |
| $K_2SO_4$ | 1.9 | 1.3 | 1.2 | - |
| $Na_2SO_4$ | 3.7 | 19.7 | 20.8 | - |
| $Na_2Cl_2$ | 61.9 | 24.3 | 24.3 | 92.6 |
| $K_2Cl_2$ | - | - | - | 0.3 |
| $MgCl_2$ | - | - | - | 3.9 |
| $CaCl_2$ | - | - | - | 1.6 |

9. Rettig (unpub.); preferred analysis; salt rose plotted.
10. Mercer (1983); salt rose plotted.
11. Rettig (unpub.); preferred analysis.
12. Rettig (unpub.); salt rose plotted.

## Table 4-6. Chemical Analysis, Salt Norm (anhydrous weight percent), and Simple Salts (weight percent) of Magenta Waters (Continued)

| | Site | | | |
|---|---|---|---|---|
| | WIPP-25[13] | WIPP-25[14] | WIPP-25[15] | WIPP-27[16] |
| Date collected | 9/4/80 | 9/4/80 | 9/17/80 | 9/20/80 |
| Density (g/cc) | 1.010 | 1.007 | 1.004 | 1.095 |
| pH | 7.5 | 7.41 | 6.9 | 6.66 |
| Chemical analysis | mg/L | mg/kg | mg/L | mg/kg |
| Mg | 240. | 248. | 260. | 1,690. |
| Ca | 910. | 893. | 905. | 3,290. |
| Sr | - | 12. | 12. | 50. |
| Li | - | 0.2 | 0.2 | - |
| Na | 3,100. | 3,340. | 2,910. | 38,900. |
| K | 0.8 | 65. | 71.5 | 7,030. |
| F | 1.5 | - | - | - |
| Cl | 5,600. | 5,460. | 5,250. | 75,500. |
| Br | - | 2.1 | 2.5 | 26. |
| $NO_3$ | 2.8 | - | - | - |
| $HCO_3$ | - | - | 180. | - |
| $SO_4$ | 1,900. | 2,480. | 2,490. | 2,830. |
| B | 1.9 | 1.4 | 1.54 | 4.9 |
| TDS | 11,800. | 12,500. | 12,100. | 129,000. |
| Balance (+/-) | 1.012 | 1.032 | 0.963 | 0.994 |
| Cl/Br | - | 2,600. | 2,100. | 2,900. |
| Salt norm | | | | |
| Magnesite | - | - | 1.0 | - |
| Anhydrite | 23.0 | 23.8 | 26.3 | 3.1 |
| Kieserite | - | 4.0 | 2.3 | - |
| Halite | 66.5 | 66.6 | 63.3 | 76.7 |
| Sylvite | - | - | - | 6.4 |
| Carnallite | <0.1 | 2.2 | 2.7 | 9.2 |
| Bischofite | 3.8 | 3.2 | 4.2 | - |
| Tachyhydrite | 6.6 | - | - | - |
| Antarcticite | - | - | - | 4.5 |

## Table 4-6. Chemical Analysis, Salt Norm (anhydrous weight percent), and Simple Salts (weight percent) of Magenta Waters (Continued)

| | Site | | | |
|---|---|---|---|---|
| | WIPP-25[13] | WIPP-25[14] | WIPP-25[15] | WIPP-27[16] |
| Simple salts | | | | |
| $MgCO_3$ | - | - | 1.0 | - |
| $CaSO_4$ | 23.0 | 23.8 | 26.4 | 3.1 |
| $MgSO_4$ | - | 4.0 | 2.3 | - |
| $Na_2Cl_2$ | 66.6 | 66.7 | 63.4 | 76.8 |
| $K_2Cl_2$ | <0.1 | 1.0 | 1.2 | 10.4 |
| $MgCl_2$ | 8.0 | 4.5 | 5.7 | 5.1 |
| $CaCl_2$ | 2.4 | - | - | 4.5 |

13. Mercer (1983).
14. Rettig (unpub.); salt rose plotted.
15. Bendix (unpub.); preferred analysis.
16. Rettig (unpub.); affected by potash inwash.

## Table 4-6. Chemical Analysis, Salt Norm (anhydrous weight percent), and Simple Salts (weight percent) of Magenta Waters (Continued)

| | Site | | |
|---|---|---|---|
| | WIPP-27[17] | WIPP-30[18] | GNOME-5[19] |
| Date collected | 9/25/80 | 9/24/80 | 11/15/61 |
| Density (g/cc) | 1.090 | 1.012 | - |
| pH | 6.3 | 8.2 | 7.6 |
| Chemical analysis | mg/L | mg/kg | mg/kg |
| Mg | 2,100. | 203. | 122. |
| Ca | 3,660. | 731. | 648. |
| Sr | 58.6 | 15. | - |
| Li | 0.34 | 0.2 | - |
| Na | 43,200. | 5,930. | 150. |
| K | 8,090. | 119. | 8.3 |
| F | - | - | 1.5 |
| Cl | 85,200. | 7,980. | 250. |
| Br | 28.3 | 2.1 | - |
| $NO_3$ | - | - | 13. |
| $HCO_3$ | 210. | - | 103. |
| $SO_4$ | 3,410. | 3,660. | 1,940. |
| B | 2.32 | 10. | 0.72 |
| TDS | 146,000. | 18,700. | 3,240. |
| Balance (+/-) | 0.986 | 1.042 | 0.993 |
| Cl/Br | 3,010. | 3,800. | - |
| Salt norm | | | |
| Calcite | 0.1 | - | - |
| Magnesite | - | - | 2.2 |
| Anhydrite | 3.3 | 7.3 | 69.4 |
| Kieserite | - | - | 14.7 |
| Polyhalite | - | 4.5 | - |
| Bloedite | - | 9.4 | - |
| Glauberite | - | 6.9 | - |
| Halite | 76.0 | 71.5 | 11.7 |
| Sylvite | 6.2 | - | - |
| Carnallite | 10.1 | - | 1.1 |
| Antarcticite | 4.2 | - | - |

## Table 4-6. Chemical Analysis, Salt Norm (anhydrous weight percent), and Simple Salts (weight percent) of Magenta Waters (Continued)

| | Site | | |
|---|---|---|---|
| | WIPP-27[17] | WIPP-30[18] | GNOME-5[19] |
| Simple salts | | | |
| $CaCO_3$ | 0.1 | - | - |
| $MgCO_3$ | - | - | 2.3 |
| $CaSO_4$ | 3.3 | 12.9 | 69.9 |
| $MgSO_4$ | - | 5.3 | 14.8 |
| $K_2SO_4$ | - | 1.4 | - |
| $Na_2SO_4$ | - | 8.6 | - |
| $Na_2Cl_2$ | 76.0 | 71.8 | 11.8 |
| $K_2Cl_2$ | 10.7 | - | 0.5 |
| $MgCl_2$ | 5.7 | - | 0.6 |
| $CaCl_2$ | 4.2 | - | - |

17. Bendix (unpub.); preferred sample; affected by potash inwash.
18. Rettig (unpub.); nonrepresentative sample; salt rose plotted.
19. USGS (unpub. Tech file); salt rose plotted.

**Remarks**

4. Preferred over 3, because it was taken according to the criteria of Colton and Morse (1985). Note conspicuous decrease in Na and Cl, probably due to prolonged purging of process brine introduced during well development.

5. Later sampling (since 1985) yielded increases in Ca and Cl (Robinson, 1987).

6. Later sampling (since 1985) yielded increases in Ca and $Cl+SO_4$ (Robinson, 1987).

7. Later sampling (since 1985) yielded decreases in Na and Cl (Robinson, 1987).

9. Although the charge balance is only slightly better, this analysis is preferred to 8 due to the availability of a bromide value. A 1985 sample (Robinson, 1987) showed decreases in most major solutes. In both sampling episodes, very little water could be collected before the well was pumped to depletion.

## Table 4-6. Chemical Analysis, Salt Norm (anhydrous weight percent), and Simple Salts (weight percent) of Magenta Waters (Continued)

13, 14, 15. Sample 15 is preferred (despite the slightly better charge balance in 14), having been collected according to the criteria of Lambert and Robinson (1984). Anomalously low K value in 13 is presumably due to a laboratory error (Robinson, 1987). Note that analysis 15 is virtually identical to the analysis for the Culebra water in the same locality (Table 5, #38), consistent with natural mixing and therefore hydraulic connection between the Magenta and Culebra at WIPP-25. The potentiometric levels are also the same (Mercer, 1983).

17. Preferred over 16, having been collected according to the criteria of Lambert and Robinson (1984), although both have been affected by inwash of potash from nearby refining operations. Note that analysis 17 is virtually identical to the analysis for the Culebra water in the same locality (Table 5, #44), consistent with natural mixing and therefore hydraulic connection between the Magenta and Culebra at WIPP-27. The potentiometric levels are also the same (Mercer, 1983).

18. A non-representative sample. Subsequent field testing (completed 12/10/80) by Lambert and Robinson (1984) revealed that continued purging was able to reduce the chloride in WIPP-30 Magenta to approximately 4,000 mg/L, which probably is closer to the true value than 8,000. Due to operational difficulties later during this test, however, together with the extremely low productivity (~50 mL/min), Lambert and Robinson were unable to collect and provide a representative sample. See Lambert and Robinson (1984) and Robinson (1987) for details.

## Table 4-7. Chemical Analysis, Salt Norm (anhydrous weight percent), and Simple Salts (weight percent) of Dewey Lake (1, 2), Triassic Dockum (3), and Quaternary Alluvium (4) Waters

| | Site | | | |
|---|---|---|---|---|
| | WALKER[1] | TWIN PAS[2] | H-5[3] | WIPP-15[4] |
| Date collected | 7/31/62 | 1/30/86 | 5/24/86 | 3/12/79 |
| Density (g/cc) | - | 0.998 | - | - |
| pH | 7.1 | 7.7 | - | - |
| Chemical analysis | mg/kg | mg/L | mg/L | mg/L |
| Mg | 145. | 22.5 | 51. | 81. |
| Ca | 613. | 80.4 | 56. | 35. |
| Sr | 8.4 | 1.06 | - | - |
| Ba | - | - | - | 0.2 |
| Li | 0.19 | - | - | - |
| Na | 140. | 25.4 | 280. | 300. |
| K | 3.6 | 3.85 | 25. | 19. |
| F | 2.0 | 0.58 | 1.2 | 2.0 |
| Cl | 325. | 44.1 | 120. | 93. |
| Br | - | 0.17 | - | - |
| $NO_3$ | 8.0 | - | 1.6 | - |
| $HCO_3$ | 134. | 230. | 240. | 988. |
| $SO_4$ | 1,790. | 75.1 | 530. | 170. |
| B | - | 0.13 | 0.89 | 1.0 |
| TDS | 3,170. | 483. | 1,310. | 1,690. |
| Balance (+/-) | 1.001 | 1.070 | 1.072 | 0.975 |
| Cl/Br | - | 259. | - | - |
| Salt norm | | | | |
| Calcite | - | 7.2 | - | - |
| Dolomite | - | 42.0 | 0.1 | 13.1 |
| Magnesite | 3.0 | - | 14.2 | 16.8 |
| Trona | - | - | - | 30.7 |
| Burkeite | - | - | - | 22.2 |
| Anhydrite | 67.1 | 29.7 | - | - |
| Kieserite | 12.6 | - | - | - |
| Glauberite | - | - | 30.3 | - |
| Aphthitalite | - | - | 5.5 | 4.4 |
| Thenardite | - | - | 32.0 | - |
| Halite | 11.5 | 16.9 | 17.1 | 12.1 |
| Sylvite | - | 0.9 | - | - |
| Carnallite | 0.5 | 2.3 | - | - |
| Bischofite | 4.3 | - | - | - |

## Table 4-7. Chemical Analysis, Salt Norm (anhydrous weight percent), and Simple Salts (weight percent) of Dewey Lake (1, 2), Triassic Dockum (3), and Quaternary Alluvium (4) Waters (Continued)

| | Site | | | |
|---|---|---|---|---|
| | WALKER[1] | TWIN PAS[2] | H-5[3] | WIPP-15[4] |
| Simple salts | | | | |
| $CaCO_3$ | - | 30.3 | 0.1 | 7.5 |
| $MgCO_3$ | 3.0 | 19.4 | 14.4 | 24.2 |
| $Na_2CO_3$ | - | - | - | 33.7 |
| $CaSO_4$ | 67.8 | 30.0 | 15.0 | - |
| $MgSO_4$ | 12.7 | - | - | - |
| $K_2SO_4$ | - | - | 4.3 | 3.6 |
| $Na_2SO_4$ | - | - | 49.1 | 18.1 |
| $Na_2I_2$ | 11.6 | 17.0 | 17.2 | 12.9 |
| $K_2Cl_2$ | 0.2 | 1.9 | - | - |
| $MgCl_2$ | 4.6 | 1.3 | - | - |

1. USGS (unpub. Tech file).
2. Bendix (unpub.)
3. Mercer (1983).
4. Sandia National Laboratories and University of New Mexico (1981).

Remarks

1. Also known as "Pocket" by Lambert (1987) and Lambert and Harvey (1987).

2. Twin Pasture Well, also known as W. M. Snyder's "Ranch Headquarters well" by Cooper and Glanzman (1971).

4. Located at the lowest topographic point in San Simon Sink.

The cation-anion charge balance for each analysis, recorded in the tables as "Balance (+/-)," is calculated by SNORM and is the ratio of the sum of cation equivalencies to the sum of anion equivalencies. Elemental boron is calculated as the borate anion. In general, the more the balance departs from unity, the less reliable the analytical data and the ensuing SNORM results. Except for the possibility of offsetting analytical errors, we are confident of the salt norm (regardless of the quality of the sample) if the balance is within $1.00 \pm 0.02$. Balances $> 1.05$ or $< 0.95$ may indicate misleading results, particularly for speciation and abundance of salts with quantities of $< 5\%$ in the normative assemblage.

The salt norm for each analysis is somewhat abbreviated to report only major salt abundances; that is, those salts composed solely of major solutes, identified as "diagnostic" in Table 4-2. Norms for salts containing one or more minor solutes are not reported. The simple-salt assemblage for each analysis, in several cases plotted on maps or illustrations as simple-salt rose diagrams, is also listed. Normative salt abundance is reported in anhydrous weight percentage and simple salt abundance in weight percentage in their respective assemblages.

Of the 63 permissible normative salts, 26 are considered diagnostic (Table 4-2), but only 22 resulted from applying the normative calculation to this data base. One of the diagnostic normative salts (picromerite) was excluded because the presence of other indicator minerals in the norm did not support its hydration state. The remaining three (arcanite, kalicinite, and pirssonite) did not appear in the norms.

We have not reported all replicate analyses. For example, we have excluded many of the analyses reported by Mercer (1983), either because they are nearly identical to S. L. Rettig's data reported here, or because they yield charge balances that deviate markedly from unity. Furthermore, none of the analyses in Mercer (1983) reports bromine concentrations. We have also not considered here the analyses, chiefly of waters from the Culebra member, that were reported by Uhland and Randall (1986) and Uhland et al. (1987); these data yield charge balances that commonly deviate appreciably from unity and

are replicated by the Bendix (now United Nuclear) Corporation (unpublished) analyses reported from the Grand Junction laboratory.

# 4.5 DISCUSSION

Fluids from the three horizons in the Rustler Formation (Tables 4-3, 4-5, and 4-6) and from surface and near-surface sites in the discharge area of Rustler waters (Table 4-4) exhibit a wide range of salinities and salt norms. This variation is attributed to multiple origins of the solutes. Retention of brines older than the present hydrologic system, diagenetic processes within the Rustler Formation, influx of younger meteoric weathering waters, and dissolution of evaporite minerals within the formation all probably contributed in various degrees to the evolution of these fluids. We also include data for four waters in units that overlie the Rustler Formation (Table 4-7) as examples of surface-derived waters that may have recharged the Rustler Formation.

To aid in the following discussion, the stable-isotope data of Lambert and Harvey (1987) are used to evaluate the possible sources of water molecules where $\delta D$ and $\delta^{18}O$ values are available for waters from the same horizon-sites that supplied solute data. Stable-isotope data allow one to distinguish the provenance of water, such as a purely meteoric source, partial evaporation, water/rock interaction, or mixing and contamination. See Lambert and Harvey (1987) for a detailed discussion of the relevant principles of stable-isotope fractionation as applied to Delaware Basin groundwaters.

## 4.5.1 Validity of Rustler Water Samples

Water samples in this data base were collected according to several different criteria under widely varying field conditions, not all of which may have yielded samples representative of formation fluid. These well conditions and criteria have been described and evaluated by Mercer and Orr (1979), Mercer (1983), Lambert and Robinson (1984), Colton and Morse (1985), Uhland and Randall (1986), Uhland et al. (1987), and Robinson (1987). In addition, Lambert and Harvey (1987), as part of their stable isotope study, identified water

samples of questionable validity based on drilling records and properties of the sampled fluids. Coupled with our own evaluation of fluid properties and site locations, samples from one or more of the Rustler horizons at three sites (WIPP-27 Magenta, WIPP-27 Culebra, and WIPP-29 Culebra, due to the likely contribution of potash-refinery outfall at these sites) have been excluded from the interpretations of natural groundwater chemistry.

Samples of questionable validity are annotated in Tables 4-3 through 4-6. The remarks also contain comments concerning which sample and/or analysis is preferable, given a choice, and the basis for the preference.

### 4.5.2 Evolution of Rustler Waters

The salt norms for the Rustler Formation fluids readily fit four water types:

- Highly concentrated primitive or primary brines, most of which have been involved in diagenetic exchange of magnesium for calcium largely associated with dolomitization (assuming a calcite precursor) and termed primitive-diagenetic waters

- Generally dilute alkali-bearing carbonate recharge fluids that obtained their solutes chiefly through carbonic acid hydrolysis of detrital silicate minerals in the weathering environment, such as the feldspars of the Quaternary Gatuña Formation (Table 4-7, #4)

- Generally dilute sulfate-rich recharge fluids in which meteoric weathering waters were modified by interaction with Rustler anhydrite along a relatively halite-free flow path

- Generally highly concentrated halite-rich dissolution brines in which meteoric waters were modified by interaction, not only with Rustler anhydrite, but also with Rustler and uppermost Salado halite.

#### 4.5.2.1 Primitive-Diagenetic Waters

The primitive endmember brine is chloride-rich with appreciable quantities of normative carnallite and bischofite coexisting with halite and anhydrite-kieserite. In salt norms of marine evaporite brines, halite abundance never exceeds 79%, and drops to as low as 15 to 25% within the halite facies. Simultaneously, kieserite is always greater in abundance than anhydrite, and bischofite is always greater in abundance than carnallite (Bodine and Jones, 1986). Primitive brines are also characterized by low Cl/Br ratios; seawater (~300) is about the maximum and values as low as 50 accompany halite precipitation (Braitsch, 1971).

None of the fluids in the three Rustler zones illustrates a truly pure, primary, primitive hypersaline brine. Some of the Rustler/Salado contact waters are hypersaline, containing normative halite abundance equal to or less than that in the seawater norm, exhibiting the characteristic normative carnallite-bischofite association, and having a Cl/Br ratio of ~300 or less. However, their norms contain tachyhydrite rather than kieserite. Thus, these brines have been modified to a varying degree by diagenetic fluid/rock reaction. In less productive horizons of wells that have been extensively treated with process brines during development, the "diagenetic" process that enriched $CaCl_2$ in solution may have been leaching of concrete behind the casing. $CaCl_2$ is commonly used as an additive to cement mixes in the well service industry. This is likely the case in P-18 Rustler/Salado (Table 4-3, #21) and Culebra (Table 4-5, #35). Also, P-18 was drilled with KCl-saturated brine, which may have contributed some KCl to the relatively small amount of fluid swabbed from the formation. Nevertheless, even if the $CaCl_2$ and KCl are contaminants, it is difficult to ascribe the $MgCl_2$ in the carnallite to a contaminant source. The percentage of carnallite in the norm is consistent with other primitive norms (e.g., P-17).

The extent of diagenetic exchange through dolomitization is reflected in the norm by loss of kieserite and appearance of tachyhydrite, with concomitant decrease in normative bischofite. The loss of normative kieserite can be expressed by the equation:

$$Mg^{2+} + SO_4^{2-} + 2CaCO_3 = CaMg(CO_3)_2 + CaSO_4 \quad [1]$$

brine — calcite — dolomite — anhydrite (or gypsum)

wherein calcium released by dolomitization is precipitated as calcium sulfate. After sulfate concentration is reduced and normative kieserite is eliminated, the further exchange of calcium for magnesium through the reaction:

$$Mg^{2+} + 2CaCO_3 = Ca^{2+} + CaMg(CO_3)_2 \quad [2]$$

results in normative tachyhydrite and eventually antarcticite at the expense of bischofite. With increased calcium concentration, additional loss of sulfate is required to maintain saturation with gypsum or anhydrite.

An example of a primitive hypersaline norm possibly showing limited diagenesis is the Rustler/Salado contact brine from H-5 (Table 4-3, #6 and #7); only enough Ca excess has arisen to eliminate kieserite and produce minor tachyhydrite in the norm. In contrast, there is sufficient Ca in the Rustler/Salado contact brine from P-18 (Table 4-3, #21) for tachyhydrite to dominate the norm with only minor bischofite remaining. It is unclear whether this excess Ca, appearing in the simple salt norm as chloride, is due to natural exchange of dissolved magnesium for calcium, or if the extremely low productivity at sites such as P-18 has simply not been sufficient to purge $CaCl_2$-bearing wellbore additives from the formation in the immediate vicinity of the wellbore. Note in Figure 4-5 that this latter brine is not purely meteoric in origin. If representative of the formation fluid, its isotopic composition is consistent with those of other Rustler/Salado brines having isotope shifts away from the meteoric field. As discussed by Lambert and Harvey (1987), such shifts may result from mixing, rock/water interaction, or both. In any case, in both the previous examples, anhydrite in the norm is low (0.1 to 0.5%), carnallite abundance is moderate (18.0 to 22.6%), and alkaline earth chloride salts (68.0 to 69.4%) dominate the assemblages. They might suggest a primary seawater evaporite brine that had progressed

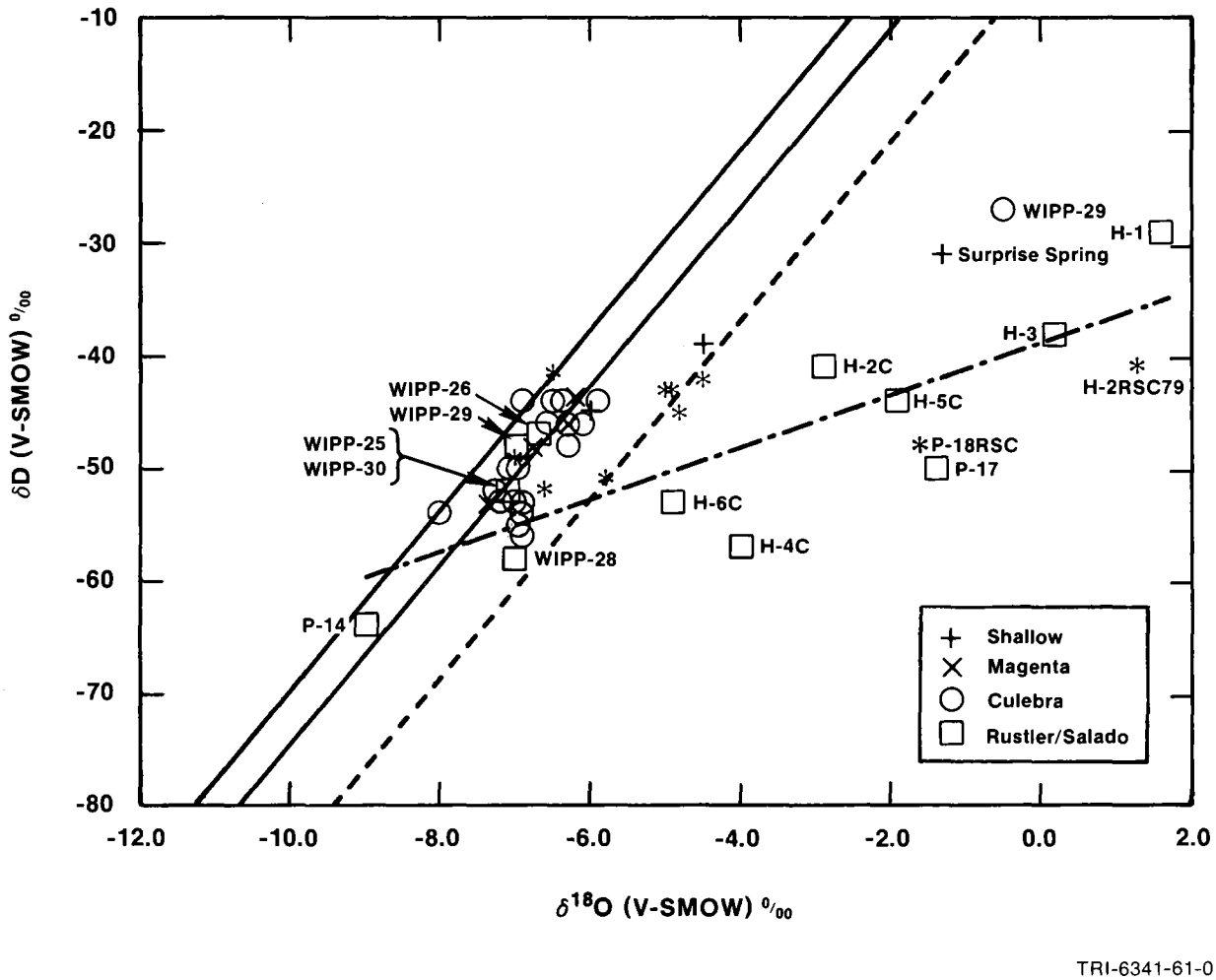


Figure 4-5. Stable-isotope compositions of waters for which solute normative calculations have been made (adopted from Lambert and Harvey, 1987).

to the end of halite facies or possibly to the early stages of bitter salt deposition. The abundance of normative carnallite suggests that little or no primary polyhalite was deposited along this evolutionary path. Such primary pore fluids might be expected in the uppermost Salado halites that overlie the ore-grade potash salts of the Salado Formation; however, radiometric studies of polyhalites from the Salado Formation indicate that latest polyhalite age is Triassic, and is not a relic of primary precipitation (Brookins et al., 1980).

Among Culebra fluids the brine from P-18, for example, (Table 4-5, #35) appears to be primitive-diagenetic; its norm is tachyhydrite-rich with coexisting carnallite-halite-bischofite-anhydrite. Unfortunately no bromine determination was made. Except for salinity, the brine is very similar to that from the Rustler/Salado contact below (Table 4-3, #21), and hence may represent similar degrees of solute contamination through similar processes involving minimal purging of units of low productivity (Mercer and Orr, 1979; Mercer, 1983). However, if the sample is representative, its isotopic composition is indistinguishable from other Culebra fluids of meteoric origin (Figure 4-5; Lambert and Harvey, 1987).

The same normative salts appear in the brine from P-14 (Table 4-5, #30 and #31) as in P-18. Although the norms are qualitatively similar for both samples of P-14, there is no reason to suspect that the later sample from the pump test is not representative of native fluid (Robinson, 1987). Even in view of possible $CaCl_2$ and KCl contamination, the Culebra salt norm from P-14 has a primitive-diagenetic character as does P-18.

#### 4.5.2.2 Recharge Waters

The other water types, the recharge waters, have meteoric normative signatures and entered the Rustler Formation from the surface with varying degrees of subsequent lateral migration. The solutes in these waters would be expected to reflect the extent and character of weathering reactions involving framework silicates (e.g., sodic feldspars) in the recharge zone and of other mineral-water interactions in the Rustler. Their isotopic compositions are consistent with a purely meteoric origin for their water molecules also

although the absolute time of their meteoric recharge is not indicated directly by either their solutes or their stable-isotopes. Figure 4-5 plots the stable-isotope compositions of waters for which solute normative calculations have been made. The tightly clustered Rustler data from confined portions of the Culebra and Magenta plot along the meteoric field (heavy solid lines). $\delta D$ deviations as large as -10% (heavy dashed line) from the meteoric field are not considered significant (Allison et al., 1985). The stable-isotope compositions of WIPP 29 Culebra, Surprise Spring, and Rustler/Salado contact waters have been discussed in detail by Lambert and Harvey (1987). Most samples of questionable validity (asterisks) have a conclusively meteoric signature, except for the Rustler/Salado samples P-18 and 1979 H-2, which appear to be part of the same trend as the other Rustler/Salado points.

The recharge-type water containing alkali carbonate would have gained solutes through dissolution of carbonate minerals and carbonic acid hydrolysis of framework silicates. A representative silicate hydrolysis reaction involving the albite component of plagioclase feldspar, for example, can be written as follows:

$$2NaAlSi_3O_8 + H_2O + 2H_2CO_3 = Al_2Si_2O_5(OH)_4 + 4SiO_2 + 2Na^+ + 2HCO_3^- \quad [3]$$

albite kaolinite quartz

in which kandite-group minerals and quartz (or hydrous or amorphous silica) are formed, and sodium and bicarbonate are added to the solution. Similar reactions can be written for the hydrolysis of potash feldspar or mafic silicate minerals yielding dissolved potassium or magnesium with the bicarbonate in the fluid. Such reactions generate salt norms with alkali-bearing carbonate/bicarbonate salts, as exemplified by the norm for a water sampled from Quaternary sediment, the Gatuña Formation, deposited in a collapse structure at WIPP-15 (Table 4-7, #4) east of the site (Figure 4-4). The presence of burkeite (Table 4-2) in the norm suggests either some sulfuric acid hydrolysis of silicates accompanying the oxidation of sulfide minerals or, more likely, dissolution of small quantities of calcium sulfate, most likely secondary gypsum. As might be expected in a halite-poor unit such as

siliclastic alluvium, the WIPP-15 fluid contains only a minor quantity of chloride, all as normative halite. The chloride most likely came from dissolution of atmospheric aerosol.

#### *4.5.2.2.1 ANHYDRITE DISSOLUTION IN THE RUSTLER*

Interaction of the alkali-bearing carbonate-type recharge water with Rustler Formation rocks that contained anhydrite, but in which halite had been either previously dissolved or not deposited, would produce the sulfate-rich recharge type. With a carbonate-rich, sulfate-poor water, such as the WIPP-15 water (Table 4-7, #4), the principal interaction would be dissolution of anhydrite and precipitation of calcite through the reaction

$$2HCO_3^- + CaSO_4 = CaCO_3 + CO_2 + H_2O + SO_4^{2-} \quad [4]$$

that decreases carbonate and/or bicarbonate salts in the norm and replaces them with sulfate salts. Because anhydrite/gypsum is considerably more soluble than calcite, calcium concentration in the fluid will be enhanced as dissolved carbonate is depressed.

Where only minor silicate hydrolysis has occurred in the weathering environment, anhydrite (or, close to the surface, gypsum) dissolution will give rise to salt norms with strikingly high relative abundances of anhydrite in the norm. Examples of this include the H-7, H-8, H-9, INDIAN, and SOUTH waters from the Culebra member (Table 4-5, #18-20, #21-23, #24-25, #56, and #62, respectively) and the GNOME-5 water from the Magenta member (Table 4-6, #19). All contain more than 55% normative anhydrite with the norm for Culebra water from SOUTH (Table 4-5, #62) containing 80% anhydrite. These waters contain, at most, only small quantities of alkali-bearing sulfate salts in the norm.

Alternatively, if silicate hydrolysis in the weathering recharge zone has been appreciable, such as for the WIPP-15 Quaternary water (Table 4-7, #4), the dissolution of anhydrite in the Rustler Formation results in the replacement of carbonate in the water by sulfate and, rather than producing norms with abundant anhydrite, yields a normative sulfate salt assemblage with a large proportion of alkali sulfate. Extreme examples of this are the

norms for the H-1 Culebra water (Table 4-5, #1) and the H-4 and H-5 Magenta waters (Table 4-6, #5 and #6) that contain normative aphthitalite and thenardite coexisting with glauberite and bloedite.

#### *4.5.2.2.2 HALITE DISSOLUTION IN THE RUSTLER*

The halite-rich recharge type of water is characterized by normative halite substantially exceeding the 78% of the seawater norm (Bodine and Jones, 1986). Examples of Rustler Formation recharge norms in which halite dissolution apparently played a dominant role include H-8, H-9, P-14, WIPP-25, WIPP-27, and GNOME-5 Rustler/Salado contact brines (Table 4-3, #12, #14, #18, #23, #27, and #35 respectively), H-5, H-11, H-12, WIPP-30, and DOE-1 Culebra fluids (Table 4-5, #14, #27, #28, #50, and #57), and the H-10 Magenta brine (Table 4-6, #12). In the case of WIPP-30 Culebra (#50), it is known that this water is a mixture of Culebra and Rustler/Salado waters, caused by a documented unintentional leak through the packer that was supposed to have isolated the two during testing of the Culebra (Lambert and Robinson, 1984); the preferred sample from this horizon-site is #51. The norms contain more than 85% halite (several more than 90%) and, as expected, these waters have Cl/Br ratios that range from 810 to 8,000, where measured. Cl/Br ratios far greater than 300, the approximate seawater value, reflect re-solution of the characteristically low bromine halites initially precipitated from marine evaporite brines.

### 4.5.2.3 Hypersaline Halite-Rich Waters Containing Recharge and Primitive Components

Halite dissolution alone, that is, absence of alkaline-earth chlorides from the norm and presence of normative alkali-bearing sulfate salts, cannot destroy a meteoric signature. This latter feature of the norm should only be diluted, not eliminated, through halite dissolution by recharge waters. Yet the above cited norms nearly always contain alkaline earth-bearing chloride salts (dominantly bischofite, represented by $MgCl_2$ in the simple salt norm). Furthermore, sodium-bearing sulfate normative salts, except in one analysis of H-8 (Table 4-3, #12), are absent from these assemblages, and the only commonly occurring

alkali sulfate-bearing normative salt is polyhalite, whose presence can actually represent the dissolution of some Rustler polyhalite. These characteristics can be attributed to recharge waters dissolving halite. Such dissolution releases intergranular and intragranular (fluid inclusion) solutes that are added to the recharge water. Thus, brines from the Rustler Formation that are rich in NaCl contain accessory solutes characteristic of primitive fluids to some degree.

The maximum amount of $MgCl_2$ derived from halite dissolution, however, is limited. Assuming (a) 1 to 2 weight percent fluid in rock salt, (b) necessarily complete dissolution of halite containing the fluid inclusions in order to release the maximum volume of fluid inclusions and their solutes, (c) the encapsulated fluid is a saturated solution of $MgCl_2$, giving a maximum possible $MgCl_2$ component in the final solution, and (d) ready access of Culebra and Magenta waters, as well as Rustler/Salado waters, to rock salt of the requisite properties, the maximum percentage of $MgCl_2$ thus derived is 0.5 to 1 weight percent. This would account for some of the norms (Table 4-3, #14, #18, #23, #27; Table 4-5, #50), but it would not account for the others in the hypersaline group having 2 to 4 weight percent $MgCl_2$ in the simple salt norm. This certainly cannot account for the higher relative $MgCl_2$ proportion (2.1%) in the preferred sample of WIPP-30 Culebra (Table 4-5, #51). In such cases, the alkaline earth chloride in hypersaline Rustler brines may be an original feature.

Mixing a sulfate-rich recharge water containing normative alkali-bearing sulfates with a primitive water containing normative bischofite and carnallite or a primitive-diagenetic fluid containing normative tachyhydrite and carnallite (with or without bischofite or antarcticite) produces considerable variation in the mixed water norm. These brines are all highly saline; nearly all contain >100,000 mg/L TDS and many, particularly those from the Rustler/Salado contact zone, contain more than 200,000 mg/L; two of the preferred Rustler/Salado analyses, WIPP-25 and WIPP-30, have TDS approaching conditions expected for NaCl saturation ( 330,000 mg/L): (Table 4-3, #23 and #34, respectively).

Significant changes in the composition and salt norm of mixed hypersaline fluids can be due to, for example, the alkali sulfate in the recharge waters reacting with the calcium chloride component of a primitive-diagenetic brine to precipitate secondary calcium sulfate. This would be the predicted result of mixing the $Na_2SO_4$-bearing water of the Castile brine reservoirs with the $CaCl_2$-bearing water of the underlying Bell Canyon Formation (Lambert, 1978), making derivation of the former from the latter impossible. Consequently, the brine-density flow dissolution mechanism proposed by Anderson (1981) is unlikely at this locality.

Similarly effective titration of a normative alkali sulfate in the recharge water by normative magnesium and potassium chloride of a primitive brine can result either in direct precipitation of polyhalite or in the replacement of primary anhydrite by polyhalite. The formation of polyhalite by fluid mixing may explain the origin of the actual polyhalite that Snyder (1985) describes in some cores of the Tamarisk member between the Magenta and Culebra members. Radiometric dating of Rustler polyhalite has not yet been undertaken, but similar Salado polyhalites are Triassic in age (Brookins et al., 1980) and are therefore not genetically related to the present episode of Rustler groundwater flow, which was probably recharged during the climatically wetter Tahokan pluvial (Lambert, 1987; Bradbury, 1981; Van Devender, 1980). If this is the case, the present groundwater in the Rustler has probably dissolved, not precipitated, polyhalite. The normative salt assemblage expected from polyhalite dissolution is polyhalite-leonite, which appears in WIPP-28 Rustler/Salado (Table 4-3, #29-30), and in all the discharge waters from USGS-8 and Anderson Lake (Table 4-4, #1-5). In addition, all these norms are hypersaline, with >89% halite.

Of course, if the mixed fluid is undersaturated, the components generated by the titration (halite and alkaline-earth sulfate) will appear in the salt norm. Only if all the other normative chloride salts of the primitive water are converted to halite can a sodium-bearing sulfate remain in the norm. The single example of this in the Rustler waters may be the preferred analysis of H-8 from the Rustler-Salado contact (Table 4-3, #12), in which the norm contains a very small fraction (0.3%) of bloedite with halite (94%) and the sulfates

anhydrite-epsomite-polyhalite (total of 5.5%). It is suggested that at most only a small increment of primitive brine mixed with the halite-dissolving recharge water; the extremely high Cl/Br ratio (8,000) in H8 is consistent with this interpretation.

Besides eliminating all normative sodium-bearing sulfate salts, a larger proportion of primitive brine in the mixed fluid will exchange potassium sulfate with calcium or magnesium chloride to produce alkaline-earth sulfate and potassium chloride until all antarcticite, tachyhydrite, or bischofite is removed from the norm. As an exception to this, however, carnallite-polyhalite is a stable salt pair and is the only instance in which the simple salts $K_2SO_4$-$MgCl_2$ coexist. The conjugate simple salt pair $K_2Cl_2$-$MgSO_4$ is much more common. It is also found with the normative salt pair carnallite-polyhalite, but is not restricted to this occurrence. Polyhalite-carnallite in the salt norm, or the $K_2SO_4$-$MgCl_2$ salt pair in the simple salt assemblage, can be diagnostic of mixing marine-derived and weathering solutes, but can also arise from simple dissolution of the naturally occurring assemblage halite-carnallite-polyhalite, known in the McNutt potash zone of the Salado Formation.

Many of the Rustler halite-dissolution fluids exhibit the carnallite-polyhalite or $K_2SO_4$-$MgCl_2$ association in the norm. For example, four of the six Rustler/Salado contact (#14:H-9; #18:P-14; #23:WIPP-25; #27:WIPP-27; all but the last of which are preferred samples or analyses) and two of the five Culebra brines (#27:H-11; #50:WIPP-30; the latter of which is second to #51 in preference) cited above contain the carnallite-polyhalite association in their norms. Other preferred analyses that give these characteristics (normative halite $>\sim$80%, high Cl/Br, normative polyhalite-carnallite and/or $K_2SO_4$-$MgCl_2$, high TDS) include the Rustler/Salado of WIPP-26, WIPP-27, WIPP-29, WIPP-30 (Table 4-3, #26, #28, #32, and #34), Laguna Grande de la Sal (Table 4-4, #6), and the Culebra of H-11 and WIPP-28 (Table 4-5, #27 and #46).

Even larger proportions of primitive or primitive-diagenetic components in the mixed fluid result in survival of alkaline earth chloride salts in the norm. The only indications of the mixed origins of these solutes are the increased abundance of halite in the norm and a

Cl/Br ratio in excess of 300. It is conceivable in principle that halite-enriched, alkaline-earth chloride norms can also be attributed to a primitive-diagenetic fluid in which halite-resolution brines from gypsum dewatering have mixed with the primitive-solute brine. Examples of such waters include H-7 and GNOME-5 from the Rustler/Salado contact zone (Table 4-3, #10 and #35), H-3, H-5, H-6, H-10, H-12, WIPP-28, DOE-1, and DOE-2 from the Culebra member (Table 4-5, #5, #12, #16, #26, #28, #45, #57, and #58; #46 is the preferred WIPP-28 sample), and H-10 from the Magenta member (Table 4-6, #12). The water molecules in the Culebra group of samples (with the exception of H-10, for which stable-isotope data are not available at this time) are known to be meteoric, however (Figure 4-5), and this precludes a significant component of water from dehydration of marine gypsum, regardless of the origin of the solutes.

#### 4.5.2.4 Less Saline Mixed Recharge-Primitive Waters

A number of samples from the Culebra and Magenta zones that suggest mixing of sulfate-rich recharge with primitive or primitive-diagenetic solutes are relatively dilute (generally <25,000 mg/L TDS). These waters have dissolved negligible to moderate amounts of halite and are confined to the Culebra and Magenta. They would not be characteristic of the Rustler/Salado contact because of the ubiquitous salt underlying that zone. Many of these waters yield norms that are difficult to interpret unequivocally, particularly those with relatively low normative chloride salt content.

For example, H-4 from the Culebra member (Table 4-5, #7-10) with approximately 20,000 mg/L TDS, contains normative alkali-bearing sulfate salts and about 60% normative halite. The water appears to be essentially a recharge fluid. However, the Cl/Br ratio ranges from 167 to 192, which is too low to be accounted for by halite re-solution alone. If the recharge water had sufficient normative alkali sulfate to eliminate any normative alkaline-earth chloride of a primitive-solute brine and still not destroy the alkali-bearing sulfate signature of the recharge water's norm, the apparent conflict between the normative assemblage and the Cl/Br ratio can be reconciled. The apparent radiocarbon age of this water was calculated by Lambert (1987) to be at least 16,000 yr.

With other examples, further contradictions develop. Samples from the Culebra (Table 4-5, #30-31) in hole P-14 with TDS of 34,000 (#30) and 25,000 (#31) yield salt norms with 60 and 45% halite (#30 and #31, respectively), and 25 (#30 and #31, respectively) to 45% antarcticite-tachyhydrite. Anhydrite ranges from 6 to 9% (#30 and #31, respectively). The available Cl/Br ratio is 201 (#31). Thus the primitive-diagenetic solute characteristics are preserved both in the salt norm and in the bromine data; dilution is apparently the result of either mixing with very dilute recharge waters or with earlier diagenetic fluids from gypsum dewatering. Its water molecules, however, are conclusively meteoric in origin (Figure 4-5). In addition, WIPP-26 Culebra, with TDS varying from 15,000 to nearly 18,000 in three analyses (Table 4-5, #40-42), contains abundant tachyhydrite and antarcticite (9.7 to 10.2% in the three analyses), moderate halite (61 to 63%), and substantial anhydrite (19-23%) in the salt norm. This fluid, however, has a Cl/Br ratio that ranges from 2,250 to 2,420, indicative of simple halite dissolution; again, the water molecules are unequivocally meteoric.

These three similar moderately saline fluids from the same stratigraphic horizon show both internal and comparative inconsistencies: H-4 has a characteristic halite-dissolution recharge salt norm, but a bromine content that suggests a primitive fluid; P-14 has a strong primitive-diagenetic signature in both the salt norm and the bromine quantity; and WIPP-26 has a salt norm that suggests a primitive-diagenetic fluid, but a Cl/Br ratio and normative anhydrite that suggests extensive evaporite re-solution by a recharge brine. The inconsistencies are possibly related to the extent and character of silicate hydrolysis and evaporite re-solution in the recharge water, which, in turn, probably reflects permeability and flow path along the recharge route. The fracture density in the Culebra is known to generally increase westward; fractures are more likely close to the Nash Draw scarp (P-14) than farther to the east (H-4), and collapse breccia occurs in the Draw itself (WIPP-26). These characteristics are all consistent with the nature of the mixtures proposed.

## 4.5.3 Areal Distribution of Salt Norms from Rustler Formation Fluids

The areal distribution of salt norms for waters from the three Rustler zones are shown by maps with simple-salt rose diagrams representing the salt norms of the water composition at each location. Because of the closely spaced boreholes within the WIPP Site (Figure 4-2), two maps have been prepared for each zone (Figures 4-6 through 4-11). The smaller scale map for each zone (Figures 4-6, 4-8, and 4-10) includes well locations near the WIPP Site, but only a selected number of boreholes within the WIPP Site, to avoid overlapping rose plots. TDS values listed in the figures in italics are as mg/kg; others are mg/L. P-18 is of questionable validity. The larger scale map for each zone (Figures 4-7, 4-9, and 4-11) contains all boreholes producing fluids for analysis within the WIPP Site.

### 4.5.3.1 Rustler/Salado Contact Zone

The salt norms and total salinities of the Rustler/Salado contact fluids reflect zonation of chloride-rich brines east to west from primitive-diagenetic types through mixed primitive-recharge solutes to waters dominated by halite-resolution recharge.

Primitive-diagenetic assemblages occupy the eastern central portion of the WIPP Site, including H-5 and H-6 to the north and west, and P-17 and H-4 to the south (Figures 4-6 and 4-7). Each Rustler/Salado contact brine within this area is hypersaline, containing <70% normative halite, and moderate to high quantities of normative tachyhydrite (2 to 31%) and bischofite (5 to 67%). The sum of normative bischofite and tachyhydrite always greatly exceeds carnallite, and the Cl/Br ratio determinations yield a range from 56 to 183. These fluids appear to be modified from brines that could have accompanied deposition of the halite or even of the initial bitter salts in the uppermost Salado Formation. Note also that these four also have isotopic compositions that are not purely meteoric (Figure 4-5); they exhibit a significant deviation from the meteoric field in $\delta D$-$\delta^{18}O$ space. The projection of the trend, including Rustler/Salado waters farther west, suggests that the

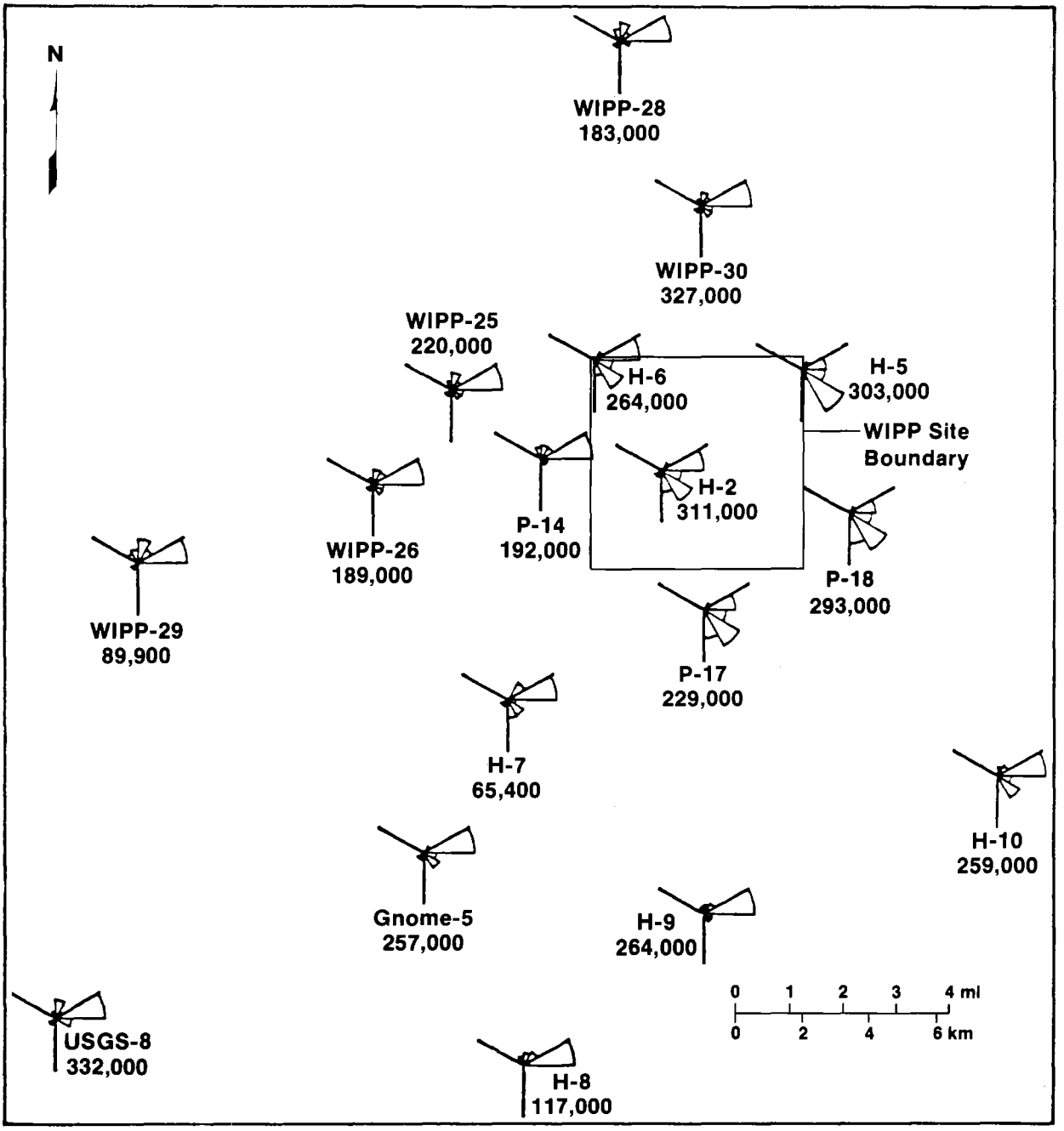


Figure 4-6. Map of the WIPP Site with simple-salt rose diagrams at sites (axes of diagrams) of selected analyzed waters from the Rustler/Salado contact zone.

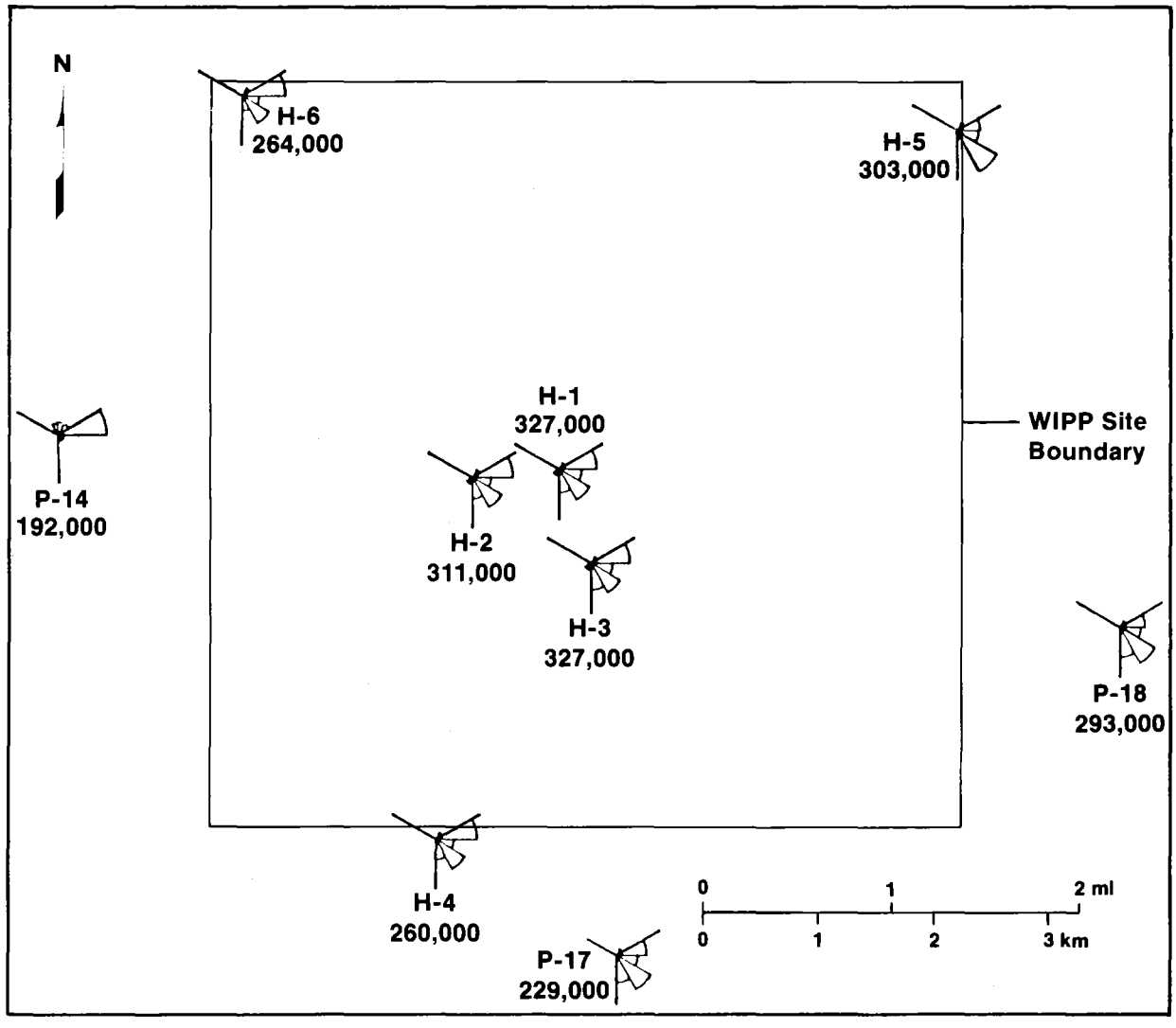


Figure 4-7. Map of the WIPP Site proper with simple-salt rose diagrams at sites (axes of diagrams) of selected analyzed waters from the Rustler/Salado contact zone.

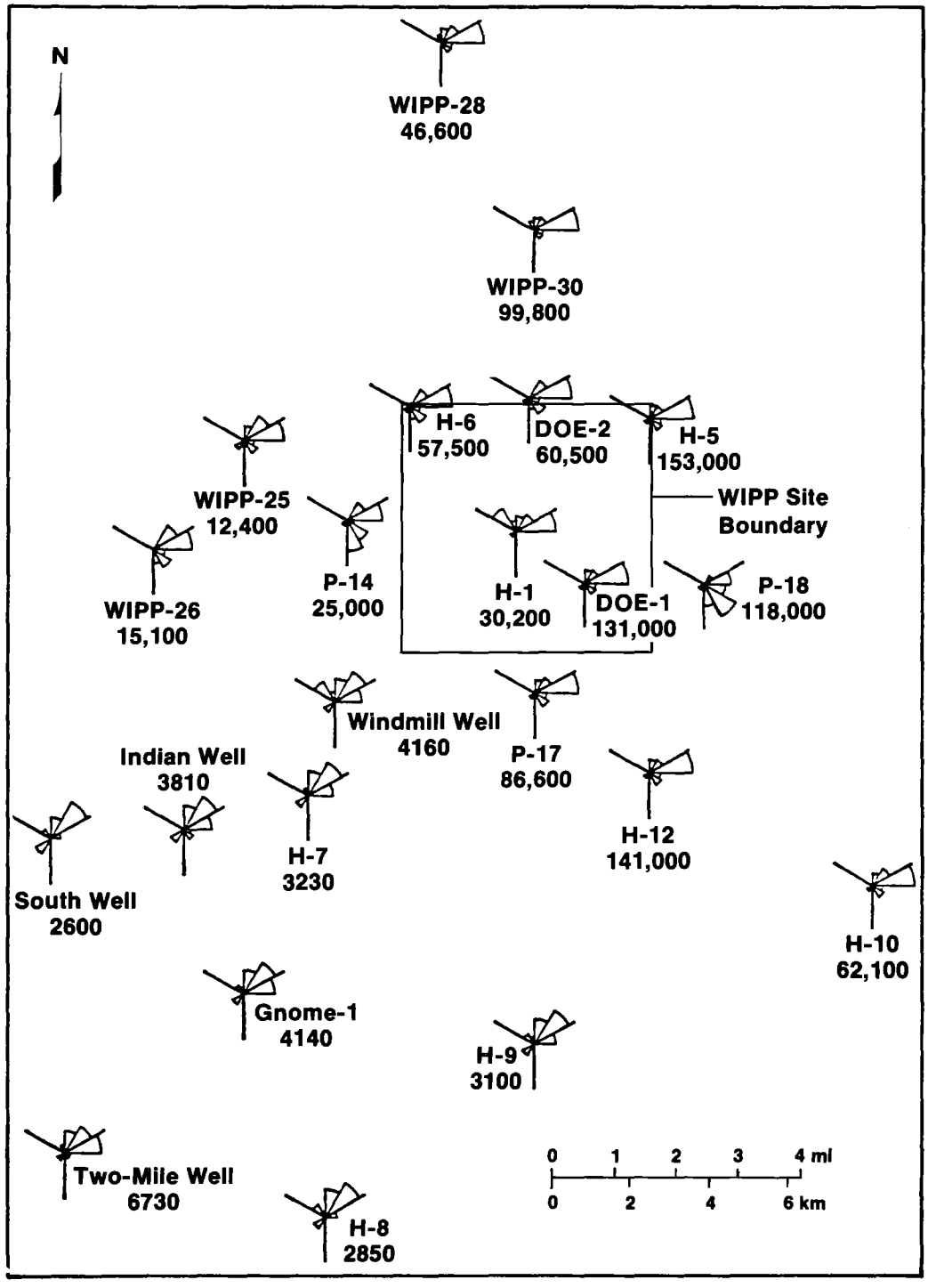


Figure 4-8. Map of the WIPP Site with simple-salt rose diagrams at sites (axes of diagrams) of selected analyzed waters from the Culebra member of the Rustler Formation.

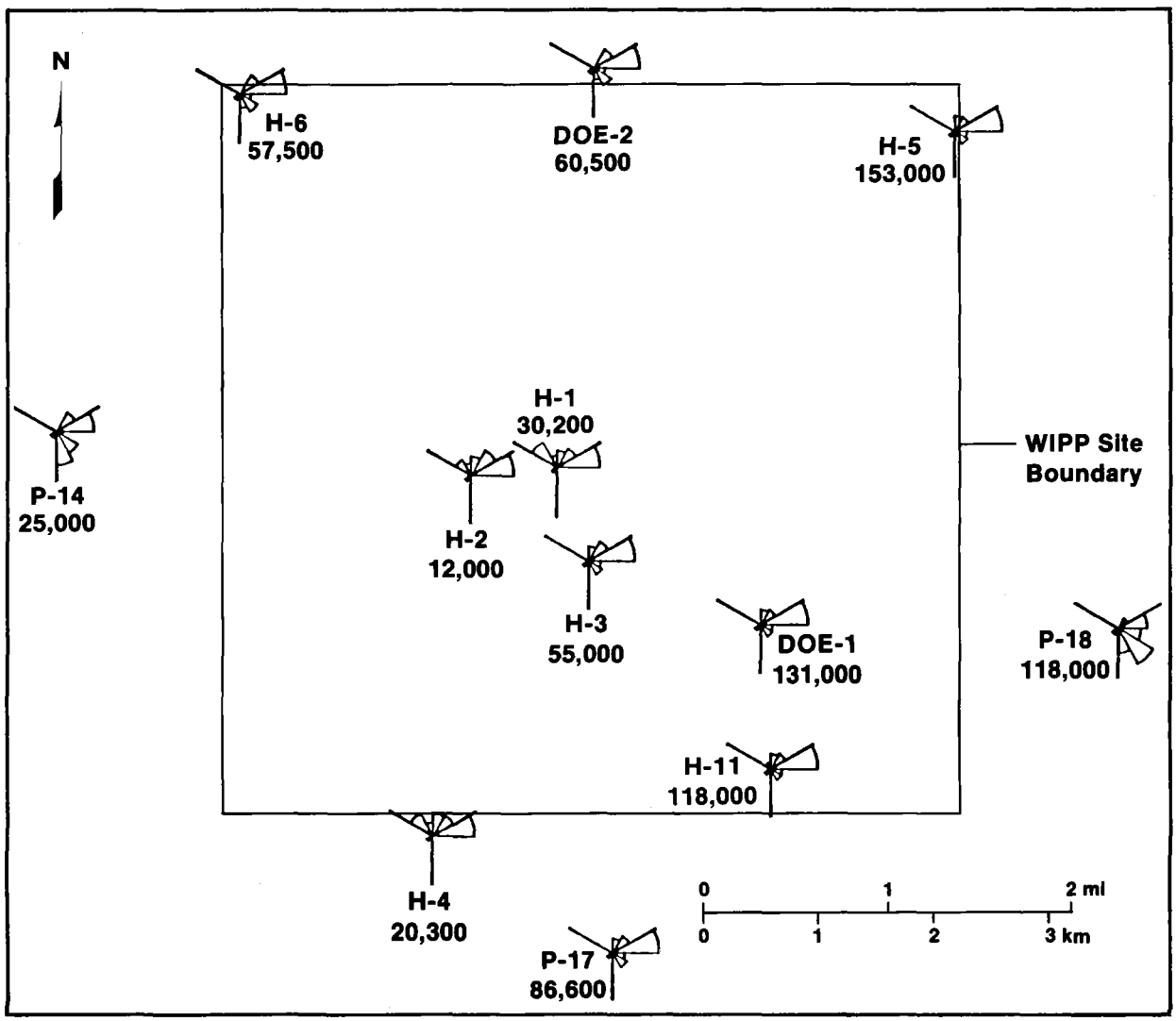


Figure 4-9. Map of the WIPP Site proper with simple-salt rose diagrams at sites (axes of diagrams) of selected analyzed waters from the Culebra member of the Rustler Formation.

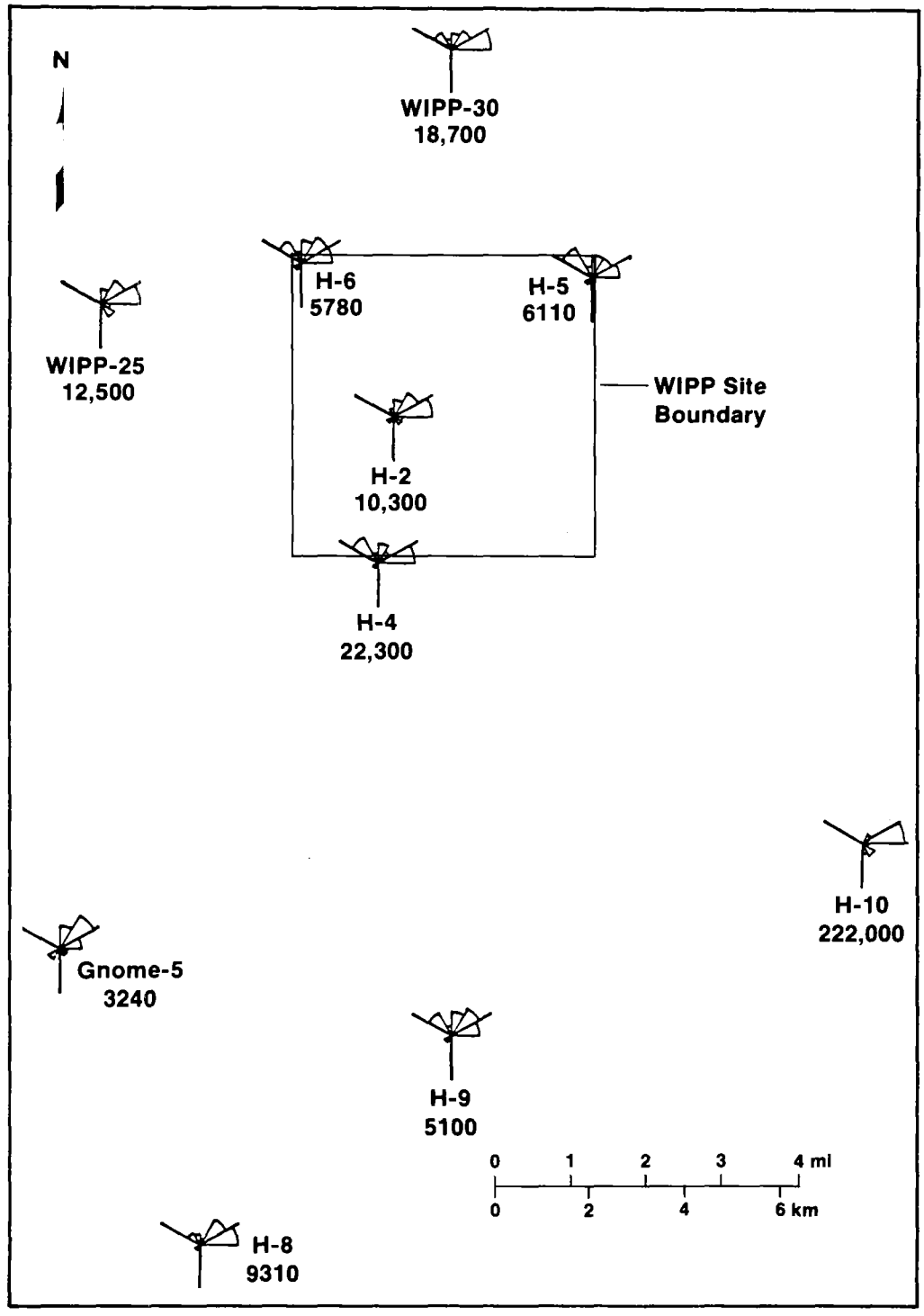


Figure 4-10. Map of the WIPP Site with simple-salt rose diagrams at sites (axes of diagrams) of selected analyzed waters from the Magenta member of the Rustler Formation.

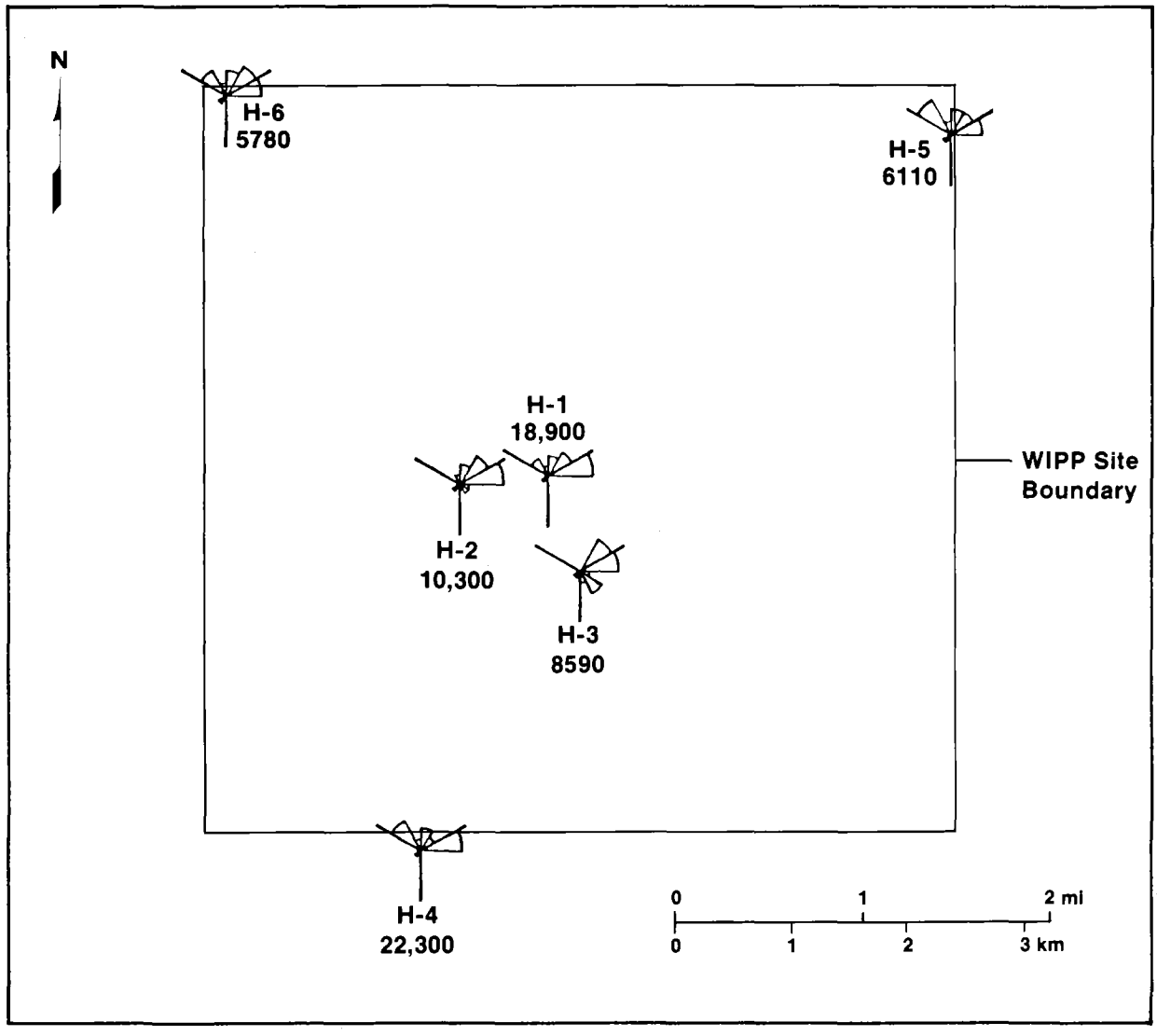


Figure 4-11. Map of the WIPP Site proper with simple-salt rose diagrams at sites (axes of diagrams) of selected analyzed waters from the Magenta member of the Rustler Formation.

water/rock interaction ratio is becoming larger toward the west, as indicated by the westward-increasing approach to a more significant meteoric component, both in terms of normative salts and $\delta D$-$\delta^{18}O$ relationships.

South and west of the WIPP Site are Rustler/Salado contact brines characterized by moderate to high salinity and a primitive-diagenetic normative salt assemblage (anhydrite, carnallite, bischofite, generally tachyhydrite, and little or no kieserite), but with a pronounced excess of halite (84 to 94%) over the seawater norm. This strongly suggests mixing of recharge waters that dissolved substantial halite with a primitive-diagenetic fluid. This group is represented by H-7, GNOME-5, and H-10 (Figure 4-6). The extent of apparent diagenesis among these waters is highly variable. Tachyhydrite in the norm ranges from none in H-10 and 0.6% in GNOME-5 to 6.5% (with 2.6% antarcticite) in H-7 (Table 4-3, #15, #35, and #9, respectively). This variation can develop through two disparate processes. One is a great variation in the extent of solute calcium exchanged for magnesium accompanying dolomitization (note the Bardawil brines; Levy, 1977, as cited by Bodine and Jones, 1986). The second is calcium precipitation as gypsum when a calcium-rich brine (primitive-diagenetic) mixes with an alkali sulfate-rich fluid (recharge). Both processes may have played a role. Alternatively, one or more of these fluids may have evolved solely as primitive-diagenetic brines in which gypsum dehydration provided fluid for halite re-solution, and dolomitization eliminated kieserite and added tachyhydrite to the norm. Although no stable-isotope data are available for these samples, this latter alternative is less likely, given the strongly meteoric isotopic signature of other known Rustler/Salado waters to the west.

The brine of H-10 (Table 4-3, #15 and #16) is an enigma, and no information is available on the degree of representativeness of this sample. It exhibits the high normative halite characterizing halite re-solution, but has a Cl/Br ratio of only 186, suggestive of a primitive fluid. One possible explanation is that a low chloride, sodium-rich fluid, such as an alkaline evaporite water from an ephemeral surface playa, mixed with a calcium-bearing primitive-diagenetic brine with resultant precipitation of calcium and increase in normative halite.

Such a water would have necessarily migrated into this part of the Rustler/Salado laterally, since the overlying Magenta and Culebra have much higher Cl/Br values; halite-re-solution water from the Magenta and Culebra did not migrate downward into the Rustler/Salado. Also, there are no nearby playas in the portion of Los Medaños containing H-10.

The proportion of halite-resolution recharge water mixed with primitive-diagenetic solutes increases progressively to the north, west, and east of the WIPP Site. In the Rustler/Salado contact brines at WIPP-30, WIPP-25, P-14, WIPP-26, and H-9 (Figure 4-6), normative halite (83 to 95%) coexists with normative polyhalite-carnallite (Table 4-3, #34, #23, #18, #26, and #14, respectively). As discussed above, such an assemblage is taken as evidence for mixed primitive marine and recharge waters. All of these fluids contain high Cl/Br (>1,900) which, along with the high normative halite abundance, indicates considerable halite re-solution by the recharge water component. In the westernmost sample sites at WIPP-28, USGS-8, and H-8 (Table 4-3, #30; Table 4-4, #2; Table 4-3, #12, respectively) all alkaline earth-bearing chlorides are absent from the norms, and at H-8 normative sodium-bearing sulfate presents an even stronger recharge signature, although the normative bloedite there is not abundant (0.3%). The normative halite abundance (84 to 94%) and high Cl/Br (>2,800) indicate an extensive proportion of re-solution halite in this group of waters.

It is not surprising that the Rustler/Salado contact fluids are highly saline; none contains <65,000 mg/kg TDS (H-7 in Figure 4-6). Given the present distribution of halite in the Rustler, this cannot be explained by postdepositional halite dissolution in the overlying Rustler Formations, for waters in this zone west of the limit of Rustler halite (Figure 4-12). Recharge waters may have percolated through the Rustler Formation, downward and/or laterally, attaining their sulfate-rich character by interaction with Rustler anhydrite but, for the most part, not becoming chloride rich until reaching the Rustler/Salado contact interval. Thereupon the recharge fluids dissolved Salado Formation halite that floors the Rustler/Salado contact interval and mixed with any available uppermost Salado primitive-diagenetic solutes.

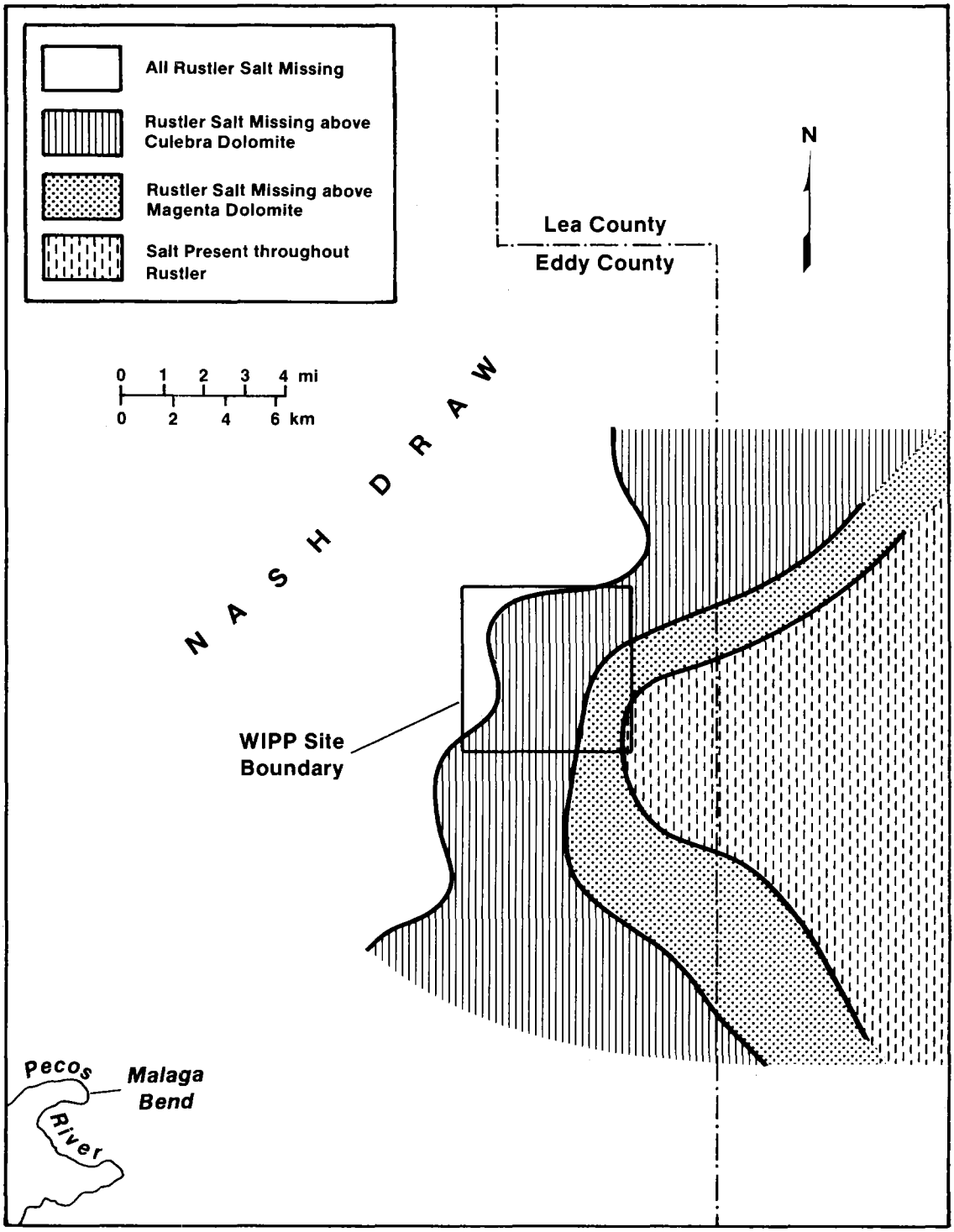


Figure 4-12. Boundaries of salt occurrences in the Rustler Formation with respect to the Culebra and Magenta dolomite members in the WIPP Site (from Mercer [1983] and Snyder [1985]).

Table 4-4 lists analyses and salt norms of Rustler and Salado waters associated with the "brine aquifer" that discharges along the Pecos River or have been retrieved by drilling. The geographic relationships among the "brine aquifer" (the best developed water-bearing zone associated with the Rustler/Salado contact), Nash Draw, Laguna Grande de la Sal, Surprise Spring (at the north end of Laguna Grande), and Malaga Bend (a discharge point for briny fluids along the Pecos River) are shown in Figure 4-13. These waters are highly saline and, except for greater concentrations of potassium, yield norms that are similar to the mixed halite re-solution recharge and primitive or primitive-diagenetic norms that are characteristic of the Rustler/Salado contact zone. The high potassium content, reflected in normative kainite and leonite (Table 4-4, #1-5) in the Malaga Bend area, or in normative sylvite-carnallite-polyhalite in the Laguna Grande de la Sal water (Table 4-4, #6), is attributed to a dominant contribution from outfall from the potash facilities to the north and east. The substantial increase in salinity of Surprise Spring water from 1938 to 1975 (Table 4-4, #6 and #7) is most likely also the result of surface-derived solutes input to the shallow groundwater system from the potash operations. The stable-isotope composition of the later Surprise Spring sample is consistent with partial evaporation of imported refining water under conditions prevailing in a shallow water-table (Figure 4-5; Lambert and Harvey, 1987; cf. Hunter, 1985).

#### 4.5.3.2 Culebra Waters

Salt norms and total salinities present an entirely different range of features for fluids from the Culebra member. Salinities generally do not exceed 100,000 and are commonly $<10{,}000$ mg/L. The salt norms are typically dominated by sulfates, and sodium-bearing sulfate salts are common. Furthermore, neither the salt norms nor the total salinities of these waters (Figures 4-8 and 4-9) yield as directional an areal pattern as do those for the Rustler/Salado contact brines.

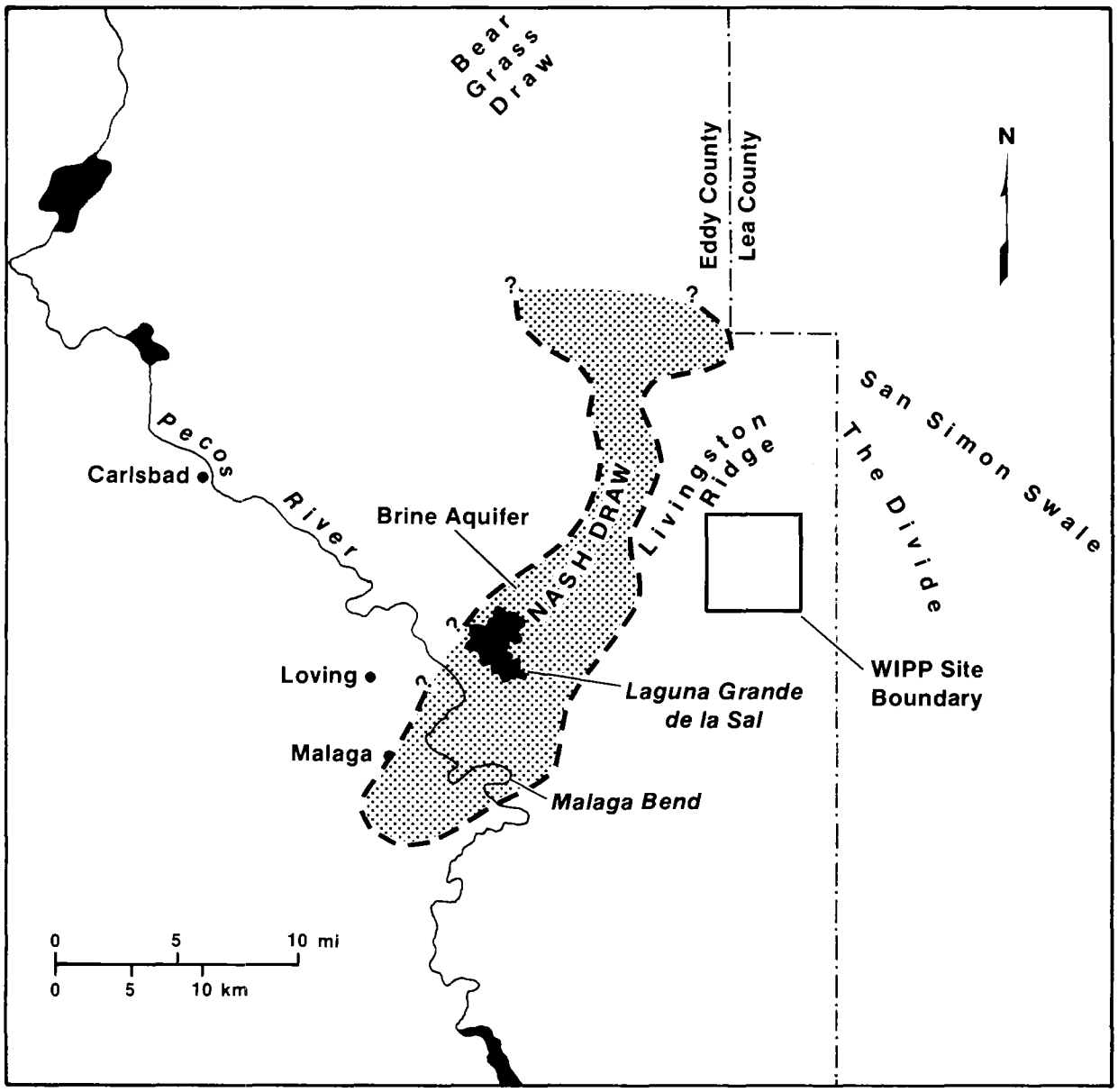


Figure 4-13. Location of the "brine aquifer" from Mercer (1983).

Only two Culebra norms can be confidently interpreted as dominantly primitive-diagenetic. The sample from P-18 (Table 4-5, #35) comes from the eastern margin of the WIPP Site (Figure 4-8). Based on the absence of extensive halite dissolution in the overlying strata of the Rustler Formation there (Snyder, 1985), its normative character is not unexpected, although the sample may not be representative due to low productivity and resultant incomplete purging of introduced wellbore fluids. Although no bromine data were obtained for this fluid, the abundances of tachyhydrite, bischofite, and carnallite (33, 21, and 24%, respectively) are characteristic of a well-developed primitive-diagenetic assemblage. Leaching a $CaCl_2$-doped well-casing concrete with a small amount of fluid, either native or introduced, may have given rise to significant quantities of tachyhydrite and antarcticite. The normative carnallite at this locality could have been augmented by the KCl-saturated brine that was used to drill the hole (Jones, 1978). The $MgCl_2$ is more difficult to explain in terms of a possible contaminant. The norm of the other primitive-diagenetic Culebra fluid, P-14 (Table 4-5, #31), is somewhat different in that antarcticite, tachyhydrite, and carnallite (24, 20, and 1%, respectively) constitute the alkaline earth-bearing chloride salts. This brine also yields a Cl/Br ratio of 201, a primitive-diagenetic value. The origin of the P-14 Culebra water itself, however, is clearly meteoric, as indicated by its isotopic composition (Figure 4-5; Lambert and Harvey, 1987). The presence of such a norm in such a locality, with a high permeability, a meteoric water source, and isolated from other such primitive-diagenetic solute signatures in the surrounding area, is anomalous.

Two features of the chemistry of these waters are noteworthy. First, both brines are well undersaturated with halite and other chloride salts; the P-18 sample contains 118,000 mg/L TDS, and the P-14 sample has only 25,000 mg/L. Either these waters were severely diluted with recharge waters that underwent negligible reaction in the weathering regime or the dilution occurred much earlier as the result of diagenetic dewatering of the primary bedded gypsum. The second mechanism is especially appealing at P-18 where it is difficult to envision downward percolating recharge fluids entering the Culebra member without dissolving substantial quantities of Rustler halite (see Figure 4-12). However, the meteoric isotopic signatures of both samples (even from P-18, which even given contamination is

meteoric-like) and the likelihood of stratabound rather than vertical flow governing recharge makes it less necessary to appeal to gypsum dehydration for a pure water source. Also, the Rustler anhydrite need not have evolved from a gypsum precursor that persisted long after deposition to be dewatered very late. Nevertheless, the primitive-diagenetic normative character of the solutes combined with the meteoric character of the water molecules suggests a local secondary influx of abundant, solute-poor water. Evidence for a locally higher abundance of meteoric water in the Rustler near WIPP-33 is discussed by Bachman (1987) and Lambert and Harvey (1987).

The second feature, restricted to the P-14 sample, is the markedly high Ca/Mg ratio when compared with the several primitive-diagenetic Rustler/Salado contact brines or the Culebra P-18 sample. In the P-14 sample, normative antarcticite is not only present, but its abundance is greater than that of tachyhydrite. Normative antarcticite does not occur in any Rustler/Salado contact brine or in the P-18 fluid from the Culebra. This may be the result of extensive dolomitization of the Culebra member by the P-14 fluid. This contrasts with the absence of bedded carbonate in the Rustler/Salado contact interval, which results in less opportunity for calcium-magnesium exchange between the fluid and the host rock and lower calcium concentrations in the fluid. The P-18 fluid from the Culebra contains no normative antarcticite and may not have been in contact with sufficient original limestone in the member to effect such extensive exchange. The extreme areal uniformity and the higher $^{13}C/^{12}C$ ratio of both Culebra and Magenta dolomites suggest that they evolved not from limestone precursors experiencing later dolomitization, but as evaporitic dolomites. In any case, no Magenta or Culebra dolomite has been found in isotopic equilibrium with the meteorically derived water now in the Rustler, so a dolomitization step, if any, would have had to predate the present Rustler fluids. Conversely, evidence of dedolomitization in the presence of Rustler-like meteoric water has been found in the Culebra at WIPP-33, between the WIPP Site and Nash Draw (Lambert and Harvey, 1987; Lambert, Chapter 5).

Eight Culebra samples from H-3, H-5, H-6, H-10, H-12, P-17, DOE-1, and DOE-2 (Table 4-5, #5, #14, #16, #17, #26, #28, #34, #57, and #58) give salt norms qualitatively indicative of a primitive or primitive-diagenetic origin (magnesite-anhydrite-kieserite-halite-carnallite-bischofite). However, the normative halite abundances (80 to 88%) and Cl/Br ratios (674 to 2,800) significantly exceed the seawater values. Each is also quite saline (55,000 to 153,000 mg/L). Based on the norms alone, three alternative origins can be ascribed to these waters. The first is that a primitive or primitive-diagenetic fluid mixed with a halite re-solution recharge water. The second is that, like one origin of the diluted primitive-diagenetic waters proposed above, early gypsum dehydration water diluted a primitive halite-precipitating brine, but in this case, effected considerable halite re-solution. The third is that the original primitive water was undersaturated with halite, and that it dissolved halite after migrating into a neighboring bedded halite. The relatively high amount of normative carnallite as contrasted with bischofite-tachyhydrite abundance in most of these waters (all but H-6 and DOE-2) favors the first alternative; that is, mixing of the primitive or primitive-diagenetic brine with a halite re-solution recharge water, in which alkali sulfate salts in the recharge water and abundant calcium in the primitive-diagenetic water interact to precipitate secondary gypsum and to decrease the normative alkaline-earth chlorides in the fluid. It appears plausible that all samples but H-6 and DOE-2 involved mixing with recharge waters, but the latter may have evolved though an earlier diagenetic process of halite re-solution accompanying diagenetic gypsum dewatering. With the exception of H-10, for which stable-isotope data are not yet available, all Culebra waters in this group are of meteoric origin. One of these, H-6, has been radiocarbon dated to have been isolated from the atmosphere for at least 12,000 yr (Lambert, 1987).

Two Culebra sites, WIPP-25 and WIPP-26 (Table 4-5, #38, #41, and #42), have normative halite quantities significantly less than seawater (63 to 65%), but have Cl/Br ratios well in excess (2,000 to 4,000) of the seawater value. Furthermore, they contain abundant normative alkaline-earth sulfate salts, chiefly anhydrite with minor kieserite in WIPP-25, and are unusually dilute (12,000 to 15,000 mg/L) for waters with carnallite-bischofite norms. These

characteristics suggest substantial straight dissolution of calcium sulfate (and perhaps some dolomite) on dilution of primitive fluids. These waters are also meteoric in origin (Lambert and Harvey, 1987).

The only remaining Culebra waters with total salinity >10,000 mg/L are H-1, H-4, H-11, WIPP-28, and WIPP-30 (Table 4-9, #1, #10, #27, #46, and #51). Three of these, H-11, WIPP-28, and WIPP-30 with 47,000 to 118,000 mg/L, contain the carnallite-polyhalite association indicating mixing of primitive or primitive-diagenetic fluids with alkali-sulfate recharge waters. The high halite contents in the norms of these three waters (84 to 91%) and the high Cl/Br (1,400 to 3,400) point toward some halite re-solution by the recharge waters. H-1, on the other hand, is less saline (30,000 mg/L) and contains normative thenardite and aphthitalite with 68% normative halite. This water is a typical anhydrite re-solution recharge water that has lost calcium to originally sodium-associated carbonate derived from silicate hydrolysis and also has dissolved minor amounts of halite. H-4, with 61% normative halite coexisting with the bloedite-glauberite association, also has an anhydrite re-solution recharge signature. The Cl/Br ratio of the fluid is only 176, suggesting mixing of a primitive-diagenetic fluid with an anhydrite re-solution recharge water that contained negligible chloride. It has been isolated from the atmosphere for at least 16,000 radiocarbon yr (Lambert, 1987), and its water molecules are meteoric in origin (Figure 4-5; Lambert and Harvey, 1987; Lambert, 1987).

Of the 13 Culebra sites with dilute solutions, 10 (H-2, H-7, H-8, H-9, ENGEL, GNOME SHAFT, GNOME-1, GNOME-4, WINDMILL, and SOUTH in Table 4-5, #3, #20, #23, #25, #29, #52, #53, #54, #60, and #62) yield norms containing sodium-bearing sulfates, either bloedite or the bloedite-glauberite pair, and halite abundances from 1.2 to 61%. One well's Culebra water, TWO-MILE (Table 4-5, #59), contains a polyhalite-carnallite association with 54% halite in the norm. Two locations (GNOME-8 and INDIAN in Table 4-5, #55 and #56) yield waters with the carnallite-bischofite association in the norm and 36 and 22% halite, respectively. All 13 fluids were probably sodium carbonate-bearing recharge waters that interacted with Rustler anhydrite, deposited secondary calcite, and,

for those with >15 to 25% chloride salts in the norm, redissolved minor amounts of Rustler halite.

Two of these 13 sites (H-8 and SOUTH) yielded waters with exceptionally low chloride content, 1.8 and 1.2% halite in otherwise chloride salt-free norms, suggesting recharge waters that did not encounter any primitive or primitive-diagenetic fluid or participate in halite re-solution accompanying migration into the Culebra. The very high abundance of anhydrite in each norm strongly suggests extensive dissolution of Rustler anhydrite.

Of this group, one (H-9) has a radiocarbon date of 15,000 yr and six (H-2, H-9, ENGEL, WINDMILL, SOUTH, and INDIAN) have stable-isotope determinations on their water molecules and are meteoric. The conclusions from the areal distribution of the norms of the Culebra waters (Figures 4-8 and 4-9) are the following: (1) that the norms reflect zonations similar to those defined by Siegel et al. (Chapter 2), and (2) that the Culebra dolomite member has extremely variable hydrologic and solute properties.

The solute norms display a conspicuous zonation. The one primitive-diagenetic, but somewhat diluted and possibly incompletely representative brine (P-18), with a dominantly tachyhydrite-bischofite-carnallite norm and very low Cl/Br ratio occurs where the Rustler Formation is the least permeable. Bedded halite is preserved above both the Culebra and Magenta members there. P-18 is surrounded by sampling sites where the Culebra waters are moderately saline with norms yielding abundant halite (>80%), coexisting with either the tachyhydrite-bischofite-carnallite assemblage (H-6 and DOE-2) or the carnallite-bischofite association (H-3, H-5, H-10, H-12, P-17, and DOE-1). This suggests that the waters mixed with anhydrite-halite re-solution and recharge waters, but preserved the alkaline earth chloride salt(s) in the normative assemblage. In Nash Draw north of the WIPP Site are two Culebra brines (WIPP-28 and WIPP-30) with normative polyhalite-carnallite indicating a larger fraction of anhydrite-halite re-solution recharge water mixing with primitive or primitive-diagenetic fluids. Finally, the large area of low-salinity Culebra waters south and west of the WIPP Site with alkali sulfate-bearing norms reflects (1) the

paucity of halite adjacent to the Culebra, (2) essentially no contribution of halite re-solution or primitive-diagenetic brines along the recharge path to the area, and (3) a relatively high degree of mixing in this region, possibly indicative of more rapid flow accompanying higher permeability. The second aspect of this low-salinity area is not consistent with derivation by confined flow from more saline areas to the north. The late-Pleistocene radiocarbon ages of Culebra and overlying Dewey Lake waters in the south are not consistent with ongoing rapid vertical recharge (Lambert, 1987). The norms, stable-isotope composition, and radiocarbon age in this area are, however, consistent with the following sequence of events: (1) near-surface weathering of sodium-feldspar-bearing alluvium (e.g., Gatuña sediments) to the northwest in Nash Draw (Bachman, 1985), (2) infiltration of the resulting alkali-carbonate recharge water into underlying erosionally-truncated Rustler beds during the late Pleistocene, and (3) lateral migration of this groundwater southeast to its present occurrence, where adjacent rocks were halite-free at the time of recharge. Alternatively, $Na_2SO_4$ in the norm can be generated as follows: (1) cation-exchange sites in the original smectite-group clay minerals in the evaporite section become saturated in Na due to their association with halitic rocks, (2) postdepositional removal of halite removes much of the soluble sodium, (3) an influx of groundwater dissolves $CaSO_4$, enriching Ca in solution, and (4) Ca displaces Na in the exchange sites in the clay minerals, giving additional Na in solution. Cationic exchange was proposed as the origin of excess Na (expressed as sulfate) in the Castile brine reservoirs (Lambert, 1978). Unfortunately, it may not be possible to identify the mineral source of exchangeable sodium necessary in such a mechanism, if (a) the exchange took place in rocks that escaped preservation in the geologic record, or (b) the exchange proceeded to completion.

The variability of the hydrologic properties of the Culebra member is illustrated by the great diversity of normative characteristics for the solutes, such as the unusual preservation of a severely diluted primitive-diagenetic brine at P-14 and its apparent mixing to the west with anhydrite-halite re-solution recharge or halite re-solution gypsum dehydration waters at WIPP-25 and WIPP-26. It is not at all clear what hydrologic conditions have preserved such normative compositions in an area where Rustler halite is absent (Figure 4-12) and

where the primitive-diagenetic brine (P-14) is clearly separated by unequivocal re-solution waters at H-1, H-2, and H-3 from the nearest likely candidate primitive-diagenetic brine (P-18). It is also not clear what hydrologic features allow a closely spaced group of sites (H-1, H-2, and H-3) near the center of the WIPP Site to yield waters of such vastly different salinities (13,000 *vs* 55,000) and normative characters (thenardite-aphthitalite association *vs* carnallite-bischofite association). Certainly hydrologic connections among them must be absolutely minimal in order for lateral mixing and homogenization not to have occurred since the Pleistocene. The norms of dilute solutions in the southwest quadrant of Figure 4-8 are relatively sulfate-rich and chloride poor, but range in normative mineralogy from carnallite-bischofite (INDIAN) to extremely abundant bloedite (WINDMILL). This strongly suggests recharge of the member by weathering waters. Local variations in the extent of silicate hydrolysis, interaction with Rustler anhydrite, and dissolution of isolated occurrences of Rustler halite, rather than evolution along a well-defined flow path, best explain the random variations of the salt norms in this area.

#### 4.5.3.3 Magenta Waters

Waters from the Magenta member of the Rustler Formation were obtained at far fewer sites than either the Rustler/Salado contact zone brines or the Culebra fluids, because the Magenta horizon is either commonly dry, such as along the eastern margin of Nash Draw, or has been removed by erosion, such as within Nash Draw and throughout much of the area southwest of the WIPP and GNOME sites (Figure 4-10).

No Magenta waters have solutes indicating a predominantly primitive origin. The only highly saline water (222,000 mg/kg) is H-10 (Table 4-6, #12) where the norm has tachyhydrite, bischofite, and carnallite, but also 93% halite. The Cl/Br ratio is 860. This is a typical mixture of a halite-rich recharge fluid and a primitive-diagenetic brine. Two other much more dilute solutions with 8,600 and 12,500 mg/L TDS (H-3 and WIPP-25 in Table 4-6, #4 and #14, respectively) give a qualitatively primitive norm: halite (46 and 67%, respectively), bischofite, carnallite, anhydrite, and either tachyhydrite (H-3) or kieserite (WIPP-25), but in both the Cl/Br ratio is high (574 and 2,600, respectively). The

low halite abundance is due to high anhydrite content (38 and 24%, respectively), rather than abundant alkaline earth-bearing chlorides in the norms. Thus, each appears to be a mixture of an anhydrite-halite re-solution recharge water with primitive or primitive-diagenetic solutes.

Two other localities yield Magenta waters with slight primitive or primitive-diagenetic normative characteristics. The sample from H-2 (Table 4-6, #2) with a total salinity of 10,000 mg/L contains small quantities of carnallite and polyhalite and 65% halite in the norm, and the GNOME-5 fluid (Table 4-6, #19) with 3,200 mg/L TDS contains 1.1% carnallite, 15% kieserite, only 12% halite, but 69% anhydrite in the norm. Bromine content was not determined in either water. Both samples are very dilute so that it is difficult to be certain of any primitive or primitive-diagenetic contribution to these waters.

The remaining seven Magenta waters show substantial quantities of sodium-bearing alkali salts in the norm and are clearly dominated by anhydrite re-solution recharge waters with a little halite re-solution. In two samples, H-4 and H-5 (Table 4-6, #5 and #6), silicate hydrolysis was apparently sufficient to yield considerable thenardite (17% in both) and some aphthitalite (1.7 and 2.5%, respectively) in their norms. The moderate amounts of normative halite (55 and 24%, respectively) and salinities (22,000 and 6,100 mg/L) indicate moderate to minor halite re-solution; unfortunately, bromine data for both are lacking. The waters from four of the remaining five sites (H-1, H-6, H-9, and WIPP-30 in Table 4-6, #1, #7, #10, and #18) contain abundant bloedite (9 to 35%), glauberite, and anhydrite in the norm. H-8 (Table 4-6, #9) contains the glauberite-syngenite-polyhalite assemblage of alkali-bearing sulfate salts. Salinities in these waters range from 5,000 to 19,000 mg/L with normative halite varying from 25 to 72%. Bromine determinations are reported for three of the waters (H-8, H-9, and WIPP-30) with Cl/Br ratios of 4,300, 300, and 3,800, respectively. Only the value for H-9 is anomalous; however, because of the low normative halite abundance (25%), and the low salinity (5,000 mg/L), the Cl/Br ratio probably reflects a Cl/Br ratio generated in the weathering environment. This may be true of other waters

discussed above, especially where a low Cl/Br ratio is the only basis for inferring a component of primitive-diagenetic origin in a given sample. All Magenta samples whose isotopic compositions have been determined (H-1, H-2, H-3, WIPP-25, WIPP-27, and the WIPP-30 sample of questionable validity) are meteoric.

Lambert and Robinson (1984) could not obtain a sample of WIPP-30 Magenta that could be judged representative according to their field criteria. A serial sample examined late in the pump test gave a chloride value of approximately 4,000 mg/L, around half that of the sample used for the normative calculation. This value was part of a downward trend in chloride. The minimum value of chloride is not known, due to the low productivity and the extremely slow rate of purging of a known borehole perturbation that at one point during the pump test instantaneously (overnight) raised the chloride, total divalent cations, and calcium by a factor of 2.

The areal distribution of normative data for fluids from the Magenta member (Figures 4-10 and 4-11) locates the only highly saline water (H-10) to southeast of the WIPP Site in an area in which bedded halite presumably occurs in the strata adjacent to the Magenta dolomite (Figure 4-12). This water is a mixed halite re-solution recharge and primitive-diagenetic fluid. No dominantly primitive or primitive-diagenetic Magenta fluid has been observed within the WIPP Site and surrounding area.

The remaining Magenta samples are relatively dilute (<23,000 mg/L) and represent variable but lesser proportions of primitive and primitive-diagenetic solutes as compared to anhydrite-dissolution recharge solutes. Halite re-solution is negligible to minor. As with the Culebra fluids, no definitive areal pattern occurs in the norms of these dilute waters. Thus, most solutes are probably locally controlled, and are not well mixed laterally throughout the zone. For example, the norms for the closely spaced cluster of wells, H-1, H-2, and H-3 within the WIPP Site, show considerable variation (Table 4-6, #1, #2, and #4; Figure 4-11), just as in the Culebra. H-3 has a strong component of primitive-diagenetic signature (normative tachyhydrite-bischofite) with a lesser fraction of anhydrite

re-solution recharge. H-2 shows a greater fraction of anhydrite re-solution recharge fluid (a polyhalite-carnallite signature), whereas H-1 with normative bloedite-anhydrite is characteristic of a water that dissolved minor amounts of halite and is dominated by anhydrite re-solution recharge solutes.

Other variations in the norms of Magenta fluids within the WIPP Site and surrounding area, particularly WIPP-25 with its characteristic primitive normative mineralogy and evidence of halite re-solution (Table 4-6, #14 and Figure 4-11), further document the variability of the member. Note that this norm and individual solute values are virtually identical to those in the underlying Culebra (Table 4-5, #38). This is another indication, together with identical hydraulic properties (Mercer, 1983), stable-isotope compositions (Lambert and Harvey, 1987), and uranium-isotope activity ratios (Lambert and Carter, 1987), that the Magenta and Culebra are interconnected at WIPP-25. This, together with WIPP-27, is one of the few places where such well-developed interconnection occurs.

### 4.5.4 Salt Norm Variations Among Rustler Zones

Because the distribution of Rustler salt norms in the WIPP Site and surrounding area, particularly the Culebra and Magenta norms, indicates highly variable hydrologic properties and variable degrees of hydrologic connection with adjacent strata, the variation of salt norms among the three zones at each site has been examined where more than one Rustler horizon was sampled. These comparisons are shown on Figure 4-14 for twenty sampling localities.

The general features are well illustrated. Most sites show a progressive drop in fluid salinities upward from the Rustler/Salado contact zone through the Culebra dolomite and into the Magenta dolomite. There is an upward progression in the norms at most sites, representing some aspect of the succession from primitive or primitive-diagenetic to anhydrite re-solution to meteoric recharge, with minor halite re-solution characteristics. Waters from H-5 (Figure 4-14), for example, illustrate both trends over broad ranges. The

| Well Name | Magenta | Culebra | Rustler-Salado |
|---|---|---|---|
| H-1 | 18,900 | 30,200 | 327,000 |
| H-2 | 10,300 | 12,000 | 311,000 |
| H-3 | 8590 | 55,000 | 327,000 |
| H-4 | 22,300 | 20,300 | 260,000 |
| H-5 | 6110 | 153,000 | 303,000 |
| H-6 | 5780 | 57,500 | 264,000 |
| H-7 | | 3230 | 65,400 |
| H-8 | 9310 | 2850 | 117,000 |
| H-9 | 5100 | 3100 | 264,000 |

| Well Name | Magenta | Culebra | Rustler-Salado |
|---|---|---|---|
| H-10 | 222,000 | 62,100 | 259,000 |
| P-14 | | 25,000 | 192,000 |
| P-17 | | 86,600 | 229,000 |
| P-18 | | 118,000 | 293,000 |
| Gnome-5 | 3240 | | 257,000 |
| WIPP-25 | 12,500 | 12,400 | 220,000 |
| WIPP-26 | | 15,100 | 189,000 |
| WIPP-28 | | 46,600 | 183,000 |
| WIPP-30 | 18,700 | 99,800 | 327,000 |

TRI-6341-57-0

Figure 4-14. Simple-salt rose diagrams comparing waters from the Magenta, Culebra, and Rustler/Salado contact zones for those sites in the WIPP Site with analyzed samples from more than one horizon.

Rustler/Salado contact sample is strongly hypersaline, 303,000 mg/kg, and is dominated by primitive-diagenetic solutes yielding a bischofite-tachyhydrite salt norm with minor halite. The overlying Culebra water is substantially less saline, 153,000 mg/L, with a bischofite-carnallite association and 88% halite in the norm that is diagnostic of a mixed primitive-recharge fluid having dissolved substantial halite. On the other hand, the uppermost Magenta water is dilute, 6,100 mg/L, with the thenardite-aphthitalite pair and 23.7% halite in the norm. This is characteristic of an anhydrite re-solution recharge fluid that has picked up little primitive brine and has dissolved only minor amounts of halite at most.

Although about half the waters do not strictly follow both these trends, a number of the perturbations, particularly when comparing dilute fluids, are minor and reflect only differences in the proportion of the recharge-primitive solute mix, the amount of halite dissolution, and the extent and character of silicate hydrolysis effected by the recharge fluid. Those sequences that deviate markedly from the general trend, H-10, P-14, WIPP-25, and WIPP-26, have already been discussed above.

Relationships in solutes and normative salts between the Magenta and Culebra in the south part of the area, particularly at H-8 and H-9, may be relevant to the degree of vertical mass transport in this area. Although the salinities are generally low compared to most of the Rustler to the north, the Magenta contains significantly more TDS than the Culebra at both wells (~9000 *vs* ~2900 mg/L at H8; ~5100 *vs* 3100 mg/L at H9). A zone of higher salinity overlying a zone of lower salinity is anomalous, if groundwater flow is proceeding directly downward from the surface. There is little reason to doubt the quality of the analysis, since two different laboratories obtained comparable results on the same samples. Similarly, it is difficult to argue for contamination of the less productive Magenta zone with borehole fluid, since the dominant solutes are sulfates rather than the chlorides commonly found in borehole additives.

Because of the likelihood that some NaCl-bearing drilling brine had not been purged from the H-8 and H-9 Magenta samples and for the purposes of further comparisons of the

norms, the simple-salt norms were recalculated without halite. Since halite was the only normative chloride mineral, all chloride was assigned to halite, and the TDS value was reduced by both the chloride and an equivalent amount of sodium to yield a halite-free TDS value. The results of this recalculation are given in Table 4-8. Note that even after the removal of NaCl from the TDS values, the Magenta still contains significantly more solutes than the Culebra at both localities. At H-8, downward mass trasport from the Magenta to the Culebra requires a loss in $CaSO_4$, $K_2SO_4$, and $Na_2SO_4$, and a significant gain in $MgSO_4$. At H-9, derivation of Culebra solutions by vertical mass transport from the Magenta requires a gain in $CaSO_4$ and a tenfold loss in $Na_2SO_4$. If the samples and analyses are reasonably reliable for these dilute solutions, the norms are not consistent with a derivation of the Culebra by vertical downward flow from the Magenta. At H-8, the gain in Mg is not sufficient to offset the loss in Ca to yield a downward-increasing TDS trend, as might be expected in vertical recharge to the Culebra. Similarly, at H-9, it is difficult to envision a mechanism of rock/water interaction that would decrease Mg sulfate and TDS during downward flow from Magenta to Culebra. Thus, even though the normative signatures of the H-8 and H-9 waters are meteoric-recharge, the norms and TDS trends are not entirely consistent with direct vertical infiltration from the surface to the Culebra in the area of fresher groundwaters south of the WIPP Site. Significant mass transport from the surface to the Culebra at H-9 is also not consistent with the radiocarbon date, which shows that this water has been isolated from the atmosphere at least 14,900 radiocarbon yr. This is neither significantly older nor appreciably younger than dates from the more saline parts of the Culebra farther north. Thus, the groundwater solutions here have probably not arisen from ongoing dilution due to active recharge entailing downward mass transport from the Magenta to the Culebra.

## Table 4-8. Recalculated Halite-Free Simple-Salt Norms and TDS for H-8 and H-9

| | Normative simple salts, wt% | | | | | |
|---|---|---|---|---|---|---|
| | $MgCO_3$ | $CaSO_4$ | $MgSO_4$ | $K_2SO_4$ | $Na_2SO_4$ | TDS mg/L |
| H-8 | | | | | | |
| Magenta[1] (#9) | 0.8 | 83.3 | 1.3 | 5.0 | 9.7 | 3500 |
| Culebra[2] (#23) | 2.4 | 68.4 | 24.8 | 0.3 | 4.1 | 2800 |
| H-9 | | | | | | |
| Magenta (#11) | 0.8 | 48.7 | 21.5 | 1.6 | 27.4 | 3860 |
| Culebra (#25) | 2.8 | 73.9 | 20.5 | 0.6 | 2.2 | 2780 |

1. See Table 4-6 for original Magenta analyses and norms.
2. See Table 4-5 for original Culebra analyses and norms.

# 4.6 REFERENCES

Allison, G. B., W. J. Stone, and M. W. Hughes. 1985. "Recharge in Karst and Dune Elements of a Semi-Arid Landscape as Indicated by Natural Isotopes and Chloride." *Journal of Hydrology*, Vol. 76:1-25.

Anderson, R. Y. 1981. "Deep-Seated Salt Dissolution in the Delaware Basin, Texas and New Mexico." *Environmental Geology and Hydrology in New Mexico*. S. G. Wells and W. Lambert, ed. N. M. Geol. Soc. Spec. Publ. 10:133-145.

Bachman, G. O. 1984. "Regional Geology of the Ochoan Evaporites, Northern Part of the Delaware Basin." Circular 184:1-22. Socorro, NM: New Mexico Bureau of Mines and Mineral Resources.

Bachman, G. O. 1985. *Assessment of Near-Surface Dissolution at and Near the Waste Isolation Pilot Plant (WIPP), Southeastern New Mexico*. SAND 87-7178. Albuquerque, NM: Sandia National Laboratories.

Bachman, G. O. 1987. *Karst in Evaporites in Southeastern New Mexico*. SAND84-7078. Albuquerque, NM: Sandia National Laboratories.

Bodine, M. W., Jr., and B. F. Jones. 1986. *The Salt Norm: A Quantitative Chemical-Mineralogical Characterization of Natural Waters*. Water Resources Investigation Report 86-4086. Reston, VA: US Geological Survey.

Bradbury, J. P. 1981. "Report on Quaternary Fossils from San Simon Sink, Lea County, New Mexico." *Sandia National Laboratories and University of New Mexico, Basic Data Report for Drillhole WIPP 15 (Waste Isolation Pilot Plant--WIPP)*. SAND79-0274. Albuquerque, NM: Sandia National Laboratories.

Braitsch, O. 1971. *Salt Deposits, Their Origin and Composition.* New York: Springer-Verlag.

Brookins, D. G., J. K. Register, and H. Krueger. 1980. "Potassium-Argon Dating of Polyhalite in Southeast New Mexico." *Geochimica et Cosmochimica Acta*, Vol. 44:635-637.

Collins, A. G. 1975. *Geochemistry of Oilfield Waters.* Amsterdam: Elsevier Scientific Publishing Co.

Colton, I. D., and J. G. Morse. 1985. *Water Quality Sampling Plan.* WIPP DOE-215. Carlsbad, NM: Waste Isolation Pilot Plant Project Office.

Cooper, J. B., and V. M. Glanzman. 1971. *Geohydrology of Project Gnome Site, Eddy County, New Mexico.* Paper 712-A. Washington, DC: US Geological Survey.

Cross, W., J. P. Iddings, L. V. Pirsson, and H. S. Washington. 1902. "A Quantitative Chemico-Mineralogical Classification and Nomenclature of Igneous Rocks." *Journal of Geology*, Vol. 10:555-690.

Eugster, H. P., C. E. Harvie, and J. H. Weare. 1980. "Mineral Equilibria in the Six-Component Sea Water System, Na-K-Mg-$SO_4$-Cl-$H_2O$, at 25°C." *Geochimica et Cosmochimica Acta*, Vol. 44:1335-1348.

Eugster, H. P., and B. F. Jones. 1979. "Behavior of Major Solutes During Closed-Basin Brine Evolution." *American Journal of Science*, Vol. 279:609-631.

Gonzalez, D. D. 1981. "Hydrologic Data." *Sandia National Laboratories and University of New Mexico, Basic Data Report for Drillhole WIPP 15 (Waste Isolation Pilot Plant--WIPP).* SAND79-0274. Albuquerque, NM: Sandia National Laboratories.

Hem, J. D. 1970. *Study and Interpretation of the Chemical Characteristics of Natural Waters.* Water Supply Paper 1473. Washington, DC: US Geological Survey.

Hiss, W. L. 1975. *Chloride-Ion Concentration in Ground Water in Permian Guadalupian Rocks, Southeast New Mexico and West Texas.* Resource Map 4. Socorro, NM: New Mexico Bureau of Mines and Mineral Resources.

Hunter, R. L. 1985. *A Regional Water Balance for the Waste Isolation Pilot Plant (WIPP) Site and Surrounding Area.* SAND84-2233. Albuquerque, NM: Sandia National Laboratories.

Johnson, K. S. 1986. *Salt Dissolution and Collapse at the Wink Sink in West Texas.* BMI/ONWI-598. Office of Nuclear Waste Isolation.

Jones, C. L. 1978. *Test Drilling for Potash Resources: Waste Isolation Pilot Plant Site, Eddy County, New Mexico.* Open File Report 78-592. Denver, CO: US Geological Survey.

Kunkler, J. L. 1980. *Evaluation of the Malaga Bend Salinity Alleviation Project.* Open File Report 80-1111. Denver, CO: US Geological Survey.

Lambert, S. J. 1978. "Geochemistry of Delaware Basin Ground Waters." *Geology and Mineral Deposits of Ochoan Rocks in Delaware Basin and Adjacent Areas.* G. S. Austin, ed. Circular 189:33-38. Socorro, NM: New Mexico Bureau of Mines and Mineral Resources.

Lambert, S. J. 1983. *Dissolution of Evaporites in and Around the Delaware Basin, Southeastern New Mexico and West Texas.* SAND82-0461. Albuquerque, NM: Sandia National Laboratories.

Lambert, S. J. 1987. *Feasibility Study: Applicability of Geochronologic Methods Involving Radiocarbon and Other Nuclides to the Groundwater Hydrology of the Rustler Formation.* SAND86-1054. Albuquerque, NM: Sandia National Laboratories.

Lambert, S. J., and J. A. Carter. 1987. *Uranium-Isotope Systematics in Groundwaters of the Rustler Formation, Northern Delaware Basin, Southeastern New Mexico.* SAND87-0388. Albuquerque, NM: Sandia National Laboratories.

Lambert, S. J., and D. M. Harvey. 1987. *Stable-Isotope Geochemistry of Groundwaters in the Delaware Basin of Southeastern New Mexico.* SAND87-0138. Albuquerque, NM: Sandia National Laboratories.

Lambert, S. J., and K. L. Robinson. 1984. *Field Geochemical Studies of Groundwaters in Nash Draw, Southeastern New Mexico.* SAND83-1122. Albuquerque, NM: Sandia National Laboratories.

Levy, Y. 1977. "The Origin and Evolution of Brine in Coastal Sabkhas, Northern Sinai." *Journal of Sedimentary Petrology*, Vol. 47:451-462.

Mercer, J. W. 1983. *Geohydrology of the Proposed Waste Isolation Pilot Plant Site, Los Medaños Area, Southeastern New Mexico.* Water Resources Investigation Report 83-4016. Albuquerque, NM: US Geological Survey.

Mercer, J. W., and B. R. Orr. 1979. *Interim Data Report on the Geohydrology of the Proposed Waste Isolation Pilot Plant Site, Southeast New Mexico.* Waste Resources Investigations Report 79-98. Albuquerque, NM: US Geological Survey.

Nicholson, A., Jr., and A. Clebsch, Jr. 1961. *Geology and Ground-Water Conditions in Southern Lea County, New Mexico.* Ground-water Report 6. Socorro, NM: New Mexico Bureau of Mines and Mineral Resources.

Powers, D. W., S. J. Lambert, S. E. Shaffer, L. R. Hill, and W. D. Weart, ed. 1978. *Geological Characterization Report, Waste Isolation Pilot Plant (WIPP) Site, Southeastern New Mexico*. SAND78-1596. Albuquerque, NM: Sandia National Laboratories.

Rankama, K., and T. G. Sahama. 1950. *Geochemistry*. Chicago: University of Chicago Press.

Robinson, K. L. 1987. *Analysis of Solutes in Groundwaters from the Rustler Formation at and near the WIPP Site*. SAND86-0917. Albuquerque, NM: Sandia National Laboratories.

Snyder, R. P. 1985. *Dissolution of Halite and Gypsum, and Hydration of Anhydrite to Gypsum, Rustler Formation, in the Vicinity of the Waste Isolation Pilot Plant, Southeastern New Mexico*. Open File Report 85-229. Denver, CO: US Geological Survey.

Snyder, R. P., and L. M. Gard, Jr. 1982. *Evaluation of Breccia Pipes in Southeastern New Mexico and Their Relation to the Waste Isolation Pilot Plant (WIPP) Site*. Open File Report 82-968. Denver, CO: US Geological Survey.

Uhland, D. W., and W. S. Randall. 1986. *1986 Annual Water Quality Data Report for the Waste Isolation Pilot Plant*. DOE-WIPP-86-006. Carlsbad, NM: Westinghouse Electric Corporation.

Uhland, D. W., W. S. Randall, and R. C. Carrasco, 1987. *1987 Annual Water Quality Data Report for the Waste Isolation Pilot Plant*. DOE-WIPP-87-006. Carlsbad, NM: Westinghouse Electric Corporation.

Van Devender, T. R. 1980. "Holocene Plant Remains from Rocky Arroyo and Last Chance Canyon, Eddy County, New Mexico." *The Southwestern Naturalist*, Vol. 25:361-372.

# CHAPTER 5:

# ISOTOPIC CONSTRAINTS ON THE RUSTLER AND DEWEY LAKE GROUNDWATER SYSTEMS

Steven J. Lambert
Sandia National Laboratories

## ABSTRACT

Interpretations of the groundwater hydrology of the Rustler Formation and Dewey Lake Red Beds overlying the Waste Isolation Pilot Plant (WIPP) Facility are constrained by the isotopic record: (1) groundwaters largely confined within dolomitic units of the Rustler Formation contain negligible tritium; (2) confined Rustler waters and some Dewey Lake waters are depleted in heavier oxygen and hydrogen isotopes relative to potential recharge water; (3) one possibly perched Dewey Lake water and three confined Rustler waters were sufficiently uncontaminated to yield calculable radiocarbon model ages (times of isolation from the atmosphere) ranging from 12,000 to 16,000 years; and (4) these dated waters belong to the population of groundwaters depleted in heavier isotopes relative to modern recharge, suggesting that recharge more depleted in D and $^{18}O$ was in a wetter, perhaps cooler late-Pleistocene pluvial period. Rustler water radiocarbon ages and stable-isotope compositions are independent of salinity or solute assemblage, suggesting a slug-type recharge event. Dissolved uranium concentrations and $^{234}U/^{238}U$ activity ratios have trends different from those predicted for confined steady-state Culebra flow. Implications of these results are that (1) the Rustler groundwater system is not at steady-state with respect to either flow direction or recharge; instead, the system has largely been draining since the Pleistocene; (2) recharge was rapid relative to the time required for mixing and homogenization of solutes due to groundwater flow; (3) recharge had a

significant eastward component, conflicting with the principally north-to-south flow predicated on potentiometric measurements; (4) travel time for Rustler water from its recharge point to the eastern part of the WIPP Site has been at least several thousand years. Strontium- and hydrogen-isotope ratios of secondary gypsum in the Rustler and Dewey Lake indicate that (1) the contribution of near-surface derived mineral material to the Rustler has been minimal, except in the water-bearing zones; (2) the water/rock ratio during gypsification has been relatively large within present water-bearing zones, but much smaller above and below, implying more stratabound fluid movement and minimal vertical movement; (3) the Dewey Lake Red Beds contained a paleohydrologic system largely independent from the Rustler, involving greater degrees of material transport from the surface.

# CONTENTS

# CONTENTS (Continued)



# FIGURES

# FIGURES (Continued)



# TABLES

# CHAPTER 5.0

## 5.1 INTRODUCTION

### 5.1.1 Importance of the Rustler Formation

The Rustler Formation is the uppermost evaporite-bearing unit in the Ochoan (Permian) sequence in the Delaware Basin of southeastern New Mexico. It is important because it contains interbeds of fractured brittle rock that carry the most abundant and regionally persistent occurrences of groundwater above the Waste Isolation Pilot Plant (WIPP) Facility. The Rustler is the unit of most concern for radionuclide transport to the accessible environment by means of groundwater flow. Therefore, an understanding of the geologic history of groundwater in the Rustler Formation (Permian, Ochoan) is fundamental to the evaluation of the ability of the bedded evaporite environment at the WIPP to contain waste radionuclides for the requisite time.

### 5.1.2 Interpretive Problems Unique to Groundwater Geochemistry

Water is a mobile phase. In its natural occurrence, a groundwater solution may or may not behave as a closed system at various points along its flow path in geographic space, or along its evolutionary path in thermodynamic space. At any given time or locality, it is sampled as a homogeneous phase, whether it be a grab-sample at the surface or a groundwater sample pumped or bailed from a well. The chemical and isotopic composition may reflect the combined results of numerous episodes of water/rock interaction. Since several possible evolutionary paths can give rise to any given observed chemical or isotopic composition, it is generally not possible to infer a unique evolutionary path simply from its composition. Similarly, it is generally not possible to infer a unique flow path simply from the geographic distribution of any single groundwater constituent in a regional flow system.

The fundamental principles governing the behavior of some geochemical constituents (elemental, molecular, or isotopic) may be simpler or better understood than others. Some

constituents may be more inert relative to some processes of rock/water interaction than others. Thus, some constituents may have responded to their host rocks via rock/water interaction to greater or lesser degrees. All constituents are not expected to respond to each episode of rock/water interaction to the same degree, and some may not respond at all. Thus, it is likely that some constituents will preserve some parts of the history of the groundwater solution and others will not. For these reasons, any geochemical study of groundwater systems needs to consider many different methods of study and attempt to synthesize the results into a mutually consistent descriptive model.

It may not be possible, however, to fully reconcile all the data with a single existing hypothesis. If this is the case, hypotheses probably need to be sought to allow such reconciliation. This work will attempt such reconciliation with the hypotheses that seem most appropriate at the present state of scientific understanding, taking note of the internal mutual consistencies in various geological, hydrological, and geochemical interpretations of the Rustler and Dewey Lake groundwater systems, as well as considering some of the remaining inconsistencies.

### 5.1.3 Nuclide Systems in Groundwaters and Host Rocks

Several nuclide systems have been examined for possible application to the groundwater hydrology of the Rustler Formation. These nuclide systems include the stable isotopes in the water molecules (deuterium and $^{18}O$), tritium occurring as part of the water molecules, and nuclides represented in soluble species ($^{14}C$, $^{36}Cl$, $^{234}U$, and $^{238}U$). This chapter is a synthesis of studies and conclusions previously reported by Lambert and Harvey (1987), Lambert (1987), Lambert and Carter (1987), and Brookins and Lambert (1988).

The stable oxygen and hydrogen isotopes reflect the climatic conditions under which the groundwaters precipitated from the atmosphere (Lambert and Harvey, 1987), while the low to intermediate half-life nuclides can be, when free from contamination, indicative of the period of time during which the groundwater has been isolated from some atmospheric source for the nuclides (Lambert, 1987). Isotopes of uranium have been used to evaluate

the nature of past and ongoing interactions between groundwater and host rock (Lambert and Carter, 1987). In addition, some nuclide systems have been useful in unraveling various aspects of the history of interaction between groundwaters and their host rocks; the host rocks themselves preserve certain characteristics of the waters they carried. For example, the $^{87}Sr/^{86}Sr$ ratio of the rock may reflect the secondary deposition of surface-derived material in a host rock invaded by water (Brookins and Lambert, 1988). Similarly, the observed D/H ratios in hydrous minerals crystallized or recrystallized in the presence of water will be determined in part by the D/H ratio of the water, even if the water is no longer present. Whereas most Rustler isotopic studies were originally reported in the references cited, the preliminary studies of D/H ratios in Rustler and Dewey Lake gypsum constitute new work and have not been previously reported.

## 5.2 Stable Isotopes in Groundwaters and Host Rocks

### 5.2.1 Sources of Samples

Surface- and groundwater samples from the northern Delaware Basin in southeastern New Mexico have been analyzed for their stable-isotope compositions (D/H and $^{18}O/^{16}O$ ratios). Fourteen carbonates from groundwater host-rocks were analyzed for their $^{18}O/^{16}O$ and $^{13}C/^{12}C$ ratios.

Most groundwaters were taken from pump- or bail-tests of wells in the Rustler Formation near the WIPP Site (Robinson, 1987). Three fluid-producing horizons in the Rustler Formation have been extensively hydraulically tested, sampled, and analyzed for various solution parameters. Because these horizons occur near the WIPP Site and nearby Nash Draw (a solution valley developed in the Rustler outcrops to the west), they have been identified as likely transport media for radionuclide-contaminated groundwaters (Mercer, 1983). These three units are, in descending stratigraphic sequence, the Magenta member, the Culebra dolomite member, and the zone including the basal Rustler and upper Salado

Formations, commonly called the Rustler/Salado contact. The Salado Formation contains the evaporite sequence in which the WIPP subsurface facility is being constructed.

The hydrologic subunit that appears to have the most regionally persistent productivity is the Culebra. It has supplied the most water (n=37) and aquifer-rock (n=9) samples in this study. Three Culebra waters have been radiocarbon-dated using a model yielding a high degree of internal consistency, and tritium measurements have been performed on five Culebra waters and one Magenta water (Lambert, 1987). Rustler groundwaters are under confined conditions at the WIPP Site and in many parts of east-central Nash Draw, at least on the time scale of the hydrologic testing during which samples were recovered. In addition to the Rustler Formation, the overlying Dewey Lake Red Beds have been sampled in three localities near the WIPP Site. One of these samples has been radiocarbon-dated. Water in the Dewey Lake is believed to be perched in many localities and is not regionally persistent in its occurrence (Mercer, 1983). However, the presence of unsaturated domains beneath known saturated occurrences within the Dewey Lake has been difficult to demonstrate.

For comparison, several other groundwaters in the region were analyzed. These include four samples from the Capitan Limestone where it is under confined conditions, 12 from Carlsbad Caverns in the northern Guadalupe Mountains (a vadose zone in the Capitan), and one from alluvium. Two surface waters (the Pecos River and a summer rainstorm) and water from Surprise Spring (discharging from the Tamarisk member of the Rustler Formation in southwestern Nash Draw) complete the suite of major water-sampling. In addition, water was sampled from nine municipal wells tapping the Ogallala Formation in southeastern New Mexico, and their $\delta D$ values were measured for comparison with Ogallala waters from the neighboring Southern High Plains of Texas.

### 5.2.2 Validity of Data

According to geological, hydrological, and geochemical criteria, several samples from pump- or bail-tests were judged to be not representative of the fluid reservoir at depth, due

to probable mixing and contamination. These include, but might not be restricted to the Magenta water from WIPP-30; the Culebra water from P17, P15, and P18; and Rustler/Salado contact water from P15, P18, and WIPP-27. Even though some of these water samples were analyzed in the absence of additional criteria for evaluating their validity, their δ-values, if available, were not used in the interpretations (Lambert and Harvey, 1987). Also, some sampling episodes (separated in time by several months or years) at various borehole localities gave less reliable samples than at other times, dependent on prevalent borehole conditions (Lambert and Robinson, 1984; Lambert and Harvey, 1987; Robinson, 1987). How well a sample represents the subsurface reservoir, rather than how well a laboratory measurement characterizes a sample, generally governs the validity of an analytical result for a given subsurface location (Lambert and Harvey, 1987).

### 5.2.3 Unmodified Groundwater of Direct Meteoric Derivation

The $\delta D/\delta^{18}O$ relationships of the Capitan, Dewey Lake, alluvial, most Rustler, and surface waters analyzed indicate a direct meteoric origin (Figure 5-1). Their isotopic compositions in $\delta D/\delta^{18}O$ space fall along the meteoric field (the heavy lines) defined by Craig (1961) and Epstein et al. (1965; 1970), with little alteration by partial evaporation or rock/water interaction (Lambert, 1978; Lambert, 1983; Lambert and Harvey, 1987). Since groundwaters are known in semi-arid areas whose $\delta D/\delta^{18}O$ values plot below and to the right of the meteoric field (cf. Allison et al., 1985), as much as -10% relative to surface precipitation (delimited by the heavy dashed line labeled "a"), small deviations of these groundwaters from the meteoric field are not considered significant. In this context the term "meteoric" implies only an inferred origin from precipitation, not that the time of such origin is necessarily modern.

The meteoric groundwaters fall into one of two distinct populations of D and $^{18}O$ values. The dichotomy in δ-values is related to local hydrologic conditions and is illustrated in Figure 5-1. Confined Rustler and confined Capitan groundwaters (i.e., having potentiometric levels at higher elevations than the upper boundary of the producing unit) fall

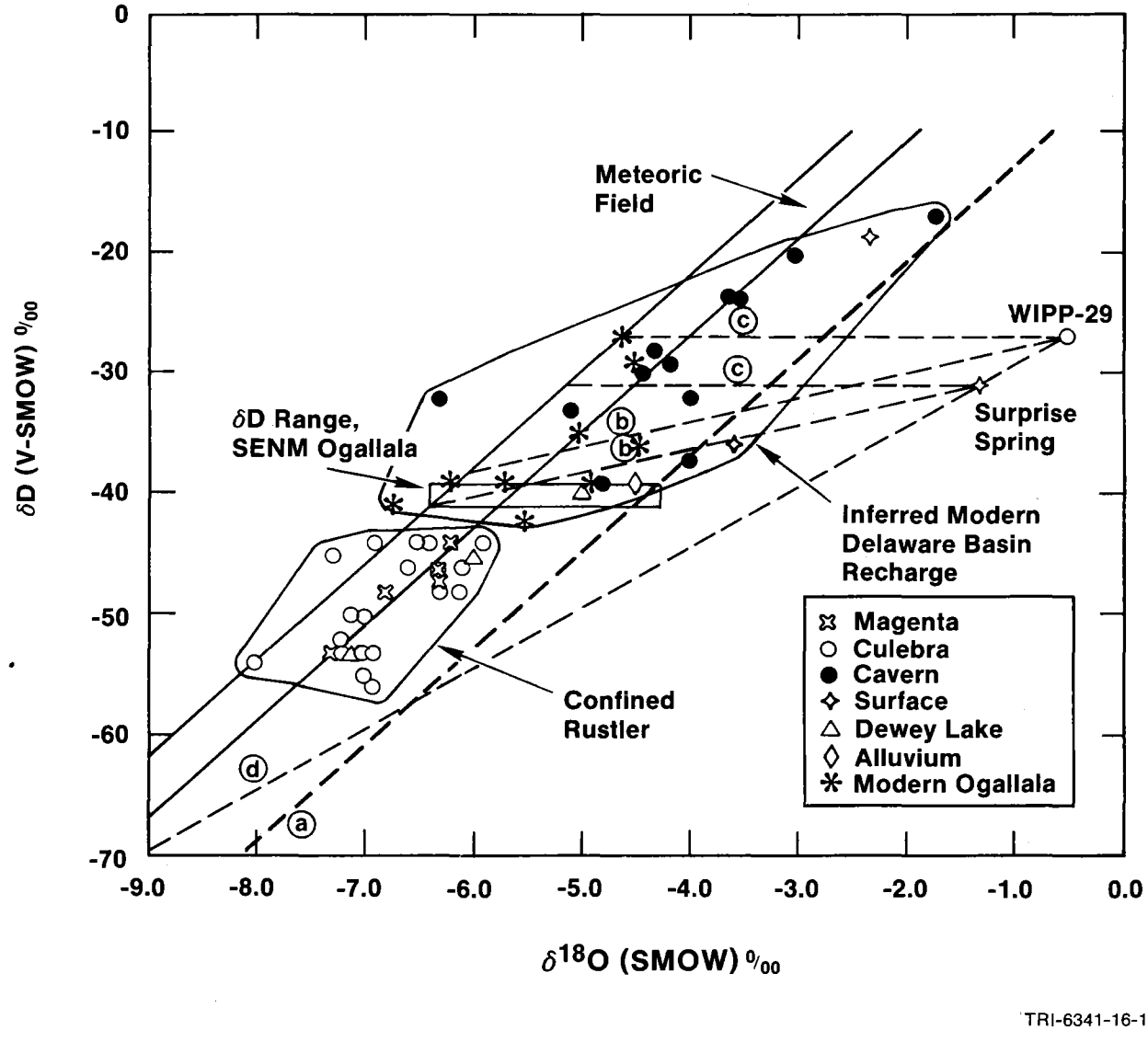


Figure 5-1. Stable-isotope compositions of groundwaters from the Rustler Formation and related units (adapted from Lambert and Harvey [1987]).

into the range of more negative δD and $\delta^{18}O$ values, having δD values more negative than -43‰. Meteoric waters from the vadose Capitan and water-table conditions in alluvium define the more positive range of isotopic compositions, and have δD values more positive than -41‰ and $\delta^{18}O$ values generally more positive than -5.5‰. Both populations came from areas in the northern Delaware Basin that have a relatively uniform climate typical of the northern Chihuahuan desert, where surface elevations are 3000 to 4500 ft. The three waters from the Dewey Lake are split: one from the isotopically heavier population and two from the lighter. One of the lighter Dewey Lake waters has been radiocarbon dated; it contains a major component that has been out of contact with the atmosphere for at least 14,000 radiocarbon years (Section 3.5.3; Lambert, 1987). Three of the confined Rustler waters from the Culebra near the WIPP Site, falling in the lighter $\delta D/\delta^{18}O$ population, have radiocarbon dates between 12,000 and 16,000 radiocarbon years (Section 3.5.3; Lambert, 1987). The mean δD value of the groundwater sample population more depleted in $\delta^{18}O$ and δD (26 data), which contains the four late Pleistocene groundwater dates, is -50‰.

The isotopically heavier population of meteoric groundwater and surface samples (16 data) overlap the δD values of nine groundwater samples from the Ogallala sandstone tapped by southeastern New Mexico municipal wells (the rectangle in Figure 5-1), which have δD values between -39 and -41‰ (C. J. Yapp, University of New Mexico, unpublished). These Ogallala waters have δD values similar to some of those reported by Nativ and Smith (1987) for the Southern High Plains of Texas. There, only Ogallala waters having δD values more positive than -42‰ have significant levels of tritium (>10 tritium units [TU]), indicating that modern recharge there is relatively enriched in deuterium (Figure 5-2). Nativ and Smith (1987), Osterkamp and Wood (1987), and Wood and Osterkamp (1987) have concluded that the Ogallala groundwater of the Southern High Plains (a) is recharged rapidly through playas representing localities of dissolved caliche caprock, (b) does not experience significant partial evaporation prior to recharge, and (c) contains a preferential concentration of heavier isotopes relative to the entire range of isotopic compositions of High Plains rainfall. Significantly high tritium concentrations in High Plains Ogallala

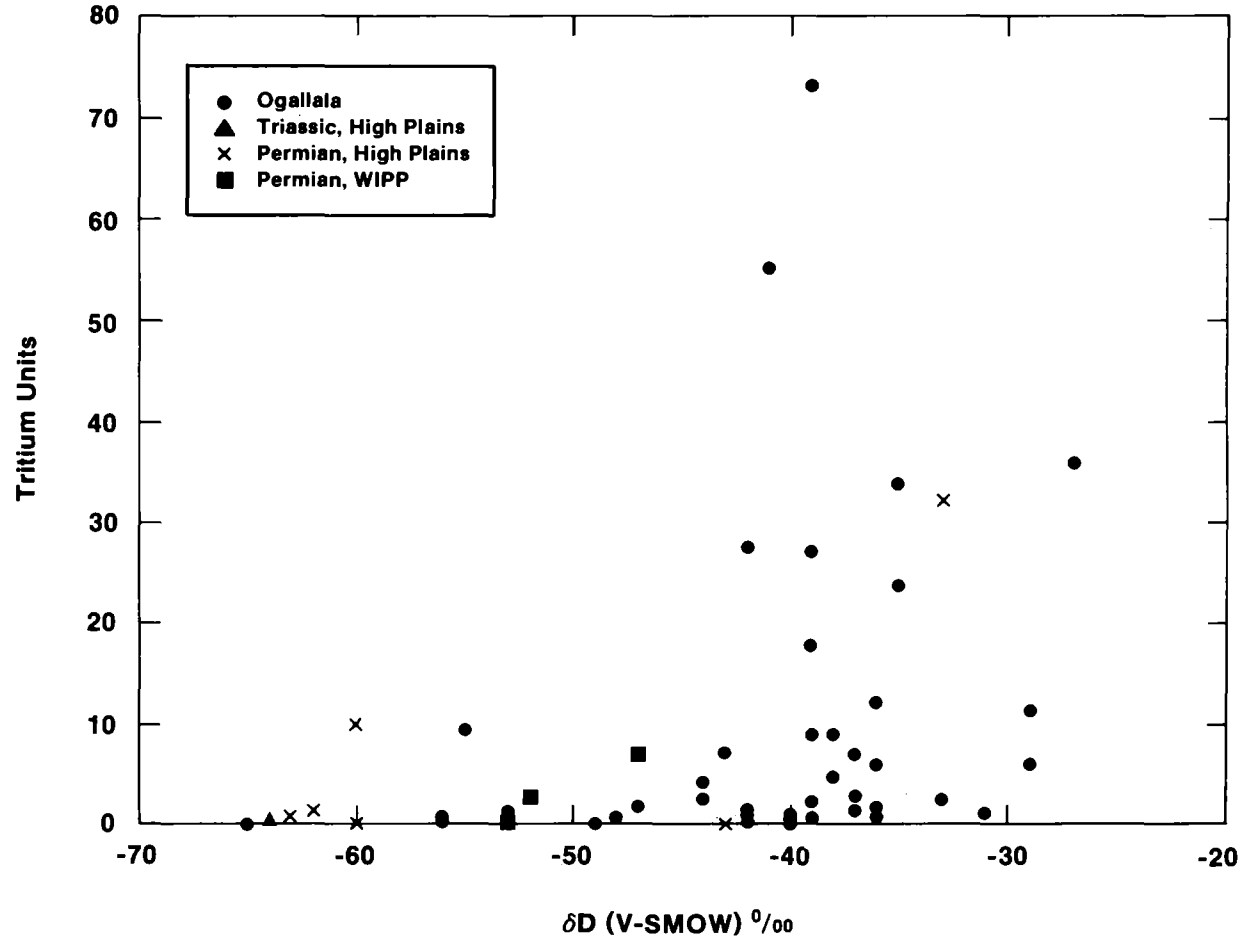


Figure 5-2. Tritium and deuterium concentrations in groundwaters from the Southern High Plains, Texas, and the Delaware Basin, southeastern New Mexico. High Plains data are from Nativ and Smith (1987); WIPP data are from Lambert and Harvey (1987) and Lambert (1987).

waters (>10 TU), indicating derivation from a meteoric source since 1950, are restricted largely to groundwaters having δD values more positive than about -42‰ (Figure 5-2). Ogallala waters from nearby southeastern New Mexico have δD values between -39 and -41‰, corresponding with δD values of modern groundwater recharge in the Texas High Plains. Hydrogen-isotope characteristics of groundwaters from the nearby climatically similar Delaware Basin (Rustler waters labeled "Permian, WIPP" in Figure 5-2), having more negative δD values and little tritium, are not consistent with significant post-1950 recharge. Instead, modern groundwater recharge in the Delaware Basin is better represented by δD values more positive than -42‰ and not by the confined Rustler waters having more negative D values (see Figure 5-1). Since the elevations, climate, and vegetative cover are similar in the Southern High Plains and the northern Delaware Basin, it is here concluded that regional groundwaters more enriched in deuterium (δD> -42‰) represent modern recharge at the latitude and elevation of the Delaware Basin of southeastern New Mexico.

Figure 5-3 is a histogram of δD values of unmodified meteoric southeastern New Mexico groundwater samples. The population less depleted in deuterium includes the nine Ogallala data of Yapp. Although $\delta^{18}O$ values are not available for the New Mexico Ogallala samples, these groundwaters are also assumed to have unmodified meteoric isotopic compositions. The deuterium-enriched population, inferred to have direct modern hydraulic connections to surficial sources of meteoric recharge, has a mean δD value of -33‰ (Lambert and Harvey, 1987) and is here taken to represent the isotopic composition of meteoric water that has recharged shallow groundwater systems under present climatic conditions at elevations of 3000 to 4500 ft in southeastern New Mexico. This elevation range includes the elevation of the WIPP Site, 3300 to 3550 ft.

Confined Rustler and Capitan groundwaters showing no isotope shift from the meteoric field have a mean δD value of -50.3% (n = 46), with confidence limits (at the 95% level) of

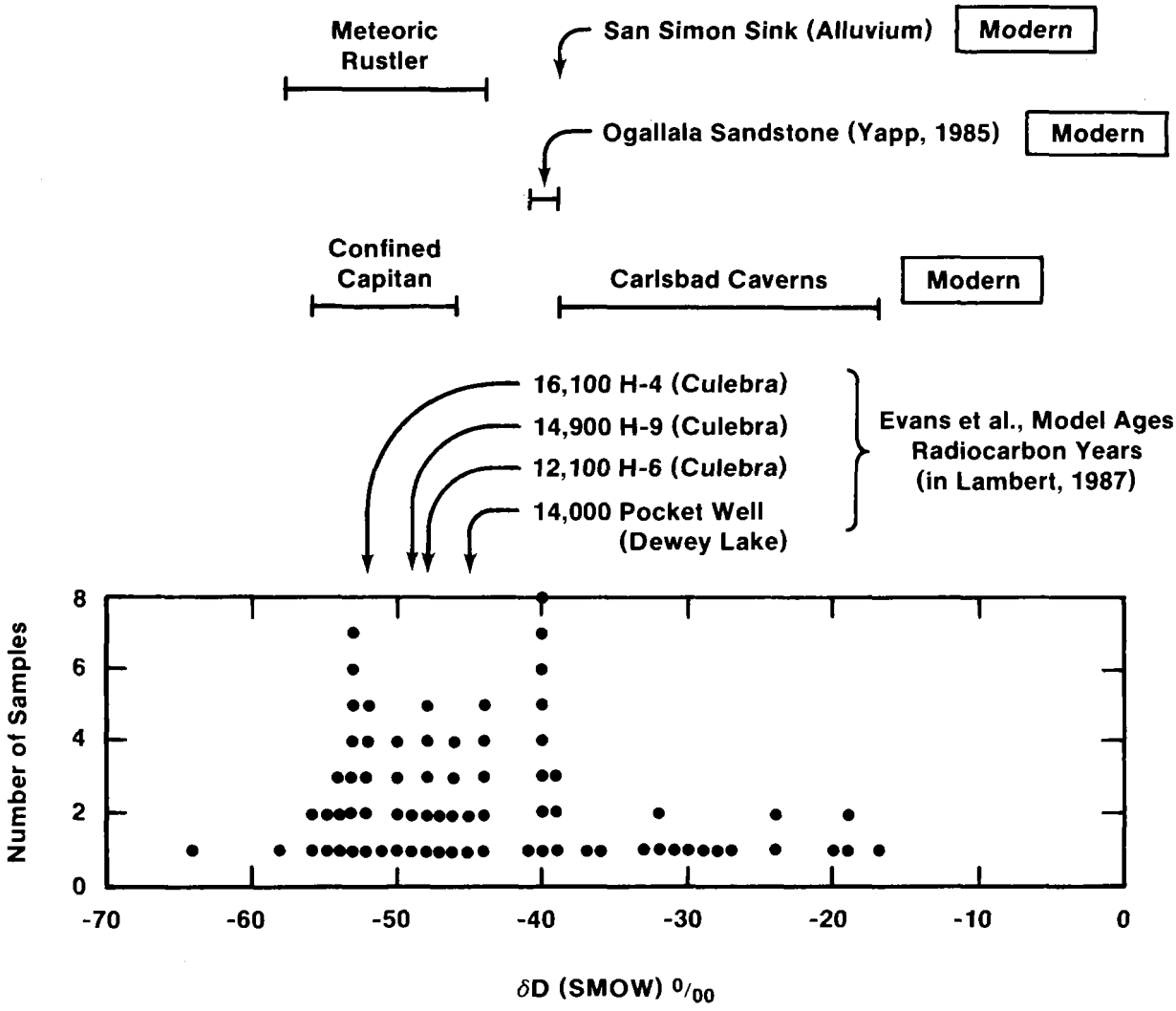


Figure 5-3. Histogram of δD values for meteoric groundwaters in the Delaware Basin (from Lambert and Harvey [1987]).

-42 to -59‰. These confidence limits do not statistically overlap with δD values of groundwaters from water-table (San Simon Sink, Ogallala sandstone) or vadose (Carlsbad Caverns) conditions, all of which have δD values more positive than -42‰. Also, four confined groundwaters from the more negative δD range have radiocarbon ages of 12,000 to 16,000 years. The nonoverlap of the isotopic compositions of the two populations in Figure 5-3 suggests that climatic conditions governing recharge have not been identical for both populations in the Delaware Basin. Both populations of groundwaters are expected to have received recharge over at least several years; hence, their isotopic compositions would be expected to represent recharge over several cycles of year-to-year variations and might reflect the dominance of recharge during certain seasons rather than necessarily coinciding with the isotopic composition of total weighted mean precipitation. Consequently, the shallow (unconfined) groundwaters, including those reported by Nativ and Smith (1987), are taken to represent the seasonally integrated average isotopic composition of modern meteoric recharge in the Delaware Basin and nearby climatically-similar areas.

The tight clustering of δ-values in the isotopically lighter (largely confined) groundwater population (Figures 5-1 and 5-3) is indicative of more complete mixing and homogenization, due either to long residence time or to long flow paths. This is consistent with the absence of tritium in Rustler and some Dewey Lake waters near the WIPP Site and the late Pleistocene radiocarbon ages of isolation from the atmosphere of some of these waters (Section 3.5.3; Lambert, 1987). Conversely, greater scatter observed in the δ-values of the isotopically heavier population is consistent with shorter (mostly local) recharge paths or less mixing and homogenization of seasonal variation in δ-values of recharge water.

A separation in mean δD values as small as 10‰ was used by Yapp (1985) to infer that Albuquerque Basin groundwaters more depleted in deuterium are relics of a previous recharge event typifying past (possibly wetter and/or cooler) climatic conditions. The difference in mean δD between the two populations defined here on the basis of hydraulic environment, confined versus less confined, (-50‰ versus -33‰) is 17‰. Further, the nonoverlap of the two populations suggests that mixing between the two, especially in the

confined Rustler units, has been minimal. The late Pleistocene radiocarbon ages (three from the Culebra and one from the Dewey Lake) obtained for groundwaters in the isotopically lighter Delaware Basin population (Figure 5-3) are consistent with the hypothesis that groundwaters now under confined conditions in the Rustler and Capitan were recharged during, and perhaps in response to, a past climatic event. These groundwater ages correspond to ages of local late-Pleistocene packrat middens (Van Devender, 1980), which preserve evidence of floral assemblages consistent with a cooler and/or moister environment than is reflected in the modern plant community. The extremely low tritium levels in Rustler groundwaters near the WIPP Site, which correspond to more negative δ-values (Figure 5-2), suggest that the groundwaters are receiving little if any active recharge at the present time. The four apparent late Pleistocene ages derived from radiocarbon measurements of waters more depleted in $\delta^{18}O$ and δD suggest that the isotopically lighter population represents southeastern New Mexico paleowater, distinct from recharge under modern climatic conditions, analogous to the findings of Gat and Issar (1974) for groundwater in the Sinai Desert.

### 5.2.4 Groundwaters Modified by Rock/Water Interactions

Confined groundwaters from the Rustler/Salado contact in Nash Draw have meteoric isotopic compositions typical of other Rustler waters. Toward the east, over the WIPP Site, however, the isotopic composition of water from the Rustler/Salado contact shows progressively more positive deviation in δ-value ("isotope shift") from typical Rustler meteoric values (Figure 5-4). Shift-contours roughly parallel the boundaries drawn by Snyder (1985) (dotted line in Figure 5-4) delineating the stratigraphic positions of halite occurrence in the Rustler. The zero-shift contour parallels the scarp defining Nash Draw at Livingston Ridge. The magnitude of the shift is correlative with measured decreases in transmissivity (cf. Mercer, 1983), increasing distance from the eastern dissolution scarp of Nash Draw (cf. Bachman, 1985; 1987), and an increasing amount of halite surviving in the Rustler Formation (cf. Snyder, 1985).

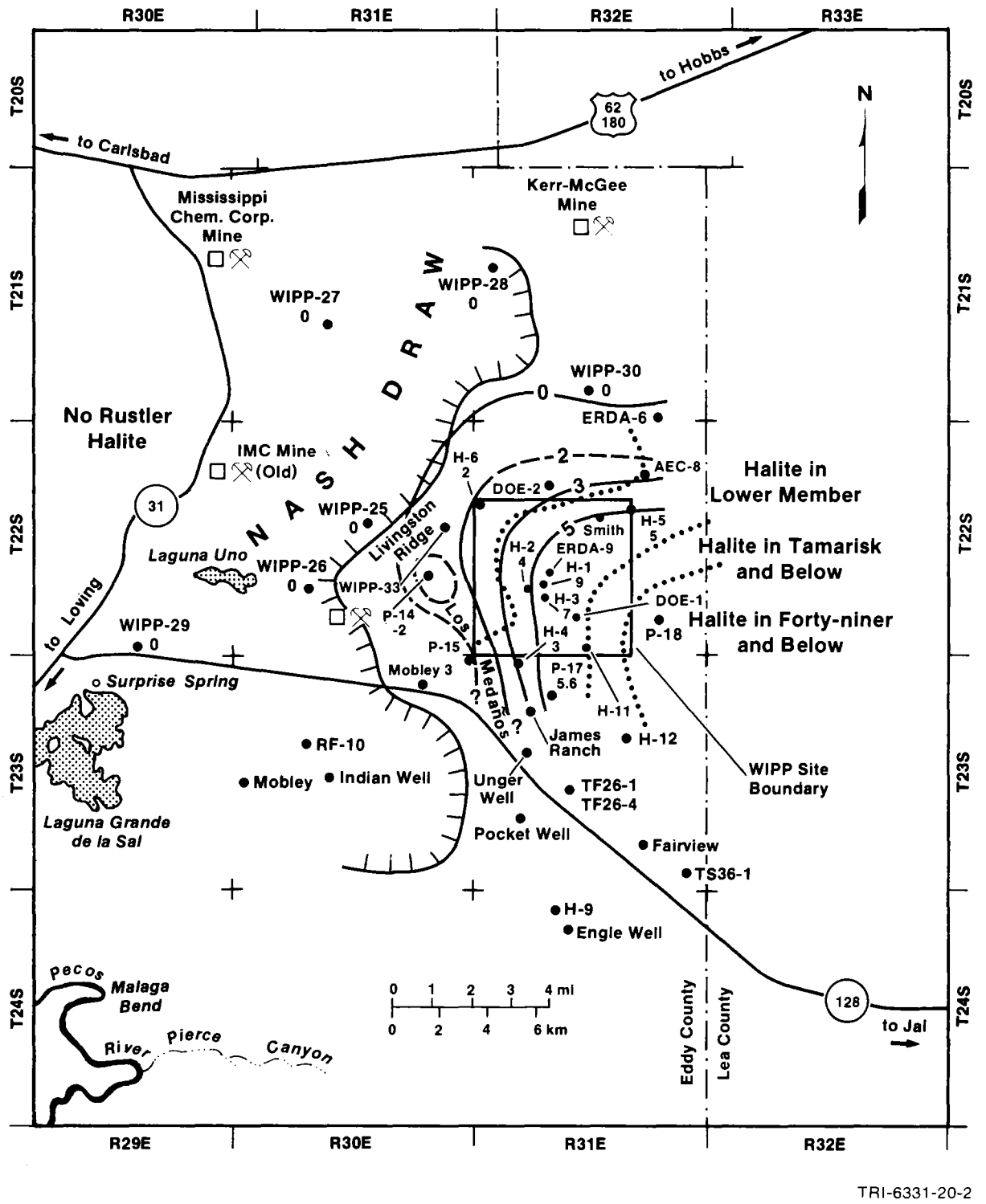


Figure 5-4. Contour map of oxygen-isotope shift in confined groundwaters at the Rustler/Salado contact, relative to -7% (from Lambert and Harvey [1987]).

Assuming an eastward-progressing halite-dissolution front, total removal of halite by dissolution in the Rustler has been faster than eastward scarp retreat, development of increased permeability due to subsidence-induced fracturing, and flushing of isotopically shifted water. The isotope shift is attributable to an increasing amount of rock/water interaction accompanying a diminishing water/rock ratio (cf. Clayton et al., 1966). The precise mechanism of isotope exchange and the reactant solid phase have not been identified, but the potential effect of anhydrite hydration to gypsum or the contribution of a relatively large reservoir of exchangeable water of crystallization in existing gypsum relative to a smaller amount of groundwater should not be overlooked.

### 5.2.5 Discharging Groundwater

It has been proposed (Robinson and Lang, 1938; Hale et al., 1954) that the more permeable units in the Rustler drain the WIPP Site and Nash Draw and discharge into the alluvium and ultimately into the Pecos River near Malaga. It has also been proposed (Chapman, 1986) that the Rustler draining this area discharges to the surface a significant distance upgradient from Malaga through a series of springs in southwestern Nash Draw. The best known of these is Surprise Spring on the northern, shore of Laguna Grande de la Sal (described by Robinson and Lang, 1938), the only perennial lake that existed prior to potash-refining activities.

The isotopic compositions of the shallow Culebra water from WIPP-29 (12 ft below surface) and Surprise Spring water issuing from the Tamarisk member of the Rustler Formation are similar. This similarity suggests that similar mechanisms governed the evolution of isotopic compositions of their water molecules, assuming that they were derived from a common source (Figure 5-1; Lambert and Harvey, 1987). However, WIPP-29 Culebra and Surprise Spring waters are probably derived by evaporation with a $\delta D/\delta^{18}O$ slope of 2 (Figure 5-1, lines "b"; cf. Allison et al., 1982), from water imported from the nearby Ogallala aquifer for use in nearby potash-refining operations. These waters are

derived under conditions typical of a shallow local water table, having a δD value of about -40‰ (rectangle). Hunter (1985) indicated that much of this water so imported is subsequently dumped into the shallow groundwaters of Nash Draw. Their isotopic compositions are also consistent with derivation from modern-type recharge water by oxygen-isotope shift (Figure 5-1, horizontal dashed lines "c"). The isotopic compositions are less consistent with their having been derived directly by partial evaporation of confined Rustler-type water from a free-standing surface (lake) under arid conditions (Figure 5-1, dashed line "d" slope = 5; cf. Craig et al., 1963).

A combination of geological, isotopic, and solute arguments has been used by Lambert and Harvey (1987) to assess the possible genetic relationships between Surprise Spring and WIPP-29 Culebra waters. Evolution of a water similar to WIPP-29 Culebra by evaporation of many other Rustler waters (entailing an increase in both chloride and $\delta^{18}O$) is possible in principle. Various hypothetical flow paths in the Culebra from other parts of Nash Draw and the WIPP Site to Surprise Spring pass through or near the near-surface occurrence of the Culebra at WIPP-29 (Lambert and Harvey, 1987). WIPP-29 would intercept groundwater flowing to Surprise Spring from occurrences of confined Rustler groundwaters to the north and east in Nash Draw and at the WIPP Site. However, Figure 5-5 shows that derivation of Surprise Spring from WIPP-29 Culebra requires a large dilution with water having essentially no chloride and a $\delta^{18}O$ value of -1.4‰, which is significantly different from other Rustler waters ($\delta^{18}O \approx -7‰$). This hypothetical dilution trend is shown as the heavy dashed line in Figure 5-5 connecting the WIPP-29 and Surprise Spring data points and intercepting the $\delta^{18}O$ axis at zero chloride concentration. Solute (including potassium) and stable-isotope relationships indicate that WIPP-29 Culebra water is derived from imported potash-refinery water by evaporation, not by evaporation directly from the Rustler. Thus, discharge at Surprise Spring does not now contain an appreciable component of upgradient Rustler water from Nash Draw or near the WIPP Site.

Waters at Surprise Spring and WIPP-29 Culebra are probably of local, near-surface derivation, at least partially anthropogenic. Neither their isotopic and solute compositions nor

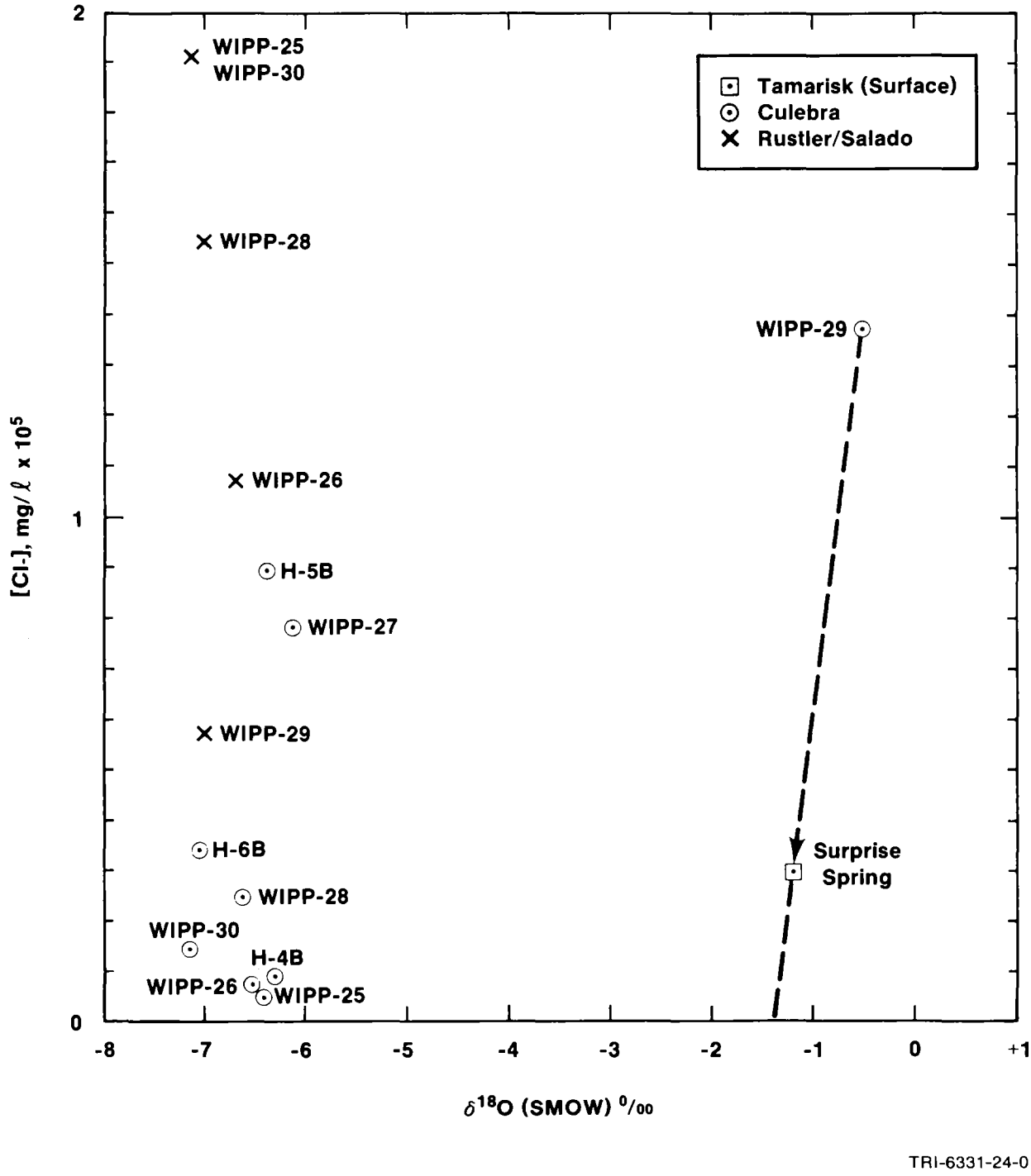


Figure 5-5. Total dissolved chloride versus $\delta^{18}O$ for Rustler groundwaters in Nash Draw and at the WIPP Site (from Lambert and Harvey [1987]).

their geological occurrences are consistent with the proposal that they have been derived from other Rustler waters by simple evaporation. Consequently, these localities presently are not significant discharge points for groundwater at the WIPP Site or in east-central Nash Draw. They appear to be, instead, discharge points for a local shallow (probably water-table) groundwater system manifest partly in the numerous ponds that have formed from a water table that has risen since the 1930's (Hunter, 1985). The recharge for this local system appears to be potash-refinery spillage and local natural recharge entering the near-surface gypsum karst developed in the Tamarisk member of the Rustler Formation. In any case, the fluid volumes involved in the local system in southwestern Nash Draw overwhelms any possible contributions from Rustler water flowing from farther east.

### 5.2.6 Isotopic Compositions of Host Rocks

Rock/water interactions sufficient to result in isotopic shifts in waters of the Rustler Formation are largely restricted to the Rustler/Salado contact zone (Section 5.2.4). Secondary calcite, however, has apparently precipitated in isotopic equilibrium (according to the relationship of O'Neil et al., 1969) at ambient temperatures with typical meteoric Rustler water in the Culebra member at WIPP-33, a borehole drilled in a circular collapse feature located between the WIPP Site and Nash Draw (Bachman, 1981; 1985; 1987). None of the other analyzed aquifer rocks have isotopic compositions that reflect similar alteration of dolomite (Figure 5-6; Lambert and Harvey, 1987), but dissolution of some dolomite has probably occurred (Lambert, 1987). Dolomite $\delta^{18}O$ and $\delta^{13}C$ values for both Magenta and Culebra are all very uniform (33.4‰ and 6.1‰; 95% confidence limits ±1.0‰ and ±1.1‰, respectively). Figure 5-6 lists $\delta^{18}O$ values for coexisting carbonates and waters in the Rustler Formation. Observed carbonate/water oxygen-isotope fractionation factors ($\alpha$) are shown for each carbonate/water pair. Since WIPP-29 water is not representative of unmodified meteoric water, the WIPP-29 fractionation factor has questionable geological significance. No water sample was recovered from WIPP-33, so the mean local Rustler water $\delta^{18}O$ value, -6.8‰, was used to calculate $\alpha$ at WIPP-33. These values are

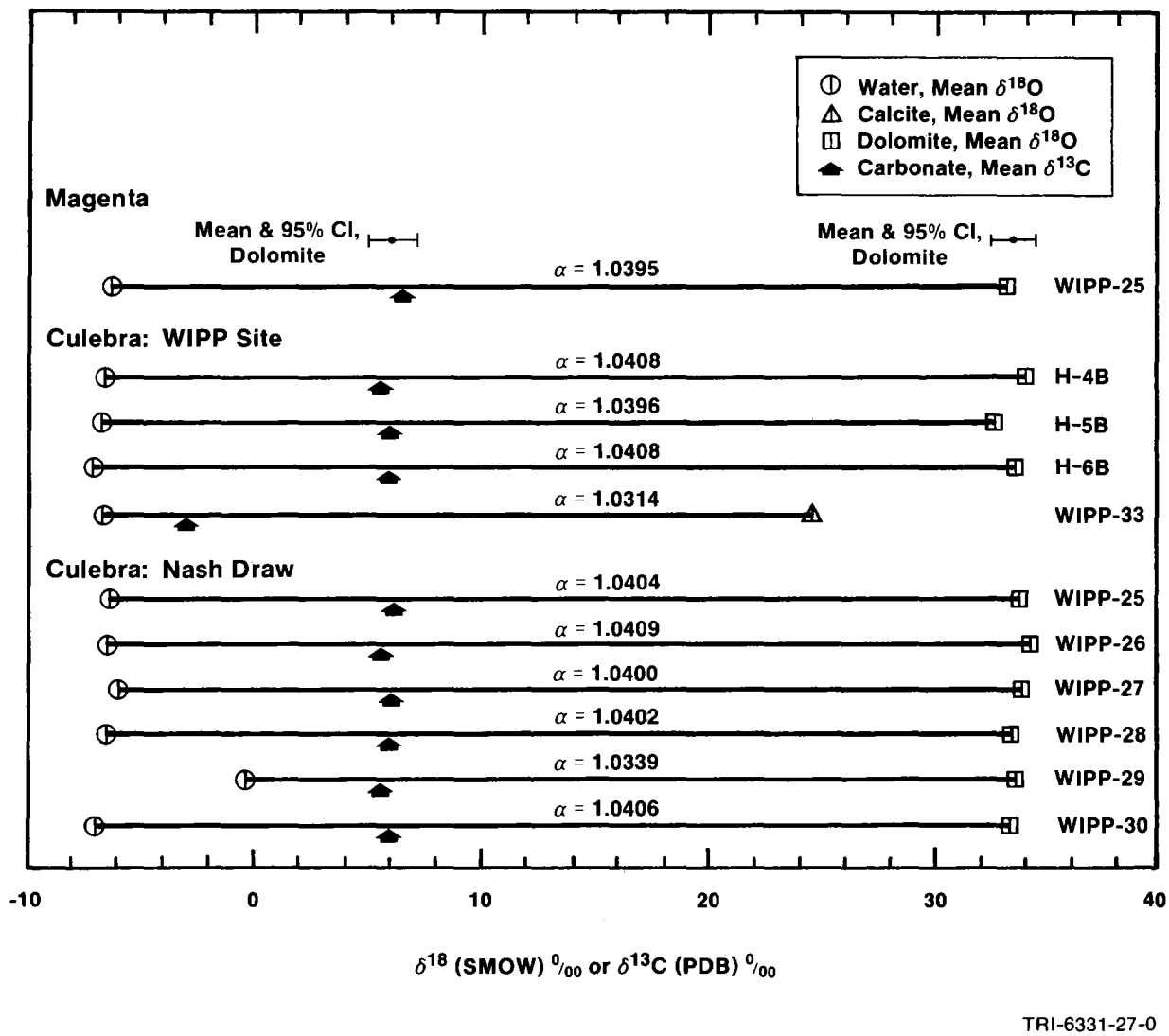


Figure 5-6. $\delta^{18}O$ values for coexisting carbonates and waters in the Rustler Formation (from Lambert and Harvey [1987] and Lambert [1987]).

suggestive of evaporitic, rather than purely biogenic dolomite precipitated under uniform conditions. Except for WIPP-29 Culebra, which shows both oxygen- and hydrogen-isotope shift, all the waters have a uniform $\delta^{18}O$ value of -6.6‰ (95% confidence limits ~ ±0.8‰). Calculated dolomite/water oxygen-isotope fractionation factors (α-values) are between 1.0395 and 1.0409, too high to reflect isotopic equilibrium (Northrup and Clayton, 1966; Clayton et al., 1968). The only carbonate mineral that appears to be at isotopic equilibrium with typical meteoric Rustler groundwater at ambient temperature (O'Neil et al., 1969) is the calcite in the Culebra rubble from WIPP-33 ($\alpha = 1.0314$). There is no other indication of carbonate recrystallization in the Rustler in isotopic equilibrium with meteoric Rustler groundwater.

### 5.2.7 Summary: Stable Isotopes, Recharge, and Climatic Change

The late Pleistocene epoch was a time of significantly different climate in southeastern New Mexico, as indicated by the juniper-oak plant community preserved in the packrat middens of Last Chance Canyon and Rocky Arroyo at elevations of 3700 ft (Van Devender, 1980). At the same elevation, desert-scrub grassland now predominates. A climate that supported a juniper-oak community 10,000 to 10,500 radiocarbon years ago (the age of the packrat middens) would presumably be more conducive to groundwater recharge if the juniper-oak community developed in response to higher rainfall. At several times in the geologic past, southeastern New Mexico has had higher rainfall than at present (Figure 5-7; Bachman, 1980; 1981; 1984; 1985; 1987). Presumably those wetter intervals have been more conducive to groundwater recharge than the present climate; such intervals may also have been more conducive to more negative δ-values in groundwaters (cf. Yapp, 1985).

The Rustler groundwater system is not at steady state; instead, discharge currently exceeds recharge. Present-day hydrologic measurements characterize a system in a transient stage that may continue to change its characteristics (e.g., potentiometric surface, permeability, etc.) in the future. Groundwater flow (and evaporite dissolution) in the Rustler may presently be at temporally low volumes and rates, relative to the past, and

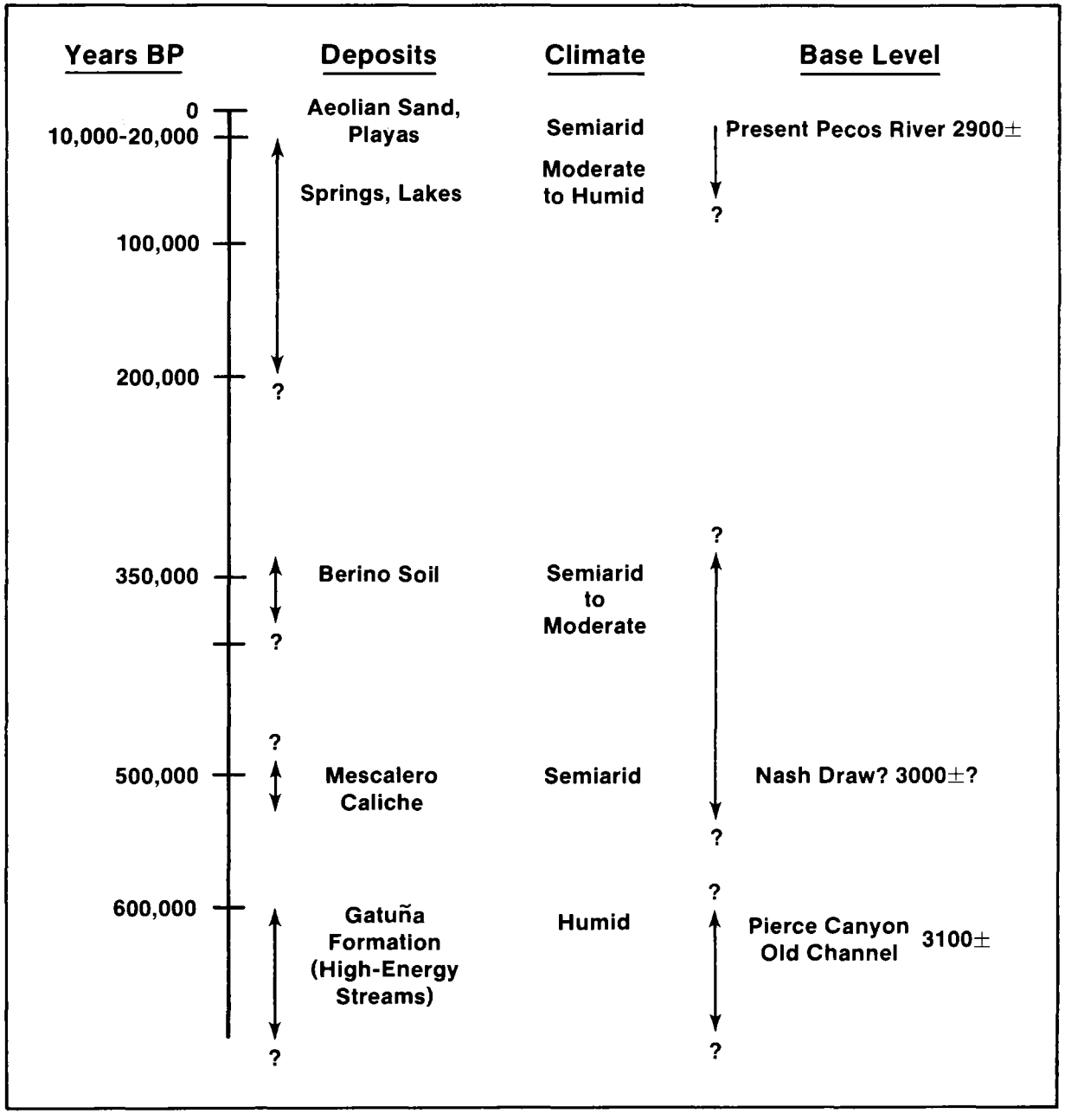


Figure 5-7. Diagram of variations in type of surficial deposits, climate necessary to produce them, and inferred base level at various times since the middle Pleistocene in southeastern New Mexico (from Lambert and Carter [1987]).

may increase should a wetter climate again prevail in the next 10,000 years. These present conditions imply little or no modern recharge to the Rustler groundwater near the WIPP Site. The absence of indicated recharge near the WIPP Site does not itself preclude modern recharge to the same geologic units in other areas where the units are close to the surface and under less confined conditions.

# 5.3 ATMOSPHERICALLY GENERATED NUCLIDES IN THE RUSTLER FORMATION

## 5.3.1 Systems of Nuclides

Several systems of nuclides have been examined for the potential for determining the age of groundwater isolation from the atmosphere. One class of atmospherically generated nuclides of interest in groundwater studies includes $^{3}H$ (tritium), with a half-life of about 12 years. Since tritium is generated principally by atmospheric testing of nuclear weapons, its presence is not to be expected in groundwaters that have been out of contact with the atmosphere since before 1950. Another class of atmospherically generated nuclides arises principally from neutron-activation or spallation reactions involving cosmic rays; these also can be generated by nuclear bomb effects and some subsurficial neutron-activation. This class includes $^{14}C$ (half-life 5730 years) and $^{36}Cl$ (300,000 years).

## 5.3.2 Sampling, Contamination, and Mixing

Samples of wellbore fluids to be analyzed for these nuclides were collected from the three regionally persistent water-producing units in the Rustler (Magenta and Culebra dolomite members and the basal Rustler zone near the contact with the underlying Salado Formation). Specific procedures were designed to minimize contamination of major and certain minor solutes arising from wellbore effects (Lambert and Robinson, 1984). The contamination associated with newly emplaced hydrologic test holes designed for maximum core recovery, however, is not limited to simple mixing of fluids, but also includes microbial metabolism of solid cellulosic material introduced to control lost circulation. This carbon

apparently contributed a more or less steady infusion of modern anthropogenic carbon to the total dissolved carbon in the wellbore effluent. This inoculation has probably persisted in southeastern New Mexico since the advent of potash-coring surveys in the early 1930's, since which time organic materials have been introduced into more permeable units (including Rustler wet zones) to allow recovery of circulation during drilling down to the intervals to be cored.

Nuclide systems generated in the atmosphere from neutron activation by cosmic rays are of naturally low abundance (pre-1950 concentrations of $^{14}C$ are of the order of 1 part in $10^{12}$; Zeuner, 1972). These systems are particularly susceptible to contamination by even small amounts of modern sources, especially organic carbon in the case of radiocarbon. In southeastern New Mexico groundwaters, this contamination is illustrated by a linear mixing relationship (Figure 5-8; Lambert, 1987) involving percent modern carbon (PMC) and dissolved carbon concentration (represented here by the alkalinity, which is approximately equal to bicarbonate). The PMC/[$HCO_3^-$] line has a positive slope, which shows that $^{14}C$-rich carbon has been added to the baseline value of dissolved carbon in the Rustler Formation. If the low-PMC values in this relationship had arisen through dilution with dead carbon, the slope would be negative. In the absence of any solid/liquid interaction, the slope would be vertical. The excellent linear correlation shown in Figure 5-8 indicates mixing between two reservoirs of carbon, one with nearly 0 PMC and one with nearly 100 PMC.

Whereas the PMC/bicarbonate relationship indicates simple binary mixing between reservoirs of low- and high-PMC, the actual number of carbon reservoirs is greater than two. This is indicated by the nonsystematic variation of $\delta^{13}C$ values (which are indicative of carbon source, i.e., rock carbonate versus organic material) with bicarbonate (Figure 5-9). There is no linear relationship between $\delta^{13}C$ and dissolved carbon concentration, as would be the case if there were only two reservoirs of carbon.

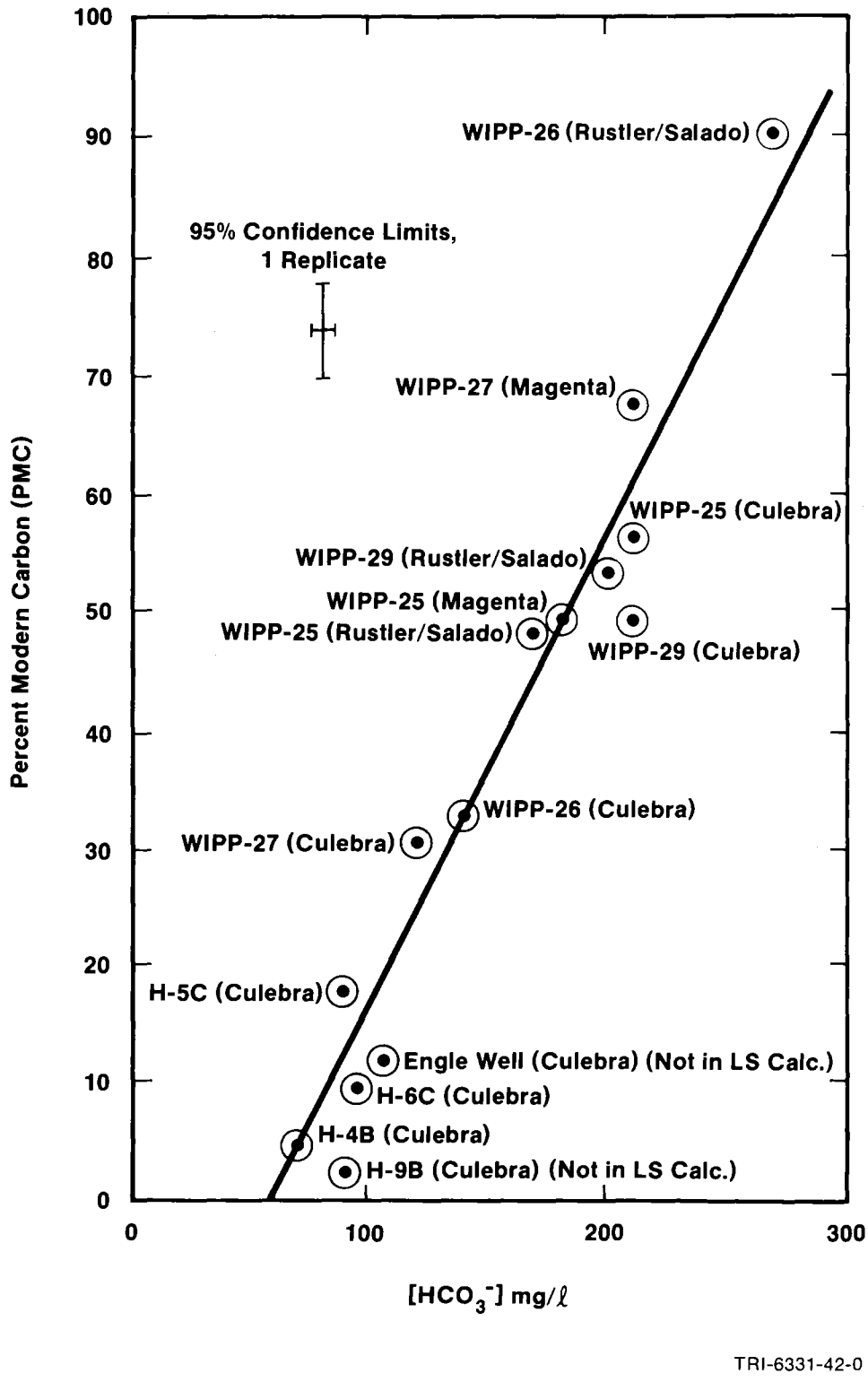


Figure 5-8. PMC values plotted versus dissolved carbon as bicarbonate (from Lambert [1987]).

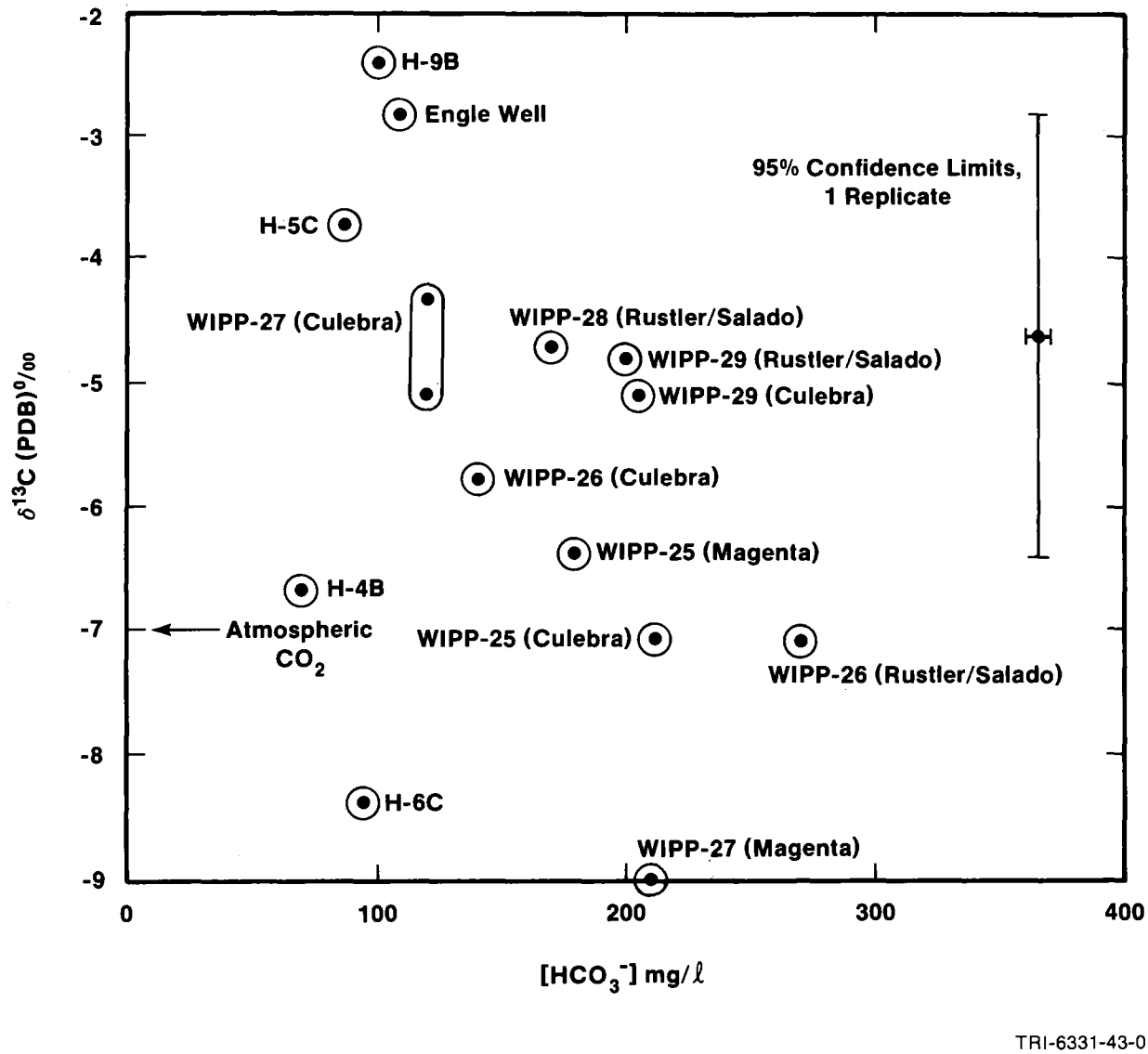


Figure 5-9. $\delta^{13}C$ values plotted versus dissolved carbon as bicarbonate (from Lambert [1987]).

Figure 5-10 shows two separate linear trends in PMC versus $\delta^{13}C$, one for samples with PMC values greater than 10 (12 boreholes, 17 data) and one for samples with PMC values less than 10 (four boreholes, four data). The two trends appear to converge near PMC = 0 and $\delta^{13}C = 0$. The distribution of PMC and $\delta^{13}C$ values from groundwaters in this study is consistent with three-component mixing of various reservoirs of carbon, whose expected ranges of PMC and $\delta^{13}C$ values are shown. The data from the wells with >10 PMC suggest that their PMC and $\delta^{13}C$ values have arisen dominantly from mixing of two endmembers: carbonaceous species dissolved from the host carbonate rock, and modern organic material introduced during water-well development. One could argue that contamination had taken place dominantly during well development, but anthropogenic contamination in the Rustler was probably present at some measurable level in the vicinity since the earlier days of coring for potash.

The other trend (PMC<10) appears to be a mixture of dissolved rock carbon and carbon derived from ancient organic material dissolved in the water at the time of recharge. Although dissolved rock carbon and contaminant carbon dominate the samples having PMC>10, such samples probably contain some component of original dissolved (recharge) carbon. Note that a small amount of high-PMC modern organic carbon introduced by artificial contamination can significantly increase the PMC values of low-PMC carbon derived from older organics, with essentially no change in $\delta^{13}C$. Consequently it is assumed here that the contaminated waters were derived from the original widespread low-PMC waters. In view of the likely effects of contamination of the Rustler, the lower limit of resolution for PMC measurements may represent the baseline value of radiocarbon in the Rustler groundwater system, especially since the confidence limits of lowest PMC values (based on replicate samples and analyses) include zero (Lambert, 1987). These confidence limits are based on replicates as required by the method of Natrella (1963), reflecting varying degrees of mixing and/or contamination, which should be expected to be independent of PMC value. The true confidence limits, based on replicate samplings, are therefore much greater than the relatively small (up to a few tenths PMC) standard

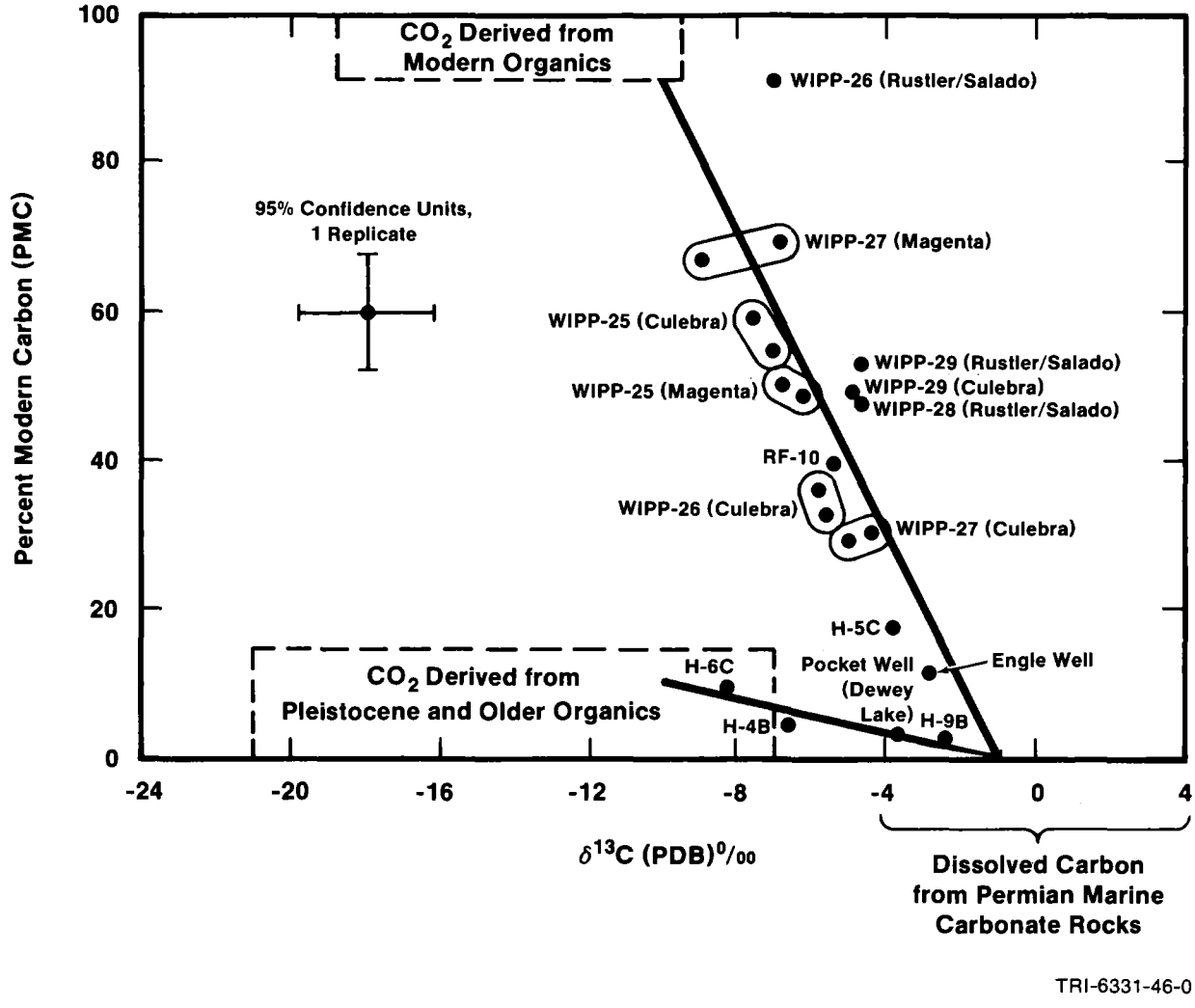


Figure 5-10. PMC values plotted versus $\delta^{13}C$ (from Lambert [1987]).

deviation arising from counting. This latter, smaller confidence limit may be dependent on the absolute PMC value. Thus, the minimum age of recharge of the Rustler groundwater system at the WIPP Site and in eastern Nash Draw, in view of the probable drilling-induced carbon contamination of even low-PMC waters, is likely to be greater than 30,000 years, the practical limit of radiocarbon dating for groundwaters. The results of attempted application of various radiocarbon dating models to these groundwater data are summarized in Section 5.3.5.

### 5.3.3 Tritium

The tritium concentrations (reported in Tritium Units; 1 TU = 1 tritium atom in $10^{18}$ hydrogen atoms) in groundwaters from the Rustler Formation (n=6) and the overlying Dewey Lake Red Beds (n=1) are all less than 7 TU. Figure 5-11 shows tritium and radiocarbon concentrations in Rustler and Dewey Lake groundwater. Concentrations include one value of about 7 TU from the Magenta in Nash Draw, one value of about 3 TU (from a sample that has an apparent radiocarbon age of about 16,000 yr), and five less than 0.3 TU. The extremely low values show that the confined groundwaters in the Rustler and some perched waters in the Dewey Lake have not received significant amounts of recharge from meteoric precipitation since 1950. TU values as high as 7 are attributable to contamination, in view of the demonstrated radiocarbon contamination in the well that produced this TU value (WIPP-27, just below a potash-refinery spoils pile). A significant modern component in the groundwater would yield values of 20 TU or more; values less than 10 TU are not considered conclusively indicative of a large degree of hydraulic connection with the surface (Isaacson et al., 1974). Low tritium concentrations alone, however, do not preclude the possibility of surface-derived recharge in the recent past before 1950. Unless otherwise specified in the figure as Dewey Lake (DL) or Magenta (MA), measurements (all from Lambert, 1987) apply to water from the Culebra member of the Rustler Formation. Tritium units are enclosed in rectangles.

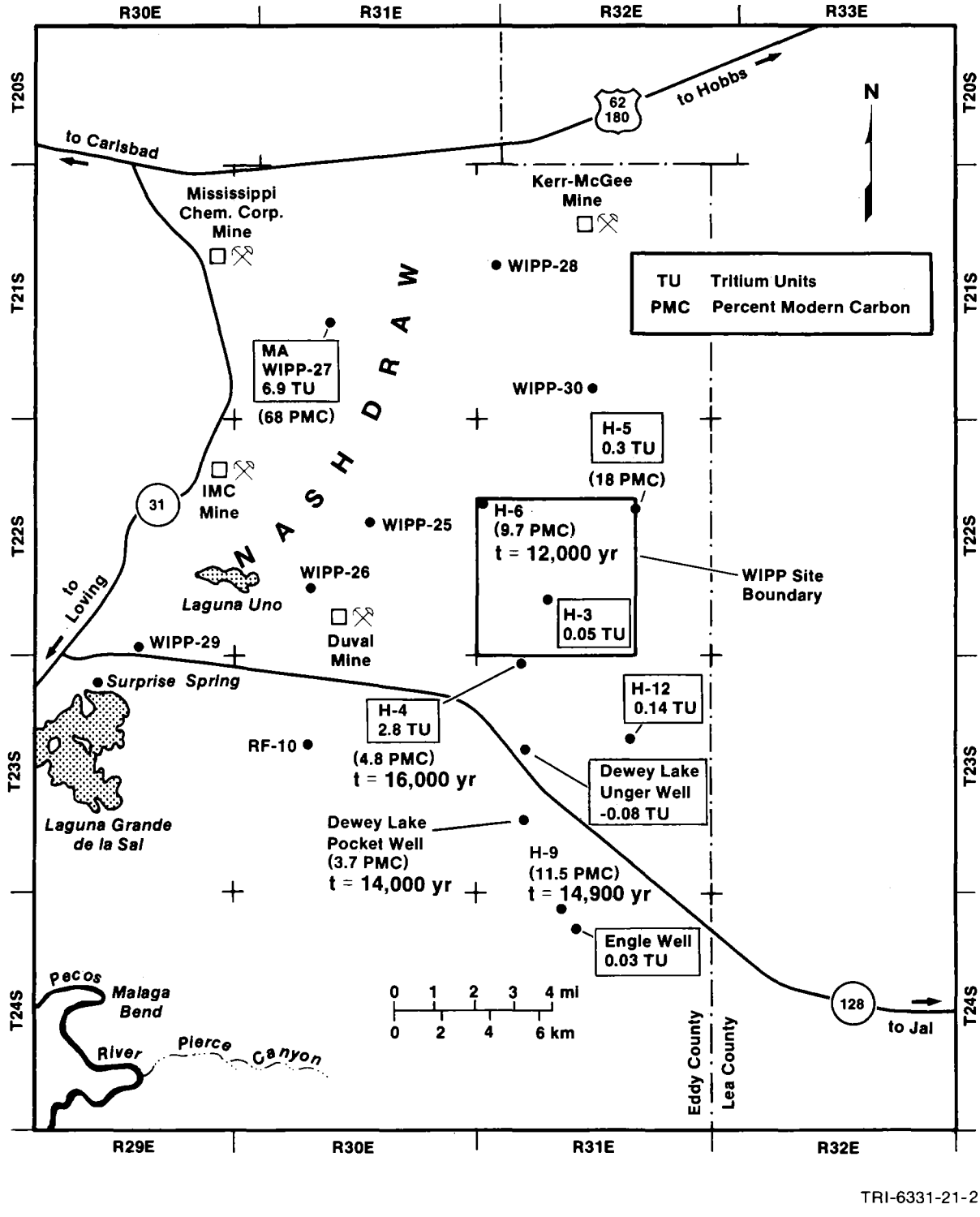


TRI-6331-21-2

Figure 5-11. Tritium and radiocarbon in Rustler and Dewey Lake groundwaters (adapted from Lambert and Harvey [1987]).

### 5.3.4 Chlorine-36

The $^{36}Cl$ concentrations in groundwaters of this study were below the limit of detectability, 1 part $^{36}Cl$ in $10^{15}$ parts $^{35}Cl$ (Lambert, 1987), even with high-sensitivity accelerator mass spectrometry. Despite claims of very low detection limits allowed by such instruments as accelerator mass spectrometers, the overwhelming amount of $^{35}Cl$ and $^{37}Cl$ (as chloride most likely dissolved from Permian halite) in Rustler waters makes inapplicable the assumption of a known initial concentration of chloride (including $^{36}Cl$) that is entirely atmospheric in origin. Thus, with the breakdown of assumptions fundamental to dating models (such as mixing and contamination as have been demonstrated here for radiocarbon, tritium, and $^{36}Cl$), analyses of the atmospherically generated nuclides alone will aid little in the determination of Rustler flow-paths, groundwater velocity, and the recharge/discharge areas. If the effects of contamination can be somehow mitigated, the radiocarbon age may be indicative of time of isolation from the atmosphere, recharge time, or residence time.

### 5.3.5 Assumptions and Limitations in Models for Radiocarbon Age

#### 5.3.5.1 The Danger Inherent in an Isolated Result

An age calculation should not be made on the basis of a single nuclide measurement with only its inferred initial value at time of recharge and half-life. Such a simplistic approach does not account for nuclide sources introduced at times since that of recharge or for decreases in nuclide activity due to processes other than radioactive decay. An isolated groundwater date resulting from an atmosphere-based method such as radiocarbon is not highly reliable. Overinterpreting a single result is especially misleading in slow-moving groundwater systems in carbonates and evaporites where the purging effect (cf. Lambert and Robinson, 1984) during sampling is small and the contamination effect can be large due to the relatively small amount of natural water available in the system. For any single point in PMC/$\delta^{13}C$ space (Figure 5-10), the degree of natural, unperturbed, uncontaminated geochemical evolution will be indistinguishable from simple ternary mixing. Greater confidence can be placed in similar radiocarbon results arising from samples from

somewhat spaced localities. One isolated result, in view of ternary mixing, is not interpretable as a unique date characteristic of the groundwater system. Similarly, with only a few geographically scattered dates, it is not possible to infer flow gradients or travel times between dated localities with a high degree of confidence. Such confidence requires a large number of reliable, geographically distributed dates.

#### 5.3.5.2 Numerical Interpretive Models

Several existing radiocarbon-dating models were applied to the PMC and $\delta^{13}C$ values obtained from groundwaters believed to be minimally contaminated on the basis of their carbon-isotope systematics. The various models were first evaluated for the applicability of their necessary assumptions to the Rustler geology. The models considered include the fundamental decay equation, Vogel (1970), Tamers (1975), Pearson and Swarzenki (1974), Mook (1976), Fontes and Garnier (1979), Wigley et al. (1978), and Evans et al. (1979).

Several of the models account for dilution of the PMC value with dead carbon by dissolution of mineral carbonate; others account for the additional loss of radiocarbon by non-radioactive-decay processes such as precipitation from solution. Some of the models examined (decay equation, Fontes, Wigley) were found inapplicable, either because their necessary assumptions were not consistent with observed systematics in the Rustler Formation, or because their level of sophistication and rigor required too many inferences to account for unobtainable input data. Of the remaining models, those of Tamers, Pearson, Mook, and Evans et al. accounted for radiocarbon loss by dilution, but only that of Evans et al. handled loss by precipitation in a way that could conceivably be supported by observations of the Rustler (Table 5-1). Application of some of the models resulted in indeterminate ages (due to taking the logarithm of a negative number), indicating either failure of fundamental assumptions, or some degree of contamination even in the low-PMC waters, or both. The model of Evans et al. (1979) gives the youngest calculable radiocarbon ages for groundwaters believed to be minimally contaminated with drilling-introduced

## Table 5-1. Model Radiocarbon Ages for Groundwaters[1]

| Locality | PMC | $\delta^{13}C$ | Tamers[2] | Pearson | Mook | Evans |
|---|---|---|---|---|---|---|
| **ADJUSTMENTS INVOLVING DISSOLUTION OF DOLOMITE ($\delta^{13}C$ = +5.7‰)** | | | | | | |
| H-4 | 4.82 | -6.7 | 19300 | 17300 | 12000 | 16100 |
| H-6 | 9.7 | -8.4 | 13600 | 12600 | 10600 | 12100 |
| H-9 | 2.22 | -2.4 | 25700 | 20200 | indet[3] | 14900 |
| Pocket | 3.67 | -3.8 | 21600 | 17400 | indet | 14000 |
| **ADJUSTMENTS INVOLVING DISSOLUTION OF CALCITE ($\delta^{13}C$ = -2.9‰)** | | | | | | |
| H-4 | 4.82 | -6.7 | | 10100 | indet | 3819 |
| H-6 | 9.7 | -8.4 | | 7400 | indet | 4600 |
| H-9 | 2.22 | -2.4 | | indet | indet | indet |
| Pocket | 3.67 | -3.8 | | 500 | indet | indet |

1. Ages, in radiocarbon years, calculated according to models used as follows:
   Tamers: Tamers (1975)
   Pearson: Pearson and Swarzenki (1974)
   Mook: Mook (1976)
   Evans: Evans et al. (1979)
2. The model of Tamers (1976) is independent of $\delta^{13}C$ values.
3. Indeterminate, due to resulting negative amount of logarithm.

modern carbon (i.e., PMC<10), and part of the same carbon-isotope systematics. The numerical model of Evans et al. for calculating the radiocarbon age of groundwaters in carbonate units, however, yields the "correct" radiocarbon age only under the following conditions:

- The PMC value is less than 50 (i.e., there is no contamination of the water by modern carbon introduced after the initial infiltration).

- The steady, progressive equilibration of the $^{13}C/^{12}C$ ratio of dissolved carbon with the equivalent ratio in the rock has not been perturbed by an event that adds nonradioactive carbon dioxide to the water by instantaneous leaching (congruent dissolution) of the rock.

- There has been no mixing of waters of significantly different age to produce the water sampled for radiocarbon measurement.

If any of these conditions have been violated, the radiocarbon age is indeterminate. For the cases of severe contamination (PMC > 10 in these data), significant negative ages (-1000 to -8000 years) were calculated (Lambert, 1987). If independent information is not available to show that none of the above conditions has been violated, a high degree of confidence should not be placed in resulting maximum positive radiocarbon ages, since any amount of anthropogenic contamination will cause a model calculation to give spuriously young dates. Model calculations are already structured to minimize and account for effects of processes likely to yield spuriously old apparent radiocarbon ages.

The radiocarbon dating method cannot be applied to groundwaters without a consideration of the geological/geochemical context. Despite the detailed development of the method in easily characterized sandstone units (e.g. Pearson et al., 1983), spurious results are likely to ensue if the method is blindly applied to any other system, especially carbonate units. Radiocarbon dating of groundwater should not be attempted without a reasonably complete understanding of the carbon-isotope systematics in the groundwater system and a due consideration of the effects of mixing and contamination (Evans et al., 1978; Lambert, 1987).

#### 5.3.5.3 Isolation Time of Groundwaters

The age of the minimally contaminated carbon reservoir (PMC < 10) is estimated to be at least 13,000 years, and probably in excess of 20,000 to 30,000 years (Lambert, 1987).

Applying the confidence limits to the least contaminated waters having less than about 6 PMC implies that these values are statistically indistinguishable from 0 PMC. In other words, the true "age" (time of isolation from the atmosphere) of the natural carbon in these waters may actually exceed the limit of resolution of the radiocarbon method.

The minimum estimated age of surface-derived recharge for groundwaters in the Rustler (boreholes H4, H5, and H6) and parts of the Dewey Lake (Pocket well) aquifers near the WIPP Site is 12 to 16 ka; the mean of these four ages is 14 ka, with 95% confidence limits of 5 ka (Lambert, 1987). These confidence limits indicate that the four ages are statistically indistinguishable. Further, there is no monotonic age gradient from north to south across the WIPP Site, and hence no trending of significantly younger water toward some recharge area. These four PMC/$\delta^{13}C$ pairs can be numerically treated as members of a single isochronous evolutionary path according the model of Evans et al. (1979). The late Pleistocene age range (12 to 16 ka) is supported by other paleoclimatic evidence in the region, such as fossil packrat middens. The recharge may actually be part of an earlier Pleistocene event older than the age range of the radiocarbon method, about 30 ka, given the possibility of even a small amount of contamination of these waters by modern carbon introduced during well development, which would make apparent radiocarbon ages spuriously young. Barring such mixing, these results are not consistent with a hypothesis proposing meteoric recharge of Rustler groundwater since the late Pleistocene in the confined units near the WIPP Site or Nash Draw.

There are several difficulties associated with using the geographic distribution of these ages to calculate a travel time for Rustler groundwater across the WIPP Site. First, residence times of the four least contaminated groundwaters show no coherent trends of becoming significantly younger toward some recharge point (Figure 5-11). Second, residence times (or ages of isolation from the atmosphere) of least contaminated groundwaters are statistically indistinguishable from one another, and may represent pulse recharge in a discrete event rather than continuous flow away from a recharge area. Third, the carbon isotopic compositions of these four sampling localities, including one Dewey Lake datum, suggest

that they have a common evolutionary path according to the model of Evans et al. (Figure 5-12). Finally, the relatively uniform residence times of least contaminated groundwaters in the Rustler and parts of the Dewey Lake may have arisen through homogenization after recharge.

Figure 5-12 (from Lambert, 1987) is a hypothetical reconstruction of the quantitative evolution of carbon-isotope systematics for these four waters. The model of Evans et al. is approximately linear in PMC and $\delta^{13}C$ along an isochron, and the assumption is made that all four waters are isochronous. The least squares line in PMC/$\delta^{13}C$ space has been extrapolated back to a $\delta^{13}C$ value of -10.15‰, from which an original PMC value of 10.4 was inferred for the groundwater system represented by H-6C, H-4B, and H-9B (from the Culebra) and Pocket (from the Dewey Lake). This extrapolated PMC value was assumed to have been diluted by a factor of two during congruent dissolution of host rock upon entry of water to the groundwater system. Hence, 20.8 is the hypothetical PMC value of the decaying organic matter in the soil through which the infiltrating groundwater was thought to have passed, and from which the water obtained its dissolved carbon before entering the carbonate host rock. The radiocarbon age of this organic matter is calculated to be 13,000 a, and is taken to be the age of the recharge to the groundwater system. The wide geographic separation of wells containing water of age > 10,000 a suggests that water of this apparent age was originally widespread throughout the area near the WIPP Site.

Calculations of maximum age should not be done on any individual value of PMC available for the Rustler Formation groundwaters, since it is impossible to eliminate the effects of anthropogenic contamination or natural mixing for any individual value. This contamination has had the effect of raising the PMC values significantly above probable native values, and lowering the apparent age. This is the opposite effect that is usually obtained in groundwater systems involving exchange of carbon species between water and host rock. If contamination due to well development had not occurred, one would expect to find a

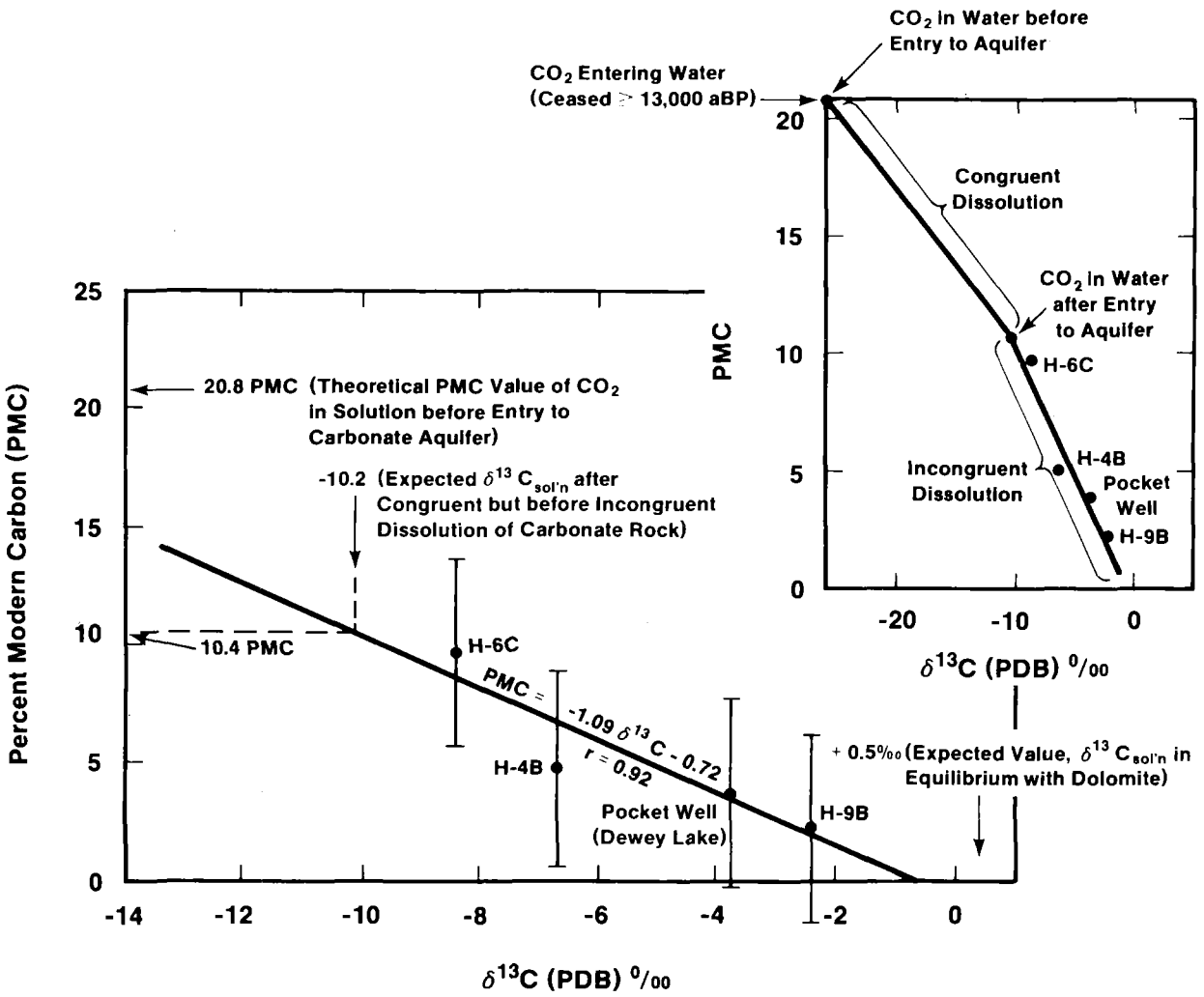


Figure 5-12. PMC and $\delta^{13}C$ values for waters that give finite positive apparent radiocarbon ages according to the model of Evans et al. (1979) (from Lambert [1987]).

decrease in PMC with increasing bicarbonate, owing to the dilution and sorption of radiocarbon as carbon dissolved from the host rock. In such cases, the lowering of the PMC value by rock-water interactions would give a spuriously old apparent age, unless the PMC value could be corrected for rock-water interactions.

According to the models of Tamers (1975) and Evans et al. (1978), the maximum PMC value for dissolved carbon in carbonate aquifers is 50. In some of the high-PMC contaminated samples, insufficient time had elapsed between well development (the time of contaminant inoculation) and sampling to allow for dilution of modern contaminants to the expected 50 PMC value.

### 5.3.6 Summary

Out of sixteen sets of radiocarbon measurements in the Rustler and Dewey Lake (Figure 5-10), ten were uninterpretable due to severe contamination; four gave calculable ages according to more than one interpretive model; two were problematical (H5 and Engle). Circumstantial evidence inferred from the nearby H9 hole indicates that Engle is certainly contaminated (Lambert, 1987). WIPP-26 gave the most severe contamination (91 PMC at the Rustler/Salado contact), but is not associated with potash-refinery discharge, since it lies well uphill from such ponding. Taken as a group, these radiocarbon data indicate mixing phenomena between a source of dead carbon, probably in the rock carbonate, and modern carbon, probably in the organic matter introduced during drilling and developing wells. There is no indication of a preponderance of original soil- or atmosphere-derived carbon dioxide in most of these wells. The most comprehensive applicable model for interpreting radiocarbon data as ages fails for most of the data because of the complex mixing phenomena. Given the highly variable climatological history of the Delaware Basin, and the fact that the area was once dominated by a more humid climate and the resulting plant community, organic soil components cannot be excluded as an important source of the original carbon dioxide introduced into the groundwater system.

Enhanced analytical capabilities designed to allow detection of smaller amounts of radiocarbon do not make PMC values more interpretable as ages, since the effects of contamination and mixing in groundwater systems of nonuniformly low productivity cannot be precisely quantified.

The usefulness of the class of weapons-generated nuclides (e.g., tritium and krypton) is limited due to surface contamination associated with the venting of the Gnome event in the area. Furthermore, the relatively small content of native radiocarbon shows that the Rustler groundwater has been out of contact with the atmosphere for so long (at least several half-lives) that no native tritium should be observable. If significant concentrations of tritium were observed in the population of groundwaters more depleted in $^{18}O$ and deuterium (Section 5.2.3), they would be attributed to contamination. D/H and $^{18}O/^{16}O$ ratios are better methods of identifying meteoric waters.

Because of the questionable validity of the assumptions necessary to apply radiocarbon and radiochloride dating methods to the evaporite environment of southeastern New Mexico, and because of the previously demonstrated susceptibility of these components to contamination not associated with natural recharge in this groundwater system, these methods cannot refine the estimates of groundwater travel times across the WIPP Site or define the recharge area with confidence. Any radiocarbon investigation needs to include tests of the validity of the assumption that the PMC measurements are representative of the carbon native to the groundwater.

The four mutually consistent, tightly clustered radiocarbon ages of groundwaters spread out from north to south across the WIPP Site along the flow direction inferred from the hydraulic gradient do not indicate a conspicuous systematic aging along the flow path, but rather are consistent with a late Pleistocene pulse recharge event. The absence of rapid vertical influx to the Rustler Formation and parts of the Dewey Lake Red Beds near the WIPP Site in the Holocene Epoch as indicated by D/H, $^{18}O/^{16}O$, T, and $^{14}C$ measurements does not, however, preclude lateral groundwater flow within the water-bearing units.

# 5.4 URANIUM-ISOTOPE DISEQUILIBRIUM IN RUSTLER GROUNDWATERS

## 5.4.1 Distribution of U-Concentration and U-Isotope Ratios

Uranium concentrations and $^{234}U/^{238}U$ activity ratios for groundwaters and aquifer host rocks from the Rustler Formation have been previously reported and interpreted by Lambert and Carter (1987), and their results are summarized here. Aqueous total-U concentrations in Culebra waters (Figure 5-13) range from about 0.02 to about $40 \cdot 10^{-9}$ g/g (parts per billion [ppb]). The total-U concentrations increase monotonically westward toward Nash Draw, generally mimicking the flow directions inferred from potentiometric levels in Permian rocks by Cooper and Glanzman (1971). The flow directions inferred by Mercer (1983) indicate a more southward component from the WIPP Site to the southeastern re-entrant of Nash Draw.

Large deviations from the expected secular-equilibrium activity ratio value of 1 are observed in the confined Culebra groundwaters at the WIPP Site (Figure 5-14). The activity ratios decrease westward and somewhat southward, from extremely high values (>6) near the WIPP Site to lower values (<3) toward Nash Draw, again generally mimicking the flow patterns inferred from some potentiometric level distributions. Control on contouring east of the WIPP Site is not particularly tight, due to the scarcity of wells suitable for sampling in the eastern low-permeability region of the Culebra. Similarly, control is not tight south of the WIPP Site, because data there are not yet available. Consequently, due to the lack of control in the southern portion of Figure 5-14, the activity ratio distributions may or may not mimic the southward component of flow apparently leading from the WIPP Site (Mercer, 1983; LaVenue et al., 1988).

West of the WIPP Site, in central Nash Draw (a dissolution valley underlain by outcrops of Rustler Formation evaporites), well-mixed high-permeability hydrologic systems are

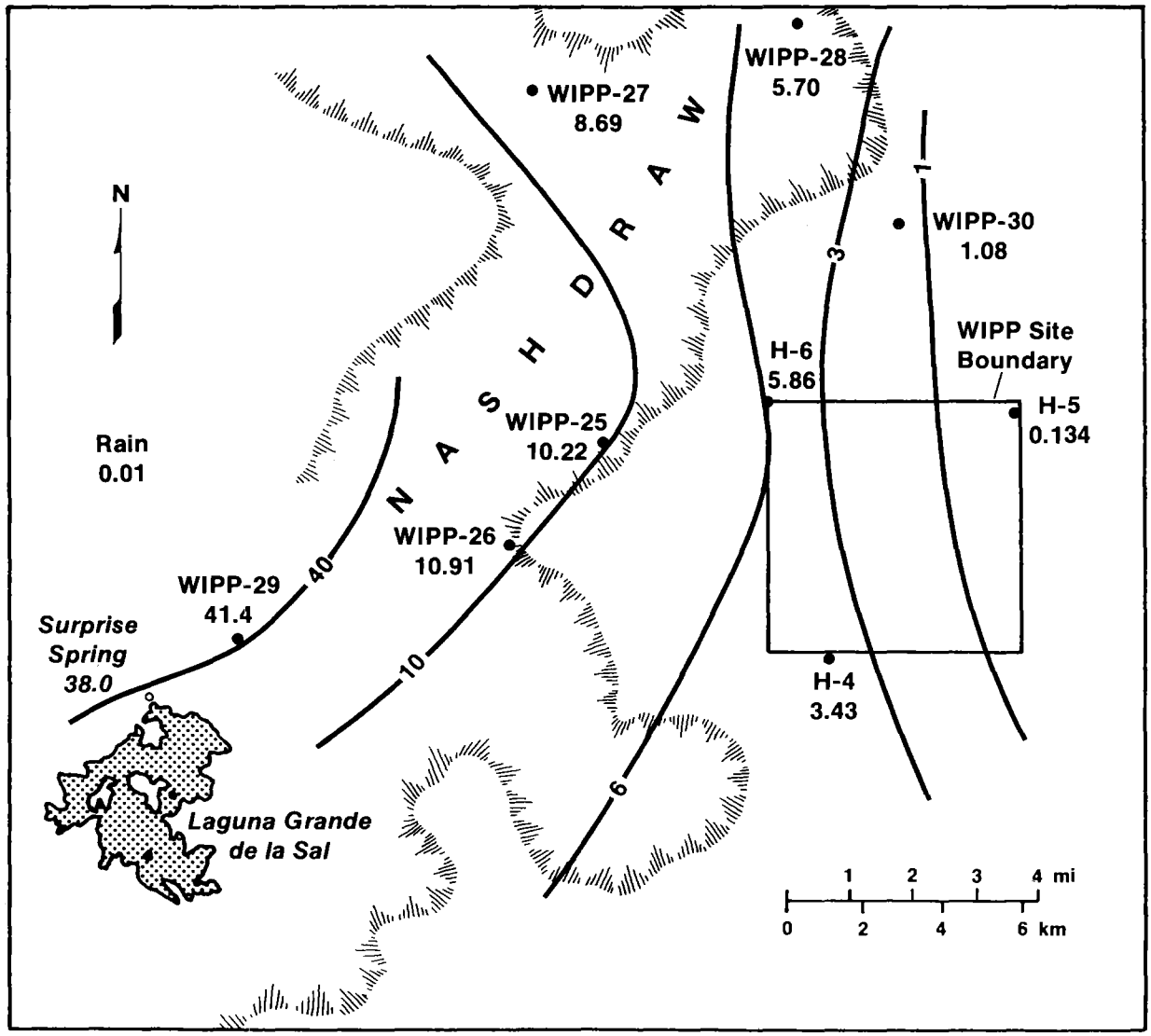


Figure 5-13. Contour map of total uranium concentration in groundwater from the Culebra dolomite member of the Rustler Formation (from Lambert and Carter [1987]). Total U is expressed in terms of $10^{-9}$ g/g, or ppb.

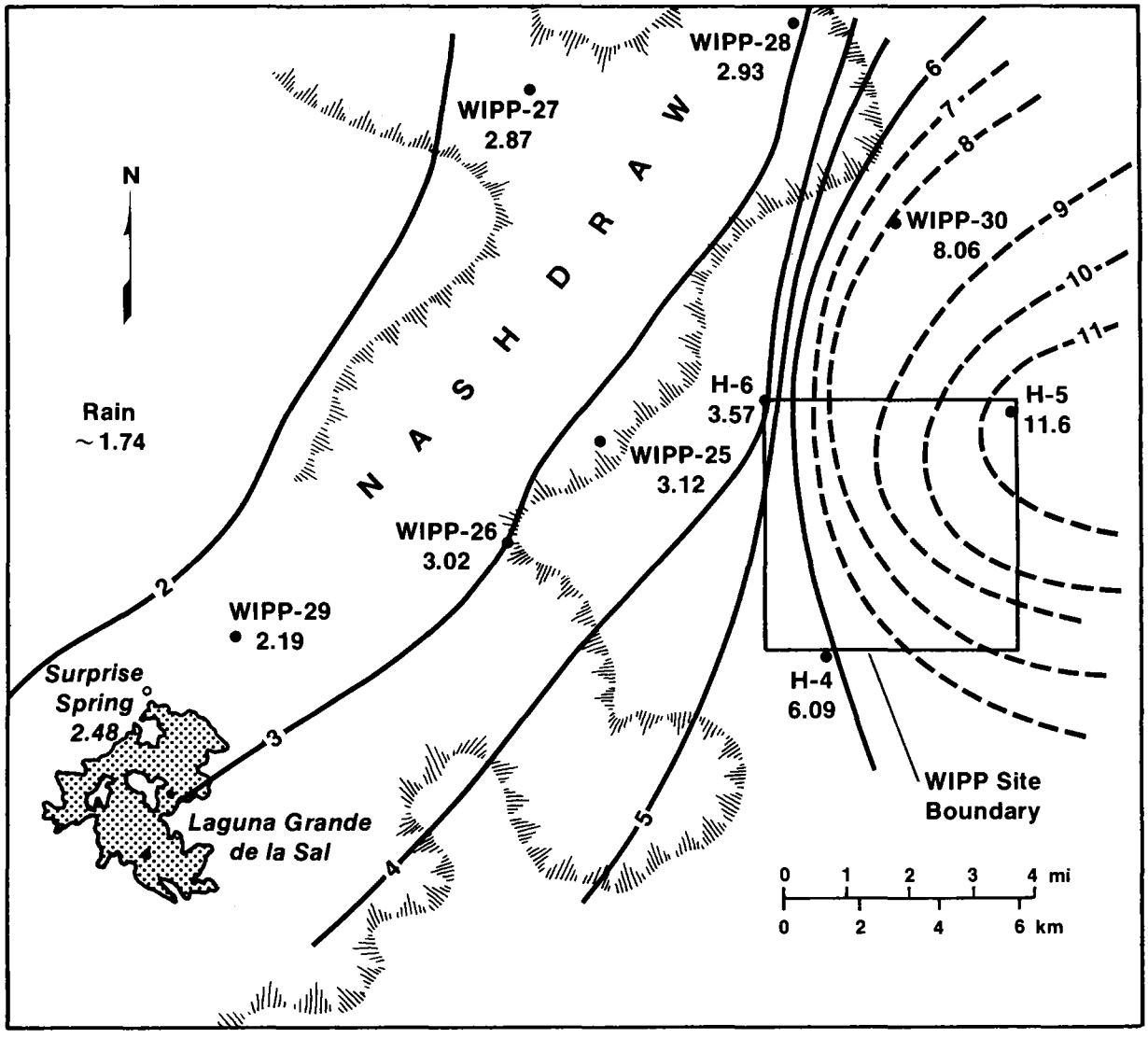


Figure 5-14. Contour map of $^{234}U/^{238}U$ activity ratio in groundwater from the Culebra dolomite member of the Rustler Formation (from Lambert and Carter [1987]).

developed in the Culebra dolomite member and near the Rustler/Salado contact zone. This mixing has resulted in relatively uniform aqueous total-U concentrations of about 10 ppb, and activity ratio values between 2 and 3. In the southwestern part of Nash Draw, where the Culebra member carries groundwaters very near the surface, the total-U has its highest observed aqueous value of about 40 ppb. Southwestern Nash Draw is dominated by a shallow hydrologic system that is recharged by water imported for potash refining. The high total-U and low activity ratio values are consistent with a large amount of congruent dissolution, without isotopic fractionation, of uranium and other constituents from soluble evaporites (Osmond and Cowart, 1976).

In the Culebra groundwaters, total U increases monotonically from east to west toward Nash Draw. The activity ratio decreases westward from maximum values of 6 to 12 near the WIPP Site, in the same direction as potentiometric levels decrease and total U increases. Geographic variations in groundwater total U and activity ratios from the Rustler/Salado contact mimic those in the Culebra (Lambert and Carter, 1987), although the activity ratio variations are smaller and the number of reliable control points, particularly near the WIPP Site, is small. The overall total-U concentrations are lower at the Rustler/Salado contact. Reliable total-U and activity ratio values for Magenta waters at WIPP-25 and -27 (in Nash Draw) are similar to those of Culebra waters there, and are consistent with a well-developed degree of vertical interconnection at those points (Lambert and Robinson, 1984; Lambert and Carter, 1987).

### 5.4.2 Model for U-Concentration and Activity Ratios in Groundwater

The evolution of uranium concentration and activity ratio is generally explained by a multi-legged path (Figure 5-15). Water moves from the oxidizing recharge zone (I) congruently dissolving uranium from rock (AR = 1) without isotopic fractionation until the redox barrier is reached. There the oxidation potential drops, congruently precipitating uranium. As water moves through the reducing zone (II), the $^{234}U/^{238}U$ activity ratio increases due to preferential leaching of $^{234}Th$, which has undergone recoil during the $\alpha$-decay

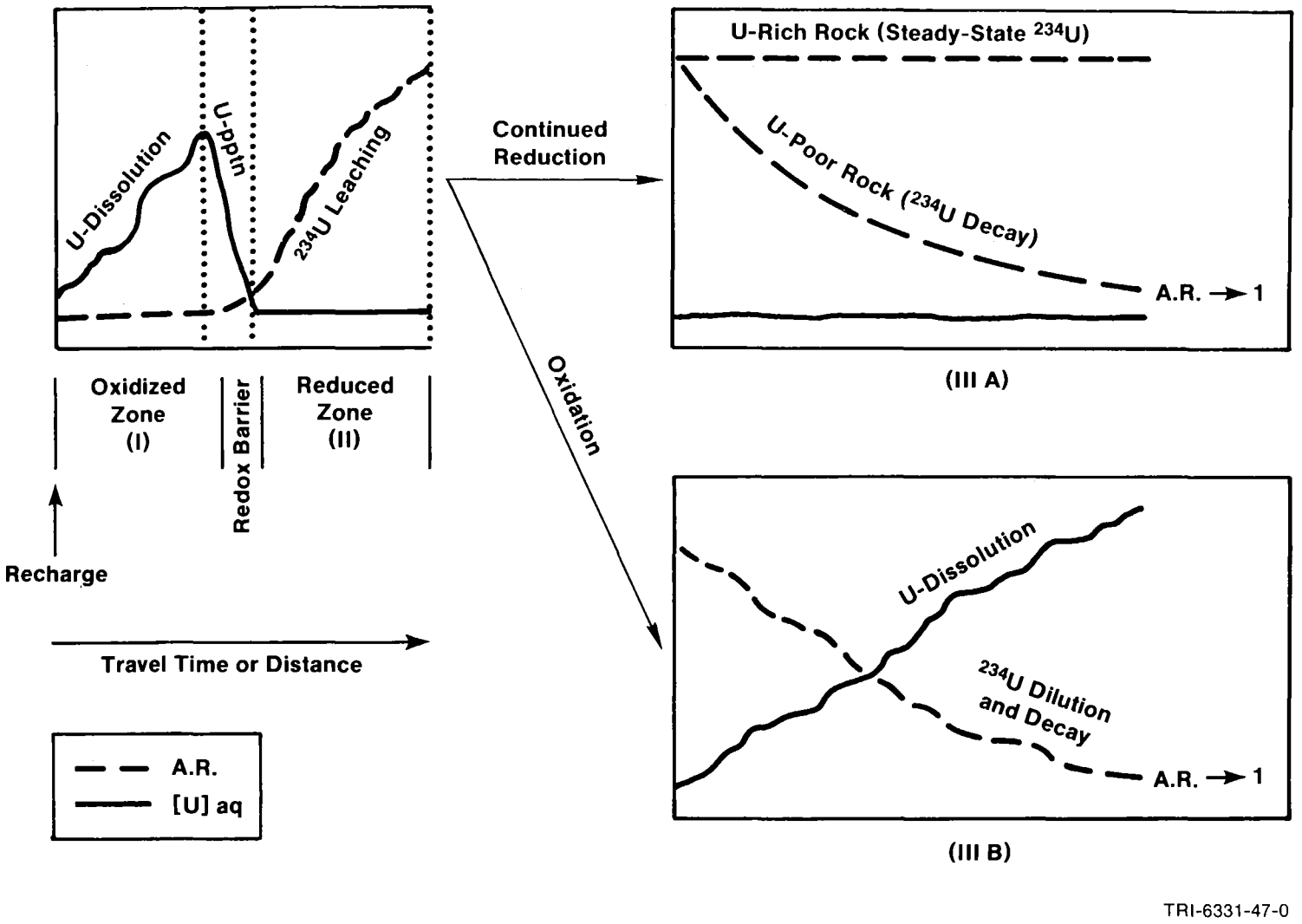


Figure 5-15. Schematic diagram of evolutionary paths for uranium concentrations and $^{234}U/^{238}U$ activity ratios in groundwaters (from Lambert and Carter [1987], based on the model described by Osmond and Cowart [1976]).

of its parent nucleus, $^{238}U$. The $^{234}Th$ quickly decays to $^{234}U$. If reducing conditions prevail along the flow path, very little additional $^{238}U$ is introduced into solution, but the activity ratio can increase profoundly, due to the enhanced leachability of $^{234}U$ and its parent $^{234}Th$, which has damaged its local lattice environment during recoil. If groundwater remains under reducing conditions, either the activity ratio achieves a steady-state value, or else a diminished supply of leachable $^{234}Th$ allows the activity ratio to decrease by preferential decay of $^{234}U$ (IIIA) toward secular equilibrium. If groundwater with a high activity ratio encounters oxidizing conditions, resumption of congruent dissolution of uranium from rock with a low activity ratio dilutes the aqueous activity ratio while increasing the total uranium concentration (IIIB).

Thus, in a confined aquifer under reducing conditions, activity ratios in solution can increase along the flow path. The rate-determining step in this process is the initial decay of $^{238}U$ to $^{234}Th$, rather than any subsequent process of decay or leaching. The steady-state value of the activity ratio depends on the initial total-U concentration, the amount of leachable uranium provided by rock surfaces, and the time spent on the evolutionary path.

## 5.4.3 Interpretation of U-Concentrations and Activity Ratios

### 5.4.3.1 $^{234}U$ Decay and Congruent Dissolution of Uranium

From the eastern scarp of Nash Draw westward, increasing total aqueous U (Figure 5-13) and decreasing activity ratio (Figure 5-14) trends along the generalized flow direction are consistent with ongoing congruent dissolution of uranium from the host rock. This is inconsistent with zone II in Figure 5-15, but may be indicative of zone IIIB. Near the WIPP Site, the total-U and activity ratio systematics cannot be described by such simple mixing. Some of the high activity ratio values near the WIPP Site may have been lowered from initially higher values by congruent dissolution of low-activity ratio rock. In fact, Kronfeld et al. (1979) used trends of decreasing activity ratio values to infer flow directions. High activity ratio values, however, can be generated only at distal, not proximal, points along the flow path in confined, reducing systems, according to the model of Osmond and Cowart

(1976). Thus, the increase in activity ratio value (dominantly eastward) in a direction different from that of the modern Culebra flow direction (dominantly southward, with westward influence) indicates that flow at one time in the past had a significant west-to-east component. If the present-day permeability distribution is similar to that at the time of recharge, flow in both Magenta and Culebra was from the higher permeability area in Nash Draw toward the lower permeability area near the WIPP Site. The extremely high (>6, up to 12) activity ratio values near borehole H5 (at the eastern boundary of the WIPP Site), together with the low permeability there, are not consistent with active (present-day) recharge in the east part of the WIPP Site, even though the potentiometric levels there (LaVenue et al., 1988) are highest. The relict activity ratio distributions, if activity ratio values at one time increased along the flow direction, indicate that the principal flow direction has since changed. Changes of principal flow direction with respect to that necessary to generate eastward increasing high activity ratio, together with the late-Pleistocene radiocarbon ages and non-modern $\delta D$ and $\delta^{18}O$ values in groundwaters, all are consistent with the premise that groundwater flow in the Rustler Formation is not at steady state.

Nash Draw, a Pleistocene course of the ancestral Pecos River (Bachman, 1980), is a likely paleo-recharge area for the Rustler units, since the permeability there has been better developed than at the WIPP Site since mid-Pleistocene Gatuña time (Bachman, 1981). The permeability along the eastern flanks of Nash Draw was also high in the late Pleistocene, as recorded by the gypsite spring deposits containing late Pleistocene faunal remains (Bachman, 1981). If the Culebra had recharge characteristics similar to the Magenta, both units must have at one time had similar potentiometric distributions. Total-U and activity ratio contours for Culebra groundwaters mimic potentiometric contour orientations that imply present westward flow in the Magenta dolomite (Figure 5-16; Mercer, 1983). Magenta potentiometric distributions, are developed in rocks of lower inherent permeability than the Culebra, but it is assumed here that at one time the recharge and discharge flow directions were similar for both units. If this is the case, lower flow velocities preserving the Magenta hydraulic gradients to some degree have apparently

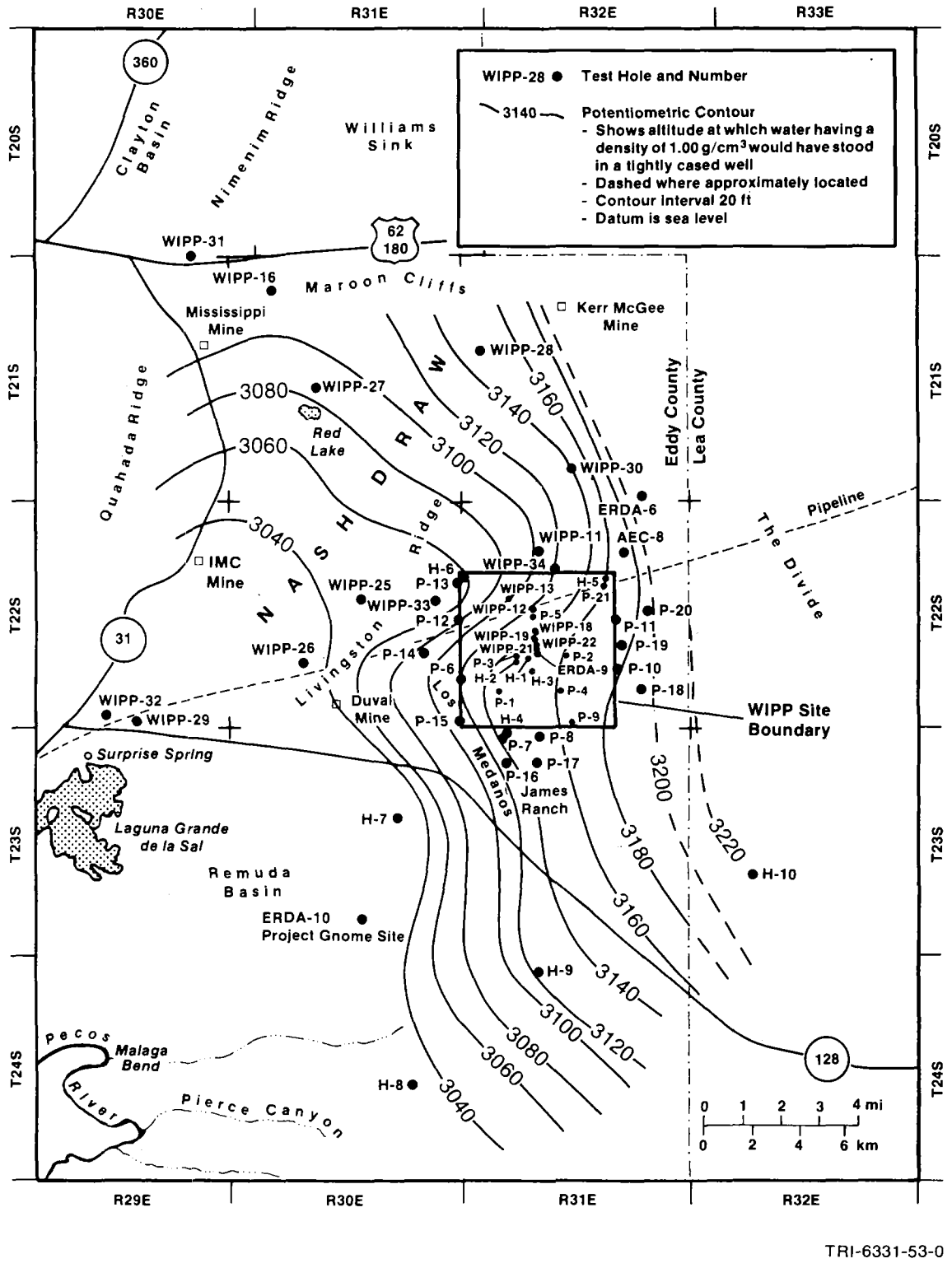


Figure 5-16. Adjusted potentiometric surface of the Magenta member of the Rustler Formation (1982) (from Mercer [1983]).

resulted in a relict Magenta potentiometric distribution. The Culebra potentiometric distributions, however, have readjusted differently since, perhaps in response to erosional and dissolutional developments in the southeastern lobe of Nash Draw. This has resulted in the capture of generally westward flow by a southward flow near the WIPP Site.

Based on decay of $^{234}U$ and assuming no additional uptake from the rock, uranium travel time during drainage from east to west along toward the high-permeability dissolution zones of Nash Draw, from the WIPP Site to a hypothetical discharge point in southwestern Nash Draw, is no more than 200,000 years. However, westward decreases in activity ratio associated with increases in total U in Nash Draw are attributable largely to dilution by congruent dissolution along a west-trending, increasingly oxidizing flow path, rather than radioactive decay.

### 5.4.3.2 Incongruent Dissolution of Uranium and $^{234}U$ Buildup

The time required for activity ratio values to have built up to observed values of 6 to 12 near the WIPP Site during an earlier eastward-flowing regime depends on the initial U concentration in solution and in rock. According to the computational method of Andrews and Kay (1982), it is not possible to achieve activity ratio values greater than 3.4 using the mean present-day U concentration (Lambert and Carter, 1987) in Culebra rock ($0.9 \cdot 10^{-6}$ g/g), and the lowest aqueous Culebra U concentration ($0.134 \cdot 10^{-9}$ g/g at H5). Using reasonably likely values of U-concentration at the time of recharge ($0.02 \cdot 10^{-9}$ g/g), and silty uranium-rich rock ($9 \cdot 10^{-6}$ g/g), which may better represent a higher U concentration on fractured rock surfaces, minimum times required to achieve the observed activity ratio values are 10,000 to 30,000 years, regardless of recharge area. This range of ages is consistent with the residence times of Culebra water in the WIPP Site area calculated by Lambert (1987) from radiocarbon measurements. The nearest likely paleo-recharge area for the old eastward-flowing system is to the west, the Rustler outcrops in Nash Draw, rather than to the north as suggested by Robinson and Lang (1938). In Nash Draw, the ancestral Pecos River drainage flowed and high permeability was developed as early as

mid-Pleistocene (Bachman, 1980; 1985). Rustler groundwater flow has since changed direction and is now probably draining toward the south (LaVenue et al., 1988) without appreciable recharge in the site area (Lambert and Harvey, 1987; Lambert, 1987).

# 5.5 STRONTIUM ISOTOPE RATIOS IN THE RUSTLER AND RELATED ROCKS

## 5.5.1 Distribution of $^{87}Sr/^{86}Sr$ Ratios

The strontium isotopic composition of the host rocks and their secondary veins were determined by analyzing anhydrite, gypsum, and other calciferous phases from the various formations in the WIPP area (Brookins and Lambert, 1988). The data are summarized in Table 5-2 and plotted in Figure 5-17. The interpretations are summarized from Brookins and Lambert (1988).

Figure 5-17 shows a systematic increase in $^{87}Sr/^{86}Sr$ upwards in the section from the Castile Formation through the Rustler Formation from 0.706879 ($Sr_{CA}$) to 0.706896 ($Sr_{SA}$) to 0.706945 ($Sr_R$). This systematic increase is predicted based on the strontium isotopic evolution curve for seawater. The very late Permian (Ochoan) is marked by a rapid increase in $^{87}Sr/^{86}Sr$, and this is reflected in the $^{87}Sr/^{86}Sr$ ratios.

$Sr_M$ and $Sr_{CU}$ data show greater range in $^{87}Sr/^{86}Sr$, higher averages than $Sr_R$, and larger standard deviations. This reflects the exchange of those dolomite units with waters flowing through them, and the higher $Sr_{CU}$ values are consistent with the meteoric $^{18}O/^{16}O$ and D/H ratios for waters contained in the dolomite units (Lambert and Harvey, 1987). There is little Sr exchange between the water-bearing Culebra dolomite and Rustler rocks above and below the Culebra (represented by $Sr_R$), further attesting to the relatively confined nature of the Culebra water in much of the area. The Sr-isotope data also suggest more interaction between rock and surface-derived water (i.e., higher $^{87}Sr/^{86}Sr$ values)

**Table 5-2. Strontium Isotopic Data for Host Rocks**

| Formation | Symbol | $^{87}Sr/^{86}Sr$ range | $^{87}Sr/^{86}Sr$ mean±SD | N |
|---|---|---|---|---|
| Caliche | $Sr_{CL}$ | 0.708417-0.708718 | 0.708623±0.000050 | 5 |
| Dewey Lake | $Sr_{DL}$ | 0.707220-0.708611 | 0.707856±0.000079 | 25 |
| Magenta | $Sr_{M}$ | 0.706986-0.707470 | 0.707152±0.000038 | 20 |
| Culebra | $Sr_{CU}$ | 0.707281-0.708101 | 0.707505±0.000088 | 15 |
| Rustler | $Sr_{R}$ | 0.706945-0.707132 | 0.706992±0.000008 | 35 |
| Salado | $Sr_{S}$ | 0.706889-0.706903 | 0.706896±0.000003 | 4 |
| Castile | $Sr_{CA}$ | 0.706870-0.706895 | 0.706879±0.000004 | 7 |

in the Culebra than in the Magenta, which is consistent with the observation that the Culebra is more likely to contain significant quantities of groundwater (i.e., a higher water/rock ratio) than the Magenta (Mercer, 1983).

The $Sr_{DL}$ data show a very wide range in Sr isotopic composition. This reflects the role of detrital Sr brought into the Delaware Basin during sedimentation and also reflects later exchange with waters. The surface caliche and gypsite spring deposits ($Sr_{CL}$) yield high $^{87}Sr/^{86}Sr$ values consistent with prediction based on mixed provenance for these occurrences. Note that the Pleistocene gypsite spring deposit (Bachman, 1981) contains high$^{87}Sr/^{86}Sr$ material more closely associated with a large component of shallow derivation, similar to the Dewey Lake veins, and is not the result of direct remobilization of the Rustler sulfates at depth. In turn, gypsum veining in the Dewey Lake Red Beds cannot be derived directly and solely from partial dissolution of Rustler sulfates, without the admixture of an apparently surficial component having a significantly higher $^{87}Sr/^{86}Sr$ ratio than the Rustler sulfates.

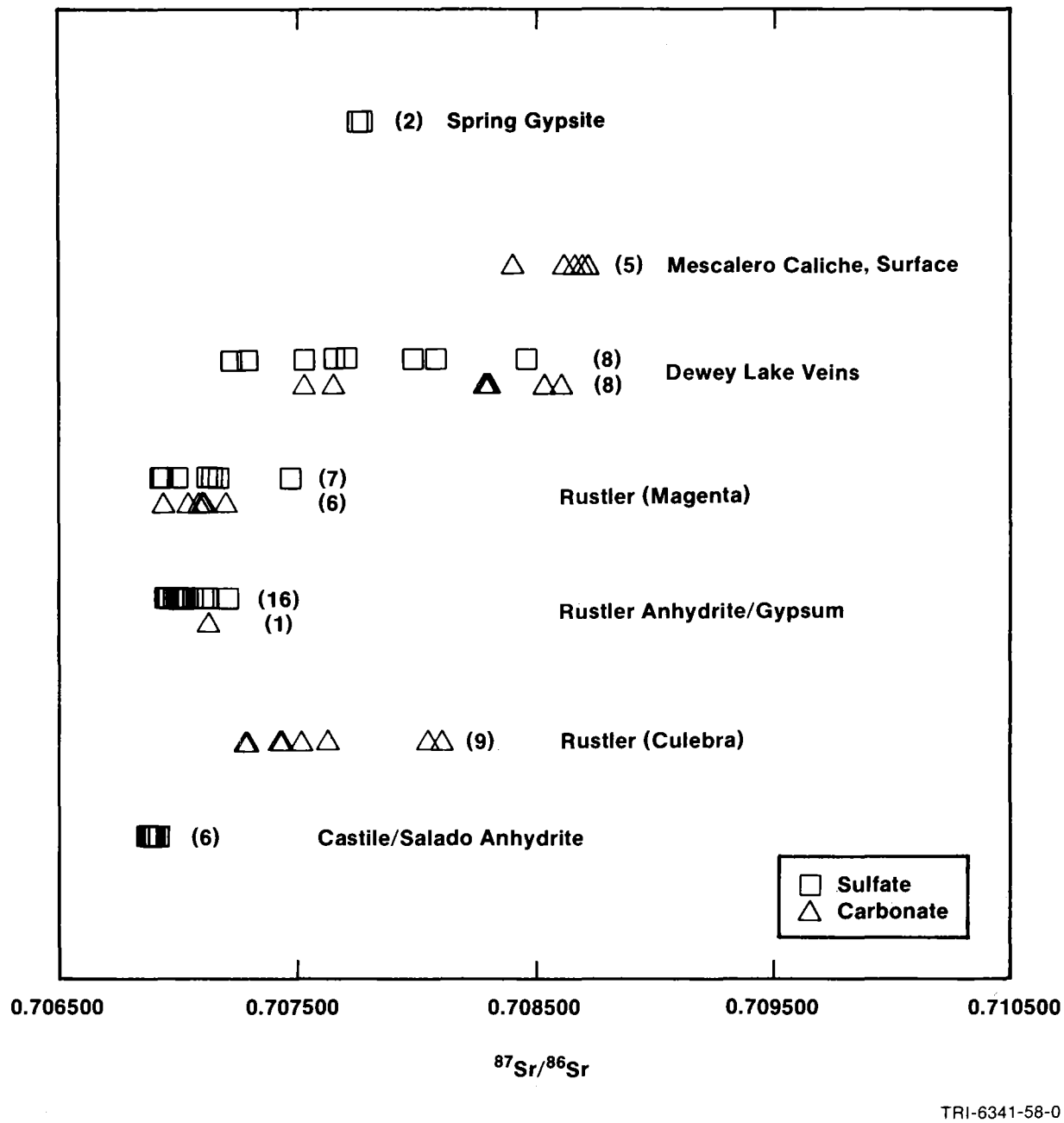


Figure 5-17. $^{87}Sr/^{86}Sr$ ratios in Ochoan and related rocks (data from Brookins and Lambert [1988]).

Variations in $Sr_{CA}$, $Sr_S$, and $Sr_R$ data of Table 5-2 are also of interest because they preclude widespread mass mobilization and homogenization due to interaction of waters with the rocks since their time of deposition. Otherwise more monotonous, uniform, and higher $^{87}Sr/^{86}Sr$ data would be observed. Thus, water/rock interaction involving relatively large amounts of water (accompanied by admixing of higher $^{87}Sr/^{86}Sr$ material) seems to have been confined to the dolomite units in the Rustler (Magenta and Culebra), the Dewey Lake Red Beds, and the various horizons inferred to be dissolution zones.

### 5.5.2 $^{87}Sr/^{86}Sr$ Relationships Between Veins and Host Rocks

The selenite or other vein and coexisting host rock $^{87}Sr/^{86}Sr$ data are plotted in Figure 5-18. It is readily apparent that despite the variation in $^{87}Sr/^{86}Sr$ from one rock sample to the next, the vein material is commonly very similar to the host rock in $^{87}Sr/^{86}Sr$ isotopic composition. In seven of the 15 coexisting vein/host rock pairs represented in Figure 5-18, the vein $^{87}Sr/^{86}Sr$ is less than that for the host rock, higher in four cases, and the vein-host values are identical in four cases. Application of the analytical uncertainty of ± 0.000008 ($2\sigma$) yields no significant difference in $^{87}Sr/^{86}Sr$ between vein and host rock in five cases. This indicates that the vein filling material (selenite in most cases, and calcite and granular gypsum in others) has derived its Sr from the surrounding rock as opposed to some extrinsic high $^{87}Sr/^{86}Sr$ surface source, as might be inferred for the spring deposits, caliche, and a component of the Dewey Lake selenite veins. This holds for selenite veins in dolomite as well as selenite veins in anhydrite or gypsum. Thus, even when sulfate is introduced, local dissolution has provided the Ca, Mg, and Sr. Even selenite veining in Rustler halite (the vein/host pair having the highest $^{87}Sr/^{86}Sr$ ratio in the Rustler anhydrite/gypsum group of Figure 5-18) contains cations derived from material more like native Rustler sulfates ($^{87}Sr/^{86}Sr < 0.7074$) and less like surficial material represented by caliche and spring gypsite ($^{87}Sr/^{86}Sr > 0.7084$).

Host rock for Dewey Lake veins is siliceous, thus requiring extrinsic derivation for vein material. Dewey Lake veins are mixtures of material from near-surface-type sources and evaporitic-type sources. The extremely limited range in $^{87}Sr/^{86}Sr$ values in Rustler and

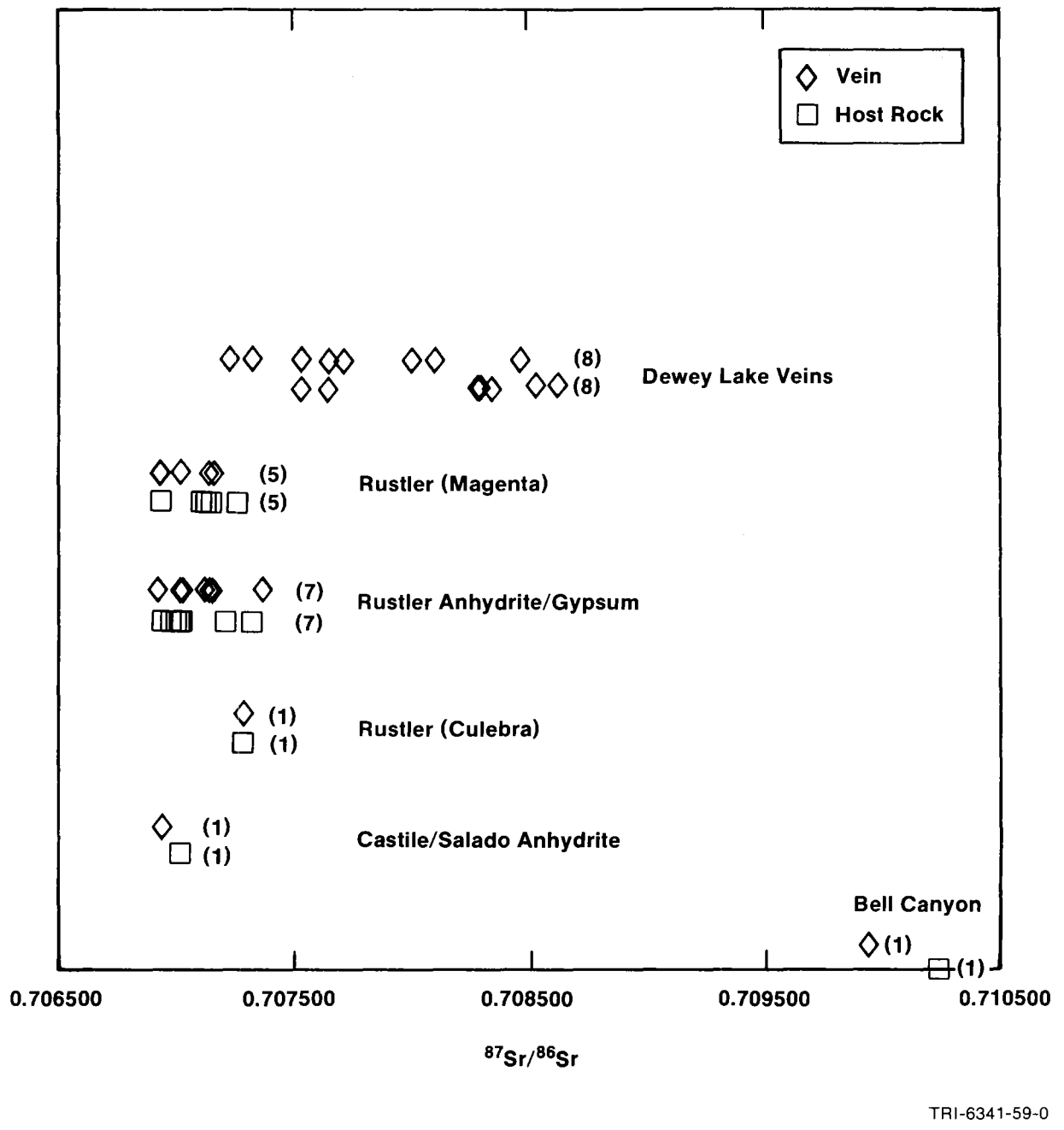


Figure 5-18. $^{87}Sr/^{86}Sr$ ratios in veins and their Ochoan host rocks (data from Brookins and Lambert [1988]).

deeper veins relative to the wide range in Dewey Lake veins indicates that the surface-related paleohydrologic system developed in the Dewey Lake did not entail unlimited groundwater circulation and rock/water interaction deeper in the section. If that were the case, $^{87}Sr/^{86}Sr$ ratios in veins would have been homogenized to very high (>0.708400) surface-type values.

# 5.6 D/H RATIOS IN RUSTLER AND DEWEY LAKE GYPSUM VEINS AND HOST ROCK

## 5.6.1 The Significance of Gypsum Occurrences

Gypsum is a common hydrated phase in the evaporites of the Rustler Formation and the overlying Dewey Lake Red Beds. Gypsum occurs as an alteration product of anhydrite where the Castile and Salado Formations have been erosionally exhumed. It also occurs near the surface within the influence of surface water and shallow groundwaters. The occurrence of gypsum in the Ochoan rocks varies from granular (variety alabaster) to euhedral or subhedral macrocrystalline (variety selenite) to fibrous (variety satin spar). The first variety is abundant as an alteration product of massive bedded anhydrite, whereas the latter two varieties are common as vein fillings. The Dewey Lake Red Beds in particular contain abundant selenite and satin spar in structures generally interpreted as fractures; the orientation of the gypsum-filled structures in the Dewey Lake is both concordant and discordant with respect to the bedding.

Gypsum occurs in the Rustler Formation largely as replacement of anhydrite, but veins are known also. The calcium in the carbonate and sulfate Rustler veins is inferred to have been directly derived from host rock, according to similarities in vein and host $^{87}Sr/^{86}Sr$ ratios (Section 5.5.2). This indicates that the Rustler Formation has been a relatively closed system with respect to mass transfer from the surface. The Dewey Lake veins, however, are inferred from $^{87}Sr/^{86}Sr$ data to be mixtures of surface-derived, perhaps relatively young, material together with remobilized calcium similar to that in the Rustler

(Section 5.5.1). The occurrence of postdepositional veining outside presently known water-bearing zones is especially significant, in that it may represent former regimes of groundwater flow within the Rustler and Dewey Lake. The degree of material transport between and within paleohydrologic units, as tracked by trace isotope distributions, may be relevant to evaluating the potential for mass transport in the Rustler water-bearing zones under present hydrologic conditions. Solute transport is traceable by variations in $^{87}Sr/^{86}Sr$ ratios (Section 5.5.1). However, small differences in $^{87}Sr/^{86}Sr$ ratios may be less sensitive to fluid transport (i.e., movement of water molecules and their subsequent interaction with host rock). Movement of water accompanied by little or no introduction of uniquely discernable solutes is better characterized by an isotopic signature of the water molecules themselves, such as D/H ratios.

### 5.6.2 Principles of D/H Fractionation between Gypsum and Water

The equilibrium partitioning of deuterium between the water of crystallization of gypsum and free water at ambient temperatures has been determined experimentally and reported by Fontes and Gonfiantini (1967) and Sofer (1978). The equilibrium fractionation factor, $\alpha$, is defined by the following ratio:

$$\alpha = \frac{(D/H)_{gypsum}}{(D/H)_{water}} \quad . \qquad [1]$$

The reported values of $\alpha$ vary from 0.980 (Sofer, 1978) to 0.985 (Fontes and Gonfiantini, 1967). In this discussion, $\alpha$ is taken conservatively as 0.980. It is also assumed that the D/H fractionation between water and gypsum during subsurface postdepositional crystallization or recrystallization takes place at equilibrium. This means that at isotopic equilibrium at ambient temperatures, the $\delta D$ value of gypsum would be very nearly 20‰ more negative than the coexisting water. Once D/H equilibrium partitioning between gypsum and water has been attained, the observed $\delta D$ value of the water of crystallization of gypsum thus preserves an indication of the water in whose presence it last recrystallized.

If the water/rock ratio is large, such that the crystallization of gypsum under the (D/H) fractionation factor of 0.980 does not change the hydrogen isotopic composition of the water, then the δD value of the resulting gypsum will be 20‰ more negative than the water. At the other extreme, if gypsum is formed from anhydrite, consuming available water at suitably low ionic strength, the water/rock ratio will be small. The relative abundance of fresher water in contact with anhydrite (i.e, the water/rock ratio during interaction) would remain small until all anhydrite is so converted. Under such conditions, the bulk δD value of the resulting gypsum will be identical to that of the water incorporated during the gypsification. If, at intermediate water/rock ratios, a pre-existing gypsum is partially recrystallized by a moving groundwater, the resulting gypsum δD values will reflect mixtures of the previous and latest episodes of gypsum/water interaction. At such intermediate water/rock ratios, free water will remain after the recrystallization, but mass-balance considerations in a local system of mineral/water interaction will result in a change in the isotopic composition of both water and gypsum (relative to their initial values) in order to yield the equilibrium fractionation factor between them. Thus, in any given episode, the δD value of gypsum will be at most 20‰ more negative than the paleowater that formed it, given the gypsum-water D/H fractionation factor of 0.980.

### 5.6.3 Distributions of D/H Ratios in Gypsums

As part of a preliminary paleoclimate study, D/H ratios were determined for the water of crystallization of several gypsums from massive occurrences in the Rustler Formation and from veins in the Dewey Lake Red Beds. Several gypsum specimens were obtained from carefully selected cores; boreholes providing core included localities known or proposed as evaporite karst features. A comprehensive discussion of evaporite karst has been provided by Bachman (1987). Some of the features, particularly the topographic depression in which the WIPP-33 borehole was drilled, have been proposed as major conduits for modern vertical migration of large amounts of surface water into the Rustler wet zones (L. C. Chaturvedi and J. B. Chapman, written communication; Barrows in Chaturvedi and Channell, 1985). If the gypsification in such features as WIPP-33 and at gravity anomalies such as at WIPP-14 and -34 are taken to be contemporaneous with the development of

known or postulated karstic features, the gypsum δD values will constrain the possible sources of water associated with such features. The AEC-8 samples are particularly significant because this locality is far removed from known shallow zones of gypsum dissolution such as Nash Draw. All of the samples discussed here have had their $^{87}Sr/^{86}Sr$ ratios determined (Section 5.5), and all have been submitted for attempts at determining the time of recrystallization using the uranium-thorium dating method. The uranium-thorium results are not available at this time.

Gypsum samples were chiseled from the center of the core (either 4-in or NX-sized) to obtain gypsum less likely to have come in contact with drilling fluid or atmospheric moisture. Each sample was examined under a binocular microscope for qualitative determinations of purity. Major impurities were removed by hand-picking. The principle non-gypsum impurities in the selenite veins from the Dewey Lake Red Beds are siliciclastics from the host rock. The most abundant non-gypsum component from the Magenta dolomite member of the Rustler Formation is dolomite, while the non-gypsum component in the selected horizons of the Forty-niner, Tamarisk, and lower members is typically anhydrite (Sewards et al., Chapter 3). The gypsum-rich separates were gently crushed to release major fluid inclusions and to minimize decrepitation during pyrolysis. The pyrolysis, extraction of hydrogen, and isotopic analysis were carried out according to a method modified from Epstein and Taylor (1970) and described by Lambert and Harvey (1987). Two replicates (reproduced within ± 2‰) were obtained for each of the other samples analyzed at Sandia National Laboratories. The AEC-8 samples (1 replicate each) were analyzed in the laboratories of Dr. Samuel Epstein at the California Institute of Technology.

The preliminary data are given in Table 5-3, together with the stratigraphic horizons for the samples. The data are plotted as a function of depth in Figures 5-19 and 5-20. Figure 5-19 shows ranges for gypsum δD values expected from crystallization or recrystallization in the presence of Rustler-type meteoric water (δD = -44 to -58‰), given a high (solid lines) and a low (dashed lines) water/rock ratio. Figure 5-20 shows ranges for gypsum δD values

## Table 5-3. Hydrogen Isotope Composition of Gypsums

| Borehole | Depth, ft | Unit | wt% $H_2O$ | D (SMOW) ‰ |
|---|---|---|---|---|
| AEC-8 | 215.7 | Dewey Lake selenite vein | 98 | -68 |
| AEC-8 | 725.0 | Rustler Tamarisk | 93 | -73 |
| WIPP-14 | 247.2 | Dewey Lake selenite vein | 92<br>94 | -57<br>-56 |
| WIPP-14 | 319.4 | Dewey Lake selenite vein | 89<br>89 | -45<br>-43 |
| WIPP-14 | 665.7 | Rustler Forty-niner | 93<br>93 | -50<br>-51 |
| WIPP-19 | 350.0 | Dewey Lake selenite vein | 93<br>94 | -41<br>-43 |
| WIPP-33 | 401.6 | Rustler Forty-niner | 90<br>88 | -72<br>-73 |
| WIPP-34 | 661.5 | Rustler Forty-niner | 81<br>83 | -50<br>-50 |
| WIPP-34 | 714.1 | Rustler Forty-niner | 82<br>83 | -62<br>-60 |
| WIPP-34 | 716.8 | Rustler Magenta | 80<br>78 | -64<br>-65 |
| WIPP-34 | 821.5 | Rustler lower | 69<br>69 | -53<br>-53 |

1. Relative to 100% $CaSO_4 \cdot 2H_2O$

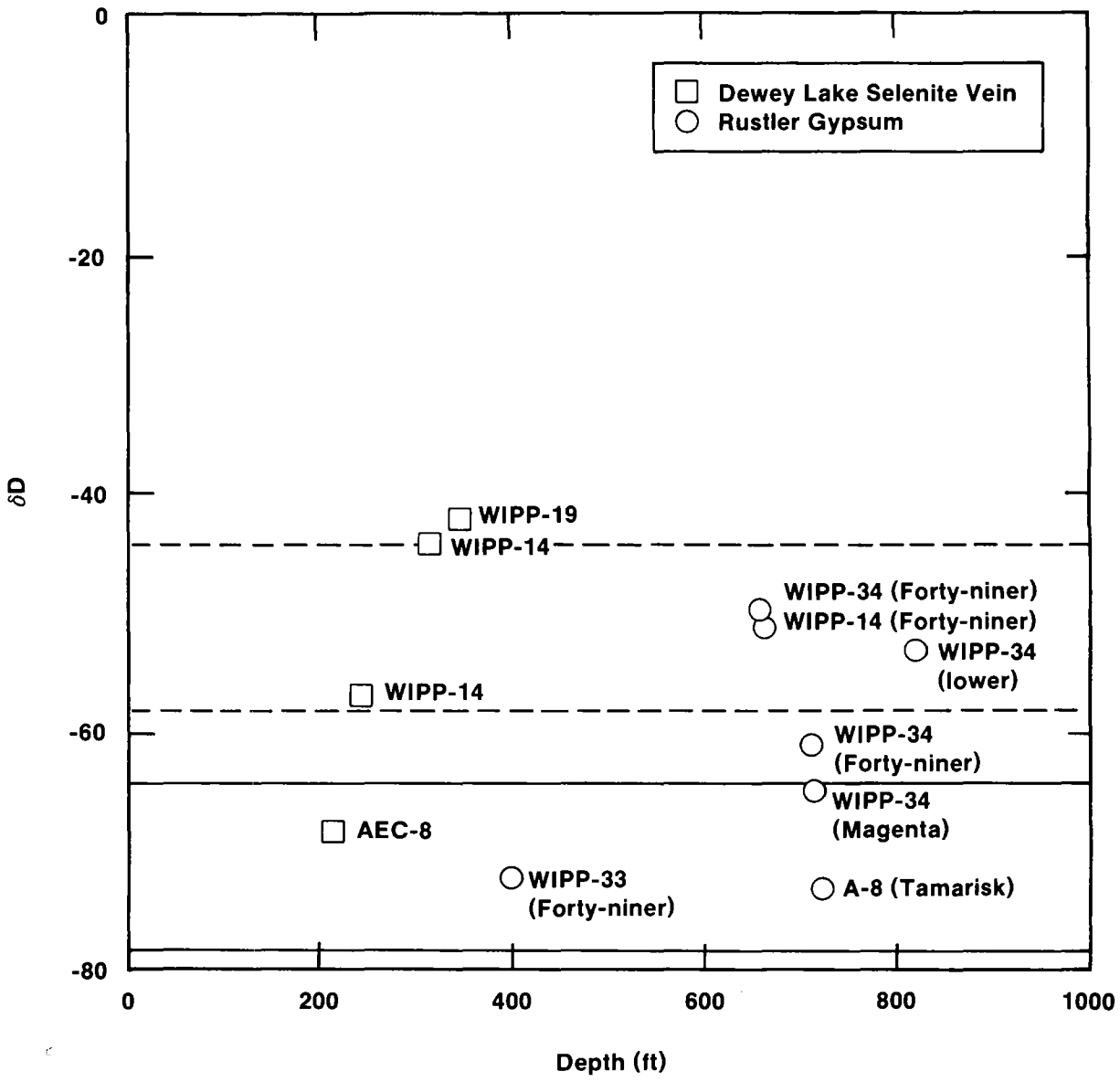


Figure 5-19. δD values of the water of crystallization in gypsums as a function of depth.

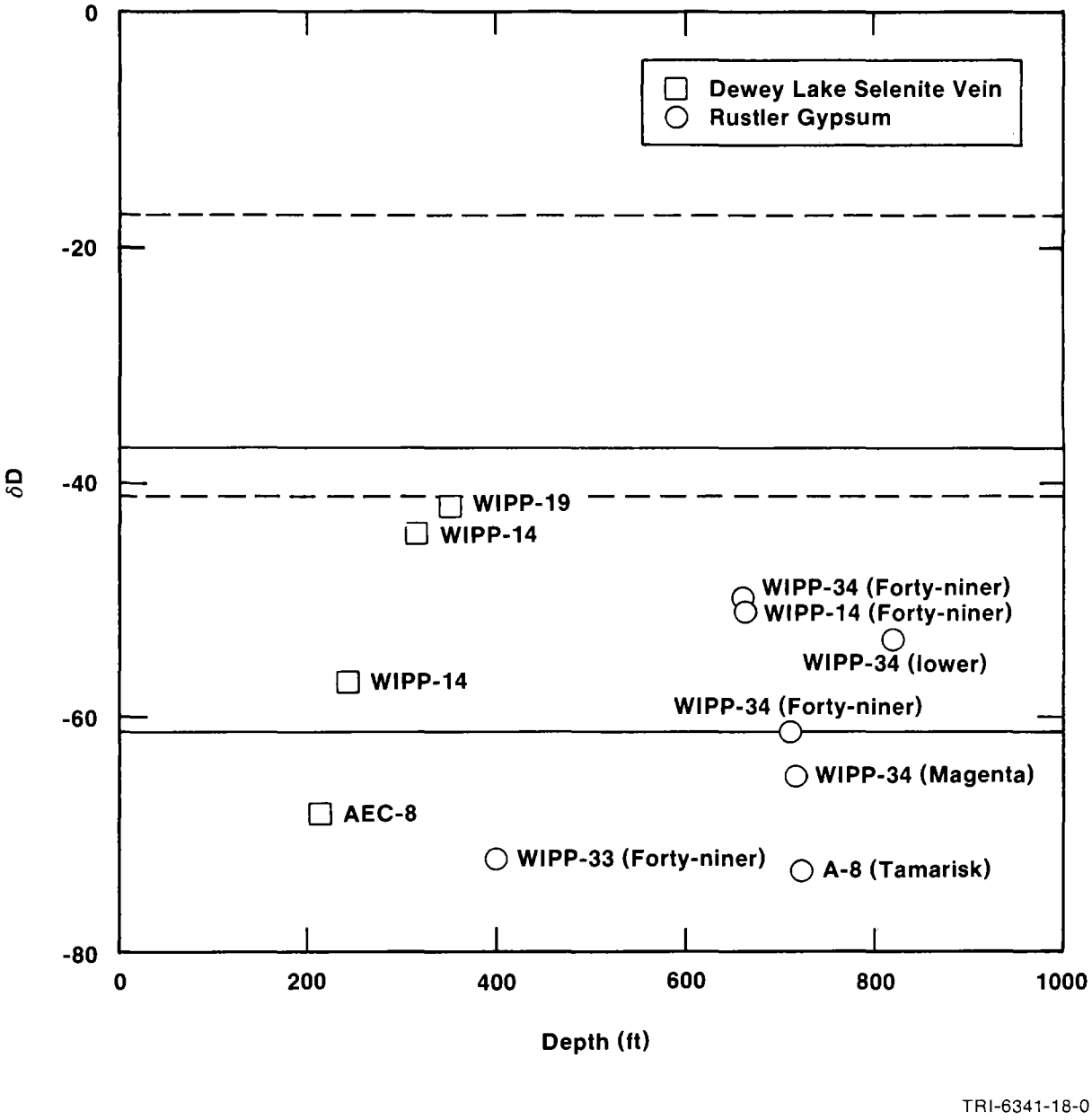


Figure 5-20. δD values of the water of crystallization in gypsums as a function of depth.

expected from crystallization or recrystallization in the presence of surface-type (possible modern) meteoric water ($\delta D$ = -17 to -41‰) given a high (solid lines) and a low (dashed lines) water/rock ratio.

None of the gypsums can have crystallized in the presence of any amount of primary evaporite mother liquor, such as Permian seawater. Gypsums formed under such conditions would have $\delta D$ values more positive than -20‰, if the seawater had a $\delta D$ value of 0‰. The $\delta D$ value of evaporite mother liquor derived from seawater would probably be more positive than 0‰, since the degree of evaporation required to precipitate primary gypsum would have left a solution significantly enriched in deuterium by kinetic fractionation during evaporation (cf. Craig et al., 1963). Thus, all gypsums reported here in the preliminary study, even from the Rustler Formation, have last recrystallized in the presence of meteoric water, whose $\delta D$ values would be expected to fall in the continental/meteoric range (cf. Friedman et al., 1964). Further, Lambert and Harvey (1987) have argued that throughout the Holocene and late Pleistocene, Delaware Basin meteoric groundwaters have been more negative than -17‰. The 11 $\delta D$ values in Figures 5-19 and 5-20 have no correlation with depth. This suggests that shallowness alone is not a sufficient condition for the penetration of modern surface-derived groundwater more enriched in deuterium (cf. Section 5.2.3), and the interaction of such water with gypsum to influence its isotopic composition.

### 5.6.4 Inferred Influxes of Meteoric Water

The reproducibility of $\delta D$ measurements on gypsums, together with the reproducibility of the water yield of the rock samples (Table 5-3), indicates little if any post-coring exchange of hydrogen isotopes in the water of crystallization of gypsum under conditions of sample storage and laboratory analysis. The analyses were carried out over a period of time during which the temperature and relative humidity were undergoing radical day-to-day changes in the laboratory, accompanying a change in the configuration in the building ventilating system (from summer to winter). The reproducibility of replicate measurements

suggests a minimal influence of ambient laboratory conditions on the gypsum D/H ratios. Thus, the D/H ratios in gypsums are taken to represent the in situ isotopic compositions and are assumed to have been determined by the last episode of recrystallization of gypsum in the presence of a given water and a given water/rock ratio.

The gypsum/water fractionation factor (Equation A) was used together with the ranges of $\delta$D values of the two different populations of water samples (confined Rustler-type versus less confined shallow-type) to calculate the expected $\delta$D values of recrystallized gypsum under varying water/rock ratios. Since the former population of waters (Rustler-type) ranges in $\delta$D value between -44 and -58‰ (Section 5.2.3), a very small water/rock ratio would yield gypsums having this same range of $\delta$D values. A large water/rock ratio would yield the range of -64 to -78‰. These ranges are depicted in Figure 5-19. Similarly, the latter population of waters (shallow-type) range in $\delta$D between -17 and -41‰, yielding this same range for gypsums expected to have formed in the presence of this water, given a small water/rock ratio. A large water/rock ratio would yield the range -37 to -61‰. These ranges are depicted in Figure 5-20.

Taken together, Figures 5-19 and 5-20 show that the $\delta$D values of Rustler gypsum and Dewey Lake selenite vein material at AEC-8 and gypsums from the WIPP-33 Forty-niner and WIPP-34 Magenta are consistent with recrystallization in the presence of a water that isotopically resembles typical Rustler meteoric water, inferred to be late Pleistocene or older (Figure 5-20). However, they are not consistent with recrystallization in the presence of shallow-type water inferred to be modern (Figure 5-20). Also, the WIPP-19 sample cannot be easily generated from Rustler-type water alone, regardless of water/rock ratio. Note that if 0.985 instead of 0.980 is used for the $\alpha$-value in Equation 1, these constraints apply to one of the WIPP-34 Forty-niner data points also. If the Rustler-type waters more depleted in deuterium are at least as old as late Pleistocene (Section 5.3.5.3), and no waters of similar isotopic composition have entered the subsurface since, then the time of recrystallization also is at least that old, since such groundwaters are not characteristic of modern recharge (Section 5.2.3). These constraints preclude both total preservation of these

gypsums as primary seawater precipitates and their recrystallization in response to infiltration typified by local modern meteoric isotopic compositions. Whereas Rustler dolomites generally have not recrystallized in isotopic equilibrium with Rustler water (except at WIPP-33; see Figure 5-6), much of the gypsum in the Ochoan section has done so.

The degree of direct vertical infiltration at localities such as WIPP-34 can be evaluated from the vertical distribution of gypsum $\delta D$ values. The gypsum $\delta D$ value in the Magenta is clearly consistent with isotopic equilibrium with a large amount of Rustler-type water (Figure 5-19), which is assumed to have occurred at WIPP-34 as elsewhere in the Rustler. Hence, a large water/rock ratio (or else no water/rock interaction at all) must have persisted at all points along the flow path leading to WIPP-34 Magenta, in order for the $\delta D$ value of water to have remained unchanged from Rustler-type values and give rise to the observed gypsum $\delta D$ value in the Magenta. If a relatively large amount of water had travelled a vertical flow path across the bedding at WIPP-34, interacting with overlying gypsiferous strata (at the two localities in the Forty-niner represented by data points), the Forty-niner gypsum $\delta D$ values would the the same as in the Magenta. Note, however, that in the gypsum only 2.7 ft above the Magenta, the $\delta D$ value is out of the range of gypsum values expected for recrystallization in the presence of Rustler-type water with a large water/rock ratio. If a downward-migrating water interacted with Forty-niner gypsum with a small water/rock ratio, giving the less negative gypsum $\delta D$ values observed in the Forty-niner, the $\delta D$ value of the water would be less negative than typical Rustler values by the time it reached the Magenta. This would result in a gypsum $\delta D$ value significantly more positive than observed in the Magenta. The gypsum $\delta D$ values suggest that the water/rock interaction ratio is lower in the Forty-niner than in the underlying Magenta. It is not geologically and hydrologically reasonable for the water/rock ratio to increase along the flow direction away from the source. It is more geologically reasonable to regard the WIPP-34 Forty-niner values as products of interaction with water leaking upward from the Magenta water, known to be a locally abundant confined water source (Mercer, 1983), resulting in a decreased water/rock ratio in the Forty-niner away from the source. A small

amount of leakage upward from confined units is expected, especially if the static potentiometric level is significantly above the producing horizon. The isotope systematics alone are consistent with a recrystallization of Forty-niner gypsum by relatively large amounts of isotopically heavier (possibly modern) water; however, the geologic/hydrologic context suggests a smaller water/rock ratio in the Forty-niner, involving Rustler-type water having leaked upward from the water-bearing Magenta dolomite unit.

Similarly, it is proposed that the more positive $\delta D$ value of the WIPP-34 lower member sample resulted from the influence of a small amount of Rustler-type water leaking downward from the Culebra, rather than the influence of a large amount shallow-type water. Otherwise, a large amount of downward-moving shallow-type water more enriched in D would be required to cross relatively permeable zones (the Magenta and Culebra). The Magenta and Culebra would probably contain an abundant pre-existing occurrence of Rustler-type water (of at least late Pleistocene age) more depleted in D. Thus, under the present hydrologic conditions the water more enriched in D would not arrive at the lower member. These relationships attest to only a limited amount of vertical fluid movement from the surface during crystallization or recrystallization of gypsum, but allow lateral incursion of larger amounts of water along the bedding, with less effect on soluble sulfates above and below. This is consistent with the conclusions based on $^{87}Sr/^{86}Sr$ studies reported in Section 5.5.

A single gypsum sample of Dewey Lake vein selenite from WIPP-19 appears to have formed under at least partial influence of shallow-type water, since its $\delta D$ value is more positive than expected from interaction only with Rustler-type water given a fractionation factor of 0.980, regardless of water/rock ratio (Figure 5-19). Note, however, that application of $\alpha = 0.985$ places the WIPP-19 sample well within the range of interaction with Rustler-type water. It is conceivable that the Dewey Lake veins in WIPP-14 also preserve some component of shallow-type water with a variable water/rock ratio. This hypothesis is consistent with the mixing between surface-derived and largely evaporitic material to yield the Dewey Lake veins, as inferred from the $^{87}Sr/^{86}Sr$ ratios (Section 5.5). Note, however,

that the δD value of the shallowest analyzed Dewey Lake vein selenite from AEC-8 is not consistent with a significant surficial influence.

Finally, the WIPP-14 Forty-niner sample, when viewed as an isolated δD value, is problematical. Its δ value is virtually identical to that of a Forty-niner specimen from WIPP-34 and is intermediate between two Dewey Lake values in WIPP-14. Geological and hydrological context suggested that the higher-deuterium WIPP-34 Forty-niner gypsum had last recrystallized with Rustler-type water and an intermediate water/rock ratio. It is tentatively proposed that, since the WIPP-14 Forty-niner sample is from the same population of Rustler specimens that show minimal shallow-type cationic component (Figure 5-17), its origin is similar to that of the higher-deuterium Forty-niner specimen from WIPP-34.

# 5.7 SUMMARY AND CONCLUSIONS

## 5.7.1 Isotopic Evidence of Transient Flow in the Rustler

Stable-isotope data reported by Lambert and Harvey (1987) indicate that modern recharge has a different isotopic composition than meteorically derived confined Rustler groundwaters. Tritium and radiocarbon data (Lambert, 1987) indicate that confined Rustler groundwaters have a minimal modern meteoric component, and have been isolated from the atmosphere for at least 12,000 to 16,000 years. Uranium systematics reported by Lambert and Carter (1987) for groundwaters in the same area suggest that groundwater flow from the probable paleorecharge area in Nash Draw was in a direction different from the dominantly southward flow inferred for the modern flow system from potentiometric measurements by LaVenue et al. (1988). The available isotopic data are consistent with the interpretation that principal recharge and groundwater flow patterns, and probably evaporite dissolution patterns, were dominated during the Pleistocene by climatic variations that represented wetter conditions than now found in the northern Delaware Basin. Thus, the Rustler hydrologic system is indicated by the isotopic systematics to be transient rather than at steady state.

The Culebra in borehole H5 northeast of the WIPP Site has a relatively high potentiometric level, but this alone is not a condition sufficient for recharge. The absence of tritium and the high (11.6) activity ratio value there implies long residence time of a significant component under confined conditions. High potentiometric level, together with the relatively low permeability there is likely to result from drainage away from this region in surrounding areas of higher permeability. This drainage without significant recharge has apparently left a relict region of high transient potentiometric level that, due to low permeability, is slow to respond to surrounding post-Pleistocene drainage.

### 5.7.2 Isotopic Constraints on Groundwater Flow

Tritium, $\delta^{18}O$, and $\delta D$ values in groundwaters of southeastern New Mexico suggest that modern localized recharge in response to rapid vertical infiltration under present climatic conditions in southeastern New Mexico at elevations of 3000 to 4500 ft has an isotopic signature significantly different from confined Rustler groundwaters near the WIPP. Although the latter do not appear to be dominated by the former, this does not preclude slower, lateral, stratabound water movement within the higher-permeability brittle interbeds in the Rustler, such as the Magenta and Culebra dolomites. Unlike the confined Rustler, some perched Dewey Lake groundwaters may have a component of modern surficial recharge fostered by present climatic conditions.

Rustler and some Dewey Lake groundwaters have a significant component at least 12,000 years old. Only four out of sixteen well-water occurrences gave internally consistent age calculations, based on the internally consistent interpretive model of Evans et al. (1979) for carbonate units. The mean age of isolation from the atmosphere is 14,000 radiocarbon years, and the 95% confidence limits are ± 5,000 years. The narrow range of ages probably does not reflect rapid flow across the WIPP Site accompanied by post-Pleistocene mixing and homogenization, because the solute distribution patterns are not consistent with such homogenization (Siegel et al., Chapter 2). These ages do not allow consistent age gradients or travel times to be inferred across the WIPP Site. Ten out the sixteen well-water occurrences were complexly contaminated. The remaining two are

problematical, but probably represent three-component mixtures including some contamination.

Packrat middens and fossil fauna in spring deposits indicate that late Pleistocene climate in southeastern New Mexico more than 10,000 to 20,000 years ago fostered vegetation now found only at higher elevations in nearby mountainous areas. Late Pleistocene climate was probably wetter and more conducive to recharge.

Generalized flow directions in confined Culebra groundwaters inferred from $^{234}U/^{238}U$ relationships have an east/west component, at an angle to the modern, dominantly north/south flow directions inferred from potentiometric heads alone. Change in flow direction during the past 10,000 to 30,000 years is likely, governed by developments in Nash Draw. In the northeastern part of the WIPP Site near H5, Culebra groundwater contains an extremely high uranium-isotope activity ratio (11.6) and no significant tritium. The Culebra rock there has low transmissivity. Despite the high potentiometric level there, these observations are not consistent with a significant amount of either modern or ancient local recharge.

$\delta^{18}O$ and $\delta^{13}C$ values of carbonates and $\delta D$ values of gypsums indicate that gypsum and occasionally calcite in the Rustler water-bearing rock have locally precipitated in equilibrium with water characteristic of the confined Rustler, but dolomite has not recrystallized. This does not preclude the dissolution of dolomite and sulfates.

$^{87}Sr/^{86}Sr$ ratios in carbonates and sulfates indicate that gypsum and calcite veining in the Dewey Lake Red Beds overlying the Rustler Formation entailed material transport from surface. However, the latest-formed occurrences of gypsum and calcite in the Forty-niner, Tamarisk, and lower members of the Rustler Formation contain little admixture of Ca from surface. Culebra, and to a lesser extent, Magenta rocks contain significant admixtures of surficial material, but are "sandwiched" between gypsic horizons that contain significantly

less surface-derived material. Thus, this limits the degree of material transport vertically across Rustler bedding.

$\delta D$ values of various occurrences of gypsum indicate that crystallization of Rustler gypsum and Dewey Lake veins entailed meteoric (not marine) water. Water (as opposed to mineral-derived solutes) may have moved vertically at some time during the gypsification, but the water/rock ratio varied, being greater in presently known saturated zones and smaller in the less-permeable adjacent beds. The resultant inferred stratification of the water/rock ratio also limits the degree of water transport (i.e., direct vertical recharge) across Rustler bedding.

# 5.8 REFERENCES

Allison, G. B. 1982. "The Relationship between $^{18}O$ and Deuterium in Water in Sand Columns undergoing Evaporation." *Journal of Hydrology*, Vol. 55:163-169.

Allison, G. B., W. J. Stone, and M. W. Hughes. 1985. "Recharge in Karst and Dune Elements of a Semi-Arid Landscape as Indicated by Natural Isotopes and Chloride." *Journal of Hydrology*, Vol. 76:1-25.

Andrews, J. N., and R. L. F. Kay. 1982. "U-234/U-238 Activity Ratios of Dissolved Uranium in Groundwaters from a Jurassic Limestone Aquifer in England." *Earth and Planetary Science Letters*, Vol. 57:139-151.

Bachman, G. O. 1980. *Regional Geology and Cenozoic History of the Pecos Region, Southeastern New Mexico*. Open File Report 80-1099. Denver, CO: US Geological Survey.

Bachman, G. O. 1981. *Geology of Nash Draw, Eddy County, New Mexico*. Open File Report 81-31. Denver, CO: US Geological Survey.

Bachman, G. O. 1984. "Regional Geology of the Ochoan Evaporites, Northern Part of the Delaware Basin." *Circular 184*. Socorro, NM: New Mexico Bureau of Mines and Mineral Resources.

Bachman, G. O. 1985. *Assessment of Near-Surface Dissolution at and near the Waste Isolation Pilot Plant, (WIPP), Southeastern New Mexico*. SAND84-7178. Albuquerque, NM: Sandia National Laboratories.

Bachman, G. O. 1987. *Karst in Evaporites in Southeastern New Mexico*. SAND86-7078. Albuquerque, NM: Sandia National Laboratories.

Brookins, D. G., and S. J. Lambert. 1988. "WIPP Site Studies: Secondary Selenite Veins in the Rustler Formation and Dewey Lake Red Beds." *Materials Research Society Symposium Proceedings*. Vol. 112:233-241.

Chapman, J. B. 1986. *Stable Isotopes in Southeastern New Mexico Groundwater: Implications for Dating Recharge in the WIPP Area*. EEG 35. New Mexico Environmental Evaluation Group.

Chaturvedi, L., and J. K. Channell. 1985. *The Rustler Formation as a Transport Medium for Contaminated Groundwater*. EEG 32. New Mexico Environmental Evaluation Group.

Clayton, R. N., I. Friedman, D. L. Graf, T. K. Mayeda, W. F. Meents, and N. F. Shimp, 1966. "The Origin of Saline Formation Waters, I. Isotopic Composition." *Journal of Geophysical Research*, Vol. 71:3869-3882.

Clayton, R. N., B. F. Jones, and R. A. Berner. 1968. "Isotope Studies of Dolomite Formation Under Sedimentary Conditions." *Geochemica et Cosmochimica Acta*, Vol. 32:415-432.

Cooper, J. B., and V. M. Glanzman. 1971. *Geohydrology of Project Gnome Site, Eddy County, New Mexico*. Paper 712-A. Denver, CO: US Geological Survey.

Craig, H. 1961. "Isotopic Variations in Meteoric Waters." *Science*, Vol. 133:1702-1703.

Craig, H., L. I. Gordon, and Y. Horibe. 1963. "Isotopic Exchange Effects in the Evaporation of Water, I. Low-temperature Experimental Results." *Journal of Geophysical Research*, Vol. 68:5079-5087.

Epstein, S., R. P. Sharp, and A. J. Gow. 1965. "Six-Year Record of Oxygen and Hydrogen Isotope Variations in South Pole Firn." *Journal of Geophysical Research*, Vol. 70:1809-1814.

Epstein, S., R. P. Sharp, and A. J. Gow. 1970. "Antarctic Ice Sheet: Stable Isotope Analyses of Byrd Station Cores and Interhemispheric Climatic Implications." *Science*, Vol. 168:1570-1572.

Epstein, S., and H. P. Taylor, Jr. 1970. "The Concentration and Isotopic Composition of Hydrogen, Carbon and Silicon in Apollo 11 Lunar Rocks and Minerals." *Proceedings of the Apollo 11 Lunar Science Conference,* Vol. 2:1085-1096.

Evans, G. V., R. L. Otlet, R. A. Downing, R. A. Monkhouse, and G. Rae. 1979. "Some Problems in the Interpretation of Isotope Measurements in United Kingdom Aquifers." *Proceedings of the International Symposium on Isotope Hydrology*. Vienna: International Atomic Energy Agency.

Fontes, J. C., and J. M. Garnier. 1979. "Determination of the Initial C-14 Activity of the Total Dissolved Carbon: A Review of the Existing Models and a New Approach." *Water Resources Research*, Vol. 15:399-413.

Fontes, J. C., and R. Gonfiantini. 1967. "Fractionement Isotopique de L'hydrogène dans L'eau de Cristallisation du Gypse." *C. R. Acad. So. Paris, Ser D.*, Vol. 265:4-6.

Friedman, I., A. C. Redfield, B. Schoen, and J. Harris. 1964. "The Variation of the Deuterium Content of Natural Waters in the Hydrologic Cycle." *Reviews of Geophysics*, Vol. 2, No.1:177-224.

Gat, J. R., and A. Issar. 1974. "Desert Isotope Hydrology: Water Sources of the Sinai Desert." *Geochimica et Cosmochimica Acta*, Vol. 38:1117-1131.

Hale, W. E., L. S. Hughes, and E. R. Cox. 1954. *Possible Improvement of Quality of Water of the Pecos River by Diversion of Brine at Malaga Bend, Eddy County, New Mexico*. Pecos River Commission, New Mexico and Texas.

Hunter, R. L. 1985. *A Regional Water Balance for the Waste Isolation Pilot Plant (WIPP) Site and Surrounding Area*. SAND84-2233. Albuquerque, NM: Sandia National Laboratories.

Isaacson, R. E., L. E. Brownell, R. W. Nelson, and E. L. Roetman. 1974. "Soil-Moisture Transport in Arid Site Vadose Zones." *Proceedings of the International Symposium on Isotope Hydrology*: 97-114.

Kronfeld, J., E. Gradsztajn, and A. Yaniv. 1979. "A Flow Pattern Deduced from Uranium Disequilibrium Studies for the Cenomanian Carbonate Aquifer of the Beersheva Region, Israel." *Journal of Hydrology*, Vol. 44:305-310.

Lambert, S. J. 1978. "Geochemistry of Delaware Basin Groundwaters." *Geology and Mineral Deposits of Ochoan Rocks in Delaware Basin and Adjacent Areas*. G. S. Austin, ed. Circular 159:33-38. Socorro, NM: New Mexico Bureau of Mines and Mineral Resources.

Lambert, S. J. 1983. *Dissolution of Evaporites in and Around the Delaware Basin, Southeastern New Mexico and West Texas*. SAND82-0461. Albuquerque, NM: Sandia National Laboratories.

Lambert, S. J. 1987. *Feasibility Study: Applicability of Geochronologic Methods Involving Radiocarbon and Other Nuclides to the Groundwater Hydrology of the Rustler Formation*. SAND86-1054. Albuquerque, NM: Sandia National Laboratories.

Lambert, S. J., and J. A. Carter. 1987. *Uranium-Isotope Systematics in Groundwaters of the Rustler Formation, Northern Delaware Basin, Southeastern New Mexico*. SAND87-0388. Albuquerque, NM: Sandia National Laboratories.

Lambert, S. J., and D. M. Harvey. 1987. *Stable-Isotope Geochemistry of Groundwaters in the Delaware Basin of Southeastern New Mexico*. SAND87-0138. Albuquerque, NM: Sandia National Laboratories.

Lambert, S. J., and K. L. Robinson. 1984. *Field Geochemical Studies of Groundwaters in Nash Draw, Southeastern New Mexico*. SAND83-1122. Albuquerque, NM: Sandia National Laboratories.

LaVenue, A. M., A. Haug, and V. A. Kelley. 1988. *Numerical Simulation of Ground-water Flow in the Culebra Dolomite at the Waste Isolation Pilot Plant (WIPP) Site*. SAND88-7002. Albuquerque, NM: Sandia National Laboratories.

Mercer, J. W. 1983. *Geohydrology of the Proposed Waste Isolation Pilot Plant Site, Los Medaños Area, Southeastern New Mexico*. Water Resources Investigation Report 83-4016. Denver, CO: US Geological Survey.

Mook, W. G. 1976. "The Dissolution-Exchange Model for Dating Groundwater With C-14." *Interpretation of Environmental Isotope and Hydrochemical Data in Groundwater Hydrology*. Vienna: International Atomic Energy Agency.

Nativ, R., and D. A. Smith. 1987. "Hydrogeology and Geochemistry of the Ogallala Aquifer, Southern High Plains." *Journal of Hydrology*, Vol. 91:217-253.

Natrella, M. G. 1963. *Experimental Statistics: National Bureau of Standards Handbook 91*, reprinted October 1966.

Northrup, D. A., and R. N. Clayton. 1966. "Oxygen-Isotope Fractionations in Systems Containing Dolomite." *Journal of Geology*, Vol. 74:174-196.

O'Neil, J. R., R. N. Clayton, and T. K. Mayeda. 1969. "Oxygen Isotope Fractionation in Divalent Metal Carbonates." *Journal of Chemical Physics*, Vol. 51:5547-5558.

Osmond, J. K., and J. B. Cowart. 1976. "The Theory and Uses of Natural Uranium Isotopic Variations in Hydrology." *Atomic Energy Review*, Vol. 14:621-679.

Osterkamp, W. R., and W. W. Wood. 1987. "Playa-Lake Basins on the Southern High Plains of Texas and New Mexico: Part I. Hydrologic, Geomorphic, and Geologic Evidence for Their Development." *Geological Society of America Bulletin*, Vol. 99:215-223.

Pearson, F. J., Jr., C. J. Noronha, and R. W. Andrews. 1983. "Mathematical Modeling of the Distribution of Natural C-14, U-234 and U-238 in a Regional Ground-water System." *Radiocarbon*, Vol. 25 #2:291-300.

Pearson, F. J., Jr., and W. W. Swarzenki. 1974. "C-14 Evidence for the Origin of Arid Region Groundwater, Northeastern Province, Kenya." *Isotope Techniques in Groundwater Hydrology*. Vienna: International Atomic Energy Agency.

Robinson, K. L. 1987. *Analysis of Solutes in Groundwaters From the Rustler Formation at and near the WIPP Site*. SAND86-0917. Albuquerque, NM: Sandia National Laboratories.

Robinson, T. W., and W. B. Lang. 1938. "Geology and Ground-Water Conditions of the Pecos River Valley in the Vicinity of Laguna Grande de la Sal, New Mexico, With Special Reference to the Salt Content of the River Water." *New Mexico State Engineer.*

Snyder, R. P. 1985. *Dissolution of Halite and Gypsum, and Hydration of Anhydrite to Gypsum, Rustler Formation, in the Vicinity of the Waste Isolation Pilot Plant, Southeastern New Mexico*. Open File Report 85-229. Denver, CO: US Geological Survey.

Sofer, Z. 1978. "Isotopic Composition of Hydration Water in Gypsum." *Geochimica et Cosmochimica Acta*, Vol. 42:1141-1149.

Tamers, M. A. 1975. "Validity of Radiocarbon Dates on Groundwater." *Geophysical Survey*, Vol. 2:217-239.

Van Devender, T. R. 1980. "Holocene Plant Remains from Rocky Arroyo and Last Chance Canyon, Eddy County, New Mexico." *The Southwestern Naturalist*, Vol. 25:361-372.

Vogel, J. C. 1970. "Carbon-14 Dating of Groundwater." *Isotope Hydrology*. Vienna: International Atomic Energy Agency.

Wigley, T. M. L., L. N. Plummer, and F. J. Pearson, Jr. 1978. "Mass Transfer and Carbon Isotope Evolution in Natural Water Systems." *Geochimica et Cosmochimica Acta*, Vol. 42:1117-1140.

Wood, W. W., and W. R. Osterkamp. 1987. "Playa-Lake Basins on the Southern High Plains of Texas and New Mexico: Part II. A Hydrologic Model and Mass-Balance Arguments for Their Development." *Geological Society of America Bulletin*, Vol. 99:224-230.

Yapp, C. J. 1985. "D/H Variations of Meteoric Waters in Albuquerque, New Mexico, USA." *Journal of Hydrology*, Vol. 76:63-84.

Zeuner, F. E. 1972. *Dating the Past: An Introduction to Geochronology*. New York: Hafner Publishing Co.

# CHAPTER 6:

# THE REDOX STATE AND THE OCCURRENCE AND INFLUENCE OF ORGANICS IN THE CULEBRA

J. Myers, P. Drez, and P. James
International Technology Corporation

## ABSTRACT

This chapter presents the results of an investigation of the redox state of groundwaters in the Culebra and a discussion of the occurrence and influence of organic compounds in groundwaters in the Culebra.

Four redox couples--arsenic(III)/arsenic(V), iodide/iodate, ammonium/nitrate, and selenium(IV)/selenium(VI)--were analyzed in Culebra samples from 21 wells in the Waste Isolation Pilot Plant (WIPP) region; redox potentials (Eh) were calculated using the analytical results and the Nernst equation. Redox equilibrium or disequilibrium cannot be firmly established for any of the samples. Waters from a group of wells in the southern part of the study area (Engle, H-7B1, H-8B, and H-9B) show a possible range of redox potentials greater than ~350 mV, whereas waters from the remaining wells (except WIPP-25 and WIPP-26) have a possible range of redox potentials less than ~350 mV. Appendix 6A presents additional analyses of redox species, evaluates the redox samples, analytical data, and calculated potentials, and discusses the implications of the evaluations.

Total organic carbon (TOC) and total organic halides (TOX) are routinely analyzed as a part of the Water Quality Sampling Program (WQSP). Results of TOC and TOX determinations in Culebra waters from 23 wells are presented. The potential influence of organic compounds in Culebra groundwaters (whether dissolved, particulate, or adsorbed on minerals) is discussed.

# CONTENTS

# FIGURES



# TABLES

# 6.1 THE REDOX STATE OF GROUNDWATERS IN THE CULEBRA

## 6.1.1 Introduction

### 6.1.1.1 The Importance of Determining the Redox State of Culebra Groundwaters

The solubilities and sorptive behavior of several key elements in transuranic waste, including uranium, neptunium, and plutonium, strongly depend on their valence state and will vary by several orders of magnitude over the range of redox conditions observed in the natural environment. As a general rule, the solubilities of these waste elements are lower in a reducing environment, and reduced species of these elements tend to strongly sorb on mineral surfaces (Jensen, 1982). If accurate redox data are unavailable, then conservative assumptions regarding the redox state of the flow path will have to be made in performance assessment: oxidizing conditions will be assumed to prevail. These assumptions will constrain an assessment of the performance to assume that no precipitation or sorption processes will occur during transport along flow paths to the environment. Although this assumption may be unrealistically conservative, it would be the only defensible one in the absence of data to the contrary.

### 6.1.1.2 History of Redox Investigations in the Culebra

The first attempt to determine the redox state of Culebra groundwaters was the measurement of platinum-electrode potentials in samples withdrawn from wells in the Nash Draw area in 1980 (Lambert and Robinson, 1984).

In 1985, routine measurements of platinum-electrode potentials as well as the analysis of ferrous/ferric iron ratios were incorporated as part of the WQSP. The goal of the WQSP (Colton and Morse, 1985) is to obtain uncontaminated groundwater samples that are representative of downhole conditions. While groundwater is continually pumped from the well, samples (called "serial" samples) are collected periodically, and several parameters

(temperature, density, pH, platinum-electrode potential, chloride, alkalinity, total divalent cations, total iron, and ferrous iron) are measured in a mobile laboratory located at the well. When these parameters stabilize (reach "steady state"), subsequent samples are assumed to be uncontaminated by drilling fluid, well casing, or drill-stem materials. However, the validity of this assumption varies for different parameters; for example, as is discussed below, it is often not valid for iron. Samples (called "final" samples) are then collected and sent to various laboratories for more complete analyses. Analytical results from the WQSP program can be found in the annual water-quality data reports (Uhland and Randall, 1986; Uhland et al., 1987; Randall et al., 1988; Lyon, 1989).

As a part of the WQSP, total and ferrous iron concentrations in serial samples are analyzed spectrophotometrically using the procedures outlined in Colton and Morse (1985). Subsequent geochemical modeling of the data from 17 Culebra samples (collected in 1985 and 1986) showed that the solutions were supersaturated with respect to iron-bearing minerals such as magnetite and hematite. This suggested that most of the iron in the solution was probably in the form of colloids and pseudo-colloids (possibly formed from metastable corrosion products of the steel pipe) and thus was not truly dissolved. Therefore, calculation of the redox state based on these ferrous/ferric ratios would yield meaningless values. In addition, the iron concentrations at some wells were seen to change as the pumping rate changed (Uhland et al., 1987), again implying that the iron concentration is controlled, in at least some cases, by reactions with the well casing or other materials in the well.

The platinum-electrode technique is subject to several interferences and needs to be verified by some independent technique (such as analyses of specific redox couples) before any confidence can be placed in the measured potentials (Lindberg and Runnells, 1984; Stumm and Morgan, 1981; Breck, 1974; Cherry et al., 1979).

At this point in the program, because the platinum-electrode and iron data were not reliable, recommendations were made to the WQSP that additional redox couples be

measured to determine if redox equilibrium exists, and if so, which couples can be used to define the redox state of the groundwater samples. Specific recommendations included analyses of As(III)/As(V), $I^-/IO_3^-$, $NH_4^+/NO_3^-$, and Se(IV)/Se(VI). As work for this chapter began, groundwater samples from 21 of the approximately 30 wells that are part of the WQSP had been analyzed for some or all of these four redox couples.

## 6.1.2 Methods and Data

### 6.1.2.1 Groundwater Sampling and Analysis

The samples for redox-couple analysis were collected as part of the WQSP in accordance with the procedures outlined in Colton and Morse (1985) and Uhland and Randall (1987) from wells shown in Figure 6-1. Samples obtained for redox analysis were collected in 500-mL, teflon-lined, stainless-steel pressure vessels (sample cylinders) that have valves fitted on both ends. After serial-sampling parameters stabilized, the pressure vessel was connected to the sampling line and groundwater was allowed to flow through the vessel. After several liters of groundwater flowed through the vessel, the downstream valve was slowly closed so that pressure increased in the vessel. The upstream valve was then closed, trapping a volume of pressurized groundwater. The vessel was then disconnected from the sampling line and sent to United Nuclear Corporation (UNC) Geotech (formerly Bendix Field Engineering Corporation), the Department of Energy (DOE) facility at Grand Junction, CO, for analysis.

Ideally, pressures would be maintained along the sampling system that are equal to or greater than the downhole pressure, in order to prevent the exsolution of dissolved gases. However, for wells that have low flow rates, a significant pressure gradient must be created by the downhole pump to stimulate flow toward the well, which makes it impossible to maintain nominal hydrostatic pressures. In these cases, the pressures are maintained as high as possible without causing damage to the downhole pump while maintaining a reasonable flow rate.

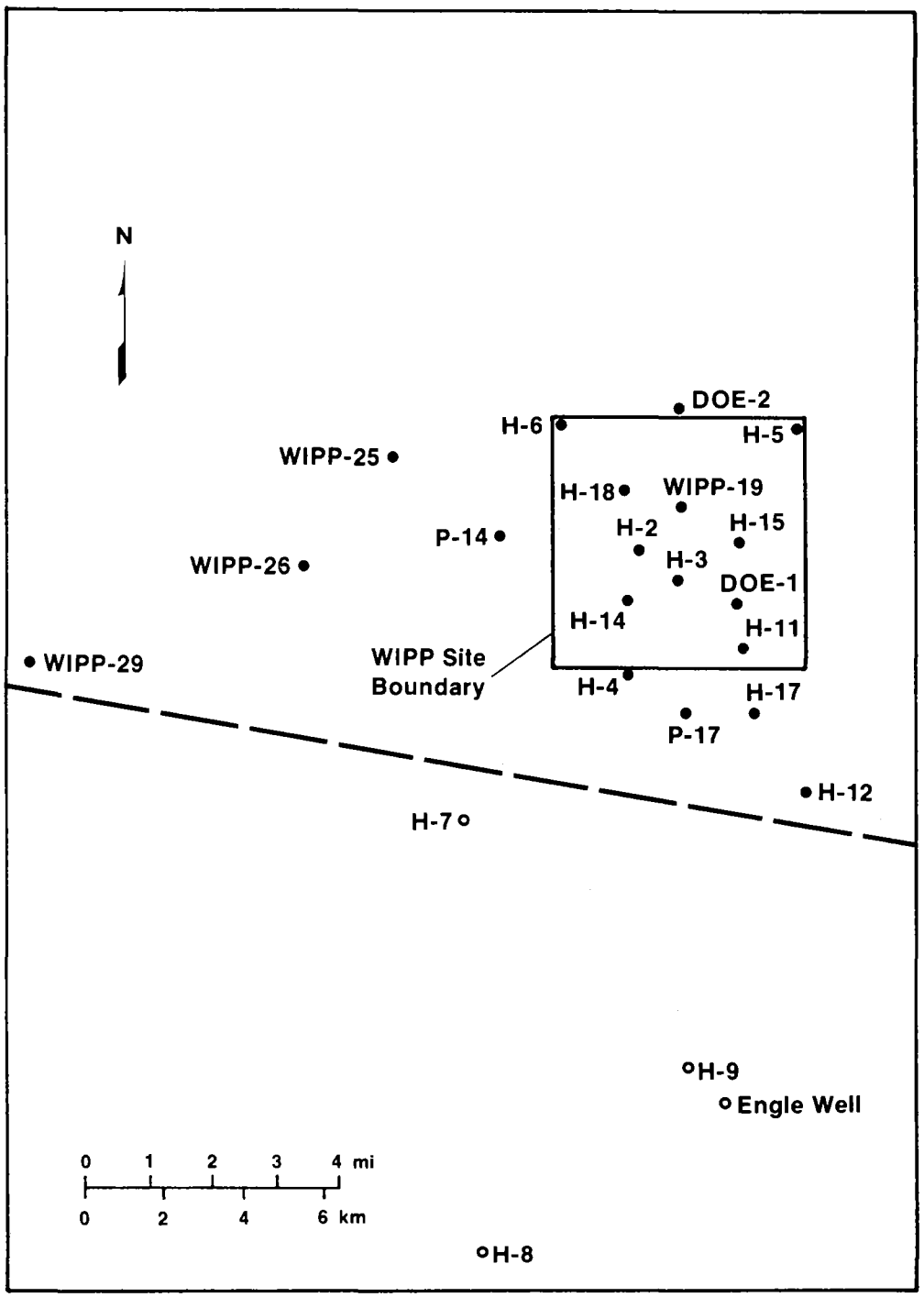


Figure 6-1. Map showing location of wells for which redox and/or organic data for Culebra groundwaters are given in this chapter.

Table 6-1 describes the analytical methods used by UNC Geotech to determine the concentrations of the redox species in the groundwater samples. Concentrations of As(V) and Se(VI) were calculated by difference assuming the following:

$$\text{As(III)} + \text{As(V)} = \text{Total As}$$
$$\text{Se(IV)} + \text{Se(VI)} = \text{Total Se}$$

Also shown in Table 6-1 are the approximate lower limits of detection for the techniques. These detection limits vary as a function of the total dissolved solid (TDS) contents of the samples.

The data used to calculate redox potentials are given in Table 6-2. (A larger data set including more recent results and some data from other sources is given and the data are evaluated in more detail in Appendix 6A.)

Table 6-2 also includes the pH values and activities of water ($a_{H_2O}$) used in the calculations of redox potentials. The pH values are from measurements performed in the field on the last serial sample collected at each well (Uhland and Randall, 1986; Uhland et al., 1987; Randall et al., 1988). The $a_{H_2O}$ values for ten of the groundwater samples were calculated using the geochemical solubility/speciation program EQ3NR (Wolery, 1983) and were based on comprehensive chemical analyses of the groundwaters (Uhland and Randall, 1986; Uhland et al., 1987; Randall et al., 1988). A linear regression of calculated $a_{H_2O}$ values versus measured specific gravity of the groundwater was used to estimate $a_{H_2O}$ values for the remainder of the samples. This empirical approach yielded a correlation coefficient of 0.9973 and produced a residual error of less than one percent in all cases.

## Table 6-1. Analytical Techniques Used to Analyze Redox Species

| Analyte | Technique | Detection Limit |
|---|---|---|
| $NO_3^-$ | Ion Chromatography | 1.0 to 10.0 mg/L |
| $NH_4^+$ | Spectrophotometry | 0.1 to 0.2 mg/L |
| $I^-$ | Polarography | 20 μg/L |
| $IO_3^-$ | Polarography | 0.1 to 20 μg/L |
| Total As | Hydride-Generation Atomic Absorption | 1.0 to 200 μg/L |
| As(III) | Hydride-Generation Atomic Absorption | 0.2 to 1.0 μg/L |
| Total Se | Hydride-Generation Atomic Absorption | 0.1 to 1.0 μg/L |
| Se(IV) | Hydride-Generation Atomic Absorption | 1.0 to 0.5 μg/L |

## Table 6-2. Concentrations of Redox Species in Culebra Groundwaters: Data Used to Calculate Redox Potentials

| Well | Coll. Date | As(tot) (mg/L) | As(III) (mg/L) | Calc'd As(V) (mg/L) | $I^-$ (ug/L) | $IO_3^-$ (ug/L) | $NH_3$ (mg/L) | $NO_3^-$ (mg/L) | Se(tot) (mg/L) | Se(IV) (mg/L) | Calc'd Se(VI) (mg/L) | pH | $a_{H_2O}$ |
|---|---|---|---|---|---|---|---|---|---|---|---|---|---|
| DOE-1 | 07/28/87 | 0.006 | 0.002 | 0.004 | 1910 | <10 | 0.59 | <10 | | | | 7.2 | 0.930 |
| DOE-2 | 08/27/86 | | | | 350 | <10 | | | | | | 6.3 | 0.968 |
| ENGLE | 03/04/85 | | | | | | <0.20 | 2.0 | | | | 7.35 | 1.000 |
| H-3B3 | 05/05/86 | | | | | | 0.33 | <1 | | | | 7.3 | 0.973 |
| H-4B | 11/13/86 | | | | 200 | <10 | 0.47 | <1 | | | | 7.59 | 0.985 |
| H-5B | 05/21/86 | | | | 200 | <10 | 2.25 | <1 | | | | 7.55 | 0.920 |
| H-6B | 07/28/86 | | | | 250 | <10 | 2.70 | <1 | | | | 7.0 | 0.970 |
| H-7B1 | 02/25/87 | | | | 65 | 52 | <0.10 | 3.1 | 0.0095 | 0.0010 | 0.0085 | 7.4 | 1.001 |
| H-8B | 02/11/87 | | | | 247 | 25 | <0.10 | 5.5 | | | | 7.22 | 1.001 |
| H-9B | 01/28/87 | | | | 247 | <10 | <0.10 | 0.50 | 0.018 | 0.0072 | 0.0108 | 7.29 | 1.000 |
| H-11B3 | 06/04/86 | | | | 230 | <10 | 1.90 | <1 | | | | 7.28 | 0.939 |
| H-12 | 01/16/87 | 0.0042 | 0.0012 | 0.0030 | 148 | 14 | 2.20 | <1 | | | | 7.45 | 0.923 |
| H-14 | 05/26/87 | | | | 610 | <10 | 0.25 | <2 | | | | 7.69 | 0.992 |
| H-15 | 05/11/87 | 0.0025 | 0.0010 | 0.0015 | 101 | <10 | 0.86 | <2 | | | | 6.87 | 0.879 |
| H-17 | 10/27/87 | 0.009 | 0.002 | 0.007 | | | 1.5 | <4 | | | | 7.0 | 0.921 |
| H-18 | 11/10/87 | | | | 103 | <20 | 0.16 | <1 | | | | 7.6 | 0.988 |
| P-14 | 06/18/87 | | | | 4940 | 935 | 0.30 | <3 | | | | 6.88 | 0.986 |
| P-17 | 12/18/86 | | | | 210 | <10 | 2.75 | <3 | | | | 7.53 | 0.953 |
| WIPP-19 | 07/14/87 | 0.003 | 0.002 | 0.001 | 2470 | <10 | 2.78 | <10 | | | | 7.01 | 0.945 |
| WIPP-25 | 04/15/87 | | | | 335 | <10 | 0.24 | 12.1 | 0.040 | 0.002 | 0.038 | 7.21 | 0.993 |
| WIPP-26 | 04/01/87 | | | | 62 | <10 | 0.10 | 19.5 | | | | 7.03 | 0.994 |

### 6.1.2.2 The Calculation of Redox Potentials

The Nernst equation provides a method for calculating redox potentials (Eh) from the concentrations of specific redox couples. The equation is usually expressed as:

$$Eh = E^o + \frac{RT}{nF} \ln \frac{a_{ox}}{a_{red}} \qquad \text{[Eqn.1]}$$

where

$$E^o = \frac{-\Delta G_r^o}{nF}$$

R = Universal gas constant,

F = Faraday constant,

T = Temperature,

n = Number of electrons transferred,

$a_i$ = Activity of species i, and

$\Delta G_r^o$ = Free energy of reaction at standard state.

The chemical reactions for the four redox couples and the equations relating the Eh (in volts) to the activities of the couple members, the pH, and the activities of water are listed below. The free energy and critical pH values for the equations were determined from Pourbaix (1974). Temperatures were assumed to be 25°C.

**Arsenic: pH below 7.26**

$$HAsO_2 + 2H_2O = H_2AsO_4^- + 3H^+ + 2e^- \qquad \text{[Rxn. 1]}$$

$$Eh = 0.666 - 0.0887\ pH + 0.0295 \log \frac{a_{As^{5+}}}{a_{As^{3+}} \cdot a_{H_2O}^2} \qquad \text{[Eqn. 2]}$$

**Arsenic: pH above 7.26**

$$HAsO_2 + 2H_2O = HAsO_4^{=} + 4H^+ + 2e^- \quad \text{[Rxn. 2]}$$

$$Eh = 0.881 - 0.1182\,pH + 0.0295 \log \frac{a_{As}^{5+}}{a_{As}^{3+} \cdot a_{H_2O}^{2}} \quad \text{[Eqn. 3]}$$

**Iodine**

$$I^- + 3H_2O = IO_3^- + 6H^+ + 6e^- \quad \text{[Rxn. 3]}$$

$$Eh = 1.085 - 0.0591\,pH + 0.0098 \log \frac{a_{IO_3^-}}{a_{I^-} \cdot a_{H_2O}^{3}} \quad \text{[Eqn. 4]}$$

**Nitrogen**

$$NH_4^+ + 3H_2O = NO_3^- + 10H^+ + 8e^- \quad \text{[Rxn. 4]}$$

$$Eh = 0.8816 - 0.074\,pH + 0.0074 \log \frac{a_{NO_3^-}}{a_{NH_4^+} \cdot a_{H_2O}^{3}} \quad \text{[Eqn. 5]}$$

**Selenium: pH below 6.58**

$$HSeO_3^- + H_2O = SeO_4^{=} + 3H^+ + 2e^- \quad \text{[Rxn. 5]}$$

$$Eh = 1.075 - 0.0886\,pH + 0.0295 \log \frac{a_{Se}^{6+}}{a_{Se}^{4+} \cdot a_{H_2O}} \quad \text{[Eqn. 6]}$$

**Selenium: pH above 6.58**

$$SeO_3^{=} + H_2O = SeO_4^{=} + 2H^+ + 2e^- \quad \text{[Rxn. 6]}$$

$$Eh = 0.880 - 0.0591\ pH + 0.0295 \log \frac{a_{Se^{6+}}}{a_{Se^{4+}} \cdot a_{H_2O}} \qquad \text{[Eqn. 7]}$$

The activity terms in the equations are, in the strict sense, equal to the product of the molality and the activity coefficient. However, because of complications in calculating activities of solutes in high ionic strength groundwaters (ionic strength >1.0 molal), a simplifying assumption that activity coefficients of the solutes (redox-couple members) equal unity, and hence that activity equals molality, is made. This assumption is justified for the following reasons:

- Since Eh is proportional to the log of the ratios of activities of the oxidized and reduced species, the activity coefficients will tend to cancel if their values are similar.

- The calculated Eh is relatively insensitive to changes in activity coefficients (see Section 6.1.2.3).

In contrast, the activity coefficients of water were not assumed to be unity. Rather, calculated or estimated activities of water ($a_{H_2O}$) were used in solving the equations to partially account for the nonideal behavior of groundwaters at high ionic strengths.

### 6.1.2.3 Effects of Uncertainties in Chemical Analyses and pH Data

A sensitivity analysis was performed to determine the effects of uncertainties in the chemical analyses on the computed redox potential, Eh. Equation 2 was solved for several ratios of As(III)/As(V); the ratio of As(III)/As(V) was varied over several orders of magnitude, while maintaining a constant total As concentration of $5.61 \times 10^{-8}$ moles per liter, a pH of 7.15, and a water activity of 0.9206, which represents groundwater from the Culebra at well H-12. The results, shown in Table 6-3, indicate that varying the As(III)/As(V) ratio by an order of magnitude (which far exceeds the expected uncertainties in the analytical data or

## Table 6-3. Effect of As(III)/As(V) Ratio on Calculated Eh

| Ratio As(III)/As(V) | Log Ratio As(III)/As(V) | Calculated[1] Eh (mV) |
|---|---|---|
| 100 | 2 | -25 |
| 10 | 1 | 4 |
| 1 | 0 | 34 |
| 0.1 | -1 | 63 |
| 0.01 | -2 | 93 |

1. Eh values were calculated using Equation 2. Other parameters, which represent Culebra groundwater at well H-12, were: pH = 7.15; $a_{H_2O}$ = 0.9206; Total As = $5.61 \times 10^{-8}$ M.

the uncertainties from assuming the activity coefficients equal unity) results in an average change in Eh of only 30 mV.

The Se couple will show the same degree of sensitivity to analytical uncertainties since the coefficient in the log of the activity ratio term has the same value (0.0295; see Equations 6 and 7). The coefficients for the I and N couples (0.0098 and 0.0074; see Equations 4 and 5) are considerably lower than those of the As and Se couples; thus the I and N couples are even less sensitive to analytical uncertainties.

This demonstrates that the calculated couple-specific potentials are relatively insensitive to reasonable uncertainties in the chemical analyses of the specific redox couples. It also demonstrates that the simplifying assumption that activity coefficients are equal to unity does not introduce large errors in calculated Eh values.

An examination of the Nernst equations derived for each of the four redox couples gives a direct indication of the sensitivity of Eh to uncertainties in the measured pH values. At 25°C the reaction most sensitive to pH is As(III)/As(V) (above pH = 7.26) which shows a decrease of 12 mV in response to an increase of 0.1 pH unit (see Equation 3). The reaction

least sensitive to pH is $NH_4^+/NO_3^-$, which shows a decrease of 7 mV in response to an increase of 0.1 pH unit (see Equation 5). Thus, small uncertainties in the measured pH (caused by degassing of $CO_2$, unknown junction potentials, etc.) should not cause large errors in the calculated Eh.

### 6.1.3 Results of Calculations of Redox Potentials

Equations 2 through 7 and the data given in Table 6-2 were used to calculate redox potentials for Culebra groundwaters from 21 locations. The results of the calculations are shown in Table 6-4. (Table 6-4 also shows the platinum-electrode potentials, relative to the standard hydrogen electrode, measured in the field. The data, however, are not considered reliable and are shown for comparison only.)

In most cases, the concentration of one of the members of a redox couple was below the lower limit of detection; however, there are some samples in which both members of the couple were detected (measured or calculated by difference). Where absolute concentrations exist for both members of a couple, a couple-specific redox potential was calculated. If one member of the couple was below the lower limit of detection, the analyses were used to set an upper or lower bound on the potential. For instance, if nitrate but no ammonium was detected, the Eh calculated using the lower limit of detection for ammonium represents a lower bound on the couple-specific potential. Or, if iodide but no iodate was detected, the Eh calculated using the lower limit of detection for iodate represents an upper bound on the couple-specific potential. (If both members of the redox couple were below the lower limit of detection, the data are not given in Table 6-2, and no Eh value was calculated. Similarly, if As(III) or Se(IV) was not detected, the Eh for the arsenic or selenium couple was not calculated.)

### 6.1.4 Discussion and Conclusions

Redox equilibrium can be thought of as a condition where all of the redox-active solutes are distributed consistently with respect to some master controlling redox potential. Under

## Table 6-4. Calculated Redox Potentials[1]

| Well | Date | N | I | As | Se | Pt Elec.[2] |
|---|---|---|---|---|---|---|
| DOE-1 | 07/28/87 | <355 | <637 | 38 | | 130 |
| DOE-2 | 08/27/86 | | <697 | | | 340 |
| ENGLE | 03/04/85 | >341 | | | | 150 |
| H-3B3 | 05/05/86 | <332 | | | | 160 |
| H-4B | 11/13/86 | <319 | <623 | | | 130 |
| H-5B | 05/21/86 | <317 | <626 | | | 50 |
| H-6B | 07/28/86 | <357 | <684 | | | 120 |
| H-7B1 | 02/25/87 | >341 | 645 | | 470 | 250 |
| H-8B | 02/11/87 | >356 | 647 | | | 220 |
| H-9B | 01/28/87 | >343 | <639 | | 454 | 250 |
| H-11B3 | 06/04/86 | <337 | <641 | | | 120 |
| H-12 | 01/16/87 | <325 | 634 | 14 | | 70 |
| H-14 | 05/26/87 | <316 | <612 | | | 70 |
| H-15 | 05/11/87 | <373 | <669 | 65 | | 140 |
| H-17 | 10/27/87 | <364 | | 63 | | |
| H-18 | 11/10/87 | <321 | <628 | | | |
| P-14 | 06/18/87 | <376 | 670 | | | 40 |
| P-17 | 12/18/86 | <321 | <628 | | | 80 |
| WIPP-19 | 07/14/87 | <364 | <647 | 37 | | 150 |
| WIPP-25 | 04/15/87 | 357 | <643 | | 492 | 200 |
| WIPP-26 | 04/01/87 | 374 | <660 | | | 320 |

1. Redox potentials calculated as explained in Section 6.1.2. "N" is the $NH_4^+/NO_3^-$ couple; "I" is the $I^-/IO_3^-$ couple; "As" is the As(III)/As(V) couple; "Se" is the Se(IV)/Se(VI) couple. "<" indicates an upper bound; ">" indicates a lower bound.

2. Pt Elec. = Field measurement of the platinum-electrode potential (in mV relative to standard hydrogen electrode). The data are not considered reliable and are shown for comparison only.

this condition, analysis of any redox couple should yield the same potential. The currently available redox-couple data for the Culebra show no evidence that redox equilibrium exists in these groundwater samples. And even if redox equilibrium among several redox couples could be demonstrated, it would still not be valid to assume that a contaminant such as uranium introduced into this environment would conform to a master redox potential unless the kinetics of redox reactions for uranium were known to be rapid.

Even though a quantitative redox potential cannot be assigned to the Culebra groundwater from each well, qualitative arguments can be made about groups of wells that show similar redox characteristics. These characteristics are discussed below, after a brief discussion of each of the four redox couples employed in this investigation.

### 6.1.4.1 The Redox Behaviors Of Arsenic, Iodine, Nitrogen, and Selenium

Arsenic

From thermodynamic data it can be shown that the pentavalent arsenate species $H_2AsO_4^-$ and $HAsO_4^=$ are the stable forms at equilibrium in an oxidizing environment over the pH range of most natural waters. The species $H_2AsO_4^-$ predominates below a pH of 7.26 and $HAsO_4^=$ above (Hem, 1970). In a reducing environment, however, the trivalent form $HAsO_2$(aq) is stable. At a pH of 7.0, the Eh at which the change from As(III) to As(V) occurs is approximately 50 mV (Pourbaix, 1974). An experimental investigation on the use of arsenic as a groundwater redox indicator (Cherry et al., 1979) concluded that the kinetics of redox equilibria in the As(III)/As(V) system is ideal for this purpose. The investigation concluded that equilibration occurs on a time scale in the range of months to years and that it should be possible to sample groundwater, return the sample preserved with acid to the laboratory, and carry out the analysis without fear of perturbing the As(III)/As(V) ratio, providing the entire operation is carried out within a week or two.

Iodine

The two most common forms of iodine found in the natural environment are iodide ($I^-$) and iodate ($IO_3^-$). The species iodine ($I_2$) and tri-iodide ($I^{-3}$) are only stable in the presence of high total iodine concentrations (tens of mg/L), which are not usually found in the natural environment, except in some oil field brines and geothermal springs. The use of the iodide/iodate redox system as an indicator of redox conditions in seawater was first proposed by Liss et al. (1973). As is also the case with the nitrogen system (discussed below), it is difficult to generalize about the redox kinetics of chemical systems strongly

affected by biochemical reactions. However, the transfer of six electrons required for the oxidation of $I^-$ to $IO_3^-$ can in general occur faster than the eight electron transfer required for the oxidation of sulfide to sulfate, but will occur much slower than the oxidation of ferrous to ferric iron.

Nitrogen

The oxidation and reduction of aqueous nitrogen species are closely tied to biologic activity, and both the paths followed and the end products of such reactions depend very strongly on kinds and numbers of biota present (Hem, 1970). This dependence on biologic activity makes it difficult to generalize on the kinetics of redox reactions in this system. The nitrite ion ($NO_2^-$) has a redox state intermediate between nitrate and ammonium. However, its stability field in Eh-pH space is extremely narrow and is bounded by parallel reactions for nitrate/nitrite and nitrite/ammonium (Pourbaix, 1974). This limited field allows the consideration of a nitrate/ammonium redox couple despite the theoretical presence of an intermediate species. The pH at which the transformation of aqueous ammonia to ammonium ion is half complete is about 9.24 (Sillen and Martell, 1964), well above the pH values observed in the Culebra. It is assumed for the purpose of this investigation that the significant aqueous nitrogen species are nitrate and ammonium and that their ratio can be used to calculate a couple-specific redox potential.

Selenium

The redox chemistry of selenium is quite complex due to the occurrence of four valence states observed in the natural environment. Selenide (-2 valence) is stable at very low redox potentials; the elemental form is stable in a narrow field at a potential around zero volts; selenite (+4 valence) is stable above zero volts; and selenate (+6 valence) is stable at conditions close to air saturation. The hexavalent species anticipated in groundwaters under oxidizing conditions (close to air saturation) is $SeO_4^=$. At slightly reducing conditions the anticipated tetravalent species are $HSeO_3^-$ at pH below 6.58, and $SeO_3^=$ at pH above 6.58

(Pourbaix, 1974). The reversibility of selenium redox reactions in complex groundwater systems is poorly understood.

### 6.1.4.2 Redox Conditions in Culebra Groundwaters

The following discussion assumes that the data used to calculate the redox potentials were valid; that is, that the samples were representative of unperturbed downhole conditions when they were collected; that the redox couples were not perturbed by the methods of collection, storage, shipment to the laboratory, or analysis; and that the analyses were appropriately accurate. This assumption was reasonable at the time this work (the redox-potential calculations) was done because the small amount of data then available offered no indications to the contrary. But as is discussed in Appendix 6A, a larger database and further evaluation of the data now indicate that at least some of the data may be questionable. We believe, nonetheless, that the following discussion offers some useful insights and hypotheses.

Ranges of Redox Potentials

The results of the redox calculations are given in Table 6-4 and are shown in Figure 6-2. On the figure, the shaded areas show the possible range of Eh values that are consistent with the calculated values or limits. The platinum-electrode data are also shown, but are not considered reliable and are shown solely for comparison with the calculated redox potentials.

The following assumptions are used to define the length of the ranges of Eh values (that is, the shaded areas) shown in Figure 6-2. The potentials calculated as upper and lower limits are assumed to bound the range of possible Eh values, but the actual points (values determined from analyses where concentrations were obtained for both members of a couple) are assumed to have some unspecified uncertainty. Thus, the ranges are primarily bounded by the limits, and the actual points are consistent with the range if they lie within it. For

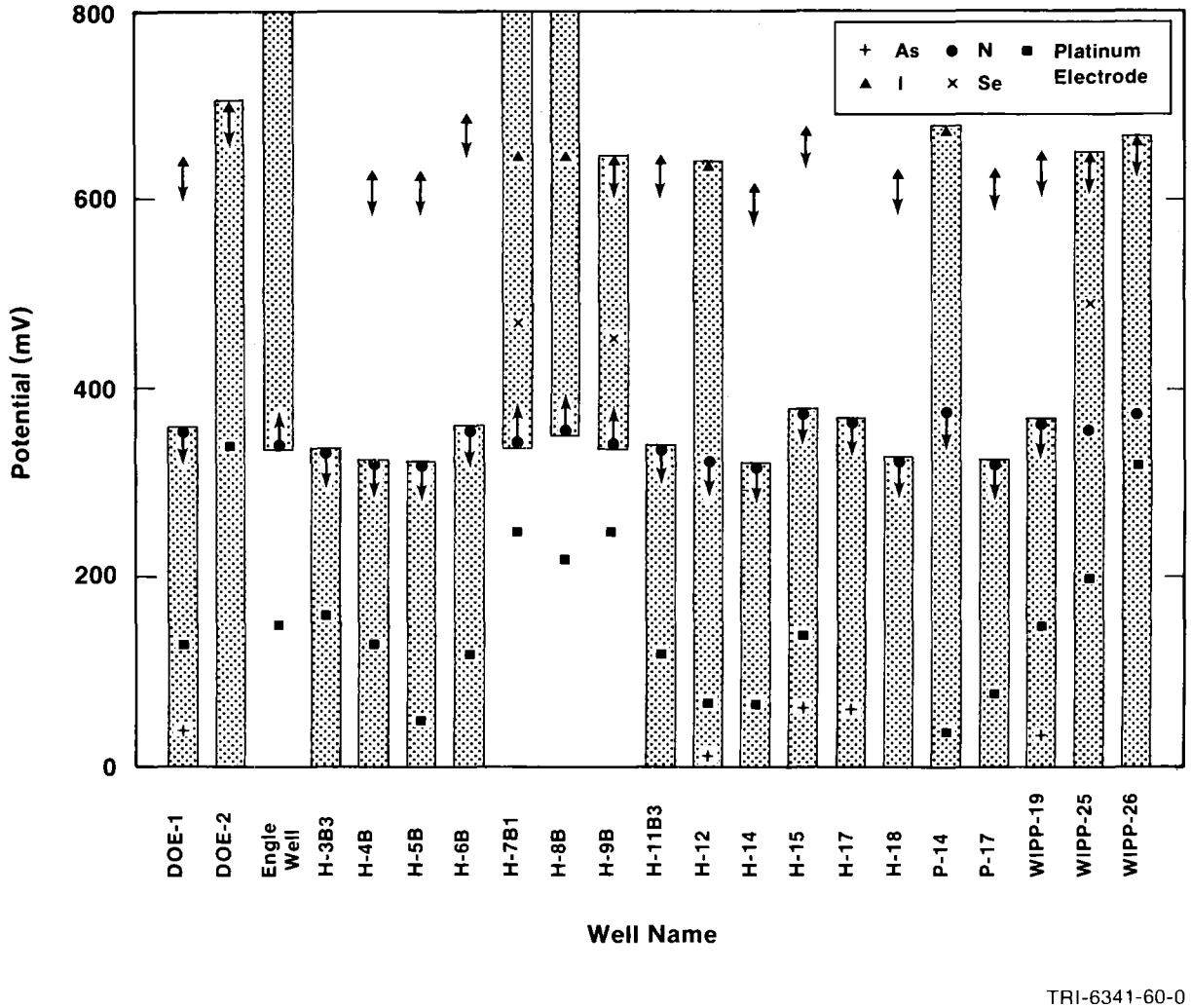


Figure 6-2. Calculated redox potentials in Culebra groundwaters.

most of these samples, the upper or lower bound is defined by the N couple, and the I, Se, and As couples provide either a consistency check or an additional bound to the range. For example, the redox state of H-7B1 is assumed to be above 341 mV because of the absence of detectable ammonium. The actual points defined by the Se and I couples provide confirmation of the range because the values lie within the range bounded by the N couple.

Spatial Distribution of Redox Characteristics

As can be seen on Figure 6-2, the wells fall into four groups. The nitrogen couple distinguishes three groups, one of which is then further divided based on the iodine couple.

The waters in one group, from Engle, H-7B1, H-8B, and H-9B, all contained measurable amounts of nitrate, whereas ammonium was below the detection level. The nitrogen couple thus gives a lower bound of ~350 mV for the ranges for these samples. These wells will be called the "oxidized" group for purposes of this discussion.

The waters from the group consisting of WIPP-25 and WIPP-26 contained measurable amounts of both nitrate and ammonium. The ranges are defined, however, by the iodine couple, with measurable iodide, but no measurable iodate.

The waters from the other wells contained measurable ammonium, whereas nitrate was below the detection level. A subgroup consisting of H-12 and P-14 has iodine data that are apparently inconsistent with the other couples. This inconsistency could be caused by a condition of redox disequilibrium; however, as is discussed in Appendix 6A, the iodate data are probably invalid. The remaining wells have redox values below ~350 mV, based on the nitrogen couple. These wells will be called "reduced" group for purposes of this discussion.

The locations of the wells are shown in Figure 6-1. In Figure 6-1, the northwest-southeast trending line separates the oxidized group (shown as open circles) from the reduced group (shown as closed circles). The oxidized groundwaters have additional characteristics in

common that distinguish them from the other groundwaters. These characteristics include low specific gravity, low TDS, and low sodium and chloride concentrations (Uhland and Randall, 1986; Uhland et al., 1987; Randall et al., 1988).

The oxidized nature of the groundwaters in the wells in the southern area of the region, as well as the radically lower TDS, could suggest either a hydrologic divide separating these two populations of wells, or a region of recharge in the southern area providing a source of air-saturated, low-TDS groundwater to the Culebra. This recharge could result from downward seepage from the overlying Tamarisk or Magenta units or perhaps even from the surface. At H-7, the Culebra is encountered at 232 feet below ground surface; whereas in the northern wells, the Culebra is found at 500 to 900 feet. Such recharge may be currently active or may have ceased at the close of the Pleistocene when rainfall was considerably higher than it is currently.

# 6.2 THE OCCURRENCE AND INFLUENCE OF ORGANICS IN GROUNDWATERS IN THE CULEBRA

## 6.2.1 Naturally Occurring and Nonhalogenated Organic Compounds

### 6.2.1.1 Introduction

Actinides and other metals can form complexes with three kinds of organic matter: dissolved organic matter, suspended organic matter, and organic matter adsorbed on sediment.

Metal ions can complex with all three types of organic matter because they all have similar functional groups. The following functional groups are arranged in order of their affinities for metal ions (Charberek and Martell, 1959):

$$-O^- > -NH_2 > -N=N > -COO^- > -O^- > -C=O \ .$$

Most metals can accept more than one ligand (pair of electrons) and form ring structures

(chelation). Naturally occurring organics (e.g., humic and fulvic acids) and many man-made chelating agents (e.g., EDTA) form very stable complexes with many metals, including actinides.

Previous work on the Culebra has not involved characterization of the suspended or sorbed organics on the host rock. The following sections describe the initial analyses to characterize the total organic carbon (TOC) in groundwaters from the Culebra.

#### 6.2.1.2 Sample Collection Procedure

As a part of the Water Quality Sampling Program (WQSP), TOC is routinely analyzed in Culebra groundwater samples that are collected after serial sampling. The samples are collected in amber glass bottles to prevent possible contamination from plastic bottles, acidified with concentrated $H_2SO_4$ to a pH <2, and cooled to 4°C during shipment and storage to minimize bacterial activity and oxidation of the organics. Analyses are done by the International Technologies laboratory (IT Analytical Services, Murraysville, PA).

#### 6.2.1.3 Analytical Procedure

Samples are analyzed by Method 9060 (US EPA, 1986). The method uses catalytic combustion or wet chemical oxidation of the organic carbonaceous material to carbon dioxide ($CO_2$). The $CO_2$ is then measured by an infrared detector.

The method is applicable for quantitative analysis of TOC in groundwater, surface and saline waters, and domestic and industrial wastes (US EPA, 1986). However, the American Society for Testing and Materials (ASTM, 1985) indicates that the method is applicable to waters that range from 2 to 20,000 mg/L TDS. At higher concentrations, the wet chemical oxidation procedure is subject to interferences due to the oxidation of other ions in solution (particularly Cl), thereby exhausting the oxidant necessary for the organics. Addition of mercuric nitrate can minimize this effect (ASTM, 1985). Examination of spike recoveries for several Culebra wells with varying TDS indicates that this is not a problem with the present analyses.

The forms of carbon that can be measured by Method 9060 are (US EPA, 1986):

- Soluble, nonvolatile organic carbon (e.g., natural sugars).
- Soluble, volatile organic carbon (e.g., mercaptans, alkanes, low molecular weight alcohols).
- Insoluble, partially volatile carbon (e.g., low molecular weight oils).
- Insoluble, particulate carbonaceous materials (e.g., cellulose fibers).
- Soluble or insoluble carbonaceous materials adsorbed or entrapped on insoluble inorganic suspended matter (e.g., oily matter adsorbed on silt particles).

#### 6.2.1.4 Analytical Results

The TOC data are included in the WQSP annual reports (Uhland and Randall, 1986; Uhland et al., 1987; Randall et al., 1988; and Lyon, 1989) and are given in Table 6-5. The values for TOC range from <1 to 7 mg/L, excluding two higher values that appear to be outliers. Values of TOC at two Culebra locations, H-8B and H-12, are 14 mg/L and 15 mg/L, respectively--at least twice as high as any other Culebra values. These values are probably outliers, perhaps due to contamination (for example, from drilling fluids or additives). Additional evidence that these two values may be outliers is that values of <1 mg/L have been measured in samples from the same wells during different sampling rounds (Table 6-5).

## Table 6-5. Total Organic Carbon (TOC), Total Organic Halide (TOX), and Chloride Concentrations in Culebra Groundwaters

| Well | Avg $Cl^-$ (mg/L) | TOC (mg/L) | TOX (mg/L) | Sample Collection Date |
|---|---|---|---|---|
| DOE-1[1] | 75,000 | <1 | 0.84 | 04/25/85 |
| | | <1 | 2.3 | 07/03/86 |
| | | 1, 1 | 9.7 | 07/28/87 |
| DOE-2[1] | 33,000 | 1 | -- | 03/12/85 |
| | | 5 | 0.61 | 08/27/86 |
| | | 1, <1 | 2.1, 1.9 | 05/19/88 |
| ENGLE | 230 | 2 | <0.1 | 03/04/85 |
| H-2A | 5,300 | 7 | 0.14 | 04/21/86 |
| | | 5, 5 | <0.05, <0.05 | 08/12/87 |
| H-3B3[1] | 29,000 | 2 | 0.3 | 02/04/85 |
| | | 2 | 0.42 | 05/05/86 |
| | | <1, <1 | 1.9, 1.3 | 08/24/87 |
| H-4B | 7,700 | 3 | 0.46 | 07/20/85 |
| | | 3 | 0.09 | 11/13/86 |
| | | 5, 4 | 0.44, 0.83 | 09/25/87 |
| H-5B[1] | 87,000 | <1, <1 | 1.7 | 08/27/85 |
| | | 2 | 1.6 | 05/21/86 |
| | | 4, 3 | 8.2, 7.0 | 02/24/88 |
| H-6B[1] | 33,000 | <1 | 0.97 | 09/15/85 |
| | | <1 | 0.92 | 07/28/86 |
| | | 6, 4 | 2.0, 3.0 | 11/16/87 |
| H-7B1 | 320 | <1 | 0.21 | 03/27/86 |
| | | <1, 1 | <0.05, <0.05 | 02/25/87 |
| | | <1, <1 | <0.05, <0.05 | 04/25/88 |
| H-8B | 32 | 14 | <0.05 | 01/22/86 |
| | | <1 | <0.05 | 02/11/87 |
| | | <1, <1 | <0.05, <0.05 | 06/08/88 |
| H-9B | 190 | 2 | 0.22 | 11/14/85 |
| | | 3 | <0.05 | 01/28/87 |
| | | <1, <1 | <0.05, <0.05 | 06/21/88 |

## Table 6-5. Total Organic Carbon (TOC), Total Organic Halide (TOX), and Chloride Concentrations in Culebra Groundwaters (Continued)

| Well | Avg $Cl^-$ (mg/L) | TOC (mg/L) | TOX (mg/L) | Sample Collection Date |
|---|---|---|---|---|
| H-11B3[1] | 66,000 | 2 | 1.5 | 06/04/85 |
| | | <1 | 0.88 | 06/04/86 |
| | | 2, <1 | 11, 15 | 09/15/87 |
| H-12[1] | 80,000 | <1 | 1.4 | 08/09/85 |
| | | 15 | 0.18 | 01/16/87 |
| | | <1, <1 | 1.0, 0.72 | 12/14/88 |
| H-14 | 8,500 | 1, <1 | 0.08 | 05/26/87 |
| | | 2, 2 | 1.2, 0.98 | 01/27/88 |
| H-15[1] | 130,000 | 1, 2 | 8.1, 6.7 | 05/11/87 |
| | | 2, 1 | 2.5, 2.8 | 01/13/88 |
| | | <1, <1 | 1.3, 1.1 | 11/07/88 |
| H-17[1] | 88,000 | 1, 1 | 6.5, 7.8 | 10/27/87 |
| H-18 | 12,000 | 1, 1 | 0.35, 0.46 | 11/10/87 |
| | | <1, <1 | <0.05, <0.05 | 04/07/88 |
| P-14 | 14,000 | 2 | 0.76 | 02/27/86 |
| | | 1, 2 | 1.0, 2.0 | 06/18/87 |
| | | 2, 1 | 0.25, 0.41 | 03/16/88 |
| P-17[1] | 49,000 | 2 | 0.23 | 03/17/86 |
| | | <1 | 1.8 | 12/18/86 |
| | | 1, 1 | 2.1, 2.9 | 10/21/87 |
| WIPP-19 | 52,000 | 7, 7 | 0.79, 1.1 | 07/14/87 |
| | | 7, 7 | 1.1, 1.6 | 02/12/88 |
| | | 5, 5 | 1.6, 4.8 | 08/29/88 |
| WIPP-25 | 5,700 | 2 | 0.38 | 02/12/86 |
| | | 4, 4 | <0.05, <0.05 | 04/15/87 |
| | | <1, <1 | <0.05, <0.05 | 03/28/88 |
| WIPP-26 | 7,100 | <1 | 0.07 | 11/25/85 |
| | | 2, 2 | <0.05, 0.08 | 04/01/87 |
| | | <1, <1 | <0.05, <0.05 | 04/14/88 |
| WIPP-29[1] | 160,000 | <1 | 0.54 | 12/14/85 |
| | | 2, 3 | 2.8 | 03/11/87 |

1. Inorganic-halide/organic-halide ratios >20,000.

The concentration range for TOC in the Culebra groundwaters is similar to the range of values (0.2 to 15 mg/L) found by Leenheer et al. (1974) for 100 groundwater samples in 27 states. There does not appear to be any correlation between TOC and chloride concentration (Table 6-5).

## 6.2.2 Halogenated Organic Compounds

### 6.2.2.1 Sample Collection Procedure

After serial sampling, samples for analysis of TOX are collected in amber glass bottles to prevent possible contamination from plastic bottles, acidified with concentrated $H_2SO_4$ to a pH <2, and cooled to 4°C during shipment and storage to minimize bacterial activity and oxidation of the organics. Analyses are done by the IT laboratory.

### 6.2.2.2 Analytical Procedure

Samples were analyzed by Method 9020 (US EPA, 1986). This method is applicable for determination of TOX in drinking and groundwaters when the inorganic-halide concentration does not exceed the organic-halide concentration by more than 20,000 times (U.S. EPA, 1986). Method 9020 detects all organic halides containing chlorine, bromine, and iodine that are absorbed by granular activated carbon under the conditions of the method. Fluorine-containing species are not determined by this method. This method will not measure TOX of compounds adsorbed to undissolved solids (US EPA, 1986). Samples with ratios of inorganic-halide/organic-halide <20,000 can be analyzed by this technique if the granular activated carbon is backwashed to remove absorbed halides (APHA et al., 1985).

### 6.2.2.3 Analytical Results

The TOX data are included in the WQSP annual reports (Uhland and Randall, 1986; Uhland et al., 1987; Randall et al., 1988; and Lyon, 1989) and are given in Table 6-5; the average chloride concentrations for each location are also included in Table 6-5.

The data in Table 6-5 demonstrate a slight positive relationship between TOX and chloride content, possibly due to an analytical interference. In addition, all TOX values are suspect when the inorganic-halide/organic-halide ratio >20,000. Because of the known interference and apparent positive correlation of TOX and chloride, the halogenated organics will be dismissed from the remainder of the discussion.

### 6.2.3 Potential Influence of Organics in Culebra Groundwaters

Organic compounds in the Culebra groundwater (dissolved, particulate, or adsorbed on minerals) could have an important effect on the redox state of the system. Thurman (1985) reports the following approximate percentages for different classes of organic compounds in groundwaters:

| COMPOUND | PERCENTAGE |
|---|---|
| Humic Acids | 6 |
| Fulvic Acids | 20 |
| Identifiable Compounds (carboxylic acids, amino acids, carbohydrates, volatile hydrocarbons and other simple compounds) | 25 |
| Hydrophilic Acids (fatty, hydroxy and complex polyelectrolytic acids with many hydroxyl and carboxyl functional groups) | 49 |

Reactions between actinides and organic complexes in solution can cause selective reduction of actinides, regardless of the overall redox state of the system (Morse and Choppin, 1986). For example, Pu(VI) could be reduced to Pu(IV) as a result of interaction between Pu(VI) and an organic ligand. Torres and Choppin (1984) have shown that humate complexes of trivalent actinides (e.g., americium) could predominate in naturally occurring groundwaters because the stabilities of metal-humate complexes are much larger than those of hydroxide and carbonate complexes (Table 6-6). These calculations do not consider the competition between americium and other cations in the groundwaters for the humate. In saline groundwaters (such as many of the Culebra samples considered in this

## Table 6-6. Speciation of Americium Complexes in the Presence of Humates

| Solution pH | 6.0[1] | 6.0 | 8.0[1] | 8.0 |
|---|---|---|---|---|
| $CO_3^{2-}$ concentration | $10^{-4}$ M | $10^{-6}$ M | $10^{-4}$ M | $10^{-6}$ M |
| Humate concentration | $10^{-7}$ eq/L | $10^{-7}$ eq/L | $10^{-7}$ eq/L | $10^{-7}$ eq/L |
| Am(humate) | 98.94% | 99.99% | 99.99% | 99.99% |
| $Am(CO_3)^+$ | 0.25% | $10^{-3}$% | $10^{-3}$% | $10^{-3}$% |
| $Am(CO_3)_2^-$ | 0.80% | $<10^{-4}$% | $10^{-3}$% | $<10^{-4}$% |
| Am total hydrolyzed aqueous species | $<10^{-4}$% | $<10^{-4}$% | $<10^{-4}$% | $<10^{-4}$% |

1. Overestimated value of carbonate for comparison.

work), the high concentrations of competing cations such as $Na^+$ and $Ca^{2+}$ may prevent an appreciable fraction of the radionuclides from complexing with the humate.

Sorption of actinide aqueous species on solid surfaces, including colloidal particulates, can be an important process that could have a direct impact on the apparent solubility and mobility in natural systems (Choppin and Allard, 1985). The interaction of trace elements in aqueous solutions with solid surfaces can be attributed to a combination of one or more idealized processes (Benes and Mayer, 1981; OECD/NEA, 1983; Choppin and Allard, 1985):

- Physical adsorption - Attraction of a solute onto a sorbent by non-specific forces. This sorption process is rapid and reversible, with a dependency on concentration in the solution.

- Chemisorption - Chemically-specific interaction between the solute and the sorbent. Most chemisorption interactions occur between anion groups on the

sorbent and the cationic solutes. The reactions are usually slow, partly reversible, and selective. For actinides, $OH^-$, $F^-$, and $PO_4^-$ are examples of sparingly soluble complexes in solution. On solid surfaces, these anionic groups could act as chemisorption agents.

- Electrostatic adsorption - Sorption due to coulombic attraction between charged solute species and sorbent (ion exchange). The sorbent usually carries a net charge, which is dependent on pH and the ionic strength of the solution. This process is usually rapid, partly reversible, and concentration dependent. The properties of the solid (ion exchange) as well as the ionic strength of the solution are very important.

Depending on the relative importance of actinide-organic interactions in the Culebra, naturally occurring organics (dissolved, suspended, or absorbed on particulate surfaces) could either increase or decrease the solubility of actinides if a release occurs. However, if a release of waste does occur, the organics in the waste matrix could be expected to overwhelm any naturally occurring organics due to the high amount of organics present in the waste package (Clements and Kudera, 1985).

# 6.3 REFERENCES

APHA, AWWA, WPCF. 1985. *Standard Methods for the Examination of Water and Wastewater.* 16th ed. Washington, DC: American Public Health Association.

ASTM. 1985. *1985 Annual Book of ASTM Standards.* Section 11, Vol. 11.02. Philadelphia: American Society for Testing and Materials.

Benes, P., and V. Mayer. 1981. *Trace Chemistry of Solutions.* Oxford: Elsevier.

Breck, W. G. 1974. *Redox Levels in the Sea.* Vol. 5. E. D. Goldberg, ed. New York: Wiley Interscience.

Charberek, S., and A. E. Martell. 1959. *Organic Sequestering Agents.* New York: John Wiley and Sons.

Cherry, J. A., A. U. Shaikh, D. E. Tallman, and R. V. Nicholson. 1979. "Arsenic Species as an Indicator of Redox Conditions in Groundwater." *Journal of Hydrology*, Vol. 43:373-392.

Choppin, G. R., and B. Allard. 1985. "Complexes of Actinides with Naturally Occurring Organic Compounds." *Handbook of the Physics and Chemistry of the Actinides.* A. J. Freeman and C. Keller, ed.

Clements, T. L., and D. E. Kudera. 1985. *TRU Waste Sampling Program: Volume 1 - Waste Characterization.* EGG-WM-6503. Idaho Falls, ID: Idaho National Engineering Laboratory.

Colton I. D., and J. G. Morse. 1985. *Water Quality Sampling Plan.* WIPP-DOE-215. Carlsbad, NM: Waste Isolation Pilot Plant Project Office.

Hem, J. D. 1970. *Study and Interpretation of the Chemical Characteristics of Natural Water.* 2nd ed. Water Supply Paper 1473. Albuquerque, NM: US Geological Survey.

Jensen, B. S. 1982. *Migration Phenomena of Radionuclides Into the Geosphere.* New York: Harwood Academic Publishers.

Lambert, S. J., and K. L. Robinson. 1984. *Field Geochemical Studies of Groundwaters in Nash Draw, Southeastern New Mexico.* SAND83-1122. Albuquerque, NM: Sandia National Laboratories.

Leenheer, J. A., R. L. Malcolm, P. W. McKinley, and L. A. Eccles. 1974. "Occurrence of Dissolved Organic Carbon in Selected Groundwater Samples in the United States." *U.S. Geological Survey Journal of Research*, Vol. 2:361-369.

Lindberg, R. D., and D. D. Runnells. 1984. "Ground Water Redox Reactions: An Analysis of Equilibrium State Applied to Eh Measurements and Geochemical Modeling." *Science*, Vol. 225:925-927.

Liss, P. S., J. R. Herring, E. D. Goldberg. 1973. "The Iodide-Iodate System in Seawater as a Possible Measure of Redox Potential." *Nature, Phys. Sci.*, Vol. 242, No. 120:108-109.

Lyon, M. L. 1989. *Annual Water Quality Data Report for the Waste Isolation Pilot Plant.* DOE-WIPP-89-001. Carlsbad, NM: Waste Isolation Pilot Plant Project Office.

Morse, J. W., and G. R. Choppin. 1986. "Laboratory Studies of Plutonium in Marine Systems." *Marine Chemistry*, Vol. 20:73-89.

OECD/NEA. 1983. "Sorption - Modeling and Measurement for Nuclear Waste Disposal Studies." *Proceedings of NEA Workshop, June 1983, Paris, RWM-4.* Paris: Organization for Economic Cooperation and Development, Nuclear Energy Agency.

Pourbaix, M. 1974. *Atlas of Electrochemical Equilibria in Solutions.* Houston: National Association of Corrosion Engineers.

Randall, W. S., M. E. Crawley, and M. L. Lyon. 1988. *Annual Water Quality Data Report.* DOE-WIPP-88-006. Carlsbad, NM: Waste Isolation Pilot Plant Project Office.

Robinson, K. L. 1988. *Analysis of Solutes in Groundwaters from the Rustler Formation at and near the WIPP Site.* SAND86-0917. Albuquerque, NM: Sandia National Laboratories.

Sillen L. G., and A. E. Martell. 1964. *Stability Constants for Metal-Ion Complexes.* Spec Pub. 17. London: Chemical Society.

Stumm, W., and J. P. Morgan. 1981. *Aquatic Chemistry.* 2nd ed. New York: John Wiley and Sons.

Thurman, E. M. 1985. *Organic Geochemistry of Natural Waters.* Dordrecht: Martinus Nijhoff/Dr. W. Junk Publishers.

Torres, R. A., and G. R. Choppin. 1984. "Europium (III) and Americium (III) Stability Constants with Humic Acid." *Radiochimica Acta,* Vol 35:143-148.

Uhland, D. W., and W. S. Randall. 1986. *Annual Water Quality Data Report.* DOE-WIPP-86-006. Carlsbad, NM: Waste Isolation Pilot Plant Project Office.

Uhland, D. W., W. S. Randall, and R. C. Carrasco. 1987. *Annual Water Quality Data Report*. DOE-WIPP-87-006. Carlsbad, NM: Waste Isolation Pilot Plant Project Office.

Uhland, D. W., and W. S. Randall. 1987. *Geotechnical and Geoscience Procedure Manual Section 5.3, Collection of Final Samples*. WP 07-230. Carlsbad, NM: Waste Isolation Pilot Plant Project Office.

UNC Geotech. 1988. "Data Report on the Analysis of 12 Samples from Nine WIPP Project Wells." Unpublished.

UNC Geotech. 1989. "Analytical Report for WIPP Groundwater Samples H-5B, H-6B, H-6C, H-17, H-18, WIPP-30, DOE-1, H-2A, H-4B, H-11B3, H-12, P-14, WIPP-19, WIPP-25, WIPP-26 Wells and AIS/Collection Ring and AIS/Hole 2." Unpublished.

US EPA. 1986. *Test Methods for Evaluating Solid Waste*. 3rd ed., Revision 0. US Environmental Protection Agency, SW-846.

Wolery, T. J. 1983. *EQ3NR, A Computer Program for Geochemical Aqueous Speciation-Solubility Calculations: User's Guide and Documentation*. UCRL-53414. Livermore, CA: Lawrence Livermore National Laboratory.

# APPENDIX 6A
# A PRELIMINARY EVALUATION OF REDOX DATA FOR CULEBRA GROUNDWATERS

Karen L. Robinson
Sandia National Laboratories

## 6A.1 Purpose

This appendix has three purposes:

- To present all data available (as of August, 1989) to K. Robinson for the arsenic, iodine, nitrogen, and selenium redox couples.
- To give a preliminary evaluation of these data--that is, attempt to determine how reliable the data are.
- To briefly discuss the effect of this evaluation on conclusions reached in Chapter 6.

## 6A.2 Data

The primary sources of redox-couple data are the analyses by UNC Geotech (formerly Bendix Field Engineering Corporation; Grand Junction, CO) of samples collected by the WQSP specifically for redox-couple analyses. Details of the sample-collection procedures are given in Section 6.1.2.1, and the analytical methods used by UNC Geotech are summarized in Table 6A-1.

Although no other samples are collected specifically for the determination of redox couples, other laboratories determine some of the redox species in samples collected and analyzed for other purposes. Comparing these data with the other redox data is sometimes helpful in evaluating the redox data.

## Table 6A-1. Summary of Analytical Methods Used by UNC and ITAS[1]

| Analyte | Sample: Redox<br>Lab: UNC<br>Method | Sample: SNL<br>Lab: UNC<br>Method | Sample: WQSP<br>Lab: ITAS<br>Method |
|---|---|---|---|
| $NO_3^-$ | Ion Chromatography | Ion Chromatography | Flow Injection Analysis |
| $NH_4^+$ | Spectrophotometry | -- | -- |
| $I^-$ | Polarography | Polarography | Titration |
| $IO_3^-$ | Polarography | Polarography | -- |
| Total As | Hydride-Generation Atomic Absorption | Hydride-Generation Atomic Absorption | Graphite-Furnace Atomic Absorption |
| As(III) | Hydride-Generation Atomic Absorption | -- | -- |
| As(V) | Calculation: As(V) = As(tot) - As(III) | -- | -- |
| Total Se | Hydride-Generation Atomic Absorption | Hydride-Generation Atomic Absorption | Graphite-Furnace Atomic Absorption |
| Se(IV) | Hydride-Generation Atomic Absorption | -- | -- |
| Se(VI) | Calculation: Se(VI) = Se(tot) - Se(IV) | -- | -- |

1. Methods used by UNC are described in Robinson (1988) and unpublished reports from UNC to SNL (UNC Geotech, 1988, 1989, etc.). ITAS methods are given in unpublished data reports from ITAS to the WQSP and are filed at the WIPP Site (Lyon, 1989). The ITAS methods given here were used on samples analyzed in 1987; different methods may have been used on previous or subsequent samples. A thorough search of the records to determine which method was used for each analyte in each sample is beyond the scope of this appendix.

UNC Geotech, for example, determines iodide (and occasionally iodate, total arsenic, and total selenium) in general-chemistry samples collected by the WQSP for Sandia National Laboratories (SNL). The anion samples are filtered at the time of collection into plastic bottles. The cation samples are filtered at the time of collection into plastic bottles and acidified (to pH <2) with high-purity nitric acid. The collection procedures are described in Colton and Morse (1985) and Uhland and Randall (1987). The analytical methods used by UNC Geotech are summarized in Table 6A-1.

The IT Analytical Services laboratory (ITAS, Murraysville, PA), on the other hand, routinely determines iodide, nitrate, total arsenic, and total selenium in general-chemistry samples collected by and for the WQSP. The collection procedures are the same as those summarized above for the SNL samples (Colton and Morse, 1985; Uhland and Randall, 1987). The analytical methods used by ITAS are summarized in Table 6A-1.

The data are presented in Table 6A-2. The results of the UNC analyses of the redox samples, as well as the results of the ITAS analyses of the WQSP general-chemistry samples, are from a series of annual water-quality data reports (Uhland and Randall, 1986; Uhland et al., 1987; Randall et al., 1988; Lyon, 1989). The results of the UNC analyses of SNL's general chemistry samples are from Robinson (1988) and some unpublished reports from UNC Geotech to SNL (UNC Geotech, 1988; 1989).

Most wells have been sampled at least twice. Many of the solutes were analyzed in duplicate by the labs, and the replicate results are included in Table 6A-2. The data generated specifically for the redox studies are shown in boldface type, and those data used to calculate redox potentials in Sections 6.1.2 and 6.1.3 are marked with a superscript 4. Well locations are shown on Figure 6-1.

## Table 6A-2. Concentrations of Selected Redox Species in Culebra Groundwaters Part A: Arsenic and Selenium Data

| Well | Date | Lab[1] | Total As (mg/L) | As(III) (mg/L) | Total Se (mg/L) | Se(IV) (mg/L) |
|---|---|---|---|---|---|---|
| DOE-1 | 04/25/85 | IT | 0.006; 0.018; 0.014 | | <0.001; <0.001 | |
| | 07/03/86 | Rdx | <0.005 | | <0.001 | |
| | | IT | 0.034; 0.034 | | 0.230; 0.136 | |
| | 07/28/87 | Rdx | 0.006[4] | 0.002[4] | 0.002 | <0.001 |
| | | IT | <0.5; <0.5 | | <0.5; <0.5 | |
| DOE-2 | 03/12/85 | IT | 0.024; 0.026 | | 0.048 | |
| | 08/27/86 | Rdx | <0.005 | | <0.001 | |
| | | IT | <0.01 | | <0.01 | |
| | 05/19/88 | Rdx | 0.002; 0.002 | <0.001; <0.001 | <0.001; <0.001 | |
| | | IT | <0.05; <0.05 | | <0.5 | |
| Engle | 03/04/85 | IT | <0.001 | | 0.10 | |
| H-2A | 04/21/86 | Rdx | <0.005 | | <0.001 | |
| | | IT | <0.01; <0.01 | | <0.01; <0.01 | |
| | 08/12/87 | Rdx | 0.006 | 0.004 | 0.002 | <0.001 |
| | | IT | 0.015; 0.013[2] | | <0.05; <0.05 | |
| H-3B3 | 02/04/85 | IT | 0.024; 0.025 | | 0.067; 0.098 | |
| | 05/05/86 | Rdx | <0.005 | | <0.0001 | |
| | | IT | 0.039 | | <0.1 | |
| | 08/24/87 | Rdx | <0.001 | | <0.001 | |
| | | IT | <0.005 | | <0.5; <0.5 | |
| H-4B | 07/20/85 | IT | 0.04 | | <0.01 | |
| | 11/13/86 | Rdx | 0.008 | 0.005 | <0.001 | |
| | | IT | 0.02 | | 0.03 | |
| | 09/25/87 | Rdx | 0.006 | 0.003 | <0.001 | |
| | | IT | <0.05; <0.05 | | <0.5; <0.5 | |
| H-5B | 08/27/85 | IT | 6.7 | | 7.3 | |
| | 05/21/86 | Rdx | <0.005 | | <0.001 | |
| | | IT | 0.042; 0.042 | | <0.1; <0.1 | |
| | 02/24/88 | Rdx | 0.0022 | 0.0014 | <0.001 | |
| | | IT | <0.024[3] | | <0.024[3] | |
| H-6B | 09/15/85 | IT | 78 | | 1.3 | |
| | 07/28/86 | Rdx | <0.005 | | <0.001 | |
| | | IT | <0.1; <0.1 | | <1; <1 | |
| | 11/16/87 | Rdx | 0.002 | <0.001 | 0.002 | 0.001 |
| | | IT | <0.5; <0.5 | | <0.05; <0.05 | |

## Table 6A-2. Concentrations of Selected Redox Species in Culebra Groundwaters
## Part A: Arsenic and Selenium Data (Continued)

| Well | Date | Lab[1] | Total As (mg/L) | As(III) (mg/L) | Total Se (mg/L) | Se(IV) (mg/L) |
|---|---|---|---|---|---|---|
| H-7B1 | 03/27/86 | Rdx | <0.005 | | <0.001 | |
| | | IT | 0.005 | | 0.006 | |
| | 02/25/87 | Rdx | 0.0024 | <0.0002 | 0.0095[4] | 0.001[4] |
| | | IT | <0.05 | | <0.05 | |
| | | UNC | 0.006; 0.005 | | 0.009; 0.009 | |
| | 04/25/88 | Rdx | 0.001; 0.001 | | 0.010; 0.010 | <0.001 |
| | | IT | 0.005 | | 0.012 | |
| H-8B | 01/22/86 | Rdx | <0.004 | | | |
| | | IT | 0.002; <0.001 | | <0.001; <0.001 | |
| | 02/11/87 | Rdx | <0.0005 | | 0.0008 | <0.0005 |
| | | IT | <0.005 | | <0.5 | |
| | 06/08/88 | Rdx | <0.001; <0.001 | | <0.001; <0.001 | |
| | | IT | <0.02[3] | | <0.04[3] | |
| H-9B | 11/14/85 | Rdx | <0.005 | | | |
| | | IT | <0.01; <0.01 | | <0.01; <0.01 | |
| | 01/28/87 | Rdx | <0.0005 | | 0.018[4] | 0.0072[4] |
| | | IT | <0.005 | | 0.012 | |
| | 06/21/88 | Rdx | <0.001; <0.001 | | <0.001; <0.001 | |
| | | IT | <0.005; <0.005 | | <0.5; <0.5 | |
| H-11B3 | 06/04/85 | IT | 0.15; 0.15 | | <0.001; <0.001 | |
| | 06/04/86 | Rdx | 0.013 | 0.015 | <0.001 | |
| | | IT | 0.040; 0.040 | | <0.1; <0.1 | |
| | 09/15/87 | Rdx | 0.01 | 0.008 | <0.001 | |
| | | IT | <0.05; <0.05 | | <5; <5 | |
| H-12 | 08/09/85 | IT | 18 | | 0.60 | |
| | 01/16/87 | Rdx | 0.0042[4] | 0.0012[4] | <0.001 | |
| | | IT | 0.17[2] | | <0.5 | |
| | 12/14/88 | Rdx | 0.0072; 0.0072 | 0.0013; 0.0014 | 0.001; 0.001 | 0.001 |
| | | IT | <0.05 | | <0.5 | |
| H-14 | 05/26/87 | Rdx | <0.001 | | <0.001 | |
| | | IT | <0.05 | | <0.05 | |
| | 01/27/88 | Rdx | 0.003 | 0.002 | <0.001 | |
| | | IT | <0.05; <0.05 | | <0.05; <0.05 | |
| H-15 | 05/11/87 | Rdx | 0.0025[4] | 0.001[4] | <0.001 | |
| | | IT | <0.5 | | <0.5 | |
| | 01/13/88 | IT | <1; <1 | | <0.05; <0.05 | |
| | 11/07/88 | Rdx | 0.002; 0.002 | <0.001; <0.001 | <0.001; <0.001 | |
| | | IT | <0.05; <0.05 | | <5; <5 | |

## Table 6A-2. Concentrations of Selected Redox Species in Culebra Groundwaters
## Part A: Arsenic and Selenium Data (Continued)

| Well | Date | Lab[1] | Total As (mg/L) | As(III) (mg/L) | Total Se (mg/L) | Se(IV) (mg/L) |
|---|---|---|---|---|---|---|
| H-17 | 10/27/87 | Rdx | 0.009[4] | 0.002[4] | <0.001 | |
| | | IT | <0.05; <0.05 | | <5; <5 | |
| H-18 | 11/10/87 | Rdx | 0.001 | <0.001 | 0.001 | |
| | | IT | <0.5; <0.5 | | <0.05; <0.05 | |
| | 04/07/88 | Rdx | <0.001; <0.001 | | <0.001; <0.001 | |
| | | IT | <0.005; <0.005 | | <0.5; <0.5 | |
| P-14 | 02/27/86 | IT | <0.1; <0.1 | | <0.1; <0.1 | |
| | 06/18/87 | Rdx | <0.001 | | <0.001 | |
| | | IT | <0.05 | | <0.05; <0.05 | |
| | 03/16/88 | Rdx | 0.001 | <0.001 | <0.001 | |
| | | IT | <0.05; <0.05 | | <0.5; <0.5 | |
| P-17 | 03/17/86 | IT | 0.32; 0.29 | | <1.0 | |
| | 12/18/86 | Rdx | 0.0035;0.0032 | 0.0015; 0.0012 | <0.001; <0.001 | |
| | | IT | 0.17 | | 0.033 | |
| | | UNC | 0.005; 0.004 | | <0.001 | |
| | 10/21/87 | Rdx | 0.003 | <0.001 | <0.001 | |
| | | IT | <0.005; <0.005 | | <0.05; <0.05 | |
| WIPP-19 | 07/14/87 | Rdx | 0.003[4] | 0.002[4] | 0.003 | <0.001 |
| | | IT | <0.5; <0.5 | | <0.5; <0.5 | |
| | 02/12/88 | Rdx | 0.0024 | 0.0016 | <0.001 | |
| | | IT | <0.5; <0.5 | | <0.5; <0.5 | |
| | 08/29/88 | Rdx | 0.0075;0.0072 | 0.0025; 0.0024 | <0.001 | |
| | | IT | <0.02; <0.02[3] | | <0.04; <0.04[3] | |
| WIPP-25 | 02/12/86 | Rdx | <0.005 | | | |
| | | IT | 0.27 | | <0.1 | |
| | 04/15/87 | Rdx | 0.0025 | <0.001 | 0.040[4] | 0.002# |
| | | IT | <0.05 | | <0.05 | |
| | 03/28/88 | Rdx | 0.0025 | <0.001 | 0.018 | 0.002 |
| | | IT | <0.005 | | <0.5 | |
| WIPP-26 | 11/25/85 | Rdx | <0.005 | | | |
| | | IT | <0.01; <0.01 | | <0.1; <0.1 | |
| | 04/01/87 | Rdx | <0.001 | | 0.018 | <0.001 |
| | | IT | <0.5 | | <0.05 | |
| | 04/14/88 | Rdx | 0.001; 0.001 | | 0.019; 0.018 | <0.001 |
| | | IT | <0.005; <0.005 | | 0.022 | |
| WIPP-29 | 12/14/85 | Rdx | <0.02 | | | |
| | | IT | <1; <1 | | <1; <1 | |
| | 03/11/87 | Rdx | 0.012 | 0.003 | 0.0034 | <0.001 |
| | | IT | <5 | | <0.5 | |

## Table 6A-2. Concentrations of Selected Redox Species in Culebra Groundwaters
## Part B: Iodine and Nitrogen Data

| Well | Date | Lab[1] | $I^-$ (mg/L) | $IO_3^-$ (mg/L) | $NH_4^+$ (mg/L) | $NO_3^-$ (mg/L) |
|---|---|---|---|---|---|---|
| DOE-1 | 04/25/85 | Rdx | | | 1.2; 1.4 | <5 |
| | | IT | <1; <1 | | | <0.4; <0.4 |
| | 07/03/86 | Rdx | 0.21 | <0.010 | <0.1; <0.1 | <1; <1 |
| | | IT | 1.2 | | | 0.4; 0.4 |
| | 07/28/87 | Rdx | 1.91[4] | <0.010[4] | 0.59; 0.59[4] | <10; <10[4] |
| | | IT | <2; <2 | | | 15 |
| | | UNC | 0.113; 0.106 | | | |
| DOE-2 | 03/12/85 | Rdx | | | <0.2; <0.2 | <2 |
| | | IT | <1 | | | <0.4 |
| | | UNC | 0.24; 0.21; 0.23 | | | |
| | 08/27/86 | Rdx | 0.35[4] | <0.010[4] | 0.3; <0.1 | <1; <1 |
| | | IT | <1 | | | <0.4 |
| | 05/19/88 | Rdx | 0.12; 0.13 | <0.020 | 0.2; 0.2 | <1; <1 |
| | | IT | <2; <2 | | | <0.09 |
| Engle | 03/04/85 | Rdx | | | <0.2[4] | 2.0[4] |
| | | IT | <1 | | | 2.2 |
| | | UNC | 0.11; 0.12; 0.12 | | | |
| H-2A | 04/21/86 | Rdx | 0.105 | <0.010 | 0.70; 0.74 | <1 |
| | | IT | 1 | | | 1.3 |
| | | UNC | 0.077; 0.086; 0.081 | | | |
| | 08/12/87 | Rdx | <0.020 | <0.020 | <0.1 | <1 |
| | | IT | 8; 7 | | | <0.9 |
| | | UNC | 0.075; 0.090 | | | |
| H-3B3 | 02/04/85 | IT | 1 | | | <0.4 |
| | | UNC | 0.13; 0.14; 0.15 | | | |
| | 05/05/86 | Rdx | 0.15 | <0.010 | 0.31; 0.34[4] | <1[4] |
| | | IT | <1 | | | 0.4 |
| | 08/24/87 | Rdx | <0.020 | <0.020 | 0.37 | <4 |
| | | IT | <2; <2 | | | <0.9 |
| H-4B | 07/20/85 | Rdx | | | 1.0 | <1 |
| | | IT | 1.1 | | | <0.4[4]; <0.4 |
| | 11/13/86 | Rdx | 0.20[4] | <0.010[4] | 0.47[4] | <1[4] |
| | | IT | 2; 0 | | | <0.4; <0.4 |
| | 09/25/87 | Rdx | 0.163 | <0.020 | 0.03 | <3 |
| | | IT | <2; <2 | | | <0.4 |
| | | UNC | 0.188; 0.214 | | | |

## Table 6A-2. Concentrations of Selected Redox Species in Culebra Groundwaters
## Part B: Iodine and Nitrogen Data (Continued)

| Well | Date | Lab[1] | $I^-$ (mg/L) | $IO_3^-$ (mg/L) | $NH_4^+$ (mg/L) | $NO_3^-$ (mg/L) |
|---|---|---|---|---|---|---|
| H-5B | 08/27/85 | Rdx | | | 1.3; 1.3 | <5; <5 |
| | | IT | 1.1; 1.1 | | | 1.8; 1.8 |
| | | UNC | 0.20; 0.18 | | | |
| | 05/21/86 | Rdx | 0.20[4] | <0.010[4] | 2.3; 2.2[4] | <1; <1[4] |
| | | IT | 1.3 | | | 0.4; <0.4 |
| | 02/24/88 | Rdx | 0.15; 0.15 | <0.015 | 1.26 | <4 |
| | | IT | <2; <2 | | | 0.18 |
| | | UNC | 0.072; 0.085 | | | |
| H-6B | 09/15/85 | Rdx | | | <0.1; <0.1 | <10; <10 |
| | | IT | <1; <1 | | | 0.9; 0.9 |
| | | UNC | 0.100; 0.090; 0.097 | 0.10 | | |
| | 07/28/86 | Rdx | 0.25[4] | <0.010[4] | 2.7[4] | <1[4] |
| | | IT | 0.9 | | | 0.9; 0.9 |
| | 11/16/87 | Rdx | 0.158 | <0.020 | 0.19; 0.21 | <2 |
| | | IT | <2; <2 | | | <0.9 |
| | | UNC | 0.178; 0.186 | | | |
| H-7B1 | 03/27/86 | Rdx | 0.054 | 0.077 | 0.14; 0.12 | 2.8 |
| | | IT | <1 | | | 3.1; 3.1 |
| | | UNC | 0.053; 0.052 | | | |
| | 02/25/87 | Rdx | 0.065[4] | 0.052[4] | <0.1[4] | 3.2; 3.0[4] |
| | | IT | <2 | | | 3.5 |
| | | UNC | 0.074; 0.069 | | | |
| | 04/25/88 | Rdx | 0.070; 0.080 | <0.020;<0.020 | <0.1; <0.1 | 2.5; 2.6 |
| | | IT | <2 | | | 3.1 |
| H-8B | 01/22/86 | Rdx | 0.16 | <0.010 | 0.3 | 6.4 |
| | | IT | <1 | | | 6.2 |
| | | UNC | 0.15; 0.14 | | | |
| | 02/11/87 | Rdx | 0.247[4] | 0.025[4] | <0.1; <0.1[4] | 5.5; 5.4[4] |
| | | IT | <2 | | | 6.2 |
| | 06/08/88 | Rdx | 0.12; 0.12 | <0.020;<0.020 | <0.1; <0.1 | 5.0; 5.0 |
| | | IT | <2; <2 | | | 4.0 |
| H-9B | 11/14/85 | Rdx | 0.12 | <0.010 | 0.56 | <1 |
| | | IT | <1 | | | 0.9 |
| | | UNC | 0.11; 0.11 | | | |
| | 01/28/87 | Rdx | 0.247; 0.247[4] | <0.010;<0.010[4] | <0.1; <0.1[4] | 0.5; 0.5[4] |
| | | IT | <1; <1 | | | 2.2; 1.8 |
| | 06/21/88 | Rdx | 0.10; 0.10 | <0.020;<0.020 | <0.1; <0.1 | <1; <1 |
| | | IT | <2 | | | 0.49; 0.53 |

## Table 6A-2. Concentrations of Selected Redox Species in Culebra Groundwaters
## Part B: Iodine and Nitrogen Data (Continued)

| Well | Date | Lab[1] | $I^-$ (mg/L) | $IO_3^-$ (mg/L) | $NH_4^+$ (mg/L) | $NO_3^-$ (mg/L) |
|---|---|---|---|---|---|---|
| H-11B3 | 06/04/85 | IT | 1.1 | | | <0.4; <0.4 |
| | 06/04/86 | Rdx | 0.23[4] | <0.010[4] | 1.8; 1.9[4] | <1; <1[4] |
| | | IT | 0.48 | | | <0.4; <0.4 |
| | 09/15/87 | Rdx | <0.020 | <0.020 | 0.85 | <13 |
| | | IT | <2; <2 | | | <1.3 |
| | | UNC | 0.129; 0.128 | | | |
| H-12 | 08/09/85 | Rdx | | | 2.6 | <10 |
| | | IT | 1.6 | | | <0.4; <0.4 |
| | 01/16/87 | Rdx | 0.148[4] | 0.014[4] | 2.2[4] | <1[4] |
| | | IT | <1 | | | 3.5; 4.0 |
| | | UNC | 0.222; 0.206 | | | |
| | 12/14/88 | Rdx | 0.25; 0.28 | <0.015; <0.015 | 2.32; 2.32 | <0.5; <0.5 |
| | | IT | <2; <2 | | | <0.09; <0.09 |
| H-14 | 05/26/87 | Rdx | 0.61[4] | <0.010[4] | 0.20; 0.30[4] | <2.5; <2.0[4] |
| | | IT | <2; <2 | | | 1.8 |
| | | UNC | 0.054; 0.049 | | | |
| | 01/27/88 | Rdx | 0.070; 0.070 | <0.015 | 0.26 | <1 |
| | | IT | <2; <2 | | | <0.09 |
| H-15 | 05/11/87 | Rdx | 0.101[4] | <0.010[4] | 0.85; 0.86[4] | <2; <2[4] |
| | | IT | <2; <2 | | | 2.2 |
| | | UNC | <0.01 | | | |
| | 01/13/88 | IT | <2 | | | <0.09 |
| | 11/07/88 | Rdx | 0.30; 0.30 | <0.015; <0.015 | 0.85; 0.85 | <1; <1 |
| | | IT | <2; <2 | | | <0.09 |
| H-17 | 10/27/87 | Rdx | <0.020[4] | <0.020[4] | 1.5[4] | <4[4] |
| | | IT | <2; <2 | | | <0.9 |
| | | UNC | 0.104; 0.100 | | | |
| H-18 | 11/10/87 | Rdx | 0.103[4] | <0.020[4] | 0.16[4] | <1[4] |
| | | IT | <2 | | | <0.9 |
| | | UNC | 0.113; 0.123 | | | |
| | 04/07/88 | Rdx | 0.080; 0.070 | <0.020; <0.020 | <0.1; <0.1 | <0.5; <0.5 |
| | | IT | <2 | | | <0.09 |

## Table 6A-2. Concentrations of Selected Redox Species in Culebra Groundwaters
## Part B: Iodine and Nitrogen Data (Continued)

| Well | Date | Lab[1] | $I^-$ (mg/L) | $IO_3^-$ (mg/L) | $NH_4^+$ (mg/L) | $NO_3^-$ (mg/L) |
|---|---|---|---|---|---|---|
| P-14 | 02/27/86 | IT | <1 | | | 0.9 |
| | | UNC | 0.42; 0.41 | | | |
| | 06/18/87 | Rdx | 4.94[4] | 0.935[4] | 0.29; 0.32[4] | <3; <3[4] |
| | | IT | <2; <2 | | | 2.7 |
| | 03/16/88 | Rdx | 0.57 | <0.015 | 0.35; 0.39 | <1; <1 |
| | | IT | <2; <2 | | | 0.13 |
| | | UNC | 0.410; 0.389 | | | |
| P-17 | 03/17/86 | IT | 7.3; 7.3 | | | 1.3 |
| | | UNC | 0.18; 0.17 | | | |
| | 12/18/86 | Rdx | 0.21[4] | <0.010[4] | 2.73; 2.77[4] | <3; <3[4] |
| | | IT | <1 | | | 0.4; 0.9 |
| | | UNC | 0.052; 0.050 | | | |
| | 10/21/87 | Rdx | 0.023 | <0.020 | 2.59 | <2 |
| | | IT | <2 | | | <0.9 |
| WIPP-19 | 07/14/87 | Rdx | 2.47[4] | <0.010[4] | 2.79; 2.77[4] | <10; <10[4] |
| | | IT | <2; <2 | | | 4.0 |
| | | UNC | <0.15 | | | |
| | 02/12/88 | Rdx | 0.24; 0.24 | <0.015; <0.015 | 1.7 | <2 |
| | | IT | <2; <2 | | | 0.49; 0.53 |
| | | UNC | 0.207; 0.223 | | | |
| | 08/29/88 | Rdx | <0.20; <0.20 | <0.020; <0.020 | 1.36; 1.35 | <1; <1 |
| | | IT | <2; <2 | | | <0.09 |
| WIPP-25 | 02/12/86 | Rdx | 0.10 | <0.010 | 0.5; 0.6 | 13 |
| | | IT | <1 | | | 15.9; 15.5 |
| | | UNC | 0.038; 0.043; 0.045[4] | | | |
| | 04/15/87 | Rdx | 0.335[4] | <0.010[4] | 0.25; 0.23[4] | 12.0; 12.2[4] |
| | | IT | <2 | | | 13.3 |
| | 03/28/88 | Rdx | 0.12 | 0.025 | 0.02; 0.05 | 13.1 |
| | | IT | <2 | | | 11.5 |
| | | UNC | 0.052; 0.056 | | | |
| WIPP-26 | 11/25/85 | Rdx | 0.078 | 0.020 | 0.38 | 16; 15.3 |
| | | IT | <1; <1 | | | 25.7; 24.8 |
| | | UNC | 0.069; 0.070 | | | |
| | 04/01/87 | Rdx | 0.062[4] | <0.010[4] | 0.10; 0.09[4] | 19.3; 19.7[4] |
| | | IT | <2; <2 | | | 23; 23.5 |
| | 04/14/88 | Rdx | 0.060; 0.060 | <0.020 | <0.1; <0.1 | 13.3; 13.6 |
| | | IT | <2; <2 | | | 15.9 |
| | | UNC | 0.075; 0.076 | | | |

## Table 6A-2. Concentrations of Selected Redox Species in Culebra Groundwaters
## Part B: Iodine and Nitrogen Data (Continued)

| Well | Date | Lab[1] | $I^-$ (mg/L) | $IO_3^-$ (mg/L) | $NH_4^+$ (mg/L) | $NO_3^-$ (mg/L) |
|---|---|---|---|---|---|---|
| WIPP-29 | 12/14/85 | **Rdx** | **0.55** | **<0.010** | **2.7** | **<1** |
| | | IT | 2.1 | | | 0.4 |
| | | UNC | 0.039; 0.38 | | | |
| | 03/11/87 | **Rdx** | **0.358** | **0.076** | **4.3; 4.3** | **3.0; 3.0** |
| | | IT | <2 | | | 6.6; 7.1 |

1. Information in the "Lab" column indicates both which agency arranged for the analyses and which laboratory performed them. All samples were collected by WQSP personnel.
   - Rdx: samples collected specifically for redox analyses; analyses by UNC Geotech for the WQSP. Values are boldfaced in the table.
   - IT: samples collected for general chemical analyses (anions and cations); analyses by IT Analytical Services for the WQSP.
   - UNC: samples collected for general chemical analyses (anions and cations); analyses by UNC Geotech for SNL.
2. Data flagged in WQSP annual report as being doubtful.
3. Analysis done after analytes were pre-concentrated by ion-exchange method (see Lyon, 1989).
4. Data (single values or averages of replicates) used to calculate redox potentials (Tables 6-2 and 6-4 in Section 6.1.2).

# 6A.3 Discussion

## 6A.3.1 Methods of Evaluating the Data

Solute data may be incorrect--that is, not representative of the unperturbed groundwater--for any of three reasons (Robinson, 1988). First, the groundwater sample itself may not have been representative with respect to the parameters of interest, perhaps because it was contaminated at depth or because it was perturbed as it was pumped from depth to the surface. Second, the concentrations of some species may increase or decrease between the time of collection and the time of analysis. Third, the analysis may be inaccurate.

In this work, we attempted to evaluate the representativeness and the stability of the samples by comparing results of analyses of samples collected at different times from the same locations. Inherent in this approach is the assumption that the redox state of the Culebra groundwater in the region did not change during the program (that is, since 1985). There also are difficulties with using this approach in this work because many of the analytical results are reported as less than some detection level (as an upper limit).

We attempted to evaluate the quality of the analyses by considering results of replicate analyses (multiple analyses of the same sample by a laboratory) and by comparing results for different samples collected at the same time from the same location. Again, this was sometimes difficult in this work because many of the analytical results are reported as upper limits.

## 6A.3.2 Arsenic and Selenium

Representativeness and stability of the samples

The concentration of iron in some Culebra waters has been observed to change with varying pumping rates (Uhland et al., 1987), apparently because of interactions between the groundwater and materials in the well (such as the casing and the pump). Therefore,

the representativeness of the samples with respect to all trace metals is considered questionable. The assumption that the samples are representative of the unperturbed groundwater with respect to total arsenic and total selenium should be tested before it is accepted. In addition, we do not have enough information at this time to evaluate whether the ratios of As(III)/As(V) or Se(IV)/Se(VI) changed as the samples were pumped from depth or between the times of collection and analysis.

Quality of the analyses

The ITAS As and Se analytical data for samples collected before 1988 are not considered reliable. Many of those results are higher (by one to two orders of magnitude) than the UNC Geotech results or the more recent ITAS results. The WQSP and ITAS personnel were aware of some of the problems with the trace metal data; the third annual report (Randall et al., 1988) identified some data as doubtful. In 1988, the WQSP and ITAS began developing some better methods for trace-metal analyses in waters with high concentrations of TDS (Lyon, 1989); the methods involve preconcentrating the trace metals by an ion-exchange method before analysis.

The ITAS As and Se results for samples collected in 1988 agree reasonably well (Table 6A-2) with the UNC Geotech results, and the analyses (but not necessarily the samples) are tentatively considered reliable.

Evaluation of calculated redox potentials

Redox potentials based on the arsenic couple were calculated for samples from DOE-1, H-12, H-15, H-17, and WIPP-19. The representativeness of the DOE-1 sample collected in 1987 is questionable because a sample collected in 1986 contained no detectable arsenic (see Table 6A-2). The data for the H-12, H-15, and WIPP-19 samples may be reasonable based on comparisons of samples collected in different years (see Table 6A-2). H-17 was only sampled once.

Thus, if the samples collected were representative of the unperturbed groundwater and if the As(III)/As(V) ratios did not change before analysis (during collection, preservation, transportation, or storage) or during analysis, then the calculated arsenic-redox potentials for the DOE-1, H-12, H-15, H-17, and WIPP-19 samples may be meaningful.

Redox potentials based on the selenium couple were calculated for samples from H-7B1, H-9B, and WIPP-25. The representativeness of the H-7B1 sample collected in 1987 is questionable for two reasons. First, Se was not detectable in the 1986 sample, and second, Se(IV) was not detectable in the 1988 sample (see Table 6A-2). The representativeness of the H-9B sample collected in 1987 is also questionable because the 1988 sample had no detectable Se (see Table 6A-2). The data for the WIPP-25 sample appear to be reasonable based on comparisons of samples collected in 1987 and 1988 (see Table 6A-2).

Thus, if the samples collected were representative of the unperturbed groundwater and if the Se(IV)/Se(VI) ratios did not change before analysis (during collection, preservation, transportation, or storage) or during analysis, then the calculated selenium-redox potentials for the H-7B1, H-9B, and WIPP-25 samples may be meaningful.

### 6A.3.3 Iodine

Representativeness and stability of the samples

The samples are assumed to be representative of the unperturbed groundwater with respect to iodide because at many locations we observe the same concentrations of iodide in samples collected over a period of several years (Table 6A-2). In addition, we know of no reason to suspect that samples would be contaminated with either iodide or iodate as a result of interactions between the groundwaters and materials in the borehole.

Iodate was detected in samples from a few locations, but usually not in previous or subsequent samples from the same location (Table 6A-2). Only at H-7B1 was iodate found twice, in 1986 and 1987, but not in 1988. Because iodate is detected only intermittently at most locations, we suspect that the $I^-/IO_3^-$ ratio in some samples may be perturbed by the

sampling procedure or between the time of collection and analysis. Thus, the samples with detectable iodate are not considered representative with respect to iodate.

Quality of the analyses

The UNC iodide results, with three exceptions, are tentatively considered reliable. This is based on the general good agreement between samples collected from the same location at different times and between samples collected for SNL and the redox program from the same location at the same time (Table 6A-2). The three exceptions are the results from DOE-1 (1987), P-14 (1987), and WIPP-19 (1987), all of which are an order of magnitude higher than other results from the same locations. The problem may be a dilution-factor error on the part of the analyst or a sample-contamination problem.

The ITAS iodide results, which are often much higher than the UNC results, are not considered reliable.

There is no reason to doubt the accuracy of the iodate analyses. However, as was explained above, the representativeness and stability of the samples with respect to iodate are questioned.

Evaluation of calculated redox potentials

Although the iodide results for the samples from DOE-1, P-14, and WIPP-19 are probably high (by a factor of 10), the calculated potentials are not very sensitive to order-of-magnitude changes in iodide concentrations (see Equation 4 and Section 6.1.2.3). Because the detected iodate values are questionable, the calculated redox potentials for the samples from H-7B1, H-8B, H-12 and P-14 should be considered upper limits. For all other samples, the calculated upper limits may be meaningful.

### 6A.3.4 Nitrogen

Representativeness and stability of the samples

The samples are tentatively assumed to be representative of the unperturbed groundwater with respect to nitrate because at many locations we observe the same concentrations of nitrate in samples collected over a period of several years (Table 6A-2). In addition, we know of no reason to suspect that samples would be contaminated with either nitrate or ammonium as a result of interactions between the groundwaters and materials in the borehole.

However, we tentatively conclude that some samples may have gained or lost ammonium between the times of collection and analysis, because at many wells (notably DOE-1, H-2A, H-4B, H-6B, H-8B, H-9B, H-14, WIPP-25, and WIPP-26), the ammonium concentrations varied by one to two orders of magnitude from year to year (Table 6A-2).

Quality of the analyses

Ammonium was analyzed only by UNC Geotech and only in the redox samples. Based on the general good agreement between replicate analyses on the same samples (Table 6A-2), we tentatively conclude that the analytical results are reasonable. We note, however, a rough positive correlation between ammonium concentration and TDS concentration; such a correlation may be real, but could also represent an analytical interference.

Most of the nitrate results from UNC Geotech and ITAS are either in reasonable agreement or at least do not contradict each other (Table 6A-2). The UNC Geotech results are tentatively considered reliable, because they agree with detected concentrations reported by ITAS. Some of the ITAS results--the concentrations that are confirmed by the UNC Geotech data--are also tentatively considered reliable. However, for many samples, ITAS reported measureable concentrations that were lower than the detection levels reported by UNC Geotech; these data cannot be evaluated at this time.

Evaluation of calculated redox potentials

Based on the presence of detectable ammonium and nitrate, redox potentials were calculated for the samples from WIPP-25 and WIPP-26 (both from 1987). The nitrate results are tentatively considered accurate as was explained above. The ammonium concentrations, on the other hand, varied from year to year. Calculated potentials, however, are relatively insensitive to errors in the concentrations of ammonium and nitrate (see Equation 5 and Section 6.1.2.3). Thus, if the ammonium concentrations are accurate within one or two orders of magnitude, then the calculated nitrogen-redox potentials for WIPP-25 and WIPP-26 may be meaningful.

Based on the presence of detectable nitrate and the absence of detectable ammonium, lower bounds were calculated for the redox potentials of the samples from H-7B1, H-8B, H-9B, and Engle Well. The nitrate results are tentatively considered accurate as was explained above. Ammonium, however, was detected in some other samples from these wells. If the actual ammonium concentrations are close to the detection limits used in the calculations, then the nitrogen-redox potentials for the samples from H-7B1, H-8B, H-9B, and Engle may be very close (within ~50 mV) to the calculated lower bounds.

Based on the presence of detectable ammonium and the absence of detectable nitrate, upper bounds were calculated for the redox potentials of the samples from the remaining wells. The ammonium concentrations at many locations varied from year to year; as we mentioned above, however, calculated redox potentials are relatively insensitive to errors in the concentrations of the redox species. Nitrate in these samples was present in concentrations below the UNC detection level, but was sometimes detected by ITAS. Thus, if the ammonium concentrations are accurate within one or two orders of magnitude and if the ITAS nitrate results are accurate to within one or two orders of magnitude, then the nitrogen-redox potentials for these samples may be very close (within ~50 mV) to the calculated upper bounds.

# 6A.4 Summary and Conclusions

Representativeness and stability of samples

The main conclusions about the representativeness and stability of the samples are the following:

- The representativeness and stability of the samples with respect to arsenic and selenium are questioned, but cannot be evaluated with the data available.

- In general, the samples are considered representative and stable with respect to iodide and nitrate, but not iodate.

- The stability of ammonium in some of the samples is questioned.

Quality of the analyses

The main conclusions about the quality of the analyses are the following:

- The results from the UNC Geotech laboratory are tentatively considered reliable.

- Some of the ITAS results are tentatively considered reliable: the As and Se results for samples collected in 1988 and most of the nitrate results (some of the nitrate results cannot be evaluated).

- Some of the ITAS results are not considered reliable: the As and Se results for samples collected before 1988 and the iodide results.

Calculated redox potentials

The main conclusions (with their caveats) about the calculated redox potentials are the following:

- If the samples collected were representative of the unperturbed groundwater and if the As(III)/As(V) ratios did not change before analysis (during collection, preservation, transportation, or storage) or during analysis, then the calculated arsenic-redox potentials for the DOE-1, H-12, H-15, H-17, and WIPP-19 samples may be meaningful. Similarly, if the samples collected were representative of the unperturbed groundwater and if the Se(IV)/Se(VI) ratio did not change before analysis (during collection, preservation, transportation, or storage) or during analysis, then the calculated selenium-redox potentials for the H-7B1, H-9B, and WIPP-25 samples may be meaningful.

- The calculated upper limits for the iodine-redox potential may be meaningful.

- If the ammonium concentrations are accurate within one or two orders of magnitude, then the calculated nitrogen-redox potentials for WIPP-25 and WIPP-26 may be meaningful. Also, if the actual ammonium concentrations are close to the reported detection limits, then the nitrogen-redox potentials for the samples from H-7B1, H-8B, H-9B, and Engle may be very close (within ~50 mV) to the calculated lower bounds. Finally, if the ammonium concentrations are accurate within one or two orders of magnitude and if the ITAS nitrate results are accurate to within one or two orders of magnitude, then the nitrogen-redox potentials for all other samples (that is, all but H-7B1, H-8B, H-9B, WIPP-25, WIPP-26, and Engle) may be very close (within ~50 mV) to the calculated upper bounds.

Effect on conclusions drawn in Chapter 6

An important conclusion of Chapter 6 was that redox conditions are more oxidizing to the south of the dashed line on Figure 6-1 and more reducing to the north. This conclusion is based on two observations: the presence of detectable nitrate and lack of detectable ammonium to the south, and the presence of detectable ammonium and lack of detectable nitrate to the north (except at WIPP-25 and WIPP-26).

But these observations may actually be analytical artifacts. The presence of nitrate to the south but not the north may reflect the lower detection level for nitrate in the southern waters (which have lower concentrations of TDS) rather than an absence of nitrate to the north. Similarly, although the increase in observed ammonium concentrations with increasing concentrations of TDS may be real, it may also reflect an analytical interference.

Thus, to state with confidence that there is a difference between redox conditions (as represented by the ammonium/nitrate couple) in the southern and northern areas (or perhaps some trend across the region), the stability of the ammonium samples needs to be verified, the analytical technique for ammonium needs to be validated, and the detection level of the analytical technique for nitrate needs to be improved for high-TDS waters.

Another suggestion in Chapter 6 was that data do not indicate a condition of redox equilibrium and in fact may indicate a condition of redox disequilibrium. If the arsenic and selenium potentials mentioned above were meaningful and if the nitrogen potentials were meaningful, then we would have evidence of redox disequilibrium. To demonstrate redox disequilibrium using these redox couples, the representativeness and stability of the arsenic and selenium samples must be verified and the nitrogen data must be verified as discussed in the previous paragraph.

## FEDERAL AGENCIES

U. S. Department of Energy, (5)
Office of Civilian Radioactive Waste
Management
Attn: Deputy Director, RW-2
Associate Director, RW-10
Office of Program Administration
and Resources Management
Associate Director, RW-20
Office of Facilities Siting
and Development
Associate Director, RW-30
Office of Systems Integration
and Regulations
Associate Director, RW-40
Office of External Relations
and Policy
Forrestal Building
Washington, DC 20585

U. S. Department of Energy (3)
Albuquerque Operations Office
Attn: J. E. Bickel
R. Marquez, Director
Public Affairs Division
P.O. Box 5400
Albuquerque, NM 87185

U. S. Department of Energy
Attn: National Atomic Museum Library
Albuquerque Operations Office
P. O. Box 5400
Albuquerque, NM 87185

U. S. Department of Energy (4)
WIPP Project Office (Carlsbad)
Attn: Vernon Daub
J. A. Mewhinney
P.O. Box 3090
Carlsbad, NM 88221

U. S. Department of Energy
Research & Waste Management Division
Attn: Director
P. O. Box E
Oak Ridge, TN 37831

U.S. Department of Energy
Richland Operations Office
Nuclear Fuel Cycle & Production Division
Attn: R. E. Gerton
P.O. Box 500
Richland, WA 99352

U. S. Department of Energy (1)
Attn: Edward Young
Room E-178
GAO/RCED/GTN
Washington, DC 20545

U. S. Department of Energy
Engineering and Geosciences Division, ER-15
Office of Basic Energy Sciences
Attn: W. C. Luth
Washington, DC 20545

U. S. Department of Energy (6)
Office of Environmental Restoration
and Waste Management
Attn: Jill Lytle, EM30
Mark Frei, EM-34 (3)
Mark Duff, EM-34
Clyde Frank, EM-50
Washington, DC 20585

U. S. Department of Energy (3)
Office of Environment, Safety and Health
Attn: Ray Pelletier, EH-231
Kathleen Taimi, EH-232
Carol Borgstrom, EH-25
Washington, DC 20585

U. S. Department of Energy
Ecological Research Division, ER-75
Office of Health and Environmental Research
Office of Energy Research
Attn: F. J. Wobber
Washington, DC 20545

U. S. Department of Energy (2)
Idaho Operations Office
Fuel Processing and Waste
Management Division
785 DOE Place
Idaho Falls, ID 83402

U.S. Department of Energy
Savannah River Operations Office
Defense Waste Processing
Facility Project Office
Attn: W. D. Pearson
P.O. Box A
Aiken, SC 29802

U. S. Department of the Interior (6)
Attn: N. Trask (MS 410)
T. Coplen (MS 431)
G. C. Curtin (MS 913)
B. F. Jones (MS 432)
L. N. Plummer (MS 432)
I. J. Winograd (MS 432)
Geological Survey
National Center
Reston, VA 22092

U.S. Department of the Interior (6)
Attn: S. Asher-Bolinder (MS 939)
J. S. McLean (MS 406)
R. P. Snyder (MS 913)
S. Bartsch-Winkler (MS 905)
S. Williams-Stroud (MS 939)
O. Raup (MS 939)
Box 25046
Denver Federal Center
Denver, CO 80225

U. S. Department of the Interior
Attn: J. Thomas
Geological Survey
705 N. Plaza Street
Carson City, NV 89701

U. S. Department of the Interior
Attn: Librarian
National Park Service
Carlsbad Caverns National Park
3225 National Parks Highway
Carlsbad, NM 88220

U. S. Environmental Protection Agency (4)
Attn: Ray Clark (2)
Mark Cotton (2)
Office of Radiation Programs (ANR-460)
Washington, DC 20460

U.S. Geological Survey
Conservation Division
Attn: W. Melton
P.O. Box 1857
Roswell, NM 88201

U.S. Geological Survey (4)
Water Resources Division
Attn: Kathy Peter (2)
Roger Ferriera
Scott Anderholm
Suite 200
4501 Indian School NE
Albuquerque, NM 87110

U.S. Nuclear Regulatory Commission (8)
Attn: Joseph Bunting, HLEN 4H3 OWFN
Ron Ballard, HLGP 4H3 OWFN
Michael Bell
David Brooks
Tin Mo
Jacob Philip
John Randall
NRC Library
Mail Stop 623SS
Washington, DC 20555

Office of Nuclear Regulatory Research (4)
U. S. Nuclear Regulatory Commission
MS: NL-005
Washington, DC 20555
Attn: G. F. Birchard
L. A. Kovach
T. J. Nicholson
J. D. Randall

Department of the Army (2)
Attn: T. Poole
L. Wakeley
Waterways Experiment Station
Corps of Engineers
Structures Laboratory
Concrete Technology Division
3909 Halls Ferry Road
Vicksburg, MS 39180-6199

## BOARDS

Defense Nuclear Facilities Safety Board
Attn: Dermot Winters
Suite 675
600 E Street, NW
Washington, DC 20004

U. S. Department of Energy
Advisory Committee on Nuclear
Facility Safety
Attn: Merritt E. Langston, AC21
Washington, DC 20585

Nuclear Waste Technical
Review Board (2)
Attn: Dr. Don A. Deere
Dr. Sidney J. S. Parry
Suite 910
1100 Wilson Blvd.
Arlington, VA 22209-2297

Richard Major
Advisory Committee on Nuclear Waste
Nuclear Regulatory Commission
7920 Norfolk Avenue
Bethesda, MD 20814

## STATE AGENCIES

Environmental Evaluation Group (3)
Attn: Library
Suite F-2
7007 Wyoming Blvd., N.E.
Albuquerque, NM 87109

New Mexico Bureau of Mines
and Mineral Resources (2)
Attn: F. E. Kottolowski, Director
J. Hawley
Socorro, NM 87801

NM Department of Energy & Minerals
Attn: Librarian
2040 S. Pacheco
Santa Fe, NM 87505

NM Environmental Improvement Division
Attn: Deputy Director
1190 St. Francis Drive
Santa Fe, NM 87503

## LABORATORIES/CORPORATIONS

Battelle Pacific Northwest Laboratories (8)
Attn: D. J. Bradley, K6-24
J. Relyea, H4-54
R. E. Westerman, P8-37
K. Krupa, K2-57
H. C. Burkholder, P7-41
E. Murphy
L. Pederson, K6-47
J. Serne
Battelle Boulevard
Richland, WA 99352

Geohydrology Associates
Attn: T. E. Kelly
4015 Carlisle Blvd NE
Albuquerque, NM 87110

Savannah River Laboratory (6)
Attn: N. Bibler
E. L. Albenisius
M. J. Plodinec
G. G. Wicks
C. Jantzen
J. A. Stone
Aiken, SC 29801

George Dymmel
SAIC
101 Convention Center Dr.
Las Vegas, NV 89109

INTERA Inc. (3)
Attn: G. E. Grisak
J. F. Pickens
A. Haug
Suite #300
6850 Austin Center Blvd.
Austin, TX 78731

INTERA Inc.
Attn: Wayne Stensrud
P.O. Box 2123
Carlsbad, NM 88221

INTERA Inc.
Attn: A. Marsh LaVenue
8100 Mountain Road
Suite #204D
Albuquerque, NM 87110

IT Corporation (3)
Attn: R. F. McKinney
J. Myers
R. Holt
Regional Office - Suite 700
5301 Central Avenue, NE
Albuquerque, NM 87108

IT Corporation (2)
Attn: D. E. Deal
P.O. Box 2078
Carlsbad, NM 88221

Arthur D. Little, Inc. (3)
Attn: C. R. Hadlock
Scot Foster
Philip Rury
Acorn Park
Cambridge, MA 02140-2390

Los Alamos National Laboratory (10)
Attn: A. Meijer
D. Broxton
B. Carlos
D. Eggert
D. Hobart
E. Springer
I. Triay
J. F. Kerrisk
D. T. Vaniman
K. Wolfsberg
P. O. Box 1663
Los Alamos, NM 87545

Lawrence Berkeley Laboratory (4)
Attn: F. Hale
S. L. Phillips
H. Nitsche
H. Wollenberg, Jr.
University of California
Berkeley, CA 94720

Oak Ridge National Laboratory (8)
Attn: R. E. Blanko
E. Bondietti
J. A. Carter
C. Claiborne
D. R. Cole
G. Jacobs
G. H. Jenks
R. Meyer
Box 2009
Oak Ridge, TN 37831

RE/SPEC, Inc.
Attn: W. Coons
P. F. Gnirk
P.O. Box 14984
Albuquerque, NM 87191

RE/SPEC, Inc. (7)
Attn: L. L. Van Sambeek
G. Callahan
T. Pfeifle
J. L. Ratigan
P. O. Box 725
Rapid City, SD 57709

Center for Nuclear Waste Regulatory Analysis (6)
Attn: J. L. Russell (3)
W. Murphy
R. Pabalan
Library
Southwest Research Institute
6220 Culebra Road
San Antonio, TX 78228-0510

Environmental Engineering and Science (2)
Attn: J. O. Leckie
S. W. Park
Department of Civil Engineering
Stanford University
Stanford, CA 94305

Science Applications
International Corporation
Attn: Howard R. Pratt,
Senior Vice President
10260 Campus Point Drive
San Diego, CA 92121

Science Applications
International Corporation
Attn: Michael B. Gross
Ass't. Vice President
Suite 1250
160 Spear Street
San Francisco, CA 94105

Serata Geomechanics
Attn: Dr. Shosei Serata
4124 Lackside Drive
Richmond, CA 94806-1941

Systems, Science, and Software (2)
Attn: E. Peterson
P. Lagus
Box 1620
La Jolla, CA 92038

Westinghouse Electric Corporation (7)
Attn: Library
Lamar Trego
W. P. Poirer
W. R. Chiquelin
V. F. Likar
D. J. Moak
R. F. Kehrman
P. O. Box 2078
Carlsbad, NM 88221

Weston Corporation
Attn: David Lechel
Suite 1000
5301 Central Avenue, NE
Albuquerque, NM 87108

## UNIVERSITIES

Arizona State University
Attn: L. P. Knauth
Department of Geology
Tempe, AZ 85287-1404

University of Arizona
Attn: J. G. McCray
Department of Nuclear Engineering
Tucson, AZ 85721

Cornell University
Department of Physics
Attn: Dr. R. O. Pohl
Clark Hall
Ithaca, NY 14853

Florida State University (2)
Attn: J. B. Cowart
J. K. Osmond
Department of Geology
Tallahassee, FL 32308

University of Minnesota
Department of Energy and Materials Science
Attn: R. Oriani
151 Amundson Hall
421 Washington Ave SE
Minneapolis, MN 55455

University of New Mexico (2)
Geology Department
Attn: C. J. Yapp
Library
Albuquerque, NM 87131

New Mexico Institute of Mining and Technology (3)
Attn: L. Brandvold
G. W. Gross
F. Phillips
Socorro, NM 87801

Pennsylvania State University
Materials Research Laboratory
Attn: Della Roy
University Park, PA 16802

Princeton University
Department of Civil Engineering
Attn: George Pinder
Princeton, NJ 08540

Texas A&M University
Center of Tectonophysics
College Station, TX 77840

University of Texas at Austin
Attn: Edward C. Bingler
Deputy Director
Texas Bureau of Economic Geology
Austin, TX 78712

Environmental Engineering and Science (2)
Attn: J. O. Leckie
S. W. Park
Department of Civil Engineering
Stanford University
Stanford, CA 94305

INDIVIDUALS

G. O. Bachman
4008 Hannett Avenue NE
Albuquerque, NM 87110

Carol A. Hill
Box 5444A
Route 5
Albuquerque, NM 87123

Harry Legrand
331 Yadkin Drive
Raleigh, NC 27609

Dennis W. Powers
Star Route Box 87
Anthony, TX 79821

Bob E. Watt
1447 45th St.
Los Alamos, NM 87544

## LIBRARIES

Thomas Brannigan Library
Attn: Don Dresp, Head Librarian
106 W. Hadley St.
Las Cruces, NM 88001

Hobbs Public Library
Attn: Ms. Marcia Lewis, Librarian
509 N. Ship Street
Hobbs, NM 88248

New Mexico State Library
Attn: Ms. Ingrid Vollenhofer
P.O. Box 1629
Santa Fe, NM 87503

New Mexico Tech
Martin Speere Memorial Library
Campus Street
Socorro, NM 87810

Pannell Library
Attn: Ms. Ruth Hill
New Mexico Junior College
Lovington Highway
Hobbs, NM 88240

WIPP Public Reading Room
Attn: Director
Carlsbad Public Library
101 S. Halagueno St.
Carlsbad, NM 88220

Government Publications Department
General Library
University of New Mexico
Albuquerque, NM 87131

## WIPP PEER PANEL

G. Ross Heath, Chairman
College of Ocean & Fishery Sciences
University of Washington
Seattle, WA 98185

Robert J. Budnitz
President, Future Resources Associates, Inc.
Suite 418
2000 Center Street
Berkeley, CA 94704

Thomas A. Cotton
4429 Butterworth Place NW
Washington, DC 20016

Patrick A. Domenico
Geology Department
Texas A&M
College Station, TX 77843-3115

Charles D. Hollister
Dean for Studies
Woods Hole Oceanographic Institute
Woods Hole, MA 02543

Thomas H. Pigford
Department of Nuclear Engineering
4153 Etcheverry Hall
University of California
Berkeley, CA 94270

John Mann
Department of Geology
245 Natural History Building
1301 West Green Street
University of Illinois
Urbana, IL 61801

## THE SECRETARY'S BLUE RIBBON PANEL ON WIPP

Dr. Thomas Bahr
New Mexico Water Resources Institute
New Mexico State University
Box 3167
Las Cruces, NM 88003-3167

Mr. Leonard Slosky
Slosky and Associates
Suite 1400
Bank Western Tower
1675 Tower
Denver, CO 80202

Mr. Newal Squyres
Eberle and Berlin
P. O. Box 1368
Boise, ID 83701

Dr. Arthur Kubo
Vice President
BDM International, Inc.
7915 Jones Branch Drive
McLean, VA 22102

Mr. Robert Bishop
Nuclear Management Resources Council
Suite 300
1776 I Street, NW
Washington, DC 20006-2496

## NATIONAL ACADEMY OF SCIENCES, WIPP PANEL

Dr. Charles Fairhurst, Chairman
Department of Civil and
Mineral Engineering
University of Minnesota
500 Pillsbury Dr. SE
Minneapolis, MN 55455

Dr. John O. Blomeke
Route 3
Sandy Shore Drive
Lenoir City, TN 37771

Dr. John D. Bredehoeft
Western Region Hydrologist
Water Resources Division
U.S. Geological Survey (M/S 439)
345 Middlefield Road
Menlo Park, CA 94025

Dr. Karl P. Cohen
928 N. California Avenue
Palo Alto, CA 94303

Dr. Fred M. Ernsberger
250 Old Mill Road
Pittsburgh, PA 15238

Dr. Rodney C. Ewing
Department of Geology
University of New Mexico
200 Yale, NE
Albuquerque, NM 87131

B. John Garrick
Pickard, Lowe & Garrick, Inc.
2260 University Drive
Newport Beach, CA 92660

John W. Healy
51 Grand Canyon Drive
Los Alamos, NM 87544

Leonard F. Konikow
U.S. Geological Survey
431 National Center
Reston, VA 22092

Jeremiah O'Driscoll
505 Valley Hill Drive
Atlanta, GA 30350

Dr. D'Arcy A. Shock
233 Virginia
Ponca City, OK 74601

Dr. Christopher G. Whipple
Electric Power Research Institute
3412 Hillview Avenue
Palo Alto, CA 94303

Dr. Peter B. Myers, Staff
Director
National Academy of Sciences
Committee on Radioactive
Waste Management
2101 Constitution Avenue
Washington, DC 20418

Dr. Geraldine Grube
Board on Radioactive
Waste Management
GF462
2101 Constitution Avenue
Washington, DC 20418

Dr. Ina Alterman
Board on Radioactive Waste
Management
GF462
2101 Constitution Avenue
Washington, DC 20418

## FOREIGN ADDRESSES

Studiecentrum Voor Kernenergie
Centre D'Energie Nucleaire
Attn: Mr. A. Bonne
SCK/CEN
Boeretang 200
B-2400 Mol
BELGIUM

Atomic Energy of Canada, Ltd. (2)
Whiteshell Research Estab.
Attn: Peter Haywood
John Tait
Pinewa, Manitoba, CANADA
R0E 1L0

Dr. D. K. Mukerjee
Ontario Hydro Research Lab
800 Kipling Avenue
Toronto, Ontario, CANADA
M8Z 5S4

Department of Earth Sciences and
Quaternary Sciences Institute
Attn: T. W. D. Edwards
University of Waterloo
Waterloo, Ontario
CANADA N2L 3Gl

Mr. Francois Chenevier, Director (2)
ANDRA
Route du Panorama Robert Schumann
B.P.38
92266 Fontenay-aux-Roses Cedex
FRANCE

Mr. Jean-Pierre Olivier
OECD Nuclear Energy Agency
Division of Radiation Protection
and Waste Management
38, Boulevard Suchet
75016 Paris, FRANCE

Claude Sombret
Centre D'Etudes Nucleaires
De La Vallee Rhone
CEN/VALRHO
S.D.H.A. BP 171
30205 Bagnols-Sur-Ceze
FRANCE

Bundesministerium fur Forschung und
Technologie
Postfach 200 706
5300 Bonn 2
FEDERAL REPUBLIC OF GERMANY

Bundesanstalt fur Geowissenschaften
und Rohstoffe
Attn: Michael Langer
Postfach 510 153
3000 Hanover 51
FEDERAL REPUBLIC OF GERMANY

Hahn-Meitner-Institut fur Kernforschung
Attn: Werner Lutze
Glienicker Strasse 100
100 Berlin 39
FEDERAL REPUBLIC OF GERMANY

Institut fur Tieflagerung (4)
Attn: K. Kuhn
Theodor-Heuss-Strasse 4
D-3300 Braunschweig
FEDERAL REPUBLIC OF GERMANY

Kernforschug Karlsruhe
Attn: K. D. Closs
Postfach 3640
7500 Karlsruhe
FEDERAL REPUBLIC OF GERMANY

Physikalisch-Technische Bundesanstalt
Attn: Peter Brenneke
Postfach 33 45
D-3300 Braunschweig
FEDERAL REPUBLIC OF GERMANY

Hermann Gies
Institut fur Tieflagerung, Gruppe Geochemie
Gesellschaft fur Strahlen und Umweltforschung mbH
Theodor-Heuss-Strasse 4
D-3300 Braunschweig
FEDERAL REPUBLIC OF GERMANY

British Geological Survey (3)
Hydrogeology Group
Attn: G. Darling
R. A. Downing
R. L. F. Kay
Maclean Building
Crowmarsh Gifford
Wallingford
Oxfordshire OX10 8BB
GREAT BRITAIN

U. K. Atomic Energy Authority (3)
Attn: M. Ivanovich
R. Otlet
A. J. Walker
Centre for Nuclear Applications
Isotope Measurement Laboratory
Harwell
Oxfordshire OX11 ORA
GREAT BRITAIN

D. R. Knowles
British Nuclear Fuels, plc
Risley, Warrington, Cheshire WA3 6AS
1002607 GREAT BRITAIN

Shingo Tashiro
Japan Atomic Energy Research Institute
Tokai-Mura, Ibaraki-Ken
319-11 JAPAN

Netherlands Energy Research Foundation
ECN (2)
Attn: Tuen Deboer, Mgr.
L. H. Vons
3 Westerduinweg
P.O. Box 1
1755 ZG Petten, THE NETHERLANDS

Svensk Karnbransleforsorjning AB
Attn: Fred Karlsson
Project KBS
Karnbranslesakerhet
Box 5864
10248 Stockholm, SWEDEN

SANDIA INTERNAL

400 L. D. Tyler
1510 J. C. Cummings
1512 K. L. Erickson
1520 C. W. Peterson
1521 J. G. Arguello
1521 H. S. Morgan
3141 S. A. Landenberger (5)
3151 Supervisor (3)
3154-1 C. L. Ward, (10) for DOE/OSTI
6000 D. L. Hartley
6200 B. W. Marshall
6230 R. K. Traeger
6232 W. R. Wawersik
6233 D. J. Borns
6233 J. L. Krumhansl
6233 S. J. Lambert (5)
6233 C. L. Stein
6300 T. O. Hunter
6310 T. E. Blejwas, Acting
6312 G. E. Barr
6313 L. E. Shephard

6315 F. B. Nimick, Acting
6315 R. J. Glass
6315 M. D. Siegel (15)
6340 W. D. Weart
6340A A. R. Lappin
6340 S. Y. Pickering
6341 R. C. Lincoln
6341 Staff (9)
6341 Sandia WIPP Central Files (10)
6342 D. R. Anderson
6342 Staff (11)
6343 T. M. Schultheis
6343 Staff (2)
6344 E. Gorham
6344 C. F. Novak (10)
6344 Staff (9)
6345 B. M. Butcher, Acting
6345 K. L. Robinson (5)
6345 Staff (9)
6346 J. R. Tillerson
6346 Staff (7)
8524 J. A. Wackerly (SNLL Library)
9300 J. E. Powell
9310 J. D. Plimpton
9320 M. J. Navratil
9325 L. J. Keck (2)
9330 J. D. Kennedy
9333 O. Burchett
9333 J. W. Mercer
9334 P. D. Seward



☆ U.S. GOVERNMENT PRINTING OFFICE 1991 - 573-122/40203